

10TH INTERNATIONAL CONFERENCE
ON
SIMULATION AND MODELLING
IN THE
FOOD AND BIO-INDUSTRY
2018

FOODSIM'2018

EDITED BY

Jan F.M. Van Impe

and

Monika E. Polańska

APRIL 8-12, 2018

GHENT, BELGIUM

A Publication of EUROSIS-ETI

Printed in Ghent, Belgium

10th International Conference on
Simulation and Modelling
in the
Food and Bio-Industry

GHENT, BELGIUM

APRIL 8-12, 2018

Organised by

ETI

The European Technology Institute

In Cooperation with

13th International Trends in Brewing Symposium

Katholieke Universiteit Leuven
Technology Campus Ghent

Sponsored by

EUROSIS

The European Simulation Society

Ghent University

University of Skövde

Hosted by

Katholieke Universiteit Leuven
Technology Campus
Ghent, Belgium

EXECUTIVE EDITOR

**PHILIPPE GERIL
(BELGIUM)**

EDITORS

General Conference Chairs

Jan F.M. Van Impe, KU Leuven, Campus Gent, Belgium - IPC Chair
Monika E. Polańska, KU Leuven, Campus Gent, Belgium - OC Chair

OC - Organizing Committee

Monika E. Polańska - OC Chair
Simen Akkermans
Maria Baka
Gerda Friant
Philippe Nimmegeers
Cindy Smet
and all staff of
BioTeC+ Chemical and Biochemical Process Technology and Control
KU Leuven, Campus Gent, Belgium
<https://cit.kuleuven.be/biotec>

IPC - International Programme Committee

Jan F.M. Van Impe, KU Leuven, Campus Gent, Belgium - IPC Chair
Simen Akkermans, KU Leuven, Campus Gent, Belgium
Antonio Alonso, CSIC-IIM, Vigo, Spain
Lourdes Amigo, CSIC, Madrid, Spain
Maria Baka, KU Leuven, Campus Gent, Belgium
Serafim Bakalis, University of Nottingham, Nottingham, United Kingdom
Eva Balsa-Canto, CSIC-IIM, Vigo, Spain
Ursula Gonzales Barron, Instituto Politécnico de Bragança, Bragança, Portugal
Paula Bourke, Dublin Institute of Technology, Dublin, Ireland
Teresa Brandão, Universidade Católica Portuguesa, Porto, Portugal
Bert Bredeweg, Universiteit van Amsterdam, Amsterdam, The Netherlands
Vasco Cadavez, Instituto Politécnico de Bragança, Bragança, Portugal
Enda Cummins, UCD, Dublin, Ireland
Luis Dias, Instituto Politécnico de Bragança, Bragança, Portugal
Juliette Dibie-Barthélemy, UMR AgroParisTech/INRA, Paris, France
Ilija Djekic, University of Belgrade, Belgrade, Republic of Serbia
Ferruh Erdogan, Ankara University, Ankara, Turkey
Matthias Filter, Bundesinstitut für Risikobewertung, Berlin, Germany
Denis Flick, UMR AgroParisTech/INRA, Paris, France
Ourania Gouseti, University of Nottingham, Nottingham, United Kingdom
Anet Režek Jambrak, University of Zagreb, Zagreb, Croatia
Alexandros Koulouris, Alexander TEI of Thessaloniki, Thessaloniki, Greece
Kostas Koutsoumanis, Aristotle University of Thessaloniki, Thessaloniki, Greece
Ivan Leguérinel, Université de Bretagne Occidentale, Quimper, France
Evelyne Lutton, INRA-Grignon, Thiverval-Grignon, France
Isabel Mafra, University of Porto, Porto, Portugal

IPC - International Programme Committee

Bart Nicolai, KU Leuven, Leuven, Belgium
Philippe Nimmegeers, KU Leuven, Leuven, Belgium
Nathalie Méjean Perrot, INRA-Grignon, Thiverval-Grignon, France
Artemio Plana-Fattori, UMR AgroParisTech/INRA, Paris, France
Cristina Luisa Silva, Universidade Católica Portuguesa, Porto, Portugal
Panagiotis Skandamis, Agricultural University of Athens, Athens, Greece
Torstein Skåra, Nofima, Stavanger, Norway
Cindy Smet, KU Leuven, Campus Gent, Belgium
Petros Taoukis, National Technical University of Athens, Athens, Greece
Bas Teusink, Vrije Universiteit Amsterdam, Amsterdam, The Netherlands
Efstathia Tsakali, University of West Attika (TEI-Athens), Athens, Greece
John Tsaknis, University of West Attika (TEI-Athens), Athens, Greece
Vasilis Valdramidis, University of Malta, Msida, Malta
Eirina Velliou, University of Surrey, Guildford, United Kingdom
Pieter Verboven, KU Leuven, Leuven, Belgium
Olivier Vitrac, INRA, Paris, France
Dana Ziuzina, Dublin Institute of Technology, Dublin, Ireland

© 2018 EUROSIS-ETI

Responsibility for the accuracy of all statements in each peer-referenced paper rests solely with the author(s). Statements are not necessarily representative of nor endorsed by the European Simulation Society. Permission is granted to photocopy portions of the publication for personal use and for the use of students providing credit is given to the conference and publication. Permission does not extend to other types of reproduction, nor to copying for incorporation into commercial advertising nor for any other profit-making purpose. Other publications are encouraged to include 300- to 500-word abstracts or excerpts from any paper contained in this book, provided credits are given to the author and the conference.

All author contact information provided in this Proceedings falls under the European Privacy Law and may not be used in any form, written or electronic, without the written permission of the author and the publisher. Infringements of any of the above rights will be liable to prosecution under Belgian civil or criminal law.

All articles published in these Proceedings have been peer reviewed

EUROSIS-ETI Publications are ISI-Thomson, IET, SCOPUS and Elsevier Engineering Village referenced
Legal Repository: Koninklijke Bibliotheek van België, Keizerslaan 4, 1000 Brussels, Belgium
CIP 12.620 D/2011/12.620/1

Selected papers of this conference are published in scientific journals.

For permission to publish a complete paper write EUROSIS, c/o Philippe Geril, ETI Executive Director, Greenbridge Science Park, Ghent University Ostend Campus, Wetenschapspark 1, Plassendale 1, B-8400 Ostend, Belgium.

EUROSIS is a Division of ETI Bvba, The European Technology Institute, Torhoutsesteenweg 162, Box 4, B-8400 Ostend, Belgium

Printed and bound in Belgium by Reproduct NV, Ghent, Belgium
Cover Design by Grafisch Bedrijf Lammaing, Ostend, Belgium
Cover pictures are reproduced under Wikimedia Commons

EUROSIS-ETI Publication
ISBN: 978-9492859-01-3
EAN: 978-9492859-01-3

PREFACE

Dear Colleagues,

Welcome (back) in Gent on KU Leuven's local Technology Campus, to attend the FOODSIM'2018 conference!

Apart from being organized in one of the most friendly cities worldwide, this 10th edition of the FOODSIM conference (an anniversary!) offers a very attractive scientific programme to all colleagues interested in mathematical modeling, simulation, and model based design and optimization of food products and processes. Besides a variety of Technical Sessions devoted to Sustainable Food Systems Engineering, Food Safety and Spoilage, Quantitative Risk Assessment, Food Process Systems Engineering, Innovative Food Production and Processing Technologies, Food Business and Economics, a dedicated session presents recent advances in Multi-Scale Modeling Methods. Other programme highlights include 3 state-of-the-art Tutorial and Workshop presentations and a Poster Session organized by the Erasmus Mundus MSc students (European Master BiFTec - Food Science, Technology and Business), thus highlighting the importance of Quantitative Food Science in both teaching as well as training of early stage researchers.

The organizing KU Leuven/BioTeC+ team celebrates its 25th anniversary. Quite a few presentations highlighting our recent experimental and computational work are integrated into the various sessions.

As in the previous edition, FOODSIM is running in parallel with another food related event on our campus, Trends in Brewing. The organizers of both events expect significant synergies. First of all, participants can easily attend lectures or even full sessions from the parallel event, including Workshops and Poster Sessions. Second, FOODSIM participants may be interested in visiting the attractive Trends in Brewing Technical Exhibition, while the 3 FOODSIM Keynote Lectures are definitely of interest to a new TiB audience as well. Third, an extra FOODSIM (musical) Keynote open to all is organized at the occasion of 25 years of KU Leuven/BioTeC+ and 10 years of FOODSIM. Last but not least, both events share the Social Programme, with specialty beer tasting as one of the daily highlights and the optional visit to a Belgian brewery to conclude the conference in style.

The FOODSIM programme has all ingredients needed to provide you with a rewarding experience at the interface of science and "savoir vivre". The organizers look forward to lively discussions and hope to provide you with a forum for networking and intensified collaboration. Many thanks to all involved in the organization and in the reviewing process!



Jan F.M. VAN IMPE, IPC Chair & Monika E. POLAŃSKA, OC Chair &
KU Leuven/BioTeC+ Research Division



Preface	VII
Scientific Programme	1
Author Listing	307

Keynotes

Constraint-Based Models of Microbial Physiology: Surprisingly Versatile Bas Teusink, Bob Planqué, Douwe Molenaar and Frank Bruggeman	5
--	----------

Human in the Loop for Modelling Food and Biological Systems: a Novel Perspective coupling Artificial Intelligence and Life Science Nathalie Méjean Perrot, Nadia Boukhelifa, Alberto Tonda, Thomas Chabin, Marc Barnabé, Dominique Swennen, Alice Roche, Thierry Thomas-Danguin and Evelyne Lutton	11
--	-----------

Non-thermal Food Processing: Modelling of Processes towards Safety, Quality and Sustainability Anet Režek Jambrak, Ilija Djekić and Jan Van Impe	19
--	-----------

Tutorial and Workshop Presentations

Sustainability in Food Industry: Towards a Unified Multi-Objective Decision Making Framework Philippe Nimmegeers, Satyajeet Bhonsale, Carlos André Muñoz López, Ihab Hashem and Jan Van Impe	25
--	-----------

Application of Dynamic Optimization for Food Systems using Pomodoro: A Tutorial Satyajeet Bhonsale, Dries Telen, Philippe Nimmegeers and Jan Van Impe	29
---	-----------

E-CAM: a European Infrastructure for Advanced Simulation Software Development, Training and Industry Collaboration from Food and Pharma to Advanced Materials Donal Mac Kernan	33
--	-----------

Modeling and Simulation in Sustainable Food Systems Engineering

Position Paper: Needs Analysis and Trends in Sustainable Food Systems within Higher Education Monika Polańska, Paula Bourke, Enda Cummins, Wolfram Schnäckerl, Vasilis Valdramidis and Jan Van Impe	41
---	-----------

CONTENTS

Modelling Multicriteria Argument Networks about reduced Meat Consumption Nicolas Salliou and Rallou Thomopoulos.....	46
Consumer Demand for Sustainable versus Low-Cost Food Products: An Agent-based Modelling Approach Rallou Thomopoulos and Serafim Bakalis	52
Multi-objective Optimization of the Formulation of Barley Bread using Artificial Neural Network and Genetic Algorithm Predrag Kojić and Milica Pojić.....	57
Numerical Study of Airflow and Temperature Distribution in a loaded Cold Store Pierre Coldrey, Jean Moureh, Graciella Alvarez, Denis Leducq, Alain Foster, Mohammed Youbi-Idrissi, Alain Damas and Judith Evans.....	60
 Modeling and Simulation in Quantitative Risk Assessment	
A Quantitative Human Exposure Assessment Model for Antibiotic Resistant <i>Escherichia Coli</i> through Tap Water Consumption Eithne O' Flaherty, José Luis Balcázar, Carles M. Borrego and Enda Cummins	71
Modelling the Persistence of Nano Silver through Drinking Water Treatments David Shevlin and Enda Cummins.....	74
Quantitative Risk Assessment of Antimicrobials in the Feed to Food Chain Rachel Clarke, Mark G Healy, Owen Fenton and Enda Cummins.....	77
Next Generation Microbiological Risk Assessment: Next Generation Sequencing (NGS) for the Determination of Fish Flesh Microbiota Theofania Tsironi, Vassiliki Nefel Simou, Afrodite Mexi, Lougovois Vladimirov, Koussissis Stamatis and Dimitra Houhoula.....	81
 Modeling and Simulation in Food Safety and Spoilage	
Kinetic Modelling of Scavenger Reactions: Parameter Estimation for a Gallic Acid Based Oxygen Scavenger Astrid F. Pant and Matthias Reinelt.....	89
Efficient Data Collection for Modelling the Growth Rate as a Function of the Environmental Conditions Simen Akkermans, Philippe Nimmegeers and Jan F. Van Impe.....	95

The Role of Control Strategies for the Implementation of Food Safety in Hospital and Health Units, as a Tool for HACCP Assistants and Simulators Efstathia Tsakali, Olga Gortzi, George Boskou, Andreas Souliotis, Dimitrios Timpis and John Tsaknis	104
Modelling of Temperature, Water Activity and Microbial Growth on the Surface of a Pork Leg during Refrigerated Transportation Mouna Merai	108
Quantitative Anti-Fungal Activity Assessment of ZnO Nanoparticles: Towards the Design and Development of Novel Air Filtration Systems Vasilis P. Valdramidis, Davide Sardella and Ruben Gatt	113
Effect of Food Microstructure on Thermal Inactivation Dynamics of <i>Listeria Monocytogenes</i> Davy Verheyen, Maria Baka, Torstein Skåra and Jan F. Van Impe	117
A Simple Method for growing <i>Pseudomonas Fluorescens</i> Biofilms on a Hydrophobic Polystyrene Surface Valeria Angarano, Cindy Smet, Maria Baka, Simen Akkermans, Andre Chieffi and Jan Van Impe	125
Stochastic Methods to model Bacterial Growth and Food Safety Risks: Some Perspectives Míriam R. García and Antonio A. Alonso	130
Growth/No Growth Models of Different Stress adapted <i>Listeria Monocytogenes</i> Strains Pantelis Stathopoulos, Dimitra Houhoula, Dimitris Timpis, Efstathia Tsakali, Jan F.M. Van Impe and Spiridin Konteles.....	135
Modeling and Simulation in Food Process Systems Engineering	
PSE4GUT: Influence of a Low Calories Diet Shift on Gut Microbiota Dynamics – Towards a Process Systems Engineering Approach Theodora Akritidou, Cindy Smet, Philippe Nimmegeers, Simen Akkermans and Jan F.M. Van Impe.....	145
Simultaneous Data Scaling and Training of Data Driven Regression Models for Quality Control of Batch Processes Carlos André Muñoz López, Philippe Nimmegeers and Jan Van Impe.....	150
Smart Sensors to assess and to anticipate Fish Quality Evolution Carlos Vilas, Míriam R. García, Eva Balsa-Canto and Antonio A. Alonso.....	158

CONTENTS

Industrial Process design for Microwave Pasteurization of Liquid Foods: a Computational Study Huseyin Topcam and Ferruh Erdogan	166
A Coupled CFD-Heat Transfer Model for In-Package Solid Food Pasteurization Clarissa Detomi de Albuquerque, Sébastien Curet and Lionel Boillereaux.....	172
Numerical Modelling of Airflow and Heat Transfer in a Vented Pallet of Cheese Anh Thu Pham, Jean Moureh and Denis Flick.....	177
Edible Oil Hydrogenation: Revisited Viscosity Prediction for Accurate Process Simulation Pierre Albrand, Anne-Marie Billet, Carine Julcour and Vincent Gerbaud	181
Optimal Control of Fructo-Oligosaccharide Production J. Schorsch, M. Kinnaert, R. Fekih-Salem, L. Dewasme, C.C. Castro and A. Vande Wouwer	184
Modeling and Simulation in Innovative Food Production and Processing Technologies	
Modelling and Validation of Time Temperature History and Enzyme Inactivation in the Continuous Flow Microwave assisted Pasteurization of Apple Juice Érica S. Siguemoto, Carmen C. Tadini and Jorge A. W. Gut.....	189
A Long-Short-Term Memory Network Model for Biscuit Baking Alberto Tonda and Nathalie Perrot.....	194
On the Quantification of the Impact of Natural Antimicrobials on the Growth Kinetics of <i>Listeria</i> in Complex Food Models Katherine Costello, Madeleine Bussemaker, Eirini Velliou, Jorge Gutierrez-Merino, Maria Baka and Jan Van Impe.....	199
Effect of Xhantan Gum on Physicochemical and Textural Properties of Gluten-Free Batter and Bread Christian R. Encina-Zelada, José A. Teixeira, Fernando Monteiro, Ursula Gonzales-Barron and Vasco Cadavez.....	204
Creating, Refining and Validating a Model Describing Spatiotemporal Dynamics in Cheese during Ripening Thorsten Stefan	210

Influence of Cold Atmospheric Plasma on the Microbial Dynamics of Salmonella Typhimurium during Storage at Different Temperatures Cindy Smet, Maria Baka, James Walsh, Vasilis Valdramidis and Jan F.M. Van Impe.....	214
Influence of Plasma Characteristics on the Efficacy of Cold Atmospheric Plasma (CAP) for Inactivation of Biofilms developed by <i>Listeria Monocytogenes</i> and <i>Salmonella Typhimurium</i> M. Govaert, C. Smet, M. Baka and J.F.M. Van Impe	221
Modelling Microbiological and Quality Marker Responses to Enhance Cold Plasma Cereal Grain Processing Dana Ziuzina, Agata Los, Simen Akkermans, Daniela Boehm, Patrick J. Cullen, Jan F.M. Van Impe and Paula Bourke	229
Characterization of Fish Based Model Food Systems for Microwave Heating Modeling Ferruh Erdogdu, Huseyin Topcam, Ozan Altin, Davy Verheyen, Jan F. Van Impe, Ti Kian Seow, Dagbjørn Skipnes and Torstein Skåra	235
Multi-Scale Modeling Methods	
A Semi-Automatic Modelling Approach for the Production and Freeze Drying of Lactic Acid Bacteria Thomas Chabin, Marc Barnabé, Alberto Tonda, Nadia Boukhelifa, Fernanda Fonseca, Eric Dugat-Bony, Hélène Velly, Evelyne Lutton and Nathalie Méjean Perrot	243
A Generalized NURBS Based Dynamic Metabolic flux Analysis Framework: Deciphering Intracellular Pathway Activation from Extracellular Measurements Philippe Nimmegeers, Simen Akkermans, Wouter Gijsen, Dries Telen and Jan Van Impe	248
Ghost Competition: On the Reliability of Quorum Sensing as an Information Source for Bacterial Species Ihab Hashem, Philippe Nimmegeers, Satyajeet Bhonsale, Carlos André Muñoz López and Jan Van Impe.....	253
Multi-Scale Modelling to explain Wine Fermentation D. Henriques, R. Minebois, R. Pérez-Torrado, E. Balsa-Canto and A. Querol..	259
Two-Equation Oxygen Diffusivity of Apple Cortex Tissue for Multiscale Modeling of Gas Exchange Siem Janssen, Pieter Verboven, Bart Nicolaï and Susana Zorrilla	264

CONTENTS

Estimation of Intrinsic Viscosity of Apple Cells by Numerical Simulation
Artemio Plana-Fattori, Christophe Doursat, Giana Almeida, Gabrielle Moulin,
Cassandre Leverrier, Even Ou and Denis Flick269

**Modeling of Microwave Heating in a Cylindrical Cavity System: Effect
of Rotation and Sample Location on Temperature Uniformity**
Ozan Altin, Ferruh Erdogdu, Dagbjørn Skipnes and Torstein Skåra.....277

Modeling and Simulation in Food Business and Economics

**An Evaluation of the Effect of Different Tempering Conditions on Dark
Chocolate Compositions**
Jewel Ann Joseph, Jan F.M. Van Impe and Monika Polańska.....285

**Techno-Economic Evaluation of β -Cyclodextrin Production from Cassava
Tubers**
Nikolaos Vacharakis, Anastasia Louizaki, Chrysi Charalambous,
Stylianos Raphaelides and Alexandros Koulouris.....290

Modeling a Brewery: Capacity and Cost Analysis
Alexandros Koulouris, Albert Roussos and Demetri Petrides295

Short Paper

Design and CFD Simulation of a Parabolic Solar Fruit Dryer
Joshua Wanyama, Cyrus Galyaki, John Muyonga, Nicholas Kiggundu
and Noble Banadda301

Scientific Programme

Keynotes

CONSTRAINT-BASED MODELS OF MICROBIAL PHYSIOLOGY: SURPRISINGLY VERSATILE

Bas Teusink

Bob Planqué

Douwe Molenaar

Frank Bruggeman

and all of the www.teusinkbruggemanlab.nl team

Amsterdam Institute of Molecules, Medicines and Systems

Vrije Universiteit Amsterdam

O|2 building, section Systems Bioinformatics, location code 2E51

De Boelelaan 1085, NL-1081HV Amsterdam, The Netherlands

E-mail: b.teusink@vu.nl

KEYWORDS

Model, Optimization, Microbial Physiology, Constraint-based Modeling, Systems Biology.

ABSTRACT

Microbial cells evolved a remarkable ability to adapt to environmental conditions, or to withstand otherwise detrimental mutations, which makes them often very resilient to man-made interventions. These properties arise from the integrative functioning of biological networks. Functional genomics has allowed the cost-effective measurement of the network components; however, we still mostly fail to understand how their interactions lead to cellular function and adaptation. For this, modeling is required.

Current mainstream constraint-based metabolic modeling efforts largely focus on the metabolic network only, albeit at genome-scale. They are based on reaction stoichiometry only, but nonetheless can be extremely valuable for mostly exploratory analysis of the metabolic potential of an organism. However, because these “Flux Balance Analysis” (FBA) methods lack important parts of the cell –with their associated constraints- they often fail to predict changes in common regulatory strategies.

One view that is becoming dominant in cellular physiology, is that physical and (bio)chemical constraints limits protein content and synthesis, impacting on how resources are partitioned over growth and stress processes to optimize fitness (“cellular economics”). Such constraints can lead to (evolutionary) trade-offs and can explain a large number of microbial physiological phenomena, such as overflow metabolism or catabolite repression. Current efforts in the modeling field aim to include such resource constraints into the constraint-based modeling format.

We have developed theory to understand what the solution is to a flux maximization problem under resource constraints. We found that Elementary Flux Modes (EFMs), mathematical definitions of minimal pathways, are the flux maximisers. Although the number of EFMs is enormous (in the millions), the number of active constraints determines the maximum number of active EFMs at optimum. So

complexity of the flux space seems to be determined by the constraints, not by the seemingly infinite possibilities.

Still, the resource allocation perspective is developed for steady-state growth under constant environments. What happens during *dynamic* growth conditions is largely unexplored. Such analysis requires dynamic models, one of which is dynamic FBA.

We conclude that the constraint-based modeling approach is a powerful and versatile approach to explain the physiology of a cell through the interactions of its molecular components and the governing physico-chemical and biochemical constraints.

CONSTRAINT-BASED MODELING AT STEADY STATE

Adaptations involve the consideration of wise allocation of limited resources

Cells adapt their cellular composition and protein expression according to environmental conditions. Accumulating data and theory have established that proper resource allocation is an important driver for such adaptations. In *E coli*, the expression level of the lac system maximized a benefit-minus-cost function (Dekel and Alon, 2005); overexpression of non-functional protein causes a reduction in growth rate (Snoep et al., 1995; Kurland and Dong, 1996; Shachrai et al., 2010). Ribosomal content scales linearly with growth rate (Scott et al., 2010), which is the expected optimal partitioning for growth rate (Bosdriesz et al., 2015). Protein titration studies (in labstrains grown in labmedium to which cells are quite well adapted) very often show optimality around wild type level, with strong decrease in fitness upon lowering protein level, and a decrease at higher expression level (Mijakovic et al., 2005; Teusink et al., 2011). In yeast, but also *E coli* (Ihssen and Egli, 2004) there is an inverse relationship between stress resistance and growth rate (Zakrzewska et al., 2011; Levy et al., 2012), to the extent that the general stress response is now viewed as a growth rate response (Brauer et al., 2008). One explanation is that at high growth rates less resources are being spent on stress proteins, and more on ribosomes (Dhar et al., 2013). Thus, adaptation is resource management,

weighted (or traded-off (Szekely et al., 2013)) against effectiveness (or benefit) of the possible strategies.

Models of growth: current state of the art

Current mainstream quantitative approaches in cell physiology are too limited to predict, from costs and benefits, which factors, and to what extent, contribute to the tipping of the balance into different directions. Traditionally, costs associated to unicellular growth are related to ATP use. Based on flux measurements at different growth rates, the total rate of ATP production by catabolism is estimated and equated to growth-associated ATP requirements – the ATP costs for making biomass (Neijssel and Teixeira de Mattos, 1994; Feist and Palsson, 2010). This method assumes that full coupling exists between ATP production and ATP consumption by growth-related processes and results in a growth-dependent ATP requirement and a maintenance rate at zero growth (Teusink et al., 2006). These parameters are used in the roughly two different approaches that are being used to subsequently model cellular growth:

- (i) coarse grained “Monod-type” models consisting of one equation that links growth rate to the availability of nutrients;
- (ii) stoichiometric genome-scale metabolic models that predict, most often through optimisation, the flow of material towards new cells (biomass) based on inflow of nutrients. The latter approach requires hundreds to thousands of equations for mass-balancing each metabolite in the metabolic network.

The coarse-grained models lack molecular details but incorporate (some) kinetics and hence can truly predict rates from nutrient concentrations, according to the so-called Monod equation of variants thereof. However, they are so coarse-grained that the interesting “intracellular” biology is lost. These models are most useful for predictive biology (estimating likelihood of microbial outgrowth (Peleg and Corradini, 2011)) and evolutionary models.

At the other end of the spectrum, the genome-scale metabolic models capture all the gene-to-protein-to-reaction associations of a cell, and hence have the full molecular detail of metabolism (Francke et al., 2005). However, note that only the stoichiometry of the reaction (i.e. which compounds take part in each reaction) is captured, not the kinetics of the corresponding enzymes. Workflows exist that use whole-genome sequences, bioinformatics, additional biochemical knowledge (“legacy data”) and experiments to construct and validate the metabolic network (Thiele and Palsson, 2010). It is available for a great number of organisms (Oberhardt et al., 2009), including human (Thiele et al., 2013). Given the reaction network structure, growth is subsequently modeled as a sink for biomass components, such as lipids, proteins, RNA and DNA, as specified in the biomass equation (Feist and Palsson, 2010):



Here x_i specifies how much of each component is represented in biomass, and y represents the part of the experimentally-derived growth-related ATP expenditure unaccounted for in these models (Teusink et al., 2006). Typically, these stoichiometric models can only account for about 50% of the total ATP produced by catabolism (Stouthamer and Bettenhausen, 1973; Förster et al., 2003; Teusink et al., 2006). Thus, the network should supply the biomass components and ATP in the proper ratio's, defining feasible flux distributions. In steady state, the “solution space”, i.e. the space of feasible flux distributions, is very large. Therefore, in Flux Balance Analysis (FBA), optimization is used to find optimal (steady-state) flux distributions to maximize (or minimize) some objective function, often the biomass equation (Orth et al., 2010; Santos et al., 2011). Many variants to this approach exist (Lewis et al., 2012) but FBA remains the most-often used technique.

In this formalism, two immediate limitations are at play. *First*, the solution space is necessarily bounded by constraints on uptake rates (Schuster et al., 2008; Teusink et al., 2009), as obviously, an optimum is difficult to find in an infinite space. Hence, the highest yield strategy will maximize the flux (Teusink et al., 2009). Under fixed glucose uptake, respiration will therefore always lead to higher growth rate than fermentation in this formalism (Teusink et al., 2006). *Second*, the biomass equation is fixed, even though components in the cell do change with growth rate (as discussed above). Hence, although genome-scale metabolic models have been successful in prediction of reaction essentiality and for exploring metabolic engineering strategies (Oberhardt et al., 2009), in their most-widely used form they are inherently limited in predicting metabolic adaptation strategies.

Example of a success story with FBA

We have recently (Branco Dos Santos et al., 2017) developed a metabolic reconstruction of the human pathogen *Bordetella pertussis*, the causative agent of whooping cough. We have used data from two deeply sampled batch fermentations to parametrise the energy requirements, to resolve some ambiguities in the network and to derive at a proper biomass composition. We subsequently explored the network to find all possible growth nutrient combinations that would support growth. Surprisingly, *B. pertussis* was always considered a fastidious organism requiring rich growth media, but we predicted and experimentally validated that it is able to grow –slowly– on cysteine as the only C, N and S source. In fact it grows on many rather minimal media.

Two more discoveries were made through the model; first, *B. bordetella* secretes relatively high amounts of nucleobases and nucleotides as N-products (found as means to close the N-balance in the model). Second, we found that thiosulphate could replace organic S-sources that during industrial production of pertussis toxin caused toxicity problems. In the end, a simpler growth medium led to a more than twofold increase in toxin yield (Branco Dos Santos et al., 2017).

Many aspects of cell biology are not captured in current genome-scale modeling approaches

Despite these successes, from a predictive modeling perspective there are three major shortcomings of the current mainstream genome-scale modeling approaches. *First*, the inherent kinetic limitations of enzymes is poorly represented, only via some bounds on particular (uptake) reactions rates only. In particular the role of ribosomes, the protein-synthetic machinery of the cell, sets important indirect limitations to the fluxes in the metabolic network, as it has to synthesize all the enzymes that carry out these reactions, *including itself*. The latter represent the self-replicating core of cellular growth, which we believe is an essential ingredient of a growth model (Molenaar et al., 2009). *Second*, it fails to adequately capture major other constraints on cell growth as discussed above, rooted in physics and chemistry. *Third*, ‘costs of living’ are largely ignored, and only captured in y , the growth-associated maintenance. These shortcomings are being recognized and new formats are being developed that promise to provide a rich, genome-scale perspective on growth and adaptation.

Costs of living

The costs for growth and survival, and for adaptability, relate to:

- (i) protein-synthesis related costs (protein turnover; protein misfolding; protein trafficking; protein modifications; RNA synthesis and turnover; metabolic precursors and energy for polymerisation)
- (ii) replicative costs (proofreading; DNA modifications such as methylation; chromatin remodelling)
- (iii) cell division costs (cell-wall remodeling, organel and genome partitioning)
- (iv) other maintenance costs related to e.g. ion and pH homeostasis, possibly cytoskeleton maintenance etc.
- (v) investment in stress resistance at the expense of growth-promoting proteins

Some of these will be growth-rate dependent, other most probably not. Clearly, a number of these costs will be very difficult to quantify, but for quite a few of them, high-throughput methods have been developed to provide reasonable estimates.

Genome-scale modeling approaches capturing some of these aspects

In recent years, a number of approaches have been developed to implement physicochemical constraints and costs into the genome-scale modeling framework - for review, see (Goelzer and Fromion, 2017). These include flux-minimization to favor shorter pathways (Holzhütter, 2004), upper bounds on total flux weighted by some crowding factor for protein (Beg et al., 2007; Vazquez et al., 2008), limits on membrane occupancy (Zhuang et al., 2011) or very recently bounds on protein based on catalytic activities were proposed (Adadi et al., 2012). In all cases only a limited set of all relevant costs and constraints were taken into account, and without quantitative assessment of the possible impact of others. Conversely, genome-scale

models have been used to compute (metabolic) costs of proteins for comparative purposes (Barton et al., 2010).

Recently the ME matrix was introduced, in which the Metabolic network and the network for Expression, i.e. transcription and translation, were combined in excruciating detail (Thiele et al., 2012). Thus, for flux to go through a metabolic reaction, also flux has to go through the transcription and translation reactions for the associated protein, based on “coupling constants” (Thiele et al., 2010, 2012). Other studies incorporated constraints at the level of protein expression, cell morphology and flux to enzyme level in different ways, but with the same general idea (Goelzer et al., 2015; Nilsson and Nielsen, 2016; Reimers et al., 2017).

Most of these studies use growth rate as the sink for individual proteins, which are now variables of the model that need to be balanced: thus, rather than having a fixed total protein amount in the biomass equation (see above), protein composition can and will change with growth rate. This means, however, that the growth rate now appears in mass balances, making the optimisation non-linear and hard to solve for large systems of variables. The solution to this problem is to fix the growth rate and minimise for nutrient uptake. Mathematically, the solution will be the same as for maximising the growth rate under a constraint uptake rate. However, in this way, we implicitly assume that uptake rate is indeed constraining growth! This led us to think about the expected solutions of models that aim to maximise flux under protein constraints.

Maximising flux requires thinking about elementary flux modes

When an objective flux is maximized under a total protein constraint (the so-called specific flux, with symbol q), then the optimal flux distributions are highly structured, irrespective of the kinetics and feedbacks used. We have mathematically proven that the flux will have to go through an elementary flux mode (EFM), which is a mathematical definition of a minimal pathway: EFMs connect extracellular sources and sinks through a (or combinations of) metabolic pathway in which none of the reactions can be removed without loss of steady state. The proof can be found elsewhere, but whenever the internal metabolite levels are fixed to arbitrary values (so also the optimal values), the optimisation problem becomes a linear program, and the resultant solution space is spanned by rays that represent EFMs. Optimal solutions lie on these rays, making EFMs the maximisers.

However, the approaches used in the genome-scale, stoichiometric models, do not use total protein as a constraint, but uptake rate, i.e. they assume a constraint at the membrane. This led us to think that more than one protein pool could act as a constraint. It turns out, that when flux is maximised under n protein constraints, the number of active EFMs in the optimal flux distribution is smaller or equal to n .

This result has one important consequence in the way we can think about complex metabolic networks: despite the fact that in such networks thousands of reactions occur, and millions of pathways can be defined, in the optimal state,

the degrees of freedom are determined by the number of prevailing constraints.

CONSTRAINT-BASED MODELING UNDER DYNAMIC CONDITIONS

The modeling and theory described so far dealt with microbes at steady state under constant conditions. This of course is an idealisation for most conditions in a microbe's life. There are different approaches to extend the constraint-based modeling approaches to dynamic conditions, depending on the available (kinetic) information and the time-scales.

Dynamic FBA combines population dynamics with genome-scale reconstructions

In so-called dynamic FBA ordinary differential equations describe the dynamics of both the growth-limiting nutrient(s) and the biomass. Using enzyme-kinetic functions, prevailing nutrient levels are converted into corresponding uptake constraints, and FBA is used to calculate the instantaneous, maximal steady-state growth rate under those constraints. The resulting growth rate is used to compute the biomass over time. The key assumptions of this approach are that indeed uptake is the dominant constraint for growth rate, and that the time scale of the nutrient dynamics is much larger than that of internal dynamics; this allows for pseudo steady state of the internal metabolic network.

When applied to metabolic models only, the approach really is very similar to a Monod-type model, except that the biomass yield is now well-informed by genomic details. For this reason, dynamic FBA has been applied to microbial ecosystems (Hanemaaijer et al., 2017). One of the key problems, however, is the optimisation at each time integration step, which prevents predictions of delayed return-of-investment strategies in ecosystems. Nonetheless, especially when these models become combined with resource allocation constraints that allow for shifts in growth strategies, we expect these type of models to be an important corner stone towards more realistic and molecular population dynamic models.

CONCLUSIONS

Constraint-based modeling once started with the steady state analysis of stoichiometric networks of metabolic reactions. This is still an excellent way to quickly move from genome to potential physiology. The constraints are steady state (mass balance constraints) and capacity constraint, i.e. constraints on the values of the flux. In recent years, resource allocation constraints, have been added, which on the one hand adds richness in the behaviour of the models, and on the other hand removes degrees of freedom in the potential states of the cell. Through these developments, a predictive molecular systems biology comes into reach.

REFERENCES

- Adadi, R., B. Volkmer, R. Milo, M. Heinemann, and T. Shlomi, 2012, Prediction of microbial growth rate versus biomass yield by a metabolic network with kinetic parameters: *PLoS computational biology*, v. 8, no. 7, p. e1002575, doi:10.1371/journal.pcbi.1002575.
- Barton, M. D., D. Delneri, S. G. Oliver, M. Rattray, and C. M. Bergman, 2010, Evolutionary systems biology of amino acid biosynthetic cost in yeast: *PLoS one*, v. 5, no. 8, p. e11935, doi:10.1371/journal.pone.0011935.
- Beg, Q. K., A. Vazquez, J. Ernst, M. A. de Menezes, Z. Bar-Joseph, A.-L. Barabási, and Z. N. Oltvai, 2007, Intracellular crowding defines the mode and sequence of substrate uptake by *Escherichia coli* and constrains its metabolic activity: *Proceedings of the National Academy of Sciences of the United States of America*, v. 104, no. 31, p. 12663–12668, doi:10.1073/pnas.0609845104.
- Bosdriesz, E., D. Molenaar, B. Teusink, and F. J. Bruggeman, 2015, How fast-growing bacteria robustly tune their ribosome concentration to approximate growth-rate maximization: *The FEBS journal*, doi:10.1111/febs.13258.
- Branco Dos Santos, F. et al., 2017, Probing the genome-scale metabolic landscape of *Bordetella pertussis*, the causative agent of whooping cough: *Applied and Environmental Microbiology*, doi:10.1128/AEM.01528-17.
- Brauer, M. J., C. Huttenhower, E. M. Airoidi, R. Rosenstein, J. C. Matese, D. Gresham, V. M. Boer, O. G. Troyanskaya, and D. Botstein, 2008, Coordination of growth rate, cell cycle, stress response, and metabolic activity in yeast: *Molecular biology of the cell*, v. 19, no. 1, p. 352–367, doi:10.1091/mbc.E07-08-0779.
- Dekel, E., and U. Alon, 2005, Optimality and evolutionary tuning of the expression level of a protein: *Nature*, v. 436, no. 7050, p. 588–592, doi:10.1038/nature03842.
- Dhar, R., R. Sägger, C. Weikert, and A. Wagner, 2013, Yeast adapts to a changing stressful environment by evolving cross-protection and anticipatory gene regulation: *Molecular biology and evolution*, v. 30, no. 3, p. 573–588, doi:10.1093/molbev/mss253.
- Feist, A. M., and B. O. Palsson, 2010, The biomass objective function: *Current opinion in microbiology*, v. 13, no. 3, p. 344–349, doi:10.1016/j.mib.2010.03.003.
- Förster, J., I. Famili, P. Fu, B. Ø. Palsson, and J. Nielsen, 2003, Genome-scale reconstruction of the *Saccharomyces cerevisiae* metabolic network: *Genome research*, v. 13, no. 2, p. 244–253, doi:10.1101/gr.234503.
- Francke, C., R. J. Siezen, and B. Teusink, 2005, Reconstructing the metabolic network of a bacterium from its genome: *Trends in microbiology*, v. 13, no. 11, p. 550–558, doi:10.1016/j.tim.2005.09.001.
- Goelzer, A. et al., 2015, Quantitative prediction of genome-wide resource allocation in bacteria: *Metabolic Engineering*, v. 32, p. 232–243, doi:10.1016/j.ymben.2015.10.003.
- Goelzer, A., and V. Fromion, 2017, Resource allocation in living organisms: *Biochemical Society Transactions*, v. 45, no. 4, p. 945–952, doi:10.1042/BST20160436.
- Hanemaaijer, M., B. G. Olivier, W. F. M. Röling, F. J. Bruggeman, and B. Teusink, 2017, Model-based quantification of metabolic interactions from dynamic microbial-community data: *PLoS One*, v. 12, no. 3, p. e0173183, doi:10.1371/journal.pone.0173183.
- Holzhütter, H.-G., 2004, The principle of flux minimization and its application to estimate stationary fluxes in metabolic networks: *European journal of biochemistry / FEBS*, v. 271, no. 14, p. 2905–2922, doi:10.1111/j.1432-1033.2004.04213.x.

- Ihssen, J., and T. Egli, 2004, Specific growth rate and not cell density controls the general stress response in *Escherichia coli*: *Microbiology* (Reading, England), v. 150, no. Pt 6, p. 1637–1648, doi:10.1099/mic.0.26849-0.
- Kurland, C. G., and H. Dong, 1996, Bacterial growth inhibition by overproduction of protein: *Molecular microbiology*, v. 21, no. 1, p. 1–4.
- Levy, S. F., N. Ziv, and M. L. Siegal, 2012, Bet hedging in yeast by heterogeneous, age-correlated expression of a stress protectant: *PLoS biology*, v. 10, no. 5, p. e1001325, doi:10.1371/journal.pbio.1001325.
- Lewis, N. E., H. Nagarajan, and B. O. Palsson, 2012, Constraining the metabolic genotype-phenotype relationship using a phylogeny of in silico methods: *Nature reviews. Microbiology*, v. 10, no. 4, p. 291–305, doi:10.1038/nrmicro2737.
- Mijakovic, I., D. Petranovic, and P. R. Jensen, 2005, Tunable promoters in systems biology: Current opinion in biotechnology, v. 16, no. 3, p. 329–335, doi:10.1016/j.copbio.2005.04.003.
- Molenaar, D., R. van Berlo, D. de Ridder, and B. Teusink, 2009, Shifts in growth strategies reflect tradeoffs in cellular economics: *Molecular Systems Biology*, v. 5, p. 323, doi:10.1038/msb.2009.82.
- Neijssel, O. M., and M. J. Teixeira de Mattos, 1994, The energetics of bacterial growth: a reassessment: *Molecular microbiology*, v. 13, no. 2, p. 172–182.
- Nilsson, A., and J. Nielsen, 2016, Metabolic Trade-offs in Yeast are Caused by F1F0-ATP synthase: *Scientific Reports*, v. 6, p. 22264, doi:10.1038/srep22264.
- Oberhardt, M. A., B. Ø. Palsson, and J. A. Papin, 2009, Applications of genome-scale metabolic reconstructions: *Molecular Systems Biology*, v. 5, p. 320, doi:10.1038/msb.2009.77.
- Orth, J. D., I. Thiele, and B. Ø. Palsson, 2010, What is flux balance analysis? *Nature biotechnology*, v. 28, no. 3, p. 245–248, doi:10.1038/nbt.1614.
- Peleg, M., and M. G. Corradini, 2011, Microbial growth curves: what the models tell us and what they cannot: *Critical reviews in food science and nutrition*, v. 51, no. 10, p. 917–945, doi:10.1080/10408398.2011.570463.
- Reimers, A.-M., H. Lindhorst, and S. Waldherr, 2017, A Protocol for Generating and Exchanging (Genome-Scale) Metabolic Resource Allocation Models: *Metabolites*, v. 7, no. 3, doi:10.3390/metabo7030047.
- Santos, F., J. Boele, and B. Teusink, 2011, A practical guide to genome-scale metabolic models and their analysis: *Methods in Enzymology*, v. 500, p. 509–532, doi:10.1016/B978-0-12-385118-5.00024-4.
- Schuster, S., T. Pfeiffer, and D. A. Fell, 2008, Is maximization of molar yield in metabolic networks favoured by evolution? *Journal of theoretical biology*, v. 252, no. 3, p. 497–504, doi:10.1016/j.jtbi.2007.12.008.
- Scott, M., C. W. Gunderson, E. M. Mateescu, Z. Zhang, and T. Hwa, 2010, Interdependence of cell growth and gene expression: origins and consequences: *Science (New York, N.Y.)*, v. 330, no. 6007, p. 1099–1102, doi:10.1126/science.1192588.
- Shachrai, I., A. Zaslaver, U. Alon, and E. Dekel, 2010, Cost of unneeded proteins in *E. coli* is reduced after several generations in exponential growth: *Molecular cell*, v. 38, no. 5, p. 758–767, doi:10.1016/j.molcel.2010.04.015.
- Snoep, J. L., L. P. Yomano, H. V. Westerhoff, and L. Ingram, 1995, Protein burden in *Zymomonas mobilis*: negative flux and growth control due to overproduction of glycolytic enzymes: v. 141, no. 9, p. 2329–2337.
- Stouthamer, A. H., and C. Bettenhausen, 1973, Utilization of energy for growth and maintenance in continuous and batch cultures of microorganisms. A reevaluation of the method for the determination of ATP production by measuring molar growth yields: *Biochimica et biophysica acta*, v. 301, no. 1, p. 53–70.
- Szekely, P., H. Sheftel, A. Mayo, and U. Alon, 2013, Evolutionary Tradeoffs between Economy and Effectiveness in Biological Homeostasis Systems: *PLoS computational biology*, v. 9, no. 8, p. e1003163, doi:10.1371/journal.pcbi.1003163.
- Teusink, B., H. Bachmann, and D. Molenaar, 2011, Systems biology of lactic acid bacteria: a critical review: *Microbial cell factories*, v. 10 Suppl 1, p. S11, doi:10.1186/1475-2859-10-S1-S11.
- Teusink, B., A. Wiersma, L. Jacobs, R. A. Notebaart, and E. J. Smid, 2009, Understanding the adaptive growth strategy of *Lactobacillus plantarum* by in silico optimisation: *PLoS Computational Biology*, v. 5, no. 6, p. e1000410, doi:10.1371/journal.pcbi.1000410.
- Teusink, B., A. Wiersma, D. Molenaar, C. Francke, W. M. de Vos, R. J. Siezen, and E. J. Smid, 2006, Analysis of growth of *Lactobacillus plantarum* WCFS1 on a complex medium using a genome-scale metabolic model: *The Journal of biological chemistry*, v. 281, no. 52, p. 40041–40048, doi:10.1074/jbc.M606263200.
- Thiele, I. et al., 2013, A community-driven global reconstruction of human metabolism: *Nature biotechnology*, doi:10.1038/nbt.2488.
- Thiele, I., R. M. T. Fleming, A. Bordbar, J. Schellenberger, and B. Ø. Palsson, 2010, Functional characterization of alternate optimal solutions of *Escherichia coli*'s transcriptional and translational machinery: *Biophysical journal*, v. 98, no. 10, p. 2072–2081, doi:10.1016/j.bpj.2010.01.060.
- Thiele, I., R. M. T. Fleming, R. Que, A. Bordbar, D. Diep, and B. O. Palsson, 2012, Multiscale modeling of metabolism and macromolecular synthesis in *E. coli* and its application to the evolution of codon usage: *PloS one*, v. 7, no. 9, p. e45635, doi:10.1371/journal.pone.0045635.
- Thiele, I., and B. Ø. Palsson, 2010, A protocol for generating a high-quality genome-scale metabolic reconstruction: *Nature Protocols*, v. 5, no. 1, p. 93–121, doi:10.1038/nprot.2009.203.
- Vazquez, A., Q. K. Beg, M. A. Demenezes, J. Ernst, Z. Bar-Joseph, A.-L. Barabási, L. G. Boros, and Z. N. Oltvai, 2008, Impact of the solvent capacity constraint on *E. coli* metabolism: *BMC Systems Biology*, v. 2, p. 7, doi:10.1186/1752-0509-2-7.
- Zakrzewska, A., G. van Eikenhorst, J. E. C. Burggraaff, D. J. Vis, H. Hoefsloot, D. Delneri, S. G. Oliver, S. Brul, and G. J. Smits, 2011, Genome-wide analysis of yeast stress survival and tolerance acquisition to analyze the central trade-off between growth rate and cellular robustness: *Molecular biology of the cell*, v. 22, no. 22, p. 4435–4446, doi:10.1091/mbc.E10-08-0721.
- Zhuang, K., G. N. Vemuri, and R. Mahadevan, 2011, Economics of membrane occupancy and respiro-fermentation: *Molecular systems biology*, v. 7, p. 500, doi:10.1038/msb.2011.34.

AUTHOR BIOGRAPHIES

BAS TEUSINK did his master in (bio)chemistry and a PhD in systems biology, both at the University of Amsterdam. After postdocs in biomedical research, in 2002 he moved to NIZO food research to start developing genome-scale metabolic modeling for food related bacteria. In 2008, he

became full professor in systems biology and integrative bioinformatics at the Vrije Universiteit Amsterdam. He is interested in fundamental questions about the design principles of biological networks, and applies the understanding in public-private partnerships.

BOB PLANQUE did his master in Mathematics in Leiden, and his PhD in Mathematics at the CWI in Amsterdam. After a postdoc in mathematical behavioural ecology in Bristol, UK, he joined the Mathematics Department at the Vrije Universiteit Amsterdam in 2006 as assistant professor. His main interests lie in mathematical biology, and has active collaborations with biologists from various fields, such as ecology, physiology and systems biology.

DOUWE MOLENAAR holds a PhD in microbiology from the University of Groningen, did a postdoc in theoretical biochemistry at the Netherlands Cancer Institute and worked in biotechnology research in the Forschungszentrum Jülich, the Heinrich-Heine Universität Düsseldorf, and at NIZO food research. During these periods he became proficient in bioinformatics and data analysis. He is currently a researcher at the Vrije Universiteit Amsterdam.

FRANK BRUGGEMAN obtained a PhD Degree in Systems Biology at the VU University in Amsterdam 2005. His research is focused on understanding of the adaptive strategies of microorganisms, mostly by studying single cells, using experiments and statistical biophysics theory. Currently, he holds a University Chair in Interdisciplinary Life Sciences at the VU University.

THE TEAM has steadily grown since the start in 2008 and currently comprises technicians, teachers, a data manager, PhD students and postdocs.

See www.teusinkbruggemanlab.nl for more details.

HUMAN IN THE LOOP FOR MODELLING FOOD AND BIOLOGICAL SYSTEMS: A NOVEL PERSPECTIVE COUPLING ARTIFICIAL INTELLIGENCE AND LIFE SCIENCE

Nathalie Méjean Perrot*, Nadia Boukhelifa*, Alberto Tonda*, Thomas Chabin*, Marc Barnabe*, Dominique Swennen[†], Alice Roche[‡], Thierry Thomas Danguin[‡], Evelyne Lutton*

*UMR 782 GMPA, Team *MALICES and †ECOMIC, INRA

1 av. Lucien Brétignières, 78850, Thiverval-Grignon, France

+UMR CSGA, Centre des Sciences du Gout et de l'Alimentation, INRA, CNRS, Université de Bourgogne Franche- Comté

Email: firstname.name@inra.fr

KEYWORDS

Human expertise, modelling, interactive learning, agri-food systems, visualization, optimization, machine learning

ABSTRACT

Since centuries, agriculture, food and biological systems are strongly linked to human expertise, albeit such knowledge has been capitalized and shared often at a local level, only. Since the beginning of the last century, swept away by productivism, modern agriculture and food production have put cumulated human knowledge aside. Facing new challenges like sustainability in a changing context, holistic approaches cannot be managed “manually” ab initio and there is a clear need for computing decision-support tools to tackle these new issues. Moreover, new approaches should be built centred on humans and for humans. The heart of our purpose is to shift the focus again on human and local expertise, guided by powerful computing interactive systems.

INTRODUCTION

Since centuries, agriculture, food and biological systems are strongly linked to human expertise, albeit such knowledge has been capitalized and shared often at a local level, only. Scientific and technical experts have tried to study complex food and biological systems for a while. Generally lot of heterogeneous experiments have been achieved in different conditions and statistical analysis allows extracting various characteristic features leading to a local or partial understanding of the system in the mind of the expert. Nevertheless the task is far more complex if a global understanding of those systems is needed, even if experts have sometimes partial intuitions on it (Perrot et al., 2011) (Van Mil et al., 2014)(Perrot et al., 2016). The heart of our purpose in this paper is to shift the focus on human, intuitions and local expertise, guided by powerful computing interactive systems.

If we refers to the cognitive human behavior, as it is described in the community of intelligent systems (Lucentini and Goodwin, 2015), a point widely studied is the cognitive architectures and the way that data is captured from the environment, stored and further processed. Basically, cognitive architectures refer to two paradigms: symbolic and sub-symbolic. It gives the possibility to infer, for some aspects, like experts decision for process management, data exploration, fault tolerance, learning, systematicity and so on, how the human behavior will be. It is just a question of analyzing if an architecture is based on a symbolic, sub-symbolic or mixed approach.

Symbols, as described by (Lucentini and Goodwin, 2015), “are entities which make reference to another objects by means of a totally arbitrary convention, a law or a class. They are a widely used form of representation, for example the word car is a symbol for a real car, because there is a convention that the word car in a specific language refers to those types of elements”. The sub-symbolic level, is not using symbols as the symbolic one and is more a “bottom-up” approach emerging from neuronal connections, non explicitly conscientize by the experts.

Our challenge for this article is to present experiences led in our laboratory to guide through man machine interactions, the emergence of a model integrating symbolic and sub-symbolic human knowledge. It is dedicated to food and biological complex systems.

HUMAN IN THE LOOP

For our approach, we rely on the ability of experts to create patterns giving them the possibility to reason in an uncertain environments. Indeed, experts, faced with complexity when coping with their dynamic environment and constraints, develop a considerable ability to focus their attention and organize the space of reasoning around dynamic patterns, based more on

experience than on rules (Ballester et al., 2008). Such patterns are scripts that embody in an efficient way knowledge of viable stereotyped event sequences. For example, it has been described in (Sicard et al., 2011) applied to a cheese biological ecosystem: the process is represented in the expert's mind in the form of chronological standard change patterns and drift from standard trajectories that lead to defects on the cheese, like bad odours or bacterial contaminations. This mechanism of information aggregation allows the experts to anticipate the appropriate system state to intervene in, and, if needed, to correct early drift trajectories. The experts are thus able to manage a certain amount of complexity in an uncertain environment. In multiscale living biological global systems, patterns are organized in space and time (various land parcels and climatic conditions for example for agronomic problematics such wine, wheat crop..., various space and growth time for living ecosystems for example food, marine or gut ecosystems).

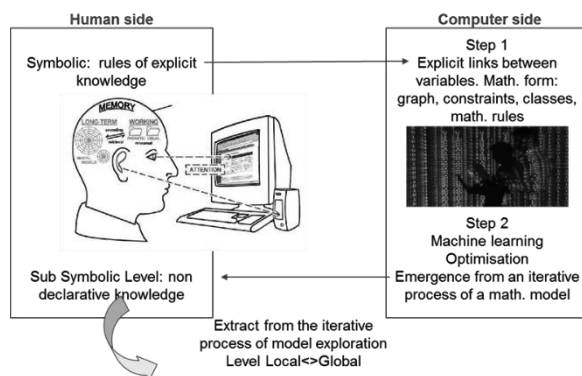


Figure 1: An approach of human integrated in the computing loop. A first step is delivered by the expert from his symbolic knowledge and integrated by the computer side in the form of explicit links, graphs, rules,... A second step emerge from the iterative interaction between human and computer through a model exploration at different level after a computing step of calculus.

One of the efficient coding mechanisms used by experts is the cognitive mechanism of 'chunk' recognition (Chase and Simon, 1973). A 'chunk' is a grouped set of clustered variables, closely related to each other, taken from a situation and associated to each other. Chunks are used to describe a part of a standard trajectory, directly linked to a particular state, which could require to be stabilized or corrected. These variables are acquired through the perceptions of experts. For example, winemakers

anticipate the quality of their wine using mental chunks based on their perception of the quality of the soil of a parcel and its localisation, the way the grapevine has been conducted, etc. Nevertheless, chunks are not easy to handle as they are not usually in the form of explicit knowledge and sometimes refer to the subsymbolic level of the expert cognition. As a consequence, very often they are not exploited as functional knowledge to create computational models suitable for decision making. Some of the patterns can be explicit on a graph or in the form of rules. For the subsymbolic ones, our hypothesis is that it can emerge from the exploration of the result of a model if relevant computing tools and visualisation techniques are implemented for man-machine interactions.

We propose a parallel between the approaches of computational cognitive (Sun, 2008)(Mc Clelland, 2009) developed to model human cognition devoted to symbolic and sub-symbolic levels and the computing tools we develop to embed human in the computing loop. From this parallel, the idea is to build a tool able to deal with and integrate those different levels of human knowledge into the loop of modeling. Every simulation model is here a way to embed a part of the human knowledge on a biological system. The challenge of this paper is more precisely to present different studies were the use of computational models in this spirit is developed. It is based on human, machine learning, optimization and visualization. The purpose, more than a compilation of studies is to enhance our vision of "the human in the loop" through different experimentations. We thus focus on the knowledge available at the different level of human cognition. We observe symbolic and sub-symbolic levels and especially the mental patterns the experts have in mind. We exemplify this approach on a series of systems like in cheese ripening process, wheat culture management, wine odor prediction or bacteria freeze drying. Two axes are explored: food and biological systems exploration and food and biological properties

The approach tested and experimented (figure 1) is an approach coupling (1) an algorithm enabling the effective description of the human symbolic knowledge in the form of rules, classes or links between variables or classes (step 1) ;(2) an approach of machine learning including a crucial optimisation step proposing different alternative of

representation (step 2) explored iteratively through a visual interface. The idea is to open from this iterative exploration process the door to the sub-symbolic knowledge emergence. Two ingredients are important for that: the way we use optimisation and visualization techniques.

OPTIMISATION AND EMERGENCE

The idea of optimisation takes its roots in the 16th and 17th centuries notion of “modernity”, when philosophers were advertising the issue of becoming “owner and master” of nature (“Discours de la méthode” (Descartes, 1637), in a mathematical framework (Galilée (Martin, 2002))). Thanks to modern computation capabilities, managing and predicting natural phenomena becomes more and more a reachable challenge. However optimality, in any domain, raises various fundamental questions, in particular regarding the purpose of optimisation (are we able to address the appropriate issues with the help of modern computational tools?) and the methods (are we able to address the right issues with the right tools?).

A subsidiary question is also: Do we not believe too much in computation? Improvement may be another perspective, more appropriate, in particular for an interactive/iterative process of problem solving involving human knowledge.

In this work, we revisit the use of stochastic optimisation heuristics and in particular Evolutionary Algorithms, exploited in an iterative and interactive context, to better address complex questions. Evolutionary Algorithms (EAs) are stochastic methods that copy, in a very abstract manner, the principles of natural evolution that let a population of individuals be progressively adapted to its environment (Goldberg, 1989). This progression results in an improvement of the fitting of the individuals to its environment, this can be exploited as an optimisation heuristic: an optimal adaptation is reached asymptotically.

An EA considers populations of potential solutions exactly like a natural population of individuals that live, fight, and reproduce, but with a natural environment pressure replaced by an artificial optimization pressure. Reproduction consists of generating new individuals-solutions using the so-called genetic operators that, by analogy with nature, are called mutation if they involve one individual, or crossover if they involve two parent solutions. A fitness function, computed for each individual, is used to drive the selection process, is

thus improved, and ultimately optimized by the EA.

In an interactive context, an improvement scheme seems adequate and enough, as the optimisation aim is often not fixed and varies with interactions with experts. Additionally, EA are convenient for building interactive schemes; there is actually a large interest of the community into interactive EA (IEA). Interactions with the optimisation/improvement EA may take place at various levels (interactive evaluation of results, reformulation of optimisation function, modification of current solutions, interactive tuning of the parameters of the algorithm).

VISUALIZATION TECHNIQUES

Visualization is a field of computer science concerned with the creation and study of visual representations of data (Card et al., 1999). It makes use of our powerful visual cortex and wealth of experience to reach insights from data, amplified through human-computer interaction. For a visualization to be interactive, it needs to support human input to control some aspects of the visual display. Additionally, a good interaction response rate needs to be met to ensure real-time perception of task execution.

Visualization can be a valuable asset in the context of modelling. For example, creating robust computational models necessitates tools to explore the behaviour of models and tune their underlying representations, but not only. From our experience visualization can empower modelling by bringing in:

- human-computer interaction methodologies that facilitate the study of the visible and hidden roles humans play in modelling (Lutton et al., 2016);
- more intuitive representations of often complex multiscale models (Chabin et al., 2017). These visualizations can facilitate collaboration between the various stakeholders involved in the modelling process (e.g. data owners, domain experts, modellers, decision makers); and
- interactive tools to explore the behaviour of the constructed models, and ultimately allowing for enrichment and modification (Sacha et al., 2016).

EXPERIENCES OF HUMAN IN THE LOOP:

Food and biological system exploration

Explore to find a camembert-type cheese ripening viable trajectory.

This experiment was led under the frame of a french ANR project (INCALIN) and a FP7 European project (DREAM). The challenge was to work with the experts and a distributed high performance calculation structure to discover relevant viable trajectories of cheese ripening (Sicard et al., 2012). The viability study is achieved on a space dimension of 5: Two control variables: relative humidity and temperature of the ripening chamber; Three state variables: the cheese mass, cheese surface temperature and respiration r_{CO_2} . The trajectories are considered relevant if the cheese are in a given target of sensory quality at the end of the process of ripening and if the ripening time is reduced.

In a first step (see Step 1, figure 1) explicit knowledge is described by the experts in terms of a constraint set, a subset of the three dimensional state space: cheese mass, cheese surface temperature and respiration level (see article (Sicard et al., 2012)). It can be represented as a tube including all the values in which the state variables should stay at each time. The bound values stem from the experimental limits and the legal norms (viability tube represented figure 2).

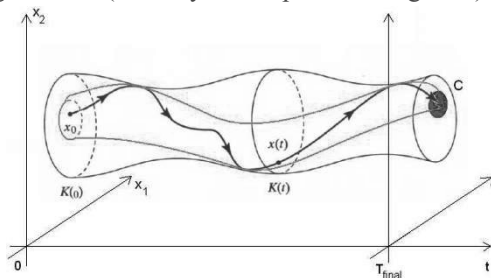


Figure 2: Viability tube of the ripening process of a camembert type cheese (upon Sicard et al., 2009).

In a second step (Step 2, figure 1), 45 654 840 simulations are performed on a computing cluster of calculus and a Pareto front of the results is explored visually by the experts. On the basis of this first exploration, new constraints are proposed, emerging from the visual exploration of the experts, and a new Pareto front is explored and iteratively, till a satisfying solution is found by the experts.

This exploration applied to a cheese ripening process, has led us to find an original viable trajectory for the industry, satisfying the manufacturing constraints while maintaining the quality target for the ripening process. This trajectory has a 8-day ripening time, whereas the standard is 12 days. This trajectory was validated on a ripening pilot. The microbial equilibrium was preserved so as the cheese sensory properties (see figure 3).

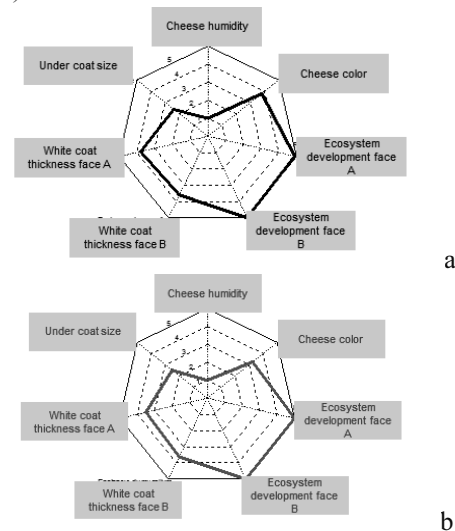


Figure 3: The cheese sensory evaluation after having tested the emergent trajectory following the exploration experiments: -a- in black: cheese sensory evaluation at the end of the ripening process for the classic trajectory (day 12); -b- in red: cheese sensory evaluation at the end of the ripening process for the classic trajectory (day 8). The cheese sensory characteristics for the two trajectories (classic and optimized) are almost the same.

Explore to find sustainable strategies for wheat culture.

We organised a Pareto front visual exploration session to help a domain expert investigate various fertilization strategies for wheat growth. Our expert had a research question pertaining to azote fertilisation strategies. In particular, she wanted to find strategies that work well regardless of the climate or the weather. To achieve this, in a first step we constructed a Pareto front from simulation files produced by the expert using an existing soil crop model called Azodyn (Jeuffroy et al., 1999). This model takes soil characteristics and predicts the consequences of azote (N) fertiliser management strategies, in terms of daily crop

growth, yield, grain protein content and N losses to the environment. The Pareto front was constructed by maximising yield, and both minimising loss and the final N dose. These objectives were selected by the experts, to help them answer their research question. In a second step, the exploration session was carried out iteratively using a large tactile display (figure 4) and an interactive visualization system coupled to an evolutionary algorithm (Cancino Tionca et al., 2012)(Boukhelifa et al., 2017) (figure 5).

Besides helping the expert answer their research question, the objectives of this workshop were three-fold: (a) to get feedback and evaluate our approach of interactive model exploration, (b) to collect data on expertise related to each application domain, and (c) to establish opportunities for automatic learning and user interaction leverage points.



Figure 4: Model exploration session with a domain expert using interactive visualization.

During this exploration session, the domain expert reported finding interesting fertilisation strategies that she did not investigate previously (thus new research questions). More interestingly, in collaboration with this domain expert, we were able to generate decision rules for the different fertilisation strategies that she explored. In the future, we plan to test these rules, by generating a new dataset based on the new findings, and re-launching the simulation and exploration. We have also gathered a rich dataset on interactive model exploration (videos, notes and log files), which we plan to analyse.

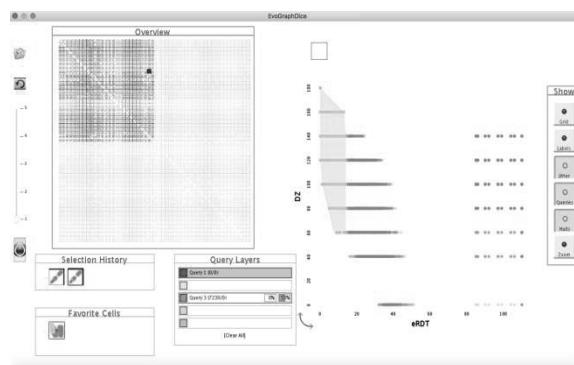


Figure 5: EvoGraphDice: The visualization tool we used for the exploration session. In this view the expert selected a view showing yield versus Azote doze. The green selection corresponds to favorable fertilization strategies according to the ‘yield’ criteria.

Food and Biological properties prediction

Predict flavor of red wine

In food science, sensory properties are important and not always easy to predict. For example the analysis of the aromatic component of food products is usually performed by separating, identifying and quantifying the molecules included in an extract. Such well-established procedure provides a list of key odorants but does not give any information about the perceptual influence of mixed compounds. This is a major problem for the prediction of the food overall sensory profile on the basis of its chemical content. To solve this issue, we developed an approach of “human in the loop”, applied to the prediction of the odor of 16 red wines (Roche et al., 2017). We worked with experts, sensory databases and computational tools coupling fuzzy logic and genetic algorithms for fuzzy model parameters optimization. This model queries analytical and sensory databases in order to predict the flavor profile (figure 6).

In a first step (see Step 1, figure 1) explicit knowledge is initially described by a panel of 4 experts (flavorists) in the form of rules. They were asked to describe in basic odor qualities 4 to 15 sensory descriptors useful to characterize red wines but not specific to it (e.g. bell pepper, blackcurrant fresh, cherry cooked, cherry stone, strawberry fresh). Basic odor qualities are also linked to analytical data by the experts in the form of ontologies (A. Roche, N. Perrot, T. Thomas-Danguin, “Odor perceptual space: From odorant descriptors to odor qualities”, in writing).

In a second step (see step 2, figure 1), a model is proposed linking all the knowledge in a model coupling ontologies, fuzzy reasoning to compute the rules proposed by the flavorists and a genetic algorithm performing an optimization of the fuzzy rules parameters using a data basis collected during experiments. It estimates the intensity of each sensory descriptor for a wine on the basis of its composition in terms of odor active compounds. After several iterations with experts, a final model is proposed to predict the wine sensory properties. Applied to a series of datasets on 16 red wines. The results of prediction are in good agreement with the actual values with the two projections on the first two principal components of a PCA, statistically significantly correlated (Monte-Carlo test $p = 0.003$).

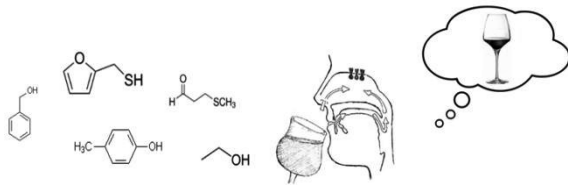


Figure 6: From analytical data to flavor perception of red wines: a question of human in the loop.

Predict and discover knowledge of a multiscale involved process: a “theory building tool” applied to bacteria freeze drying

In many real-world modelling case studies, the amount of data available is often not enough to apply fully automated tools such as black-box machine learning algorithms. At the same time, additional knowledge on the problem is usually available, in the form of implicit proficiency developed by experts of the domain. In such situations it is fundamental to allow human users to interact with the machine learning tools, and make their knowledge explicit. LIDEOGRAM (Life-based Interactive DEvelopment Of GRaphical Models) (Chabin et al., 2017) is a tool implementing this specific vision: The goal is to provide experts with a design tool for modelling complex system processes. In LIDEOGRAM, each non-input variable for a case study is modelled as a mathematical formula dependent on other variables in the problem. Interacting with a graphical representation of the system, users are involved in three steps: In a first step (see step 1, figure 1), sets of variables and classes grouping some or all the variables can be created, and a first graph of links between those variables and classes can be

proposed. Starting from the relationships described by the user-defined graph, in a second step (see step 2, figure 1), a machine learning approach based multi-linear regression will propose mathematical formulas, each one a different trade-off between complexity and fitting. This process ultimately creates a multi-scale model, where each part of the process is defined with respect to variables at a lower scale, following the dependencies given by the initial user-defined graph. In a final step, experts select mathematical formulas of their choice, iteratively, until a satisfactory result is reached. LIDEOGRAM has been successfully applied to a case study involving freeze-drying of bacteria, where a model developed interacting with a human expert was able to deliver better result than one obtained through a purely automatic approach (see Figure 7 for a screenshot of the interface used in the experiments).

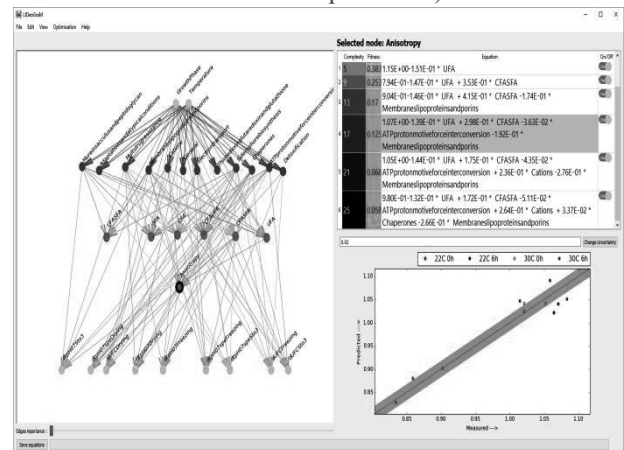


Figure 7: Screenshot of LIDEOGRAM. The left side shows a graphical model representing the meanness of the local models obtained by symbolic multi-linear regression. The top-right part is the list of equations proposed for the selected node, and the bottom-right part shows a plot of the measured versus predicted data associated to the selected equation.

Computational models such a LIDEOGRAM are useful tools for hypothesis generation: through simulations, users can explore unseen scenarios, and ultimately exploit the model as a theory-building device (Sun, 2008). At the same time, this approach can be used to create new knowledge by summarizing information, in a process similar to chunking in cognitive models (Lucentini and Goodwin, 2015). While we advocate for the use of models to explore the implications of ideas, especially for assessing their sufficiency, optimality, and empirical adequacy, such explorations must nevertheless be carried out with

care. Reaching broad conclusions from the shortcomings of particular models, in particular, is difficult: Even if a modeler can show that a model fits all available data perfectly, the work still cannot tell us that it correctly captures the processes in the tasks that it addresses (McClelland, 2009).

CONCLUSIONS

In this paper, an approach centered on human and human embedded in the computing loop is presented. It is based on human, machine learning, optimisation and visualisation. Different studies were the use of computational models interacting with human are presented. Those experimentations, show clearly the value added of such a paradigm and open a road for future research in food and biological modelling.

REFERENCES

- Ballester, J., Patris, B., Symoneaux, R., & Valentin, D. (2008). Conceptual vs perceptual wine spaces: does expertise matter? *Food quality Quality and Preference*, 19(3), 267–276.
- Boukhelifa, N., Bezerianos, A., Cancino, W., Lutton, E. (2017). Evolutionary visual Exploration: evaluation of an IEC framework for guided visual search. *Evolutionary Computation*, 25(1), 55-86.
- Cancino Tionca, W.G., Boukhelifa, N., Lutton, E. (2012). EvoGraphDice: Interactive evolution for visual analytics. In: 2012 IEEE Congress on Evolutionary Computation, (p. 1-8).
- Card, S. K., Mackinlay, J. D., Shneiderman, B. (1999). *Readings in Information Visualization: Using Vision to Think*. Morgan Kaufmann Publishers.
- Chabin, T., Barnabé, M., Boukhelifa, N., Fonseca, F., Tonda, A., Velly, H., Lemaître, B., Perrot, N., Lutton, E. (2017). LIDeOGraM: An interactive evolutionary modelling tool. *International Conference on Artificial Evolution (Evolution Artificielle)*, 25-27 October 2017.
- Charpentier, J. (2010). Among the trends for a modern chemical engineering, the third paradigm: the time and length multiscale approach as an efficient tool for process intensification and product design and engineering. *Chemical Engineering Research and Design*, 88, 248-254.
- Chase, W., & Simon, H. A. (1973). Perception in chess. *Cognitive Psychology*, 4, 55–81.
- McClelland, J.L. (2009). The Place of Modeling in Cognitive Science. *Topics in Cognitive Science*, 1, 11–38.
- Descartes R., *Le discours de la méthode*, La Haye, 1637, http://classiques.uqac.ca/classiques/Descartes/discours_methode/Discours_methode.pdf.
- Goldberg D.A., 1989. *Genetic Algorithms in Search, Optimization, and Machine Learning*. Addison-Wesley Publishing Company, inc., Reading, MA.
- Hintzman, D. (1990). Human learning and memory: Connections and dissociations. In: *Annual Review of Psychology*, pp.109-139. Annual Reviews Inc, Palo Alto, CA.
- Jeuffroy, M-H., and Recous. S (1999). Azodyn: a simple model simulating the date of nitrogen deficiency for decision support in wheat fertilization. *European journal of Agronomy* 10(2), 129-144
- Lucentini, D.F., Gudwin, R.R. (2015). A Comparison Among Cognitive Architectures: A Theoretical Analysis. *Procedia computer science*. Volume 71, 2015, Pages 56–61.
- Lutton, E., Tonda, A., Boukhelifa N., Perrot, N. (2016). *Complex Systems in Food Science: Human Factor Issues*. FOODSIM, Catholic University Leuven, Ghent, Belgium.
- Martin M.-É., *La nature est un livre écrit en langage mathématique*, Galilée, Pleins Feux, 2002.
- Perrot, N., De Vries, H., Lutton, E., Van Mil, H.G.J., Donner, M., Tonda, A., Martin, S., Alvarez, A., Bourguine, P., van der Linden, E. Axelos, M. (2016). Some remarks on computational approaches towards sustainable complex agri-food systems. *Trends in Food Science and Technology*. 48, 88-101.
- Perrot, N., Baudrit, C., Trelea, I.C., Trystram, G., Bourguine, P. (2011). Modelling and analysis of complex food systems: state of the art and new trends. *Trends in Food Science and Technology*, 22(6), 304-314.
- Roche, A., Perrot, N., Chabin, T., Villière, A., Symoneaux, R., Thomas-Danguin, T. (2017), In silico modelling to predict the odor profile of food from its molecular composition using experts' knowledge, fuzzy logic and optimization: Application on wines, 2017 ISOCs/IEEE International Symposium on Olfaction and Electronic Nose (ISOEN), Montreal, QC, 2017, pp. 1-3. doi: 10.1109/ISOEN.2017.7968875.
- Sacha, D., Sedlmair, M., Zhang, L., Lee, J.A., Weiskopf, D., North, S., Keim, D. (2016). "Human-centered machine learning through interactive visualization." *ESANN*.
- Sicard, M., Perrot, N., Baudrit, C., Bourguine, P., Alvarez, I., Martin, S. (2009). The viability theory to control food processes. *European Conference on Complex Systems*.
- Sicard, M., Perrot, N., Reuillon, R., Mesmoudi, S., Alvarez, I., Martin, S. (2012). A viability approach to control food processes: Application to a Camembert cheese ripening process. *Food Control*, 23,312-319.
- Stuart K. Card, Jock D. Mackinlay and Ben Shneiderman (1999). *Readings in Information Visualization: Using Vision to Think*, Morgan Kaufmann Publishers.
- Sun, R. (2008). Introduction to computational cognitive modeling. In R. Sun (Ed.), *Cambridge handbook of*

computational psychology (pp. 3–19). New York: Cambridge University Press.

Van Mil H., Foegeding E., Windhab E., Perrot, N., Van der Linden, E. (2014). A *complex system approach to address world challenges in food and agriculture*”, Trends in Food Science and Technology, 40 (1), 20-32.

NON-THERMAL FOOD PROCESSING: MODELLING OF PROCESSES TOWARDS SAFETY, QUALITY AND SUSTAINABILITY

Anet Režek Jambrak¹, Ilija Djekić², Jan Van Impe³

1. Faculty of Food Technology and Biotechnology, University of Zagreb, Pierotti street 6, Zagreb, Croatia

2. Department of Food Safety and Quality Management, University of Belgrade - Faculty of Agriculture, Belgrade, Republic of Serbia

3. KU Leuven, Department of Chemical Engineering, 3000 Leuven, Belgium

E-mail: anet.rezek.jambrak@pbf.hr

KEYWORDS

non-thermal processing, modelling, safety, quality, and sustainability

ABSTRACT

There is significant progress and spread of use of non-thermal processing applications in research and industry. United Nations (UN) has issued the 2030. Agenda for Sustainable Development (2015) with 17. Sustainable Development Objectives that should have impact to the development projects and future programs in the world. Regarding those objectives scientists and researchers are starting to use novel techniques in order to obtain valuable output products. Likewise, in food industry engineers and scientist are trying to develop processes and methods in order to assure food safety, have quality product and “save the planet” - to be sustainable. Therefore, one need to see the whole picture, from raw material, through process, product and waste by means of energy, economy and environment.

INTRODUCTION

Non-thermal processing techniques include: electrotechnologies, UV light, cold pressure (high pressure processing), hydrodynamic cavitation, ionizing radiation, ozonation, oscillating magnetic fields, pulsed light, supercritical and subcritical fluid processing, biopreservation, electrohydrodynamic processing and electron beam processing (Jambrak, Herceg, Šubarić et al., 2010).

Technologies such as high pressure, UV light, pulsed light, ozone, power ultrasound and cold plasma (advanced oxidation processes) have shown promising results for inactivation of microorganisms. The purpose of using non-thermal technologies is to assure food safety using shorter processing time, lower energy uptake, lower carbon footprint and lower temperatures. The efficacy of inactivation of microorganisms is greatly enhanced by combination of conventional (thermal) with non-thermal, or non-thermal with another non-thermal technique. The key advantages offered by non-thermal processes in combination

with sub lethal mild temperature (<60°C) can inactivate microorganisms synergistically (Jambrak and Herceg, 2014).

MODELLING OF PROCESSES TOWARDS SAFETY, QUALITY AND SUSTAINABILITY

In order to assure food safety mathematical modelling is an essential tool. More specifically, predictive microbiology focusses on the quantitative description of the microbial behavior in food products, for a given set of environmental conditions. Therefore, by combining experimental data, microbial knowledge and mathematical techniques, inactivation following non-thermal technologies can be accurately predicted and controlled.

Predictive models can be classified in different ways: (i) black box (empirical) vs. white box (mechanistic) models, (ii) based on spatial scale (macroscopic- mesoscopic-microscopic models), (iii) based on data collection methods (e.g., viable plate counts, flow cytometry) and (iv) kinetic and probabilistic models.

However, overall quality of food products (juices, nectars, milk etc.) can be deteriorated (Jambrak, Šimunek, Petrović et al., 2017). Aromatic profile and sensory characterisation of ultrasound treated cranberry juice and nectar. *Ultrasonics Sonochemistry* 38: 783-793.. The aim of this use of mathematical modelling is use quality index in evaluating effects of each non-thermal technology on quality characteristics of food material that is processed. For that purpose mathematical models for calculating a total quality index (TQI) can be introduced. Mathematical index of TQI in order to evaluate total quality can be calculated.

Fruit juice example

All parameters have to be transformed where the relationship between quality index and optimal values is considered as linear. Linearity is also only an assumption because it is difficult to demonstrate its existence, particularly around the limit values (Molnár, 1995).

Parameters of the first kind for which there is a target value, i.e. the measured value of untreated juice . The following rule applies - the nearer to the target values the parameter is, the better the quality is, equation 1:

$$QI = \left| \frac{2 * (x_i - T)}{x_{max} - x_{min}} \right| \quad /1/$$

Where: QI – quality index for a parameter; x_i – measured value in the subset of values; T - target value; x_{max} – maximal value in the subset of values; x_{min} – minimal value in the subset of values. The following quality parameters can be included in this group (viscosity, conductivity, aroma profile, pH etc.).

Parameters of the second kind have the following rule: the smaller the value is, the better the quality is. For this type of parameters, QI is calculated based on equation 2:

$$QI = \frac{x_i}{x_{max}} \quad /2/$$

Where:

QI – quality index for a specific quality parameter; x_i – measured value in the subset of values; x_{max} – maximal value in the subset of values. Two aroma profile parameters can be included in this group (ester group, aldehyde group i.e).

Parameters of the third kind have the following rule: The higher its value, the better the quality is. For this type of parameters, QI is calculated based on equation 3:

$$QI = \frac{x_{max} - x_i}{x_{max} - x_{min}}; x_i \leq x_{max} \quad /3/$$

Where:

QI – quality index for a specific quality parameter; x_i – measured value in the subset of values; x_{max} – maximal value in the subset of values. Antioxidant potential parameter can be included in this group.

We can assume a new Euclidean space R^N (N is the number of quality parameters) where all quality indexes are considered as vectors $QI = (QI_1, QI_2, \dots, QI_N) \in R^N$ (Horn and Johnson, 1985). Upon calculation of all QIs, the Euclidean norm of the vector, whose components are the indexes QI_N , will represent the total quality index (TQI) equation (4) (Finotti et al., 2007). Optimal values for all three types of indexes are “0”.

$$TQI = \sqrt{\sum_{j=1}^N (QI_j)^2} \quad /4/$$

As a conclusion, the “rule of thumb” is that the farther from the origin the vector, the worse is its “TQI” and the nearer the origin the vector, the better is its “TQI” (Finotti et al., 2007).

Model 1 – Normalized index

Every component of the vector represents the normalized distance of the parameters from its optimal or target value (Finotti et al., 2007). Depending on the values, for equation (1) it is theoretically possible to have values $QI \geq 1$, bearing in mind that the higher the QI is, the worse is its quality. Therefore in some occasions it is recommended to normalize the index meaning that when $QI \geq 1$ we normalize it by assigning the value $QI=1$.

Total quality index - Model 2

Molnar proposed a slightly different approach assuming normalized values between 0 and 1, with 0 representing the worst and 1 the best food quality (Molnár, 1995). The transformation equation $QI = f(x_i)$ needs to fulfil the requirement that the maximum measured value is ascribed to 1, and the minimum value to 0 in the case of desirable attribute, and vice versa for undesirable attribute (Curic et al., 2008).

For the purpose of this paper, the following equation was used:

$$QI = 1 - \frac{|T - x_i|}{x_{max} - x_{min}} \quad /5/$$

Where:

QI – quality index for a specific quality parameter; x_i – measured value in the subset of values; x_{max} – maximal value in the subset of values, x_{min} – minimal value in the subset of values. T – target value - values from i.e. untreated juice.

Total quality index was calculated as a sum of normalized quality indexes relative to the ideal quality of a product (untreated juices), equation 6:

$$TQI = \frac{(\sum_{j=1}^N QI_j)_{sample}}{(\sum_{j=1}^N QI_j)_{target}} \quad /6/$$

Several properties of main quality characteristics of juices, beverages, liquid foods and nectars are sensory properties, rheological properties, °Brix, acidity, color etc.. The complexity of food matrix like juices/nectars in relation to various non-thermal treatments (with the purpose of assuring food safety) and quality parameters becomes a challenge for researchers to develop (mathematical) models and analyze data in terms of a quality score.

Quality function deployment (QFD) is another innovative quality tool introduced in Japan in the 60s. It was defined as a “method for developing a design quality aimed at satisfying the customer and then translating the customer’s demands into design targets and major quality assurance points to be used throughout the production phase”. Its customer centricity to product/process innovation emphasizes its benefit. But even if we assure food safety and preserve food quality we need to take care to have low carbon food print of non-thermal process comparing to traditional one, and to have “zero waste” or to re-use it.

Life Cycle Assessment is the main methodology applied to assess the environmental impact of products and it has been increasingly applied to products of the agri-food. It is a scientific method that includes the following steps outlined in ISO 14040: mapping the process, setting the scope and boundaries, collecting data, calculating, evaluating and interpreting the results with the aim to propose environmental improvements. The LCA, simplified LCA or non-LCA models have the objectives to quantify the environmental performances in the whole food product chain. Regarding the approach three main types occur: LCA, variations of LCA and non-LCA models. Depending on the model, the following criteria apply: (i) if the model is

generic or specific for food industry; (ii) if it is user friendly/or not; (iii) if it is free/payable; (iv) if it is focused on one environmental impact or several; (v) besides environment, if it focuses on some other sustainability dimension (economic, social) (vi) if it requires specific environmental knowledge, etc. LCA has great potential for driving the development of products and processes. Through LCA novel processing can be compared with existing commercial alternatives and environmental hotspots can be also identified.

For non-thermal technologies, when they are evaluated from an environmental point of view there are many difficulties like lack of real data for the inventory phase (lab scale information or theoretical data) and the definition of the novel foods, since new products or processes might have unique properties. Therefore, there is need for an approach for the environmental analysis of non-thermal food technologies. Through evaluating environmental impacts through LCA of some traditional and novel food preservation technologies, we can contribute to the development of more sustainable food products. Some general improvements can be defined towards environmental issues in order to select the more adequate preservation method when designing new food products.

CONCLUSION

By performing modelling and optimization of non-thermal processing and subsequent sustainability evaluation approach (life cycle assessment) it will be feasible that this approach allows minimization of environmental impact as well as significant reduction of energetic needs. The whole picture needs to be looked from fundamental approach (basic interdisciplinary science), raw materials, through processes and technologies, and then to final product taking care of waste (by-product) and management for its re-usage. Usage of non-thermal processing and their combination (synergy) will ultimately focus of reduction of waste and energy necessities while producing high quality products with minimal environmental and naturally social impact. Scientists need to assure e^3 (ecologic, economic and environmentally friendly) non-thermal process in order to assure safety, quality, and sustainability.

REFERENCES

- Curic D, Novotni D, Skevin D, et al. (2008) Design of a quality index for the objective evaluation of bread quality: Application to wheat breads using selected bake off technology for bread making. *Food Research International* 41(7): 714-719.
- Finotti E, Bersani AM and Bersani E. (2007) Total quality indexes for extra-virgin olive oils. *Journal of Food Quality* 30(6): 911-931.
- Horn RA and Johnson CR. (1985) *Matrix Analysis* Cambridge University Press. New York.
- Jambrak AR and Herceg Z. (2014) Application of Ultrasonics in Food Preservation and Processing. *Conventional and Advanced Food Processing Technologies*. John Wiley & Sons, Ltd, 515-536.
- Jambrak AR, Herceg Z, Šubarić D, et al. (2010) Ultrasound effect on physical properties of corn starch. *Carbohydrate Polymers* 79(1): 91-100.

Jambrak AR, Šimunek M, Petrović M, et al. (2017) Aromatic profile and sensory characterisation of ultrasound treated cranberry juice and nectar. *Ultrasonics Sonochemistry* 38: 783-793.

Molnár PJ. (1995) A model for overall description of food quality. *Food Quality and Preference* 6(3): 185-190.

BIOGRAPHY

ANET REŽEK JAMBRAK, Associate professor, was born on 26 December 1980. in Zagreb. She graduated from the Faculty of Food Technology and Biotechnology of the University of Zagreb in 2002. and in year 2008. she defended her doctoral dissertation (thesis) titled "*Influence of Ultrasound on Physical and Functional Properties of Whey Proteins*". According to the decisions of the Biomedical Sciences Committee, she was titled Scientific Research Officer on 18 January 2011, and in the position of Scientific Advisor (permanent title) on 24.11.2017. She became Associate professor in 2013 at the same Faculty. She also has strong international collaboration with renowned scientists. She was trained abroad in 2005. at the Faculty of Health and Life Sciences at Coventry University, UK through the scholarship "British scholarship trust" and in 2009. at the University of Avignon, France, as a invited lecturer and researcher in the field of "green" ultrasound and microwave extractions. In the period from 2007. Anet Režek Jambrak has published over 80 significant scientific papers, published in top scientific journals with high impact factors (citation more than 1100, h-index 18). She is also a co-author of 10 chapters in scientific books, most of which are renowned world publishers Elsevier, Springer, Wiley-Blackwell and Nova Science Publisher. She is the winner of many awards and acknowledgments, most notably the 2016. Young Scientist Award from the International Union of Food Science and Technology (IUFoST). In 2011. she received award for Young Scientist "Vera Johanides" from Croatian Academy of Engineering and 2009. State Prize for Science for Young Scientists awarded by the Parliament of the Republic of Croatia and the Government of the Republic of Croatia. Since 2016. she is a member of the International Academy of Food Science and Technology (IAFoST) - Early Career Scientist.

Tutorial and Workshop Presentations

Sustainability in food industry: Towards a unified multi-objective decision making framework

Philippe Nimmegeers, Satyajeet Bhonsale, Carlos André Muñoz López, Ihab Hashem, Jan Van Impe
BioTeC+ & OPTEC, Department of Chemical Engineering, KU Leuven
CPMF2, Flemish Cluster Predictive Microbiology in Foods
Gebroeders de Smetstraat 1, B-9000 Gent, Belgium
E-mail address: Jan.VanImpe@kuleuven.be

KEYWORDS

Sustainability, Multi-objective optimization, Decision making, food industry

ABSTRACT

The growth of world population, the associated societal challenges and regulations push the food industry to become more sustainable. Improvements are required on multiple aspects: sustainable use of resources, limiting environmental impact and competitiveness, while ensuring safe process operation, food quality and food safety. Existing food manufacturing systems are mainly designed to maximize the production without keeping other aspects of sustainability in mind. Model-based optimization techniques accounting for sustainability indicators can be used to improve the in these aspects. In addition, many sustainability measures exist related to one or more of the three sustainability pillars (society, environmental and economic). These sustainability measures are often conflicting, as optimizing one of these measures often worsens the performance of another measure. Hence, achieving sustainable operation can therefore be seen as a multi-objective problem. Many advanced techniques have been developed in different fields, but these do not find their way to food industry. Furthermore, a generic, standardized approach is missing. Therefore, there is a need for a unified framework that can be used for sustainable design, operation optimization and decision making in food industry. In this article, the current state of the art with respect to sustainability in food industry and multi-objective optimization are presented. In addition, software tools developed at KU Leuven/BioTeC+ are introduced in the frame of enabling a sustainable food process design and operation. To conclude a strategy for developing a multi-objective decision making framework has been proposed.

INTRODUCTION

In 2015, the world population reached 7.3 billion and predictions of the United Nations state that the world population will reach 9.7 billion and 11.2 billion by 2050

and 2100 respectively according to the United Nations' report on the world population prospects (2015). Consequently, food demand will increase as it is expected that prosperity and healthcare will do the same. As a limited amount of natural resources is available, an efficient and complete use is required. Hence, a sustainable food industry is of utmost importance Zisopoulos et al. (2017).

It has been proven that dynamic optimization and computer aided process engineering (CAPE) can improve food production and processing Banga et al. (2003). During design and operation of (bio)chemical plants, optimal decisions have to be taken considering multiple and often conflicting sustainability objectives (e.g., maximizing production while minimizing greenhouse gases emissions).

Several mathematically equivalent trade-off solutions exist for these multiobjective optimization problems. The systematic generation and efficient presentation of these optimal alternatives to decision makers becomes a key step in the optimal design and operation of (bio)chemical/food (processing) plants. Hence, decisions have to be made in an efficient and well informed manner as (i) the economic profitability has to be enhanced; (ii) socio-environmental impacts must be computed, reduced and reported and (iii) trade-offs between risk and process performance, originating from model uncertainties, have to be accounted for Azapagic and Clift (1999).

Major challenges for computer-aided decision making (CADM) in the design and operation of food processes in view of sustainability are:

1. Inclusion of socio-environmental sustainability objectives. Up till now mainly economic return is considered in model-based process design and operation. A systematic inclusion of socio-environmental indicators, resulting in a MOO frame, is thus desirable.
2. Availability of interactive methods and software tools. To support DMs, a user-friendly tool combining efficient solvers for MOO problems with interactive visualization methods is required. The tool has to be compatible with widely spread CAPE tools.

3. Validation for industrial applications. To convince industry, the methods and tools have to be validated on a challenging industry relevant case study, which preferably exhibits complex characteristics such as a large scale, nonlinear and dynamic model.

Research on these aspects will spread the use of sustainability indicators in computer aided decision making in food industry and enable to systematically quantify and assess the trade-offs among these sustainability indicators.

In the next section, the current state of the art is discussed with respect to sustainability in food industry. The third section covers the concept of multi-objective optimization. Subsequently, multi-objective optimization tools developed at KU Leuven/BioTeC+ are presented in the frame of enabling a sustainable food process design and operation. To conclude a strategy for developing a multi-objective framework is proposed.

SUSTAINABILITY IN FOOD INDUSTRY

The assessment of sustainability in food industry has gained interest throughout the last decade. Examples of efforts that have recently been taken in food industry are summarized in this section. Two main streams can be considered. On the one hand, exergy analysis is a valuable tool to draft Sankey or Grassmann diagrams and identify parts of the studied process in which energy is wasted. On the other hand life cycle assessment techniques are popular to assess the environmental impacts of a studied food process.

Zisopoulos et al. (2017) have reviewed exergy analysis and exergy indicators as a tool to assess sustainability in food industry and identify opportunities to avoid the production of waste streams, or reusing waste streams along the whole food chain. However, currently used approaches lack clarity and care should also be taken with respect to nutrition aspects. Therefore, Zisopoulos et al., (2017) stress the need for a systematic framework for exergy analysis in food industry.

Pardo and Zufa (2012) studied the environmental impacts of four thermal and non-thermal food preservation techniques (autoclave pasteurization, microwaves, high hydrostatic pressure and modified atmosphere packaging) through life cycle assessment with SimaPro using the ReCiPe methodology Goedkoop et al. (2009; 2013). In Do et al. (2014) a decision support framework for selecting thermal process technologies in the food industry has been developed by combining a rule-based technique and a fuzzy analytic hierarchy process. The selection comprises two steps and results in the ranking of potential technologies for a particular product. This decision support aims at helping in the selection of thermal process technologies at an early development phase.

Tran et al. (2017) recently presented an optimized

integer-programming mathematical model by applying an integrated environmental indicator for selecting alternatives in cleaner production programs, based on goal programming. This model has been validated with a cassava starch factory.

These examples indicate that different strategies are used for assessing the sustainability of food manufacturing processes. Furthermore, different different sustainability measures can be used. In the next section a multi-objective optimization formulation is presented to cover different indicators in making decisions regarding the design or operation of food manufacturing processes.

MULTI-OBJECTIVE OPTIMIZATION

In multiobjective optimization (MOO) two or more, typically conflicting, objectives are simultaneously optimized (e.g., maximizing productivity while minimizing energy losses). A multi-objective optimization problem could be written as follows:

$$\min_{\mathbf{u} \in R^{n_u}} [J_1(\mathbf{x}, \mathbf{u}), \dots, J_n(\mathbf{x}, \mathbf{u})] \quad (1a)$$

subject to:

$$0 = \mathbf{f}(\mathbf{x}, \mathbf{u}) \quad (1b)$$

$$0 \geq \mathbf{g}(\mathbf{x}, \mathbf{u}) \quad (1c)$$

with $\mathbf{J} = [J_1, \dots, J_n] \in R^n$ the set of objective functions defined by (independent) optimization variables $\mathbf{u} \in R^{n_u}$ and states $\mathbf{x} \in R^{n_x}$, with $\mathbf{f} \in R^{n_x}$ denoting the right hand side of the model equations and \mathbf{g} denoting the n_c equality and inequality constraints.

The solution of such a multi-objective optimization problem is a Pareto front, showing the optimal trade-off solutions. These trade-off solutions indicate that there cannot be improved with respect to one objective, without worsening with respect to another objective.

The *feasible space* Ω of the optimization problem is defined as the set of states and optimization variables which satisfy all the constraints and bounds set in Equations (1b) and (1c) Vallerio et al. (2015).

Different approaches to solve multi-objective optimization problems and constructing a Pareto front are summarized in Logist et al. (2010):

Numerous applications exist with respect to multi-objective optimization in food industry. War (2016) presented a survey on solving optimization problems in food manufacturing industry.

Validi et al. (2014) presented a multi-objective optimization approach minimizing CO₂ emissions from transportation and total costs in the distribution chain for a two layer supply chain in the distribution of milk in Ireland using NSGA-II.

In Sendín et al. (2010) an efficient and robust multi-objective optimization technique has been presented and applied to the thermal sterilization of canned tuna fish and pork puree.

TOOLS DEVELOPED AT KU LEUVEN/BIOTEC+

At KU Leuven/BioTeC+ multi-objective optimization is one of the key research topics. This research has resulted in the development of two toolkits which can be applied to food manufacturing processes: Pomodoro Bhonsale et al. (2016) and INPROP Muñoz López et al. (2018).

If a mathematical model equations and parameters are known for a studied food manufacturing process, the inhouse developed software toolkit Pomodoro could be used. Pomodoro is a Python-based toolkit which can be used to solve dynamic optimization problems using state of the art discretization schemes with orthogonal collocation as default. The user needs to specify the process model, objective functions and any applicable constraints and Pomodoro discretizes the problem and solves it. Furthermore, Pomodoro contains a multiobjective toolkit which contains state of the art gradient-based multiobjective optimization algorithms and a ParetoBrowser Vallerio et al. (2015) that can be used for the visualization. Pomodoro uses `casADi` Andersson (2013) to compute exact Hessians and Jacobians and passes it to IPOPT Wächter and Biegler (2006) which solves the optimization problem.

INPROP Muñoz López et al. (2018) is a free Matlab-based INterface for PROcess OPTimization that provides a platform to apply gradient-based multiobjective optimization of processes simulated in Aspen Plus. Starting from the process implemented in the equation oriented mode of Aspen Plus, INPROP uses `Activex(.COM)` protocols to link the simulation backup file (*.bkp) and the Open Object Model Framework (OOMF) to transfer the required model information to the optimization framework in Matlab. The user needs to specify the location of the simulation files, define the subset of dependent and independent variables that are required for the formulation of the objective functions and constraints and define these functions. INPROP uses vectorization methods, Normal Boundary Intersection (NBI) and Normalized normal constraint (NNC) to reformulate the multiobjective problem and to allow the use of NLP solvers. INPROP transfers the models gradient information from the equation oriented engine of Aspen Plus and uses Casadi to analytically determine Jacobians and approximate the Hessians to finally pass them to IPOPT (which solves the optimization problem). This approach allows using INPROP to efficiently optimize the process regarding diverse objectives (e.g. exergy, economics, LCA, logistics).

A FRAMEWORK FOR MULTI-CRITERIA DECISION MAKING IN FOOD INDUSTRY

The problem of enabling a uniform strategy for sustainable interactive decision making in the food industry could be addressed by developing a user-friendly (soft-

ware) platform which integrates methods and tools to improve process sustainability.

Firstly, a set of standardized tools could be developed to aid decision makers (DMs) in quantifying and comparing sustainability indicators in process design and operation. With respect to this multi-objective optimization allows to trade off incommensurable quantities without using aggregate objectives (i.e., Cost-Benefit Analysis (CBA) Pearce et al. (1989)), a step often used in Life Cycle Assessment (LCA) leading to subjective and sub-optimal solutions Azapagic and Clift (1999). This involves the inclusion of widespread indicators (e.g., carbon footprint Wright et al. (2011)) and less used ones (e.g., exergy efficiency Rosen and Dincer (2001)).

Secondly, efficient numerical methods are required for the solution of MOO problems, enabling real time interactive decision-making. This should allow DMs to solve and interpret complex decision problems by interactive exploration of multidimensional Pareto sets. The graphical representation of Pareto sets poses significant cognitive hurdles for DMs, especially if high-dimensional Pareto sets are involved. The efficient visualization of high-dimensional data is a problem encountered in many different fields and applications (e.g., data representation and exploration). Minimization of risk due to model uncertainties should also be considered in the MOO framework, leading to trade-offs with process performance.

Once the numerical tools are developed, an interface for computer aided decision making tool would be a next step. Such a computer aided decision tool allows to make trade-offs in a practical setting as for instance the tradeoff between production and energy recovery. This tool should be developed in collaboration with stakeholders in food industry to match the features of the decision making tool with the practical DM's needs.

CONCLUSIONS

The aim of this article was to highlight the importance of model-based multi-objective optimization in the frame of achieving a more sustainable food industry. An overview of the current state of the art with respect to sustainability in food industry and multi-objective optimization have been presented. Furthermore, two software tools, Pomodoro and INPROP both developed at KU Leuven/BioTeC+, are introduced in the frame of enabling a sustainable food process design and operation. Finally a strategy for the development of a multi-criteria decision making framework has been proposed. The work required to converge to such framework requires the involvement of different stakeholders in food industry.

ACKNOWLEDGEMENTS

This work was supported by KU Leuven [PFV/10/002] Center-of-Excellence Optimization in Engineering (OPTEC) and the Belgian Science Policy Office (DYSCO) [IAP VII/19]. CAM holds a VLAIO-Baekeland [HBC.2017.0239] grant. IH is supported by FWO-SB grant 1S54217N. SB holds a IWT-Baekeland [IWT 150715] grant.

REFERENCES

2016. *A survey on metaheuristics for optimization in food manufacturing industry*. *Applied Soft Computing*, 46, 328–343.
- Andersson J., 2013. *A General-Purpose Software Framework for Dynamic Optimization*. PhD thesis, Arenberg Doctoral School, KU Leuven, Department of Electrical Engineering (ESAT/SCD) and Optimization in Engineering Center, Kasteelpark Arenberg 10, 3001-Heverlee, Belgium.
- Azapagic A. and Clift R., 1999. *The application of life cycle assessment to process optimisation*. *Computers & Chemical Engineering*, 23, no. 10, 1509–1526.
- Banga J.R.; Balsa-Canto E.; Moles C.G.; and Alonso A.A., 2003. *Improving food processing using modern optimization methods*. *Trends in Food Science & Technology*, 14, no. 4, 131–144.
- Bhonsale S.; Vallerio M.; Telen D.; Vercammen D.; Logist F.; and Van Impe J., 2016. *SolACE: An Open Source Package for Nonlinear Model Predictive Control and State Estimation for (Bio)Chemical Processes*. In *Proceedings of the 26th European Symposium on Computer Aided Process Engineering*. Portoroz, Slovenia., June 12th - 15th.
- Do T.T.H.; Schnitzer H.; and Le T.H., 2014. *A decision support framework considering sustainability for the selection of thermal food processes*. *Journal of Cleaner Production*, 78, 112 – 120.
- Goedkoop M.; Heijungs R.; Huijbregts M.; De Schryver A.; Struijs J.; and Van Zelm R., 2009. *ReCiPe 2008, A Life Cycle Impact Assessment Method Which Comprises Harmonised Category Indicators at the Midpoint and the Endpoint Level*.
- Goedkoop M.; Oele M.; Leijting J.; Ponsioen T.; and Meijer E., 2013. *SimaPro 8. Database Manual*. *Methods Library*. Pré Consultants.
- Logist F.; Houska B.; Diehl M.; and Van Impe J., 2010. *Fast Pareto set generation for nonlinear optimal control problems with multiple objectives*. *Structural and Multidisciplinary Optimization*, 42, 591–603.
- Muñoz López C.A.; Telen D.; Nimmegeers P.; Cabianca L.; Logist F.; and Van Impe J., 2018. *A process simulator interface for multiobjective optimization of chemical processes*. *Computers & Chemical Engineering*, 109, 119 – 137.
- Pardo G. and Zufa J., 2012. *Life cycle assessment of food-preservation technologies*. *Journal of Cleaner Production*, 28, 198 – 207.
- Pearce D.; Markandya A.; and Barbier E., 1989. *Blueprint for a green economy*. Earthscan.
- Rosen M. and Dincer I., 2001. *Exergy as the confluence of energy, environment and sustainable development*. *Exergy, An International Journal*, 1, no. 1, 3–13.
- Sendín J.O.H.; Alonso A.A.; and Banga J.R., 2010. *Efficient and robust multi-objective optimization of food processing: A novel approach with application to thermal sterilization*. *Journal of Food Engineering*, 98, no. 3, 317–324.
- Tran T.V.; Schnitzer H.; Braunegg G.; and Le H.T., 2017. *Development of an optimization mathematical model by applying an integrated environmental indicator for selecting alternatives in cleaner production programs*. *Journal of Cleaner Production*, 154, 295 – 308.
- Validi S.; Bhattacharya A.; and Byrne P., 2014. *A case analysis of a sustainable food supply chain distribution system: A multi-objective approach*. *International Journal of Production Economics*, 152, 71 – 87.
- Vallerio M.; Hufkens J.; Van Impe J.; and Logist F., 2015. *An interactive decision-support system for multi-objective optimization of nonlinear dynamic processes with uncertainty*. *Expert Systems with Applications*, 42, 77107731.
- Wächter A. and Biegler L., 2006. *On the Implementation of a Primal-Dual Interior Point Filter Line Search Algorithm for Large-Scale Nonlinear Programming*. *Mathematical Programming*, 106, no. 1, 25–57.
- Wright L.; Kemp S.; and Williams I., 2011. *'Carbon footprinting': towards a universally accepted definition*. *Carbon Management*, 2, no. 1, 6172.
- Zisopoulos F.K.; Rossier-Miranda F.J.; van der Goot A.J.; and Boom R.M., 2017. *The use of exergetic indicators in the food industry: A review*. *Critical Reviews in Food Science and Nutrition*, 57, no. 1, 197–211.

Application of dynamic optimization for food systems using Pomodoro: A Tutorial

Satyajeet Bhonsale, Dries Telen, Philippe Nimmegeers, Jan Van Impe*
BioTeC+ & OPTEC, Department of Chemical Engineering, KU Leuven
CPMF2, Flemish Cluster Predictive Microbiology in Foods
Gebroeders De Smetstraat 1, B-9000 Gent, Belgium
*E-mail: Jan.VanImpe@kuleuven.be

KEYWORDS

Optimal control, optimal experiment design, software toolkit

Abstract

The aim of this tutorial is to introduce the tool Pomodoro which has been developed to solve (multiobjective) dynamic optimization arising in various fields. We aim to present the user-friendliness of Pomodoro through case studies relevant to the food and brewing sector. The optimal experiment design of fed-batch bioreactor for production of baker's yeast is considered as the tutorial case study.

INTRODUCTION

Optimal control or *dynamic optimization*, which deals with calculation of time varying trajectories which optimize a given objective for a system of differential equations, has found a variety of applications in a number of engineering disciplines. Applications of *off-line* optimal control in the (bio)-chemical industry vary ranging from calculation of optimal feeding profiles of fed-batch bioreactors (e.g., Liu et al. 2013), optimal operation profiles for batch reactors (e.g Benavides and Diwekar 2012) to parameter estimation and optimal experiment design (e.g., Telen et al. 2014).

Pomodoro is a toolkit based on CasADi (Andersson 2013). Pomodoro equipped to handle not only single objective dynamic optimization problems, but also multiobjective, and model predictive control and model based estimation problems. In this tutorial we will focus on the single objective case and the multiobjective Pareto Browser will not be considered. Pomodoro provides an efficient framework for researchers and engineers without a background in optimal control to implement their case studies in a straightforward symbolic way. The toolkit can be obtained from <https://cit.kuleuven.be/biotec/software/pomodoro>

Mathematical background and methods

This section serves to give a brief mathematical overview of the problem classes which can be solved using

Pomodoro along with the various techniques which can be used to solve them.

Dynamic Optimization

Formulation

The optimal control or dynamic optimization problem (OCP) is described as

$$\underset{\mathbf{x}(\cdot), \mathbf{u}(\cdot), \mathbf{p}}{\text{minimize}} \quad J = \int_{\xi_0}^{\xi_f} \mathcal{L}(\mathbf{x}(\xi), \mathbf{u}(\xi), \mathbf{p}) d\xi + \mathcal{M}(\mathbf{x}(\xi_f), \mathbf{p}) \quad (1a)$$

$$\text{subject to} \quad 0 = \mathbf{f}(\dot{\mathbf{x}}(\xi), \mathbf{x}(\xi), \mathbf{u}(\xi), \mathbf{p}, \xi); \quad \xi \in [\xi_0, \xi_f] \quad (1b)$$

$$0 = \mathbf{b}_i(\mathbf{x}(0), \mathbf{p}) \quad (1c)$$

$$0 \geq \mathbf{c}_p(\mathbf{x}(\xi), \mathbf{u}(\xi), \mathbf{p}, \xi) \quad (1d)$$

$$0 \geq \mathbf{c}_t(\mathbf{x}(\xi_f), \mathbf{u}(\xi_f), \mathbf{p}, \xi_f) \quad (1e)$$

where \mathbf{x} represents the state variables, \mathbf{u} the control variables, and \mathbf{p} the fixed parameters. The process dynamics are defined by a set dynamic equations \mathbf{f} over the interval of the independent variable $\xi \in [\xi_0, \xi_f]$. It has to be noted that although the optimal control solution is obtained over the interval of the independent control variable, the final value (ξ_f) may also be an optimization variable, e.g., final time in batch operation. The initial conditions of the system are contained in the equality constraints of Eq. 1c, while the Eq. 1d-1e represent the path and terminal constraints acting on the system. The objective functional can consist of both the Lagrange term \mathcal{L} and the Mayer term \mathcal{M} . It is assumed throughout this paper that all the functions are twice differentiable.

Numerical solution

The most common approach to solve the OCP is the direct approach which converts the optimal control problem into a nonlinear program (NLP), which is then solved using appropriate algorithms. The proposed software utilizes the *orthogonal collocation* of Biegler (2007). There exist other direct methods like the single shooting and multiple shooting which make use of numerical integrators to solve the ODE systems. Orthogonal collocation, on the other hand, fully discretizes the state and control variables which act as the optimization variables

in the NLP. Due to the large size of the NLP obtained by such discretization, dedicated optimization algorithms which exploit the structure of the system efficiently are required.

Software framework

In this section the design details of the software `Pomodoro` are discussed. The entire software consists of three main blocks which interact with each other and with `CasADi` to generate the solution. These blocks are `Pomodoro` itself, `Pareto Browser`, and `SolACE`. In this tutorial we will focus on `Pomodoro`.

Pomodoro

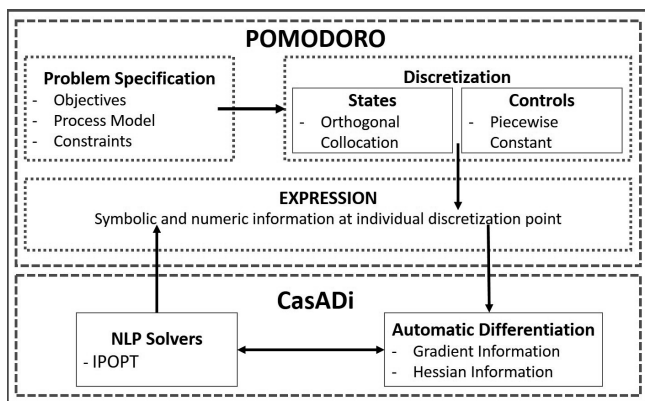


Figure 1: Outline of `Pomodoro`. `Pomodoro` utilizes `CasADi` to formulate the dynamic optimization problems. The discretization routines for controls and states inherit from the class `Expression` which allows the user to impose constraints on individual collocation points.

The basic structure of `Pomodoro` is outlined in Figure 1. The entire `Pomodoro` tool is written in `Python` which also acts as the interface of the software. The problem specifications are input by the user in the `Python` symbolically. `Pomodoro` then contains the routines which convert these symbolic equations into an NLP. Following the orthogonal collocation strategy, the state variables are discretized by third order polynomials using Radau collocation points (in the class `LagrangeStates`), while the control variables are discretized as piecewise constant (in the class `PiecewiseConstant`). These classes inherit properties from their base class `Expression`. `Expression` allows the user to get and pass information on any individual collocation (or discretization) point, or at any time instance. This is a major advantage as now a constraint can be imposed easily at any time instance in the problem. This is helpful especially during parameter estimation problems when equidistant sampling times are not possible.

The class `Problem` acts like a buffer to collect all the

information about the (discretized) states and controls, system ODEs, objective functions, and constraints. The problem is then passed to the `Solver` class which initializes the NLP solver, and on command the solve problem. The default solver is set to be IPOPT (Wächter and Biegler 2006), although other solvers like `CasADi`'s inbuilt SQP solver can also be used. It is, however easily possible to extend this class to include other solvers available commercially or as open source. `CasADi` provides the solver with exact jacobian and hessian information by efficiently exploiting the automatic differentiation techniques. The solution of the NLP is passed back to the class `Problem` through the `Expression` routine, which makes the numerical solution at any individual collocation point available.

Case Study

The case study in consideration is the optimal experiment design (OED) of a fed-batch fermentation of baker's yeast (Barz et al. 2010). The goal of OED is to design excitation such that maximum information can be obtained out of the experiment. For further details on OED the reader is referred to Telen et al. (2014). In this example, the aim of the experiment is to obtain data for parameter estimation. The fed batch bioreactor system is modeled by a dynamic system with Contois kinetics as follows:

$$\frac{dx_1}{dt} = (r - p_2 - u_1)x_1 \quad (2)$$

$$\frac{dx_2}{dt} = -\frac{rx_1}{p_1} + u_1(u_2 - x_2) \quad (3)$$

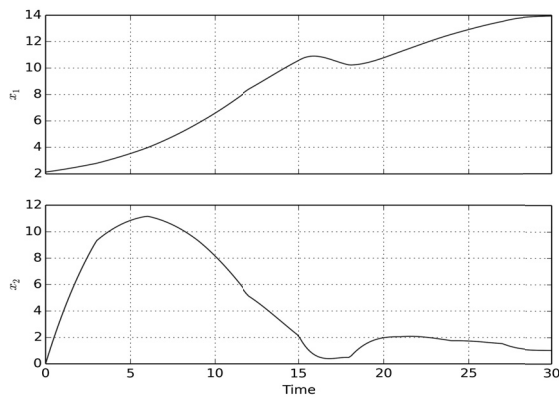
$$r = \frac{\theta_1 x_2}{\theta_2 x_1 + x_2} \quad (4)$$

Here, x_1 and x_2 denote the biomass and substrate concentrations in g/L. The parameters to be estimated are $[\theta_1, \theta_2]$. The nominal values used in computation are $\theta_* = [0.30, 0.03]$. The other parameters are assumed to be known as $\mathbf{p} = [0.55, 0.03]$. The initial substrate concentration is fixed at 0.01 g/L and the initial biomass concentration is obtained as a result of the optimization. The objective function used is the A criterion which considers minimization of the trace of inverse of the Fisher Information Matrix .

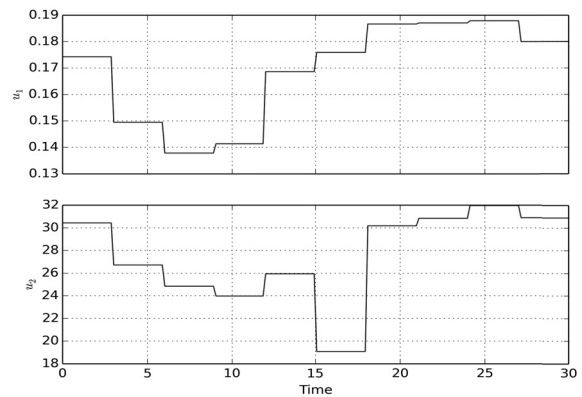
$$J = \min [\text{trace} (\mathcal{F}^{-1})] \quad (5)$$

Figure 2 shows the result of the optimization. The control profiles obtained lead to the maximum information content as defined by the A-criterion.

During the tutorial, the OED problem will be formulated and solved using `Pomodoro`. We will go through the case step by step and show details of implementation.



(a) State trajectories for the OED problem. x_1 is the biomass and x_2 is the substrate concentration. The time is given in hours.



(b) Control trajectories for the OED problem. u_1 is the dilution and u_2 is the substrate concentration in the feed. Time is given in hours.

Figure 2: OED results yielding the maximum information content. Pomodoro

Conclusions

The software toolkit Pomodoro for optimal control was discussed and used to solve an relevant case study. In the presentation, the audience will be shown step by step implementation of the case study.

Acknowledgements

This work was supported by the Belgian Science Policy Office (DYSCO) [IAP VII/19] and KU Leuven PFV/10/002 Center-of-Excellence Optimization in Engineering (OPTEC). SB holds a IWT-Baekeland [IWT 150715] grant

References

- Andersson J., 2013. *A General-Purpose Software Framework for Dynamic Optimization*. PhD thesis, Arenberg Doctoral School, KU Leuven.
- Barz T.; Arellano-Garcia H.; and Wozny G., 2010. *Handling Uncertainty in Model-Based Optimal Experimental Design*. *Industrial and Engineering Chemistry Research*, 49, 5702 – 5713.
- Benavides P.T. and Diwekar U., 2012. *Optimal control of biodiesel production in a batch reactor: Part I: Deterministic control*. *Fuel*, 94, 211 – 217. ISSN 0016-2361.
- Biegler L.T., 2007. *An overview of simultaneous strategies for dynamic optimization*. *Chemical Engineering and Processing: Process Intensification*, 46, no. 11, 1043–1053.

Liu C.; Gong Z.; Shen B.; and Feng E., 2013. *Modelling and optimal control for a fed-batch fermentation process*. *Applied Mathematical Modelling*, 37, no. 3, 695 – 706. ISSN 0307-904X.

Telen D.; Vercammen D.; Logist F.; and Van Impe J., 2014. *Robustifying optimal experiment design for non-linear, dynamic (bio)chemical systems*. *Computers & Chemical Engineering*, 71, 415 – 425. ISSN 0098-1354.

Wächter A. and Biegler L., 2006. *On the Implementation of a Primal-Dual Interior Point Filter Line Search Algorithm for Large-Scale Nonlinear Programming*. *Mathematical Programming*, 106, no. 1, 25–57.

Code listing for the OED problem

```

1 import time
2 import numpy as NP
3 #import pomodoro
4 from pomodoro.problem.problem import Problem
5 from pomodoro.solver.solver2 import Solver2
6 from pomodoro.discs.expression import
  Expression
7 from casadi import *
8 t = time.time()
9 prob = Problem()
10 p1 = 0.55;p2 = 0.03
11 lb = [0.0,0.0,-1.0e7,-1.0e7,-1.0e7,-1.0e7,-1.0
12 e7,-1.0e7,-1.0e7]
13 ub = [25.0,25.0,1.0e07,1.0e07,1.0e07,1.0e07,1.0
14 e07,1.0e07,1.0e07]
15 tend = prob.setTimeRange(0.0,30.0)
16 x = prob.addStates(9,lb,ub,method=['
17 LagrangeStates',10])
18 x.load('OED_BY.state')
19 u = prob.addControls(2,[0.05,5.0],[0.20,35.0],
20 method=['PiecewiseConstant',10])
21 x0 = prob.addParameters(1,1.0,10.0,2.0)
22 t = prob.addFixedParameters(2,[0.3,0.03])

```

```

19 u.load('OED_BY_control')
20 x1 = x[0]; x2 = x[1]; dx1dt1 = x[2]
21 dx1dt2 = x[3]; dx2dt1 = x[4]; dx2dt2 = x[5]
22 F11 = x[6]; F12 = x[7]; F22 = x[8]
23 t1 = t[0]; t2 = t[1]
24 rhs = Expression(SX.zeros(9))
25 r = (t1*x2)/(t2*x1 + x2)
26 drdt1 = x2/(t2*x1 + x2) + t1*((dx2dt1*(t2*x1 +
    x1) - x2*(t2*dx1dt1 + dx2dt1))/((t2*x1 + x2)
    *(t2*x1 + x2)))
27 drdt2 = (t1*dx2dt2*(t2*x1 + x2) - t1*x2*(x1 +
    t2*dx1dt2 + dx2dt2))/((t2*x1 + x2)*(t2*x1 +
    x2))
28 rhs[0] = (r - p2 - u[0])*x1
29 rhs[1] = (-1/p1)*r*x1 + u[0]*(u[1] - x2)
30 rhs[2] = x1*drdt1 + r*dx1dt1 - p2*dx1dt1 - u
    [0]*dx1dt1
31 rhs[3] = x1*drdt2 + r*dx1dt2 - p2*dx1dt2 - u
    [0]*dx1dt1
32 rhs[4] = (-1/p1)*(r*dx1dt1 + x1*drdt1) - u[0]*
    dx2dt1
33 rhs[5] = (-1/p1)*(r*dx1dt2 + x1*drdt2) - u[0]*
    dx2dt2
34 rhs[6] = dx1dt1*dx1dt1 + dx2dt1*dx2dt1
35 rhs[7] = dx1dt1*dx1dt2 + dx2dt1*dx2dt2
36 rhs[8] = dx1dt2*dx1dt2 + dx2dt2*dx2dt2
37 prob.addOde(x, rhs)
38 prob.addConstraints(x1(0) - x0, 0.0)
39 prob.addConstraints(x2(0), 0.01)
40 prob.addConstraints(x[2:](0), 0.0)
41 Acrit = (F11(-1) + F22(-1))/(F11(-1)*F22(-1) -
    F12(-1)*F12(-1))
42 prob.addObjective(Acrit)
43 solver = Solver2(prob, printlevel=5, max_iter
    =10000)
44 solver.solve()

```

E-CAM: a European Infrastructure for Advanced Simulation Software Development, Training and Industry Collaboration from Food and Pharma to Advanced Materials

Donal Mac Kernan
School of Physics
University College Dublin
Dublin 4, Ireland
E-mail: Donal.MacKernan@ucd.ie

KEYWORDS

Food Science, Molecular Dynamics, Rare-event methods, Coarse Grained Models, meso-scale, Multi-scale, Electronic Structure, Machine Learning

ABSTRACT

Molecular mechanisms play a key role, both at a fundamental and processing level, in innovative taste systems, functional and nutritional ingredients, and integrated solutions for the food, beverage and pharmaceutical markets. Incorporating an understanding of such mechanisms into data coming from experiment and consumer preferences can provide greater insight to, and control of the relevant processes at play. This work will touch on several examples where advanced simulation at a molecular, meso- and multi-scale level can shed light into the mechanisms at play.

INTRODUCTION

From a field of wheat or a herd of cows, the industry research laboratory or the processing plant, to the kitchen the mouth, and digestion, the complexity and centrality of food to life is second only to life itself. Food manufacturers are faced by six key challenges, their products must be: tasty, healthy, safe, affordable, have consumer appeal, and be sustainable. Each of these demands poses significant scientific challenges ranging from:

- (a) Quantum effects such as the creation and breakage of covalent bonds entailed in the hydrolysis of sugars, fats and proteins; and,
- (b) Classical effects occurring at nanometer length scales such as the folding and unfolding of proteins as can occur in the processing of milk, or the non-covalent binding of tastants to receptors in the tongue; and,
- (c) mesoscale properties of colloids, gels and foam, important for example for storage, rheology, and perceptions of texture.

While experimental methods play a central role in food, elucidating nanoscale effects is difficult and in most cases impractical. However, computer based simulation at these length and time scales is possible, provided suitable statistical methods, algorithms/software and massively parallel platforms are available, combined with people having the requisite skills for their exploitation.

Software Development Infrastructure for Simulation

E-CAM, the European Union H2020 Centre of Excellence mission is to address these needs, as an infrastructure for Advanced Simulation Software Development, Training, & Industry Collaboration in applications ranging from Food and Pharmaceuticals to Advanced Materials. The E-CAM infrastructure is built on four pillars: State of the Art Workshops, Industry Scoping Workshops, Long term Industry Pilot Projects, and extended software development workshops (ESDW's). ESDW's combine software module generation with "training by doing" bringing modern programming standards and techniques into the work practices of the participants, in its four core scientific areas: classical molecular dynamics (MD), electronic structure, quantum dynamics, and meso/multi-scale modeling. Participation to E-CAM workshops is essentially open to anyone with a genuine interest in the themes of each meeting, and free. This is possible because E-CAM is in fact a partnership of 16 CECAM (Centre Européen de Calcul Atomique et Moléculaire) nodes, 3 PRACE (Partnership for Advanced Computing in Europe) Centres, and 1 Centre for Industrial Computing.

FOOD SCIENCE AND INDUSTRY CHALLENGES TO SIMULATION

The six key challenges faced by food manufacturers mentioned earlier pose equally interesting and significant challenges to science. To address the demand that a product be tasty, healthy and safe, one must consider the processes involved: these include taste perception; the absorption of nutrients occurring during the disassembly of food structures involved in digestion, and generally some form of heat treatment.

The Complex Sensation of Taste

The sensation of taste is extremely complex, involving mastication and saliva, the release of volatile compounds, olfactory receptors (one cannot completely separate the sense of taste from the sense of smell), taste receptors, the texture of food, neuroscience, and indeed genetics. What can a simulator do when confronted by such complexity? At a molecular level, it is now possible to simulate at least in part G-Protein Coupled Receptors (GPCR's) and ion-channel receptors that play a central role in olfaction and taste. GPCR's are trans-membrane proteins that consist of three domains: the extracellular domain (ECD), which lies

outside the cell (ligands such as tastants or odorants bind to it), the so called transverse membrane domain (TMD), and the intracellular domain (ICD), to which G-proteins are attached. When agonist or antagonist ligands bind to the ECD, a complex set of conformational changes ensue, which can lead to release from the ICD of parts of the G-protein (although they remain bound to the plasma domain), and a complex set of down-stream intra-cellular and even inter-cellular signaling. A full molecular dynamics simulation of a single GPCR protein including model membranes and water under physiological conditions typically requires a unit cell of 20-30 nanometers on each side, and about a million atoms. In addition, a reasonable initial condition for the atomic co-ordinates of GPCR structure is also needed, which can be provided in part (but rarely fully) via X-RAY and NMR data, bio-informatics and homology. With current hardware, 100-200 computing core per day are needed to simulate just 20-30 nanoseconds of real time. One can do a bit better if one combines CPU with GPGPU's. Nevertheless, it should be clear that to reach biologically relevant timescales using brute force simulation methods even for super computers is still very much beyond us, but all is not lost. It is in fact now frequently possible to overcome this timescale challenge by using sophisticated statistical sampling methods, which are collectively known as rare-event methods, and are the focus of the first E-CAM core scientific area, classical MD.

Rare-event Methods & Taste Receptors

Many processes in nature and technology are characterized by rare but important events, which occur on time scales orders of magnitudes longer than basic molecular motions (essentially 10^{-15} seconds which is the timescale associated with vibrations of hydrogen bonds). Examples of such rare-events can include transitions from one meta-stable conformation to another. Rare-event methods allow nearby conformations of the GPCR to be explored including quantitative information regarding their relative free energies, reaction mechanisms such as the complex conformational changes that occur on ligand binding, and associated time-scales. Rare-event methods provide in principle, the means to identify the dominant relevant conformations, order parameters, and reaction paths, and to validate the correctness of the latter. In this context, statistical/machine learning tools such as cluster analysis are also being increasingly used. Taste receptors frequently are found as dimers or other complexes allowing the sensing of a very wide combination of tastes. An alternative to detailed molecular simulation of GPCR systems via simulation known as Coarse Graining is also possible, and can be quite effective (Ponzoni et al 2017), despite the fact that many details of the GPCR may not be known.

Meso-scale/Multiscale Modeling and Taste Receptors

Coarse graining (CG) also known as meso-scale modeling involves mapping many atoms to a single coarse grained effective atom, and building a simulation scheme for the coarse grained representation of proteins and macro-

molecules. There is a diversity of such mapping schemes, and great debate regarding their relative merits and capabilities. CG may include water explicitly or in may treat water implicitly. Where it is reasonable to using a CG mapping where each amino acid is represented by a single CG atom, and water is treated implicitly, biologically relevant time scales can be reached. Indeed it is also possible to combine rare-event methods with CG. Another alternative is to treat certain degrees of freedom at a full atomistic level of detail, and others at a coarse grained level, trying to combine computational speed with atomic detail where it is critical.

Machine Learning

Despite the great progress that has taken place regarding the development of rare-event methods, predicting the sensation of taste that an individual may have for a tastant is daunting. One very novel approach that has developed over the last 5 years is to combine molecular and meso-scale simulation with machine learning and Quantitative Structure Activity Relationships. These allow physiological response data, or even the opinions of human tasters to be combined with atomistic, molecular and meso-scale descriptors. The interest in doing this is that molecular structures can be modified through minor changes in their chemistry, and processing.

Safe Food

Ensuring food is safe and free of pathogens is a critically important step in food processing. Heat treatment remains the main approach. Heating also plays a crucial role to make many foods palatable and digestible for humans. But excessive heating can also destroy the nutritional benefits of some foods, and give rise to unpleasant tastes. Molecular Simulation and in particular rare-event methods can be used to determine whether a given protein is likely to irreversibly unfold to conformations that may limit bio-availability, or be associated with unpleasant tastes.

Food Safety & Diagnostics

From the perspective of molecular simulation, at a molecular level, Food, Pharma, and biology pose very similar challenges, and as a consequence, the methods used to explore their properties are often the same. This is also true for a wide array of diagnostic tools used primarily for food safety, including: Rapid Microbiological Methods; Molecular (DNA/RNA) Diagnostics; and immune-diagnostics. In the context of food, such methods are used to detect pathogens, allergens, pollutants, and to confirm the genetic origins of food. As these diagnostic tools operate at a molecular level, it should not be surprising that simulation can greatly facilitate their development and optimization, as has been demonstrated by one of the E-CAM industry pilot projects in the development of a molecular switch sensor technology which can be used for detecting analytes/biomarkers for pathogens/allergens etc. in food. It integrates recognition and labeling (i.e. flagging the presence/absence

of the target) and switch into a single simple modular recombinant protein (see Fig. 1 for an example involving single chain variable fragment antibodies and fluorescent proteins). In model simulation studies the switch gives rise to an order of magnitude reduction in the error associated with the measurement of bio-marker concentrations in assays.



Figure 1: A snap-shot of the molecular switch sensor where the sensing elements are ScFv antibody fragments

Enzymatic Hydrolysis

Proteins, carbohydrates and fats normally must be broken down to small molecular units before they can be absorbed into the cell and be of nutritional benefit via enzymatic hydrolysis. This entails the combined use of water and enzymes to break constituent bonds. A key type of enzyme in the context of fat, are lipase proteins, an example of which is illustrated below in Fig. 2.



Figure 2: is an example of a lipase enzyme involved in the hydrolysis of fat

The breaking of bonds involves quantum mechanical effects, albeit primarily of the electronic ground state, which is the focus of one of the scientific core areas of E-CAM. That said, a full brute force simulation of enzymatic hydrolysis is really not feasible at the moment with quantum methods, as the number of atoms involved would be impractical, probably of the order of 50000 atoms at least. However it is possible to use a hybrid simulation scheme that combines molecular dynamics for most degrees of freedom where a quantum description is not necessary, with a quantum description of the much smaller set. An alternative approach is to use molecular dynamics with a semi-empirical probabilistic scheme, which breaks and even creates bonds

depending on the local conditions around reactive sites. And yet another approach is to use machine learning, where quantum simulation is used to train an effective force-field, allowing molecular simulation to be performed which can be virtually indistinguishable from a quantum description, provided the system does not significantly encounter environments to which it was not trained. The latter are being developed within E-CAM, and elsewhere.

Affordable Food

Several factors can affect the relative affordability of food. These include the costs of: the raw material, processing, storage, and transport. While the choice for example of protein source, based on animal protein is an important issue, we shall focus our attention to processing, storage, and transport, and consider a few representative examples. One of the key steps in much of food processing is drying, for instance of milk and other proteins. Apart from the obvious benefit of reduction in volume or weight, it also can increase substantially the lifetime of a food, facilitating storage and transport. However the process of drying can cause proteins to unfold, revealing hydrophobic residues, which in hydrated form of the protein are not in contact with water. In such cases, when the dried food is re-hydrated, it may not return to its original stage, but instead be transformed irreversibly into a hydrophobic and indigestible complex.

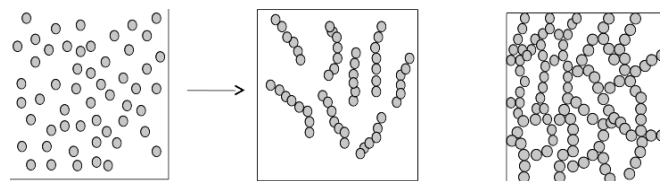


Figure 3: Aggregation can depend critically on hydration

Predicting when aggregation will occur can be difficult. In the context of protein aggregation, one problem is that salt and protonation/deprotonation of titratable sites (typically acidic or basic amino acids) can occur as the pH of a solution is varied, and simultaneously proteins may fold or unfold, and when proteins are at their iso-electric point, which corresponds in principle to when the pK of the protein equals the pH of the solution, they may suddenly aggregate (see Fig. 3). But for large proteins the situation can be very complex. Nevertheless there exist several computational schemes which frequently give reasonable results including lambda-dynamics (Donnini et al 2016) (which builds on classical molecular dynamics), and a simple but surprisingly effective coarse grained method (Barroso da Silva and Mac Kernan 2017).

One of the E-CAM industry pilot projects is working on this problem, which turns out to be closely related from a physical and chemical perspective to solubility, which is important for food and pharma, for example, in the purification of nutraceuticals (food grade molecules known

to be of significant health benefit, typically phytochemicals) and active pharmaceutical ingredients. In the context of nutraceuticals (and pharmaceuticals), another important question is ensuring bio-availability. Frequently nutraceuticals either are poorly soluble, or have a very unpleasant taste. One approach that has been developed over the last ten years or so is to encapsulate the nutraceutical in a soluble matrix or gel. Classical MD can be used to estimate the diffusion rates of active ingredient through the ematrix, while mesoscale simulation can be used to determine the relative stability of the encapsulating structure.

Adsorption of proteins onto steel surfaces

The issue of solubility is also closely related to the fouling of metals pipes by organic matter, such as can occur in the heat treatment of milk, and other proteins. In principle this is a question that can be addressed using rare-event methods, provided a reasonable accurate force-field is known for metal-organic matter interactions. E-CAM is developing such a force field by combining molecular dynamics, electronic structure calculations, with machine learning. The advantage of this approach is that once the force field is parameterized, it offers the possibility of simulation metal-organic matter and water interactions at the cost of classical molecular dynamics, which otherwise would be prohibitive for large systems.

FREE ENERGY METHODS

Many processes in nature and technology are characterized by rare but important events, which occur on time scales orders of magnitudes longer than basic molecular motions (Dellago et al 2017). Such processes, which, for instance, include chemical reactions, protein folding and first order phase transitions, are difficult to simulate with classical molecular dynamics (MD) simply because of the extreme time scales involved. The main goal of E-CAM in this context is to develop software tools capable of dealing with rare events and complex free energy properties, thus extending the time scales accessible with regular MD.

Two fundamental problems of statistical mechanics are intimately tied to the time scale problem of classical molecular dynamics simulation. (1) The calculation of the populations of meta-stable states of an equilibrium system. Such populations can be expressed in terms of free energies and hence this problem boils down to the efficient calculation of free energies. (2) The sampling of transition pathways between long-lived (meta-stable states and the calculation of reaction rate constants.

Whereas the first problem is a static one and does not necessarily require the “real” dynamics of the system to be followed, free energies are often computed using molecular dynamics. Since the understanding of rare but important events also requires the calculation of free energy barriers, which are related to rare configurations, such simulations are affected by the rare event problem. In principle, this can

be solved by running MD simulations for a very long time. In the best of cases such simulations will be expensive, but often they are simply unfeasible on current computers. Similarly, rare transitions between long-lived states can be found by running an MD simulation until the transition of interest occurs. However, within the accessible computing time the event may never happen. In the past decades, several powerful algorithms have been developed to overcome the time scale problem both for free energy computation and for rare event sampling. Typically, these methods apply an appropriately constructed bias or constraint, which artificially increases the likelihood of the rare event in a way such that it is possible to correct for the bias and restore the true probability of the event. In contrast to straightforward molecular dynamics, for which a number of excellent software packages are available (e.g., LAMMPS, Charmm, Gromacs, NAMD, etc.), methods for free energy computation and, in particular, for rare event sampling have not yet been implemented, with the required efficiency and scalability, into widespread simulation packages. One objective of E-CAM is to close this gap and develop well tested and robust software modules for free energy computation and rare event sampling.

ELECTRONIC STRUCTURE METHODS

The intelligent design and exploitation of materials for technological applications, or of new drugs, relies on our ability to describe and manipulate matter at a microscopic level. To do this, it is essential to know how atoms interact to form molecules and more complex materials. Interactions can be described empirically by creating models that reproduce known macroscopic properties of the material (e.g. melting temperature). They can also, in principle, be computed by solving the microscopic equation that describes the physics of interacting electron and nuclei in atomic systems. This equation, known as the time-independent Schrödinger equation, is one of the cornerstones of quantum mechanics. It is unfortunately too complex to solve, in general, both analytically and numerically. Several approximate methods then exist to tackle the problem. Currently, the best compromise between efficiency and accuracy is provided by a framework known as Density Functional Theory (DFT), which has been successfully applied to determine a wide range of properties of atoms, molecules, and complex materials. The software modules developed in the electronic structure work package in E-CAM, tackle specific ingredients necessary for DFT calculations of the interactions. They have been conceived to be transferable (i.e. they can be incorporated in many of the codes in use) and scalable (i.e. they can be used on computers at the highest end of current technologies), and are available to the entire community of practitioners in the field. As mentioned earlier, the use of machine learning to develop neural network based potentials trained using quantum data allows large systems to be simulated using classical MD essentially reproducing exactly the quantum properties of the system (in the sense of the method used to train the neural network). Currently such simulations are limited to at most four different atomic species. However

other neural network based approaches are also being developed within E-CAM which while less precise, and capable of modeling more species and important metal-protein interactions.

MESOSCALE & MULTISCALE SIMULATION

The inclusion of atomistic or electronic detail and the short time-steps required in most quantum and classical MD calculations limit the system size and the total time accessible with these methods. For phenomena of relevance to academia and industry that occur on longer time and distance scales (such as protein folding and docking, polymer and surfactant structuring, lubrication and blood flow) it is useful to integrate out some of the underlying degrees of freedom and to develop coarse-grained models. These meso-scale models can be studied using suitably adapted simulation techniques from classical simulations and by developing new techniques that go beyond the particle-based description. Equally important and challenging is the requirement to work across more than one length or timescale at the same time, using multi-scale simulation techniques targeted at the production of new materials with tailored macroscopic properties (for example, dislocations, grain and phase boundaries, active sites). While considerable theoretical work exists in this domain, there is no generally accepted code in the community that covers a sufficient range of length scales and phenomena.

The most recent E-CAM state-of-the-art workshop aimed to identify (i) current challenges, (ii) the existing software solutions and their limitations, and (iii) need for further development of meso- and multiscale methods and codes. This approach was motivated by the desire to propose the kind of software required to bridge different descriptions (quantum, classical, continuum) in a systematic bottom-up scheme, in which input parameters are computed at the higher resolution and then used in the lower resolution model. Explorations of new directions led to discussions on the methodologies of systematic static and dynamic coarse-graining, including inverse Monte Carlo, Newton inversion, discretisation, Mori-Zwanzig formalism etc.

Several moderated round table discussions took place during the meeting that helped provide a focus on key difficulties and challenges for meso-scale/multiscale simulation. Here we highlight one relevant to food science.

Industrial manufacturing typically involves processing where materials are in far from equilibrium conditions. Yet virtually all simulation methods have been developed for systems that are either in equilibrium or close enough to it that the corresponding force-field parameters and initial conditions are a good estimate of reality, for instance, in regimes where linear response is valid. However, such assumptions are frequently not valid, for example, for complex glassy polymeric systems, or driven systems and so on. An additional complication is that there is no theory on how such systems can be treated, despite their great practical industrial importance.

E-CAM INDUSTRY PILOT PROJECTS & FOOD

There is one E-CAM pilot project that is focused on Food and Pharmaceutical Proteins. The goals of this project are as follows. 1. To study the changes in structure and function that occur to protein complexes, antibodies and pharmaceuticals due to changes in hydration, salt and pH levels; 2. Optimize the functionality of a class of novel protein based biosensors including the effect of the changes above; and, 3. Build and develop further R&D interactions with industry. The technical problem and solution of building rationally designed protein based sensors of biomarkers that are cheap, easy-to-use, accurate, robust for use either in the living cell or in miniature low cost devices forms the core of our innovation.

ACKNOWLEDGEMENTS

DM is grateful to Jean Christoph Jacquier and Dolores O’Riordan from the UCD Institute of Food and Health, and from Fernando Barosso Da Silva (Univ Sao Paolo), for providing great insight into the complexities of Food Science. The work of DM is supported by the European Union under grant Number 676531 corresponding to the H2020 E-CAM Centre of Excellence.

REFERENCES

- Barroso da Silva, F. L., Mac Kernan, D. 2017. “Benchmarking a fast proton titration scheme in implicit solvent for biomolecular simulations”, *J. Chem. Theory and Comp.* 13 (6), 2915-2929
- Dellago, C, Swenson, D., Mac Kernan, D., Everaers, R. Castagna, J., 2017. “Identification/selection of E-CAM MD Codes or development”, Report to the European Union, DOI 10.5281/zenodo.841694
- Donnini, S. Ullmann, T., Groenhof, G. and Grubmüller, H, 2016. ”Charge-neutral constant pH molecular dynamics simulations using a parsimonious proton buffer.” *J. Chem. Theory Comput.* 2016; 12:1040-1051.
- Ponzoni, L., Rossetti, G., Maggi, L, Giorgetti, A., Carloni, P. and Micheletti, C., 2017. “Unifying view of mechanical and functional hotspots across class A GPCRs“, *PLOS Computational Biology.*

WEB REFERENCES

WWW.CECAM.ORG

WWW.E-CAM2020.EU

Modeling and Simulation in Sustainable Food Systems Engineering

POSITION PAPER: NEEDS ANALYSIS AND TRENDS IN SUSTAINABLE FOOD SYSTEMS WITHIN HIGHER EDUCATION

Monika Polanska¹, Paula Bourke², Enda Cummins³, Wolfram Schnäckerl⁴, Vasilis Valdramidis⁵, Jan Van Impe¹

¹ BioTeC+ & OPTEC & BiFTec, Faculty of Engineering Technology, KU Leuven
Gebroeders De Smetstraat 1, B-9000 Gent, Belgium - Monika.Polanska@kuleuven.be

² Dublin Institute of Technology, School of Food Science and Environmental Health, Ireland

³ University College Dublin, School of Biosystems & Food Engineering, Ireland

⁴ Anhalt University of Applied Sciences, Faculty of Agriculture, Nutrition & Landscape Development, Bernburg, Germany

⁵ University of Malta, Faculty of Health Sciences, Msida, Malta

KEYWORDS

sustainable food systems, simulation in food systems, Erasmus Mundus, joint master

ABSTRACT

Food production has to take into account a number of global challenges, such as growing demand for food worldwide, climate change, food loss, changing diets, and water scarcity, as well as competing claims, including the need for animal feed, fibre for clothing and biofuels for energy. Global warming is likely to lead to greater incidence of agricultural yield shocks in certain regions, land fragility, and seed fragility, and will add to the complexity of the challenges at hand.

A Master's course with a specific integrated and international outlook would fill an increasing need and result in the transfer of knowledge, experience and standards to developing countries, as well as promote an excellence of European education. Hence, the project group developed a unique proposal within the Erasmus Mundus framework, European Master of Science in Sustainable Food Systems Engineering (FOOD4S - 'food force').

Quality assurance and monitoring of the programme is of utmost importance for the management board. The survey on 'satisfaction analysis on teaching performance' is currently being performed for the preceding Erasmus Mundus programme, on which the FOOD4S proposal has been built. The results will be used to improve the ongoing and perspective programme in terms of particular aspects.

INTRODUCTION

The general aim of Erasmus Mundus, as a co-operation and mobility programme in the field of higher education, is to promote the European Union as a centre of excellence in learning around the world. By supporting European top-quality Masters Courses it enhances the visibility and attractiveness of European higher education in third countries. Selected courses intend to offer high quality education, promote the European dimension in higher education through joint curricular development, inter-institutional co-operation in teaching and supervising

students, inter-institutional transfer of knowledge, joint recognition of qualifications, support mobility streams within Europe and between the EU and third countries, and finally contribute to the worldwide attractiveness and competitiveness of the European Higher Education Area (EHEA). Promotion of European co-operation within the Erasmus Mundus programme aims to develop long-lasting collaborative models among European universities for the delivery of international joint study (training / research) programmes with an integrated mobility component, and is in line with the objectives of the Bologna Declaration.

The newly proposed programme contributes also to strengthening European Innovation Capacity by providing knowledge in an area where many gaps exist. The tangible embedding of food safety and energy sustainability; environmental impacts of food production (Life Cycle Assessment); effects of climate change on food safety, sustainable food production and quality; predictive modelling and quantitative (microbial, chemical) risk assessment, providing predictive tools for the food industry, policy makers and managers to formulate and implement risk management policies and controls with the view to protecting human health, will also have a major impact on uplifting Europe's innovation capacity. Current quality assurance and control tools are insufficient in dealing with the emerging threat of climate change, demonstrating the need for a concerted multidisciplinary effort to address this issue. In response to this challenge, predictive modelling tools can be applied to evaluate the effects of climate change on food safety with regard to managing this new treat for all stakeholders, including industry, government and regulatory agencies.

Not a single course currently exists, where the essential elements of risk assessment, predictive modelling and computational optimisation are brought together with both sustainability principles of food production and food processing as well as energy and food chain concepts, within one coherent structure at a level for master's students.

NEEDS ANALYSIS

Transformations are taking place in agribusiness like never seen before. As global population and income rises, agriculture has become a key focus in a world that needs

more food and energy. The industry is facing challenges driven by the globalization of food production and distribution, growing food price volatility, the rising importance of environmental sustainability, rapid technological innovation and new demands for biofuels (Munang et al. 2011). There are many different views as to what constitutes a 'sustainable' food system, and what falls within the scope of the term 'sustainability'. Strictly speaking sustainability implies the use of resources at rates that do not exceed the capacity of the Earth to replace them. For food, a sustainable system might be seen as encompassing a range of issues such as security of the supply of food, health, safety, affordability, quality, a strong food industry in terms of jobs and growth and, at the same time, environmental sustainability, in terms of issues such as climate change, biodiversity, water and soil quality (Thompson et al. 2010; Frison et al. 2011). The value of world agriculture and agri-food trade has also increased in response to recent trade liberalization and economic growth. Producers are operating in a changing landscape of increased international competition, evolving consumer needs, supply and production challenges and complex legal requirements.

On the one hand, awareness of consumer and product safety has probably never been so high. Food safety and energy sustainability has become a priority research area worldwide as the global food supply evolves. The consumers are now warier about the origin, traceability and safety of the food they eat. At the same time, making improvements to the food chain to reduce energy consumption and to 'prolong shelf life is essential for food security and sustainability but represents a significant challenge for the industry. Food safety and quality worldwide faces increased pressures and challenges arising from the globalisation of food trade, intensive production systems and changing consumer preferences (King et al. 2017).

On the other hand, it is estimated that the food chain is causing significant environmental impacts due to CO₂ emissions and enormous food waste (Adekomaya et al. 2016; Wittman et al. 2016; Acevedo et al. 2018). Most of this can be avoided, and the vast majority of the remainder used as a resource into the food chain. Life Cycle Assessment (LCA) and related tools (such as carbon or water footprints) have proved to be an essential element on the evaluation of the environmental performance of food value chains (Biswas et al. 2010; Abecassis 2018).

In response to this challenge, predictive modelling tools can be applied to evaluate the effects of climate change on food safety with regard to managing this new treat for all stakeholders, including industry, government and regulatory agencies. Predictive modelling and quantitative (microbial/chemical) risk assessment play a crucial role in food quality and safety, providing tools which are used by the food industry, policy makers and managers to formulate and implement risk management policies and controls with the view to protecting human health and environment (Tamplin 2017; Acevedo et al. 2018). As highlighted in the EU SCAR report (2015), ICTs dominate innovation in our times and it can not only be supportive in innovation processes but also change research. Also in the farm sector and the food chain, the use of ICT has increased significantly over the last decade. However, this is just the

start of what could become a revolution in agriculture. It has the potential to change the way farms are operated and managed and it will change the farm structure as well as the food chain in unexplored ways. ICT could support labour efficiency, resource efficiency and close the gap between the producer and the consumer. It is therefore not only relevant for conventional farming but also for organic farming and short supply chains. This means that an agenda for research and innovation topics should be based on a careful mapping of agricultural issues (challenges and opportunities) with the potential contribution of ICTs (favoured over other solutions) and to see where development of those ICTs then makes sense.

NEW PROGRAMME AND ITS STRUCTURE

The long lasting cooperation and the existing fully complementary expertise of six European partners (**KU Leuven, Dublin Institute of Technology, University College Dublin, Anhalt University of Applied Sciences, University of Malta, and French National Institute for Agricultural Research - INRA**) evolved into the development of novel and unique project, **European Master of Science in Sustainable Food Systems Engineering (FOOD4S 'food force')**. This interdisciplinary programme in innovative fields assembles a broad coverage of areas and subjects that could not be provided at any single institution alone. It offers an education which is at the same time broad and in-depth aiming to foster and develop knowledge and awareness of scientific trends in food science, safety and quality, food product and process design, sustainable production, ecological footprint and quantitative methods and risk analysis in food systems in a global context as 4S stands for Science, Sustainability, Safety and Simulation. The needs analysis revealed there is a requirement for such oriented programmes in education and professional field. The proposal is also in line with the strategic objectives of the WHO European action plan for food and nutrition policy in protecting the food chain, prevention and control of foodborne contamination and food safety management, which makes FOOD4S very topical. Participation in the programme is not only beneficial to graduates but to the European Union as a centre of excellence in learning and is strengthening European Innovation Capacity.

FOOD4S is designed as a 2-years master programme of 120 ECTS. The Programme will commence with four compulsory modules (total of 30 ECTS) offered by KU Leuven, Technology Campus Ghent. These courses will provide students with the fundamentals of the programme, which are captured by the 4 S's: Science, Sustainability, Safety and Simulation. Then students are given a choice between two blocks of modules (to be taken as a whole). University College Dublin (UCD) offers a module block on (Computational) Risk & Safety and Dublin Institute of Technology (DIT) offers a module block on Innovative Technology. Each path in Ireland is awarding another 30 ECTS. In the second year of studies, students will select a module block of University of Malta (UMalta) or Anhalt University of Applied Sciences (UANhalt) dealing with, respectively Energy & Food Chains or Sustainable

production. The module blocks organised by UCD and UMalta are primarily computationally oriented while the module blocks of DIT and UAnhalt are mainly technology oriented. Students can freely combine a module block of DIT or UCD on the one hand with one of UMalta or UAnhalt on the other hand, thus aiming towards a computational orientation or technological orientation, or a mixture of these. This allows students to differentiate based on the knowledge and skills they desire to develop (Figure 1).

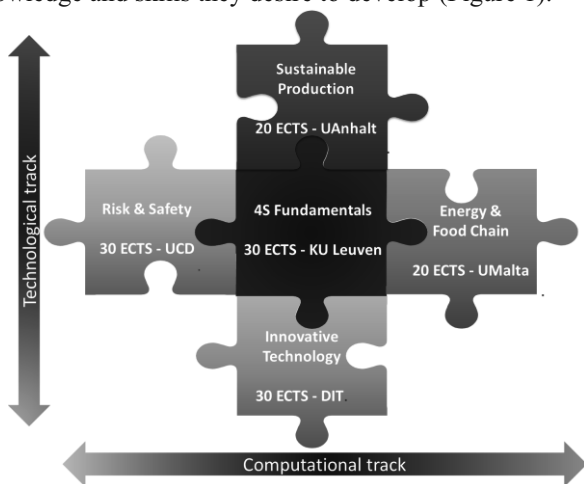


Figure 1. Taught modules tracks

The programme will also require the students to undertake a professional competence module as well as to work on a scientific project (and to submit a thesis) in one of the partner institutions. Proper selection of the professional competence module location and the Master thesis subject further allows strengthening of the computational, technological, or mixed profile. The award of the European Master of Science degree will be based on the successful completion of the modules (80 ECTS), professional competence module (10 ECTS) and the Master thesis (30 ECTS). It is envisaged to deliver a joint degree to all successful graduates.

QUALITY ASSURANCE SYSTEM

The consortium is committed to maintaining its academic standards across all courses and enhancing the quality of its learning and teaching provision. Quality assurance will be based on both internal and external assessment measures. The KU Leuven system of internal quality review will be fully implemented throughout the course, and will be supervised by the quality management service of the coordinating partner KU Leuven

(<https://www.kuleuven.be/english/education/quality/>):

- COBRA - INTERNAL QUALITY ASSURANCE METHOD - stands for Cooperation, Reflection and Action, with attention for Checks & Balances. KU Leuven has various instruments to monitor and stimulate the development of educational quality (e.g. student university-wide surveys, blueprint and programme action plan)
- EXTERNAL QUALITY ASSURANCE – Programme assessment and accreditation - KU Leuven takes care of and accounts for the quality of its educational policy and quality assurance.

In addition to the central quality system of KU Leuven, the FOOD4S course will also apply an additional joint

questionnaire on **Satisfaction analysis for students on lecturers and teaching methods**, which allows for an immediate and individual electronic fast-format assessment of every lecturer in every module. These actions will be conducted both for the course units taught at KU Leuven and the course units taught in the other consortium partner institutions. Essentially, this tool provides the lecturer with an idea of the perception by students on their teaching activities and hence, identifying ways to improve teaching performance. The short questionnaire includes questions on the teaching style and methods, the teaching materials and content and the appropriateness of that lecture/topic in the module. At the end of each module, all students are requested to fill in the online questionnaire for each lecturer who was active in this module. Students fill in the survey anonymously using an online learning platform Toledo.

The proposed project is yet to be approved for funding by the EACEA upon submission with the current call for proposals [EAC/A05/2017](#). The satisfaction analysis has been thereby based on the preceding programme, European Master in Food Science, Technology and Business (BiFTec), on which the current FOOD4S proposal has been built (www.biftec.org).

SATISFACTION ANALYSIS RESULTS

32 lecturers teaching to three cohorts of students (2015 to 2017) in 12 different modules offered among the consortium partners have been assessed by this means. 80% of students responded to each online questionnaire on the specific teaching staff. The results have been gathered and presented in Figures 2-10.

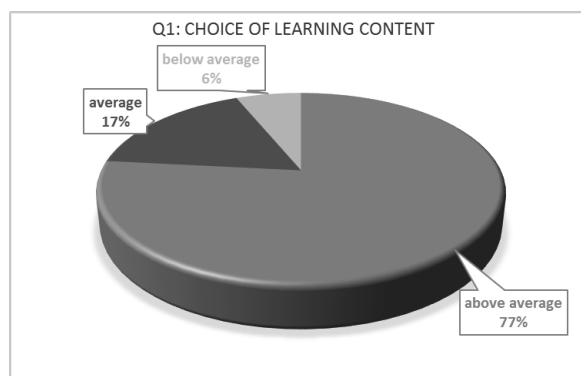


Figure 2. Satisfaction analysis on Choice of Learning Content

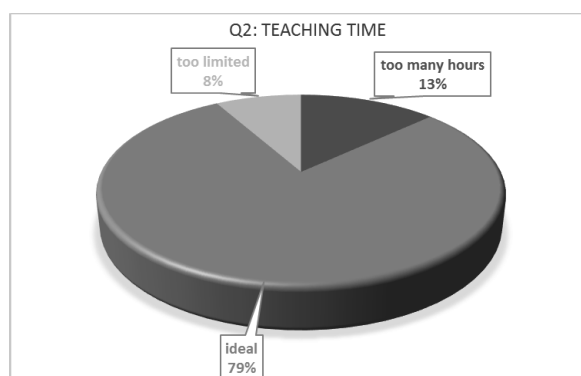


Figure 3. Satisfaction analysis on Teaching Time

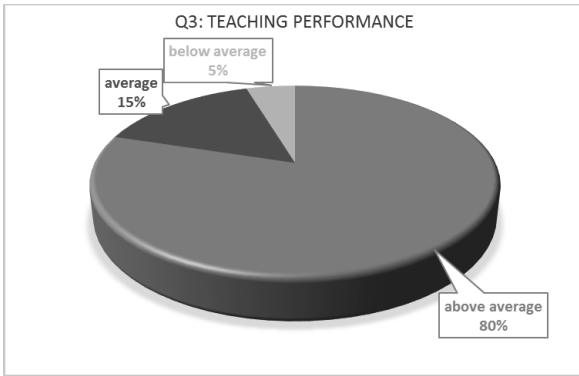


Figure 4. Satisfaction analysis on Teaching Performance

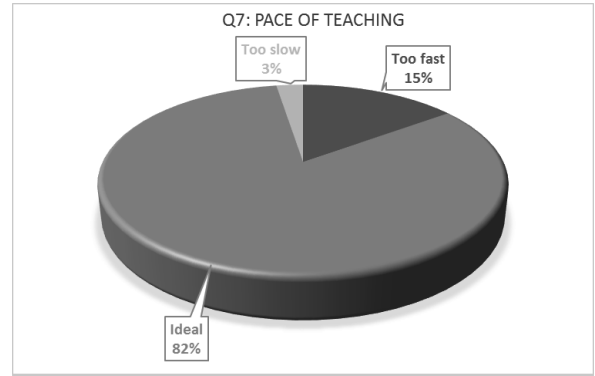


Figure 8. Satisfaction analysis on Pace of Teaching

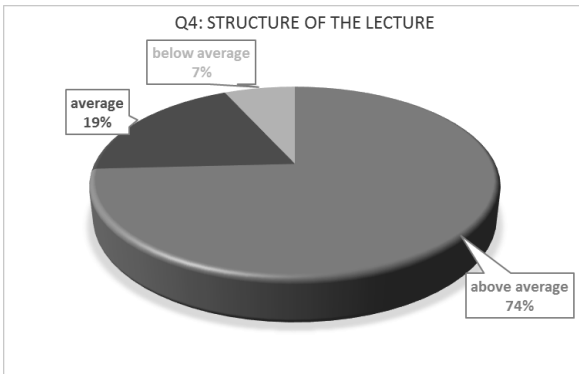


Figure 5. Satisfaction analysis on Structure of the Lecture

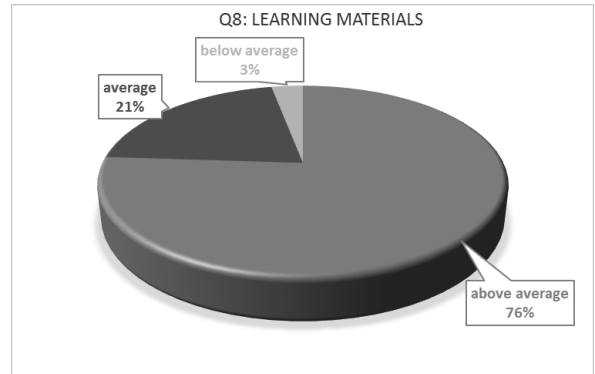


Figure 9. Satisfaction analysis on Availability of Learning Materials

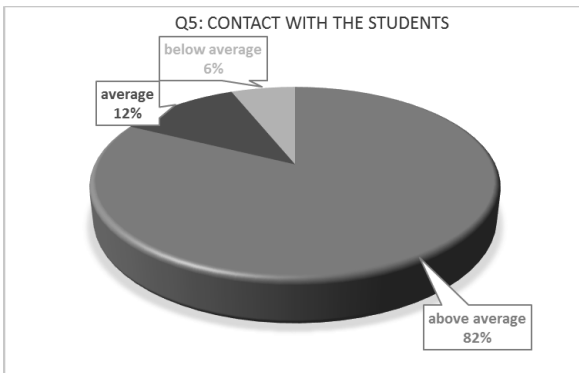


Figure 6. Satisfaction analysis on Contact with the Students

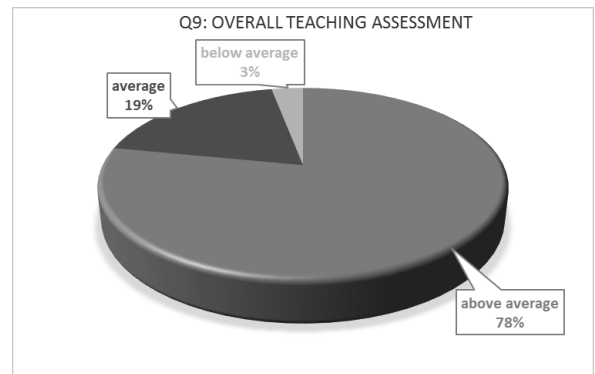


Figure 10. Overall Teaching Assessment

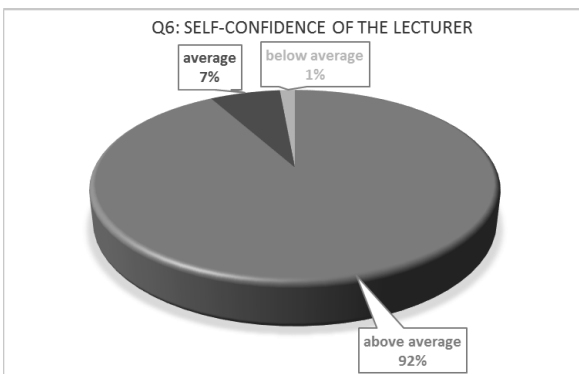


Figure 7. Satisfaction analysis on Self-confidence of the lecturer

Overall analysis of the satisfaction on the teaching performance and its particular aspects show that on average 78% of the students evaluate the course content, lecturers and their teaching methods as ‘above average’, following 19% found it ‘average’ and 3% assessed it as ‘below average’ (Fig. 10). 79% of the respondents found the teaching time and 82% pace of teaching ideal. 13% of the students considered teaching time took too many hours (Fig. 3) and 15% found pace of teaching too fast (Fig. 8). With this respect, slower pace of teaching can be recommended to particular lecturers as corrective actions. All other single aspects were evaluated as ‘above average’ by 80% of the responding students and in particular choice of learning content was positively assessed by 77% of the students, teaching performance by 80%, structure of the lecture by 74%, contact with the student by 82%, self-confidence of the lecturer(s) by 92%, available learning materials by 76% (Fig.

2, Fig. 4, Fig. Fig. 5, Fig. 6, Fig. 7, Fig. 9, respectively) . Remaining 15% of the respondents evaluated all the specific components of the teaching activities as ‘average’ and 5% (3 students out of the 67 responding) as ‘below average’. Structure of particular lecture(s) and availability of learning materials could be further improved to increase the overall satisfaction. Upon careful analysis of the particular outcomes for the individual teaching staff, the results are a base for personal face-to-face discussion with the lecturers as well as overall summary. Corrective actions and suggestions will be made to improve the delivery of each module and its components in the future for the following cohort of students. The results of the questionnaires will then be compared with the present findings to verify the efficiency of taken corrective actions. The questionnaires are part of the internal quality assurance system successfully applied by the programme and it is envisaged to continue with this system for the proposed FOOD4S programme.

CONCLUSIONS

Based on the needs analysis and current trends in food industry, the European Master of Science in Sustainable Food Systems Engineering has been developed by six consortium partners. The FOOD4S course is unique in its modular format and also in the range of topics and experiences which students will undergo in completing the individual modules. International mobility is a characteristic which is inherent to the course. This interdisciplinary programme in innovative fields assembled a broad coverage of areas and subjects and offers an education which is at the same time broad and in-depth aiming to foster and develop knowledge and awareness of scientific trends in food science, safety and quality, food product and process design, sustainable production, quantitative methods and risk analysis in food science in a global context. The course seeks to expand the scope of the theoretical, research, and policy debates over sustainable agriculture and food production. It will offer a better understanding of ecological and food systems dynamics and strategies in terms of regenerating natural systems, providing predictive tools for the food industry. Predictive modelling tools can be applied to evaluate the effects of climate change on food safety with regard to managing this new treat for all stakeholders, including industry, government and regulatory agencies. The objectives of the course are to be achieved by an education which is at the same time broad in its compulsory modules and in-depth in the optional modules (selected track of studies) and area for master thesis research. The professional competences module offers an integrative approach for linking academic competences to professional competences by inserting in the programme a practical placement in a production or research environment in industry or academia. Satisfaction analysis of the teaching staff performed among the three latest cohorts of students of the preceding Erasmus Mundus programme revealed that overall teaching performance is considered as ‘above average’ by 78% responding students, ‘average’ by following 19%, ‘below average’ by 3%. Corrective actions are applied on an annual basis serving for continues improvement of the ongoing

programme, in addition these results will also provide a good basis when setting up teaching staff for the new project.

ACKNOWLEDGEMENTS

The BiFTec programme is co-funded by the Erasmus+ Programme of the European Union.

REFERENCES

- Abecassis, J.; Cuq, B.; J-L. Escudier; G. Garric; A. Kondjoyan; V. Planchot; J-M. Salmon; H. de Vries. 2017. “Food chains; the cradle for scientific ideas and the target for technological innovations.” *Innovative Food Science & Emerging Technologies*, In Press.
- Acevedo, M.F.; D.R. Harvey; F.G. Palis. 2018. “Food security and the environment: Interdisciplinary research to increase productivity while exercising environmental conservation.” *Global Food Security*, In Press.
- Adekomaya, O.; T. Jamiru; R. Sadiku; Z. Huan. 2016. „Sustaining the shelf life of fresh food in cold chain – A burden on the environment.” *Alexandria Engineering Journal*, Vol. 55 (2), 1359-1365.
- Biswas, W.K.; J. Graham; K. Kelly; M.B. John. 2010. “Global warming contributions from wheat, sheep meat and wool production in Victoria, Australia – a life cycle assessment.” *Journal of Cleaner Production*, vol. 18(14), 1386-1392.
- EU SCAR (2015), Agricultural Knowledge and Innovation Systems Towards the Future – a Foresight Paper, Brussels.
- Frison, E.A.; J. Cherfas; T. Hodgkin. 2011. “Agricultural Biodiversity Is Essential for a Sustainable Improvement in Food and Nutrition Security.” *Sustainability*, No.3, 238-253.
- King, T.; M. Cole; J.M. Farber; G. Eisenbrand; D. Zabarar; E.M. Fox; J.P. Hill. 2017. “Food safety for food security: Relationship between global megatrends and developments in food safety.” *Trends in Food Science & Technology*, Vol. 68, 160-175.
- Munang, R.T.; I. Thiaw; M. Rivington. 2011. “Ecosystem Management: Tomorrow’s Approach to Enhancing Food Security under a Changing Climate.” *Sustainability*, No.3, 937-954.
- Tamplin, M.L. 2017. “Integrating predictive models and sensors to manage food stability in supply chains.” *Food Microbiology*, In press.
- Thompson, H.E.; L. Berrang-Ford; J.D. Ford. 2010. “Climate Change and Food Security in Sub-Saharan Africa: A Systematic Literature Review.” *Sustainability*, No.2, 2719-2733.
- Wittman, H.; M.J. Chappell; D.J. Abson; R.B. Kerr; J. Blesh; J. Hanspach; I. Perfecto; J. Fischer. 2016. “A social–ecological perspective on harmonizing food security and biodiversity conservation.” *Regional Environmental Change*, 1–11.

WEB REFERENCES

- www.biftec.org
https://eccea.ec.europa.eu/erasmus-plus/funding/key-action-1-erasmus-mundus-joint-master-degrees-2018_en
<https://www.kuleuven.be/english/education/quality>

MODELLING MULTICRITERIA ARGUMENT NETWORKS ABOUT REDUCED MEAT CONSUMPTION

Nicolas Salliou^(✉)
Independent research scientist
Donneville, France
✉ nicolas.salliou@gmail.com

Rallou Thomopoulos
IATE, Univ Montpellier, INRA, CIRAD,
Montpellier SupAgro, INRIA GraphIK
2, place Pierre Viala
34 060, Montpellier, France

KEYWORDS

Food diet modelling, Argumentation systems, Animal food product, Consumer, Food choice criteria.

ABSTRACT

A second nutrition transition seems to emerge towards more plant-based diets, curbing meat consumption in developed countries in the beginning of the XXI century. This shift suggests that logical arguments tend to influence more and more individuals towards vegetarian diets. This paper proposes a methodology to model a network of arguments around vegetarian diets by an abstract argumentation approach. Each argument, formalized by a node is connected with other arguments by arrows formalizing relationships between arguments. Thanks to this methodology we were able to formalize an argument network about vegetarian diets and identify the foremost importance of health argument compared with ethical or other type of arguments. This methodology also identified key arguments due to their high centrality in being challenged or challenging other arguments. These first results from this argument network construction suggest that any controversy surrounding vegetarian diets may polarize around such high centrality arguments about health. Even though ethical arguments appear of low importance in our network, the key issue of the necessity of animal products for human health may be essential for ethical choices towards vegetarian diets.

INTRODUCTION

The first nutrition transition involved the rise of sugar, fat, meat and processed products in human diets (Popkin 1993) and is the dominant nutritional model today. Vranken (2014) identified a second nutrition transition happening in the most developed countries where meat consumption is

currently curbing down. Transition towards reducing meat consumption covers a wide variety of practices ranging from occasional vegetarianism to veganism (also called “strict vegetarian”) (Bearsworth & Kiel 1991). Rationale for such transition mainly implies ethical and health concerns (Jabs et al. 1998) but environmental impact of meat consumption is also stressed on a lower degree (Ruby 2012). MacDonald (2000) conducted individual interviews with vegans and found that their nutritional transition depended on a catalytic experience orienting individual towards information acquisition and ultimately conducting to a decision for change. However, the information acquisition leading to decision is not precisely known among vegetarians. In this paper we present a methodology to explore main arguments and their relations between them that transitioning individuals may face during this process.

METHOD

General approach

In order to model arguments involved with vegetarian transitions we used an abstract argumentation approach (Dung 1994, Rahwan & Simari 2009, Thomopoulos & Paturel 2017). We extracted arguments in favor or not of reducing animal product consumption. Our sources of arguments are newspapers, grey literature and top ten google research (“vegetarian diet”; “vegan diet”; “vegetalism argument”). The latter inquiry added to the pool popular scientific papers, webmedia articles and blog posts. We read thoroughly each source and extracted all arguments as expressed by their author. For each argument we attributed a criterion (“Nutritional”; “Economic”; “Environmental”; “Anthropological”; “Ethical”; “Health” or “Social”) and noted the source expressing this argument (“Journalist”; “Scientist”; “Philosopher”; “Blogger”, etc.). We consequently obtained 114 arguments.

The argumentation formalism

Let us recall that an argumentation system is usually represented as an oriented graph where nodes are arguments and edges are attack relations between arguments (Figure 1).

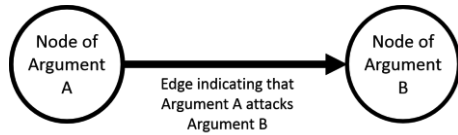


Figure 1: General graphical representation of an argumentation system

Considering Dung's seminal work on argumentation (1995), an argument and the attack relation are abstract and can be instantiated and defined in different ways in different contexts (Walton, 2009). Dung himself stated: "an argument is an abstract entity whose role is solely determined by its relations to other arguments. No special attention is paid to the internal structure of the arguments". For example, an argument can be a set of statements composed of a conclusion and at least one premise, linked by an inference or a logical relation. Attacking an argument can be achieved in different ways: 1) by raising doubts about its acceptability through critical questions; 2) by questioning its premises; or 3) by putting forward that the premises are not relevant to the conclusion or 4) by presenting an argument with an opposing conclusion. In all these cases an attack relation is said to exist (e.g Figure 2).

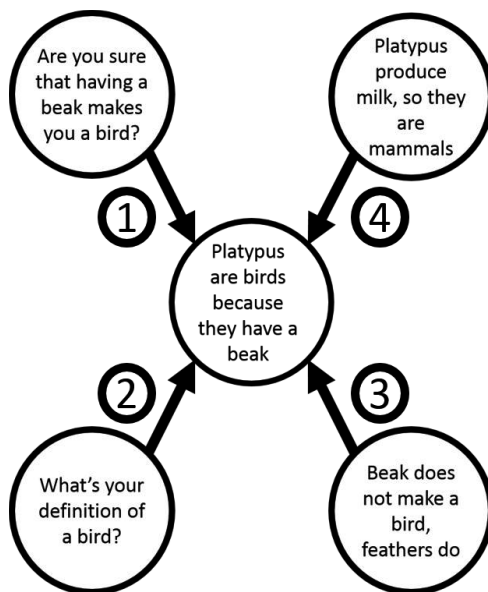


Figure 2: Examples of four types of attacks. 1: Raising doubts; 2: Questioning premises; 3: Irrelevant premises; 4: Opposing conclusions

Even though Dung's framework is theoretically sound it is not straightforward to apply in real life situations. Indeed, one of the initial difficulty is to how to define an argument in order to properly reflect stakeholders' statements in a debate. Unfortunately, there is still no general model that can be used to formalize a natural argument (i.e. an argument stated by a stakeholder during a discussion in natural language) and input in an abstract argumentation framework in a real decision-making context. Quoting Baroni and Giacomin (2009): « *While the word 'argument' may recall several intuitive meanings, like the ones of 'line of reasoning leading from some premise to a conclusion' or of 'utterance in a dispute', abstract argument systems are not (even implicitly or indirectly) bound to any of them: an abstract argument is not assumed to have any specific structure but, roughly speaking, an argument is anything that may attack or be attacked by another argument* ». Indeed, the structure of an abstract argument does not correspond to the intuitive understanding of what an argument is. Moreover, the notion of "attack between arguments" does not have a natural and direct correspondence to practical expressions used by stakeholders when debating. Moreover, representing arguments as an oriented graph can be a difficult task for stakeholders: when the number of arguments and/or attacks is large, the graph becomes illegible and difficult to interpret by stakeholders.

In our project, we needed to find a practical way of defining arguments that are used in the process of decision making. In such a context arguments can be intuitively thought of as being statements to support, contradict, or explain opinions or decisions (Amgoud & Prade, 2009). More precisely, in decisional argumentation frameworks (Ouerdane et al., 2010), the argument definition is enriched with additional features, namely the decision (also referred to as 'action', 'option' or 'alternative') and the goal (also referred to as 'target'). In other studies arguments are also associated with specific actors. An application of a decision-oriented argumentation framework to a real-life problem concerning food policy can be found in Bourguet et al. (2013), where a recommendation regarding the provision of whole-grain bread was analyzed a posteriori. In this case, each argument is associated with the action it supports. Based on the above rationale, we chose to specify an argument as a tuple composed of an identifier, a type, an explanation, a criterion, an option and a sub-option.

Formally:

An argument is a tuple $a = (I;T;S;R;C;A;Is;Ts)$ where:

- I is the identifier of the argument;
- T is the type of the argument (with values *in favour of*, denoted by '+', or *against*, denoted by '-', the vegetarian option);
- S is the statement of the argument, i.e. its conclusion;
- R is the rationale underlying the argument, i.e. its hypothesis;
- C is the criterion which the argument relies on;

- A is the actor who proposes the argument;

-Is is the information source containing the argument;

- Ts is the type of source the argument comes from.

For any argument a , we denote by $I(a)$, $T(a)$, $S(a)$, $R(a)$, $C(a)$, $A(a)$, $Is(a)$, $Ts(a)$ respectively the identifier, the type, the statement, the rationale, the criterion, the actor, the information source and the information type of argument a .

As an illustration, Table 1 displays a sample of the set of arguments considered in our case study.

Table 1: Sample of Arguments Tuples about Reduced Meat Consumption (I: Identification; T: Type; Is : Information source; Ts: Type of source)

I	T	Statement	Rationale	Criterion	Actor	Is	Ts
1	-	Vegan diet is deficient in B12 vitamin	Vegetal proteins do not contain B12 vitamin	Nutritional	Journalist	Canard Enchaîné - 144 - Juillet 2017	Newspaper
15	-	Plant proteins trigger allergies	Plant-based food are more regularly allergic	Nutritional	Innovation cluster	Valorial	Powerpoint
23	+	Vegetarian diet is good for health	Diabetes, cancer and coronary risks are reduced	Health	Scientists	Tilman & Clark 2014	Scientific paper
28	+	Properly planned vegan or vegetarian diets fits all stages of the life cycle	Nutrient needs are satisfied and growth is normal	Health	American Dietetic Association	Craig et al. 2009	Scientific paper
43	+	Vegan diet improves the rheumatoid arthritis activity	A diet-induced faecal flora change was observed	Health	Scientists	Peltonen et al. 1997	Scientific paper
55	+	Eating meat is not in human's nature	It was sometimes necessary in the past to eat meat, not nowadays	Anthropological	Blogger pro-vegan	Blog - Eleusis et Megara	Blog post
56	+	Stop eating animals does not mean animal extinction	Deforestation for the cultivation of animal feed provokes species extinctions;	Environmental	Blogger pro-vegan	Blog - Eleusis et Megara	Blog post
59	+	Animals suffer when eaten, not plants	A nervous system is needed to suffer, which plants do not have.	Ethical	Blogger pro-vegan	Blog - Eleusis et Megara	Blog post
71	-	No study is favorable to the vegan diet	One good quality study show that Atkins diet is better that Ornish diet	Health	Journalist	Signs Of The Times	Internet article
77	-	No health reason justifies to avoid animal products	Human body is adapted to eat animal products for millions of years	Health	Journalist	Signs Of The Times	Internet article

Now, let us consider the attack relation. In structured argumentation (i.e. logic based argumentation frameworks where arguments are obtained as instantiations over an inconsistent knowledge base) three kinds of attacks have been defined: undercut, rebut and undermine (Besnard & Hunter, 2008). The intuition of these attack

relations is either to counter the premise of the opposing argument ('undercut'), the conclusion ('rebut') or to attack the logical steps that allowed the inference between the argument's premise and conclusion (undermine). In abstract argumentation the set of attacks is simply considered as provided *a priori*. Another possibility that can be considered is

MAIN LESSONS AND PERSPECTIVES

Our argument network structure reveals in particular two main elements. First, one can notice that arguments about Health are by far the majority of arguments identified. They represent 47% of all 114 arguments identified and 63% of arguments involved in at least one attack. As a matter of comparison ethical arguments represent only 3% of all arguments identified. Second, some key arguments are emerging due to their centrality. Two arguments are involved in more than 3 attacks. The first argument, grouped under identification numbers 28, 57, 108 and 111 (the black node in Figure 3), refers to a scientific paper from the American Dietetic Association stating that “Properly planned vegetarian or vegan diets fits all stage of life” (Craig & Mangels 2009). The second argument, identification number 71 and 72 grouped together, is a journalist statement that “No study is favorable to the vegan diet”. Both arguments would probably be key arguments in potential controversy about vegetarian diets due to their generality.

The major importance of health issues surrounding vegetarian diets are in line with findings in Ruby’s (2012) review of vegetarian studies. On the opposite, the importance of ethical arguments which was stressed by Ruby (2012) did not appear in such modelling. This could be explained by the more complex nature of ethical arguments as well as our choice of research keywords in Google which focused on diets. However, from an ethical perspective it seems that the health issue (whether or not vegetarian diets are healthy) is actually central as animal rights may be defended from the baseline of animal products not being necessary for human health (Francione & Charlton 2013).

In this research we built the network and proposed a structural analysis. Abstract argumentation opens further analysis and in particular the rejection of attacked arguments without any argument to defend them. Such analysis allow for new indicators such a polemical indicators based on rejected argument ratios (Thomopoulos & Paturel 2017) which can better identify potential controversies. Following the theoretical approach of Xie et al. (2011) such argument network could also be used together with agent-based modelling to explore emergent establishment of new social norms on the concrete case of vegetarianisms. Such model could help to understand the conditions under which such arguments could spread in a population and favor vegetarian diets normalization.

CONCLUSION

The method presented in this paper formalizes arguments and attacks around vegetarian diets using an abstract argumentation approach. The argument network revealed the foremost importance of health issues surrounding vegetarian diets. The centrality of some argument of the network allows for identification of potential key arguments and/or controversies. The importance of health arguments in relation with ethical argument should be further researched.

REFERENCES

- Amgoud L., Prade H. (2009). Using arguments for making and explaining decisions. *ArtificialIntelligence*, 173(3-4):413–436.
- Baroni P., Giacomin M. (2009). Semantics of Abstract Argument Systems In *Simari G., Rahwan I. (eds) Argumentation in Artificial Intelligence*. Springer, Boston, MA : 25-44.
- Beardsworth, A. D., & Kiel, E. T. (1991). Vegetarianism, veganism, and meat avoidance: recent trends and findings. *British Food Journal*, 4(93), 19-24.
- Besnard P., Hunter A. (2008). *Elements of argumentation*, volume 47. MIT Press, Cambridge.
- Bourguet J-R., Thomopoulos R., Mugnier M-L., Abécassis J. (2013) An artificial intelligence-based approach to deal with argumentation applied to food quality and public health policy, *Expert Systems with Applications*, 40, 4539-4546.
- Craig, W., & Mangels, A. (2009). Position of the American Dietetic Association: Vegetarian Diets. *Journal of the American Dietetic Association*, 109(7), 1266-1282. <https://doi.org/10.1016/j.jada.2009.05.027>
- Dung, P. M. (1995). On the acceptability of arguments and its fundamental role in nonmonotonic reasoning, logic programming and n-person games, (77), 321-357.
- Francione, G., & Charlton, A. (2013). *Eat Like You Care: An Examination of the Morality of Eating Animals* (Exempla Press).
- Jabs, J., Devine, C. M., & Sobal, J. (1998). Model of the process of adopting vegetarian diets: Health vegetarians and ethical vegetarians. *Journal of Nutrition Education*, 30(4), 196–202.
- McDonald, B. (2000). « Once You Know Something, You Can’t Not Know It » An Empirical Look at Becoming Vegan. *Society & Animals*, 8(1), 1–23.
- Ouerdane W., Maudet N., Tsoukias A. (2010). Argumentation Theory and Decision Aiding. In J. Figueira, S. Greco, and M. Ehrgott, editors.

International Series in Operations Research and Management Science 1(142), Trends in Multiple Criteria Decision Analysis, Springer, 177-208.

Popkin, B. M. (1993). Nutritional Patterns and Transitions. *Population and Development Review*, 19(1), 138. <https://doi.org/10.2307/2938388>

Rahwan, I., & Simari, G. (Éd.). (2009). *Argumentation in Artificial Intelligence*. Boston, MA: Springer US. <https://doi.org/10.1007/978-0-387-98197-0>

Ruby, M. B. (2012). Vegetarianism. A blossoming field of study. *Appetite*, 58(1), 141-150. <https://doi.org/10.1016/j.appet.2011.09.019>

Thomopoulos, R., & Paturel, D. (2017). Multidimensional Analysis Through Argumentation? In S. Benferhat, K. Tabia, & M. Ali (Éd.), *Advances in Artificial Intelligence: From Theory to Practice* (Vol. 10351, p. 268-274). Cham: Springer International Publishing. https://doi.org/10.1007/978-3-319-60045-1_29

Vranken, L., Avermaete, T., Petalios, D., & Mathijs, E. (2014). Curbing global meat consumption: Emerging evidence of a second nutrition transition. *Environmental Science & Policy*, 39, 95-106. <https://doi.org/10.1016/j.envsci.2014.02.009>

Walton D., Macagno F. (2015). A classification system for argumentation schemes. *Argument & Computation*, 6(3):219–245.

Xie, J., Sreenivasan, S., Korniss, G., Zhang, W., Lim, C., & Szymanski, B. K. (2011). Social consensus through the influence of committed minorities. *Physical Review E*, 84(1). <https://doi.org/10.1103/PhysRevE.84.011130>

BIOGRAPHIES

SALLIOU NICOLAS was born in Rennes, France, and has been trained in agricultural development at AgroParisTech and specialized into social change and participatory modelling. He obtained his PhD in 2017 at the Institut National Polytechnique of Toulouse where he conducted a participatory modelling process about farmer's agroecological transitions.

THOMOPOULOS RALLOU has been INRA Research Scientist since 2004, permanent member and co-creator of the GraphIK lab at INRIA. She defended her HDR (habilitation to conduct research groups and PhDs) in 2013 at the University of Montpellier. She has dual skills in computer science and the agri-food sector. Her research topics are in knowledge representation and decision support, focused on argumentation systems, about agri-food systems. She was a Guest Research Scientist at Laval University (Canada) in 2015-2016 and previously 5 year Assistant Professor at AgroParisTech.

CONSUMER DEMAND FOR SUSTAINABLE VERSUS LOW-COST FOOD PRODUCTS: AN AGENT-BASED MODELLING APPROACH

Rallou Thomopoulos¹✉ & Serafim Bakalis²

¹ IATE, Univ Montpellier, INRA, CIRAD, Montpellier SupAgro, INRIA GraphIK
2 place Pierre Viala
34 060 Montpellier, France
✉ rallou.thomopoulos@inra.fr

² University of Nottingham,
School of Chemical and Environmental Engineering
Nottingham NG7 2RD, United Kingdom
serafim.bakalis@nottingham.ac.uk

KEYWORDS

Sustainable food systems, Agent-based modelling, Simulation, Consumer choice, Product price.

ABSTRACT

This paper introduces a first agent-based modelling attempt to food system simulation. It aims to capture the balance of supply and demand for sustainable versus low-cost food products. It contributes in modelling consumer choice and more specifically understanding the tensions between price and sustainability.

INTRODUCTION

With global population reaching 9bn by 2050 and significant environmental challenges, there is an increasing need to increase sustainability of the food chain. Although consumers demand more sustainable products, price is often driving consumer choice (Hoek *et al.*, 2016; Asioli *et al.*, 2017). Sustainable products are typically at a higher cost leaving them to a competitive disadvantage. There has been a lot of effort in understanding and modelling consumer choice and more specifically understanding the tensions between price and sustainability. A range of theoretical frameworks have been proposed (Ho *et al.*, 2006; Asioli *et al.*, 2017). Higher prices of sustainable products do not only involve higher costs of raw materials but also costs of production as they tend to be specialized small scale production units. It would be of interest to explore a scenario where by adoption of sustainable products from consumers costs are reduced.

Agent-based models (ABMs) offer a way of taking into account actor heterogeneity, social interaction

and interdependence, adaptation, and decision-making at different levels. In land use-related environmental science, they have affirmed as a way to capture complex characteristics of socio-ecological systems (Epstein and Axtell 1996, Berger 2001, Parker *et al.* 2003, Mathiews *et al.* 2007, Rammel *et al.* 2007, An 2012, Filatova *et al.* 2013). In this family of ABM works, ecology and geography predominate (Grimm 1999, Parker *et al.* 2003, Verburg and Veldkamp 2005, Castella *et al.* 2005, Railsback *et al.* 2006). However social sciences are also present in such ABM approaches to assess and explain the complexity of human decision-making processes and behaviors (Schelling 1971, Epstein and Axtell 1996, Simon 1997, Janssen *et al.* 2000, Janssen and Ostrom 2006, Robinson *et al.* 2007).

In food science, historically based on process-oriented studies, ABMs are absent from the range of models used to approach food quality and, as a more recent concern, food sustainability. Recent studies related to multi-agent systems applied to the agri-food sector are those based on the argumentation theory (Bourguet *et al.* 2013, Thomopoulos *et al.* 2015, Thomopoulos and Paturel 2017), some of them coupled with system dynamics simulation (Thomopoulos *et al.* 2017). Social issues are deeply involved in food system sustainability. Consumer demand, environmental awareness, willingness to pay, acceptability of products, spreading of new food habits, are key compounds to analyze the system. Therefore, there is a pressing need and a real challenge to take into account food-related social behaviors and integrate them in decision making.

In this paper, a first ABM attempt to food system simulation is proposed. It aims to model the balance of supply and demand for sustainable versus low-cost food products. More specifically we aim to

understand the dynamics of adoption of a certain product (namely sustainable vs low-price) including the scenario of changing price with an increase of consumption.

METHODS

Agent-based modelling

Agent-based models are computational models used to simulate the actions and interactions of autonomous agents, individual or collective, in order to assess their effects on the system as a whole. They attempt to reproduce and predict the emergence of complex phenomena induced from the micro-scale of systems to a macro-scale. Their principle is that simple local behavioral rules generate complex global behavior. An overview of their early history can be found in Samuelson (2000) and more recent developments in Samuelson and Macal (2006).

The CORMAS platform

The CORMAS platform (<http://cormas.cirad.fr/>) used for the model construction was specially developed by CIRAD for simulating natural resource management and is oriented towards the representation of interactions between stakeholders about resource use. In CORMAS, entities are categorized into three types: spatial entities describing the space at different aggregation levels, passive entities, which are objects that can be manipulated by social agents, and social entities which can make decisions, move, and interact with other agents.

Our hypotheses

- A cognitive theory of food perceptions and needs, explained in the following scenario description.
- 3 triggers for sustainable/low-price product demand: (i) environmental crises; (ii) neighborhood effect; (iii) low-price attractiveness.

Scenario description

The system we intend to model is a country made of a population of N citizens. Two products are sold in this country: low-cost products, which have a constant and low price, and sustainable products, whose price is initially higher but may vary in time. Each citizen is characterized by: (i) a constant level of need for sustainability regarding food

(environment preservation, ethics, health, etc.); (ii) a variable level of perception of sustainable products. Depending on these two levels, citizens have a behavior regarding their food product demand, either sustainable if their perception exceeds their needs, or low-cost if their needs exceed their perception. Moreover, each citizen has some resistance to change.

Environmental crises break out with a given frequency. Then all citizens get the information, all the more since they are close to the crisis event. Their perception of sustainable products may be impacted. Each citizen also communicates with his/her direct neighbors and may change his/her diet depending on theirs. Finally, citizens are influenced by low-price attractiveness.

The objective of the simulation model is to provide a view of the evolution of both food behaviors and product prices in time. Initial parameters subject to stochasticity are the distribution of need and perception levels in the population, with respect to some initial proportions of sustainable and low-cost buyers.

RESULTS

Conceptual model

Figure 1 displays the UML class diagram associated with the simulation model.

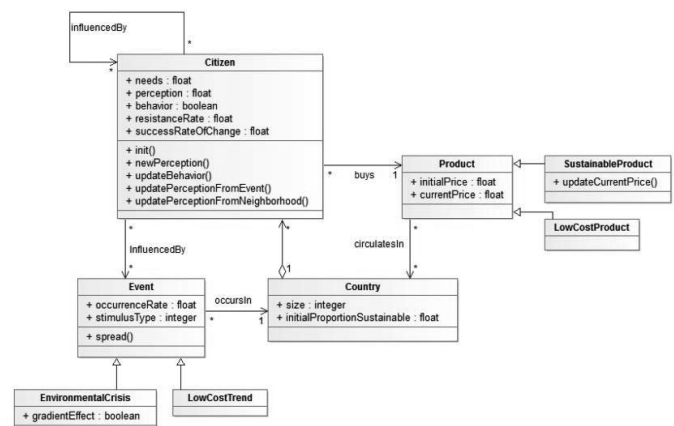


Figure 1: Class diagram

Modelling choices for price-related variables

In this scenario and for simplicity we selected a linear decrease of price with the volume of sales/consumers.

- Price function for the sustainable product: linear function of the number of buyers, from the initial price of the sustainable product when

the number of buyers is reduced (e.g. 5% as an initialization), to the low-cost product price if the whole population buys the sustainable product.

- Feedback influence of price on consumer perception: linear function from ‘no effect’ when the price of sustainable products is high (initial situation) to ‘total effect’ when the price of sustainable products decreases to the level of low-cost products.

When a consumer’s perception surpasses this consumer’s needs for sustainable products, this consumer becomes a sustainable buyer, which participates in reducing the price of sustainable products.

Simulation results

Figure 2 displays a running simulation. Each step has been calibrated to correspond to about one month, so that the whole simulation corresponds to 15 to 20 years approximately. The associated evolutions of the volumes of sales and of product prices are given in the graphs of Figure 3.

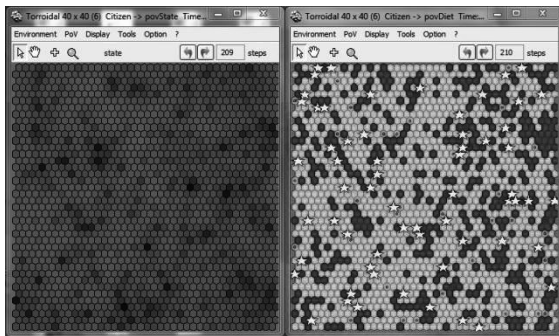


Figure 2: A running simulation. The left part shows consumer perceptions of sustainable products (the darker, the higher). The right side displays resulting consumer behaviors, green for sustainable buyers, purple for low-cost buyers. The yellow stars materialize the occurrence of an environmental crisis which tends to increase people’s perceptions of sustainable products, all the more since the crisis localization is close.

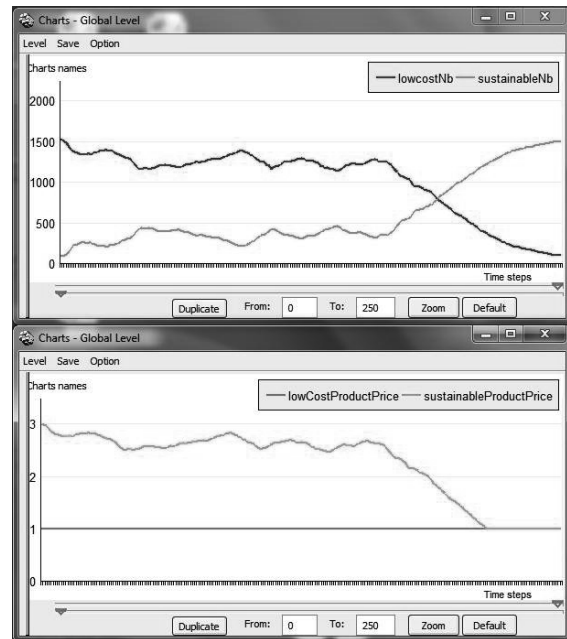


Figure 3: In the top part, evolution of the number of low-cost buyers (in red) and of sustainable buyers (in pink). In the bottom, evolution of the prices of the sustainable product (in green) and of the low-cost product (in blue).

DISCUSSION

We can see in this simulation, after some initial period of oscillations, a decrease of the price of the sustainable product until it reaches the low product price, jointly with a decrease of low-price buyers and an increase of sustainable buyers.

We showed that this result is depending on the ratio between environmental crisis frequency and low-price attractiveness. The latter is represented in our model as the ratio between the initial sustainable price and the initial low-product price (which remains constant). This is illustrated in Figure 4.

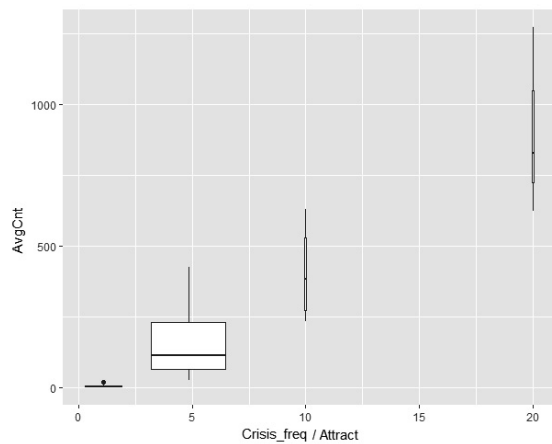


Figure 4: Sensitivity analysis shows that a stability in the simulation results obtained is reached for a given ratio between environmental crisis frequency and low-price attractiveness. This ratio seems to be close to the ratio between the initial product prices (sustainable price/low-cost price).

CONCLUSION

The overall work demonstrates the potential to develop an ABM to predict the dynamics of change of a food chain. Environmental crisis has led to adoption of sustainable products from consumers. We also evaluated the effect of a reduction of product price with an increasing volume. After a certain period where oscillations in the number of adopters of sustainable products occurred and once a critical mass of consumers was adopted we observed that the number of adopters increased dramatically. The above results indicate that there is the potential of extending the reach of sustainable products by reaching a critical mass. An interesting issue to further investigate is how the public opinion is formed in case of environmental crisis, including situations where the assumptions that the whole population is well informed and the news reliable do not hold.

REFERENCES

An L. (2012). Modeling human decisions in coupled human and natural systems: review of agent-based models, *Ecological Modelling* 229: 25-36.

Asioli D, Aschemann-Witzel J, Caputo V, et al. (2017). Making sense of the “clean label” trends: A review of consumer food choice behavior and discussion of industry implications. *Food Res Int.* 99: 58-71. doi:10.1016/j.foodres.2017.07.022

Berger T. (2001). Agent-based spatial models applied to agriculture: a simulation tool for

technology diffusion, resource use changes and policy analysis. *Agricultural Economics* 25: 245–260.

Bourguet J-R., Thomopoulos R., Mugnier M-L., Abécassis J. (2013) An artificial intelligence-based approach to deal with argumentation applied to food quality and public health policy, *Expert Systems with Applications*, 40, 4539-4546.

Castella, J. C., Tran Ngoc Trung, and S. Boissau. (2005). Participatory simulation of land-use changes in the northern mountains of Vietnam: the combined use of an agent-based model, a role-playing game, and a geographic information system. *Ecology and Society* 10(1): 27.

Epstein J.M., Axtell R., (1996). Growing artificial societies: social science from the bottom up. Complex adaptive systems, Washington, D.C.; Cambridge, Mass.; London: Brookings Institution Press: MIT Press.

Filatova T., Verburg P.H., Parker D.C., Stannard C.A. (2013). Spatial agent-based models for socio-ecological systems: Challenges and prospects, *Environmental Modelling & Software* 45: 1-7.

Grimm V. (1999). Ten years of individual-based modelling in ecology: what have we learned and what could we learn in the future? *Ecological Modelling* 115 (2-3): 129-148.

Ho TH, Lim N, Camerer CF (2006). Modeling the Psychology of Consumer and Firm Behavior with Behavioral Economics. *J Mark Res* 43(3): 307-331. doi:10.1509/jmkr.43.3.307

Hoek AC, Pearson D, James SW, Lawrence MA, Friel S (2017). Healthy and environmentally sustainable food choices: Consumer responses to point-of-purchase actions. *Food Qual Prefer* 58: 94-106. doi:10.1016/j.foodqual.2016.12.008

Janssen M.A., Ostrom E. (2006). Empirically based, agent-based models, *Ecology and Society* 11(2):37, [online] URL: <http://www.ecologyandsociety.org/vol11/iss2/art37/>

Janssen, M.A., Walker, B.H., Landgride, J., Abel, N. (2000). An adaptive agent model for analysing co-evolution of management and policies in a complex rangeland system, *Ecological Modelling* 131: 249–268.

Matthews R.B. et al. (2007). Agent-based land-use models: a review of applications. *Landscape Ecology* 22: 1447-1459.

Parker, D.C., Manson, S.M., Janssen, M.A., Hoffmann, M.J., and Deadman, P. (2003). Multi-agent systems for the simulation of land-use and land-cover change: a review, *Annals of the Association of American Geographers* 93 (2):314-337.

Railsback, S.F., Lytinen, S.L., Jackson, S.K. (2006). Agent-based simulation platforms: review and development recommendations, *Simulation* 82 (9): 609–623.

Rammel C., Stagl S., Wilfing H. (2007). Managing complex adaptive systems — A co-evolutionary perspective on natural resource management, *Ecological Economics* 63: 9-21.

Robinson D.T., Brown D.G., Parker D.C., Schreinemachers P., Janssen M.A., Huigen M., Wittmer H., Grotts N., Promburom P., Irwin E., Berger T., Gatzweiler F., Barnaud C. (2007). Comparison of Empirical Methods for Building Agent-Based Models in Land Use Science, *Journal of Land Use Science* 2(1):31–55.

Samuelson D (2000). Designing Organizations. OR/MS Today, Institute for Operations Research and the Management Sciences.

Samuelson D, Macal C (2006). Agent-Based Modeling Comes of Age. OR/MS Today, Institute for Operations Research and the Management Sciences.

Schelling T.C. (1971). Dynamic models of segregation, *The Journal of Mathematical Sociology* 1 (2): 143-186.

Simon H. A. (1997). Models of Bounded Rationality: Empirically Grounded Economic Reason. Cambridge: MIT Press.

Tamani, N., Mosse, P., Croitoru, M., Buche, P., Guillard, V., Guillaume, C., Gontard, N. (2015). An argumentation system for eco-efficient packaging material selection. *Computers and Electronics in Agriculture* 113, 174–192.

Thomopoulos R., Croitoru M., Tamani N. (2015) Decision Support for Agri-Food Chains: A Reverse Engineering Argumentation-Based Approach, *Ecological Informatics* 26(2): 182-191.

Thomopoulos R., Moulin B., Bedoussac L. (2017). Combined Argumentation and Simulation

to Support Decision: Example to Assess the Attractiveness of a Change in Agriculture. In: S. Benferhat et al. (Eds.): IEA/AIE 2017, Part II, *Lecture Notes in Artificial Intelligence* 10351: 275–281, Springer. doi:10.1007/978-3-319-60045-1_30

Thomopoulos, R., & Paturel, D. (2017). Multidimensional Analysis Through Argumentation? Contributions from a Short Food Supply Chain Experience. In: S. Benferhat et al. (Eds.): IEA/AIE 2017, Part II, *Lecture Notes in Artificial Intelligence* 10351: 268-274, Springer. doi:10.1007/978-3-319-60045-1_29

Verburg, P.H., Veldkamp, A. (2005). Editorial: spatial modeling to explore land use dynamics, *International Journal of Geographical Information Science* 19: 99–102.

BIOGRAPHIES

Rallou THOMOPOULOS is INRA Research Scientist in Montpellier and permanent member of the GraphIK lab at INRIA. She has dual skills in computer science and the agri-food sector. Her research topics are in knowledge representation and decision support, focused on argumentation systems and complemented by simulation approaches. She was a Guest Research Scientist at Laval University (Canada) in 2015-2016 and previously Assistant Professor at AgroParisTech.

Serafim BAKALIS has expertise in processing, transport phenomena and modelling of processes occurring in digestion and in general in use of consumer products. Prof. Bakalis has recently moved to the University of Nottigham to establish a group in Food Process Engineering. Prof. Bakalis has published over 100 papers and 150 conference publications.

MULTI-OBJECTIVE OPTIMIZATION OF THE FORMULATION OF BARLEY BREAD USING ARTIFICIAL NEURAL NETWORK AND GENETIC ALGORITHM

Predrag Kojić
Faculty of Technology Novi Sad,
University of Novi Sad,
Bulevar Cara Lazara 1, 21000 Novi
Sad, Serbia
E-mail: kojic@tf.uns.ac.rs

Milica Pojić
Institute of Food Technology,
University of Novi Sad,
Bulevar Cara Lazara 1, 21000 Novi
Sad, Serbia
E-mail: milica.pojic@fins.uns.ac.rs

KEYWORDS

Multi-objective optimization, Neural network, Barley bread

ABSTRACT

The objective of this study was to highlight the importance of using multi-objective method in order to obtain the best additive content and combination to improve the quality of the barley bread. Also, this research extends our knowledge of impact OSA starch, wheat gluten and xylanase on the bread volume, crumb hardness and crumb chewiness.

INTRODUCTION

Recently, researches have focused on the improvement of the barley bread quality. Production of the leavened bread with barley flour is very hard to obtain due to weak dough viscoelasticity and gas retention capability (Newman and Newman, 2008). Mixing barley flour even up to 30% with wheat flour significant improve the nutritional profile of the baked products at the expense of decrease of bread volume and increase of crumb firmness and cohesiveness (Newman and Newman, 2008). To solve this issue, considerable economic efforts due to the high cost of experiments with the valuable raw materials and endless combinations of process parameters are needed. Therefore, the development of the optimization models undoubtedly is required. In this study we used multi-objective optimization (MOO) model. MOO uses evolutionary algorithms such as genetic algorithm (GA) to solve multiobjective problems (Rangaiah and Bonilla-Petriciolet, 2013). The solutions are a set of several equally good (non-dominated) optimal solutions, called a pareto front. The GA is based on a natural selection process that mimics biological evolution (Goldberg and Holland, 1988). It is adaptive heuristic search algorithm used to generate accurate or approximate solutions to optimization problems. The algorithm recurrently modifies a population of individual solutions. At each step, the GA randomly selects individuals from the current population and uses them as parents to produce the children for the next generation. The population evolves over successive generations toward an optimal solution. So, the objective of this study was to use MOO in order to obtain the best additive content and combination to improve the quality of pure barley bread.

MATERIALS AND METHODS

Experimental design, bread making procedure and the determination of the response parameters are explained in our earlier paper (Pojić et al., 2017). In this study, we used those data to feed the artificial neural network (ANN) that will

predict the desired outputs. The inputs were *OSA* starch, wheat gluten (*GL*) and xylanase (*Xyl*), while the outputs were specific bread volume (*SV*), crumb hardness (*Hard*) and crumb chewiness (*Chew*). Successful creation of the ANNs and obtained weight matrices provide the determination of the relative importance (*RI*) of the input values and its effect on *SV*, *Hard* and *Chew* by using partitioning methodology. In this study, the following Yoon's equation was used (Yoon et al., 1993):

$$RI_{ij} [\%] = \frac{\sum_{k=0}^n (w_{ik} w_{kj})}{\sum_{i=0}^m abs \sum_{k=0}^n (w_{ik} w_{kj})} 100 \%$$

where RI_{ij} is the relative importance of the i th input variable on the j th output, w_{ik} is the weight between the i th input and the k th hidden neuron, and w_{kj} is the weight between the k th hidden neuron and the j th output. This analysis proved that the decision variables have the conflicting influence on the performance parameters, and it is not possible to maximize the *SV*, and minimize the *Hard* and *Chew*, simultaneously. Thus, to achieve the optimal content and combination of additives to solve this problem, we used the multi-objective optimization with built in functions "gamultiobj" in Matlab R2016b.

RESULTS AND DISCUSSION

Artificial Neural Network

The three feed-forward back propagation ANNs were used to predict the experimental values for *SV*, *Hard* and *Chew*, respectively. The ranges of the ANNs inputs were: $0 < OSA < 10\%$, $0 < GL < 2\%$ and $0 < Xyl < 5$ gr/100kg. The numbers of neurons were 8, 6 and 7 in the hidden and 1 in the output layer, respectively for ANN1, ANN2 and ANN3. To improve the quality of the ANN, both input and output data were normalized. The networks were trained with Bayesian regularization back propagations algorithm that achieved slightly better prediction than others training algorithms (Levenberg-Marquardt, BFGS Quasi-Newton, Scaled Conjugate Gradient, etc.). Bayesian regularization algorithm updates the weights and bias values according to the Levenberg-Marquardt optimization by minimizing a combination of weights and squared errors in order to find best combinations, so the resulting network generalizes well. Moreover, Bayesian regularization uses all data and the validation data set does not need to be separate from the training data set, this makes it very applicable for small number of experimental data (Foresee and Hagan, 1997). The transfer function was the linear transfer function (purelin) at output layer and the

tangent sigmoid transfer function (tansig) at hidden layer. All data points were randomly used to train and develop the ANN; 85% of data points for training and 15% of data for testing the process. ANN results, including the weight and bias values depend on the initial assumptions of parameters necessary for ANN construction and fitting. In the same way, the different number of hidden neurons can give different ANN outcomes. In this context, and to prevent overfitting a series of different topologies were used, in which the number of hidden neurons were varied from 1 to 10 and the training process of each network was run forty times with random initial values of weights and biases. Creation of 400 ANN in total was the result of this procedure. The quality of the fit with the respect of coefficient of determination (R^2) and mean absolute error (MAE) is presented in the Table 1 for the best fitting ANNs. Fig. 1 shows the parity plot of the experimental and predicted SV , $Hard$ and $Chew$ using ANN with best performance.

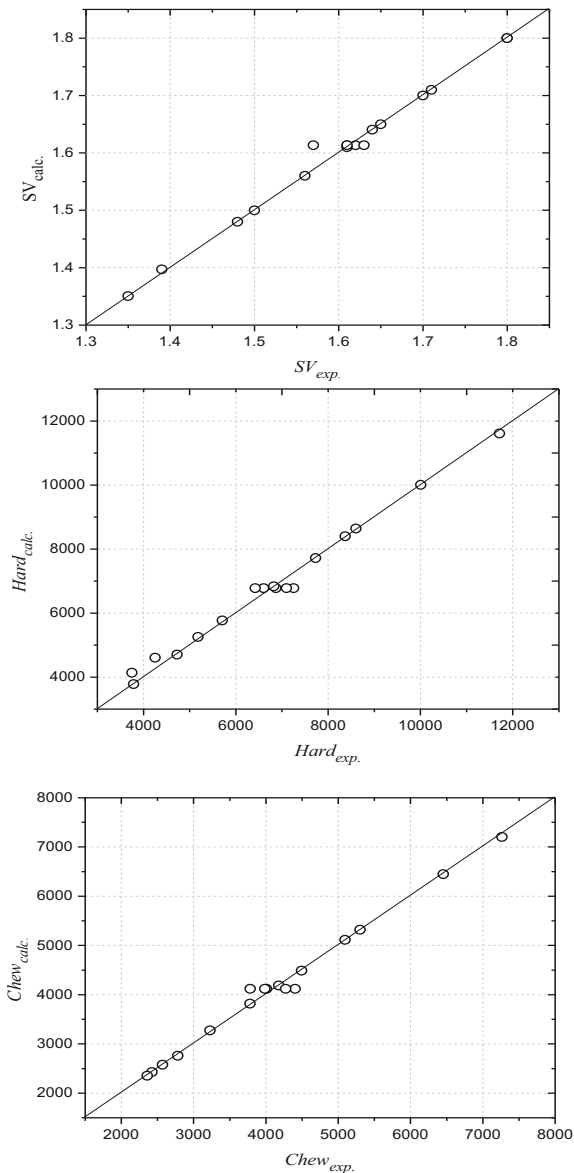


Figure 1: Parity Plot of Predicted Values of the SV , $Hard$ and $Chew$ using ANN

Table 1. Quality of the Fit

Quality of the fit	R^2	MAE
ANN1	0.9909	0.0049
ANN2	0.9905	148.1495

ANN3 0.9913 73.9448

Relative Importance of the Input Parameters on the SV , $Hard$ and $Chew$

The obtained relative importance values and standard deviations are presented in the Figs. 2, 3 and 4. Low variability of RI % makes the explanation of the input influence acceptable.

From Fig. 2 it can be seen that the increasing content of the OSA , GL and Xyl affected the increase in specific bread volume. Also, it was found that the OSA concentration affected specific bread volume more than other two parameters. The positive impact of OSA on the specific volume of barley bread is attributed to the morphology of OSA starch granules which were disrupted by drum drying pre-gelatinization and its greater capacity to develop bread structure and volume.

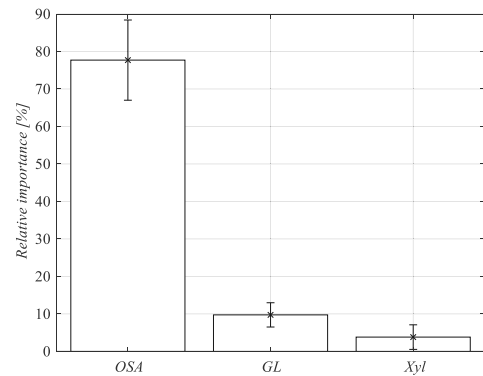


Figure 2: Relative Influence of Input Parameters on Specific Bread Volume

The OSA starch was the most influential parameter on the crumb hardness (Figure 3). With increasing the content of OSA , Gl and Xyl crumb hardness is decreased.

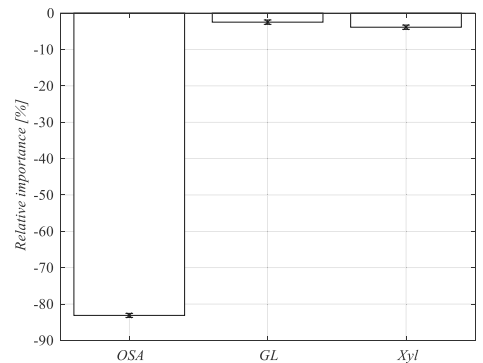


Figure 3: Relative Influence of Input Parameters on Crumb Hardness

From Fig. 4 it can be seen that the OSA starch has the greatest influence on the crumb chewiness. With increasing the OSA the crumb chewiness of the bread decreased. The second most influential parameter was Xyl , it also has a negative effect on the $Chew$, while on the other hand the GL expressed the positive effect. The fact that gluten addition affected decrease in crumb hardness and increase in crumb chewiness can be associated with the influence of bread volume and density of bread loaves on large-scale deformation hardness measurements (Goesaert et al., 2008). Therefore, the decrease in crumb hardness with addition of gluten can be explained as

a influence of bread volume increase and cell density decrease.

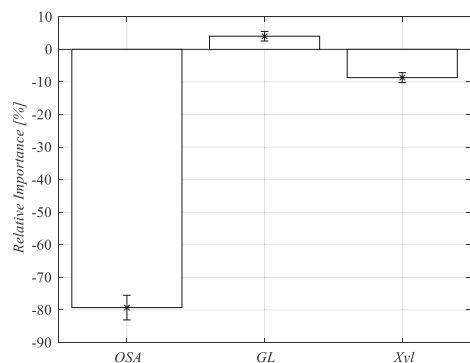


Figure 4: Relative Influence of Input Parameters on Crumb Chewiness

Multi-Objective Optimization by Genetic Algorithm

Trained and validated ANNs were also implemented in the MOO with GA as the evaluation function for the *SV*, *Hard* and *Chew*. The GA finds the Pareto optimal set within the experimental parameters boundary. GA solves three-objective problem where *SV* has to be maximal and the *Hard* and *Chew* minimal as a set of optimal solutions in which an improvement in one objective requires a degradation of another. The pareto plot of this multi-objective problem is shown in Fig. 5. Pareto points are replotted in Fig. 6 and represent the trade-off between the *Hard* and *Chew* with increasing *SV*. It is evident that the tradeoff between *Hard* and *Chew* for *SV* values from 1.76 to 1.79 ml/g are better than for the rest of pareto points. Within this region *SV* increased (desired), *Hard* decreased (desired), but *Chew* increased (undesired) meaning two objectives were improved while one deteriorated. One of the best pareto points for this process of bread making appears to be the individual minima for *Hard* (2878 g) and its correspond values for *SV* of 1.76 ml/g and *Chew* of 2615 g. This pareto solution showed an increase in *SV* of 10% and decrease in *Hard* and *Chew* of about 60% and 30% compared to breads containing medium amounts of improvers 1% *GL*, 5% *OSA* and 2.5 g/100 kg *Xyl*, respectively. The set of decisions variables correspond to objective function values were for *OSA* from 7.6 to 10%, *GL* from 1 to 2 % and *Xyl* from 0 to 0.9 g/100 kg. It is expected that *OSA* starch has the maximal values because with increasing the *OSA* starch values for *SV* also increased while *Hard* and *Chew* decreased what is the desirable behavior.

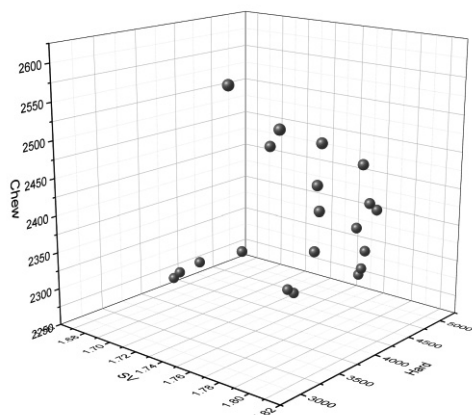


Figure 5: 3D Pareto Front for *SV*, *Hard* and *Chew*

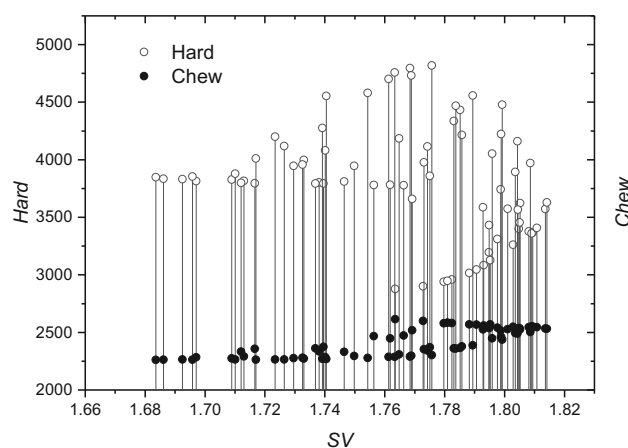


Figure 6: MOO Results of *SV* Maximization and *Hard* and *Chew* Minimization

CONCLUSION

This study has identified optimal points from Figs. 5 and 6 obtained by the MOO, which decision maker can choose, depending on the process situations. For example, values for *SV* of 1.76 ml/g, *Chew* of 2615 g and *Hard* of 2878 g give an increase in *SV* of 10% and decrease in *Hard* and *Chew* of about 60% and 30% compared to breads containing medium amounts of improvers 1% *GL*, 5% *OSA* and 2.5 g/100 kg *Xyl*, respectively. Moreover, Yoon's model revealed that *OSA* starch showed the most pronounced effect on *SV*, *Hard* and *Chew*.

ACKNOWLEDGEMENT

This research was supported by the COST action for mathematical and computer science methods for food science and industry. (Project No. CA 15118).

REFERENCES

- Foresee, F.D., Hagan, M.T., 1997. Gauss-Newton approximation to Bayesian learning, in: *Neural Networks, 1997.*, International Conference on. IEEE, pp. 1930–1935.
- Goesaert, H., Leman, P., Delcour, J.A., 2008. Model approach to starch functionality in bread making. *J. Agric. Food Chem.* 56, 6423–6431.
- Goldberg, D.E., Holland, J.H., 1988. Genetic algorithms and machine learning. *Mach. Learn.* 3, 95–99.
- Newman, R.K., Newman, C.W., 2008. Barley for food and health: *Science, technology, and products*. John Wiley & Sons.
- Pojić, M., Dapčević Hadnađev, T., Hadnađev, M., Rakita, S., Torbica, A., 2017. Optimization of additive content and their combination to improve the quality of pure barley bread. *J. Food Sci. Technol.* 54, 579–590.
- Rangaiah, G.P., Bonilla-Petriciolet, A., 2013. Multi-objective optimization in chemical engineering: developments and applications. John Wiley & Sons.
- Yoon, Y., Swales, G., Margavio, T.M., 1993. A Comparison of Discriminant Analysis versus Artificial Neural Networks. *J. Oper. Res. Soc.* 44, 51–60.

NUMERICAL STUDY OF AIRFLOW AND TEMPERATURE DISTRIBUTION IN A LOADED COLD STORE

Pierre Coldrey^a, Jean Moureh^a, Graciela Alvarez^a, Denis Leducq^a, Alain Foster^b, Mohammed Youbi-Idrissi^c,
Alain Damas^c, Judith Evans^b

^aIRSTEA, 1 rue Pierre-Gilles de Gennes, CS 10030; 92761 Antony Cedex,

^bLondon South Bank University; 103, Borough Road; SE10AA London

^cChemin de la porte des Loges, 78354 Les Loges en Josas

KEYWORDS

Airflow, Cold store, Cold distribution, Ventilation, Numerical modelling, Computational fluid dynamics

ABSTRACT

The aim of this study is to analyze the effects of ventilation and cooling power distribution on air temperature and products temperature levels in a cold store by means of computational fluid dynamics. The refrigerated space under study has a set of six fans and six heat exchangers (HEs) with different mass flow rates and blowing velocities arranged back to back at the middle of the domain. For this purpose, three cases have been simulated with different operating conditions involving various combinations between HEs and fans, while maintaining the same cooling power in the warehouse. In the author's knowledge, very few articles have been written on airflow in loaded enclosures ventilated by several heat exchangers.

NOMENCLATURE

P.....Power kW

T.....Temperature °C

$y^+ = y \sqrt{v \left(\frac{\partial u}{\partial y} \right)_{y=0}}$Dimensionless wall unit

SUBSCRIPTS

max Maximum

min Minimum

in Inlet of the HE

out Outlet of the HE

ave Average

INTRODUCTION

In refrigerated enclosures, the conservation of the organoleptic and sanitary quality of foodstuffs is directly governed by the temperature field which depends of the airflow patterns inside the cool

store. Hence, the analysis of the airflow is very meaningful from the point of view of the sanitary quality. The main industrial issue is to increase the temperature homogeneity of products at appropriate levels inside the refrigerated warehouse. With the increasing availability and power of computers, Computational Fluid Dynamics (CFD) became a very convenient tool to investigate the air and thermal distribution in a cold store.

Many studies have been performed to characterize numerically and/or experimentally the influence of enclosure's geometry and stacking arrangement of HEs inlet temperature and of HEs location on airflow and temperature distribution in rather small cold stores ($< 100 \text{ m}^3$) (M.T. Karimipana, 1999; Jing Xie and al., 2006; Mitoubkieta Tapsoba and al. 2007; M.K. Chourasia T.K. Goswami, 2007; Hsin Yu, 2006; Brajesh Tripathi S.G. Moulic, 2007; Hsin Yu and al., 2007; B. Bjerg and al., 2002; Son H. Ho and al., 2010). However, this paper focuses on the particular case of a large cold store ($57\,344 \text{ m}^3$) refrigerated by different types of HEs and ventilated by several fans. To the author's knowledge, very few articles concerning 3D CFD simulations on a large warehouse refrigerated by several heat exchangers with different mass flow rates and inlet temperatures have been performed.

Many articles deal with the influence of enclosure geometry on air flow patterns. M. Tapsoba and al. (2007) show that the presence of product in a typical refrigerated truck configuration modifies strongly the flow patterns even if the velocity levels are similar with the empty enclosure. It leads to a reduction of the jet penetration and a diminution of recirculation especially at the rear part of the enclosure. Jing Xie and al., (2006) demonstrate that design parameters as corner's smoothness or presence of stacked foodstuff strongly affect the flow field and temperature field. Smoothness of the corners affect adverse pressure gradient favorable to the reverse flow in the enclosure. The more round these corners are the less adverse pressure gradient there is and the more homogeneous the temperature is distributed. Eventually, presence of a loading in the middle of the room increases greatly the number of eddy and breaks the flow field

homogeneity. This will be the case in this paper because we have only modelled a large loaded warehouse filled with 25 pallets rows.

Another parameter affecting the air-jet trajectory is the inlet temperature of the HEs. In most CFD modelling, HEs are considered as non-isothermal jets. The influence of inlet temperature on the airflow can be characterized by the dimensionless Archimed number (Ar) comparing buoyancy forces with inertial forces. (Hsin Yu, 2006; Brajesh Tripathi S.G. Moulic, 2007; Hsin Yu and al., 2007) have numerically and experimentally determined several critical values of Ar corresponding to different forms of airflow patterns for a jet in an enclosure. Typically, if $Ar < 0.005$ the air flow pattern is fully rotary and if $Ar > 0.018$ the jet falls immediately at the entry (Brajesh Tripathi S.G. Moulic, 2007; Hsin Yu, 2006). Hsin Yu managed to predict analytically the trajectory of a horizontally diffused wall jet, in the primary flow region, depending of the Archimed number. Yu emphasizes that at high Ar , air-jet trajectory becomes analytically unpredictable because of the predominance of buoyancy forces over inertial forces and because of the apparition of a secondary recirculation making the trajectory simulation more complex. In this paper it is difficult to calculate an overall Archimed number because of the different blowing temperature of the HEs. Moreover, the interactions between the fans and the HEs help the cold jets not to fall directly at the entry even if the local Archimed number is above 0.018.

Unsteady simulations were performed in loaded small enclosures where stacked products are modelled as porous medium (M.K. Chourasia T.K. Goswami, 2006; M.K. Chourasia T.K. Goswami, 2007). These calculation allow the investigation of the rate of metabolic heat generation, porosity of the bulk medium, resistance of the product skin preventing moisture loss and cool down time. It has been demonstrated that the higher the porosity of the medium, the lower the cool down time is. But even for a porosity of 0.5, cool down time is about 50h (M.K. Chourasia T.K. Goswami, 2006). Such calculation can be performed in a small 2D enclosure (grid size $< 500\ 000$ cells) but not in a large 3D refrigerated warehouse (grid size $> 10\ 000\ 000$ cells) due to too important computational time and computational resources it would take. Thus, this CFD study will be made in stationary regime.

In order to take into account turbulence effects impacting the airflow, one must properly choose the turbulence model. Many authors find very different results when comparing turbulence models on the non-isothermal jets in confined enclosure (E. Pula H.A. Ersan, 2015; F. Kuznik and al., 2007). H.A.

Ersan compares three two-equations turbulence models on a 2D non-isothermal jet confined in an enclosure with inlet and outlet located face to face. If RNG k - ϵ model fits well with the experimental data, predicting a clockwise recirculation, std k - ω and SST k - ω fail to predict the correct behavior. Instead, they predict the fall of the jet at directly at the entry and the formation of a counter clockwise recirculation in the enclosure. More discrepancy is found on the velocity profiles for the cold confined wall jet modelled with k - ϵ model (F. Kuznik and al., 2007). Near the inlet the velocity and temperature profiles are in good agreement but the numerical model is less reliable as the profile is far from the air inlet overestimating the maximal velocity and miss-predicting the location of this maximum. The author note that these discrepancies only occur for the cold wall jet, otherwise the turbulence model correctly predicts velocity and temperature profiles for the hot and the isothermal jet. This last remark echo Hsin Yu (2006) on the difficulty to predict the air-jet trajectory for cold wall jets in confined enclosure far from the inlet region.

Many studies use the first order closure standard k - ϵ model described by Launder and Spalding (1974), since it is easy to program and has a large field of application. However, particular effects appear in confined enclosure as high streamlines curvature effects and secondary recirculation. For these complex flows, different authors (M.L. Hoang and al., 2000; J. Moureh, D. Flick, 2003; M. Tapsoba and al., 2007) agree on the superiority of second order closure models as RSM to predict airflow patterns.

In 2000, M.L. Hoang and al. used computational fluid dynamics (CFD) to investigate the airflow pattern in an operational cold store for the long-term storage of fruits and vegetables. The cold store is rather small (2.5m x 2.7m x 4.5m) and ventilated by only one heat exchanger. 3D numerical simulations were performed for the empty cold store and the loaded cold store filled with 4 wooden pallet boxes. Validation was made by a comparison of the calculated time-averaged velocity magnitudes with the measured mean velocities. An important averaged difference of 40% between calculations and measured velocities has been found for k - ϵ model in the empty cold store. Model predictions for the loaded cold store were better with an absolute difference between measurement and numerical results of 26% for k - ϵ model. RNG model gave less precise prediction with an absolute difference of 28.5%. The authors hope that enhanced turbulence models such as Reynold Stress models (RSM) could contribute to improve the numerical predictions.

J.Moureh and D.Flick study the wall air-jet characteristics and the airflow patterns within a slot ventilated enclosure in 2003. Three turbulence models were compared: SKE, RNG and the second order closing model RSM. The latest is a second order closure model is generally more precise on the modelling of flows with strong anisotropic behavior, high streamline curvature and flow separation. Only the RSM allows predicting the complexity of airflow leading to the jet separation from the ceiling and the creating of two contra-rotative recirculations in accordance to experimental data obtained on a scale model. On the contrary, the other models fail to predict the jet separation which, in turn, leads to one recirculation within the whole enclosure. This clearly underlines the superiority of RSM for internal flows including adverse pressure gradient, turbulence anisotropy and streamline curvature.

In 2007, M. Tapsoba and al. performed experiment on a reduced scale model and CFD simulations to study an enclosure loaded with slotted box supplied by a ceiling-jet. They compared experimental measurements on velocities with predictions given by two turbulence models: RSM and k-y. The results on velocity field were very similar in high velocity zones. However, RSM gave better predictions on the adherence point of Couanda effect as well as on the penetration distance and the deflection of the jet. The authors think that this clearly indicates that k-y model lacks sensitivity with respect to the adverse pressure gradient located at the rear part of the enclosure.

According to the previous articles, RSM seems to be the best model for the prediction of turbulent flow patterns inside enclosures. Thus, we choose RSM for the turbulence modelling in all our computations.

WAREHOUSE GEOMETRY

Warehouse's geometry involves 6 heat exchangers, 6 fans, 50 rows of stacked products and one door for a total volume of $57,165 m^3$ ($64m \times 56m \times 16m$) and a maximal capacity of 3 900 pallets. Due to the presence of a symmetry plane in the warehouse, we only model half the cold store to save computational time. Thus, the new geometry is twice as small: $28,582 m^3$ ($32m \times 56m \times 16m$), involves 3 heat exchangers, 3 fans, 25 rows of stacked products and half a door. Fig.1 shows a top view sketch of the warehouse and a 3D modelling of the half the geometry that is used as computational domain. Moreover, two sectional views are presented Fig.2 to indicate the main geometrical characteristic of the cold store. Note that heat is extracted from the warehouse by two types of heat exchangers (type 1 and 2), their

different characteristics are listed in the boundary condition part.

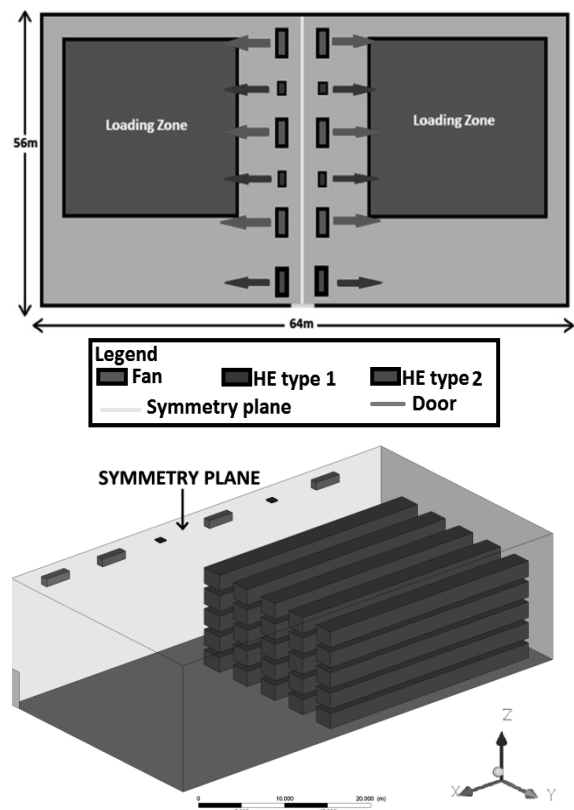


Fig.1. Geometry modelling of the cold store. Sketch of the whole geometry, top view (top). 3D modelling of half geometry, isometric view (bottom).

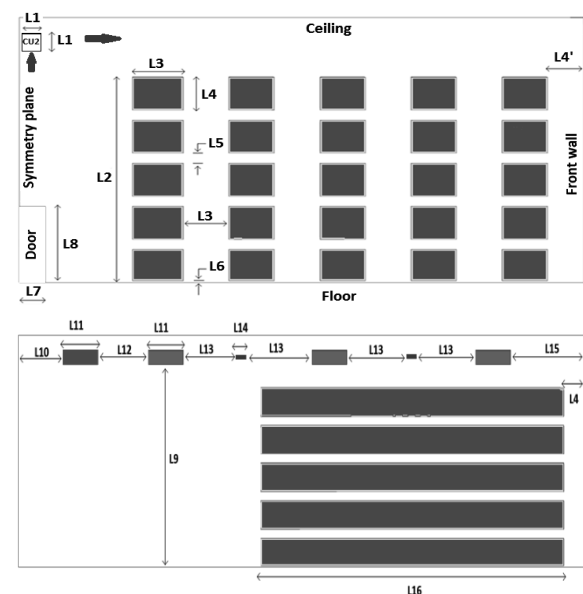


Fig.2. Cross sections showing the main dimensions of the warehouse. ZY plane (top); XZ plane (bottom).

The relevant lengths L1 through L16 are given in the following values: L1=0.98m, L2=12.5m, L3=2.5m, L4=L4'=2.0m, L5=0.6m, L6=0.1m, L7=1.4m, L8=4.6m, L9=14.0m, L10=4.0m, L11=3.5m, L12=5.0m, L13=6.0m, L14=1.0m, L15=7.0m, L16=30.0m. Eventually, velocity field will be displayed on the blowing plane of the jets presented Fig.3.

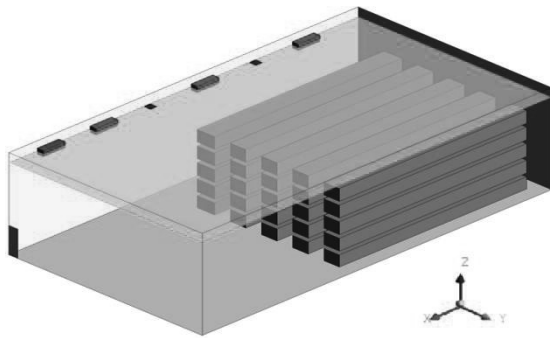


Fig.3. Location of the blowing plane of the loaded cold store ($z = 14.5\text{m}$)

MESHING, NUMERICAL SIMULATIONS AND BOUNDARY CONDITIONS

Meshing

Meshing was realized on ICEM, a mesh generator specialized in hexahedral meshes. The same mesh, composed of 13 806 606 cells, has been used for every simulations. Wall's refinement is used for the good implementation of wall functions in the flow computation. These wall functions generally model flow behavior at near wall region by use of a logarithmic law between the mean velocity and the dimensionless wall distance. That is the case of FLUENT Standard Wall Function which is the most widely used wall function for industrial flows. In this study, Standard Wall Function will be used in every simulation. For RSM, the log-law between the mean velocity and the dimensionless wall distance is valid in regions where $30 < y^+ < 300$, with y^+ the dimensionless wall distance. For all configurations, $y^+ < 300$ on the ceiling, except for some cells in the rear part of the ceiling where $y^+ < 30$ due to small wall shear stress. In this case, FLUENT applies the laminar stress-strain relationship which is a proportionality equation between the wall distance and the mean velocity of the fluid.

Refined zones correspond to first layer size of 1 cm. Non-refined zones have a first cell size of 13 cm which is the maximum length cell of all the configurations performed. Due to the small space between the bottom of the pallets and the floor (10

cm), we slightly refined the mesh near the floor in order to have at least 3 layers between the floor and the pallet. We refined the ceiling, the top of the highest pallets and the vertical walls of the pallets close to the air inlets. Fig.4 shows a transversal section of the mesh and the mesh refinement at the top of the pallets.

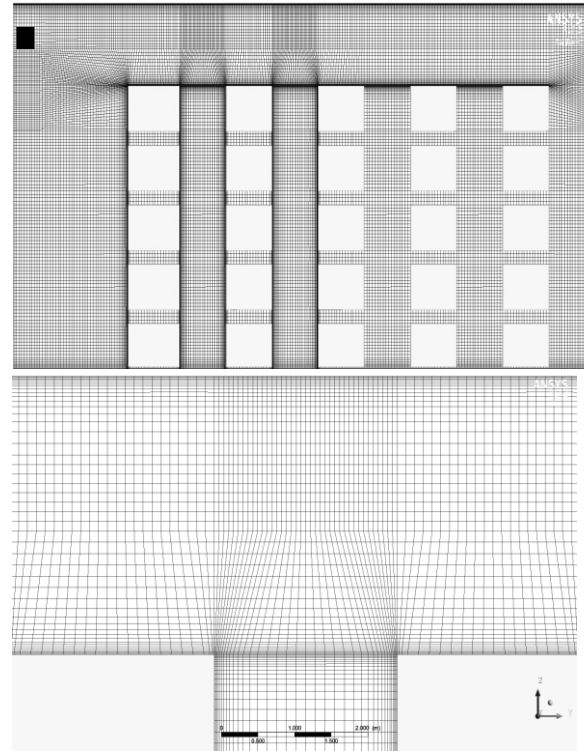


Fig.4. Transversal section of the mesh. Overall lateral view (top), pallets close up (bottom). Pallets colored in yellow.

Numerical simulation

Simulations were performed with the finite volume method CFD code ANSYS Fluent 17.2 on a 64 bits Windows7 computer with a 3.70 GHz Intel® Xeon® CPU E5-1630 v4 and 192 Go (RAM). Calculations were first launched in stationary mode with pressure-velocity coupling scheme "COUPLED". First, we decreased the under-relaxation factors for few hundred iterations. Then, default under-relaxation factors were applied for few hundred iterations more. Eventually, pseudo transient mode is activated for few hundred iterations to improve heat balance. A total of one thousand iterations is needed to satisfy convergence criteria.

In order to analyze the effects of cold distribution and ventilation on air temperature and product temperature levels in a cold store, three cases have been simulated:

- The first one (reference case) one with six HEs and six fans working,
- The second one with only four HEs and six fans working and
- The last one with six HEs and no fans working.

It is important to note that, in every case, the overall cooling power distributed in the warehouse is the same: $P = 68 \text{ kW}$. In order to check the numerical solution, global energy balance was performed by applying the first law of thermodynamics. For the steady state problems under study, the rate of heat gained from the walls, the ceiling, the floor and the door should equal the rate of equivalent heat extracted from the HEs. This relationship can be expressed as:

$$P_{floor} + P_{walls} + P_{ceiling} + P_{door} = P_{HE}$$

Global energy balance was satisfied with a reasonably low error: maximal error of 1.5% for case1.

Boundary Conditions

At the inlets of fans and heat exchangers, uniform distribution is assumed for velocity components. All HEs and fans are blowing in the positive y direction. Fans have the same properties than type 2 HEs except they blow at warehouse's ambient temperature (they generate no cold). HEs characteristics are listed tab.1 for all cases. External temperature is set to 25°C and heat transfer coefficient on the walls and the ceiling is $0.1 \text{ W}\cdot\text{m}^{-2}\cdot\text{K}^{-1}$. The floor is at constant temperature of -17°C . No slip condition is applied on every wall and on the surface of the pallets. A symmetry condition is put on the symmetry plane. Heat load of the products was ignored but heat coming from door opening has been taken into account: $P = 9,7 \text{ kW}$ (according to A.M. Foster, 2003, [4]). The number of door openings was estimated at one opening every two minutes. Eventually, natural convection is taken into account (ideal gas law).

	HE Type 1	HE Type 2
Blowing Section (m^2)	0.13	3.38
Air flow rate ($\text{m}^3\cdot\text{h}^{-1}$)	2 500	23 000
Inlet Velocity ($\text{m}\cdot\text{s}^{-1}$)	5.2	1.9
Blowing Temperature case 1 ($^\circ\text{C}$)	-23.2	-21.4
Blowing Temperature case 2 ($^\circ\text{C}$)	-27.7	-21.4

Blowing Temperature case 3 ($^\circ\text{C}$)	-22.7	-21.4
---	-------	-------

Tab.1 Physical characteristics of the different types of HEs for all configurations

RESULTS AND DISCUSSION

Fig.5 presents the streamlines generated by HEs for the three cases. Comparing cases 1 and 2, we notice a strong reduction of the penetration distance for jet flowing from type 1 HEs (blue streamlines) in case 2. This could be explained by the greater temperature differences between the ambient air ($T_{ave} \sim -18.3^\circ\text{C}$) and the air coming from the HEs (case 1: $T_{in} = -23.2^\circ\text{C}$; case 2: $T_{in} = -27.7^\circ\text{C}$) causing an increase of jet's deflection by buoyancy effect.

Comparing cases 1 and 3, we also see a lateral deviation of the jets towards the positive x direction in case 3. This deviation is due to dynamic interaction between the primary jet flow and a free thermal air convection generated upwards along the rear and lateral walls generating a deviation of the jets in the lateral direction.

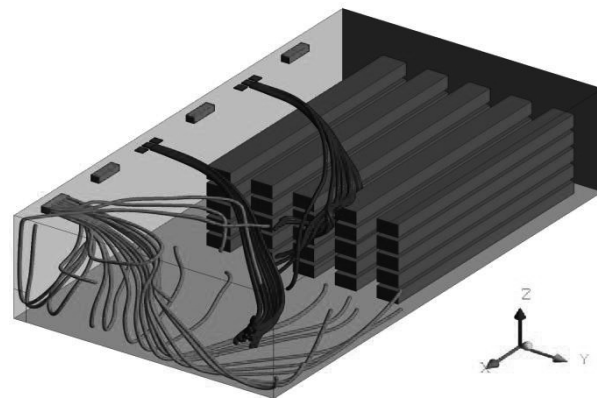
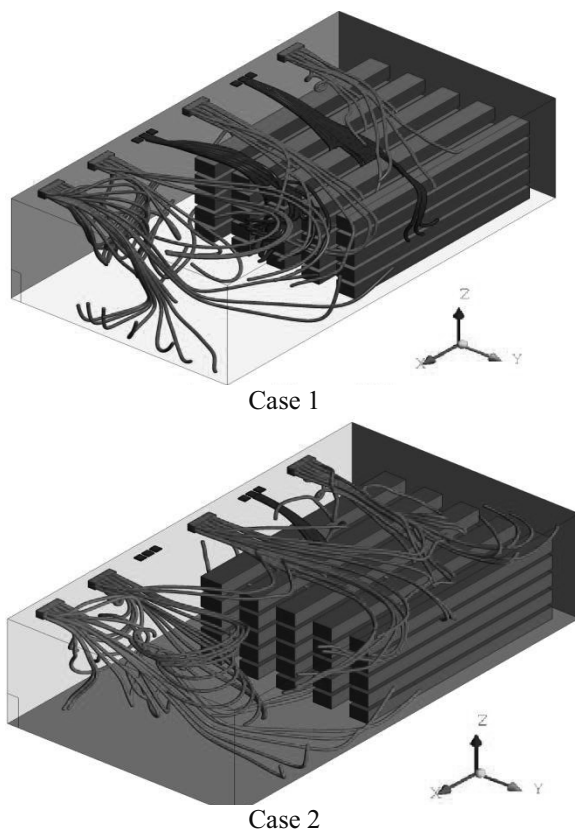
To better illustrate dynamic interactions between jets, Fig.6 presents the top view of velocity contours over the blowing plane for all cases. We see that the jets close to the lateral walls tends to be deviated towards the center of the enclosure. Moreover, we notice an increase of jets lateral deviation coming from type 1 HEs in case 3 compared to case 1. This clearly indicates that ventilation generated by the additional fans tends to stabilize the longitudinal jet development and acts like a dynamic air barrier preventing lateral interactions with crossflow coming from lateral walls. As a consequence, the use of additional fans increases the stability and the penetration distance of primary jets while limiting their lateral interactions.

Fig.7 presents temperature contours over the pallets in isometric view and product's extremal temperatures. Even if the overall cooling power is the same in every simulation ($P=68 \text{ kW}$), we observe an increase of vertical thermal stratification and temperature heterogeneity from case 1 to case 2 as cold is distributed to fewer HEs: $\Delta T = 1.57^\circ\text{C}$ for case 1, $\Delta T = 2.60^\circ\text{C}$ for case 2. Thus, cold distribution has a notable impact on products temperature homogeneity. On the other hand, there is no significant difference on products temperature between case 1 and 3 indicating that fan's ventilation has no meaningful incidence on pallets temperature levels. For all cases, maximal temperature zone is located at the bottom of the pallets. Indeed, in the thin zone between the floor

and pallet's bottom (10 cm), velocities are very low and air is rapidly warmed up by the floor ($T_{floor} = -17^{\circ}C$), creating hot spots. Eventually, the average temperature on the pallets is the same for every case and is really close to the ambient temperature of the warehouse ($T_{ave} \sim -18.3^{\circ}C$).

To better illustrate local effects generated by the additional fans, Fig. 8 (a) compares air temperature contours over the blowing plane of the middle fan ($x = -3m$) for cases 1 and 3. We clearly see an increase of thermal heterogeneity and vertical thermal stratification near the ceiling in case 3. Obviously, the lack of ventilation gives rise to stagnant air zones in the upper parts of the warehouse and enhances the thermal stratification by buoyancy effect. Fig.8 (b) compares velocity vector field colored by temperature for cases 1 and 3. A zoom has been made near the front wall to better visualize air currents. In case 3, we see upwards currents rising all along the front wall due to free thermal air convection along the wall.

In case 1, , whereas primary jet flow mainly governs the airflow in the upper regions inducing downward currents near the front wall and upwards currents only appear near the floor. Thus, ventilation reduces the impact of natural convection on airflow in the rear part of the cold store and extends the primary jet flow region.



Case 3

Fig.5 Streamlines coming from the HE. Mechanical HE (red), Blueeze (blue), secondary refrigerant HE (green). Isometric view

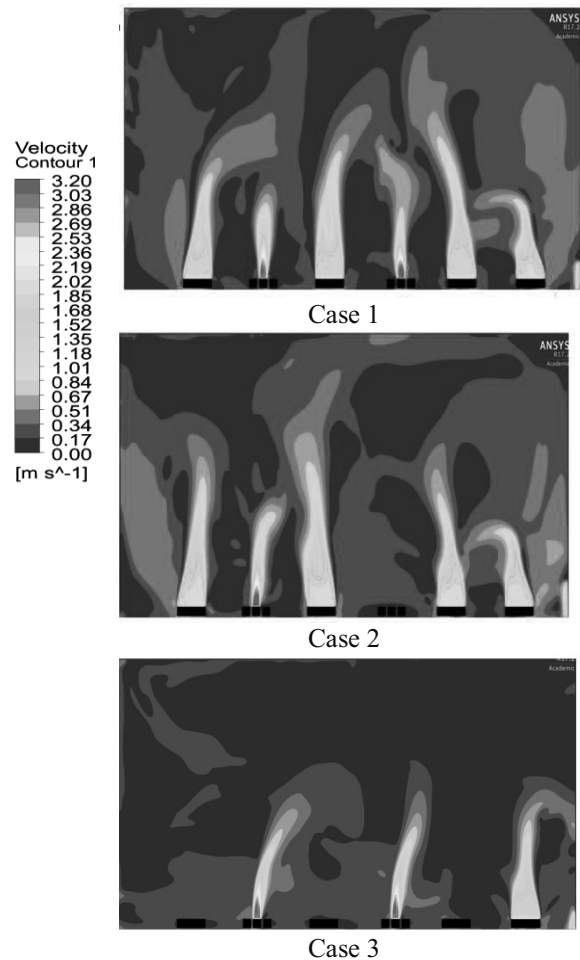


Fig.6 Velocity contours in blowing plane. Half warehouse, top view.

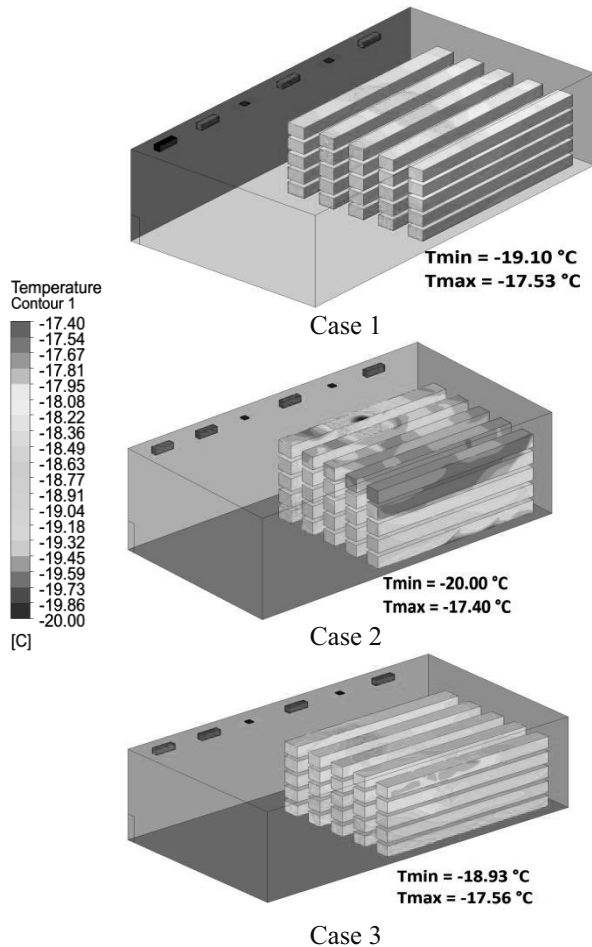


Fig.7 Temperature contours on the pallets. Isometric views

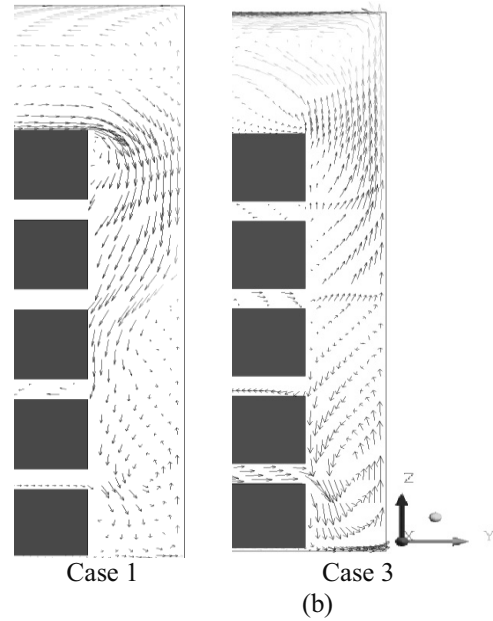
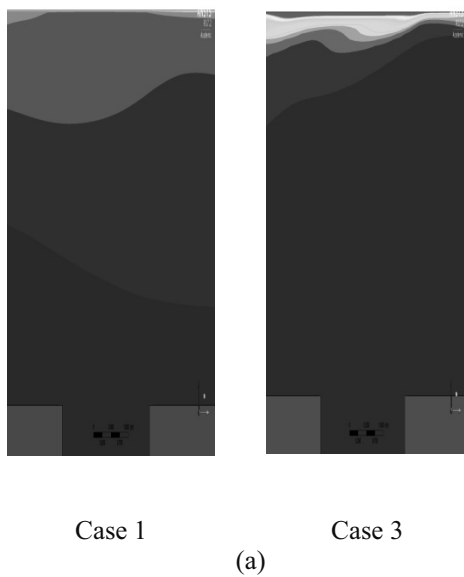


Fig.8 (a) Temperature contours in the blowing plane of the middle fan for cases 1 and 3, zoom near the ceiling. (b) Velocity vector field colored by temperature in the blowing plane of the middle fan for cases 1 and 3, zoom near the front wall. Pallets colored in brown.

CONCLUSION

In this study, numerical simulations performed using the CFD code Fluent were carried out in order to analyze the effect of cold distribution and fans ventilation on temperature and flow patterns in a large cold store loaded with pallets.

Results show that, for a fixed cooling power $P=68\text{kW}$, reducing the number of HEs (case 2) requires to decrease jet's blowing temperature causing the jets to deflect by buoyancy effect, reducing their penetration distance in the warehouse. Moreover, in case 2, temperature heterogeneity and thermal stratification on the pallets increases compared to case 1, even if the global temperature levels are similar in all cases. Thus, cooling power need to be more homogeneously distributed in the warehouse in order to lower temperature differences and natural convection effects such as jet's deflection and thermal stratification. In case 3, the lack of ventilation generated by the fans increase lateral deviation, decrease the jet penetration and enhances thermal stratification in the upper part and natural convection in the rear part of the warehouse.

CALCULATION NOTE

We find in the literature (A.M Foster, M.J Swain, R. Barrett and S.J. James; (2003) [18]) an analytical

expression of the outgoing debit I during the opening of the doors:

$$I = 0.333K_{fL}A(gH)^{0.5} \left(\frac{\rho_i - \rho_o}{\rho_i} \right)^{0.5} \left(\frac{2}{1 + (\rho_o/\rho_i)^{0.333}} \right)^{1.5}$$

with $K_{fL} = 0.48 + 0.004(T_o - T_i)$, the indications i and o meaning respectively inside and outside. A indicates the surface of the door, H its height and g the acceleration of gravity. We took $\rho_i = 1.4 \text{ kg.m}^3$, $T_i = -18.5 \text{ }^\circ\text{C}$, $\rho_o = 1.2 \text{ kg.m}^3$ and $T_o = 25.0 \text{ }^\circ\text{C}$. We find $I = 11.36 \text{ m}^3.\text{s}^{-1}$.

The number of door openings was estimated, using a previous study, at one opening every two minutes. The door puts 5 seconds to open, remains open during 10 seconds and closes in 5 seconds and there is 1 opening every 2 minutes. We counted 12 hours of activity in a day. Moreover, according to Foster, during opening and closing time we have to reduce by a half the incoming debit. Eventually, we find that $61\,344 \text{ m}^3$ of air is exchanged through the door every day.

Multiplying this volume by the heat capacity of air, the air density and temperature difference between the inside and the outside of the warehouse, we find that $4.3 \cdot 10^9 \text{ J}$ of heat is delivered by the door in the warehouse every day. Dividing this quantity by the number of seconds in a day and by the surface of the door we finally find the average heat power density on the door: $P_s = 1486 \text{ W.m}^{-2}$.

REFERENCES

Bjerg, B., Svidt, K., Zhang, G., Morsing, S., Johnsen, J.O., 2002. Modeling of air inlets in CFD prediction of airflow in ventilated animal houses. *Computers and Electronics in Agriculture* 34 223 – 235

Chourasia, M.K., Goswami, T.K., 2006. Simulation of Transport Phenomena during Natural Convection Cooling of Bagged Potatoes in Cold Storage, Part II: Mass Transfer. *Biosystems Engineering* 94 (2), 207–219

Chourasia, M.K., Goswami, T.K., 2007. Simulation of Effect of Stack Dimensions and Stacking Arrangement on Cool-down Characteristics of Potato in a Cold Store by Computational Fluid Dynamics. *Biosystems Engineering* 96 (4), 503–515

Chourasia, M.K., Goswami, T.K., 2007. Three dimensional modeling on airflow, heat and mass transfer in partially impermeable enclosure containing agricultural produce during natural convective cooling. *Energy Conversion and Management* 48 2136–2149

Chourasia, M.K., Goswami, T.K., 2007. CFD simulation of effects of operating parameters and

product on heat transfer and moisture loss in the stack of bagged potatoes. *Journal of Food Engineering* 80 947–960

Foster, A.M., Swain, M.J., Barrett, R., James, S.J., 2003. Experimental verification of analytical and CFD prediction of infiltration through cold store entrances. *International Journal of Refrigeration* 26 918-925

Ho, S. H., Rosario, L., Rahman, M.M., 2010. Numerical simulation of temperature and velocity in a refrigerated warehouse. *International Journal of Refrigeration* 33 1015 – 1025

Hoang, M.L., Verboven, P., De Baerdemaeker, J., Nicolaï, B.M., 2000. Analysis of the air flow in a cold store by means of computational fluid dynamics. *International Journal of Refrigeration* 23 127-140

Karimipana, M.T., 1999. Deflection of wall-jets in ventilated enclosures described by pressure distribution. *Building and Environment* 34 329-333

Kuznik, F., Rusaouen, G., Brau, J., 2007. Experimental and numerical study of a full scale ventilated enclosure: Comparison of four two equations closure turbulence models. *Building and Environment* 42 1043–1053

Lauder, B.E., Spalding, D.B., 1974. The numerical computation of turbulent flows. *Computer Method in Applied Mechanics and Energy* 3, 269-289.

Moureh, J., Flick, D., 2003. Wall air-jet characteristics and airflow patterns within a slot ventilated enclosure. *International Journal of Thermal Sciences* 42 703–71

Pula, E., Ersan, H.A., 2015. Numerical simulation of turbulent airflow in a ventilated room: Inlet turbulence parameters and solution multiplicity. *Energy And Buildings* 93 227–235

Tapsoba, M., Moureh, J., Flick, D., 2007. Airflow patterns in a slot-ventilated enclosure partially loaded with empty slotted boxes. *International Journal of Heat and Fluid Flow* 28 963-977

Tripathi, B., Moulic, S.G., 2007. Investigation of the buoyancy affected airflow patterns in the enclosure subjected at the different wall temperatures. *Energy and Buildings* 39 906–912

Yu, H., 2006. A Modified Estimation of a Plane Wall Jet Trajectory Horizontally diffused from a Ceiling Slot in Non-isothermal Ventilated Enclosures. *Biosystems Engineering* 95 (2), 255–269

Yu, H., Liao, C.M., Liang, H.M., Chiang, K.C., 2007. Scale model study of airflow performance in a ceiling slot-ventilated enclosure: Non-isothermal condition. *Building and Environment* 42 1142–1150

Xie, J., Qu, X.H., Shi, J.Y., Sun, D.W., 2006. Effects of design parameters on flow and temperature fields of a cold store by CFD simulation. *Journal of Food Engineering* 77 355–363

Modeling and Simulation in Quantitative Risk Assessment

A QUANTITATIVE HUMAN EXPOSURE ASSESSMENT MODEL FOR ANTIBIOTIC-RESISTANT *ESCHERICHIA COLI* THROUGH TAP WATER CONSUMPTION

Eithne O'Flaherty¹

¹ School of Biosystems and Food Engineering,
University College Dublin,
Belfield, Dublin 4,
Ireland

José Luis Balcázar²

²Catalan Institute for Water Research,
Scientific and Technological Park,
University of Girona,
Girona, Spain

Carles M. Borrego^{2,3}

³Group of Molecular Microbial Ecology,
Institute of Aquatic Ecology,
University of Girona,
Girona, Spain

Enda Cummins¹

School of Biosystems and Food Engineering,
University College Dublin,
Belfield, Dublin 4,
Ireland

KEYWORDS

Antibiotic-resistant bacteria, *Escherichia coli*, tap water

ABSTRACT

Clean drinking water is an essential necessity for life, however, antibiotic-resistant bacteria (ARB) have been found in tap water globally. The presence of ARB in tap water could lead to serious infections that are difficult to treat. A quantitative human exposure assessment model was created examining the human exposure to antibiotic resistant *Escherichia coli* (*E. coli*) through drinking water. Both scientific literature and site specific data were used to create the model. Data were collected on the concentration of ARB at a European surface water site located near a drinking water treatment plant (DWTP), the effect of environmental factors, the effect of drinking water treatments and the quantity of human tap water consumption. The results show the human exposure to AR *E. coli* ranged between 3.44×10^{-7} and 2.95×10^{-1} CFU/day. To surpass the EU Drinking Water Directive (0 CFU/100ml of *E. coli* in tap water) a concentration of between 1 and 5 log CFU/ml is required in the source water. The results from this model could be used to recommend water treatments that provide the best reduction of human exposure to ARB.

INTRODUCTION

Serious life threatening infections are being caused by ARB globally. Research shows the presence of ARB in drinking water around the world (Bai et al. 2015; Khan et al. 2016; Xu et al. 2016). This could lead to direct human exposure through the consumption of tap water or indirect exposure through washing fruit and vegetables with tap water. DWTPs are a vital safety mechanism that can help to prevent human exposure to ARB. However, ARB are escaping some water treatment

processes, therefore it is important to identify the most suitable and best combinations of water treatments that can eliminate ARB. A quantitative exposure assessment model was created to examine the human exposure to antibiotic resistant (AR) *E. coli* through tap water consumption.

MATERIAL AND METHODS

Water sampling

Water samples were taken in summer and winter from a European source water site located near the abstraction point of a drinking water treatment plant. Samples were tested for *E. coli* resistant to amoxicillin (Amox), ciprofloxacin (Cipro) and cefotaxime (Cefo). Cefo resistant *E. coli* was not detected at the surface water site.

Model development

The structure and steps involved to create the human exposure assessment model are shown in Figure 1. The first step in the model was finding the concentration of AR *E. coli* at the surface water site. Best fit probability distributions were used to characterise the initial levels of AR *E. coli* found at the surface water site. Scientific literature and site specific data were used to model the effect of environmental factors on the bacteria. Mancini's equation was used, where the equation estimates the decay rate of *E. coli* as an effect of water temperature, surface solar radiation, light extinction coefficient, salinity and depth of water (Mancini 1978). Data from scientific literature were used to model the effect of coagulation, flocculation, sedimentation (Coag/Flocc/Sed), sand filtration, carbon filtration, chlorination, ozone and UV on AR *E. coli* (Langenbach et al. 2009; Pang et al. 2016; Miranda et al. 2016; Lüddecke et al. 2015). Data on the quantity of human tap water consumption per day at the study region were collected from scientific literature (de Francisco

and Martínez Castela 2010). The human exposure to AR *E. coli* through tap water were then estimated by multiplying the concentration of AR *E. coli* after treatment by the amount of tap water consumed. Probability distributions were used to account for uncertainty and variability in the input data.

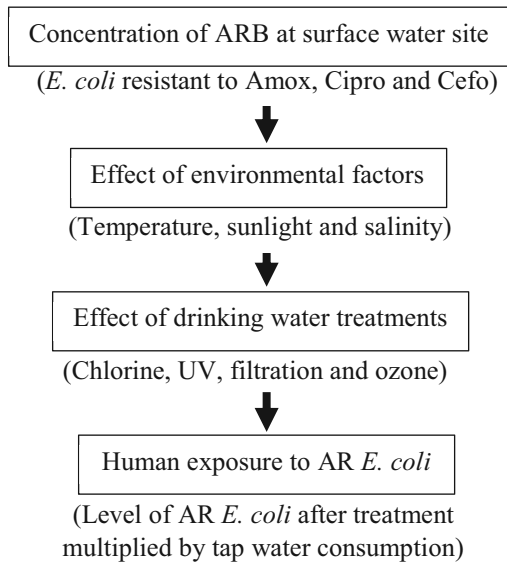


Figure 1: Steps Involved in the Model

Scenario analysis

Scenario analysis was used to investigate the effect of different combinations of water treatments on the AR *E. coli* concentration. Table 1 shows five typical water treatment combinations used in Europe. The water treatment combination used at the study site is scenario 1.

Table 1: Water Treatment Scenarios

Scenario	Water treatment scenarios
1	Coag/Flocc/Sed; Rapid Sand Filtration; Carbon Filtration and Chlorination
2	Coag/Flocc/Sed; Carbon Filtration; Rapid Sand Filtration; Ozone and Chlorination
3	Coag/Flocc/Sed; Slow Sand Filtration and UV
4	Chlorination; Coag/Flocc/Sed; Rapid Sand Filtration; Ozone; Carbon Filtration and Chlorination
5	Coag/Flocc/Sed; Rapid Sand Filtration and Chlorination

Software and Model Run

Monte Carlo Simulation was performed for 10,000 iterations on the model output data, this was done to characterise uncertainty and variability in the model input data. The Spearman's rank order

correlation was performed to examine how the model predictions are dependent on variability and uncertainty in the model input parameters. A back calculation was performed to investigate the concentration of AR *E. coli* required at the abstraction point of the DWTP in order for the EU Drinking Water Directive (Council Directive 98/83/EC, 0 CFU/100ml of *E. coli* in tap water) to be exceeded in the tap water.

RESULTS AND DISCUSSION

Human exposure

Overall the mean human exposure levels to *E. coli* resistant to Cipro and Amox were between 3.44×10^{-7} and 2.95×10^{-1} CFU/day. Scenario 1 (Coag/Flocc/Sed, sand filtration, and UV) provided the lowest human exposure level to AR *E. coli*. Unfortunately the infection dose of AR *E. coli* hasn't been identified and this type of data is critically required to quantify the probability of illness from ARB (Xi et al. 2009; Manaia 2017). If contracted an AR infection is a much more serious infection to treat in comparison to an antibiotic sensitive infection.

Sensitivity analysis

Figure 2 represents the results from the sensitivity analysis examining human exposure to Cipro resistant *E. coli* from the summer samples using scenario 2 water treatments. The results show the largest reduction of AR *E. coli* were from the water treatments, Coag/Flocc/Sed (-0.39); carbon filtration (-0.40), sand filtration (-0.29); ozone (-0.40) and chlorination (-0.34). The positive correlation coefficient value (0.40) for the initial levels of Cipro resistant *E. coli* shows the important of protecting source water sites. The quantity of tap water consumed also had a positive correlation value (0.20). The environmental factors did not have a significant effect on the level of AR. *E. coli* (results not shown, correlation coefficient values were between -0.1 to 0.1).

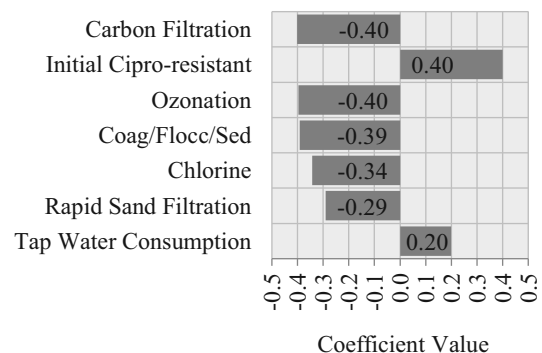


Figure 2: Sensitivity Analysis Results

Back Calculation

To surpass the EU Drinking Water Directive (0 CFU/100ml of *E. coli* in tap water) a concentration of between 1 and 5 log CFU/ml is allowed in the source water depending on the water treatment used. Scenario 1 required the highest quantity of contamination and scenario 5 (Coag/Flocc/Sed; Rapid Sand Filtration and Chlorination) required the least amount of contamination for the EU directive to be exceeded.

CONCLUSION

This model estimated the mean human exposure levels to AR *E. coli* were between 3.44×10^{-7} and 2.95×10^{-1} CFU/day. This model also identified water treatment combinations that provided the largest reduction of AR *E. coli*. The model can help to inform policy makers on the maximum levels of ARB acceptable at source water sites.

FUTURE RESEARCH

To examine the human exposure to AR *E. coli* through recreational and irrigation water.

ACKNOWLEDGEMENT

This work has been financed through the project funded by the Irish Environmental Protection Agency and the Spanish Ministry of Economy and Competitiveness (MINECO) in the frame of the collaborative international consortium of the project TRACE (2014-W-MS-17 and JPIW2013-129) of the Water Challenges for a Changing World Joint Programming Initiative (Water JPI) Pilot Call. CBM and JLB also acknowledge funds from the European Union through the European Regional Development Fund (FEDER) and the Generalitat de Catalunya (2014 SGR 291).

REFERENCES

- Bai, X., Ma, X., Xu, F., Li, J., Zhang, H. and Xiao, X. 2015. "The drinking water treatment process as a potential source of affecting the bacterial antibiotic resistance." *Science of the Total Environment*, 533, 24–31.
- de Francisco, A.L.M. and Martínez Castela, A. 2010. "The Bahía 2008 Study: hydration barometer in the Spanish population." *Nefrología*, 30(2), 220–6
- Khan, S., Knapp, C.W. and Beattie, T.K. 2016. "Antibiotic Resistant Bacteria Found in Municipal Drinking Water." *Environmental Processes*, 3, 541–552.
- Langenbach, K., Kuschk, P., Horn, H. and Kästner, M. 2009. "Slow Sand Filtration of Secondary Clarifier Effluent for Wastewater Reuse." *Environmental Science & Technology*, 43(15), 5896–5901.
- Lüddeke, F., Heß, S., Gallert, C., Winter, J., Güde, H.

and Löffler, H. 2015. "Removal of total and antibiotic resistant bacteria in advanced wastewater treatment by ozonation in combination with different filtering techniques." *Water Research*, 69, 243–251

- Mancini, J.L. 1978. "Numerical Estimates of Coliform Mortality Rates under Various Conditions." *Water Pollution Control Federation*, 50(11), 2477–2484.
- Miranda, A.C., Lepretti, M., Rizzo, L., Caputo, I., Vaiano, V., Sacco, O., Lopes, W.S. and Sannino, D. 2016. "Surface water disinfection by chlorination and advanced oxidation processes: Inactivation of an antibiotic resistant *E. coli* strain and cytotoxicity evaluation." *Science of The Total Environment*, 554–555, 1–6.
- Pang, Y., Huang, J., Xi, J., Hu, H. and Zhu, Y. 2016. "Effect of ultraviolet irradiation and chlorination on ampicillin-resistant *Escherichia coli* and its ampicillin resistance gene." *Frontiers of Environmental Science & Engineering*, 10(3), 522–530.
- Xu, L., Ouyang, W., Qian, Y., Su, C., Su, J. and Chen, H. 2016. "High-throughput profiling of antibiotic resistance genes in drinking water treatment plants and distribution systems." *Environmental Pollution*, 213, 119–126.

AUTHOR BIBLIOGRAPHIES

EITHNE O'FLAHERTY received an Honor's Bachelor degree in Microbiology from the National University of Ireland, Galway, and a Master's Degree in Sustainable Energy and Green technologies from the University College Dublin. She is currently doing a PhD in quantitative risk assessment in the University College Dublin. Email: eithne.o-flaherty@ucdconnect.ie

CARLES BORREGO obtained a Doctoral Degree in Microbiology from the University of Girona. He is Associate Professor of Microbiology at the University of Girona and Research Professor at the Catalan Institute for Water Research. He has expertise on microbial ecology of inland waters and artificial systems related to the urban water cycle. His current work is focused on the effect of anthropogenic pollution on the aquatic environment. Email: cborrego@icra.cat

JOSÉ LUIS BALCÁZAR received his Ph.D. in Animal Pathology from the University of Zaragoza (Spain) in 2006. Since 2009, Dr. Balcázar holds a research scientist position at the Catalan Institute for Water Research (ICRA). He has expertise in environmental microbiology, with a focus on antibiotic pollution and the prevalence and spread ARGs amongst bacteria in aquatic environments. Email: jlbalcazar@icra.cat

MODELLING THE PERSISTENCE OF NANO SILVER THROUGH DRINKING WATER TREATMENTS

David Shevlin & Enda Cummins
Biosystems & Food Engineering,
University College Dublin,
Belfield, Dublin 4,
Ireland
E-mail: david.shevlin@ucdconnect.ie

KEYWORDS

Nanosilver, filtration, water treatment, health.

ABSTRACT

Emerging contaminants such as nano silver (nAg) are likely being released during their use and disposal and maybe accumulating in the environment. This increases the likelihood of nAg entering freshwater environments and contaminating drinking water sources. Water abstraction for drinking water from these sources will likely lead to unintentional abstraction of nAg prior to water purification. Therefore, there is a reliance on drinking water treatment systems to adequately remove nAg prior to human consumption. This model attempts to estimate efficiencies of standard and advanced progressive drinking water treatments by determine residual concentrations of nAg following these treatments. An initial input value to the model is based on a probability distribution with a mean value of $3.67E^{-2}$ $\mu\text{g/L}$ estimated representing a worst-case scenario for Irish waters. Post conventional treatment indicated persisting concentrations of nAg ranging between $1.31E^{-2}$ to $4.85E^{-3}$ $\mu\text{g/L}$ depending on the coagulant used. Total removal was not observed during conventional treatment but was significantly removed to below tolerable ingestion levels. Residual concentrations were then subjected to advance filtration methods through several progressive scenarios to estimate removal following each advanced treatment.

INTRODUCTION

Nanomaterials are entering the environment in ever increasing volumes and likely accumulating in water sources (Shevlin *et al.* 2018). Oxidizable nano silver (nAg), an engineered nanomaterial is utilized in numerous products and processes due in part to its antimicrobial properties and the functional performance of nano scale silver. Nanomaterials are classified as materials in the scale of 1 – 100 nm in at least one dimension (Shevlin *et al.* 2018). Presence and accumulation of these materials in drinking water sources increases the potential for these reactive materials to be inadvertently recovered during drinking water abstraction. Abstracted water from lakes, rivers and reservoirs is subjected to drinking water treatment prior to distribution in the water network. Conventional water treatment used to remove contaminants and biological entities may be ineffective or inefficient for removal of nAg (Chalew *et al.* 2013). Therefore, advanced and costly treatments may need to be employed to remove the potentially increasing concentrations of nAg likely to be present in source water. Adequate treatment must be ensured to reduce the risks to human health through inadvertent exposure to nAg present in treated drinking water. Nano Ag can penetrate cellular

membranes and potentially interfere with cellular functions inducing a human toxicity concern.

Treatment processes

Conventional water treatment is divided into primary and secondary treatment followed by disinfection prior to distribution in the water network.

Primary treatment

Abstracted water is initially subjected to preliminary treatment for the removal of macro scale entities prior to the primary treatment. During primary treatment, chemicals are added to the system to aid the coagulation of colloid and particulate matter (U.S. Epa 2011). Coagulation is followed by flocculation whereby coagulated material clusters together to form larger flocs. Increase in flocculants increases mass and density which will cause eventual sedimentation of the floc. Entrapment of nAg within flocs will aim in removal of nAg to sediment.

Secondary treatment

Filtration is the next step in water purification following primary treatment and is performed through slow or rapid sand filtration. This process removes biological and fine particulate matter and likely to capture nAg through absorption.

Advanced treatments

Microfiltration – low pressure technology using a pore size between 0.1 and 10 μm .

Ultrafiltration – low pressure technology using a pore size between 0.01 and 0.4 μm .

Nanofiltration and Reverse osmosis– High pressure technology used for the removal of dissolved contaminants.

Ingestion of silver

Currently no guideline limits are attributed to the nanoform of silver, so it was necessary to draw from data relating to the macroform as set by governing bodies. The World Health Organisation (WHO) and the US-EPA set guideline limits of $0.005 \text{ mg/kg/d}^{-1}$ while the European Food Safety Authority (EFSA) set a guideline of 0.05 mg/kg in food and water (Scenihr 2013). The WHO limit is based on a No Observable Adverse Effect Level (NOAEL) for humans. This limit value is based on a lifetime exposure (70 yrs. or 25550 days) giving a NOAEL of $0.39 \text{ mg / person / day}$ or (bw = 70 kg) $0.005 \text{ mg/kg bw/d}^{-1}$.

METHODOLOGY

Surface water concentrations

Measured data pertaining to surface water concentrations of nAg in Irish waters is not available. Therefore, an estimate of surface water concentrations is represented through a Triangular probability distribution using estimates from available literature sources representing a worst-case scenario for Irish waters. A mean value of $3.67E^{-2}$ was used as the initial input value ($A_{\text{surface conc}}$) to the model. All model simulations were developed using the Microsoft Excel add on software @Risk7 (Palisade Software, Ithaca, NY, USA) and run for 10,000 iterations.

Model framework

A mass balance model (fig. 1) was developed using the $A_{\text{surface conc}}$ value as the initial input value. Percentage reductions following each treatment scenario was then assessed to calculate the likely residual concentrations.

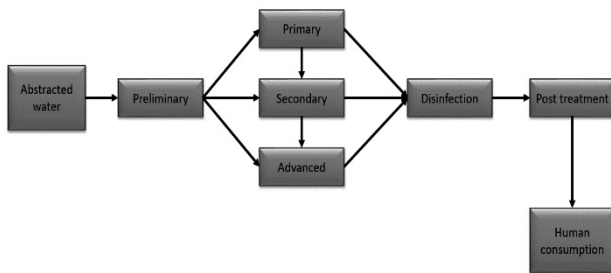


Fig. 1 Schematic overview of model showing water abstraction from surface waters and subsequent drinking water treatment processes applied for removal of nAg.

Estimating nAg removal during treatment

When estimating the removal of nAg through each process it was necessary to bridge data gaps due to insufficient studies primarily focusing on nAg. This was done with other nano scaled materials or bulk forms of metals. Probability distribution were developed for each process based on available data and are represented in Table 1.

Table.1 Probability distributions for the estimation of removal potential through each treatment process in the presence of coagulant.

Process	Coagulant	Distribution	Mean
Primary	Alum	Normal (0.80,0.13)	0.80
	FeCl ₃	Uniform (0,0.91)	0.91
	FeSO ₄	Uniform (0,0.9)	0.92
Secondary	n/a	Uniform (0.35,0.4)	0.38

Estimated removal through advanced treatments

Residues of nAg present in post-secondary treatment were then subjected to further reduction through advanced treatments. Estimates of removal are presented (Table 2)

through probability distributions to account for the variability and uncertainty in the data.

Table 2. Model inputs with probability distributions estimating the removal potential progression through each treatment.

Description	Symbol	Unit	Distribution/model
Initial concentration	$A_{\text{surface conc}}$	µg/L	($3.67E^{-2}$ mean)
Primary treatment	P_t	%	Table 1
Secondary treatment	S_t	µg/L	Table 1
Post secondary treatment	PS_t	µg/L	$PS_t = PP_t \times (1 - S_t)$
Microfiltration	M_f	*Prob	Normal (0.47,0.98)
Post microfiltration	PM_f	µg/L	$PM_f = PS_t \times (1 - M_f)$
Ultrafiltration	U_f	*Prob	Normal (0.982,9.024)
Post ultrafiltration	PU_f	µg/L	$PU_f = PM_f \times (1 - U_f)$
Nanofiltration	N_f	*Prob	Uniform (0.47,0.98)
Post nanofiltration	PN_f	µg/L	$PN_f = PU_f \times (1 - N_f)$
Reverse osmosis	R_o	*Prob	Uniform (0,0.993)
Post reverse osmosis	PR_o	µg/L	$PR_o = PN_f \times (1 - R_o)$

*Probability distributions

Advanced filtration scenarios

Following conventional primary and secondary treatment, residual nAg concentrations were subjected to advanced filtration methods through several scenarios (Table 3).

Table 3. Scenarios for modelled treatments

Scenario	Treatment	Equation
1	$P_t + S_t$	$= PP_t \times PS_t$
2	$S_t + M_f$	$= PP_t \times PS_t \times (1 - M_f)$
3	$S_t + M_f + U_f$	$= PP_t \times PS_t \times PM_f \times (1 - U_f)$
4	$S_t + M_f + U_f + N_f$	$= PP_t \times PS_t \times PM_f \times PU_f \times (1 - N_f)$
5	$S_t + M_f + U_f + N_f + R_o$	$= PP_t \times PS_t \times PM_f \times PU_f \times PN_f \times (1 - R_o)$

Exposure assessment

Exposure levels through human consumption of post treated water for each demographic group was calculated using formula (1) with daily ingestion volumes for drinking water for the Irish population.

$$D = C \times IR / BW \quad (1)$$

Where: D = Exposure dose (mg/kg/d⁻¹)
 C = Contaminant concentration (mg/L)
 IR = Intake rate of contaminated water (L/d⁻¹)
 BW = Body weight (kg)

Table.4 Daily drinking water patterns for Irish population

Demographic group age (yrs.)	(IR) Mean ± SD	(BW) Mean ± SD
Adult male (18-64)	0.58 ± 0.67	86.2 ± 15
Adult female (18-64)	0.55 ± 0.56	70 ± 13.7

RESULTS AND DISCUSSION

Predicted nAg removal through the conventional treatment processes reduced the $A_{\text{surface conc}}$ by 1-2 orders of magnitude which is significantly lower than the guideline limits set by the WHO, EFSA and US-EPA for silver in drinking water. The continued reduction of $A_{\text{surface conc}}$ residuals through each treatment stage are presented in Table 5.

Table 5. Residuals mean values after water treatments with 5th and 95th percentiles.

Treatment		Mean ($\mu\text{g/L}$)	5 th	95 th
Scenario 1	Alum	2.35E ⁻⁴	0	8.40E ⁻⁴
Scenario 2		3.37E ⁻⁵	0	1.51E ⁻⁴
Scenario 3		6.34E ⁻⁷	0	4.12E ⁻⁶
Scenario 4		1.74E ⁻⁷	0	1.15E ⁻⁶
Scenario 5		3.08E ⁻⁸	0	2.07E ⁻⁷
Scenario 1	FeCl ₃	2.13E ⁻³	0	7.83E ⁻³
Scenario 2		3.08E ⁻⁴	0	1.39E ⁻³
Scenario 3		5.65E ⁻⁶	0	3.69E ⁻⁵
Scenario 4		1.58E ⁻⁶	0	1.01E ⁻⁵
Scenario 5		2.78E ⁻⁷	0	1.83E ⁻⁶
Scenario 1	FeSO ₄	1.90E ⁻³	2.81E ⁻⁴	4.46E ⁻³
Scenario 2		2.76E ⁻⁴	0	8.97E ⁻⁴
Scenario 3		5.17E ⁻⁶	0	2.71E ⁻⁵
Scenario 4		1.42E ⁻⁶	0	7.97E ⁻⁶
Scenario 5		2.49E ⁻⁷	0	1.41E ⁻⁶

Human exposure through drinking water ingestion

Preliminary exposure estimates through consumption of drinking water for the demographic groups incorporated in this assessment were calculated using (equation 1) for their daily drinking water consumption patterns (Table 4). The greatest exposure was observed for both demographic groups following consumption of water treated with conventional treatments. Exposure was significantly reduced with each additional advanced treatment. Adult male (18 – 64 years) exposure to residual nAg in post treated water for scenario 1 (Alum Coagulant) indicated a mean exposure of 1.62E⁻⁹ (90th percentile range 0 - 7.29E⁻⁹) mg/L. Exposure was significantly lowered in scenario 5 (incorporating Reverse osmosis) with mean exposure of 2.08E⁻¹³ (90th percentile range 0 - 1.21E⁻¹²) mg/L. Water treated with FeCl₃ coagulant resulted in a mean exposure level of 1.46E⁻⁸ (0 - 6.48E⁻⁸) mg/L to 1.89E⁻¹² (0 - 1.12E⁻¹¹) mg/L for scenarios 1 and scenario 5, respectively. Water treated with FeSO₄ coagulant indicated a mean exposure of 1.32E⁻⁸ (4.63E⁻¹⁰ - 4.63E⁻⁸) mg/L to 1.71E⁻¹² (0 - 9.29E⁻¹²) mg/L for scenario 1 and scenario 5, respectively.

Adult female (18 – 64 years) exposure to residual nAg in post treated water for scenario 1 (Alum Coagulant) indicated a mean exposure of 1.92E⁻⁹ (90th percentile range 0 – 8.31E⁻⁹) mg/L. Exposure was significantly lowered in scenario 5 (incorporating Reverse osmosis) with mean exposure of 2.55E⁻¹³ (90th percentile range 0 - 1.55E⁻¹²) mg/L. Water treated with FeCl₃ coagulant resulted in a mean exposure level of 1.76E⁻⁸ (0 – 7.93E⁻⁸) mg/L to

2.27E⁻¹² (0 - 1.44E⁻¹¹) mg/L for scenario 1 and 5, respectively. Water treated with FeSO₄ coagulant indicated a mean exposure of 1.57E⁻⁸ (9.21E⁻¹⁰ – 5.36E⁻⁸) mg/L to 2.08E⁻¹² (0 – 1.12E⁻¹¹) mg/L in scenario 1 and 5, respectively.

Exposure levels of residual nAg in post treated water predicted in this model are significantly below levels likely to result in an acute toxicity concern for human health through consumption of treated drinking water. The chronic exposure to residual nAg is still uncertain.

CONCLUSION

Conventional treatment indicated in this model that AgNPs are sufficiently removed to below levels likely to cause an acute toxicity concern to human health. Advanced treatment is therefore unnecessary at this juncture for removal of nAg based on current estimated concentrations of nAg in water sources. Although, as environmental concentrations increase these may need to be reassessed.

ACKNOWLEDGEMENTS

The authors would like to acknowledge financial support from the Irish Environmental Protection Agency for this work under the EPA Research Program 2014-20.

REFERENCES

- Chalew, T.E.A., Ajmani, G.S., Huang, H., Schwab, K.J. (2013) 'Evaluating Nanoparticle Breakthrough during Drinking Water Treatment', *Environmental Health Perspectives*, 121(10).
- Scenihr (2013) *Nanosilver: Safety, Health and Environmental Effects and Role in Antimicrobial Resistance*, Biochemical Pharmacology.
- Shevlin, D., O'Brien, N., Cummins, E. (2018) 'Silver engineered nanoparticles in freshwater systems – Likely fate and behaviour through natural attenuation processes', *Science of The Total Environment*, (621C), 1033–1046.
- U.S. Epa (2011) 'Drinking Water Treatment Plant Residuals. Management Technical Report. Summary of residuals generation, treatment and disposal at large community water systems.', (September 2011), 378.

BIOGRAPHY

David Shevlin was born in Dublin, Ireland. Obtained his degree in 2015 from Dundalk Institute of Technology (DKIT), Ireland and went on to further studies in University College Dublin (UCD), Ireland.

QUANTITATIVE RISK ASSESSMENT OF ANTIMICROBIALS IN THE FEED TO FOOD CHAIN

Rachel Clarke
School of Biosystems and Food
Engineering, University College Dublin,
Dublin, Ireland
Email: Rachel.clarke.1@ucdconnect.ie

Mark G Healy
Civil Engineering, National University
Of Ireland, Galway, Ireland

Owen Fenton
Teagasc, Environmental
Research Centre, Co. Wexford, Ireland

Enda Cummins
School of Biosystems and Food
Engineering, University College
Dublin, Dublin, Ireland

KEYWORDS

Biosolids, Contaminants, foodchain, human exposure, risk

ABSTRACT

A feed to food chain risk assessment model was developed to assess the fate of the contaminants triclosan (TCC) and triclocarban (TCC) from spreading biosolids on land. The model considered parameters such as; concentration in soil, plant uptake, bio-transfer into milk and beef, and resulting human exposure. Transfer of TCS and TCC from biosolid application, biotransfer into milk and beef followed by human consumption was considered minimal. From the scenarios considered, the greatest exposure of TCC was through milk for infants and beef for teens (mean values 1.14×10^{-7} mg kg⁻¹ bw d⁻¹, 7.41×10^{-8} mg kg⁻¹ bw d⁻¹, respectively). TCS and TCC levels were well below the estimated acceptable daily intake (ADI). Therefore, the concentrations of TCS and TCC in beef and milk represent a minor exposure pathway for humans.

INTRODUCTION

The use of biosolids on grasslands could be a pathway through which emerging contaminants may be taken up by plants and enter the foodchain *via* grazing animals. This may result in potential human exposure *viz* consumption of animal derived food products (e.g. milk, meat). Once an emerging contaminant is released into the soil it may be degraded by biological, physical or chemical processes, leach through to groundwater, transported to surface waters, stick to the soil particles or be uptaken by plants (Boxall 2012). The transfer of emerging contaminants from soil to plant has been well documented (Boxall et al., 2006, Sabourin et al., 2012, Prosser and Sibley, 2015). However, there are significant knowledge gaps regarding the uptake of emerging contaminants from plant to animal and subsequent human exposure. The antimicrobials triclosan (TCS) and triclocarban (TCC) may have the potential to bioaccumulate in soil-dwelling organisms and thus exert toxic effects on higher organisms through trophic transfer (Clarke et al., 2016). TCS and TCC are highly hydrophobic and bioaccumulate in organisms living in aquatic systems exposed to effluent from wastewater treatments (Halden et al., 2017). The aim of this study was to develop a feed to

food chain risk assessment model to estimate the potential of antimicrobials (triclosan and triclocarban) to translocate from biosolids applied to agricultural land with transmission into plants (grass), animal forage and potential human exposure through consumption of products of animal origin (e.g. milk and meat).

MATERIALS AND METHODS

Predicted environmental concentration in soil

Following an application of biosolids to agricultural land the level of contaminant in the soil (C_{soil} ; mg kg⁻¹) was calculated according to Eq. 1 (EC 2003a). This incorporates many farm level management practices (e.g. application rate, mixing depth) and soil characteristics (e.g. bulk density).

$$C_{soil} = (C_{sludge} \times APPL \times (1 - f_{int}/100)) / (D \times BD) \quad (1)$$

Where:

C_{sludge} is the concentration of TCS and TCC in biosolids (mg kg⁻¹). APPL is the application rate of biosolids on agricultural land for one application (kg m⁻²). f_{int} is the fraction intercepted by the crop expressed as a percentage (%). D is the depth (m). BD is the soil bulk density (kg m⁻³).

The effective concentration of contaminants available for plant uptake was adapted from Chişescu et al. (2014) to suit Irish conditions (i.e. organic matter content) and was calculated according to Eq. 2.

$$PEC_{porewater} = PEC_{soil} / (F_{oc} \times K_{oc}) \quad (2)$$

Where $PEC_{porewater}$ is the concentration of TCS and TCC in the pore water (mg kg⁻¹). F_{oc} is the fraction of organic matter content (F_{oc}) in the soil; and K_{oc} is the soil organic carbon-water partitioning coefficient of the contaminants. K_{oc} is the organic carbon-soil sorption coefficient (L kg⁻¹).

The passive transport of organic contaminants from soils to plants is calculated using a partition-limited model (Chiou et al., 2001).

$$C_{pt} = \alpha_{pt} \times PEC_{porewater} \times [f_{pw} + f_{ch} \times K_{ch} + f_{lip} \times K_{lip}] \quad (3)$$

Where C_{pt} is the concentration of the contaminant in the whole plant or in a specific part of that plant on a fresh weight base (mg kg^{-1}); f_{pw} , f_{lip} and f_{ch} are the weight fraction of the water, lipids and the sum of carbohydrates, cellulose, and proteins in the plant that are assumed to have approximately the same partition coefficients K_{ch} ; K_{lip} is the partition coefficient for the lipids fraction of the plant assumed to be equal to the log K_{ow} ; α_{pt} is the quasi-equilibrium factor, the ratio of the respective concentrations in plant water and external water, with $\alpha_{pt} = 1$ denoting the state of equilibrium. The magnitude of $\alpha_{pt} < 1$ is a measure of the distance to equilibrium (Chiou et al., 2001). It was assumed that organic compound partitions between plant and water and various organic components were also concentration-independent, as such the α_{pt} values are approximately independent of contaminant concentrations in soil (Chiou and Kile, 1998).

Transfer model

Potential intake of TCS and TCC by bovines relates both to feed consumption and soil ingestion. According to Chişescu et al., (2014) the daily intake of TCS or TCC by cow's can be calculated by:

$$DI = PEC_{soil} \times F_{soil} + C_{pt} \times F_{pt} + C_{plant} \times F_{pt} \quad (4)$$

Where DI is the daily intake of TCS or TCC for grazing animals (Cows and sheep) (mg d^{-1}); F_{soil} is the daily intake of soil by grazing animals (cows and sheep). F_{pt} is the daily intake of feed by grazing animals (cows and sheep). Values of 0.1 kg d^{-1} (Chişescu et al., 2014) and 0.9 kg d^{-1} (Duarte Davidson and Jones 1996) were used to account for the cow's consumption of soil and a uniform distribution (min 0.1, max 0.9) was assigned to account for the uncertainty. It has been reported that a cow can consume between 12 and 18 kg d^{-1} dry matter (Mc Gilloway and Mayne 1996). To account for variability and uncertainty, a uniform distribution was also assigned.

The bio-transfer factor

The BTF represents the ratio of the concentration of a contaminant found in animal tissues such as beef or milk to the animal's daily intake of the contaminant/chemical in mass of contaminant per day (USEPA 2005).

Equations 5 and 6 show the BTF's for each chemical in beef (BTF_b) and milk (BTF_m) as follows:

$$\text{Log BTF}_b [\text{mgkg}^{-1}/\text{mg d}^{-1}] = -7.735 + 1.033 \times \text{log}K_{ow} \quad (5)$$

$$\text{Log BTF}_m [\text{mgkg}^{-1}/\text{mg d}^{-1}] = -8.056 + 0.992 \times \text{log}K_{ow} \quad (6)$$

Measured concentrations of TCS and TCC in beef or milk fat are converted to a fresh meat or whole milk basis. The

residue concentrations of TCS and TCC in beef and milk are calculated by:

$$C_{m/b} = \text{BTF}_{(b, m)} \times \text{DI} \times \text{FC}_{(\text{milk, beef})} \quad (7)$$

Where C_m and C_b is the TCS and TCC residue concentrations in beef and milk (mg kg^{-1}); The average fat content of milk and beef is denoted by FC_{milk} and FC_{beef} , respectively. It was reported that the average fat content of milk (FC_{milk}) is 3.7% (ICOS) (2009) with a value of 4% reported by Chişescu et al. (2014). Uncertainty in the data was accounted for by incorporating a uniform distribution. Hendriks et al., (2007) reported that the average fat content in beef tissue can range extensively from 7.5% to over 27%. To account for uncertainty a uniform distribution (7.5, 27) was also used.

Human Exposure

The level of human exposure (HE) is calculated based on the quantity of milk and beef consumed using equation 8.

$$\text{HE} = C_{m/b} \times M_c / \text{bw} \quad (8)$$

Where HE denotes human exposure ($\text{mg kg}^{-1} \text{ BW d}^{-1}$); M_c is the consumption of milk or beef a day, and BW represents the body weight of the individual. The Irish Universities Nutrition Alliance (IUNA) database on nutritional surveys was used to obtain data on milk and beef consumption values of the various age groups. A log normal distribution was used to model the uncertainty regarding the intake of milk and beef.

Acceptable daily intake

The ADI is defined as the approximate exposure incurred daily over an entire lifetime (expressed on a bodyweight basis) without appreciable risks to health multiplied by an appropriate safety factor (EC 2003). The European Commission Health and Consumer Protection Directorate-General (2005) suggest a safety factor of 300 composing of three factors; 10 is for each intra-species, 10 is for each inter-species and 3 is for a limited database of studies (Prosser et al., 2015).

$$\text{ADI} (\text{mg kg}^{-1} \text{ BW d}^{-1}) = \text{NOAEL} / 10 \times 10 \times 3 \quad (9)$$

Sensitivity analysis

A Sensitivity analysis was used to identify the sources of uncertainty that exert the most influence on the risk assessment outputs. Microsoft Excel 2010 with the add-on package @Risk (version 6.0, Palisade Corporation, New York, USA) was used to perform the simulation using Monte Carlo sampling with 10,000 iterations. The model resulted in a number of output distributions which can be used to predict daily risk of exposure.

RESULTS AND DISCUSSION

Table 1 shows the concentration of TCS and TCC in soil (PEC_{soil}) following one application of biosolids to agricultural land. TCC had a greater concentration in biosolids compared to TCS (mean values $3.89 \times 10^{-2} \text{ mg kg}^{-1}$

¹,TCC and 2.42×10^{-2} mg kg⁻¹ for TCS) (Table 1). Fu et al., (2016) reported that biosolid amendment changes soil physio-chemical properties, which in turn alters the persistence of TCS and TCC, hence the risk for secondary contaminantion such as plant uptake.

Table 1. Concentrations (mean, 5th and 95th percentiles) of TCS and TCC in soil, plant tissue and daily intake

Compound	Mean PECsoil (mg kg ⁻¹)	Mean Concentration Plant Tissue (mg kg ⁻¹)		Daily Intake (mg d ⁻¹)
		(5 th , 95 th percentile)		
Triclosan	2.42E-02 (5.12E-03, 5.30E-02)	1.22E-05 (6.28E-07,497E-05)		1.23E-02 (1.73E-03, 3.33E-02)
Triclocarban	3.89E-02 (8.67E-03, 8.79E-02)	1.40E-05 (1.20E-06, 4.52E-05)		1.98E-02 (2.66E-03, 5.41E-02)

Mean concentration of TCS and TCC in plant tissue show that TCC had a greater concentration. Fu et al., (2016) reported an inhibitory effect of biosolids on plant uptake of TCS suggesting that TCS became less bioavailable in biosolid-amended soils. TCC had a greater daily intake rate, with a mean value of 1.98×10^{-2} mg d⁻¹ compared to TCS with 1.23×10^{-2} mg d⁻¹ (Table 1).

The results for mean residue concentrations show that TCC had the greatest concentration in beef and milk (mean values 1.36×10^{-4} mg kg⁻¹, and 7.77×10^{-6} , respectively). The results indicate the potential for bioaccumulation (log k_{ow} 4.9 and 4.6, respectively). The results for predicted mean human exposure to TCS and TCC in beef and milk are shown in Table 2. Human exposure to TCC in beef was greater for the teen group (mean value 7.41×10^{-8} mg kg⁻¹ bw d⁻¹). Human exposure to TCC in milk was greater for the infant group (mean value 1.14×10^{-7} mg kg⁻¹ bw d⁻¹) (Table 2). However, all human exposure values were below the ADI threshold values of 0.10 mg kg⁻¹ bw d⁻¹ for TCS and 0.13 mg kg⁻¹ bw d⁻¹ for TCC.

Table 2. Mean exposure to TCS and TCC from beef and milk (mg kg⁻¹ bw d⁻¹)

	Infant (mg kg ⁻¹ bw d ⁻¹)	Child (mg kg ⁻¹ bw d ⁻¹)	Teen (mg kg ⁻¹ bw d ⁻¹)	Adults (mg kg ⁻¹ bw d ⁻¹)
Beef				
TCS	3.53E-10 (4.55E-12,1.37E-09)	5.08E-10 (6.64E-12,1.89E-09)	1.37E-09 (4.10E-11,5.16E-09)	6.71E-10 (1.78E-11,2.65E-09)
TCC	1.89E-08 (1.04E-12,6.85E-08)	2.70E-08 (1.24E-12,8.67E-08)	7.41E-08 (7.23E-12,3.21E-07)	3.58E-08 (3.18E-12,1.46E-07)
Milk				
TCS	2.66E-09 (1.74E-10,9.38E-09)	5.95E-11 (1.66E-12,2.26E-10)	3.17E-11 (1.16E-12,1.20E-10)	3.14E-11 (1.08E-12,1.21E-10)
TCC	1.14E-07 (2.90E-11,5.82E-07)	2.75E-09 (3.53E-13,1.12E-08)	1.29E-09 (2.26E-13,5.82E-09)	1.49E-09 (2.05E-13,6.44E-09)

Sensitivity analysis was measured by Spearman's rank order correlation. Analysis indicated that the Kow was the most important input (correlation coefficient value 0.90) that affected the variance in model predictions. This indicates the importance of the persistence of TCS and TCC and the potential to accumulate in sludge and soil in affecting exposure estimates. The initial concentration of the contaminants in sludge (C_{sludge}) (correlation coefficient value 0.20) was another input of importance. This indicates the importance of removal during wastewater treatment,

thus, limiting the potential transmission of TCS and TCC from biosolid application through to the food chain.

Conclusion

In this study a quantitative feed to food chain risk assessment model was developed to assess the concentrations of TCS and TCC in biosolids, plant uptake, animal transfer and subsequent human exposure. Biosolid spreading is considered to be the main route of these compounds to the environment. Concentrations of TCC were greater in all environmental compartments and human exposure pathways. The study showed that infants and teens had the highest level of exposure from milk and beef, respectively. However, predicted human exposure values were well below the ADI. Sensitivity analysis indicated the importance of the Kow and the physio-chemical factors that influence the persistence of TCS and TCC in the sludge. Cross-resistance to antibiotics stimulated by TCS and TCC has also been investigated and discovered in many pathogenic bacteria. Therefore, more research is needed to understand the role of TCS and TCC have on human health.

Acknowledgement

The authors acknowledge the training support of the ERASMUS + programme of the European Union (grant 2014-1-MT01-K200-000327)

REFERENCES

- BOXALL, A. B. A., JOHNSON, P., SMITH, E. J., SINCLAIR, C. J., STUTT, E. & LEVY, L. S. 2006. Uptake of Veterinary Medicines from Soils into Plants. *Journal of Agricultural and Food Chemistry*, 54, 2288-2297.
- BOXALL, A. B. A. 2012. New and Emerging Water Pollutants arising from Agriculture. OECD. Available at <http://www.oecd.org/tad/sustainable-agriculture/49848768.pdf>
- CHIOU C. T. and Kile D. E. 1998. Deviations from Sorption Linearity on Soils of Polar and Nonpolar Organic Compounds at Low Relative Concentrations *Environmental Science & Technology*, 32 (3), 338-343 DOI: 10.1021/es970608g
- CHIOU, C. T., SHENG, G. & MANES, M. 2001. A partition-limited model for the plant uptake of organic contaminants from soil and water. *Environmental science & technology*, 35, 1437-1444.
- CHIȚESCU, C. L., NICOLAU, A. I., RÖMKENS, P. & VAN DER FELS-KLERX, H. J. 2014. Quantitative modelling to estimate the transfer of pharmaceuticals through the food production system. *Journal of Environmental Science and Health, Part B*, 49, 457-467.
- CLARKE, R. M. & CUMMINS, E. 2014. Evaluation of "Classic" and Emerging Contaminants Resulting from the Application of Biosolids to Agricultural Lands: A Review. *Human and Ecological Risk Assessment: An International Journal*, 21, 492-513.

- CLARKE, R., HEALY, M. G., FENTON, O. & CUMMINS, E. 2016. A quantitative risk ranking model to evaluate emerging organic contaminants in biosolid amended land and potential transport to drinking water. *Human and Ecological Risk Assessment: An International Journal*, 22, 958-990.
- DUARTE-DAVIDSON, R. & JONES, K. C. 1996. Screening the environmental fate of organic contaminants in sewage sludge applied to agricultural soils: II. The potential for transfers to plants and grazing animals. *Science of The Total Environment*, 185, 59-70.
- EC (European Commission). 2003a. Technical Guidance Document on Risk Assessment in support of Commission directive 93/67/EEC on Risk Assessment for new notified substances. Commission regulation (EC) No1488/94 on Risk Assessment for Existing substances, Directive 98/8/EC of the European Parliament and of the Council concerning the placing of biocidal products on the market. Available at https://echa.europa.eu/documents/10162/16960216/tgdpa_r2_2ed_en.pdf. Accessed March 2016.
- EC (European Commission). 2003b. Introduction to risk assessment. Available at http://ec.europa.eu/health/ph_projects/2003/action3/docs/2003_3_09_a23_en.pdf. Accessed July 2016.
- EC (European Commission). 2005. Health and Consumer Protection Directorate-General, 2005. Scientific Committee on Consumer Products - Opinion on Triclocarban. European Commission Health and
- FU, Q., WU, X., YE, Q., ERNST, F. & GAN, J. 2016. Biosolids inhibit bioavailability and plant uptake of triclosan and triclocarban. *Water Research*, 102, 117-124.
- HALDEN, R. U., LINDERMAN, A. E., AIELLO, A. E., ANDREWS, D., ARNOLD, W. A., FAIR, P., BLUM, A. (2017). The Florence Statement on Triclosan and Triclocarban. *Environmental Health Perspectives*, 125(6),064501. <http://doi.org/10.1289/EHP1788>
- ICOS (Irish Cooperative Organisation Society). (2009). International milk production comparisons. Available at <http://www.icos.ie/supply-chain/transport-quality/>. Accessed July 2016.
- MC GILLOWAY D.A. and MAYNE C.S. (1996). The importance of grass availability for the high genetic merit dairy cow. In: 'Recent Advances in Animal Nutrition' 1996; Eds. P.C. Garnsworthy, J. Wiseman and W. Haresign. Chp. 8, 135-169.
- PROSSER, R. & SIBLEY, P. 2015. Human health risk assessment of pharmaceuticals and personal care products in plant tissue due to biosolids and manure amendments, and wastewater irrigation. *Environment international*, 75, 223-233.
- SABOURIN, L., DUENK, P., BONTE-GELOK, S., PAYNE, M., LAPEN, D. R. & TOPP, E. 2012. Uptake of pharmaceuticals, hormones and parabens into vegetables grown in soil fertilized with municipal biosolids. *Science of The Total Environment*, 431, 233-236.
- USEPA (U.S. Environmental Protection Agency). (2005). Methodology for predicting cattle biotransfer factors, EPA Contract Number 68-W-03-042, Research Triangle Institute. Available at <https://archive.epa.gov/epawaste/hazard/tsd/td/web/pdf/btfreportfull05.pdf>. Accessed February 2016. Accessed June 2016.

BIOGRAPHY

Rachel Clarke was born in County Dublin, Ireland and went to Trinity College Dublin where she obtained her degree in environmental science in 2011. She went on to obtain a Masters in Science degree in Sustainable Energy and Green Technologies from University Collge Dublin She has completed a PhD in 2017 in the area of emerging contaminants in biosolids and risk assessment from University College Dublin. She currently works for the Environmental Protection Agency in health and wellbeing research management.

NEXT GENERATION MICROBIOLOGICAL RISK ASSESSMENT: NEXT GENERATION SEQUENCING (NGS) FOR THE DETERMINATION OF FISH FLESH MICROBIOTA

Theofania Tsironi, Vassiliki Nefel Simou, Afrodite Mexi, Lougovois Vladimiros, Koussissis Stamatis and Dimitra Houhoula

Department of Food Technology
Faculty of Food Technology and Nutrition
Technological Educational Institute of Athens,
Agiou Spyridonos 12210, Athens Egaleo, Greece
E-mail: dhouhoula@teiath.gr

KEYWORDS

Fish, next-generation sequencing, spoilage bacteria, pathogens, 16S rRNA.

ABSTRACT

The objective of the study is the assessment of the microbial ecology and safety of fisheries in Greece using next-generation sequencing (NGS). 14 fish samples were obtained from local fish stores (Greece) within 1 day from capture. The initial microbiota in fish flesh was determined using next-generation sequencing (NGS). The main pathogenic bacterial species identified in the tested fish samples included *Vibrio* spp., *Clostridium* spp., *Staphylococcus*, *Flavobacterium* and *Janthinobacterium* representing both native freshwater habitats and contaminants arising from different sources, including sewage and direct contamination by wild animals, livestock, and feed. The initial spoilage microbiota of fish consisted of various psychrotrophic Gram-negative bacteria, mainly *Pseudomonas*, *Acinetobacter*, *Moraxella*, *Shewanella*, *Psychrobacter*, *Lactobacillus*, *Brochothrix* and *Photobacterium*. The results of the study indicate the applicability and usefulness of NGS for the determination of microbial flora associated with food-borne diseases and spoilage in fish products.

INTRODUCTION

Food borne diseases represent a threat for both public health and the economy in Europe. Overall, there are more than 250 different food borne diseases. Most of them are bacterial infections. A number of bacterial illnesses might be attributed to seafood consumption that has been contaminated either at source or either during processing and/or retail display. Such illness cases may be related to infection with bacteria or the ingestion of toxins having been produced in the food product prior to consumption. Along with human non-pathogenic bacteria and natural microflora relevant to the aquatic environment, pathogenic bacteria are often isolated from fish. According to the European Food Safety Authority and the literature, pathogens such as *Campylobacter*, *Salmonella*, *Yersinia*, *E. coli*, and *Listeria*

monocytogenes are responsible for major foodborne outbreaks worldwide (Leisner & Gram, 1999; Novoslavskij et al., 2016). Fish is also the most commonly implicated food category in outbreaks. Each year in the United States, ~260,000 people get sick from contaminated fish (Barrett et al., 2015). According to FAO (2018), disease or illness outbreaks from fish and shellfish in the EU between 1983 and 1992 ranged from 1.9 percent of total food-borne outbreaks in United Kingdom (Scotland) to 12.4 percent in Denmark. When the known food source was identified the range of fish and shellfish outbreaks was from 4.4 percent in the United Kingdom (England/Wales) to 16.1 percent in Finland. However, not all pathogens are associated with foodborne outbreaks through the consumption of contaminated fish and fish products.

At the same time, there is an increasing consumer demand worldwide for high quality fish products. However, fresh fish is a significantly perishable food product due to its composition and its spoilage is attributed mainly to bacterial activity. Hygiene practices and temperature during handling, transportation and storage are the most important factors that determine fresh fish safety and quality up to the consumer level. *Pseudomonas* spp. is reported as the dominant spoilage microorganism in aerobic storage of fresh, chilled fish (Giuffrida et al., 2013). *Pseudomonas* spp. growth has also been reported as an adequate quality index for shelf life evaluation of aerobically stored Mediterranean fish, such as gilthead seabream (*Sparus aurata*) (Tsironi and Taoukis, 2010; Tsironi and Taoukis, 2012 and 2014). However, changes in storage conditions, including temperature and packaging, results in significant modifications in the spoilage mechanisms and determine the specific spoilage bacteria of the fish product. For example, the microflora of modified atmosphere packaged fish is dominated mainly by various Gram-positive microorganisms, mainly lactic acid bacteria as they are more resistant to CO₂ (Sivertsvik et al., 2002). A codominance of lactic acid bacteria and *Brochothrix thermosphacta* in gilthead seabream stored under 40% CO₂ has been reported by Drosinos et al. (1997), while Dalgaard et al (1997) reported considerable contribution of *Photobacterium phosphoreum* in the spoilage of chilled modified atmosphere packaged cod, trout and tuna. Because of recent crises in food quality and safety, food monitoring is regarded as one of the top priorities of the EU-

Commission. The White Paper on Food Safety reinforces the need for controls “from the farm to the fork”, which includes: (i) official controls, (ii) raised food safety standards according to the microbiological criteria of the Codex Alimentarius, and (iii) improved detection methods and laboratory quality control. The introduction of next generation sequencing (NGS) represents one of the most significant and fundamental technological advances in the biological sciences since the development of the polymerase chain reaction (PCR) in the mid-1980s. It has provided powerful new tools for the determination and study of non-culturable or poorly characterized organisms and emerging pathogens and it has enabled rapid and open-ended profiling of genotypic and diagnostic markers for virulence and antimicrobial resistance (Peters et al., 2004; Diaz-Sanchez et al., 2013).

The objective of the study is the assessment of the microbial ecology and safety of fisheries in Greece by next-generation sequencing (NGS).

MATERIALS AND METHODS

A representative number of fish samples (10 samples/species) were obtained from local fish stores (Greece) and transported to the Department of Food Technology (TEI of Athens, Greece) within 1 day from capture. 14 different species were studied in total, i.e. (1) Atlantic salmon (*Salmo salar*), (2) Albacore tuna (*Thunus alalunga*), (3) European anchovy (*Engraulis encrasicolus*), (4) Chub mackerel (*Scomber japonicus*), (5) Atlantic mackerel (*Scomber scombrus*), (6) European pilchard (*Sardina pilchardus*), (7) Grey mullet (*Mugil cephalus*), (8) European hake (*Merluccius merluccius*), (9) Gilthead seabream (*Sparus aurata*), (10) European sea bass (*Dicentrarchus labrax*), (11) Picarel (*Spicara smaris*), (12) Comber (*Serranus cabrilla*), (13) Dentex (*Dentex macrophthalmus*) and (14) Striped red mullet (*Mullus surmuletus*).

Samples were transported directly to the laboratory in polystyrene boxes with appropriate quantity of flaked ice (0°C). Upon receipt, fish was aseptically homogenized in a laminar flow hood.

DNA extraction was performed using the NucleoSpin Tissue kit (Macherey-Nagel, GmbH & Co. KG, Germany) according to the manufacturer’s instructions, with the addition of a Proteinase K overnight incubation step at 65°C. Extracted DNA was quantified using a spectrophotometer at 260nm and 280nm. After DNA extraction, 16S rRNA genes were amplified using domain-level bacterial primers that contain sequencing adapters and unique, sample-specific sequences.

RESULTS

In the present study the dominant initial microbiota of 14 fish species obtained from the Greek fish market within one day from capture were evaluated. 16S rRNA gene sequence analysis gave information at both species and strain levels (Tables 1-14).

Table 1: Representative sequencing information of bacterial genera identified by NGS for fresh Atlantic salmon (*Salmo salar*)

Sequencing information	
Total number of reads	2903
Identified bacteria (genus)	% valid reads
<i>Blastococcus</i>	0.35
<i>Kosuria</i>	0.24
<i>Propionibacterium</i>	0.22
<i>Brochothrix</i>	0.78
<i>Streptococcus</i>	1.1
<i>Janthinobacterium</i>	0.65
<i>Shewanella</i>	8.26
<i>Acinetobacter</i>	9.13
<i>Psychrobacter</i>	0.26
<i>Pseudomonas</i>	38.53

Table 2: Representative sequencing information of bacterial genera identified by NGS for fresh albacore tuna (*Thunus alalunga*)

Sequencing information	
Total number of reads	17215
Identified bacteria (genus)	% valid reads
<i>Chryseobacterium</i>	5.65
<i>Flavobacterium</i>	1.11
<i>Soonwooa</i>	5.75
<i>Sphingobacterium</i>	2.85
<i>Paracoccus</i>	4.6
<i>Comamonas</i>	2.36
<i>Acinetobacter</i>	6.42
<i>Enhydrobacter</i>	0.59
<i>Moraxella</i>	0.56
<i>Psychrobacter</i>	2.21
<i>Pseudomonas</i>	2.98
<i>Stenotrophomonas</i>	1.09
<i>Xanthomonas</i>	2.45

Table 3: Representative sequencing information of bacterial genera identified by NGS for fresh European anchovy (*Engraulis encrasicolus*)

Sequencing information	
Total number of reads	15927
Identified bacteria (genus)	% valid reads
<i>Corynebacterium</i>	1.75
<i>Microbacterium</i>	2.01
<i>Propionibacterium</i>	1.41
<i>Staphylococcus</i>	2.87
<i>Lactobacillus</i>	0.83
<i>Streptococcus</i>	1.97
<i>Aeromonas</i>	0.22
<i>Shewanella</i>	2.1
<i>Acinetobacter</i>	7.28
<i>Enhydrobacter</i>	1.42
<i>Psychrobacter</i>	2.4
<i>Pseudomonas</i>	3.16
<i>Aliivibrio</i>	2.0
<i>Photobacterium</i>	0.56
<i>Vibrio</i>	3.99

Table 4: Representative sequencing information of bacterial genera identified by NGS for fresh chub mackerel (*Scomber japonicus*)

Sequencing information	
Total number of reads	7726
Identified bacteria (genus)	% valid reads
<i>Corynebacterium</i>	1.25
<i>Propionibacterium</i>	2.4
<i>Staphylococcus</i>	1.94
<i>Aeromonas</i>	0.15
<i>Acinetobacter</i>	17.73
<i>Psychrobacter</i>	19.55
<i>Pseudomonas</i>	5.6

Table 5: Representative sequencing information of bacterial genera identified by NGS for fresh Atlantic mackerel (*Scomber scombrus*)

Sequencing information	
Total number of reads	11825
Identified bacteria (genus)	% valid reads
<i>Streptococcus</i>	0.67
<i>Acinetobacter</i>	10.79
<i>Psychrobacter</i>	19.87
<i>Pseudomonas</i>	0.8
<i>Photobacterium</i>	1.52

Table 6: Representative sequencing information of bacterial genera identified by NGS for fresh European pilchard (*Sardina pilchardus*)

Sequencing information	
Total number of reads	18381
Identified bacteria (genus)	% valid reads
<i>Corynebacterium</i>	1.28
<i>Propionibacterium</i>	5.16
<i>Brochothrix</i>	0.04
<i>Staphylococcus</i>	3.34
<i>Lactobacillus</i>	1.49
<i>Lactococcus</i>	0.68
<i>Streptococcus</i>	0.88
<i>Aeromonas</i>	1.84
<i>Shewanella</i>	0.05
<i>Acinetobacter</i>	8.47
<i>Psychrobacter</i>	14.83
<i>Pseudomonas</i>	3.12
<i>Vibrio</i>	0.05

Table 7: Representative sequencing information of bacterial genera identified by NGS for fresh grey mullet (*Mugil cephalus*)

Sequencing information	
Total number of reads	14208
Identified bacteria (genus)	% valid reads
<i>Propionibacterium</i>	3.54
<i>Flavobacterium</i>	0.6
<i>Brochothrix</i>	2.16
<i>Staphylococcus</i>	3.22
<i>Lactobacillus</i>	6.72
<i>Streptococcus</i>	7.62

<i>Sphingobium</i>	1.55
<i>Janthinobacterium</i>	0.3
<i>Acinetobacter</i>	10.75
<i>Psychrobacter</i>	3.97
<i>Pseudomonas</i>	4.28

Table 8: Representative sequencing information of bacterial genera identified by NGS for fresh European hake (*Merluccius merluccius*)

Sequencing information	
Total number of reads	10488
Identified bacteria (genus)	% valid reads
<i>Flavobacterium</i>	2.68
<i>Brochothrix</i>	0.64
<i>Streptococcus</i>	0.62
<i>Shewanella</i>	0.09
<i>Acinetobacter</i>	18.98
<i>Psychrobacter</i>	12.02
<i>Pseudomonas</i>	20.21

Table 9: Representative sequencing information of bacterial genera identified by NGS for fresh gilthead seabream (*Sparus aurata*)

Sequencing information	
Total number of reads	11777
Identified bacteria (genus)	% valid reads
<i>Flavobacterium</i>	1.93
<i>Brochothrix</i>	0.77
<i>Lactobacillus</i>	20.29
<i>Streptococcus</i>	0.15
<i>Janthinobacterium</i>	0.72
<i>Shewanella</i>	1.01
<i>Acinetobacter</i>	19.62
<i>Psychrobacter</i>	1.5
<i>Pseudomonas</i>	18.53

Table 10: Representative sequencing information of bacterial genera identified by NGS for fresh European sea bass (*Dicentrarchus labrax*)

Sequencing information	
Total number of reads	15
Identified bacteria (genus)	% valid reads
<i>Shewanella</i>	9.62

Table 11: Representative sequencing information of bacterial genera identified by NGS for fresh picarel (*Spicara smaris*)

Sequencing information	
Total number of reads	23066
Identified bacteria (genus)	% valid reads
<i>Chryseobacterium</i>	1.01
<i>Acinetobacter</i>	31.95
<i>Enhydrobacter</i>	6.95
<i>Moraxella</i>	2.08
<i>Pseudomonas</i>	1.92
<i>Photobacterium</i>	0.84
<i>Vibrio</i>	0.19

Table 12: Representative sequencing information of bacterial genera identified by NGS for fresh comber (*Serranus cabrilla*)

Sequencing information	
Total number of reads	15526
Identified bacteria (genus)	% valid reads
<i>Flavobacterium</i>	5.69
<i>Janthinobacterium</i>	0.2
<i>Shewanella</i>	0.1
<i>Acinetobacter</i>	16.81
<i>Enhydrobacter</i>	0.85
<i>Psychrobacter</i>	31.01
<i>Pseudomonas</i>	1.78
<i>Photobacterium</i>	1.04

Table 13: Representative sequencing information of bacterial genera identified by NGS for fresh dentex (*Dentex macrophthalmus*)

Sequencing information	
Total number of reads	9399
Identified bacteria (genus)	% valid reads
<i>Propionibacterium</i>	1.66
<i>Streptococcus</i>	2.67
<i>Acinetobacter</i>	1.05
<i>Pseudomonas</i>	32.51

Table 14: Representative sequencing information of bacterial genera identified by NGS for fresh striped red mullet (*Mullus surmuletus*)

Sequencing information	
Total number of reads	12195
Identified bacteria (genus)	% valid reads
<i>Propionibacterium</i>	2,28
<i>Flavobacterium</i>	0,8
<i>Staphylococcus</i>	0,95
<i>Streptococcus</i>	4,73
<i>Janthinobacterium</i>	0,24
<i>Shewanella</i>	0,06
<i>Acinetobacter</i>	1.59
<i>Psychrobacter</i>	1.23
<i>Pseudomonas</i>	44.27

The main pathogenic bacterial species identified in the tested fish samples included *Vibrio* spp., *Clostridium* spp., *Staphylococcus*, *Flavobacterium* and *Janthinobacterium* representing both native freshwater habitats and contaminants arising from different sources, including sewage and direct contamination by wild animals, livestock, and feed. The initial spoilage microbiota of fish consisted of various psychrotrophic Gram-negative bacteria, mainly *Pseudomonas*, *Acinetobacter*, *Moraxella*, *Shewanella*, *Psychrobacter*, *Lactobacillus*, *Brochothrix* and *Photobacterium*.

Several researchers have studied the spoilage microbiota of iced fish caught from the Mediterranean area by using a classical approach and concluded that *Pseudomonas* and *Shewanella* are the most predominant spoilage microorganisms grown on plates. The results of the present study are in agreement with previous studies investigating the initial spoilage microbial flora of fish (Gram & Dalgaard, 2002; Koutsoumanis et al., 2002; Tsironi & Taoukis, 2012). *Psychrobacter* spp., which was identified in most of the studied species, was first reported as part of the initial microbiota of fish from Greek waters by a recent study by Parlapani et al. (2015) in sea bream using 16S rRNA gene analysis. A high prevalence of *Staphylococcus* spp. was also observed, as also reported by Chaillou et al. (2014). Few applications on NGS have been reported recently for the determination of microbial flora in food products, i.e. dairy products (Ribani et al., 2018), fish (red drum) (Silbande et al., 2018) and shrimp (Yang et al., 2017).

CONCLUSIONS

It is necessary to study the prevalence of bacteria in fish to ensure a better understanding of ecology and distribution of pathogens and spoilage microorganisms in the food chain. The determination of fish microbiota is currently carried out mainly by phenotypic tests (morphological, biochemical) after the isolation of microorganisms using various non-selective and/or selective growth media. In this study, the application of NGS for the microbial assessment of fisheries was introduced. The conventional methods for determination of microbial flora in food products have been proven to detect species when the potential microorganisms are already known or expected in advance as the discriminatory analytical methods for their identification have to be specifically tailored for their identification. On the other hand, NGS technologies have changed the way to analyse DNA by combining sequencing and quantification of DNA in a single step. By using universal primers to amplify several regions, it is possible to obtain an internal validation of the results derived by the concordance of the assigned reads to a species.

Technological developments in the field of microbiology, such as NGS techniques and the omics approach in general, have significantly enhanced our understanding of the behaviour of microorganisms and particularly their physiological state. These innovative approaches could reveal patterns of responses that cannot be detected by classical methods and have the potential to ultimately uncover new and powerful methods to control hazards in food and feed. This may potentially bring more insight than just the usual 'snapshot' in the farm-to-fork contamination process analysis and therefore contribute to the next generation of risk assessment (den Besten et al., 2018). Under this context, the present study might be a baseline for further investigation of the pathogenic and spoilage potential of the identified microorganisms present in Greek (and consequently Mediterranean) fish products.

ACKNOWLEDGEMENT

This study was supported by the IKY FELLOWSHIPS OF EXCELLENCE FOR POSTGRADUATE STUDIES IN GREECE - SIEMENS PROGRAM: "Next generation sequencing for the diagnosis of pathogenic bacteria in Greek fisheries: A novel technique, common to face major public health issues" (Thematic area: Health, Field: Biotechnology-Molecular biotechnology, 2016-2017).

REFERENCES

- Barrett K.A., Nakao J.H., Eggers C., Gould L.H. (2015). Fish-associated foodborne disease outbreaks: United States, 1998-2015. *Foodborne Pathogens and Disease*, 14(9), 537-543.
- Chaillou S., Chaulot-Talmon A., Caekebeke H., Cardinal M., Christeans S., Denis C., Desmouts M.H., Dousset X., Feurer C., Hamon E., Joffraud J.J., La Carbona S., Leroi F., Leroy S., Lorre S., Macé S., Pilet M.F., Prévost H., Rivollier M., Roux D., Talon R., Zagorec M., Champomier-Vergès M.C. (2014). Origin and ecological selection of core and food-specific bacterial communities associated with meat and seafood spoilage. *International Society for Microbial Ecology*, 1(14), 1751-7362.
- Dalgaard, P., Mejlholm, O., Christiansen, T. J., Huss, H. H. (1997). Importance of *Photobacterium phosphoreum* in relation to spoilage of modified atmosphere-packed fish products. *Letters in Applied Microbiology*, 24, 373-378.
- Den Besten, H.M.W., Amézquita A., Bover-Cid S., Dgnas S., Ellouze M., Guillou S., Nychas G., O'Mahony G., Pérez-Rodríguez F., Membre J.M. (2018). Next generation of microbiological risk assessment: Potential of omics data for exposure assessment. *International Journal of Food Microbiology* (In press, doi: j.ijfoodmicro.2017.10.006)
- Diaz-Sanchez S., Hanning I., Pendleton S., D'Souza D. (2013). Next-generation sequencing: The future of molecular genetics in poultry production and food safety. *Poultry Science*, 92 (2), 562-572.
- Drosinos E.H., Lambropoulou K., Mitre E., Nychas G.J.E. (1997). Attributes of fresh gilt-head seabream (*Sparus aurata*) fillets treated with potassium sorbate, sodium gluconate and stored under modified atmosphere at 0±1°C. *Journal of Applied Microbiology*, 83, 569-575.
- FAO (2018). Seafood-borne disease and illness. (Available at <http://www.fao.org/docrep/003/x0465e/x0465e04.htm>, accessed on 11 March 2018).
- Giuffrida A., Valenti D., Giarratana F., Ziino G., Panebianco A. (2013). A new approach to modelling the shelf life of gilthead seabream (*Sparus aurata*). *International Journal of Food Science and Technology*, 48 (6), 1235-1242.
- Gram L., Dalgaard P. (2002). Fish spoilage bacteria: problems and solutions. *Current Opinion in Biotechnology*, 13, 262-266.
- Koutsoumanis K.P., Taoukis P.S., Drosinos E.H., Nychas G.-J.E. (2000). Applicability of an Arrhenius model for the combined effect of temperature and CO₂ packaging on the spoilage microflora of fish. *Applied and Environmental Microbiology*, 66, 3528-3534.
- Leisner J.J., Gram L. (1999). Spoilage of fish, in: Encyclopedia of Food Microbiology, ed. by Robinson RK, Batt CA and Patel PD. Academic Press, San Diego, CA, pp. 813-820.
- Novoslavskij A., Terentjeva M., Eizenberga I., Valciņa O., Bartkevičs V., Bērziņš A. (2016). Major foodborne pathogens in fish and fish products: a review. *Annals of Microbiology*, 66(1), 1-15.
- Parlapani F.F., Kormas K.A., Boziaris I.S. (2015). Microbiological changes, shelf life and identification of initial and spoilage microbiota of sea bream fillets stored under various conditions using 16S rRNA gene analysis. *Journal of the Science of Food and Agriculture*, 95, 2386-2394.
- Peters R.P., van Agtmael M.A., Danner S.A., Savelkoul P.H., Vandenbroucke-Grauls C.M. (2004). New developments in the diagnosis of bloodstream infections. *Lancet Infect Dis*, 4(12), 751-760.
- Ribani A., Schiavo G., Utzeri J.U., Bertolini F., Geraci C., Bovo S., Fontanesi L. (2018). Application of next generation semiconductor based sequencing for species identification in dairy products. *Food Chemistry*, 246, 90-98.
- Silbände A., Adenet S., Chopin C., Cornet J., Smith-Ravin J., Rochefort K., Leroi F. (2018). Effect of vacuum and modified atmosphere packaging on the microbiological, chemical and sensory properties of tropical red drum (*Sciaenops ocellatus*) fillets stored at 4°C. *International Journal of Food Microbiology*, 266, 31-41.
- Sivertsvik, M., Jeksrud, W. K., Rosnes, J. T. (2002). A review of modified atmosphere packaging of fish and fishery products-significance of microbial growth, activities and safety. *International Journal of Food Science and Technology*, 37, 107-127.
- Tsironi T., Taoukis P.S. (2010). Modeling microbial spoilage and quality of gilthead seabream fillets: Combined effect of osmotic pre-treatment, modified atmosphere packaging and nisin on shelf life. *Journal of Food Science*, 75(4), 243-251.
- Tsironi T.N., Taoukis P.S. (2012). Shelf life extension of gilthead seabream fillets by osmotic treatment and antimicrobial agents. *Journal of Applied Microbiology*, 112, 316-328.
- Tsironi T.N., Taoukis P.S. (2014). Effect of processing parameters on water activity and shelf life of osmotically dehydrated fish fillets. *Journal of Food Engineering*, 123, 188-192.
- Yang S.P., Xie J., Qian Y.F. (2017). Determination of spoilage microbiota of Pacific white shrimp during ambient and cold storage using Next-Generation Sequencing and culture-dependent method. *Journal of Food Science*, 82(5), 1178-1183.

Modeling and Simulation in Food Safety and Spoilage

KINETIC MODELLING OF SCAVENGER REACTIONS: PARAMETER ESTIMATION FOR A GALLIC ACID-BASED OXYGEN SCAVENGER

Astrid F. Pant^{1,2}

¹Technical University of Munich
TUM School of Life Sciences Weihenstephan
Freising, Germany
astrid.pant@ivv.fraunhofer.de

Matthias Reinelt²

²Fraunhofer Institute of Process Engineering
and Packaging IVV
Freising, Germany
matthias.reinelt@ivv.fraunhofer.de

KEYWORDS

Scavenger Kinetics, Food Packaging, Numerical Optimization

ABSTRACT

The software-based design of active packaging requires mathematical models of oxygen scavenger reactions. In this study we present a simple approach for describing such reactions with a second-order kinetic model and for determining the corresponding kinetic parameters. For the example of a gallic acid-based oxygen scavenger stored at 21°C and 0% RH, 75% RH and 100% RH, the model was fitted to oxygen absorption data using a downhill simplex-based algorithm for numerical optimization. As expected, the optimization results depended on the choice of the starting values. To identify the global optimum of the given parameter space, the results of multiple optimization runs with varying starting values were analyzed quantitatively. For the scavenger reactions at 75% RH and 100% RH unambiguous minima could be found. The reaction rate constants are $1.347 \cdot 10^{-7} \text{m}^3/(\text{mol} \cdot \text{s})$ and $1.496 \cdot 10^{-6} \text{m}^3/(\text{mol} \cdot \text{s})$ and the stoichiometric coefficients are 1.639 and 2.534 for 75% RH and 100% RH, respectively. However, at 0% RH, there was no detectable scavenger reaction and fitting the noisy experimental data led to ambiguous solutions without physical meaning. The analyzed method for the estimation of kinetic parameters can be applied for any scavenger reaction, thereby providing necessary information for active packaging design.

INTRODUCTION

In food packaging technology, oxygen (O_2) scavengers are used to prevent sensitive foods or food components from oxidation. O_2 scavengers are based on substances that easily react with O_2 , e.g. iron, sulfite, oxidizable polymers or natural antioxidants (Vermeiren et al. 2003, Rooney 2005). In packaging applications, O_2 scavengers can fulfill different tasks: They are used to remove O_2 from the packaging headspace and/or for improving the O_2 barrier function of polymeric packaging films.

In the last few years there has been a strong trend towards software-based packaging design. Gas transfer models have been developed that are now used to optimize packaging designs in terms of tailor-made barrier properties, e.g. packaging for fresh produce or modified atmosphere packaging (Cagnon et al. 2013, Van Bree et al. 2010, Sousa-Gallagher and Mahajan 2013). For modelling active packaging systems including O_2 scavengers, a quantitative description of the reaction kinetics of the scavenger related to typical storage parameters (e.g. relative humidity and temperature) is necessary. Thus, novel approaches for modelling scavenger kinetics have to be developed.

In this study we have a closer look at kinetic models of scavenger reactions and we focus on the determination of kinetic parameters from experimental data obtained for a gallic acid-based oxygen scavenger.

OXYGEN SCAVENGER KINETICS

The function of O_2 scavengers relies on the chemical reaction between the active substance (SC) of the scavenger and O_2 , leading to the formation of oxidation products (SC_{ox}). The overall reaction of an O_2 scavenger can be written as follows:



where n is a stoichiometric factor.

O_2 scavengers are characterized by (a) their absorption capacity, i.e. the amount of O_2 that can be absorbed by a given amount of the scavenger and (b) the time-dependent absorption of O_2 , i.e. the rate of the scavenger reaction. This information is obtained from O_2 absorption measurements. In such experiments, a defined amount of the scavenger is stored in a closed vessel under defined conditions, i.e. temperature, relative humidity (RH) and initial O_2 concentration. The decrease in O_2 concentration due to the scavenger reaction is monitored during storage. Figure 1 shows the results of an O_2 absorption experiment with a gallic acid-based scavenger.

Different approaches for modelling scavenger kinetics

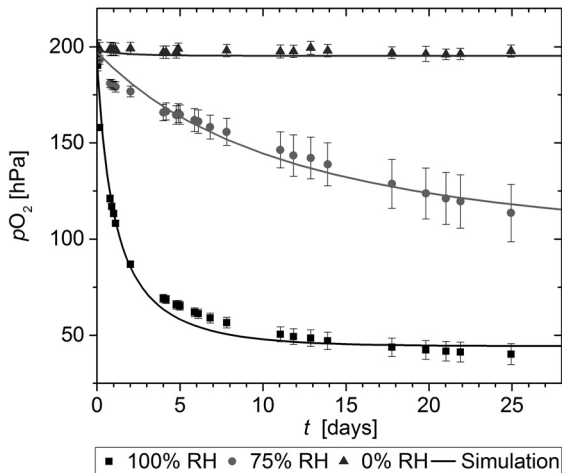


Figure 1: Oxygen Absorption of a Gallic Acid-based Scavenger at various Relative Humidities (RH)

can be found in literature. In recent years, the most common approach was to approximate scavenger kinetics with the kinetic law of a first-order elementary reaction. This approach often results in a good fit of the experimental data and is easy to apply as there are analytic solutions readily available (Charles et al. 2003, Galotto et al. 2009). However, it is based on the assumption that the reaction rate solely depends on the concentration of one reactant, i.e. O_2 or SC. This is a reasonable approximation when there is large excess of either O_2 or SC (pseudo first-order reaction). In most packaging applications, however, this assumption is not valid (i.e. there are low concentrations of O_2 and SC) so that first-order kinetic parameters cannot be transferred to other packaging systems.

For the software-based design of active packaging including O_2 scavengers, kinetic parameters independent from initial reactant concentrations are needed. Recently, some research groups have successfully applied second-order kinetic models to scavenger reactions: Dombre et al. (2015) and Di Maio et al. (2017) described the O_2 absorption of polymer-based scavengers with the kinetic law of a second-order elementary reaction. However, in these publications the method of fitting kinetic models is not discussed in detail so that there is still little knowledge about how to generate kinetic information from scavenger experiments in a way that is advantageous for packaging design and development. Whenever models with two or more free parameters have to be fitted to experimental data, manual fitting methods may fail to find optimum solutions. In this context, we closely evaluate the fitting of a second-order kinetic model to experimental data from O_2 absorption measurements in order to distinguish between different local and global minima of the objective function of the fit.

MODEL DEVELOPMENT

The active substance of the O_2 scavenger used in this study is gallic acid (3,4,5-trihydroxybenzoic acid, GA), a simple polyphenol that can be found in many plants. For the application as a scavenger, it is combined with the base sodium carbonate (Na_2CO_3) which serves as a catalyst for the oxidation. The reaction is triggered by humidity (Pant et al. 2017). Equation (1) was therefore rewritten as follows:



GA_{ox} denotes all oxidation products that are formed in this reaction, e.g. larger polyphenols. The reaction mechanism is not yet fully understood and may include a multi-step polycondensation (Tulyathan et al. 1989). The overall reaction is therefore assumed to be irreversible.

In this study, we used the kinetic law of a second-order elementary reaction as the minimal viable approximation to describe the reaction rate r :

$$r = k \cdot [GA] \cdot [O_2] \quad (3)$$

Here, r depends on the concentrations of both reactants, $[GA]$ and $[O_2]$, and k is the reaction rate coefficient. Based on this kinetic law, the net rates of consumption of GA and O_2 were described with a system of ordinary differential equations (ODE):

$$\frac{d[GA]}{dt} = -k \cdot [GA] \cdot [O_2] \quad (4)$$

$$\frac{d[O_2]}{dt} = -n \cdot k \cdot [GA] \cdot [O_2] \quad (5)$$

The net rate of production of GA_{ox} is the same as Equation (4) but with inverted sign (mass conservation).

EXPERIMENTAL DATA

Experimental data from O_2 absorption measurements with a gallic acid-based scavenger at 21°C and various relative humidities was used (Figure 1). In these experiments, 0.06 g of the scavenger were stored in closed cells with a free headspace volume of 88 cm³ or 108 cm³ and the O_2 absorption (i.e. the decrease of the O_2 partial pressure) was measured non-destructively during storage. To allow for homogenous oxygen exposition, the scavenger powder was spread in a thin layer on a glass plate. A more detailed description of the method is given by Pant et al. (2017). For all measurements, a fourfold determination was made. The experimental data (O_2 partial pressure in hPa) was transferred to O_2 concentrations $[O_2]$ in mol/m³ using the ideal gas law. The mean square deviation for each experimental condition was then calculated as follows:

$$MSE_{exp} = \sqrt{\frac{1}{N} \sum_{i=1}^m \sum_{l=1}^q ([O_2]_{exp} - [O_2]_{mean})^2} \quad (6)$$

where N is the total number of observations, m is the number of parallel experiments, q the number of observations in one experiment, $[\text{O}_2]_{\text{exp}}$ the observed oxygen concentration and $[\text{O}_2]_{\text{mean}}$ the arithmetic mean of all m observations for each l .

PARAMETER ESTIMATION

The ODE system given in Equations (4) and (5) was solved in MATLAB R2014a (The MathWorks, Inc., Natick, MA, USA) using the multistep solver `ode15s` with the default tolerances $\text{AbsTol} = 10^{-6}$ and $\text{RelTol} = 10^{-3}$. The model was fitted to the available experimental data sets reflecting different relative humidities from 0% RH to 100% RH. The fit was optimized based on the minimization of the sum of squared residuals (SSQ) to be calculated according to the following equation:

$$\text{SSQ} = \sum_{i=1}^m \sum_{l=1}^q ([\text{O}_2]_{\text{sim}} - [\text{O}_2]_{\text{exp}})^2 \quad (7)$$

where m is the number of parallel experiments, q the number of observations in one experiment, and $[\text{O}_2]_{\text{sim}}$ and $[\text{O}_2]_{\text{exp}}$ the predicted and the observed O_2 concentrations, respectively.

For the minimization of the SSQ objective function, the MATLAB function `fminsearch` was used - a function based on the Nelder-Mead downhill-simplex algorithm for local optimization as described by Lagarias et al. (1998). The termination tolerance of the function value (`TolFun`) was 10^{-4} and the lower bound on the size of a step (`TolX`) was 10^{-4} (MATLAB default settings). `Fminsearch` terminates when both stopping criteria are fulfilled.

The stoichiometric coefficient n is a measure for the O_2 absorption capacity and gives the number of absorbed molecules O_2 per molecule GA. Therefore, n must not be negative. Tulyathan et al. (1989) found an O_2 absorption capacity of 4.9 O-atoms per molecule GA. The reaction rate coefficient k , by definition, must also not be negative, but there was no previous knowledge about its order of magnitude. Thus, the parameter space was investigated in the range of $n = 0..10$ and $k = 10^{-10} \text{m}^3/(\text{mol} \cdot \text{s})..10^{10} \text{m}^3/(\text{mol} \cdot \text{s})$. To enable an effective search for k in this broad range of 20 orders of magnitude, a logarithmic scaling of k was chosen. Thereby, equal importance was attached to all possible solutions for k , regardless of their order of magnitude. For the optimization procedure, k was therefore replaced by $k = 10^{k'}$ in Equation (2).

Since the downhill-simplex optimization is known to be sensitive to the chosen starting values, the initial k and n values were varied systematically in equidistant steps over the whole parameter space so that in total 231 different combinations of k and n were tested. For all optimization results, the root mean square error (RMSE)

was calculated as a measure of the goodness of fit:

$$\text{RMSE} = \sqrt{\frac{\text{SSQ}}{N - p}} \quad (8)$$

where N is the total number of experimental observations and p the number of fitted parameters.

The results (combinations of k and n) were then sorted by their RMSE values, starting with the lowest value RMSE_{min} . All solutions with RMSE below a RMSE threshold = $\text{RMSE}_{\text{min}} + \text{MSE}_{\text{exp}}$ were considered optimum solutions, where MSE_{exp} is the experimental error of the respective experimental data set (Equation 6). With this threshold, the experimental error was taken into account.

To validate the optimization results, the k - n -parameter space was mapped out in terms of the SSQ objective function in order to visually identify minimum and maximum regions.

RESULTS

In this study, the reaction of a GA-based O_2 scavenger was described with a second-order kinetic model. The model was fitted to experimental data obtained at 21°C and various relative humidities to determine the model parameters, i.e. the reaction rate coefficient k and the stoichiometric factor n .

The simulated curves based on the best-fit sets of model parameters are shown in Figure 1. All experiments could be sufficiently described with the chosen model. The goodness of fit was adequate in relation to the experimental error; the results are given in Table 1. These results show that the GA-based scavenger is activated by humidity. While there was no detectable O_2 absorption at 0% RH, the values of k and n were significantly higher at 100% RH than at 75% RH. This may be explained by the mechanism of the scavenger reaction which includes the deprotonation of the GA and a subsequent multi-step oxidation. The availability of water, in presence of a base, is a prerequisite for the proton transfer as an initiating step. Both, the velocity of the reaction and its extent (i.e. the absorption capacity) appear to be affected by the level of RH. To determine the optimum reaction conditions of a GA-based scavenger, further research should therefore focus on analyzing the combined effect of humidity and the base on the reaction kinetics.

For a closer analysis of the fit, the complete k - n -parameter space was mapped in terms of the SSQ objective function. In the simple case of a model with two parameters, this results in a 3-D plot of the parameter space. Figure 2 shows the contour plots of the different parameter spaces for 0% RH, 75% RH and 100% RH, respectively. The SSQ values describe a mathematical surface that is defined by the model equation and the experimental data set. Parameter estimation from ex-

Table 1: Optimization Results for Experimental data at 21°C and various Relative Humidities (RH)

	MSE _{exp}	RMSE _{min} mol/m ³	n			k m ³ /(mol · s)		
			median	min	max	median	min	max
0% RH	0.116	0.038	0.06301	0.05165	3.64178	$7.54668 \cdot 10^{-7}$	$1.75341 \cdot 10^{-9}$	$9.71062 \cdot 10^9$
75% RH	0.286	0.347	1.63914	1.63908	1.63924	1.347524	$1.34741 \cdot 10^{-7}$	$1.3476 \cdot 10^{-7}$
100% RH	0.117	0.256	2.53430	2.53423	2.53439	$1.49632 \cdot 10^{-6}$	$1.49584 \cdot 10^{-6}$	$1.49651 \cdot 10^{-6}$

perimental data, formulated as a nonlinear least-squares problem, may bear the risk of multiple local optimum solutions. The related plateau phenomenon has been discussed in literature (e.g. Choi and Chiang (2009)) and was also observed in our study: The 100% RH plot shows regions with very high SSQ at low values of $\log k$ and n and a large SSQ plateau at high values of $\log k$ and n . In between these, a minimum can be presumed around $\log k = -6$ and $n = 2.5$. Although less pronounced, similar features can be observed for 75% RH. Here, a minimum can be presumed in the area of $\log k = -7$ and $n = 1.5$. At 0% RH, in contrast, there is no clearly defined minimum region; all SSQ values for $\log k < -7$ and $n < 1$ appear to be equivalent minima forming another plateau.

The described features of the k - n -parameter space are also reflected in the optimization results shown in Figure 3. For all experimental conditions it was shown that the optimization results depended on the chosen starting values, leading to apparent groups of results with different RMSE (Figure 3). This can be explained with the characteristics of the parameter space: Whenever the downhill simplex algorithm started at the plateau regions, no downhill movement was observable within the given tolerances so that the algorithm stopped, resulting in k - n -combinations with high RMSE as best-fit results (numerical local minimum). Additionally, the algorithm got stuck in other local minima (Figure 2) in the form of trenches at $n = 2$ and $\log k = -6$. Without any previous knowledge about k and n , the total minimum of the defined parameter space could only be found by multiple runs of the downhill simplex algorithm with varying initial values.

All solutions below a RMSE threshold of 0.155 mol/m³, 0.633 mol/m³ or 0.373 mol/m³ for 0% RH, 75% RH and 100% RH respectively, were considered optimum solutions. The thresholds are derived from the experimental error as described above. Table 1 gives an overview of the found optimum values for k and n . To show the distribution of the found optimum values, the median, minimum (min) and maximum (max) values are presented.

At 100% RH, there was an unambiguous minimum at $n = 2.534$ and $k = 1.496 \cdot 10^{-6}$ m³/(mol · s), which can be regarded as the global minimum given the constraints on n and k discussed above. The minimum

and maximum solutions only differed in the 3rd or 4th decimal (Table 1). Accordingly, an unambiguous minimum for 75% RH could be found at $n = 1.639$ and $k = 1.347 \cdot 10^{-6}$ m³/(mol · s).

For 0% RH, already from the experimental data it could be seen that $k = 0$ m³/(mol · s) and $n = 0$ since there was no detectable O₂ absorption. A fit of these data, however, resulted in n and k values differing by several decimal powers although characterized by similar RMSE. This example illustrates the sensitivity of the model to noisy data. The experimental data lack meaningful information, so that the issue of multiple local solutions arises. In such cases, the downhill simplex-based method fails to determine the values of the kinetic parameters.

CONCLUSION

A second-order kinetic model was developed and fitted to O₂ absorption data of a gallic acid-based O₂ scavenger. It could be shown that this model was suitable for describing oxygen absorption and the kinetic parameters could be obtained. Both, the rate coefficient k and the stoichiometric factor n were affected by the storage relative humidity. Thus, gallic acid belongs to the group of humidity-activated scavenger systems and should be used for food products with high water activity. The applied method for determining the kinetic parameters includes (a) a multiple-run local optimization and (b) a subsequent quantitative analysis of the results based on an acceptance threshold derived from the experimental error. Independent from the model to be fitted, this method can be used for searching a predefined parameter space for a global optimum. In the context of an increasing demand for active packaging solutions, the applied method provides meaningful kinetic information - a prerequisite for software-base packaging design.

ACKNOWLEDGEMENTS

The authors would like to thank Oliver Miesbauer for valuable discussions.

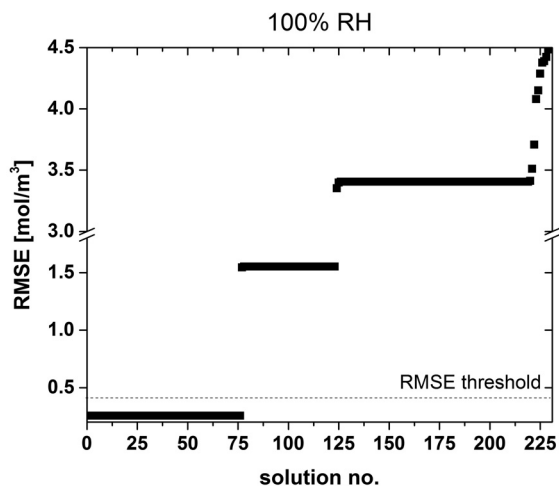
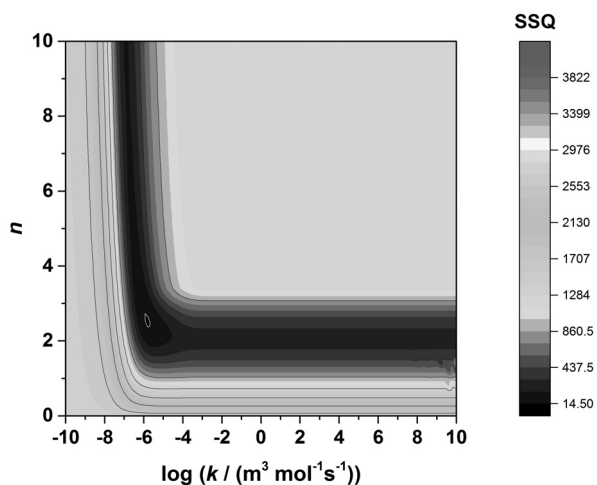
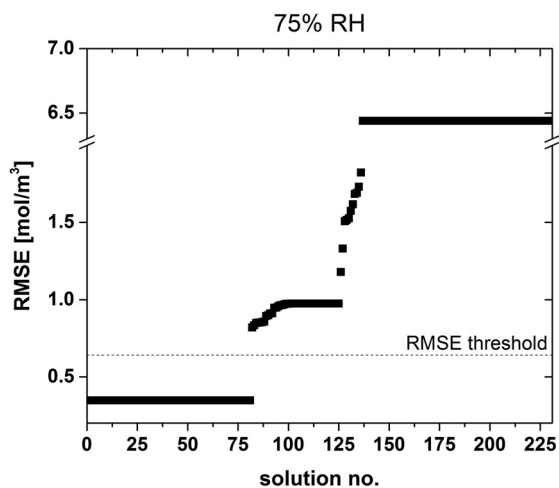
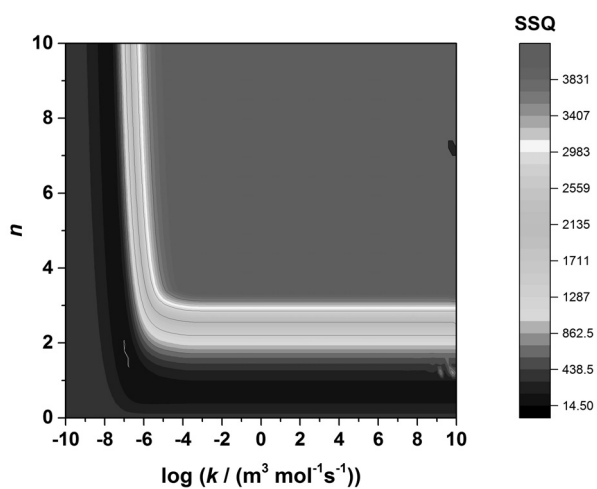
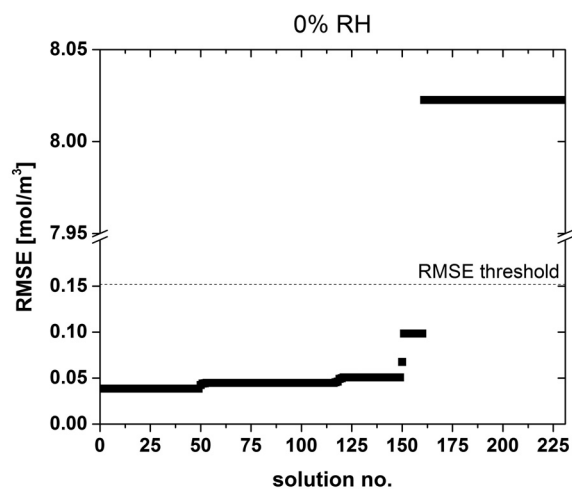
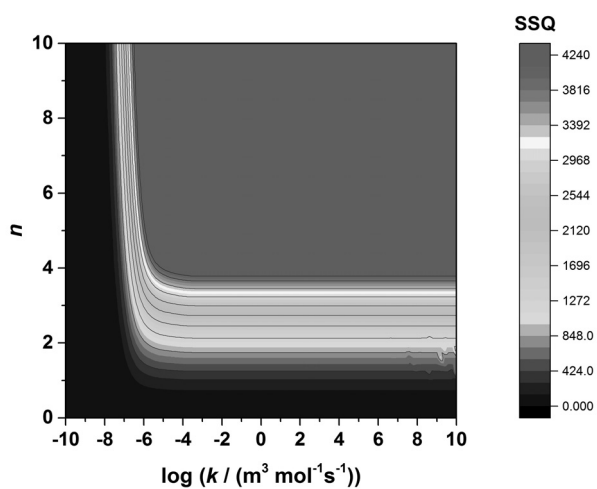


Figure 2: Contour Plots of the Parameter Spaces at various Relative Humidities (RH)

Figure 3: RMSE Values of the Optimization Results for various Relative Humidities (RH)

AUTHOR BIOGRAPHIES

ASTRID PANT studied food technology at the University of Bonn, Germany, and at the Swedish University of Agricultural Sciences in Uppsala, Sweden. Since 2010, she has been working at Fraunhofer IVV in the field of active packaging and food packaging. Currently she is pursuing her PhD studies at the Technical University of Munich with a focus on oxygen scavenger kinetics.

MATTHIAS REINELT studied chemistry at the LMU Munich and obtained his PhD at the Max Planck Institute for Plasma Physics, Munich. Since 2013 he has been working at Fraunhofer IVV in the Department of Materials Development. In his current research he focuses on the modelling and simulation of packaging systems.

REFERENCES

- Cagnon T.; Mery A.; Chalier P.; Guillaume C.; and Gontard N., 2013. *Fresh food packaging design: A requirement driven approach applied to strawberries and agro-based materials*. *Innovative Food Science & Emerging Technologies*, 20, 288–298. ISSN 1466-8564.
- Charles F.; Sanchez J.; and Gontard N., 2003. *Active modified atmosphere packaging of fresh fruits and vegetables: Modeling with tomatoes and oxygen absorber*. *Journal of Food Science*, 68, no. 5, 1736–1742. ISSN 0022-1147.
- Choi B.K. and Chiang H.D., 2009. *Multiple solutions and plateau phenomenon in measurement-based load model development: Issues and suggestions*. *IEEE Transactions on Power Systems*, 24, no. 2, 824–831.
- Di Maio L.; Marra F.; Apicella A.; and Incarnato L., 2017. *Evaluation and modeling of scavenging performances of active multilayer PET based films for food preservation*. *Chemical Engineering Transactions*, 57, 1879–1884. doi:10.3303/CET1757314.
- Dombre C.; Guillard V.; and Chalier P., 2015. *Protection of methionol against oxidation by oxygen scavenger: An experimental and modelling approach in wine model solution*. *Food Packaging and Shelf Life*, 3, 76–87. ISSN 2214-2894.
- Galotto M.J.; Anfossi S.A.; and Guarda A., 2009. *Oxygen Absorption Kinetics of Sheets and Films Containing a Commercial Iron-based Oxygen Scavenger*. *Food Science and Technology International*, 15, no. 2, 159–168. ISSN 1082-0132.
- Lagarias J.C.; Reeds J.A.; Wright M.H.; and Wright P.E., 1998. *Convergence Properties of the Nelder–Mead Simplex Method in Low Dimensions*. *SIAM Journal on Optimization*, 9, no. 1, 112–147.
- Pant A.; Saengerlaub S.; and Mueller K., 2017. *Gallic Acid as an Oxygen Scavenger in Bio-Based Multilayer Packaging Films*. *Materials*, 10, no. 5, 489. ISSN 1996-1944.
- Rooney M.L., 2005. *Innovations in Food Packaging*, Elsevier Ltd., San Diego, GA, USA, chap. Oxygen-scavenging packaging. 123–137.
- Sousa-Gallagher M.J. and Mahajan P.V., 2013. *Integrative mathematical modelling for MAP design of fresh-produce: Theoretical analysis and experimental validation*. *Food Control*, 29, no. 2, 444–450. ISSN 0956-7135.
- Tulyathan V.; Boulton R.B.; and Singleton V.L., 1989. *Oxygen uptake by gallic acid as a model for similar reactions in wines*. *Journal of Agricultural and Food Chemistry*, 37, no. 4, 844–849. ISSN 0021-8561.
- Van Bree I.; De Meulenaer B.; Samapundo S.; Vermeulen A.; Ragaert P.; Maes K.C.; De Baets B.; and Devlieghere F., 2010. *Predicting the headspace oxygen level due to oxygen permeation across multilayer polymer packaging materials: A practical software simulation tool*. *Innovative Food Science & Emerging Technologies*, 11, no. 3, 511–519. ISSN 1466-8564.
- Vermeiren L.; Heirlings L.; Devlieghere F.; and Debevere J., 2003. *Novel food packaging techniques*, book section Oxygen, ethylene and other scavengers. 22–49.

EFFICIENT DATA COLLECTION FOR MODELLING THE GROWTH RATE AS A FUNCTION OF THE ENVIRONMENTAL CONDITIONS

Simen Akkermans, Philippe Nimmegeers, Jan F. Van Impe*
BioTeC+ & OPTEC, Department of Chemical Engineering, KU Leuven
CPMF2, Flemish Cluster Predictive Microbiology in Foods
*E-mail address: Jan.VanImpe@kuleuven.be

KEYWORDS

Predictive microbiology, experimental design, D-criterion, model prediction uncertainty, secondary model

Abstract

Building secondary models that describe the growth rate as a function of multiple environmental conditions is often very labour intensive and costly. As such, the current research aims to assist in decreasing the required experimental effort by studying the efficacy of both design of experiments (DOE) and optimal experimental designs (OED) techniques. This is the first research (i) to make a comparison of these techniques based on the (relative) model prediction uncertainty of the obtained models and (ii) to compare OED criteria for the design of experiments with static (instead of dynamic) environmental conditions.

A comparison of the DOE techniques demonstrated that the inscribed central composite design and full factorial design were most suitable. Five conventional and two tailor made OED criteria were tested. The commonly used D-criterion performed best out of the conventional designs and almost equally well as the best of the dedicated criteria. Moreover, the modelling results of the D-criterion were less dependent on the experimental variability and differences in the microbial response than the two selected DOE techniques. Finally, it was proven that solving the optimisation of the D-criterion can be made more efficient by considering the sensitivities of the growth rate relative to its value as Jacobian matrix elements instead of the sensitivities of the cell density measurements.

Introduction

Building mathematical models in predictive microbiology is a data driven science. When building, e.g., secondary models describing the effect of environmental conditions on the growth rate, a large number of influencing factors is often considered. Consequently, the set of experiments required to build accurate predictive models often involves a significant work load and is associated with a high cost. As such, it is not surprising that

the development and implementation of experimental design techniques has been the topic of several publications in the field (e.g., Bernaerts et al. (2005); Balso-Canto et al. (2008); Mertens et al. (2012); Van Derlinden et al. (2013)). Two subcategories of experimental design techniques can be distinguished. On the one hand, researchers implement design of experiments (DOE) to select a set of experimental conditions that is optimised for the identification of polynomial response surface models. Even though secondary models in predictive microbiology are most often a type of polynomial equations (albeit well-constructed polynomial equations), DOE does not deliver experimental conditions that are truly optimised for the model structures at hand. On the other hand, optimal experimental design (OED) techniques deliver a tailored selection of experimental conditions based on the model structure and expected or estimated values of the model parameters. For a more in depth discussion of the use of DOE and OED in predictive microbiology, the readers are referred to Akkermans et al. (2017).

Research into the use of OED for predictive microbiology has mainly focused on the design of dynamic experiments (i.e., with time-varying experimental conditions). These dynamic experiments have often proven to be highly informative (e.g., Van Derlinden et al. (2008)). However, the implementation of dynamic conditions is often not practically feasible or requires the use of expensive equipment. As such, the current research will look into the use of OED for the selection of a combination of static experiments. The main research question dealt with in this research is whether the application of OED has an advantage over the more conventional DOE method when estimating the parameters of secondary models describing the effect of environmental conditions on the microbial growth rate. Van Derlinden et al. (2013) also compared DOE and OED techniques for parameter estimation. However, the comparison of designs in their research was limited to finding model parameters approximating the nominal parameters used for simulations. When building secondary models in practice, the most relevant property of the model is its ability to deliver accurate predictions with high confidence. As such, the current research will consider the model prediction uncertainty as a measure for the com-

parison of different experimental designs. Moreover, this research is the first to deal with the selection of an appropriate OED criterion for the design of static experiments in predictive microbiology.

Materials and methods

To carry out this research in a highly controlled manner and to be able to take abstraction of experimental noise, a simulation study was preferred over an experimental study. The research presented in this article is executed in the following steps: (i) a comparison of the available DOE techniques is carried out, (ii) five existing and two adapted criteria for OED for parameter estimation are compared and (iii) the robustness of the selected DOE and OED techniques with respect to uncertainty of the experimental measurements and variability of the microbial behaviour is studied.

Mathematical model

The mathematical model that was identified during the simulation study is discussed here. A model describing the effect of temperature, pH and water activity on the microbial growth rate was selected. The selected model is published in Akkermans et al. (2018b) and was identified using a dataset containing a total of 68 experiments at 63 distinct conditions. The primary model of Baranyi and Roberts (1994) was used to generate and describe microbial growth curves. The cardinal parameter models selected in Akkermans et al. (2018b) are used to describe the individual effect of the temperature, pH and water activity on the microbial growth rate and are combined in a simple gamma model. Model structures and parameters to describe interactions between environmental conditions were omitted in this research to reduce computational times and to work with a gamma model, which is still most commonly applied.

Simulation protocol

Measurements of microbial cell densities are generated using the mathematical model described in the previous section with the model parameters listed in Table 1. Each growth curve was simulated from the reported initial cell density until a concentration of 22.54 ln(CFU/mL) was reached. As such, all growth curves included the lag, exponential and stationary phase of growth. Twelve discrete samples were selected at equidistant time points for every growth curve. Based on the mean squared error that was obtained when identifying the model using experimental data from viable plate counts (in Akkermans et al., 2018a), normally distributed experimental noise with a mean of zero and a standard deviation of 0.356 ln(CFU/mL) was added to simulated measurements. Experiments were simulated within the range of experimental conditions reported in

Table 1: Overview of the model parameter values used to simulate the microbial behaviour using the gamma model described in Akkermans et al. (2018b). The table also presents the uniform distributions of the parameters that are proposed to study the effect of a deviation between the initial model parameters and the true microbial behaviour.

Model parameters	Values	Uniform distribution
T_{min} [°C]	2.0	0.0 - 7.0
T_{opt} [°C]	41.0	35.0 - 41.0
T_{max} [°C]	45.1	45.0 - 50.0
pH_{min} [-]	4.34	4.40 - 4.60
pH_{opt} [-]	7.04	6.50 - 7.50
pH_{max} [-]	9.06	8.60 - 10.00
$a_{w,min}$ [-]	0.9396	0.9300 - 0.9500
μ_{opt} [h ⁻¹]	2.58	2.00 - 3.00
n_0 [ln(CFU/mL)]	7.00	/
n_{max} [ln(CFU/mL)]	22.55	/
q_0	-1.00	/

Table 2: The range of environmental conditions that is studied and in which accurate model predictions are desired.

Condition	Range
T [°C]	8.0 - 43.0
pH [-]	4.70 - 8.50
a_w [-]	0.9500 - 1.0000

Table 2.

Parameter estimation

Parameter estimations were performed in the same manner as reported in Akkermans et al. (2018b). A one-step parameter estimation was applied, i.e., all primary and secondary model parameters were estimated directly on the growth curves. The advantage of using this type of parameter estimations is elaborated in Akkermans et al. (2018a).

Design of experiments

The DOE techniques considered in this research are: (i) full factorial, (ii) inscribed central composite, (iii) Doehlert, (iv) Box-Behnken, (v) circumscribed central composite, (vi) face centred central composite and (vii) Latin square design. Readers are referred to Rasch (2004) or Akkermans et al. (2017) for more detail on these designs.

Optimal experimental design

The OED technique discussed in this article is OED for parameter estimation. With this technique, experiments are selected that optimise a scalar function of the Fisher Information Matrix (F). F is calculated as follows in this research:

$$F = \frac{1}{\sigma^2} J' \cdot J \quad (1)$$

$$J = \frac{\partial n}{\partial p} \quad (2)$$

with J the Jacobian matrix containing the partial derivatives of all model predictions to all model parameters and σ^2 the variance of the measurements, which is $0.356^2 \ln(\text{CFU/mL})$. In this case, the model predictions are predicted cell densities and represented by the vector n . The model parameters are only the secondary model parameters related to the effect of temperature, pH and water activity on the microbial growth rate and are gathered in the vector p . This formulation of F is different from what has commonly been used in predictive microbiology. In this formulation, an amount of information is added to F for every measurement of the cell density that is proposed. In other research, continuous sampling was generally assumed, and F resulted from an integration over the total duration of an experiment. An example of such a calculation of F is found in, e.g., Van Derlinden et al. (2008). In this commonly used calculation, continuous sampling is assumed and the amount of information is equivalent to the amount of information obtained when taking one sample per unit of time. A result of this calculation is that the number of samples in an experiment is considered to be linearly proportional to the duration of the experiment. In practice, however, this would mean that the amount of samples becomes far too large for experiments with slow microbial growth. In this research, the sampling scheme was fixed for the experiments that were designed. This allowed the number of samples to be kept constant and allowed the calculation of the amount of information acquired by these samples. Consequently, the implementation of OED was made more realistic.

Seven objectives for OED were compared. All these objectives are calculated using the Fisher information matrix. However, two different calculations of this matrix were required. The magnitude of the sensitivity of the model output to the model parameters, as expressed by J , varies considerably between the different parameters. If, e.g., an absolute change of 0.01 was applied to both the minimum water activity and the minimum temperature for growth, the effect of the change in minimum water activity on the prediction of the growth (rate) would be much larger. Consequently, experiments would appear to result in much more information on the

minimum water activity than on the minimum temperature. To solve this issue, the model parameters can be normalised. Based on the work of Munack (1991), Bernaerts et al. (2002) performed this normalisation in similar research by multiplying the sensitivity equations with the nominal values of the model parameters. However, this normalisation is questionable when a parameter can be equal to zero (e.g., the minimum temperature for growth) which would mean that the information related to this parameter is always zero as well. In this research, the normalisation was done by multiplying the sensitivity equations (or elements of J) with the domain or image related to this parameter. E.g., the sensitivities with respect to the minimum temperature were multiplied with the difference between the maximum and minimum temperature for growth (T_{min} and T_{max} respectively) to obtain normalised sensitivities \tilde{J} :

$$\tilde{J}_{T_{min}} = (T_{min} - T_{max}) \frac{\partial n}{\partial T_{min}} \quad (3)$$

The normalised sensitivities with respect to the optimum growth rate were obtained by simply multiplying the sensitivities with the estimated value of this parameter. Criteria that were related to the calculation of the variance of the model prediction used the regular calculation of F . All other objectives were calculated based on the normalised value of F , being \tilde{F} . The different objectives and their calculations are listed below.

- **A-criterion:** $\min[\text{trace}(\tilde{F}^{-1})]$: By minimising the trace of the inverse of \tilde{F} (which is the variance-covariance matrix), this criterion minimises the sum of parameter variances.
- **D-criterion:** $\max[\det(\tilde{F})]$: The maximisation of determinant of \tilde{F} results in the minimisation of the joint confidence region of the parameter estimates.
- **E-criterion:** $\max[\lambda_{\min}\tilde{F}]$: Maximising the lowest eigenvalue causes the minimisation of the longest axis of the joint confidence region.
- **ME-criterion:** $\min[\lambda_{\min}\tilde{F}/\lambda_{\max}\tilde{F}]$: The ME-criterion is aimed at the minimisation of the ration between the longest and shortest axis of the joint confidence region.
- **G-criterion:** $\min[\max(\text{diag}(JF^{-1}J))]$: In this notation, J is the Jacobian matrix of the model predictions and $\text{diag}()$ is the main diagonal of the matrix. The model predictions are maximum specific growth rates μ_{max} , which are calculated using the secondary model identified in this case study. By using the G-criterion, the maximum variance on the model predictions is minimised. This criterion is less commonly used.
- **S_{max}-criterion:** $\min[\max(\sqrt{\text{diag}(JF^{-1}J)})/\mu_{max}]$: In this criterion, the standard deviations of the

model predictions are divided by the corresponding growth rates in the vector μ_{max} . As such, the maximum relative model prediction uncertainty (RMPU) is minimised.

- **S_{mean}-criterion:** $\min[\text{mean}(\sqrt{\text{diag}(JF^{-1}J)}/\mu_{max})]$: This criterion is similar to the S_{max}-criterion with the difference that the mean of the RMPU is minimised.

Experimental design comparison

To evaluate the experimental designs tested in this research, the resulting models were evaluated. Considering the application, it was considered most relevant to study the model prediction uncertainty as a measure for the quality of the obtained model. However, the model prediction uncertainty is evaluated for a specific set of conditions. Obviously, to evaluate the model itself, the model prediction uncertainty over the entire range of relevant conditions should be considered. For this purpose a full factorial design with 7 equidistant levels for every environmental conditions was constructed and the model prediction uncertainty was evaluated at all conditions in this design. The range for the full factorial design was equal to that for the experimental conditions and is reported in Table 2. For this calculation, the variance-covariance matrix of the model predictions V_y is required:

$$V_y = JF^{-1}J \quad (4)$$

The width of the model prediction uncertainty U for 95% confidence intervals is then calculated as:

$$U_k = 2 \cdot 1.96 \cdot \sqrt{V_y(k, k)} \quad (5)$$

In case of predictions of the microbial growth rate for food safety and quality assessment, relative errors of the growth rate should be compared. When making simulations at conditions with a low growth rate, the simulation times will be longer than at high growth rates. As a result, the same absolute error in the growth rate will cause a larger deviation in the predicted growth for low growth rates. Consequently, the relative model prediction uncertainty (RMPU) u is calculated in this research:

$$u = \frac{U}{\mu_{max}} \quad (6)$$

The most relevant measures that can be derived from these RMPUs are the mean and maximum RMPU. It should be stated, that these are only the mean and maximum RMPU of the set of conditions that is considered in the full factorial design and therefore an approximation of the true mean and maximum for the full range of relevant conditions. As 7 levels were used in this calculation, it is assumed that a good approximation was

made. The same full factorial design was used as well for the model predictions considered in the G-, S_{max}- and S_{mean}-criterion.

Experimental variation

Since measurement noise was introduced when generating simulation data, the results are in part dependent on this random noise. To eliminate the influence of this noise, a Monte Carlo method with 100 iterations was implemented for each calculation of the RMPUs of the full factorial design described in the previous section. The mean values of the RMPUs over the Monte Carlo results were calculated. From these results, the overall mean and maximum RMPU was determined. The Monte Carlo simulation results were used as well to assess the influence of the experimental uncertainty on RMPU.

Initial model parameter deviation

The use of OED requires that a model structure with initial estimates of the model parameters is available. However, the quality of this initial guess of the model parameters can influence the convergence rate of the model parameter estimates and the rate with which the model prediction uncertainty decreases. The influence of the initial model parameters on the RMPU was tested using the sigma point method (Julier and Uhlmann, 1996). For this purpose, uniform distributions of the model parameters used for the simulation of the microbial behaviour were proposed (reported in Table 2). These distributions were used to determine the variation of the RMPU as a consequence of the unknown difference between the initial parameter estimates and the response of the microorganism. The mean of the model parameters \bar{p} and variance-covariance matrix of the model parameters V were calculated from the uniform distributions. Consequently, the RMPU (u) for all sigma points was calculated as follows:

$$u_0(\bar{p}) \quad (7)$$

$$u_k(\bar{p} + \sqrt{3V_k}) \text{ with } k = 1, \dots, \nu_p \quad (8)$$

$$u_{k+\nu_p}(\bar{p} - \sqrt{3V_k}) \text{ with } k = 1, \dots, \nu_p \quad (9)$$

with ν_p the number of model parameters and V_k the k^{th} column of V . The mean RMPU (\bar{u}) is then calculated as:

$$\bar{u} = \frac{1}{3} \left((3 - \nu_p)u_0 + \frac{1}{2} \sum_{k=1}^{2\nu_p} u_k \right) \quad (10)$$

The variance of the RMPU (σ_u^2) is then approximated using the following equation:

$$\sigma_u^2 = \frac{3 - \nu_p}{3} (u_0 - \bar{u})^2 + \frac{1}{6} \left(\sum_{k=1}^{2\nu_p} (u_k - \bar{u})^2 \right) \quad (11)$$

Results and discussion

Several DOE and OED techniques are tested and compared for the estimation of the parameters of secondary models for the microbial growth rate. The designs are compared based on their ability to lead to a low mean and maximum RMPUs.

Design of experiments

Initially, 7 experimental designs were considered: (i) full factorial, (ii) inscribed central composite, (iii) Doehlert, (iv) Box-Behnken, (v) circumscribed central composite, (vi) face centred central composite and (vii) Latin square design. However, only the first three were found suitable to test in the current case study. The Box-Behnken and face centred central composite designs have just 3 levels for every factor. However, in both the temperature and pH dimension, the mathematical model has 4 degrees of freedom (minimum, optimum and maximum input and optimum growth rate). As such, it is impossible to find a unique combination of model parameter estimates and impossible to provide accurate model predictions with any certainty. The circumscribed central composite design places conditions outside the experimental range. In case of the secondary models for the microbial growth rate, this would result in conditions where the mathematical model equations are not valid because they don't allow growth or even lead to inactivation. The Latin square design was proposed as a good alternative to the full factorial design by Mertens et al. (2012), when a significant number of factors and/or levels is studied, due to its low number of experimental conditions. However, the downside is that there is no unique solution to constructing a Latin square design, making it both difficult to construct and not necessarily reliable due to the various possible outcomes. Consequently, these four designs were not included in the comparison.

The full factorial design was constructed with 4 levels of temperature, 4 levels of pH and 3 levels of water activity. This results in a total of 48 experimental conditions. The number of levels was thereby limited to the minimum that would allow identifiability of the secondary model as a higher number of levels would result in an excessive number of experiments. This design has the highest number of experiments and resulted in the lowest RMPU (both mean and maximum value). RMPUs of the DOE techniques are compared in Fig. 1. The mean RMPUs are compared as well with the OED techniques in Table 3 (discussed in the following two sections). Two versions of the inscribed central composite

design were tested. In the first, a single experiment was placed on each of the experimental conditions. In the second, 9 replicates were added at the central point of the design, as commonly done in literature and as is standard in the function *ccd* of MATLAB version 9.0 (The MathWorks). These additional central points are aimed at the identification of quadratic terms (Myers et al., 2009). As such, central composite designs of both 15 and 24 experiments were tested. Comparing the results of these two central composite designs (Fig. 1) demonstrates that the addition of the central points has little advantage with respect to the RMPU. Compared to the full factorial design, the RMPU is clearly higher for the central composite designs. However, the performance of the central composite design is adequate considering that the amount of experimental data required is much lower. Finally, the Doehlert design has a relatively high mean and maximum RMPU. Considering that it requires just 2 experiments less than the central composite design, it can be said that this design performs poorly for the identification of the secondary model in this case study. As the number of experiments is not that different, the main difference between the Doehlert and central composite design is in the selection of the experimental conditions. It should be stressed, that DOE does not take into account the model structure at hand and that it is therefore possible that other examples exist in which, e.g., the Doehlert design performs better than the central composite design.

Overall, it can be said that the central composite design with 15 experiments and the full factorial design performed best. Between these two designs, a selection can be made depending on the accuracy (as expressed by the RMPU) that is desired.

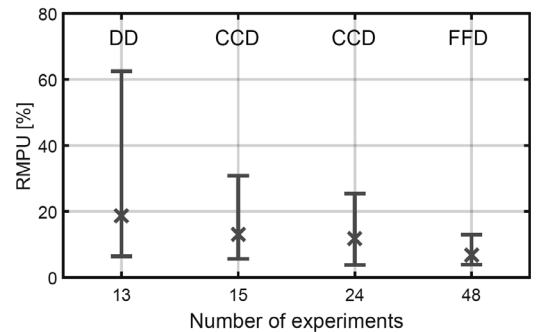


Figure 1: Comparison of the relative model prediction uncertainty resulting from different experimental designs (from left to right): (i) Doehlert design, (ii) central composite design with 15 and (iii) 24 experiments and (iv) full factorial design. Error bars represent the minimum and maximum relative model prediction uncertainty.

Table 3: Comparison of the mean relative model prediction uncertainty resulting from various applications of DOE and OED. The number of experiments required is listed at the top of each column.

Experiments	Mean relative model prediction uncertainty [%]			
	13	15	24	48
Doehlert	18.7	/	/	/
Central composite	/	13.1	11.7	/
Full Factorial	/	/	/	6.9
A-optimal	14.8	14.7	14.4	14.3
D-optimal	10.3	9.6	8.1	6.5
E-optimal	30.0	28.2	25.6	24.3
ME-optimal	27.0	25.0	21.1	18.8
G-optimal	55.8	48.8	28.5	15.5
S _{max} -optimal	11.4	10.4	8.0	5.6
S _{mean} -optimal	10.0	9.2	7.1	5.0

Optimal experimental design

In total, eight secondary model parameters need to be estimated in the current case study. As such, a minimum of 8 experiments is required for practical identifiability (although not every set of experimental conditions will allow practical identifiability). As such, to use the techniques explained the materials and methods, a set of 8 experiments was designed based on the initial guess of the model parameters. Initially, the nominal model parameters were provided as initial guess and the influence of the deviation between the initial guess and the nominal parameters was studied later. It should be stated that the experimental range was selected based on the nominal parameters as well, and therefore, the conventional DOEs had a similar advantage as the OED techniques. Convergence of the OED-criteria to their global optima for the initial experiments was aided by us of a multi-start procedure with 500.000 initialisations selected according to a Sobol sequence. After the first 8 experiments were designed, growth curves were simulated, a parameter estimation was performed and a single new experiment was designed. Parameter estimations were always performed on the full available dataset. This procedure was repeated until a total of 48 experiments were performed, i.e., the same number of experiments as required for the full factorial design.

Fig. 2 illustrates the performance of the OED objectives by comparing both the mean and maximum RMPU as a function of the number of experiments. The A-criterion provides a good mean and maximum RMPU for the first 8 experiments that are designed simultaneously (Fig. 2). However, when adding more experiments according to the A-criterion, there is little improvement in the resulting RMPU. The A-criterion focuses on minimising the sum of the variances on the model parameter estimates.

The A-criterion does not appear to provide much useful information when applied to design the additional experiments. Based on the results in Fig. 2, it can be stated that the D-criterion outperforms the four other criteria that were taken from literature (A-, E, ME- and G- criteria). The use of the D-criterion resulted in a good mean and maximum RMPU after implementing the first 8 experiments and a continuous decrease of the RMPU when adding more experiments. Both the E- and ME-criterion performed overall poorly. This may be surprising as the formulation of these criteria appears to be sound. The principle of both criteria is to reduce the size of the joint confidence region of the parameter estimates by focusing on the worst estimate or largest correlation between parameters. The D-criterion on the other hand has no specific preference as to which error to reduce first, but is rather aimed at minimising the overall size of the joint confidence region. Apparently, the focus of the D-criterion on the combination of the model parameters is more advantageous towards obtaining the low RMPUs. The results are in line with the work of Bernaerts et al. (2005) who generally found lower expected uncertainty on the parameter estimates when using D-optimal design instead of using E-optimal design. On first glance, the G-criterion appears to be most closely related to the RMPU compared to the A-, D-, E and ME-criteria. However, the G-criterion is aimed specifically at the maximum absolute error of the model prediction, in this case the microbial growth rate. As previously explained, it is the relative error and not the absolute error that should be considered when modelling the growth rate. Making this distinction is clearly an important issue as the results of the G-criterion are by far the worst of the 7 criteria tested here. With respect to the maximum RMPU, most of the results of the G-criterion were omitted from Fig. 2b to improve the clarity of this figure.

The S_{max}- and S_{mean}-criteria are two OED-criteria that were tailor made for the purpose of this research. The formulation of these two criteria corresponds to the evaluation based on respectively the maximum and mean RMPU. Consequently, both criteria gave good results as expected. The S_{mean}-criterion turns out to provide both better mean and maximum RMPUs than the S_{max}-criterion. This is due to the fact that using the mean of the discrete set of RMPUs is more robust than using the maximum. If the maximum was calculated using the continuous relationship between experimental conditions and the RMPU, the S_{max}-criterion should result in lower maximum RMPUs. This difficulty with using the maximum RMPU is also seen in the graphs of Fig. 2, which show much noisier results for the maximum than for the mean RMPU. Another surprising finding is that the results of the D-criterion are largely similar to those of the S_{max}- and S_{mean}-criteria.

Even though the S_{mean}-criterion performed slightly better than the D-criterion, the standard D-criterion is

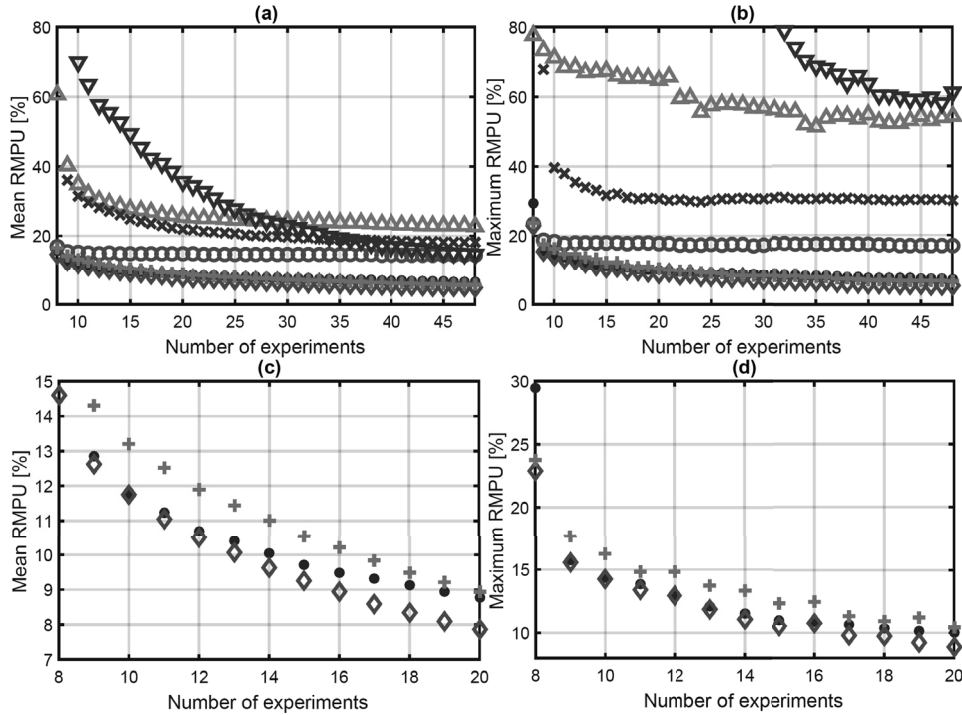


Figure 2: Comparison of the mean (a, c) and maximum (b, d) relative model prediction uncertainty resulting from the different OED objectives: A-criterion (O), D-criterion (●), E-criterion (△), ME-criterion (x), G-criterion (▽), Smax-criterion (◇) and Smean-criterion (+). Some results of the G-criterion are not shown as the relative model prediction uncertainty was significantly higher than for the other criteria and showing these results would decrease clarity of the figure.

more straightforward to implement. Consequently, it can be concluded that the D-criterion is very well suited for the purpose of selecting experimental conditions to identify secondary models that describe the microbial growth rate.

Comparison DOE and OED

A comparison between all studied DOE and OED techniques based on the mean RMPU is presented in Table 3. Based on the results on the DOE techniques, it can be said that the central composite design with 15 experiments and the full factorial design performed best out of the tested DOE techniques, compared to the experimental load. For the OED criteria, the D-optimal design was selected out of the conventional criteria. Comparing the results of the D-optimal design with the DOEs shows that the difference in mean RMPU is larger for the central composite design than for the full factorial design. It should be said that at a lower RMPU, it takes more additional effort to achieve the same absolute reduction of the RMPU than at high values. Comparing as well with the S_{mean} -criterion shows that it is possible to achieve about the same mean RMPU with just 24 experiments as the full factorial design reaches with twice as many. This emphasises the possibility of greatly reducing the experimental load by choosing highly informative experimental conditions.

Table 4: Influence of the experimental uncertainty and deviation between the initial model parameters and real microbial behaviour on the RMPU. Results are presented as standard deviations of the RMPU due to the variation that is introduced in respectively the experimental data and the model parameters used for simulations.

Design	Exp.	Influence on RMPU of:	
		Experimental uncertainty [%]	Microbial response [%]
D-optimal	15	0.56	0.24
D-optimal	48	1.22	0.59
CCD	15	1.22	0.59
FFD	48	0.56	0.70

Moreover, the two selected DOE techniques and the D-optimal OED were compared in their dependency on the experimental uncertainty and the true microbial response. In case of the OED criterion, the variability in the simulated microbial growth rate signifies specifically the importance of the choice of the initial parameter values. In case of DOE, the variability in the growth rate represents the influence of the selection of the experimental range. These results are summarised in Table 4. The RMPU was shown to be less dependent on both the

experimental uncertainty and microbial response for the D-optimal design than for the central composite and full factorial designs. The high dependence of the RMPU on the microbial response for the full factorial design is most likely due to the fact that it only contains the bare minimum number of levels and is therefore a less robust design. The more robust results for OED than for DOE are assigned to the fact that OED takes into account information on the model structure and parameters.

The main downside of OED compared to DOE is of course that it is more difficult for experimenters to find the experimental conditions because OED requires that an optimisation problem is solved. Consequently, a simplified calculation of the objective formulated in the materials and methods section was sought. The calculation of F that was used in this research was based on the objective function of the one-step parameter estimations. As such, the elements of the Jacobian matrix are calculated as the sensitivity of the predicted growth to the model parameters. Calculating these sensitivities requires the solution of differential equations. Even though these equations can be solved numerically, this step makes the computations more complex and much slower. Consequently, the sensitivities of the growth rate relative to its value are considered as Jacobian elements, to prevent the requirement of solving differential equations. J is then defined as follows:

$$J = \frac{1}{\mu_{max}} \frac{\partial \mu_{max}}{\partial p} \quad (12)$$

The normalised J and F were then calculated in the same way as explained in Eq. 3. The resulting mean RMPUs from the D-criterion with J based on cell densities and growth rates is presented in Fig. 3. These results clearly show that the simplified formulation of the objective is equivalent to the more complex.

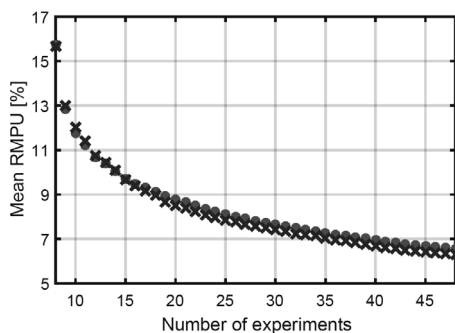


Figure 3: Comparison of the calculation of the D-criterion using the Jacobian matrix with the cell densities (\bullet) and the growth rates (\times) as model output based on the resulting mean relative model prediction uncertainty.

Conclusions

The current study compared several DOE and OED techniques based on their ability to lead to low model prediction uncertainty for secondary models for the microbial growth rate. The comparison established that the central composite and full factorial design were the most suitable DOE techniques and that the D-optimal design is the best performing OED technique available in literature. A new S_{mean} -criterion was developed as a dedicated design for the current case study. This design was demonstrated to perform better than the D-optimal design, albeit slightly. The dedicated design mainly served to demonstrate that the more simple D-optimal design performs very adequate for this application. D-optimal design is therefore advised to be used for the selection of experimental conditions to identify secondary models describing the microbial growth rate in predictive microbiology. The calculation of optimal conditions can be carried out efficiently, without solving differential equations, by considering the sensitivities of the growth rates as Jacobian elements. Finally, the results demonstrated that OED techniques can lead to a significant reduction of the experimental load compared to DOE, even for studies that are restricted to working with static environmental conditions.

Acknowledgements

This work was supported by KU Leuven [PFV/10/002] Center-of-Excellence Optimization in Engineering (OP-TEC) and the Belgian Science Policy Office (DYSCO) [IAP VII/19].

References

- Akkermans, S., Logist, F., and Van Impe, J. (2018a). Parameter estimations in predictive microbiology: Statistically sound modelling of the microbial growth rate. *Food Research International*, In Press.
- Akkermans, S., Noriega Fernandez, E., Logist, F., and Van Impe, J. (2018b). An interaction model for the combined effect of temperature, pH and water activity on the growth rate of *E. coli* K12. *Food Research International*, In Press.
- Akkermans, S., Telen, D., Nimmegeers, P., Valdramidis, V., and Van Impe, J. (2017). Model calibration based on informative experiments: DOE and OED. In Valdramidis, V., Cummins, E., and Van Impe, J., editors, *Quantitative Tools for Sustainable Food and Energy in the Food Chain*, pages 89–124. Eurosis, Ghent (Belgium).
- Balso-Canto, E., Alonso, A., and Banga, J. (2008). Computing optimal dynamic experiments for model

- calibration in predictive microbiology. *Journal of Food Process Engineering*, 31(2):186–206.
- Baranyi, J. and Roberts, T. (1994). A dynamic approach to predicting bacterial growth in food. *International Journal of Food Microbiology*, 23(3–4):277–294.
- Bernaerts, K., Gysemans, K., Nhan Minh, T., and Van Impe, J. (2005). Optimal experiment design for cardinal values estimation: Guidelines for data collection. *International Journal of Food Microbiology*, 100(1–3):153–165.
- Bernaerts, K., Servaes, R., Kooyman, S., Versyck, K., and Van Impe, J. (2002). Optimal temperature input design of the Square Root model parameters: parameter accuracy and model validity restrictions. *International Journal of Food Microbiology*, 73:145–157.
- Julier, S. and Uhlmann, J. (1996). *A general method for approximating nonlinear transformations of probability distributions*. Robotics Research Group, Department of Engineering Science, University of Oxford.
- Mertens, L., Van Derlinden, E., and Van Impe, J. (2012). Comparing experimental design schemes in predictive food microbiology: Optimal parameter estimation of secondary models. *Journal of Food Engineering*, 112:119–133.
- Munack, A. (1991). *Measuring, Modelling and Control. Biotechnology*, volume 4. VCH, Weinheim (Germany).
- Myers, R., Montgomery, D., and Anderson-Cook, C. (2009). *Response surface methodology: Process and product optimization using designed experiments*. John Wiley & Sons, Hoboken (USA), 3 edition.
- Rasch, M. (2004). Experimental design and data collection. In McKellar, R. and Xuwen, L., editors, *Modeling Microbial Responses in Food*, pages 1–20. CRC Press, Boca Raton (USA).
- Van Derlinden, E., Bernaerts, K., and Van Impe, J. (2008). Accurate estimation of cardinal growth temperatures of *Escherichia coli* from optimal dynamic experiments. *International Journal of Food Microbiology*, 128(1):89–100.
- Van Derlinden, E., Mertens, L., and Van Impe, J. (2013). The impact of experiment design on the parameter estimation of cardinal parameter models in predictive microbiology. *Food Control*, 29(2):300–308.

THE ROLE OF CONTROL STRATEGIES FOR THE IMPLEMENTATION OF FOOD SAFETY IN HOSPITAL AND HEALTH UNITS, AS A TOOL FOR HACCP ASSISTANTS AND SIMULATORS

Efstathia Tsakali
Department of Chemical Engineering
BioTeC+ & OPTEC
KU Leuven
Gebroeders De Smetstraat 1
B-9000 Gent, Belgium
E mail: efi.tsakali@kuleuven.be

Olga Gortzi
Department of Food Technology
Technological Educational
Institute of Thessaly
Terma Temponera
43100 Karditsa
Greece

George Boskou & Andreas Souliotis
Department of Nutrition-Dietetics
Harokopio University
70 El. Venizelou
17671 Athens
Greece

Dimitrios Timpis & John Tsaknis
Department of Food Technology
Technological Educational of Athens
Agiou Spiridonos
12243 Athens
Greece

KEYWORDS

Microbiological sampling, food safety, GHP.

ABSTRACT

Food safety in the catering sector of hospitals and other health care units is a very sensitive issue and can be a challenge due to several factors. Patients are particularly susceptible to foodborne illnesses because of disease, medication, malnutrition, or because their immune system is compromised as a result of age, infection or pregnancy. At the same time in hospitals it is not always possible to invest the same amounts on kitchen/ laboratory equipment and quality control, as in food industry. The ESTIASIS project -a European Union and Greece co-founded program- undertook initiatives and targeted actions in the direction of Food safety and Hygiene management in hospitals. An extended sampling plan for microbiological testing of surfaces and food was implemented in order to highlight the importance of control strategies. Final data consisted of nonparametric values so the analysis performed was for frequencies and for cross tabulation. Data mining was performed with the “a priori” algorithm in order to determine the most frequent cases and the association rules. The results demonstrate the significance of GHPs (Good Hygiene Practices) and offer valuable tools for HACCP (Hazard Analysis of Critical Control Points) simulators

INTRODUCTION

Food safety management systems are very useful tools in helping towards the elimination of foodborne outbreaks as they assist the professionals to control the conditions under which food is prepared and distributed. Developing and

implementing such systems in hospital settings can be a challenge though. The application of appropriate control and assurance measures to guarantee food safety are directly affected by several factors. The number of special recipes and their methods of preparation are considerable while patients are differentiated from the general population in terms of their needs and their resistance to lower quality foods due to their low immune system. The meals vary according to feed needs, so the final products are not as standardized as in the food industry and the supplies required cover almost the full range of the food market. On the other hand, hospital catering services are harmonised with other hospital services since they are not an exclusive activity of the institution. The staff involved in this sector are of different specialties, making proper training difficult.

Several cases of foodborne outbreaks in hospitals have been reported due to *Salmonella enterica*, *Clostridium perfringens*, *Listeria monocytogenes*, *Escherichia coli* O157, and *norovirus* (Lund and O’ Brien 2009, Tsakali et al. 2016). Cases of foodborne illnesses in hospitals, may lead to serious diseases, the treatment of which is costly and there is the possibility of spreading to other patients (Lund and O’ Brien 2009, Palmer et al. 2000). Improper practices responsible for microbial foodborne illnesses have been well documented by Egan et al. (2007) and typically involve cross-contamination of raw and cooked food, inadequate cooking, and storage at inappropriate temperatures but also poor personal hygiene and food from unsafe sources (FDA 2010). Food safety programs of the past tend to correct the hazard conditions after they have been occurred (Yousif et al. 2013). The HACCP approach is to control problems before they happen during processing and/or serving (McSwane et al. 2003). Hazard analysis and critical control points are considered as an effective and rational means of assuring food safety,

which can be applied throughout the food chain from primary production to final consumption (Domenech et al. 2008).

The Estiasis Project

The Estiasis project was a European Union and Greece co-founded program which focused on the design and the development of intervention programs for food safety management in hospitals, nursing houses and infirmaries of chronic diseases. The program lasted three years and consisted of three stages. Initially, fifteen health units in the Greek mainland were selected and assessed for the implementation of food good hygiene practices (GHP). This stage included diagnostic studies and mapping of the existing practices with in-situ visits by food safety inspectors and with a self-assessing questionnaire. Conduction of successive tests on the prevailing conditions in production areas and equipment also took place as well as consecutive microbiological and chemical analyzes in food materials, prepared meals and surfaces. All these were used for the risk identification and definition of Critical Control Points (CCP's) and finally the creation of corrective action reports for each health unit. The management and the employees involved from each health unit were informed about the results of the diagnostic studies and targeted actions were suggested in the form of a technical report. Based on the findings of the first stage a Template Manual of Food Hygiene and Safety was designed, in accordance with the requirements of ISO 22000:2005 standard. The prepared manual corresponded to actual realistic facts and it could be also used by other health units with suitable small adjustments, where appropriate (Tsaknis et al. 2014). At the same time, original informative material for the employees of the health units was prepared on the effective implementation of food hygiene and safety and the requirements of the legislation. A -10 hours-seminar for the awareness of the employees was then followed. After the completion of the corrective actions and the training of the staff, the facilities which met the requirements of the ISO 22000:2005 standard were certified by an independent agency. For the dissemination of the importance of the Estiasis actions, a web site was created, three workshops took place and there were several publications in the local press.

The aim of this paper is to present the results of the microbiological testing of food and surfaces which were used for the assessment of GHPs in the health setting prior and after the implementation of corrective actions, the training of the employees and the establishment of a realistic Food Safety Management System.

MATERIAL AND METHODS

Sampling and Examined parameters

Samples were taken from the catering areas and the relating equipment of 15 health units in Greece at two stages. The first stage was during the first visit of a food safety inspector in order to evaluate the conditions and the second after the implementation of corrective actions and training of the staff.

The period between the two stages was at least one month but no longer than four months.

Surfaces

For the microbiological sampling of the surfaces a swab technique that met the requirements of ISO18593:2004 standard, was used. As hygiene indicators, the parameters selected and tested were Total Viable Count (TVC) by ISO 4833:2003 and Coliforms by ISO 4832:2006. The surfaces included benches, disks, trays, cutlery, dishes, pots, refrigerators, handles and environmental air and were divided in three categories: surfaces of Direct Food Contact (DFC), surfaces of Indirect Food Contact (IFC) and surfaces of No Food Contact (NFC).

Food

Due to the high variation in the menus of the different health units the food samples were divided in two big categories: Raw Material for further processing (RM) and food Ready to Eat (RTE). As hygiene indicators, all food samples were tested for Total Viable Count (TVC) by ISO 4833:2003, Coliforms by ISO 4832:2006 and *Escherichia coli* by ISO 7251:2005. All food samples were also tested for the enumeration of coagulase-positive staphylococci by ISO 6888-1:1999 and *Salmonella spp.* by ISO 6579:2002. Meat and dairy samples were also tested for *Listeria monocytogenes* by ISO 11290:1996.

The amount of the samples tested per category prior and after the Estiasis intervention actions, are presented in Table 1.

Table 1: Summary Table for all Multiple Response Items

N= 876	SURFACES			FOOD		Total
	NFC	IFC	DFC	RTE	RM	
Before	79	226	149	81	21	556
After	35	101	41	79	64	320
All	114	327	190	160	85	876

Data Analysis

All the reports of microbiological analysis for food and surfaces were collected and classified. After thorough examination of all the reports the information was registered in data-sheets with the following variables: hospital code, sampling food or surface, date of sampling and the microbiological criteria. Furthermore the date was characterized as "before" or "after" according to the timing of the intervention. The food items were classified as raw materials (RM) and ready to eat (RTE) and the surfaces as direct food contact (DFC), indirect food contact (IFC), no food contact (NFC). The microbiological criteria were classified as pass or fail, according to the outcome of the analysis in reference with the EU regulations for microbiological criteria. Statistical analysis was performed with Statistica 8.0 (StatSoft Inc. 2007). Final data consisted of nonparametric values so the analysis performed was for frequencies and for cross tabulation. Data mining was performed with the "a priori" algorithm in order to determine

the most frequent cases and the association rules (minimum support 10% and minimum confidence 80%).

RESULTS AND DISCUSSION

The results of the data analysis of the microbiological testing of both surfaces and food samples are presented in Table 2. It is profound that the number of RTE food and RM that could be considered acceptable is higher after the intervention actions than it was before. Concerning surfaces the total number of samples taken after was lower than the number of samples taken before, since most of the samples were acceptable. Again, in the categories of NFC and IFC it is observed that the number of samples that failed prior to interventions is lower than after the implementation of Estiasis. However, in the case of DFC surfaces the number of unacceptable samples was greater than the accepted samples both prior and after the intervention actions. The percentage of fail even increased from 60.4 to 75.6%.

Table 2: Summary Table for all Multiple Response Items (food-surf.sta) Totals/percentages based on number of respondents (multiple identical responses were ignored)

N=873	category	Before		After	
		pass	fail	pass	fail
Surfaces	NFC	20	59	23	12
	IFC	81	145	54	47
	DFC	59	90	10	31
Food	RTE	77	3	76	1
	RM	19	2	58	6

In Table 3 some association rules that come out of the results are presented. Rule 3 and rule 9 seem to be tautological, however the difference in confidence demonstrates that it is more likely that a food sample that passed before the interventions could be raw materials and not ready to eat. The difference between rule 4 and rule 1 is that there are more cases of raw materials than ready to eat that were not acceptable at sampling after. It would be expected that rule 2 and 5 have difference with rule 5 and 6 since raw materials do not have any kind of processing so it is very possible to fail. However, rule 7 and 8 are unique and show that most of no food contact surfaces could fail before while most of the direct food contact surfaces could pass before.

Table 3: Association rules originating from the results

	IF	THEN	Support (%)	Confidence (%)
1.	after, RTE	food-pass	8.7	96.2
2.	RTE	food-pass	17.5	95.6
3.	before, RTE	food-pass	8.8	95.1
4.	after, RM	food-pass	6.6	90.6
5.	RM	food-pass	8.8	90.6
6.	before, RM	food-pass	2.2	90.5
7.	surface-pass, DFC	before	6.7	85.5
8.	NFC, surface-fail	before	6.7	83.1
9.	before, food-pass	RTE	8.8	80.2

The results indicate that the intervention actions of the Estiasis had an impact on the hygiene conditions on both surfaces and food except the case of DFC. The results could be easier interpreted when the different food categories are compared, for example to high risk food and to low risk food. In establishments where there is a lack of other means, the training of employees has more direct impact on the attention to high risk food. Tsakali et al. (2016) demonstrated that during the Estiasis project the reduction of microbiological index values was greater in processed meals where the impact of handlers' good practices is crucial. The raw materials were better preserved and showed a reduction of the total plate count value by 75.0% while ready meals were better prepared and showed a reduction of 99.5% and 99.9% for cooked meals and fresh green salads, respectively. In the case of DFC the results need further investigation since the samples after the interventions was significantly lower and any conclusions could not be considered safe.

CONCLUSIONS

The Estiasis project run for the first time an extended microbiological sampling plan for the evaluation of the conditions in the catering session of Greek health units and the impact of focused intervention programs towards food safety management. The results indicate the good initial condition of catering departments but also the importance of training and the implication of FSMS for the constant improvement of the settings. The data produced are a useful tool for further analysis by HACCP assistants and simulators.

ACKNOWLEDGEMENTS

The writers acknowledge the support they received through the Operational Program "Human Resources Development" of the National Strategic Reference Framework (NSRF)-Research Funding Program: ESTIASIS - Systemic Interventions MIS 372969, co-financed by the EU (European Social Fund – ESF) and Greek national funds

REFERENCES

- Domenech, E.; Escriche, I. and Martorell, S. 2008. "Assessing the effectiveness of critical control points to guarantee food safety." *Food Control*, No 19, 557–565.
- Egan, M.B.; Raats, M.M.; Grubb, S.M.; Eves, A.; Lumbers, M.L.; Dean, M.S. and Adams, M.R. 2007. "A review of food safety and food hygiene training studies in the commercial sector." *Food Control*, No 18, 1180–1190.
- FDA National Retail Food Team. 2004. "FDA report on the occurrence of foodborne illness risk factors in selected institutional foodservice, restaurant, and retail food store facility types."
- Gikas, A.; Kritsotakis, E.; Maraki, S.; Roubelaki, M.; Babalis, D.; Scoulica, E.; Panoulis, C.; Saloustros, E.; Kontopodis, E.; Samonis, G. and Tselentis, Y. 2007 "A nosocomial, foodborne outbreak of *Salmonella* Enterica serovar Enteritidis in a university hospital in Greece: the importance of establishing HACCP systems in hospital catering." *Journal of Hospital Infection*, No 66, 194-196.
- ISO 11290:1996: Microbiology of food and animal feeding stuffs -- Horizontal method for the detection and enumeration of *Listeria monocytogenes*
- ISO 18593:2004: Microbiology of food and animal feeding stuffs -- Horizontal methods for sampling techniques from surfaces using contact plates and swabs
- ISO 4832:2006: Microbiology of food and animal feeding stuffs -- Horizontal method for the enumeration of coliforms - Colony-count technique
- ISO 4833:2003: Microbiology of food and animal feeding stuffs -- Horizontal method for the enumeration of microorganisms -- Colony-count technique at 30 degrees C
- ISO 6579:2002: Microbiology of food and animal feeding stuffs - Horizontal method for the detection of *Salmonella spp*
- ISO 6888-1:1999: Microbiology of food and animal feeding stuffs - Horizontal method for the enumeration of coagulase-positive staphylococci (*Staphylococcus aureus* and other species) -Part 1: Technique using Baird-Parker agar medium
- ISO 7251:2005: Microbiology of food and animal feeding stuffs -- Horizontal method for the detection and enumeration of presumptive *Escherichia coli* - Most probable number technique
- Lund, B.M. and O'Brien, S.J. 2009." Microbiological safety of food in hospitals and other healthcare settings." *Journal of Hospital Infection*, No 73, 109-120.
- McSwane, D.; Rue, N. and Linton, R. 2003. *Essentials of Food Safety and Sanitation, third ed.* Pearson Education, New Jersey, USA.
- Palmer, S.; Parry, S.; Perry, D.; Smith, R.; Evans, M.; Nehaul, L.; Walapu, M. and Wright, D. 2000. "The role of outbreaks in developing food safety policy: population based surveillance of salmonella outbreaks in Wales 1986–98." *Epidemiology Infection*, No 125, 467-472.
- Tsakali, E.; Gortzi, O.; Timpis, D. and Tsaknis, J. 2016. "Food Safety and Quality Control in the Public Catering Sector- Intervention Program." *Nutrition and Food Technology Vol 2(3)*, 1-3.
- Tsaknis, J.; Timpis, D.; Gortzi, O.; Lalas, S. and Tsakali, E. 2014 *Food Hygiene and Safety in catering of Hospitals, Nursing houses and Infirmaries of Chronic Diseases. Guide book of handlers' awareness.* ELKE TEI of Athens, Greece.
- Yousif, E.I.; Ashoush, I.S.; Donia, A.A. and Hala Goma, K.A. 2013. "Critical control points for preparing chicken meals in a hospital kitchen." *Annals of Agricultural Science*, No 58(2), 203–211

AUTHOR BIOGRAPHY

Efstathia Tsakali holds a BSc in Food Technology from T.E.I. of Athens (GR), an MSc in Food Production Management from The University of Nottingham (UK) and a PhD in the domain of Functional Food of animal origin from the University of Bari (IT). She has 18 years of working experience in the food industry both as a Quality Manager but also as an FSMS auditor. She has also been a food safety seminar lecturer within several collaborations with institutes of continuous learning. Since 2012 she has been an academic associate of the department of Food Technology (T.E.I. of Athens), and since 2015 a visiting professor at the BioTeC+ & BiFTec team at KU Leuven (BE). She has published several contributions to journals and books (book chapters and international conference proceedings) and she has been a speaker at several (inter)national Conferences and Workshops.

MODELLING OF TEMPERATURE, WATER ACTIVITY AND MICROBIAL GROWTH ON THE SURFACE OF A PORK LEG DURING REFRIGERATED TRANSPORTATION

Mouna Merai
Refrigeration Process Engineering Unit-Irstea, Antony, France
E-mail: mouna.merai@irstea.fr

KEYWORDS

3D model, pork leg, temperature, water activity, microbial growth, refrigerated transportation.

ABSTRACT

European regulation previously imposed to slaughterhouses that pork carcasses must be chilled immediately to ensure a core meat temperature below 7°C before future handling operation. Recently the regulation was amended and offers the opportunity to transport carcasses with a core temperature > 7°C from the slaughterhouse to the cutting plants but with continuous refrigeration during their transportation. The purpose of this study was to evaluate the impact of the regulation modification on the microbial growth on the carcasses surface. First, the heat and mass transfer during refrigerated truck transportation were predicted using a 3D pork leg model. Predicted temperature and water activity of the carcasses surface were then used to evaluate microbial growth on the surface. The obtained results showed that in the studied conditions, the leg reached the required temperature (< 7°C) at the core after 10 hours of transportation. Small change in water content/activity was observed. Based on the proposed predictive microbiology model, the maximum microbial load increase was 2.5 log₁₀ after 30 hours of transportation.

NOMENCLATURE

a_w	water activity
$a_{w,\min}$	minimum water activity for microbial growth
C_p	air specific heat capacity (1004 J.kg ⁻¹ .K ⁻¹)
C_p	ham specific heat capacity (3200 J.kg ⁻¹ .K ⁻¹)
C_w	water concentration in the leg (mol.m ⁻³)
D_a	mass diffusivity of air (m ² .s ⁻¹)
D_w	water diffusivity inside the leg (m ² .s ⁻¹)
h	convective heat transfer coefficient (W.m ⁻² .K ⁻¹)
k	mass (water) transfer coefficient (kg.m ⁻² .Pa ⁻¹ .s ⁻¹)
Le	Lewis number of air ($Le = \frac{\alpha_a}{D_a} = 0.777$)
L_v	latent heat of water evaporation (2450 kJ.kg ⁻¹)
M_w	molar mass of water (18 g.mol ⁻¹)

N	microbial load at the surface (CFU.cm ⁻²)
P_{atm}	atmospheric pressure (101325 Pa)
P_{sat}	saturated vapor pressure (Pa)
q	heat flux (W.m ⁻²)
RH	air relative humidity (%)
t	time of transportation (s)
T	leg temperature (K)
T_{\min}	minimum temperature for microbial growth (K)
T_s	surface temperature at the muscle or rind part (K)
T_a	air temperature around the muscle or rind part (K)
X_w	water content in the leg (kg water/kg total)
Y	logarithmic microbial load at the surface log ₁₀ (N)
α_a	thermal diffusivity of air (m ² .s ⁻¹)
μ	microbial growth rate (s ⁻¹)
μ_{ref}	microbial reference growth rate (s ⁻¹)
Φ_{water}	water evaporation flux from product surface (kg.m ⁻² .s ⁻¹)
λ	ham thermal conductivity (0.45 W.m ⁻¹ .K ⁻¹)
ρ	ham density (1072 kg.m ⁻³)

INTRODUCTION

In order to prevent the contamination of meat with pathogenic during slaughter operations, legislation requires the application of refrigeration immediately after post mortem inspection of carcasses. However, it is important to control the kinetics of product temperature reduction to optimize the meat maturation (ensuring a good technological quality) and the sanitary quality (Savell et al., 2005).

French and European regulations have been enforced for the temperature of meat carcasses before and during transportation (Anonymous, 2004). According to this regulation, the meat must be chilled to reach a core temperature not exceeding 7°C as soon as possible. This refrigeration must be carried out in the cold rooms of the slaughterhouse before any carcass handling operation such as transport or cutting.

However, this strict regulation does not make the difference between the types of pathogenic and spoilage

microorganisms knowing that in the case of pork carcasses, there are essentially aerobic bacteria on the surface. Thus, in 2014, EFSA adopted a new scientific opinion which concluded that the surface temperature is an appropriate indicator of bacterial growth. Consequently, derogations have been adopted in some countries to allow the transport of carcasses or half-carcasses with a core temperature above 7°C, if the transport duration is less than 2 hours.

These derogations eventually triggered in 2016 a new scientific opinion on the growth of bacteria during the storage and transport of meat carcasses (EFSA, 2016). As some bacteria, especially *Pseudomonas* spp., can reach critical levels much faster than pathogenic bacteria, their growth kinetics may be an indicator of the temperature abuse during storage and transport.

Because of the air temperature and velocity heterogeneity in a refrigerated semitrailer, lower product temperature is often observed at the front and higher at the rear. The position of sanitary risk (zone of high temperature and low velocity) can be influenced by the semitrailer design and the carcass arrangement. Thus, an aerodynamic and thermal study in a refrigerated semitrailer loaded with meat carcasses is essential for the understanding of the airflow and the heat transfer coefficient variation at different position (Merai et al., 2018). This allows the identification of risk zones (areas where low air velocities and low convective transfer coefficients are observed).

The purpose of this study was to evaluate the impact of the regulation modification on the microbial growth on the carcasses surface. First, the heat and mass transfer during refrigerated truck transportation were predicted using a 3D pork leg model. Predicted temperature and water activity of the carcasses surface were then used to evaluate microbial growth on the surface. The developed

model can be used in the future to study the influence of transport conditions (e.g. loading temperature of carcasses and air relative humidity) on the growth of bacteria at different areas in refrigerated semitrailer.

MATERIALS AND METHODS

Our problem statement is the simultaneous heat transfer, mass (water) transfer and microbial growth in a complex geometry object such as a meat carcass exposed to different operating conditions encountered in a refrigerated semitrailer. In this case, several transport phenomena occur, heat transfer by conduction inside the product and convection between product surface and air. Water migrates from the product inside to the surface and evaporates into the surrounding air. The product temperature and the water activity at the surface are determining factors of microbial growth.

3D geometry and meshing

A 3D model developed in COMSOL® Multiphysics by Harkouss et al., 2018 of a pork leg was used in order to predict the temperature, water activity and microbial growth evolution on the muscle surface part during transportation (collaboration with INRA-Theix, France).

Based on X-ray imaging of a real pork leg, a 3D geometry was produced respecting its different parts, i.e. rind, muscles and bone (Figure 1a). A volumetric mesh was then constructed on the 3D geometry (42 cm of length; 32 cm of width and 15.8 cm of depth) (Figure 1b) consisting in 202000 tetrahedral meshes and containing the different parts.

Two zones were considered: rind part with low water evaporation and heat transfer and muscle part with water evaporation and heat transfer and microbial growth (Figure 1c).

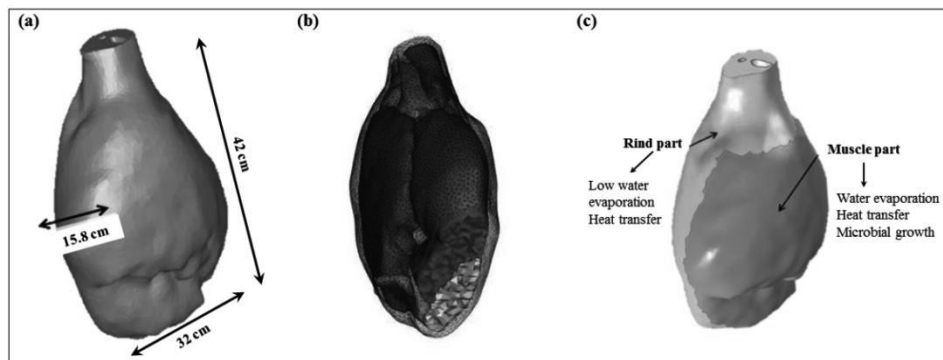


Figure 1: Views of (a) the 3D leg geometry and its dimensions, (b) the volumetric tetrahedral mesh with the different components of the leg imported into Comsol® Multiphysics software and (c) two considered zones on the leg (Harkouss et al., 2018).

Numerical models

Heat transfer modelling

In order to numerically simulate heat transfer inside the leg and predict temperature evolution during transportation, Fourier law was used:

$$\rho C_p \frac{\partial T}{\partial t} = \vec{\nabla} \cdot (\lambda \vec{\nabla} T) \quad (1)$$

This equation was applied and solved in all domains of the numerical leg, except the bone which was considered as thermally insulated.

At the air-leg interface, both the thermal convection and the energy exchanged during water evaporation were taken into account. Thus, at this boundary the heat flow rate q was calculated as follow:

$$q = -\lambda \vec{\nabla} T \cdot \vec{n} = h(T_{\text{surface}} - T_{\text{air}}) + \varphi_{\text{water}} L_v \quad (2)$$

Mass transfer modelling

The water migration inside the carcasses during transportation can be modelled by the Fick equation that was solved in all domains except in the bone:

$$\frac{\partial C_w}{\partial t} = \vec{\nabla} \cdot (D_w \cdot \vec{\nabla} C_w) \quad (3)$$

The water diffusion coefficient can be estimated by the equation presented by Ruiz-Cabrera et al. (2004) which is a function of water content (X_w):

$$D_{\text{water}} = 4 \cdot 10^{(0,625 \cdot X_w - 12)} \quad (4)$$

For the boundary condition (product surface), water evaporation flux was calculated using the following equation:

$$\varphi_w = -D_w \cdot \vec{\nabla} C_w \cdot \vec{n} = k (a_w P_{\text{sat}, T_s} - \frac{RH}{100} P_{\text{sat}, T_a}) \quad (5)$$

Water evaporation was assumed to occur only on the muscle part of the leg. k was calculated from the convective heat transfer coefficient using the Chilton Colburn analogy (Kondjoyan and Daudin, 1997):

$$k = \frac{h \cdot M_{\text{water}}}{C_{p, \text{air}} \cdot M_{\text{air}} \cdot P_{\text{atm}} \cdot Le^{2/3}} \quad (6)$$

$$\text{and } P_{\text{sat}, T} = \exp\left(-\frac{6764}{T} - 4.915 \cdot \log T + 58.75\right) \quad (7)$$

Water activity was expressed as a function of water content (Rougier et al., 2007):

$$a_w = 0.993 \exp(-0.0204 X_w^{-1.96}) \quad (8)$$

Air temperature and relative humidity profiles were measured during real pork carcasses transportation. The convective heat transfer coefficient h was measured in a laboratory scale on the muscle part of the leg.

For the simulation, air temperature and relative humidity around the leg were considered constant (RH = 97 %, $T_a = 4.5^\circ\text{C}$). Initial water content in the pork leg of 0.75 kg water/kg total and initial temperature of 15°C were assumed. Heat convection coefficient was fixed at $20 \text{ W} \cdot \text{m}^{-2} \cdot \text{K}^{-1}$.

Microbial growth modelling

In order to highlight the influence of surface temperature and water activity evolution on a possible microbial growth, a simple preliminary model without lag phase was used (eq.9).

$$\frac{\partial Y(t)}{\partial t} = \mu(T, a_w) \quad (9)$$

where μ was obtained using a secondary model that takes into account temperature and water activity evolution:

$$\mu = \mu_{\text{ref}} (T - T_{\text{min}})^2 \left(\frac{a_w - a_{w, \text{min}}}{1 - a_{w, \text{min}}} \right) \quad (10)$$

No growth is assumed for $T < T_{\text{min}}$ or $a_w < a_{w, \text{min}}$. As a first approach, simulations were made for $T_{\text{min}} = 4.5^\circ\text{C}$, $a_{w, \text{min}} = 0.9$ and μ_{ref} value is fixed at 0.003 s^{-1} . These values depend on the microorganism and other food characteristics like salt concentration or pH. The T_{min} and $a_{w, \text{min}}$ values were chosen as representatives of values that characterized psychrotrophic bacterial species involved in meat spoilage (Gill & Jones, 1992).

Supplementary studies are under way to estimate these values for specific microorganisms often encountered on carcasses and meat cuts like *Pseudomonas*.

RESULTS AND DISCUSSION

Temperature evolution during transportation

To visualize the temperature evolution inside the leg for 1 h, 5 h, 10 h and 30 h transportation, 4 horizontal slices have been selected using the same temperature scale (Figure 2).

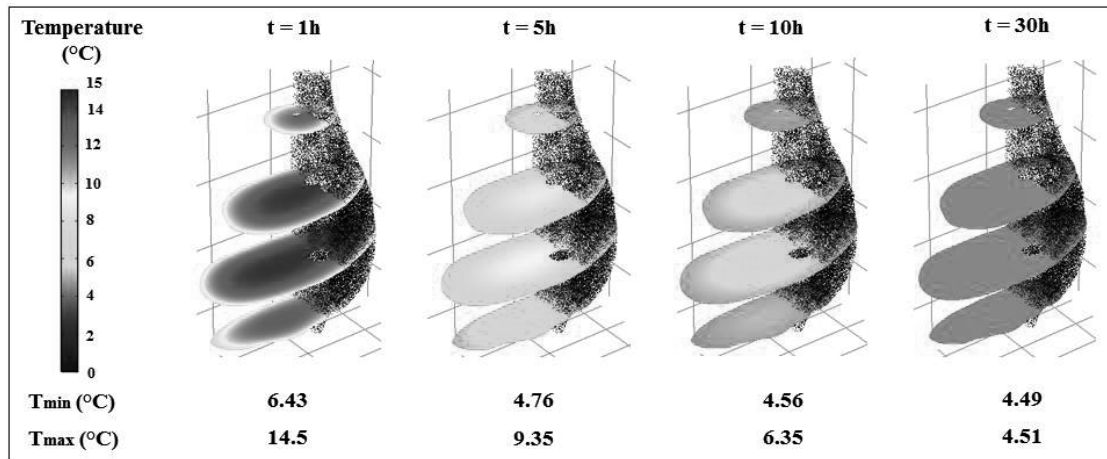


Figure 2: Temperature distribution in four horizontal slices of the carcasses' leg during transportation (t = 1 h, 5 h, 10 h and 30 h) showing the minimum and maximum temperatures.

Water activity evolution during transportation

Water activity varies slightly (results not shown) and can be considered constant around the initial value ($a_w \approx 0.96$). This small variation can be explained by the high relative humidity (97 %) of the air in the loaded refrigerated truck due to the air recycled during transportation.

According to the European legislation (EFSA, 2016), for 30 hours transportation of carcasses with initial core temperature of 15°C, the contamination should not exceed 10^4 CFU.cm⁻² (or 4 log₁₀). Predicted results showed that the logarithmic load increases: maximum value of $\log_{10}(\frac{N}{N_0})$ is lower than 2.5 after 30 hours (with $T_i = 15$ °C). To respect the regulation, the initial contamination should not exceed $10^{2.5} \approx 300$ CFU.cm⁻² in the studied conditions. This initial value of total

Microbial growth during transportation

After 10 hours of transportation, order of magnitude of transportation time in France, the microbial load increases and reaches $\log_{10}(\frac{N}{N_0}) = 1.4$ (Figure 3). This value is consistent with observed increase of total psychotropic microflora during carcass cooling (Gill and Jones, 1997; Afssa, 2009). microflora is consistent with existing literature (Gill and Jones, 1997).

Further work is to be conducted to evaluate the initial level of contamination on carcasses to accurately evaluate the final contamination.

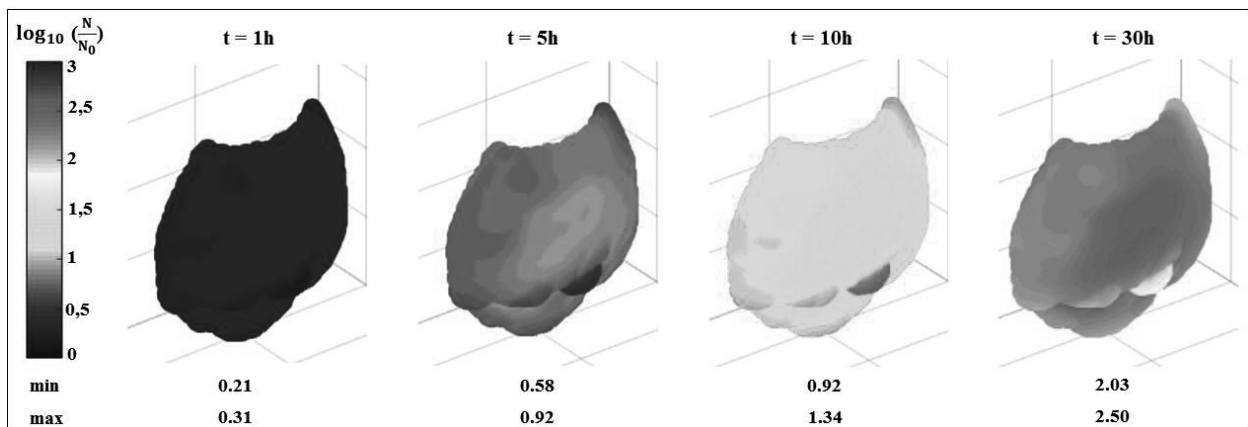


Figure 3: Microbial growth evolution during transportation (at 1 h, 5 h, 10 h and 30 h) showing the minimum and maximum values

CONCLUSION AND PERSPECTIVES

Models were developed to predict the microbial growth on the surface of the lean part of a pork leg during transportation. This choice was based on the fact that the leg is the most problematic in the whole pork carcass as it is the largest part and so it is difficult to cool.

Temperature, water content and water activity evolution were simulated for 30 hours of transportation ($T_a = 4.5$ °C, $RH = 97\%$, $h = 20 \text{ W}\cdot\text{m}^{-2}\cdot\text{K}^{-1}$, $T_0 = 15$ °C). Small changes were observed for water activity while temperature decreased rapidly at the surface of the leg (< 7 °C after 1 hour). After 10 hours of transportation the microbial load increased and reached $\log_{10} \left(\frac{N}{N_0} \right) = 1.4$.

In a future work, different scenarios will be studied varying the relative humidity, air temperature and the heat convection coefficient as a function of the position in the semi-trailer loaded with pork carcasses.

This parametric study will allow a precise prediction of the microbial growth in the most problematic zones of the semi-trailer already identified in our previous work dealing with air velocity distribution around and between the carcasses.

ACKNOWLEDGEMENT

This research work was carried out within the framework of a DIM ASTREA grant by the Regional Council of Ile-de-France (France). The authors thank Pierre-Sylvain Mirade and Jason Sicard from INRA-Theix-France for their collaboration.

REFERENCES

- Afssa, 2009. "Avis relative au transport des carcasses de porc n'ayant pas atteint la température réglementaire à la sortie de l'abattoir".
<https://www.anses.fr/fr/system/files/MIC2008sa0283.pdf>.
- Anonymous, 2004. "Règlement (CE) n°853/2004 du Parlement Européen et du Conseil du 29 avril 2004 fixant des règles spécifiques d'hygiène applicables aux denrées alimentaires d'origine animale".
- EFSA BIOHAZ Panel, 2014. "Scientific opinion on the public health risks related to the maintenance of the cold chain during storage and transport of meat. Part 1 (meat of domestic ungulates)". *EFSA Journal* 2014; 12 (3):3601, 81 pp. doi:10.2903/j.efsa.2014.3601.
- EFSA BIOHAZ Panel, 2016. "Scientific opinion on the growth of spoilage bacteria during storage and transport of meat". *EFSA Journal* 2016; 14 (6):4523, 38 pp. doi:10.2903/j.efsa.2016.4513.
- Gill, C.O., Jones, T., 1992. "Assessment of the hygienic efficiencies of two commercial processes for cooling pig carcasses". *Food Microbiology*. 9, 335-343.
- Gill, C.O., Jones, T., 1997. "Assessment of the hygienic performances of an air-cooling process for lamb carcasses and a spray-cooling process for pig carcasses". *International Journal of Food Microbiology*. 38 (2), 85-93.
- Harkouss, R., Chevarin, C., Daudin, J.D., Sicard, J., Mirade, P.S., 2018. "Development of a multi-physical finite element-based model that predicts water and salt transfers, proteolysis and water activity during the salting and post-salting stages of the dry-cured ham process". *Journal of Food Engineering*. 218, 69-79.
- Kondjoyan, A., Daudin, J.D., 1997. "Heat and mass transfer coefficients at the surface of a pork hindquarter". *Journal of Food Engineering*. 32, 225-240.
- Merai, M., Flick, D., Duret, S., Guiller, L., Laguerre, O., 2018. "Experimental characterization of airflow inside a refrigerated trailer loaded with carcasses". *International Journal of Refrigeration* (in press).
- Rougier, T., Bonazzi, C., Daudin, J.D., 2007. "Modeling incidence of lipid and sodium chloride contents on sorption curves of gelatine in the high humidity range". *LWT-Food Science and Technology*. 40, 1798-1807.
- Ruiz-Cabrera, M., Gou, P., Foucat, L., Renou, J.P., Daudin, J.D., 2004. "Water transfer analysis in pork meat supported by NMR imaging". *Meat Science*. 67, 169-178.
- Savell, J.W., Mueller, S.L., Baird, B.E., 2005. "The chilling of carcasses". *Meat Science*. 70 (3), 449-459.

QUANTITATIVE ANTI-FUNGAL ACTIVITY ASSESSMENT OF ZnO NANOPARTICLES: TOWARDS THE DESIGN AND DEVELOPMENT OF NOVEL AIR FILTRATION SYSTEMS

Vasilis P. Valdramidis^{1,2}, Davide Sardella^{1,2}, Ruben Gatt³

¹Department of Food Sciences and Nutrition,

²Centre for Molecular Medicine and Biobanking,

³Metamaterials Unit

University of Malta

MSD2080, Msida,

Malta

E-mail: vasilis.valdramidis@um.edu.mt

KEYWORDS

Filters, fungal dynamics, nanoparticles.

ABSTRACT

In this work the efficacy of filters coated with ZnO is assessed under realistic pear warehouse storage conditions. These filters are evaluated in relation to their efficacy to curtail cross-contamination by trapping spore contaminants and reducing their activity in that trapped environment. The work is built based on previous research in which the aggressiveness of different fungal contaminants was assessed and their antifungal properties were evaluated quantitatively on nutrient media and ZnO coated filters. The coated air filters, after a scaled-up operation of a six-month period, effectively trapped and inactivated any microbial contaminants after a scaled-up operation of a six month period.

INTRODUCTION

Control of particulate matter in the air is of utmost importance in industrial environments in which hygiene standards are strict, e.g., healthcare, food environments, etc. As reviewed by Brincant et al., (2016), air filtration is applied, for instance, to clean rooms, milk packaging facilities, meat production and packaging lines and in the production of soft cheese, mainly to protect the products from fungal spores, dust or any other organics matter. Consequently, the aim of most of the filters is to provide a physical barrier which particles cannot pass through, or which particles stick to (EHEDG, 2006).

Nevertheless, there are materials which are trapped by the filter forming the so-called cake. Increase of the cake's thickness, will increase the path that particles in the air stream are forced to travel through. This will increase the pressure drop across it and at some point the filter will not be efficient enough. Additionally, filters could also act as a medium in which fungi and bacteria can grow. Since physical filters only trap spores, without deactivating or destroying them, the spores immobilized on the filter can utilize the trapped organic matter as a source of food.

It is therefore imperative to identify alternative functional filtration systems that may have some or most of the following functions: (i) remove contaminating micro-organisms from the air, (ii) reduce or prevent growth of micro-organisms, (iii) prevent their ingress, (iv) curtail cross-contamination, (v) direct bioaerosols away from the food stuffs, (vi) not act as an additional source of contamination.

The aim of this work was to design and develop a novel air filtration system coated with ZnO nanoparticles, able to trap and neutralize fungal spores of pear warehouses. The specific objectives were to integrate information of the growth dynamics of the most common pear postharvest fungal isolates, the efficacy of ZnO nanoparticles against them, the antifungal properties of ZnO nanoparticles coated on commercial filters in order to design and assess the efficiency of coated filters under realistic conditions.

MATERIALS AND METHODS

Fungal growth assessment and ZnO inhibition

This information was originally presented at Sardella et al. 2016. In summary *Penicillium expansum*, *Botrytis cinerea*, *Rhizopus stolonifer* and *Alternaria alternata* used in this study. The estimated μ and λ were further expressed as a function of temperature using the Cardinal Model with Inflection (CMI)

$$\mu = \frac{\mu_{opt} (T-T_{max})(T-T_{min})^2}{(T_{opt}-T_{min})[(T_{opt}-T_{min})(T-T_{opt})-(T_{opt}-T_{max})(T_{opt}+T_{min}-2T)]} \text{ Eq. (1)}$$

$$1/\lambda = \frac{(1/\lambda_{opt})(T-T_{max})(T-T_{min})^2}{(T_{opt}-T_{min})[(T_{opt}-T_{min})(T-T_{opt})-(T_{opt}-T_{max})(T_{opt}+T_{min}-2T)]} \text{ Eq. (2)}$$

where T_{opt} , T_{min} and T_{max} ($^{\circ}\text{C}$) are the theoretical optimum, minimum and maximum temperature for growth, respectively and μ_{opt} (mm/h) and λ_{opt} (h) are the growth rate and the lag time at the optimum temperature, respectively.

Additionally, a turbidimetric assay was performed (originally presented at Sardella et al. 2017) to investigate the antifungal activity of ZnO nanoparticles. The fractional areas (coming from the analysis of O.D. versus time) were then correlated with the nanoparticles' concentration as follows:

$$fa(c) = \exp\left[-\left(\frac{c}{p_1}\right)^{p_2}\right] \text{ Eq. (3)}$$

where, p_1 is the concentration at maximum slope and p_2 is a slope parameter. The minimum inhibitory concentration (MIC), the non-inhibitory concentration (NIC) were estimated:

$$\text{MIC} = p_1 \exp\left(\frac{1}{p_2}\right) \text{ Eq. (4)}$$

$$\text{NIC} = p_1 \exp\left(\frac{1-e}{p_2}\right) \text{ Eq. (5)}$$

Antifungal properties of coated filters

HS-Alpha Pak (HS-Luftfilterbau GmbH, efficiency 40–60%, $P = 40\text{--}50$ Pa) were immersed in either of two suspensions made up of ZnO nanoparticles (Sigma Aldrich, USA) suspended in propan-2-ol having a concentration of 12 mM or 120 mM for either 0.5, 5 or 50 minutes. A modification of the slide-culture method was used to test the nanoparticles coated filters for growth inhibition

(as originally presented by Decelis et al. 2017). ZnO coated filters were soaked in nutrient agar while conidial suspensions were used to inoculate the media. Visual examination of the fungal growth in form of binary responses was reported after incubation at optimal conditions (25°C for 5 days).

Prototype development, coating and validation in realistic conditions

A filter prototype coated with 120 mM of ZnO nanoparticles (concentration was selected based on the previous efficacy studies) was tested under real conditions of an acclimatized pear warehouse. After 6 months of operation at -0.5°C , 1-3% O_2 , 0-5% CO_2 , the filter was unpacked under a fume hood and different sections of its surface were excised with a scalpel. The above mentioned filter's properties were then investigated by performing the following experimental procedures:

Method 1: Assessment of trapped microorganisms.

An air sampling system has been setup into a sterile flow cabinet in order to assess whether the spores could be detached from the filter's surface. Three different sections with a size of approximately 4.8×4.8 cm, each one coming from three different selected areas of the filter, were fitted into a plastic adapter connected to a manifold system. A $0.2 \mu\text{m}$ sterile membrane was inserted between the manifold and the adapter in order to trap the spores eventually present into the air flow. An amount of about 3000 L of sterile air (2880), coming from the flow cabinet, was sampled for each section. Hereafter, the membranes were aseptically transferred onto Czapek Yeast Agar (CYA) plates and incubated for 6 days at 25°C .

Method 2: Assessment of trapped microorganisms.

Three different areas of the filter were chosen and three sections, with a size of approximately 4.8×4.8 cm, were obtained per each area. The surface of each section was flooded with 10 mL of a sterile 0.05% Tween 80 suspension and scraped off with a sterile bent rod in order to detach spores eventually present onto the surface. Hereafter, 100 μL of the resulting suspension from each section, were spread uniformly onto the surface of CYA plates. Plates were finally incubated for 6 days at 25°C .

Method 3: Assessment of surface contaminants.

Thirty-three sections from all the four selected areas of the filter were obtained (twenty-one sections from the first three areas, twelve from the fourth one) and aseptically transferred into cell-culture flasks filled with 60 mL of CYA. Sections (three per flask) were placed onto the agar with a pair of tweezers. Sections' size was approximately 4.8 x 2.4 cm. Flasks were incubated for 6 days at 25°C. For all these studies fungal structures were observed under high power microscopy (Olympus CX31). After observing such features, keys were found in a Mycology Atlas (Atlas of Clinical Fungi: de Hoog, 1995) and were used to aid in the fungal identification.

RESULTS

From the fungal growth assessment at different temperatures, it was found that *R. stolonifer* was the most aggressive one since it showed the highest μ_{opt} value. The aggressiveness of the four isolates can be sorted as follows: *R. stolonifer* > *B. cinerea* > *A. alternata* > *P. expansum*. The four isolates were also sorted according to their lag time duration as follows: *R. stolonifer* < *A. alternata* < *P. expansum* < *B. cinerea*. Hereafter, the MIC and NIC of selective fungi were identified. In the case of *P. expansum* this was found to be MIC = 9.8 mM, NIC = 1.6 mM.

In the case of the antifungal properties of the coated filters, *Penicillium expansum* was the more sensitive organism, with no growth reported for the filters immersed in a 12 mM ZnO nanoparticles suspension for 0.5 min.

Based on these results large scale filters were coated and tested under realistic conditions by using the 3 methods presented in the Materials and Methods.

Figure 1 shows that in one section out of three, a fungal colony was present. The colony was isolated and the fungus identified was *Cladosporium* spp. This is an indication that any previously trapped microorganisms had been inactivated by the presence of the nanoparticles.

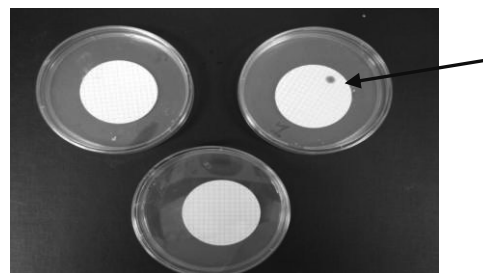


Figure 1. CYA plates with membranes for air sampling.

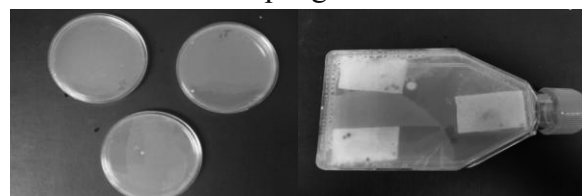


Figure 2. CYA plates following the assessment of trapped microorganisms of method 2 (left). Assessment of surface contaminants on CYA agar of method 3 (right).

With the only exception of one bacterial CFU in one plate, no growth was observed in any of the filter's sections, as shown in Figure 2. Similarly, to the previous procedure, this validated that any trapped microorganisms had been inactivated by the nanoparticles.

In the case of the third method, all the flasks showed bacterial and fungal growth onto the medium's surface, even though not abundant (Figure 2). Eleven fungal colonies were selected for identification. Seven colonies were from *Cladosporium* spp., three from *Alternaria* spp. and one from *Penicillium* spp. These results indicate that the surface of the filters, that is exposed to the external air, had some environmental contaminants. Their levels are quite low indicating that, even on the surface, the antimicrobial efficacy of the nanoparticles is pronounced.

CONCLUSIONS

These results prove that the developed air filters after an operation of a six month period effectively trapped any microbial contaminants and also reduced their levels because of the antimicrobial properties of the nanoparticles. Surface contaminants were reported to be at low levels.

ACKNOWLEDGEMENTS

This research was partially funded from the European Union's Seventh Framework Programme, REPEAR Project, under grant agreement n° 604733, FP7-SME-2013-SME AG".

REFERENCES

- Brincat, J.-P.; D. Sardella; A. Muscat; S. Decelis; J.N. Grima; V.P. Valdramidis and R. Gatt. 2016. A review of the state-of-the-art in air filtration technologies as may be applied to cold storage warehouses. *Trends in Food Science & Technology*, 50, 175-185.
- Decelis, S.; D. Sardella; T. Triganza; J.-P. Brincat; R. Gatt and V.P. Valdramidis. 2017. Assessing the anti-fungal efficiency of filters coated with zinc oxide nanoparticles. *Royal Society Open Science*, 4: 161032.
- European Hygienic Engineering & Design Group (EHEDG). 2006. Guidelines on air handling in the food industry. *Trends in Food Science & Technology*, 17, 331e3
- Sardella, D.; R. Gatt, R.; V.P. Valdramidis. 2017. Assessing the efficacy of zinc oxide nanoparticles against *Penicillium expansum* by automated turbidimetric analysis. *Mycology*, TMYC 1369187.
- Sardella, D; R. Gatt, S. Decelis, V. Valdramidis 2016. Quantitative assessment of the efficacy of ZnO nanoparticles against selected fruit fungal contaminants. *American Phytopathological Society (APS) Annual Meeting 2016*.

EFFECT OF FOOD MICROSTRUCTURE ON THERMAL INACTIVATION DYNAMICS OF LISTERIA MONOCYTOGENES

Davy Verheyen¹, Maria Baka¹, Torstein Skåra², Jan F.M. Van Impe^{1,*}
¹ BioTeC+ & OPTEC, Department of Chemical Engineering, KU Leuven
CPMF2, Flemish Cluster Predictive Microbiology in Foods
Gebroeders De Smetstraat 1, B-9000 Gent, Belgium
* E-mail address: Jan.VanImpe@kuleuven.be
² Nofima, P.O. Box 8034
4068 Stavanger, Norway

KEYWORDS

Listeria monocytogenes, thermal inactivation, sublethal injury, fish-based model systems

ABSTRACT

The effectiveness of predictive microbiology is limited by the lack of knowledge considering the influence of food microstructure on microbial dynamics. In this study, fish-based model systems with various microstructures (i.e., liquid, xanthan - a more viscous liquid system, emulsion, aqueous gel, and gelled emulsion) were used to investigate the effect of certain isolated food microstructural aspects (i.e., growth morphology of the cells, nature of the food matrix, and the presence/absence of fat droplets) and initial cell conditions (i.e., grown inside the matrix from a low inoculation level or inoculated to a high inoculation level from a fresh preculture) on thermal inactivation dynamics of *Listeria monocytogenes*, as well as on the evolution of the percentage of sublethal injury of the cells over the course of the treatment. A peak in sublethal injury always occurred when the cells were in their log-linear inactivation phase, but the level of sublethal injury at the end of the treatment was rather limited. For experiments started from cells that were grown inside the matrix, a larger maximum specific inactivation rate (k_{max}) was observed than for experiments started from a fresh preculture, although only for the viscous systems (i.e., liquid, xanthan and emulsion). Due to the greater variation among biological replicates, the residual cell density (N_{res}) was also smaller for experiments started from cells that were first grown inside the matrix. For experiments started from a fresh preculture, k_{max} was considerably larger in the viscous systems than in the gelled systems, while N_{res} was larger in gelled systems than in viscous systems, regardless of the initial condition of the cells. The presence of a small amount of fat droplets had a considerable effect on k_{max} and N_{res} , albeit of a complex nature.

INTRODUCTION

Predictive microbiology is a discipline of food microbiology in which microbial responses in food products are studied under controlled intrinsic (e.g., pH) and extrinsic (e.g., temperature) conditions in order to develop mathematical models (McMeekin et al., 2002; Van Impe et al., 2005). Well-developed models allow a realistic estimation of food safety risks, which contributes to the improvement of production processes for safe food products (Koutsoumanis et al., 2004). However, most predictive models are developed based on experiments in liquid model systems, which results in limited predictive value when the models are validated in real food products which are mostly not simple liquids (Pin et al., 1999). The completeness error

caused by the food microstructural effect which is not taken into account is an important shortcoming of predictive microbiology (Ross et al., 2000; Velliou et al., 2013; Wilson et al., 2002). A possible method to remediate this issue is the use of model systems with various microstructures for the development of predictive models and, on a more fundamental level, to get more insight into the influence of food microstructure on microbial dynamics. In this regard, Baka et al. (2016; 2017a, b) already used model systems with various microstructures (i.e., based on the classification of Wilson et al. (2002)) to study the influence of food microstructure on microbial growth dynamics. Some researchers have also used model systems with various microstructures in thermal inactivation studies (Murphy et al., 2000; Wang et al., 2017), although they mostly focussed on the comparison of two microstructures instead of the entire microstructural spectrum. Therefore, Verheyen et al. (2017) developed fish-based model systems with various microstructures among which the microstructural effect was isolated among the different systems, allowing a more systematic investigation of the isolated food microstructural effect on microbial growth and thermal inactivation dynamics.

In food industry, thermal processing remains one of the most important methods of reducing/avoiding the presence of foodborne pathogens in food products (Álvarez-Ordóñez et al., 2008; Rawson et al., 2011; Wang et al., 2017). A more detailed knowledge of the influence of a non-liquid food matrix on inactivation dynamics would therefore also be beneficial to refine conventional pasteurisation schemes used in industry (Velliou et al., 2013). Moreover, it is known that a considerable subpopulation of bacteria that is subjected to mild thermal treatments is not killed but is instead sublethally injured (Besse, 2002). Sublethal injury (SI) is defined as “a consequence of exposure to a chemical or physical process that damages but does not kill a microorganism” (Hurst, 1977). The injury can either be structural (i.e., altered membrane permeability) or metabolic (i.e., damage to functional cell components such as cellular proteins, enzymes, and nucleic acids), or a combination of both (Brashears et al., 2001; Wang et al., 2017). Since injured cells are unable to form visible colonies on selective media which are used in food diagnostics, the presence of sublethally injured cells can lead to underestimation of microbial contamination, presenting a potential threat to food safety (Jasson et al., 2007; Noriega et al., 2013). Moreover, sublethally injured cells may recover and regain their ability to multiply after thermal treatments, even leading to enhanced virulence and resistance to a wide variety of other stresses (Silva et al., 2015; Skandamis et al., 2008; Wu, 2008).

With 2,536 reported cases and a fatality rate of 16.2% in 2016, listeriosis is one of the most relevant foodborne diseases in Europe (EFSA and ECDC, 2017). The disease is caused by *Listeria monocytogenes*, a bacterium which is one of the most heat tolerant non-spore forming food pathogens (Farber and Peterkin, 1991). Therefore, ready-to-eat food products with a short shelf-life which are subjected to a mild heat treatment are very susceptible to *L. monocytogenes* contaminations (Ates et al., 2014). In this regard, fish products are especially susceptible to *L. monocytogenes* contamination (Ben Embarek, 1994), as illustrated by the fact that the bacterium was detected in 4.7% of sampled products of this category across all sampling stages (i.e., processing and retail) in Europe in 2016 (EFSA and ECDC, 2017). Due to the high resistance to various stresses, *L. monocytogenes* is also very relevant for the validation of microbial inactivation treatments (Baka et al., 2015).

In this study, the isolated influence of food microstructure on inactivation dynamics of *L. monocytogenes* at 70°C (i.e., a common pasteurisation temperature for fish products (Rosnes et al., 2011)) was investigated. In order to isolate the microstructural effect, model systems with minimum variation in compositional and physico-chemical properties were used, as developed in Verheyen et al. (2017). In contrast to previous studies, it was investigated whether there is a difference in microbial inactivation dynamics between (i) the realistic scenario of starting with a small number of microorganisms that has grown to a high level in the food product, and (ii) the experimental approach of inoculating food products with a high level of microorganisms. The influence of the heat treatments in the different microstructures on the sublethal injury of *L. monocytogenes* was also investigated.

MATERIALS AND METHODS

Model system preparation

Model systems with different microstructures (e.g., a liquid system, xanthan - a second more viscous liquid system containing xanthan gum, an emulsion, an aqueous gel, and a gelled emulsion) were prepared as described in Verheyen et al. (2017), using small vials (4mL, 45 x 14.7 mm, BGB Analytik Benelux B.V., Harderwijk, the Netherlands) containing 1 mL (height of approximately 10 mm) of viscous or structured medium. Among the different model systems, the microstructural effect was isolated by means of minimal variation in compositional and physico-chemical aspects. It is important to mention that, apart from the liquid model system which exhibits planktonic growth, all model systems exhibit submerged colony growth when homogeneously inoculated (Verheyen et al., 2017).

Microorganisms and preculture conditions

L. monocytogenes strains LMG 23773, LMG 23774, and LMG 26484, were acquired from the BCCM/LMG bacteria collection of Ghent University in Belgium. A stock culture was stored at -80°C in Brain Heart Infusion Broth (BHI, VWR International, Leuven, Belgium) and 20% (v/v) glycerol (Acros Organics, Geel, Belgium). For each strain, a purity plate was prepared separately from the frozen stock culture by spreading a loopful onto a BHI Agar plate (1.4%

(w/v), Agar Technical No3, Oxoid Ltd., Basingstoke, UK), which was afterwards incubated at 30°C for 24 h. One colony of the purity plate was carefully transferred into 20 mL of BHI. After incubating for 24 h at 30°C under static conditions, 20 µL of the stationary-phase culture was inoculated into 20 mL of fresh BHI and incubated for 24 h under the same conditions. This resulted in early stationary phase *L. monocytogenes* cultures with an inoculum level of approximately 10⁹ CFU/mL. 10 mL of the three cultures was poured together in a 100 mL Erlenmeyer in aseptic conditions and mixed, resulting in a *L. monocytogenes* strain cocktail with a cell density of 10⁹ CFU/mL.

Inoculation conditions

Model systems were inoculated with the *L. monocytogenes* strain cocktail to a cell density of approximately 10⁹ and 10² CFU/mL for experiments started from a fresh preculture and experiments started from cells grown in the matrix, respectively. In both cases, early stationary phase cells were used, since they are more heat resistant than exponentially growing populations (Noriega et al., 2013). For experiments starting from a fresh preculture, 30 mL of the *L. monocytogenes* strain cocktail was transferred to a falcon tube and centrifuged at 12,000 rpm for 10 min at 4°C. Afterwards, the supernatant was carefully removed and the pellet was added to 100 mL of the respective model system. The model system was thoroughly mixed and distributed over the small vials. For experiments started from cells growing inside the matrix, model systems were inoculated to a cell density of 10² CFU/mL, using a NaCl solution of 0.90% (w/v) as dilution medium, distributed over the small vials, and incubated at 10°C for 14 days prior to the inactivation experiment, resulting in early stationary phase cells with a cell density of approximately 10⁹ CFU/mL (unpublished results). For gelled systems, the inoculation took place prior to the initiation of the gelation reaction (Verheyen et al., 2017).

Thermal inactivation experiments

The small vials containing the inoculated model systems were placed in the water bath at 70°C, relevant for the pasteurisation of processed fish products (Rosnes et al., 2011). At different time points (i.e., 0 s, 30 s, 1 min, 80 s, 100 s, 2 min, 150 s, 3 min, 4 min, 5 min, 10 min) one vial was transferred from the water bath to an ice water bath (i.e., temperature of approximately 0°C) in order to stop the inactivation. The samples were stored in the ice water bath for maximum 3 h before further processing steps. For viscous systems (i.e., liquid, xanthan, and emulsion), serial decimal dilutions were directly prepared from an aliquot of the samples, using the NaCl solution and afterwards plated on BHI and PALCAM agar (PALCAM *Listeria* Selective Agar according to Van Netten et al. (1989), Merck Milipore, Darmstadt, Germany), employing the drop technique (Herigstad et al., 2001). For gelled systems (i.e., aqueous gel and gelled emulsion), the protocol of Hamoud-Agha et al. (2013) was used. More specifically, gels were removed from the vials and transferred into a sterile stomacher bag in aseptic conditions. Subsequently, the vials were rinsed and drained into the bag with 1.5 mL of Phosphate Buffered Saline (PBS, Sigma Aldrich, MO, USA). Afterwards, 1.5 mL of McIlkaine buffer (0.2 M Na₂HPO₄, Sigma Aldrich,

MO, USA; 0.1 M citric acid, Acros Organics, NJ, USA) was added to the bag. The mixture was homogenised for 10 min (basic masticator, Led techno, Heusden-Zolder, Belgium), after which serial decimal dilutions were prepared and plated similarly to the viscous systems. Finally, the plates were incubated at 30°C for approximately 30 h before enumeration. Every experiment was independently performed in triplicate.

Mathematical modelling

The inactivation model of Geeraerd et al. (2000), able to describe shoulder and tailing behaviour, was fitted to the experimental data. Model parameters were estimated from the set of experimental data via the minimisation of the sum of squared errors, using the lsqnonlin routine of the Optimisation Toolbox of MatLab® version R2016b (The Mathworks Inc., Natick, USA). Standard errors of parameter estimates were calculated from the Jacobian matrix. A global estimation procedure was standardised for each model system. The model of Geeraerd et al. (2000) is represented by Equation 1, 2 and 3.

$$\frac{dN(t)}{dt} = -\left(\frac{1}{1 + C_c(t)}\right) k_{max} \left(1 - \frac{N_{res}}{N(t)}\right) N(t) \quad (1)$$

$$\frac{dC_c(t)}{dt} = -k_{max} \cdot C_c(t) \quad (2)$$

$$C_c(0) = e^{k_{max} S_L} - 1 \quad (3)$$

With N [CFU/mL], the cell density at time t ; N_{res} [CFU/mL], the residual cell density; k_{max} [1/min], the maximum specific inactivation rate; C_c [-], the concentration of a critical component (intracellular or extracellular) for cell survival; $C_c(0)$ [-], the initial concentration of this critical component; and S_L [min], the shoulder length representing the period the cells need to adapt to the stress.

The theoretical data, obtained from the Geeraerd model, was used to calculate the percentage of sublethal injury (%SI) using Equation 4 according to the formula of Bush and Donnelly (1992), using BHI agar and PALCAM agar as a nonselective and selective medium, respectively.

$$\%SI = \frac{CFU \text{ on BHI agar} - CFU \text{ on PALCAM agar}}{CFU \text{ on BHI agar}} \cdot 100 \quad (4)$$

Statistical analysis

For the statistical analysis, significant differences between logarithmically transformed viable counts were determined using analysis of variance (ANOVA, single variance) test at a 95.0% confidence level ($\alpha = 0.05$). Fisher's Least Significant Difference (LSD) test was used to distinguish which means were significantly different from others. The analyses were performed using the anova1 routine of the Statistical Toolbox of MatLab® version R2016b (The Mathworks, Inc., Natick, USA). Test statistics were regarded as significant when $P \leq 0.05$.

RESULTS AND DISCUSSION

Figure 1 illustrates the inactivation dynamics and SI evolution of *L. monocytogenes* in the different model systems. It can be observed that inactivation is generally more effective (i.e., lower residual cell population) for experiments that were started from cells that were first grown inside the matrix. The aqueous gel, for which the differences between the two starting conditions are rather small, is the only exception to this observation. Even without taking the statistical analysis of the inactivation parameters into account, the differences observed among the inactivation curves for the different microstructures and inoculation conditions indicate that using simple liquid model systems inoculated with a high inoculum level of *L. monocytogenes* from a fresh preculture for inactivation experiments does not accurately simulate what takes place in real food products which can have a plethora of different microstructures and, in addition, might be contaminated with cells that have first grown inside the food matrix.

Sublethal injury assessment

Figure 1 illustrates that a peak in SI always occurred when the cells were in their log-linear inactivation phase. This is in accordance with the findings of Noriega et al. (2013) for the mild heating of *Escherichia coli*, *Salmonella* Typhimurium, and *Listeria innocua* in liquid and gelled model systems. This behaviour during the log-linear inactivation phase is caused by a mechanism of injury accumulation that culminates in cell death (Perni et al., 2007). When the stationary inactivation phase was reached, the percentage of SI remained constant at a low level. This observation is in accordance with the findings of Uyttendaele et al. (2008), who detected no significant presence of sublethally injured *L. monocytogenes* cells after a milder heat treatment of 60°C. The inactivation of freshly inoculated *L. monocytogenes* cells in the emulsion model systems is an exception to this observation, probably due to the fact that the residual population was lower than the detection limit, giving no practical value to the obtained cell counts after approximately 4 min. For the liquid and the emulsion model systems, the peak in SI percentage was higher for cells that were grown inside the matrix before the inactivation experiment. This phenomenon can possibly be explained by the adaption of the cells to their stressing environment while growing inside the matrix (Tang et al., 2015), leading to cross-protection against other stresses (Durack et al., 2013). Consequently, the cells which have experienced greater stress responses might become only sublethally injured by treatments which would completely inactivate normal cells. For the other model systems (i.e., xanthan, aqueous gel, and gelled emulsion), the influence of the initial cell condition on the evolution of the percentage of SI is rather small, even though some small differences are observed between the two conditions.

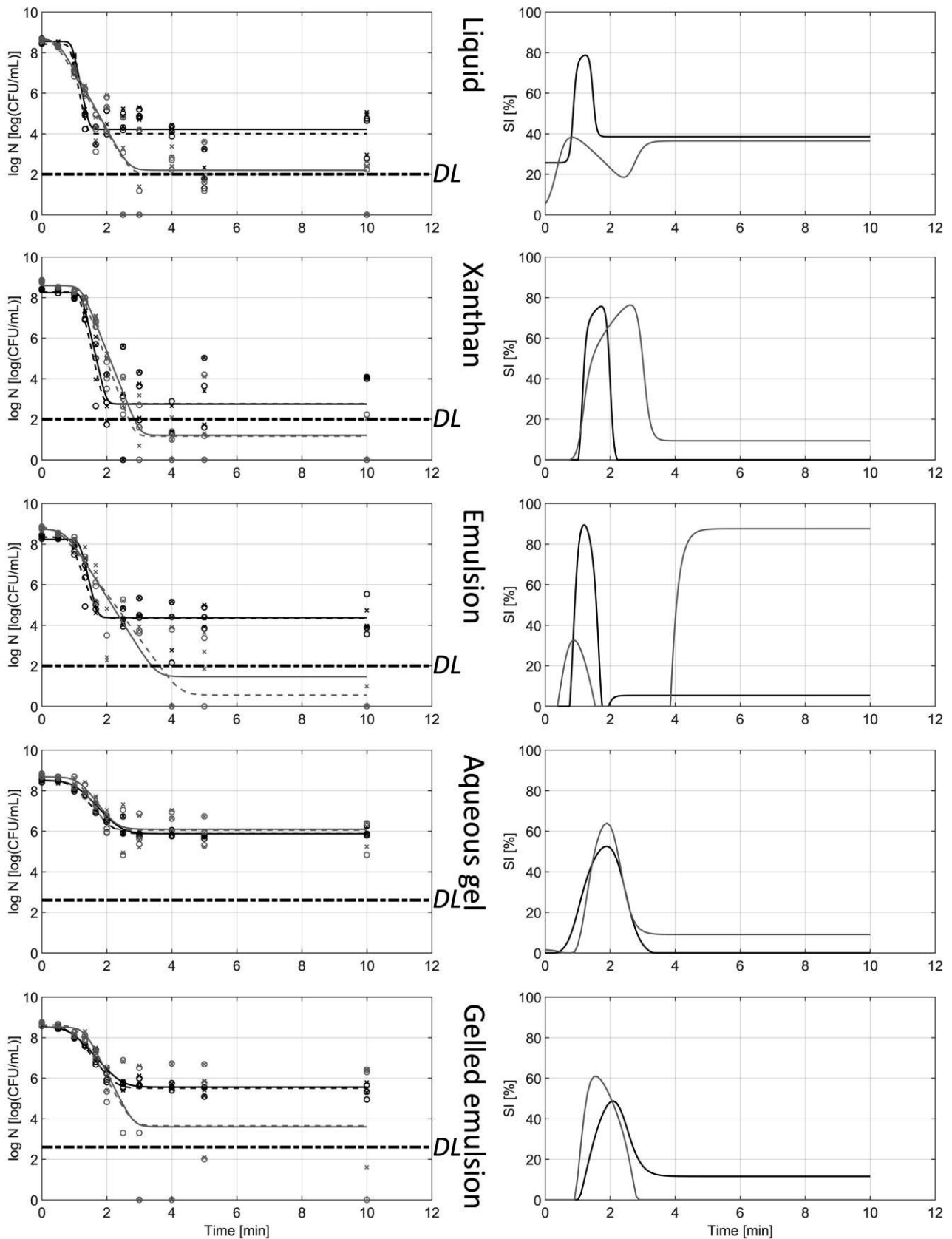


Figure 1: Inactivation dynamics and percentage of sublethal injury of *L. monocytogenes* at 70°C. The situations where the experiment started from (i) cells that were first grown in the matrix and (ii) a fresh preculture are indicated in grey and black, respectively. Symbols correspond to the experimental data, both for the nonselective (x) and the selective medium (o). Lines correspond to the global fit of the Geeraerd et al. (2000) model, both for the nonselective (-) and the selective medium (- -). The detection limit (DL) is also indicated on the graphs. SI was calculated based on Equation 4, using the values from the Geeraerd model.

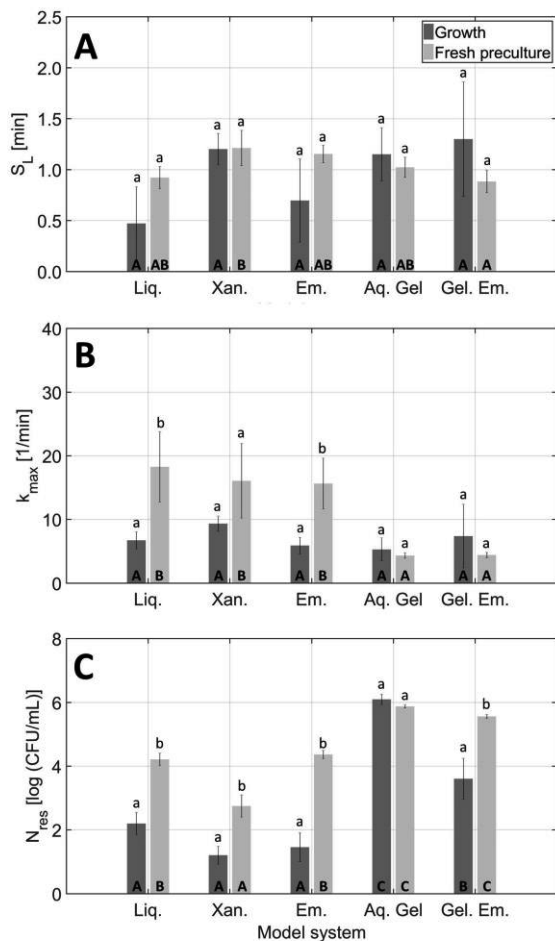


Figure 2: Statistical analysis of the shoulder length S_L (2.A), the maximum specific inactivation rate k_{max} (2.B), and the residual cell density N_{res} (2.C), according to the inactivation model of Geeraerd et al. (2000) for the thermal inactivation of *L. monocytogenes* in the five model systems (i.e., liquid, xanthan, emulsion, aqueous gel, and gelled emulsion) at 70°C. Experiments were either started from cells that were grown inside the matrix or a fresh preculture. For the different model systems with the same initial condition, bars bearing different uppercase letters are significantly different ($P \leq 0.05$). For the different starting conditions for one model system, bars bearing different lowercase letters are significantly different ($P \leq 0.05$).

Influence of initial cell condition

The thermal inactivation dynamics of *L. monocytogenes* are reported to be influenced by the growth conditions prior to the treatment (Schultze et al., 2007). Therefore, it was assessed whether the classical and simplified microbiological method of inoculating food products with high concentrations of pathogenic microorganisms for challenge testing purposes has sufficient practical relevance. Figure 2 shows the statistical analysis of the parameters of the inactivation model of Geeraerd et al. (2000), i.e., the shoulder length S_L (Figure 2.A), the maximum specific inactivation rate k_{max} (Figure 2.B), and the residual cell population N_{res} (Figure 2.C) for the experiments started from (i) cells that were grown inside the matrix and (ii) a fresh preculture.

As observed in Figure 2.A, the initial condition of the cells had no influence on S_L . The shoulder of a thermal inactivation curve can be caused by different mechanisms, i.e., cells being present in groups or clumps, cells being able to resynthesise a vital component, the presence of proteins and/or fats in the medium, and the presence of a large number of critical components that needs to be inactivated (Adams and Moss, 1995; Cerf, 1977; Geeraerd et al., 2000; Moats et al., 1971). Therefore, those causes that are related to the bacterial cells (i.e., resynthesises/presence of a vital component) are apparently not significantly influenced by the initial cell condition.

Figure 2.B shows that cells that were grown inside the matrix exhibited a larger k_{max} than those from a fresh preculture, although only for the viscous systems. The possibility of the cells to order themselves into colonies while growing in the xanthan and emulsion model systems (Verheyen et al., 2017) and the sedimentation of planktonic cells to the bottom of the liquid system (Smet et al., 2015) are possible explanations for this phenomenon. It has been reported in literature that starting from a higher cell number results in a large number of small colonies in the food matrix, while starting from a lower cell number results in a smaller number of large colonies (Velliou et al., 2013). The larger colonies which are formed when the cells are first grown inside the matrix could exhibit an enhanced heat resistance due to the higher number of cells that protect each other inside the colony. A similar effect could be created when cells sediment to the bottom of the tube and are therefore more closely packed together.

In Figure 2.C, it is illustrated that, apart from in the aqueous gel, N_{res} was larger for experiments started from a fresh preculture. Figure 1 shows that this phenomenon is caused by the large variation that is observed between the different biological replicates for the experiments that started from cells that were grown inside the matrix. A small difference in growth behaviour can apparently result in large variations in heat resistance of the cells, illustrated by the fact that some replicates exhibit similarly high or even higher cell levels as compared to when the experiments are started from a fresh preculture, while other replicates exhibit a considerably smaller number of survivors. In general, these observations show that it might be unsafe to employ the common experimental approach of using a high initial cell level for mild thermal inactivation studies with *L. monocytogenes*. Even though the residual cell population is on average larger than when the cells would be grown inside the matrix, there is a possibility that a higher number of survivors would be present in the latter more realistic scenario, resulting in a serious over-estimation of the efficacy of the inactivation procedure.

Influence of microstructural aspects on inactivation dynamics

As described in Verheyen et al. (2017), the set of model system can be used to investigate the isolated influence on microbial inactivation of three different microstructural aspects: (i) the growth morphology of the microbial cells (i.e., planktonic cells or submerged colonies), (ii) the nature

of the food matrix (i.e., viscous or gelled), and (iii) the presence/absence of fat droplets.

The effect of growth morphology is investigated by comparing dynamics between systems where the growth morphology is the sole significant difference (i.e., planktonic cells in liquid vs. submerged colonies in xanthan). As observed in Figure 2.A, the variation of S_L among the different model systems was rather small, with significant differences only being observed between the xanthan and gelled emulsion systems for experiments started from a fresh preculture. These findings suggest that the growth morphology, and the microstructural effect in general, has a negligible influence on the shoulder length. This could mean that the come-up time (i.e., the time the model systems need to reach the temperature of the water bath they are placed in) is the main reason for the presence of a shoulder phase, most likely caused by heat transfer limitations throughout the heating medium (Kotrola and Conner, 1997). The come-up time could be more accurately determined by measuring the temperature in the center of the model systems over the course of the heat treatment (Uyttendaele et al., 2008). In addition, the come-up time would have a larger influence on the shoulder phase when larger model systems would be used. Figure 2.B and Figure 2.C show that the growth morphology also has no significant influence on k_{max} and N_{res} . Consequently, the higher heat resistance which has often been observed for submerged colonies in a gelled environment as compared to planktonic cells in broth systems (Murphy et al., 2000; Velliou et al., 2013), is mostly caused by the protective effect of the gelled environment.

The effect of the food matrix on the growth dynamics of submerged colonies is studied by means of the effect of a gelled matrix (i.e., aqueous gel vs. xanthan and gelled emulsion vs. emulsion). In Figure 2.B, no statistical differences in k_{max} are observed among the different model systems for cells that were first grown inside the matrix, suggesting that the large colonies are equally heat-resistant, regardless of the nature of the food matrix in which they reside. For experiments started from a fresh preculture, on the other hand, k_{max} was considerably larger in the viscous systems than in the gelled systems, indicating submerged colonies in a gelled matrix are inactivated at a slower rate than planktonic cells and submerged colonies in the viscous systems. As observed in Figure 2.C, N_{res} was larger in gelled systems than in viscous systems, regardless of the initial condition of the cells. These findings confirm that a gelled matrix has a protective effect on *L. monocytogenes* during mild thermal inactivation. In future studies, the effect of the food matrix could be further characterised by conducting inactivation experiments in model systems with varying rheological properties, i.e., viscosity parameters of the Power law model (Reiner, 1926) for viscous systems, and the storage (G') and loss (G'') modulus for gelled systems (Verheyen et al., 2017).

By comparing inactivation dynamics between systems where the presence of a small amount (i.e., 1% fat concentration) of fat droplets is the only distinguishing factor (i.e., xanthan vs. emulsion and aqueous gel vs. gelled emulsion), the influence of the presence of fat droplets on

the thermal inactivation of *L. monocytogenes* is studied. This influence seems to be present exclusively on N_{res} , although no clear correlation can be derived from the current results. For experiments started from cells grown inside the matrix, the presence of fat droplets results in a smaller N_{res} , but only in a gelled matrix. When experiments were started from a fresh preculture, the presence of fat droplets resulted in a larger N_{res} , but only in a viscous matrix. In order to get more insight into the exact influencing mechanics of the fat droplets, future studies should focus on inactivation experiments using model systems with different fat levels and/or fat droplet size distributions, while still aiming to minimise variations in physico-chemical and compositional factors. In this regard, the influence of different fat levels on thermal inactivation of *Listeria* and *Salmonella* has already been studied, consistently leading to the conclusion that there is an influence even though further work is still needed to clarify the situation (Juneja et al., 2001; Passos and Kuaye, 2002; Schultze et al., 2007; Szlachta et al., 2010).

CONCLUSIONS AND FUTURE RESEARCH

The results of this study illustrated that, even though a peak in sublethal injury always occurred during the log-linear inactivation part on the inactivation, the percentage of sublethally injured cells at the end of the heat treatment was rather low, indicating a limited risk for food diagnostics. The cell conditions prior to the mild thermal inactivation treatment also had a significant influence on microbial inactivation dynamics, meaning that researchers should choose wisely how to inoculate their foods/model systems when conducting thermal inactivation trials. When the influence of different microstructural aspects on the parameters of the Geeraerd et al. inactivation model was investigated, the nature of the food matrix and the presence/absence of fat droplets were proven to have a significant, albeit complex, influence on the maximum specific inactivation rate k_{max} and the residual cell population N_{res} .

In future studies, the influence of the investigated microstructural aspects should be studied in more detail in order to attain an increased insight into the exact influencing mechanics. This could be achieved by conducting thermal inactivation experiments in model systems with varying rheological properties, fat levels and/or fat droplet size distributions. In those studies, one factor should be isolated at a time, while still minimising physico-chemical and compositional properties. An upscaling of the model systems and usage in relevant industrial thermal inactivation installations would also be of considerable interest for food industry.

ACKNOWLEDGEMENTS

This work was supported by the Norconserv Foundation, and the KU Leuven Research Fund (Center of Excellence OPTEC-Optimization in Engineering, project PFV/10/002). Author Maria Baka was supported by the research council of KU Leuven for post-doctoral researchers (grant PDM/16/125).

REFERENCES

- Adams, M.R., Moss, M.O., 1995. Food Microbiology. Royal Society of Chemistry, Cambridge.
- Álvarez-Ordóñez, A., Fernández, A., López, M., Arenas, R., Bernardo, A., 2008. Modifications in membrane fatty acid composition of *Salmonella* typhimurium in response to growth conditions and their effect on heat resistance. *International Journal of Food Microbiology*, 123, 212-219.
- Ates, B.M., Skipnes, D., Rode, T.M., Lekang, O., 2014. Comparison of bacterial inactivation with novel agitating retort and static retort after mild heat treatments. *Food and Bioprocess Technology*, 4(6), 833-848.
- Baka, M., Noriega, E., Tsakali, E., Van Impe, J.F., 2015. Influence of composition and processing of Frankfurter sausages on the growth dynamics of *Listeria monocytogenes* under vacuum. *Food Research International*, 70, 94-100.
- Baka, M., Noriega, E., Van Langendonck, K., Van Impe, J.F., 2016. Influence of food intrinsic complexity on *Listeria monocytogenes* growth in/on vacuum-packed model systems at suboptimal temperatures. *International Journal of food microbiology*, 235, 17-27.
- Baka, M., Vercruyssen, S., Cornette, N., Van Impe, J.F., 2017a. Dynamics of *Listeria monocytogenes* at suboptimal temperatures in/on fish-protein based model systems: Effect of (micro)structure and microbial distribution. *Food Control*, 73, 43-50.
- Baka, M., Verheyen, D., Cornette, N., Vercruyssen, S., Van Impe, J.F., 2017b. *Salmonella* Typhimurium and *Staphylococcus aureus* dynamics in/on variable (micro)structures of fish-based model systems at suboptimal temperatures. *International Journal of Food Microbiology*, 240, 32-39.
- Ben Embarek, P.K., 1994. Presence, detection and growth of *Listeria monocytogenes* in seafoods: A review. *International Journal of Food Microbiology*, 23, 17-34.
- Besse, N.G., 2002. Influence of various environmental parameters and of detection procedures on the recovery of stressed *L. monocytogenes*: a review. *Food Microbiology*, 19, 221-234.
- Brashears, M.M., Amezcua, A., Stratton, J., 2001. Validation of methods used to recover *Escherichia coli* O157:H7 and *Salmonella* spp. subjected to stress conditions. *Journal of Food Protection*, 64(10), 1466-1471.
- Busch, S.V., Donnelly C.W., 1992. Development of a repair-enrichment broth for resuscitation of heat-injured *Listeria monocytogenes* and *Listeria innocua*. *Applied and Environmental Microbiology*, 58, 14-20.
- Cerf, O., 1977. A review. Tailing of survival curves of bacterial spores. *Journal of Applied Bacteriology*, 42 (1), 1-19.
- Durack, J., Ross, T., Bowman, J.P., 2013. Characterisation of the Transcriptomes of Genetically Diverse *Listeria monocytogenes* Exposed to Hyperosmotic and Low Temperature Conditions Reveal Global Stress-Adaptation Mechanisms. *PLOS ONE*, 8(9), e73603.
- EFSA (European Food Safety Authority), ECDC (European Centre for Disease Prevention and Control), 2017. The European Union Summary Report on trends and sources of zoonoses, zoonotic agents and food-borne Outbreaks in 2016. *EFSA Journal* 2017, 15(12), 5077.
- Farber, J.M., Peterkin, P.I., 1991. *Listeria monocytogenes*, a Food-Borne Pathogen. *Microbiological Reviews*, 55(3), 476-511.
- Geeraerd, A.H., Herremans, C.H., Van Impe, J.F., 2000. Structural model requirements to describe microbial inactivation during a mild heat treatment. *International Journal of Food Microbiology*, 59, 185-209.
- Hamoud-Agha, M.M., Curet, S., Simonin, H., Boillereaux, L., 2013. Microwave inactivation of *Escherichia coli* K12 CIP 54.117 in a gel medium: Experimental and numerical study. *Journal of Food Engineering*, 116, 315-323.
- Herigstad, B., Hamilton, M., Heersink, J., 2001. How to optimize the drop plate method for enumerating bacteria. *Journal of Microbiological Methods*, 44(2), 121-129.
- Hurst, A., 1977. Bacterial Injury: A review. *Canadian Journal of Microbiology*, 23(8), 935-944.
- Jasson, V., Uyttendaele, M., Rajkovic, A., Debevere, J., 2007. Establishment of procedures provoking sub-lethal injury of *Listeria monocytogenes*, *Campylobacter jejuni* and *Escherichia coli* O157 to serve method performance testing. *Int. J. Food Microbiol.* 118, 241-249.
- Juneja, V.K., Eblen, B.S., Marks, H.M., 2001. Modeling non-linear survival curves to calculate thermal inactivation of *Salmonella* in poultry of different fat levels. *International Journal of Food Microbiology*, 70, 37-51.
- Kotrola, J.S., Conner D.E., 1997. Heat inactivation of *Escherichia coli* O157:H7 in turkey meat as affected by sodium chloride, sodium lactate, polyphosphate, and fat content. *Journal of Food Protection*, 60, 898-902.
- Koutsoumanis, K.P., Kendall, P.A., Sofos, J.N., 2004. A comparative study on growth limits of *Listeria monocytogenes* as affected by temperature, pH and a_w when grown in suspension or on a solid surface. *International Journal of Food Microbiology*, 21(1), 415-422.
- McMeekin, T.A., Olley, J., Ratkowsky, D.A., Ross, T., 2002. Predictive microbiology: Towards the interface and beyond. *International Journal of Food Microbiology*, 73(2-3), 395-407.
- Moats, W.A., Dabbah, R., Edwards, V.M., 1971. Interpretation of nonlogarithmic survivor curves of heated bacteria. *Journal of Food Science*, 36, 523-526.
- Murphy, R.Y., Marks, B.P., Johnson, E.R., Johnson, M.G., 2000. Thermal Inactivation Kinetics of *Salmonella* and *Listeria* in Ground Chicken Breast Meat and Liquid Medium. *Journal of Food Science*, 65(4), 706-710.
- Noriega, E., Velliou, E.G., Van Derlinden, E., Mertens, L., Van Impe, J.F., 2013. Effect of cell immobilization on heat-induced sublethal injury of *Escherichia coli*, *Salmonella* Typhimurium and *Listeria innocua*. *Food microbiology*, 36, 355-364.
- Passos, M.H.C.R., Kuaye, A.Y., 2002. Influence of the formulation, cooking time and final internal temperature of beef hamburgers on the destruction of *Listeria monocytogenes*. *Food Control*, 13, 33-40.
- Perni, S., Chalise, P.R., Shama, G., Kong, M.G., 2007. Bacterial cells exposed to nanosecond pulsed electric fields show lethal and sublethal effects. *International Journal of Food Microbiology*, 120 (3), 311-314.
- Pin, C., Sutherland, J.P., Baranyi, J., 1999. Validating predictive models of food spoilage organisms. *Journal of Applied Microbiology*, 87, 491-499.
- Rawson, A., Patras, A., Tiwari, B.K., Noci, F., Koutchma, T., Brunton, N., 2011. Effect of thermal and non thermal processing technologies on the bioactive content of exotic fruits and their products: Review of recent advances. *Food Research International*, 44, 1875-1887.
- Reiner, M., 1926. Über die Strömung einer elastischen Flüssigkeit durch eine Kapillare. *Kolloid Zeitschrift*, 39, 80-87.
- Rosnes, J.T., Skåra, T., Skipnes, D., 2011. Recent advances in minimal heat processing of fish: Effects on microbiological activity and safety. *Food and Bioprocess Technology*, 4(6), 833-848.
- Ross, T., McMeekin, T.A., Baranyi, J., 2000. Predictive microbiology and food safety. In: Robinson, R.K., Batt, C.A., Patel, P.D. (Eds.), *Encyclopedia of food microbiology*, Vol. 3. Academic Press, San Diego, pp. 1699-1710.
- Schultze, K.K., Linton, R.H., Cousin, M.A., Luchansky, J.B., Tamplin, M.L., 2007. Effect of preinoculation growth media and fat levels on thermal inactivation of a serotype 4b strain of *Listeria monocytogenes* in frankfurter slurries. *Food Microbiology*, 24, 352-361.

- Silva, A., Genovés, S., Martorell, P., Zanini, S.F., Rodrigo, D., Martínez, A., 2015. Sublethal injury and virulence changes in *Listeria monocytogenes* and *Listeria innocua* treated with antimicrobials carvacrol and citral. *Food Microbiology*, 50, 5-11.
- Skandamis, P.N., Yoon, Y., Stopforth, J.D., Kendall, P.A., Sofos, J.N., 2008. Heat and acid tolerance of *Listeria monocytogenes* after exposure to single and multiple Sublethal stresses. *Food Microbiology*, 25, 294-303.
- Smet, C., Noriega, E., Van Mierlo, J., Valdramidis, V.P., Van Impe, J.F., 2015. Influence of the growth morphology on the behavior of *Salmonella* Typhimurium and *Listeria monocytogenes* under osmotic stress. *Food Research International*, 77, 515-526.
- Szlachta, K., Keller, S.E., Shazer, A., Chirtel, S., 2010. Thermal Resistance of *Listeria monocytogenes* Scott A in Ultrafiltered Milk as Related to the Effect of Different Milk Components. *Journal of Food Protection*, 73(11), 2110-2115.
- Tang, S., Orsi, R.H., den Bakker, H.C., Wiedmann, M., Boor, K.J., Bergholz, T.M., 2015. Transcriptomic Analysis of the Adaptation of *Listeria monocytogenes* to Growth on Vacuum-Packed Cold Smoked Salmon. *Applied and Environmental Microbiology*, 81(19), 6812-6824.
- Uyttendaele, M., Rajkovic, A., Van Houteghem, N., Boon, N., Thas, O., Debevere, J., Devlieghere, F., 2008. Multi-method approach indicates no presence of sub-lethally injured *Listeria monocytogenes* cells after mild heat treatment. *International Journal of Food Microbiology*, 123, 262-268.
- Van Impe, J.F., Poschet, F., Geeraerd, A.H., Vereecken, K.M., 2005. Towards a novel class of predictive microbial growth models. *International Journal of Food Microbiology*, 100(1-3), 97-105.
- Van Netten, P., Perales, I., van de Moosdijk, A., Curtis, G.D.W., Mossel, D.A.A., 1989. Liquid and solid selective differential media for the detection and enumeration of *L. monocytogenes* and other *Listeria* spp. *International Journal of Food Microbiology*, 8, 299-316.
- Velliou, E.G., Noriega, E., Van Derlinden, E., Mertens, L., Boons, K., Geeraerd, A.H., Devlieghere, F., Van Impe, J.F., 2013. The effect of colony formation on the heat inactivation dynamics of *Escherichia coli* K12 and *Salmonella typhimurium*. *Food Research International*, 54(2), 1746-1752.
- Verheyen, D., Baka, M., Glorieux, S., Duquenne, B., Fraeye, I., Skåra, T., Van Impe, J.F., 2017. Development of fish-based model systems with various microstructures. *Food Research International*, in press.
- Wilson, P.D.G., Brocklehurst, T.F., Arino, S., Thuault, D., Jakobsen, M., Lange, M., Farkas, J., Wimpenny, J.W.T., Van Impe, J.F., 2002. Modelling microbial growth in structured foods: towards a unified approach. *International Journal of Food Microbiology*, 73, 275-289.
- Wu, V.C.H., 2008. A review of microbial injury and recovery methods in food. *Food Microbiology*, 25, 735-744.

A SIMPLE METHOD FOR GROWING PSEUDOMONAS FLUORESCENS BIOFILMS ON A HYDROPHOBIC POLYSTYRENE SURFACE

Valeria Angarano¹, Cindy Smet¹, Maria Baka¹, Simen Akkermans¹, Andre Chieffi² and Jan Van Impe^{1,*}

¹ BioTeC+ & OPTEC, Department of Chemical Engineering, KU Leuven

CPMF2, Flemish Cluster Predictive Microbiology in Foods

Gebroeders De Smetstraat 1, B-9000 Gent, Belgium

²Procter&Gamble Newcastle, UK

* E-mail: jan.vanimpe@kuleuven.be

KEYWORDS

Pseudomonas fluorescens, biofilm, growth curve, hydrophobic surface, primary model, biofilm reproducibility.

ABSTRACT

When bacteria are on surfaces they grow as biofilms. This means that bacteria start to produce several substances and they grow embedded in the composed Extracellular Polymeric Substances (EPSs) matrix. This work aims to develop a protocol to grow a reproducible biofilm. Reproducibility in this case refers to the same number of cells and same quantity of biofilm (biomass). *Pseudomonas fluorescens* biofilms are grown on a polystyrene (PS) surface as a drop spread on a well delimited area. The biofilm is characterised by using the crystal violet (CV) assay and the viable cell count method. The first experiments aim to determine the favourable ratio between the volume and the area on which the biofilm is spread. Moreover, the effect of the inoculum concentration and also the effect of different growth medium concentrations on biofilm growth are investigated. Cell growth dynamics is fitted with the Baranyi and Roberts (1994) primary model. The maximum cell density of a biofilm grown for 24 h at 25°C, the specific growth rate and the lag phase duration are determined. Obtaining a reproducible biofilm allows to proceed with studying innovative biofilm inactivation technologies, e.g., light treatment.

INTRODUCTION

Free-floating bacteria grow differently when they adhere to a surface and they initiate biofilm formation (Allison et al. 1998). When bacteria attach to a surface, abiotic or biotic, they organise themselves in layers of cells and they start to produce a highly complex 3D structure determined by the production of an extracellular matrix (Baum et al. 2009; Hentzer et al. 2001). This Extracellular Polymeric Substance (EPS) is composed of: (i) different biopolymers (Hung et al. 2005), (ii) extracellular DNA (Whitchurch et al. 2002), (iii) proteins and lipids (Jo et al. 2017; Raza et al. 2014). The EPS contributes to the biofilm structure and function. The function of the matrix is not only to provide a mechanical stability and protect microorganisms from desiccation, but it also acts as a barrier against chemical and biological influences (oxygen, antiseptic, antibiotics) (Hentzer et al. 2001). Moreover, this

matrix (i) contributes to the sorption and storage of nutrients, (ii) is the place where many extracellular enzymatic reactions take place and (iii) keeps the microorganisms in tight contact with each other to facilitate quorum sensing (QS) (Parsek et al. 1999).

Some biofilms can be beneficial, e.g., they can disintegrate soil and water contaminations, but in most cases they cause several problems.

Because of their ubiquitous presence they can cause (i) clinical infections (e.g., in catheters, needles), (ii) corrosion or (iii) a loss of efficiency in different processes (e.g., water processes, tooth bleaching processes (Soukos et al. 2004)), (iv) safety issues within the food industry (e.g., slaughter line of meat products, (fresh) milk and cream products, vegetables) (Lebert et al. 1997).

Nowadays, many antimicrobial agents (e.g., ampicillin, ciprofloxacin) used to avoid contamination and to cure infections in nosocomial environment (Davies 2003) are no longer effective against bacteria grown as biofilms. This is the reason why the scientific community tries to provide alternative solutions to tackle this problem, not only by chemical but also by physical means (e.g., light treatment (Ganz et al. 2005; Kim et al. 2017; Maclean et al. 2008; Papageorgiu et al. 2000), plasma treatment, in synergy or not with different (traditional) processes (Arroyo et al. 2010; Enwemeka et al. 2009; Halpin 2014; Hamblin and Hasan 2003; Rowan et al. 2015; Sun and Hong 2013;).

To microbiologically assess the impact of technologies like light or plasma treatments on biofilms, reproducible model biofilms are necessary. The Gram-negative *Pseudomonas fluorescens* bacterium is used as a model organism, because (i) it is ubiquitous in biofilms formed on different surfaces (e.g., polymers, stainless steel), (ii) it is capable of causing serious problems in the food industry (Lebert et al. 1997) and (iii) it can cause loss of efficiency in industrial processes (e.g., aqueous system).

This work aims to grow a reproducible *Pseudomonas fluorescens* biofilm. The biofilm is grown on the liquid/solid interface of a drop spread on a petri dish. The biofilm (i) area and volume, (ii) growth medium concentration and (iii) inoculum cell density, are optimised. The Baranyi and Roberts (1994) model is used to describe the biofilm evolution as a function of time.

MATERIALS AND METODS

Preculture preparation

The Gram-negative bacterium *Pseudomonas fluorescens* (ATCC13525) is used as a model organism in this study. The bacterium is cultured in Erlenmeyers: one colony is inoculated in 20 mL Tryptic Soy Broth (TSB) (VWR Chemicals, Belgium) and incubated at 25°C for 24 h under stirring conditions (160 rpm).

Inoculum preparation

The preculture (10⁹ CFU/mL) is diluted in TSB to reach a standard inoculum concentration of 10⁷ CFU/mL. Overall, a standard TSB concentration of 30 g/L is used, unless for the optimisation of the concentration of the growth media. Then, the TSB concentrations assessed are respectively: 30.0 g/L, 15.0 g/L, 3.0 g/L and 1.5 g/L.

Biofilm growth as a drop spread on a well delimited area

A drop of 400 µL is spread on a circular area of a different diameter, respectively: 2.5, 2.0 and 1.5 cm. The drop is spread on the polystyrene (PS) surface of a sterile petri dish (50 mm diameter, 8 mm height, Simport, Canada). Closed petri dishes are left for 24 h in an incubator at 25°C, facilitating biofilm growth.

Crystal violet assay

The biomass of the biofilm, which includes live and dead cells and also extracellular polymeric substances, is quantified through the Crystal violet (CV) assay. When the biofilm is mature, after 24h, the liquid is removed gently using a micropipette. The biofilm attached to the PS surface is successively rinsed gently twice with 3 mL of Phosphate Buffer Saline (PBS) at pH 7.4 in order to remove planktonic cells. Afterwards, 1.5 mL of CV solution (0.046% (v/v) of CV stain (Sigma Aldrich HT90132) in H₂O) is added. The dye is left to penetrate in the biofilm for 15 minutes, rinsed twice with 2 mL of PBS solution and left to dry for 30 minutes. Then, 1.2 mL of acetic acid solution (33% (v/v) in water) is added. After the dye is dissolved, 200 µL is transferred in a well of a 96-well microtiter plate. The quantification of the biomass is performed by reading the optical density at 590 nm using the VersaMax tunable microplate reader (Molecular devices, Berkshire, UK).

Viable cell count procedure

The viable cell count procedure consists of rinsing the mature biofilm thrice. Afterwards, 2 mL of PBS is added. The biofilm is detached from the surface using a cell scraper (Carl Roth, Germany) and by using a micropipette the solution is homogenised. The cell density of the biofilm is determined via viable plate counting on Tryptic Soy Agar (TSA) (VWR chemicals, Belgium).

Mathematical modelling biofilm growth

The model of Baranyi and Roberts (1994) is fitted to the experimental data:

$$\frac{dN(t)}{dt} = \frac{Q(t)}{1 + Q(t)} \cdot \mu_{max} \cdot \left(1 + \frac{N(t)}{N_{max}}\right) \cdot N(t) \quad (1)$$

$$\frac{dQ(t)}{dt} = \mu_{max} \cdot Q(t) \quad (2)$$

Equation (1) describes the cell density $N(t)$ (CFU/mL) as a function of time, which depends on $Q(t)$ that measures the physiological state of the cells. μ_{max} represents the maximum specific growth rate (1/h) and N_{max} the maximum cells density (CFU/mL). Equation (2) describes the evolution of the state $Q(t)$ with time.

RESULTS AND DISCUSSION

In the present work the development of a mature reproducible biofilm is obtained following different steps: by optimisation of (i) the biofilm volume and the area, (ii) the TSB concentration, and (iii) inoculum cell density. Finally, the growth curve of the biofilm is fitted with the Baranyi and Roberts (1994) model.

Optimisation of the volume and the area

First trials indicate that a volume of 400 µL is needed to allow sufficient biofilm growth. Biofilms are grown with the same inoculum volume of 400 µL on different areas (diameter 2.5, 2.0 and 1.5 cm). The biofilms with diameter 2.5 cm are generally attached to the surface after the rinsing procedure and are quite uniform on the surface. The biofilms with diameter 2.0 cm lose some part of the biofilm in the central part during the rinsing step. The samples with diameter 1.5 cm form a ring shape, due to the strong detachment of the biofilm in the central part. The optical density (OD) is proportional to the diameter of the drop (Figure 1): the larger the diameter, the larger the surface of interaction where the bacteria develop as a biofilm.

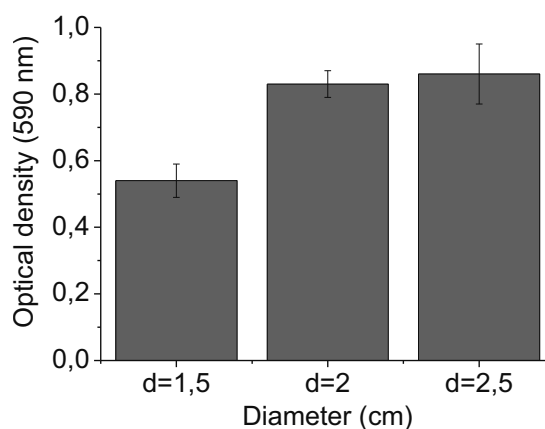


Figure 1 Optical density measured at 590 nm of biofilms grown on surfaces of diameters: 2.5, 2.0 and 1.5 cm.

Based on these experiments (area and volume), it is possible to assert that a ratio area/volume smaller than 81 guarantees a strongly-attached biofilm, which is uniform and quite reproducible in terms of optical density (Figure 2). This can be expected since *Pseudomonas fluorescens* is aerobic, and thus the oxygen diffusion in biofilm formation can have a strong influence. In fact, supposing that when the thickness of the drop varies slightly from the centre to the border, the availability of the oxygen at the liquid-solid interface remains the same. On the contrary, when the thickness of the drop is high at the centre and small at the border, the oxygen that reaches the interface liquid-solid in the centre of the drop is limited and needs a stronger diffusion process during biofilm growth (Xu et al. 1998). From now on, the biofilm will be grown on a circular area of 2.5 cm of diameter and 400 μ L of volume.

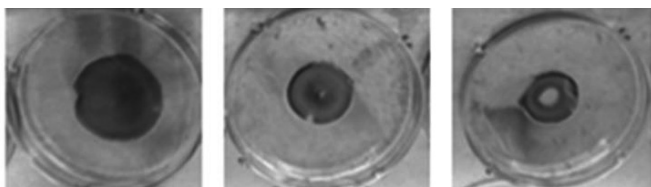


Figure 2 Biofilm grown on a surface with diameters: 2.5, 2.0 and 1.5 cm.

Optimisation of TSB concentration in the inoculum

In literature, a few works confirm that a low nutrient concentration in the inoculum can favour a stronger, thicker and faster growing biofilm (Gerstel et Romling 2001; Speranza et al 2001; Stepanović et al. 2004;). In the present work, the concentration of TSB in the inoculum is varied: 30.0, 15.0, 3.0 and 1.5 g/L. The variation of the TSB concentration indicates to determine also a variation in the superficial tension. This resulted in a “pulling back” phenomenon, which prohibited the spreading of the drop on the delimited area needed (Figure 3). For this reason the TSB concentration is fixed at 30.0 g/L.

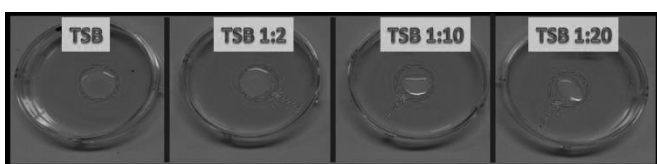


Figure 3 Drops with different TSB concentrations.

Optimisation of cell concentration in the inoculum

As illustrated in the histogram in Figure 4, the variation of the inoculum cell concentration does not impact the viable cell counts for the mature biofilm. This means that after 24 h the mature biofilms contain the same amount of cells, regardless the inoculum concentration.

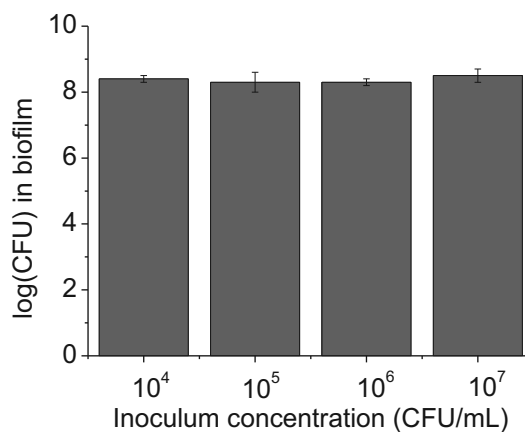


Figure 4 Viable cell counts in mature biofilms obtained with different inoculum concentrations.

Nevertheless, the biofilm seems different in terms of biomass. Quantification of the biomass by CV assay demonstrates that with a lower inoculum concentration a higher biomass is obtained (Figure 5). The biomass includes both live and dead cells and EPS substances, as typically present for bacterial biofilms. Consequently, we can claim that when the biofilm is grown starting with an inoculum concentration of 10^4 CFU/mL, the biomass is higher than the one obtained with a 10^7 CFU/mL inoculum (Figure 5). This indicates that the amount of the EPS substances produced is higher. Future research, e.g., by means of Confocal Laser Scanning Microscopy (CLSM) measurements is required to quantify the EPS and the alive and dead cells.

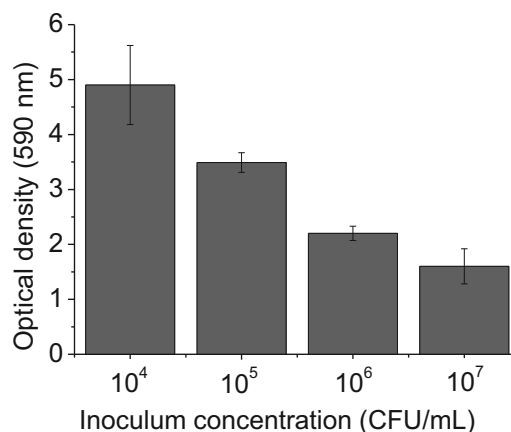


Figure 5 OD measured at 590 nm for mature biofilms obtained with different inoculum concentrations.

Growth curve and biofilm modelling

Figure 6 presents the growth curve of the biofilm of *Pseudomonas fluorescens* at 25°C fitted with the model of Baranyi and Roberts (1994). Cell density is determined via viable plate counting and the inoculum concentration used is 10^7 CFU/mL.

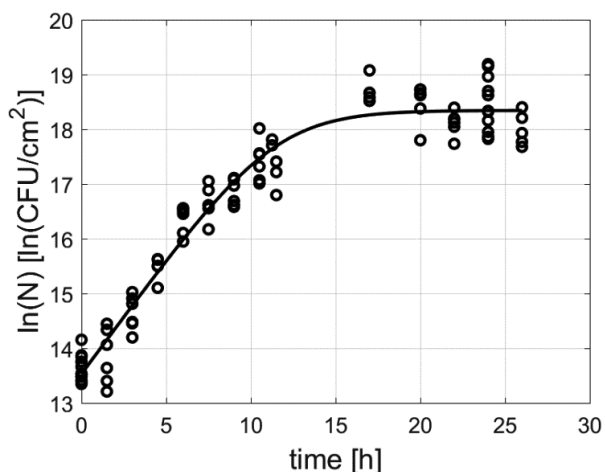


Figure 6 The growth curve of *Pseudomonas fluorescens* in biofilm at 25°C. Symbols correspond to the experimental data which are fitted with the Baranyi and Roberts (1994) growth model.

The Baranyi and Roberts (1994) fit allows to calculate the growth parameters. Resulting lag time, maximum specific growth rate and finally, the initial and the maximum cell density are listed in Table 1 including the respective standard deviations.

Table 1: Parameters obtained from the Baranyi and Roberts (1994) model.

Parameter	Estimated value
λ (h)	0.00 ± 0.00
μ_{max} (1/h)	0.42 ± 0.04
N_o (CFU/cm ²)	13.53 ± 0.11
N_{max} (CFU/cm ²)	18.35 ± 0.07

The lag time is really short, almost zero. This means that the population of cells in the biofilm starts to grow immediately. A fast cell division occurs, meaning that the bacteria do not need any time to recover the shock due to the transfer on the PS surface. This could be related to the kind of substrate that is used in this work, i.e., polystyrene. Polystyrene presents a hydrophobic surface. It is known that cells attach preferentially to hydrophobic, nonpolar surfaces (e.g., polybutylene), than to hydrophilic surfaces (e.g., stainless steel, Cu) (Assanta et al. 1998; Neu 1996). A short lag time could be a sign that bacteria condition the surface rapidly. This conditioning consists in producing a film of proteins, lipids and polysaccharide molecules which attach to the surface and facilitate biofilm formation. The “conditioning stage” represents the first stage of biofilm formation. In the specific case of study the organic molecules produced by *Pseudomonas fluorescens* (e.g., alginate) plus the molecules present in the growth medium (e.g., glucose) might cause faster surface conditioning. The organisms quickly form a layer, which neutralises excessive surface charge and surface free energy, facilitating the growth. Some studies have found that bacteria can also alter the production of some surface components (e.g., lipopolysaccharides, peptidolipids,

glycolipid, lipoteichoic acid) making the surface-cell interaction easier. Specifically, this has been observed for *Pseudomonas aeruginosa* (Neu 1996). The Baranyi and Roberts (1994) model fit indicates that after 18.35 ± 0.17 h, the biofilm is fully developed and mature (Table 1).

CONCLUSIONS

The development of the protocol for the growth of the *Pseudomonas fluorescens* biofilm is obtained. The biofilm is grown on a surface of 2.5 cm of diameter with 400 μ L of inoculum (10^7 CFU/mL) for 24 h at 25°C. Future research can evaluate novel inactivation technologies for the treatment of *Pseudomonas fluorescens* biofilms, which are characterised in this paper. One of these innovative approaches includes the assessment of the impact of different light sources on biofilms. As light has a known antimicrobial effect, it has a high potential to deal with the biofilm challenges.

ACKNOWLEDGEMENTS

This work is supported by the project Bioclean MSCA - ITN - 722871 of the HORIZON 2020 EU Framework Programme for Research and Innovation by means of KU Leuven and by Post-Doctoral Mandate (PMD/16/125) from the research council of KU Leuven for post-doctoral researchers (Maria Baka).

REFERENCES

- Allison D. G., Ruiz B., SanJose C., Jaspe A. and Gilbert P. (1998). Extracellular products as mediators of the formation and detachment of *Pseudomonas fluorescens* biofilms. FEMS Microbiology Letters 167, 179-184.
- Arroyo C., Somolinos M., Cebrián G., Condón S. and Pagán R. (2010). Pulsed electric fields cause sublethal injuries in the outer membrane of *Enterobacter sakazakii* facilitating the antimicrobial activity of citral. Letters in Applied Microbiology 51, 525-531.
- Assanta M. A., Roy D. and Montpetit, D. (1998). Adhesion of *Aeromonas hydrophila* to water distribution system pipes after different contact times. Journal of Food Protection, Vol. 61, No 10, 1321-1329.
- Baranyi J. and Roberts, T. A. (1994). Mathematics of predictive food microbiology. International Journal of Food Microbiology 95, 199-218.
- Baum M. M., Kainović A., O’Keeffe T., Pandita R., McDonald K., Wu S. and Webster P. (2009). Characterization of structures in biofilms formed by a *Pseudomonas fluorescens* isolated from soil. BMC Microbiology, 9:103.
- Davies D. (2003). Understanding biofilm resistance to antibacterial agents. Nature reviews. Drug discovery, Vol. 2, 114-22.
- Enwemeka C. S., Williams D., Enwemeka S. K., Hollosi S. and Yens, D. (2009). Blue 470-nm light kills Methicillin-Resistant *Staphylococcus Aureus* (MRSA) in vitro. Photomedicine and Laser Surgery, Vol. 27, No 2, 221-226.
- Ganz R., Viveiros J., Ahmad A., Ahmadi A., Khalil A., Tolkoff M. J., Nishioka N. S. and Hamblin M. R. (2005). *Helicobacter pylori* in patients can be killed by visible light. Lasers in Surgery and Medicine, Vol 36, 260-265.

- Gerstel U. and Römling, U. (2011). Oxygen tension and nutrient starvation are major signals that regulate agfD promoter activity and expression of the multicellular morphotype in *Salmonella typhimurium*. *Environmental Microbiology*, Vol 3, Issue 10, 638-648.
- Halpin R., Duffy L., Cregenzán-Alberti O., G Lyng J. and Noci, F. (2014). The effect of non-thermal processing technologies on microbial inactivation: an investigation into sub-lethal injury of *Escherichia coli* and *Pseudomonas fluorescens*. *Food Control*, Vol. 41, 106-115.
- Hamblin M. R. and Hasan T. (2004). Photodynamic therapy: a new antimicrobial approach to infectious disease? *Photochemical and Photobiological Sciences*, Vol. 3, 436-450.
- Hentzer M., Teitzel G., Balzer G., Heydorn A., Molin S., Givskov M. and Parsek M. (2001). Alginate overproduction affects *Pseudomonas aeruginosa* biofilm structure and function. *Journal of Bacteriology*, Vol. 183, No. 18, 5395-5401.
- Hung C.-c., Santschi P. H. and Gillow J. B. (2005). Isolation and characterization of extracellular polysaccharides produced by *Pseudomonas fluorescens* Biovar II. *Carbohydrate Polymers* 61, 141-147.
- Jo P., Rabaey K., Lovley D. R. and Vargas, M. (2017). Biofilm formation by *Clostridium ljungdahlii* is induced by sodium chloride stress: experimental evaluation and transcriptome analysis. *Plos One*, January 24.
- Kim M. J., Bang W. S. and Yuk H. G. (2017). 405 ± 5 nm light emitting diode illumination causes photodynamic inactivation of *Salmonella* spp. on fresh-cut papaya without deterioration. *Food Microbiology* 62, 124-132.
- Lebert I., Begot C. and Lebert, A. (1998). Growth of *Pseudomonas fluorescens* and *Pseudomonas fragi* in a meat medium as affected by pH (5.8–7.0), water activity (0.97– 1.00) and temperature (7–25°C). *International Journal of Food Microbiology* 39, 53-60.
- Maclean M., Macgregor S. J., Anderson J. G. and Woolsey G. (2008). High-intensity narrow-spectrum light inactivation and wavelength sensitivity of *Staphylococcus aureus*. *FEMS Microbiol Lett* 285, 227-232.
- Neu T. R. (1996). Significance of bacterial surface-active compounds in interaction of bacteria with interfaces. *Microbiological Reviews*. Vol. 60, No. 1, 151-166.
- Papageorgiou P., Katsambas A. and Chu A. C. (2000). Phototherapy with blue (415 nm) and red (660 nm) light in the treatment of acne vulgaris. *British Journal of Dermatology* 142, 973-978.
- Parsek M. R., Val D. L., Hanzelka B. L., Cronan J. E. and Greenberg E. P. (1999). Acyl homoserine-lactone quorum-sensing signal generation. *Proceedings of the National Academy of Sciences of the United States of America*, Vol. 96, 4360-4365.
- Raza W., Jun Y., Muhammad F., Shah M. A., Shen Q. and Ali, S. (2014). Partial structural linkages and physico-chemical activities of an extracellular polysaccharide produced by *Pseudomonas fluorescens* Strain WR-1. *International Journal of Agriculture & Biology*, Vol.16, No 5, 971-975.
- Rowan N. J., Valdramidis V. P. and Gómez-López, V. M. (2015). A review of quantitative methods to describe efficacy of pulsed light generated inactivation data that embraces the occurrence of viable but non culturable state microorganisms. *Trends in Food Science & Technology*, Vol. 44, 79-92.
- Soukos N. S., Som S., Abernethy A. D., Ruggiero K., Dunham J., Lee C., Doukas A. G. and Goodson J. M. (2005). Phototargeting oral black-pigmented bacteria. *Antimicrobial Agents and Chemotherapy*, Vol. 49, No. 4, 1391-1396.
- Speranza B., Corbo M. R. and Sinigaglia M. (2011). Effects of nutritional and environmental conditions on *Salmonella* sp. biofilm formation. *Journal of Food Science*, Vol 1, No 76, 12-16.
- Stepanović S., Cirković I., Ranin L. and Svabić-Vlahović M. (2004). Biofilm formation by *Salmonella* spp. and *Listeria monocytogenes* on plastic surface. *Letters in Applied Microbiology*, 38, 428-432.
- Sun G. and Hong K. H. (2013). Photo-induced antimicrobial and decontaminating agents: recent progresses in polymer and textile applications. *Textile Research Journal* 83, 532-542.
- Whitchurch C. B., Tolker-Nielsen T., Ragas, P. C. and Mattick J. S. (2002). Extracellular DNA required for bacterial biofilm formation. *Science* 295, 1487.
- Xu K. D., Stewart P. S., Fuhu, X. Huang C.-t. and McFeters G. A. (1998). Spatial physiological heterogeneity in *Pseudomonas aeruginosa* biofilm is determined by oxygen availability. *Applied and Environmental Microbiology*, Vol. 64, Issue 10, 4035-4039.

Stochastic methods to model bacterial growth and food safety risks: Some perspectives

Miriam R. García and Antonio A. Alonso
Process Engineering, IIM-CSIC, Spain
email: antonio@iim.csic.es

KEYWORDS

Stochastic process, food safety risks, modified Fokker-Planck equation, flow cytometry

ABSTRACT

Food safety risks depend on bacterial numbers. At low population numbers, the heterogeneity between individuals and its influence on the division times become critical. It has been observed experimentally that a major descriptor of bacterial growth and division is the cellular size (volume). In this work, we present a general theory to describe cellular size using stochastic differential equations. We derive its equivalent modified Fokker-Planck equation and use this partial differential equation to estimate critical parameters, like macroscopic growth rates, based on experimental size distributions measured by flow cytometry.

INTRODUCTION

Food safety risks can be evaluated using predictive microbiology theory. The aim is to develop mathematical models of growth or inactivation of pathogenic and spoilage microorganisms (Huss 2007, Baranyi and Roberts 1995). These models have been successfully applied to predict food spoilage and microbial safety (Koutsoumanis and Nychas 2000, Ross et al. 2000), smart sensing of food quality (García et al. 2015; 2017, Vilas et al. 2018), Quantitative Microbial Risk Assessment (Cassin et al. 1998, Membré and Lambert 2008) and design and control of food processes (Simpson et al. 1993, Alonso et al. 2013).

Predictive microbiology fails to predict bacterial growth when the number of cells in the initial population is low (Nicolai and Van Impe 1996, Augustin et al. 2015). The problem is that cell-to-cell differences become relevant in predicting population growth. For low population numbers, food safety depends on single-cell growth, death and division. Such stages can be described based on stochastic physiological or biochemical states of the cell, such as bacterial size. Stochastic differential equations, however, require information at the single-cell level and their resolution is computationally expensive.

The modified Fokker-Planck equation provides a methodology to link population heterogeneity with single-cell stochasticity. We develop a theory to predict

population numbers, and therefore food safety risks, using the modified Fokker-Planck equation. For the sake of clarity, we focus the equation on cell size as it provides one of the best descriptors of bacterial growth and division. Future perspectives are discussed regarding this equation and its extension to model other key physiological or biochemical states related to food safety risks.

MODELLING

For low population numbers, food safety depends on single-cell growth, death and division. In this work we will assume that microorganisms grow exponentially and hence death is negligible. Any microbial growth inside the food matrix will always be equal or slower than the assumed scenario (worse-case scenario).

Stochastic single-cell growth and division may be described using cellular size

Growth

Exponential growth of cell volume is a standard principle in bacterial physiology (Fishov et al. 1995). Based on this fact, Alonso et al. (2014) and García et al. (2018) proposed a new stochastic formulation that explains the variability observed for low inoculum concentration. The model assumes that cell growth is subject to a stochastic fluctuation δW characterized by a Wiener process:

$$\delta X^i = \mu \delta t + \xi \delta W \quad \text{with} \quad X^i = \ln(V^i), \quad (1)$$

where X^i is the volume of cell i (V^i) on a logarithmic scale and μ represents the growth rate within the exponential phase. Finally, ξ in the above expression represents the intensity of the stochastic fluctuation. It should be noted that $\xi = 0$ for deterministic growth.

Division

The trigger of bacterial division is still a matter of controversy. There are three major paradigms: the sizer, timer, and adder principle. In these paradigms, division is triggered by a certain volume, time, or after growing certain volume (Taheri-Araghi et al. 2015). As in most predictive microbiology works (Métris et al. 2005, Alonso et al. 2014, García et al. 2018), we concentrate on fully adapted cells (medium growth is kept constant)

where the sizer principle remains the reasonable assumption. For these cases, the division was modelled by adding a new cell to the population and resizing mother and newborn cell to the daughter size. The division event is triggered when the size of one or more cells is greater than a continuous random variable X_m , with statistics defined by the probability density function of mother sizes ($f_{X_m}(x)$):

$$\begin{aligned} \text{If } X^i \geq X_m \sim f_{X_m}(x), \quad X^{n+1} &\rightarrow X^i - \ln(2) \quad (2) \\ X^i &\rightarrow X^i - \ln(2) \quad (3) \end{aligned}$$

where n is the number of cells in the population, i runs from 1 to n and the daughter volume is half the mother volume ($v_d = v_m/2$). It should be stressed that for coccoid cells, the generalization needs to be corrected. Those cells divide quickly with more than one division plane, i.e., one mother gives four daughters (two division planes) or 8 daughters (three division planes) (Pinho et al. 2013, García et al. 2018). Depending on the number of planes the final arrangements of these cells are in tetrads or in clusters.

Our group used flow cytometry to determine the best probability density function describing the mother sizes $f_{X_m}(x)$ (García et al. 2018). The best agreement with the data suggests that the volume of the mothers V_m is a random variable following a log-normal distribution, supporting the theory of Amir (2014):

$$f_{X_m}(x) = \mathcal{N}(x_m, \sigma^2) \quad \text{with} \quad x_m = \ln(v_m) \quad (4)$$

We should note that for simulating the deterministic division, σ can be set to zero so that the normal distribution turns into Dirac delta function centred at the logarithm of the mother size x_m .

The modified Fokker-Plank equation of bacterial size provides directly the population main statistics

Growth

Let $n(t, x)$ be the number of individuals of volume x at time t , in the interval $x \in (\underline{x}, \bar{x})$. All individuals are in the interval so that $n(t, \underline{x}) = n(t, \bar{x}) = 0$. Let $\rho(t, x)$ be the probability distribution function satisfying the forward Kolmogorov equation:

$$\frac{\partial \rho(t, x)}{\partial t} = \frac{\xi^2}{2} \frac{\partial^2 \rho(t, x)}{\partial x^2} - \mu \frac{\partial \rho(t, x)}{\partial x} \quad (5)$$

$$\rho(t, \underline{x}) = \rho(t, \bar{x}) = 0 \quad \forall t \quad \text{boundary cond} \quad (6)$$

$$\rho(0, x) = \delta(x - x_d) \quad \forall x \quad \text{initial cond} \quad (7)$$

and define the expected number of individuals as:

$$\mathcal{M}(t) = \int_{\underline{x}}^{\bar{x}} \rho(t, x) n(t, x) dx \quad (8)$$

We differentiate the above expression in time so that:

$$\frac{d\mathcal{M}(t)}{dt} = \int_{\underline{x}}^{\bar{x}} \rho(t, x) \frac{\partial n(t, x)}{\partial t} dx + \int_{\underline{x}}^{\bar{x}} n(t, x) \frac{\partial \rho(t, x)}{\partial t} dx \quad (9)$$

This term becomes zero if there is not death or division and for this case $\frac{\partial \rho(t, x)}{\partial t} = \frac{\partial n(t, x)}{\partial t}$, otherwise:

$$\frac{d\mathcal{M}(t)}{dt} = \int_{\underline{x}}^{\bar{x}} \rho(t, x) B(n, t, x) dx \quad (10)$$

In order for (9) with the term (10) to hold for every $\rho(t, x)$ we must have:

$$\frac{\partial n(t, x)}{\partial t} = \frac{\xi^2}{2} \frac{\partial^2 n(t, x)}{\partial x^2} - \mu \frac{\partial n(t, x)}{\partial x} + B(n, t, x) \quad (11)$$

$$n(t, \underline{x}) = \rho(t, \bar{x}) = 0 \quad \forall t \quad \text{boundary cond} \quad (12)$$

$$n(0, x) = \delta(x - x_d) \quad \forall x \quad \text{initial cond} \quad (13)$$

This equation is the so-called modified Fokker-Planck equation, where $B(n, t, x)$ represents the term of division (no death is assumed during exponential growth). Sometimes, this equation can be expressed into a more convenient flux form as:

$$\frac{\partial n(t, x)}{\partial t} + \frac{\partial J(n, t, x)}{\partial x} = B(n, t, x) \quad (14)$$

where the flux relates to the field derivatives as:

$$J(n, t, x) = \frac{\xi}{2} \frac{\partial n(t, x)}{\partial x} - \mu n(t, x) \quad (15)$$

Division

For the statistics of division defined in (2)

$$B(n, t, x) = (2f_{X_d}(x) - f_{X_m}(x)) Z(n, t, x), \quad \text{with} \quad (16)$$

$$Z(n, t, x) = \int_{\underline{x}}^{\bar{x}} F_m(x) \frac{\partial J(n, t, x)}{\partial x} dx \quad (17)$$

where probability density functions f_{X_d} and f_{X_m} are truncated and their support are included in (\underline{x}, \bar{x}) .

The rate of growth of the population, $N(t)$, is obtained by integration of (14) over the domain, and using the boundary conditions so that:

$$\frac{dN(t)}{dt} = \int_{\underline{x}}^{\bar{x}} B(n, t, x) dx = Z(n, t, x) \quad (18)$$

For example for $f_{X_d} = \delta(x - X_d)$ and $f_{X_m} = \delta(x - X_m)$, the expression (18) reads:

$$\frac{dN(t)}{dt} = \frac{\partial J(n, t, x)}{\partial x} \Big|_{X_m} \quad (19)$$

The modified Fokker-Planck in fractional form

Under birth-death dynamics, equation (14) can eventually reach a stationary solution. However, this is not the case in those situations where death is practically negligible. Under those circumstances, we will be particularly interested in studying not just the evolution of the total number of individuals but the distribution of their size (volume).

To that purpose, we re-write previous equation (14) in fractional form, namely in terms of the fraction of individuals that have volume x at a given time, namely $p(t, x) : [0, \infty) \times (\underline{x}, \bar{x}) \rightarrow (0, 1)$. Both functions $n(x, t)$ and $p(t, x)$ are related as:

$$n(t, x) = p(t, x)N(t) \quad \text{where} \quad N(t) = \int_{\underline{x}}^{\bar{x}} n(t, x)dx$$

and therefore:

$$\frac{\partial p(t, x)}{\partial t} = \frac{1}{N(t)} \left(\frac{\partial n(t, x)}{\partial t} - Z(n, t, x)p(t, x) \right)$$

Finally the modified fokker-Planck in fractional form becomes:

$$\frac{\partial p(t, x)}{\partial t} = \underbrace{\frac{\xi^2}{2} \frac{\partial^2 p(t, x)}{\partial x^2} - \mu \frac{\partial p(t, x)}{\partial x}}_{\text{cell growth} = \frac{\partial J(p, t, x)}{\partial x}} \quad (20a)$$

$$+ \underbrace{(2f_{X_d}(x) - f_{X_m}(x)) Z(p, t, x)}_{\text{division}} \quad (20b)$$

$$- \underbrace{p(t, x) Z(p, t, x)}_{\text{normalization}} \quad (20c)$$

$$Z(p, t, x) = \int_{\underline{x}}^{\bar{x}} F_m(x) \frac{\partial J(p, t, x)}{\partial x} dx \quad (20d)$$

$$p(t, \underline{x}) = p(t, \bar{x}) = 0 \quad \forall t \quad \text{boundary cond} \quad (20e)$$

$$p(0, x) = \delta(x - x_d) \quad \forall x \quad \text{initial cond} \quad (20f)$$

NUMERICS

Individual-based modelling using the stochastic equation (1) with division event (2) is a bottom-up approach providing valuable information at the single-cell level. However, it requires parameters that cannot be easily measured (Augustin et al. 2015, Ferrer et al. 2009). In addition, individual-based modelling is characterised by requiring long computational times which make its use prohibitive in applications that demand many model evaluations (An et al. 2017), such as parameter estimation.

The modified Fokker-Planck equation here presented focuses on population statistics that can be directly measured by flow cytometry. The modified Fokker-Planck equation provides directly the evolution of the volume distribution without the need of predefining any probability density function. Flow cytometry provides fast

and cheap measurements of relevant population statistics like cell size distributions. Comparisons between the model and the data provide information about single-cell parameters, like distributions of division sizes, that can be used for individual-based modelling.

The precision of the modified Fokker-Planck equation depends on the discretisation method to solve the partial differential equation, but works for large and small populations whenever the assumptions of a Wiener process are satisfied (Gardiner 2004). Simulations of the modified Fokker-Planck equation are performed using the finite difference discretisation scheme presented in (Vande Wouwer et al. 2014), with a sufficiently refined mesh (consisting of 501 elements), which is enough to approximate the equation with the required accuracy. An upwind 5 points, and centred 5 points in the stencil are employed to approximate first and second order derivatives, respectively. The resulting set of ordinary differential equations may be integrated in Matlab with a standard ODE solver (ode15s).

Figure 1 compares the results and performance of the individual-based modelling (stochastic differential equations) and the modified Fokker-Planck equation (one partial derivative equation). Left panel shows that both models provide the same stationary distribution. Right panel depicts the computational times required for simulating both models. Numerical comparisons reveal that computation time of the stochastic equations grows exponentially with time, whereas the growth is linear for its equivalent modified Fokker-Planck equation (20). Note that the stochastic individual-based modelling approach requires one equation per cell and, as cells grow exponentially, computation time scales linearly with the number of cells and exponentially with time. The modified Fokker-Planck equation, however, is one partial differential equation (PDE) where the computation time depends on the degree of discretisation and the simulation time. For the examples computed in (García et al. 2018), we obtain similar order of computational times (2-10 seconds) until time 15, with a population of less than 3e4 cells, being the individual-based modelling more efficient. However from this time the modified Fokker-Planck equation becomes more efficient in orders of magnitude and different simulations will give very different computation times for the individual-based modelling. In addition, this partial derivative equation has a diffusive term allowing the use of reduced order techniques (Trefethen 2000, García et al. 2008, Vande Wouwer et al. 2014). These methods would allow reducing its computational times even further.

CONCLUSIONS AND FUTURE PERSPECTIVES

In this work a modified Fokker-Planck equation was derived to describe the dynamics of cell growth and division from an initial number of viable cells. The equation

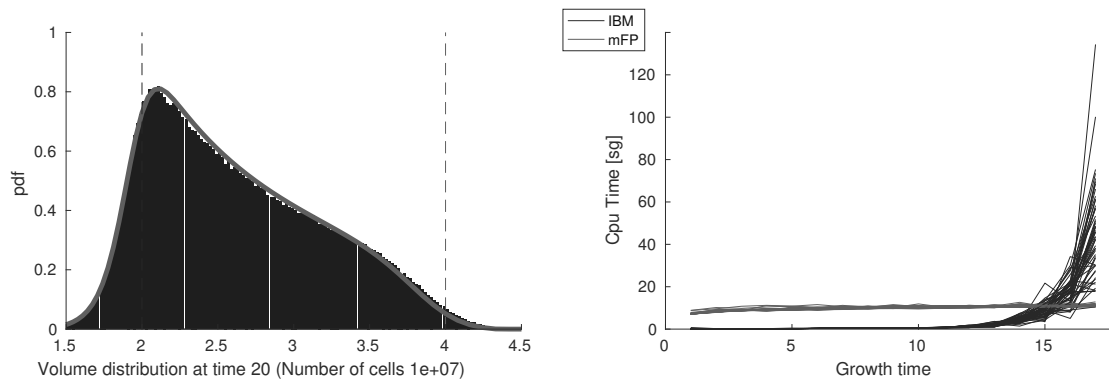


Figure 1: Comparisons between the individual-based model (IBM) and the modified Fokker-Planck equation (mFP) for $\mu = 0.7$, $\xi = 0.3$, $v_m = 4$, $\sigma = 0.05$. Left panel shows the comparisons in terms of stationary distribution. It corresponds with the distribution obtained by allowing one cell to growth and divide until time 20. Right panel depicts the differences in terms of computational time with one and another model for 50 different runs.

has been validated both numerically and experimentally with an individual based model approach that makes use of a stochastic differential Equation (SDE) formalism.

As it has been discussed, the method adopted can bring inside into the division and growth dynamical properties, giving account of possible structural changes undergoing division (e.g number of division planes).

On the other hand, the combination of the modified Fokker-Plank equation with flow cytometry data can be used to estimate macroscopic growth rates in bacterial cultures from mesoscopic bacterial size distributions. In this way, the method can provide a quick in-line way of obtaining relevant growth model parameters under different environmental conditions without the need of long and tiresome kinetic studies. It is expected that biotechnology industries and quality control departments would greatly benefit from this methodology.

The presented approach assumes that division behaves as a sizer, and therefore cells are fully adapted (exponential growth). This is a safe, and conservative, assumption since any microbial growth inside the food matrix will always be equal or slower than the assumed scenario. We are currently working in extending the theory to assume that division behaves as an adder. This will allow us to obtain better estimations of population growth during the lag phase.

ACKNOWLEDGEMENTS

The authors acknowledge financial support from the Spanish Ministry of Science and Innovation, Projects RESISTANCE DPI2014-54085-JIN and IMPROWINE AGL2015-67504-C3-2-R.

REFERENCES

- Alonso A.A.; Arias-Méndez A.; Balsa-Canto E.; García M.R.; Molina J.I.; Vilas C.; and Villafín M., 2013. *Real time optimization for quality control of batch thermal sterilization of prepackaged foods. Food Control*, 32, no. 2, 392–403. ISSN 09567135. doi:10.1016/j.foodcont.2013.01.002.
- Alonso A.A.; Molina I.; and Theodoropoulos C., 2014. *Modeling Bacterial Population Growth from Stochastic Single Cell Dynamics. Applied and environmental microbiology*, 80, no. 17, 5241–5253. ISSN 1098-5336. doi:10.1128/AEM.01423-14.
- Amir A., 2014. *Cell Size Regulation in Bacteria. Physical Review Letters*, 112, no. 20, 208102. ISSN 0031-9007. doi:10.1103/PhysRevLett.112.208102.
- An G.; Fitzpatrick B.G.; Christley S.; Federico P.; Kanarek A.; Neilan R.M.; Oremland M.; Salinas R.; Laubenbacher R.; and Lenhart S., 2017. *Optimization and Control of Agent-Based Models in Biology: A Perspective. Bulletin of Mathematical Biology*, 79, no. 1, 63–87. ISSN 0092-8240. doi:10.1007/s11538-016-0225-6.
- Augustin J.C.; Ferrier R.; Hezard B.; Lintz A.; and Stahl V., 2015. *Comparison of individual-based modeling and population approaches for prediction of food-borne pathogens growth. Food Microbiology*, 45, 205–215. doi:10.1016/j.fm.2014.04.006.
- Baranyi J. and Roberts T.A., 1995. *Mathematics of predictive food microbiology. International Journal of Food Microbiology*, 26, no. 2, 199–218. ISSN 01681605. doi:10.1016/0168-1605(94)00121-L.
- Cassin M.H.; Lammerding A.M.; Todd E.C.D.; Ross W.; and McColl R.S., 1998. *Quantitative risk as-*

- assessment for *Escherichia coli* O157:H7 in ground beef hamburgers. *International Journal of Food Microbiology*, 41, no. 1, 21–44. ISSN 01681605. doi:10.1016/S0168-1605(98)00028-2.
- Ferrer J.; Prats C.; López D.; and Vives-Rego J., 2009. *Mathematical modelling methodologies in predictive food microbiology: A SWOT analysis*. *International Journal of Food Microbiology*, 134, no. 1-2, 2–8. ISSN 01681605. doi:10.1016/j.ijfoodmicro.2009.01.016.
- Fishov I.; Zaritsky A.; and Grover N.B., 1995. *On microbial states of growth*. *Molecular microbiology*, 15, no. 5, 789–94.
- García M.R.; Cabo M.L.; Herrera J.R.; Ramilo-Fernández G.; Alonso A.A.; and Balsa-Canto E., 2017. *Smart sensor to predict retail fresh fish quality under ice storage*. *Journal of Food Engineering*, 197, 87–97. ISSN 02608774. doi:10.1016/j.jfoodeng.2016.11.006.
- García M.R.; Vázquez J.A.; Teixeira I.G.; and Alonso A.A., 2018. *Stochastic Individual-Based Modeling of Bacterial Growth and Division Using Flow Cytometry*. *Frontiers in Microbiology*, 8, 2626. ISSN 1664-302X. doi:10.3389/fmicb.2017.02626.
- García M.R.; Vilas C.; Banga J.R.; and Alonso A.A., 2008. *Exponential observers for distributed tubular (bio)reactors*. *AIChE Journal*, 54, no. 11, 2943–2956. ISSN 00011541. doi:10.1002/aic.11571.
- García M.R.; Vilas C.; Herrera J.R.; Bernárdez M.; Balsa-Canto E.; and Alonso A.A., 2015. *Quality and shelf-life prediction for retail fresh hake (*Merluccius merluccius*)*. *International journal of food microbiology*, 208, 65–74. ISSN 1879-3460. doi:10.1016/j.ijfoodmicro.2015.05.012.
- Gardiner C., 2004. *Handbook of stochastic methods: for physics, chemistry & the natural sciences*. Springer.
- Huss H.H., 2007. *Assessment and management of seafood safety and quality*. 444. Daya Books.
- Koutsoumanis K. and Nychas G.J.E., 2000. *Application of a systematic experimental procedure to develop a microbial model for rapid fish shelf life predictions*. *International Journal of Food Microbiology*, 60, no. 2-3, 171–184. ISSN 01681605. doi:10.1016/S0168-1605(00)00309-3.
- Membré J.M. and Lambert R.J.W., 2008. *Application of predictive modelling techniques in industry: From food design up to risk assessment*. *International Journal of Food Microbiology*, 128, no. 1, 10–15. ISSN 01681605. doi:10.1016/j.ijfoodmicro.2008.07.006.
- Métris A.; Le Marc Y.; Elfving A.; Ballagi A.; and Baranyi J., 2005. *Modelling the variability of lag times and the first generation times of single cells of*. *International Journal of Food Microbiology*, 100, no. 1, 13–19. ISSN 01681605. doi:10.1016/j.ijfoodmicro.2004.10.004.
- Nicolai B. and Van Impe J., 1996. *Predictive food microbiology: A probabilistic approach*. *Mathematics and Computers in Simulation*, 42, no. 2-3, 287–292. ISSN 0378-4754. doi:10.1016/0378-4754(95)00129-8.
- Pinho M.G.; Kjos M.; and Veening J., 2013. *How to get (a)round: mechanisms controlling growth and division of coccoid bacteria*. *Nature Reviews Microbiology*, 11, no. 9, 601–614. ISSN 1740-1526. doi:10.1038/nrmicro3088.
- Ross T.; Dalgaard P.; and Tienungoon S., 2000. *Predictive modelling of the growth and survival of *Listeria* in fishery products*. *International Journal of Food Microbiology*, 62, no. 3, 231–245. ISSN 01681605. doi:10.1016/S0168-1605(00)00340-8.
- Simpson R.; Almonacid-Merino S.F.; and Torres J.A., 1993. *Mathematical models and logic for the computer control of batch retorts: Conduction-heated foods*. *Journal of Food Engineering*, 20, no. 3, 283–295. ISSN 02608774. doi:10.1016/0260-8774(93)90069-V.
- Taheri-Araghi S.; Bradde S.; Sauls J.T.; Hill N.S.; Levin P.A.; Paulsson J.; Vergassola M.; and Jun S., 2015. *Cell-Size Control and Homeostasis in Bacteria*. *Current Biology*, 25, no. 3, 385–391. ISSN 09609822. doi:10.1016/j.cub.2014.12.009.
- Trefethen L.N., 2000. *Spectral Methods in MATLAB*. Society for Industrial and Applied Mathematics. ISBN 978-0-89871-465-4. doi:10.1137/1.9780898719598. URL <http://epubs.siam.org/doi/book/10.1137/1.9780898719598>.
- Vande Wouwer A.; Saucez P.; and Vilas C., 2014. *Simulation of ODE/PDE Models with MATLAB®, OCTAVE and SCILAB. Scientific and Engineering Applications*. Springer International Publishing, Cham. ISBN 978-3-319-06789-6. doi:10.1007/978-3-319-06790-2. URL <http://link.springer.com/10.1007/978-3-319-06790-2>.
- Vilas C.; Alonso A.A.; Herrera J.R.; Bernárdez M.; and García M.R., 2018. *A mathematical model to predict early quality attributes in hake during storage at low temperature*. *Journal of Food Engineering*, 222, 11–19.

GROWTH/ NO GROWTH MODELS OF DIFFERENT STRESS ADAPTED *LISTERIA MONOCYTOGENES* STRAINS

Pantelis Stathopoulos, Dimitra Houhoula,
Dimitrios Timpis

Department of Food Technology
Technological Educational Institute
Athens

Agiou Spiridonos
122 43 Athens, Greece

Efstathia Tsakali, Jan Van Impe

Department of Chemical Engineering
BioTeC+ & OPTEC
KU Leuven

Gebroeders De Smetstraat 1
B-9000 Gent, Belgium

Spiridon J Konteles

EFET Hellenic Food Authority
Regional Division of
Attica

124 Kifissias & Iatridou 2
Athens, Greece

KEYWORDS

Listeria monocytogenes, Growth/ No Growth model, stress adapted strains

ABSTRACT

Growth/No Growth models are statistical models used to quantify the combined effect of various growth inhibitors and determine the environmental conditions in which a pathogen is unable to grow. One factor affecting the development of G/NG models is the microbial intraspecies strain variability, as different strains often behave differently when one or more environmental conditions change. This obstacle is overcome by a pre-screening of the strains in order for the most resistant strain to be used. In this experiment, a pre-screening of different *Listeria monocytogenes* strains revealed that there were different strains exhibiting resistance to different stressing environmental conditions, thus making it not feasible to classify only one as the most resistant. Instead, the produced G/NG model was based on growth data of all 10 tested strains, resulting in a composite model which successfully predicted full growth of *L. monocytogenes*. Additionally, in comparison to individual strain generated models, the composite model safely predicted bacterial growth in environmental conditions where individual models failed to.

INTRODUCTION

Predictive microbiology is a systematic effort to define the effect of the initial conditions (process, environmental conditions, food composition) on the final behavior (growth, death, toxin production) of a microorganism, through statistical and mathematical approaches. It is commonly used as a scientific tool in the food industry in order to achieve production of microbiologically safe foods. In 1993, Whiting and Buchanan categorized statistical models in three distinguished types (Whiting and Buchanan, 1993). The primary models, which give a mathematical description of the growth kinetic parameters (μ_{max} , generation time, λ , y_{max}), the secondary models, which describe the effect of the various environmental factors, like pH and a_w on the microbial growth and the tertiary models, which are a combination of primary and secondary models for the production of statistical software.

A commonly used secondary model is the "Growth/No Growth" model. These models have the ability to quantify

the combined effect of various growth inhibitors and determine the conditions in which the pathogen is unable to develop (Vermeulen et al., 2007). The use of "Growth/No Growth" models gives the ability to retrieve growth data of a microorganism on synthetic substrates with final aim to reduce significantly the number of challenge tests required to determine the growth limits in real food.

This type of modeling and Predictive Microbiology in general, have been used to define how the growth of various microorganisms is affected by the use of several antimicrobial substances like nisine and essential oils (Boziaris and Nychas, 2006; Abdollahzadeh et al., 2017; Shakeri et al., 2017), the inoculum size (Vermeulen et al., 2009; Shakeri et al., 2017), the use of novel food processes as High Hydrostatic Pressure and Pulse Light (Bover-Cid et al. 2010; Hierro et al., 2011) and the strain variability (Valero et al., 2010; Lianou and Koutsoumanis, 2013; Augustin et al., 2011; Aryani et al., 2015a, b; Den Besten et al., 2017).

The latter issue has been a subject of many studies over the last years, for a variety of microorganisms, such as *Salmonella enteritica* (Sant'Ana et al., 2012; Lianou and Koutsoumanis, 2011), *Listeria monocytogenes* (Sant'Ana et al., 2012; Augustin et al., 2011; Aryani et al., 2015a, b) and *Escherichia coli* (Valero et al, 2010). The main conclusion of the above studies was that, regardless the microorganism, the variation in the growth behavior of the strains is an important factor that should be taken into account when developing a statistical model.

One of the microorganisms most commonly used for the development of statistical models is *Listeria monocytogenes*. This is due to the fact that despite not being the cause of the most food poisoning outbreaks, in comparison to other pathogens as *Salmonella* spp. (Greig and Ravel, 2009), it is a major concern for food safety because of the high mortality of the patients (Bennion et al., 2008). Therefore, there have been many studies about the minimum levels of several environmental factors, such as temperature (Walker et al., 1990), pH (Farber et al., 1989; Buchanan et al., 1993) and water activity (Farber et al., 1992; Nolan et al., 1992) that allow growth of the bacterium, while most recently, many statistical models were developed with the aim to identify the effect of various environmental factors on the growth of *L. monocytogenes* (Tienungoon et al., 2000; Koutsoumanis and Sofos, 2005; Boziaris and Nychas, 2006; Boziaris et al., 2006; Vermeulen et al., 2007, 2009).

Previous studies have demonstrated that bacterial strain variability affects the estimation of growth boundaries (George et al., 1988; Farber et al., 1989, 1992; Vermeulen et al., 2007) and therefore the development of predictive models (Tienungoon et al., 2000; Valero et al., 2010; Aryani et al., 2015a, b).

On this basis, the purpose of this study was: (i) the identification and comparison of the growth limits of 10 genetically different strains of *L. monocytogenes*, (ii) The development of a composite "Growth/No Growth" model, using growth data of all strains, skipping the screening process, (iii) The comparison of the composite Growth/No Growth model with models developed using data from individual strains.

MATERIAL AND METHODS

Strains and growth media

The 10 different strains of *L. monocytogenes* have been previously genetically serotyped (Houhoula et al., 2012). Before use, each one was resuscitated, by transferring one beam of the original culture in 10 ml of Brain Heart Infusion broth and let for overnight incubation. The initial inoculum level was confirmed by plating 1 ml in Plate Count Agar (PCA), followed by the appropriate dilutions and plate reading enumeration. The above described procedure was performed in triplicates in order to ensure results' reliability. The strains that were used as well as their source (food or clinical sample) are shown in Table 1.

Table 1: The strains of *Listeria monocytogenes* used in the experiment

<i>Code</i>	<i>Source</i>
S1	Reference Strain
S2	Food
S3	Clinical
S4	Food
S5	Clinical
S6	Clinical
S7	Food
S8	Food
S9	Clinical
S10	Reference Strain

Experimental Procedure

Growth media was adjusted to the desired pH and a_w values, following suspension in microtiter plates (Greiner Bio-One, Germany). pH was adjusted using acetic acid at 8 different levels (4.0, 4.4, 4.8, 5.2, 5.6, 6.0, 6.4 and 6.8) before autoclaving and minor corrections were made afterwards under sterile conditions. The water activity was adjusted at 6 different levels (0.89, 0.91, 0.93, 0.95, 0.97 και 0.99), with the appropriate quantities of NaCl being calculated by using calibration curves between water activity and NaCl concentrations (Dinane et al., 2002). Growth media was inoculated in 3 different levels (2, 3 and 4 log cfu/ml) and the microtiter plates were stored for 60 days at the selected experimental temperature (4 and 18°C). Growth data (visible inspection) were collected every 3 days and the experimental procedure was conducted in 4 replications in order to ensure the reliability of the results.

Development of the growth models

The type of model developed in this study was a logistic regression model. These models consist of an equation in which the right part is a polynomial expression of the examined factors influencing the growth of the microorganism, and the left part is the expression $\text{Logit}(P) = \ln(P/(1-P))$, where P is the probability of growth. The main advantage of logistic regression models is that they can easily fit binomial data because they are linear models, and they are able to incorporate any environmental factor and its interactions (Ross and Dalgaard, 2004, Halkos and Kitsos, 2010). In this case, the model tested was the following (Equation 1):

$$\text{logit}(P) = b_0 + b_1 \cdot \text{pH} + b_2 \cdot a_w + b_3 \cdot \text{iL} + b_4 \cdot \text{pH} \cdot a_w + b_5 \cdot \text{iL} \cdot \text{pH} + b_6 \cdot \text{iL} \cdot a_w \quad (\text{Eq. 1})$$

where:

P, the probability of growth of the microorganism, (0 = no growth, 1 = growth),

a_w , the water activity and,

iL (inoculum Level), expressed as the logarithmic transformation of the number of cells (log cfu/ml),

$b_0 \dots b_6$, coefficients for estimation.

These parameters are expressed linearly in the model. Water activity was not transformed into $\ln a_w = (1 - a_w)^{0.5}$ (Gibson et al., 1994; Koutsoumanis et al., 2004) because this method did not lead to a better fit of our data. The use of the main variables' squares (pH^2 , a_w^2 and iL^2) was entirely rejected, as their estimated parameters were statistically insignificant. That is because, their calculated coefficients corresponded to high P-values, greater than 0.800. The only parameter not being rejected despite having $P > 0.05$ was the inoculum level (iL) as well as its interactions (iL x pH and iL x a_w), as we considered that a higher P-value would indicate the extent of the effect of the inoculum level on bacterial growth.

RESULTS AND DISCUSSION

The effect of environmental factors on bacterial growth

The analysis of results reveals that there is variability among the 10 different *L. monocytogenes* strains tested, regarding their growth limits set. This inter-strain growth variability was not an unexpected phenomenon, as it has been demonstrated in various researches (Doyle et al., 2001; Lianou and Koutsoumanis, 2013; Aryani et al., 2015).

After incubation for 60 days, the minimum pH values where bacterial growth was observed were 6.0 and 5.2 at 4°C and 18°C respectively (Tables 2 and 3). Similarly, the minimum water activity values were 0.95 and 0.91 at 4°C and 18°C respectively, with the results being similar to those reported in the past (George et al., 1988; Farber et al., 1989, 1992; McClure et al., 1989; Cole et al., 1990; Parente et al., 1998; Tienungoon et al., 2000; Le Marc et al., 2002; Koutsoumanis et al., 2004; Boziaris and Nychas, 2006; Boziaris et al., 2006; Vermeulen et al., 2007). The increase of the experimental temperature benefited the bacterial growth and broadened the observed growth limits, as expected. Similar growth promoting beneficial effects were observed when the initial bacterial inoculum size was increased from 2 cfu/ml to 3 cfu/ml and subsequently to 4 cfu/ml.

Table 2: Minimum pH and a_w where growth observed for 10 strains of *L. monocytogenes*, after 60 days incubation at 4 °C.

4°C		Water activity																	
Strains		0.89	0.91	0.93	0.95	0.97	0.99	0.89	0.91	0.93	0.95	0.97	0.99	0.89	0.91	0.93	0.95	0.97	0.99
pH	S1	-	-	-	-	6.0	6.0	-	-	-	-	6.0	6.0	-	-	-	-	6.0	6.0
	S2	-	-	-	-	6.0	6.0	-	-	-	-	6.0	6.0	-	-	-	-	6.0	6.0
	S3	-	-	-	-	6.0	6.0	-	-	-	-	6.0	6.0	-	-	-	-	6.0	6.0
	S4	-	-	-	-	6.0	6.0	-	-	-	-	6.0	6.0	-	-	-	-	6.0	6.0
	S5	-	-	-	-	6.0	6.0	-	-	-	-	6.0	6.0	-	-	-	6.8	6.0	6.0
	S6	-	-	-	-	6.0	6.0	-	-	-	-	6.0	6.0	-	-	-	6.4	6.0	6.0
	S7	-	-	-	-	6.0	6.0	-	-	-	-	6.0	6.0	-	-	-	-	6.0	6.0
	S8	-	-	-	-	6.0	6.0	-	-	-	-	6.0	6.0	-	-	-	-	6.0	6.0
	S9	-	-	-	-	6.0	6.0	-	-	-	-	6.0	6.0	-	-	-	-	6.0	6.0
	S10	-	-	-	-	6.0	6.0	-	-	-	-	6.0	6.0	-	-	-	-	6.0	6.0
Inoculum Level		2 log cfu/ml						3 log cfu/ml						4 log cfu/ml					

Table 3: Minimum pH and a_w where growth observed for 10 strains of *L. monocytogenes*, after 60 days incubation at 18°C.

4°C		Water activity																	
Strains		0.89	0.91	0.93	0.95	0.97	0.99	0.89	0.91	0.93	0.95	0.97	0.99	0.89	0.91	0.93	0.95	0.97	0.99
pH	S1	-	6.0	6.0	5.6	5.6	5.6	-	6.0	5.6	5.6	5.2	5.2	-	6.0	5.6	5.6	5.2	5.2
	S2	-	-	6.0	5.6	5.6	5.6	-	-	6.0	5.6	5.6	5.6	-	6.4	6.0	5.6	5.6	5.6
	S3	-	6.4	6.0	5.6	5.6	5.6	-	6.0	6.0	5.6	5.6	5.6	-	6.0	6.0	5.6	5.2	5.2
	S4	-	-	6.0	5.6	5.2	5.2	-	-	6.0	5.6	5.2	5.2	-	-	6.0	5.6	5.2	5.2
	S5	-	6.8	6.0	5.6	5.2	5.2	-	6.8	6.0	5.6	5.2	5.2	-	6.4	6.0	5.6	5.2	5.2
	S6	-	6.8	6.0	5.6	5.6	5.6	-	6.4	6.0	5.6	5.2	5.2	-	6.4	6.0	5.6	5.2	5.2
	S7	-	6.0	6.0	5.6	5.2	5.2	-	6.0	6.0	5.6	5.2	5.2	-	6.0	6.0	5.6	5.2	5.2
	S8	-	6.4	6.0	5.6	5.2	5.2	-	6.0	6.0	5.6	5.2	5.2	-	6.0	6.0	5.6	5.2	5.2
	S9	-	-	6.0	5.6	5.6	5.6	-	6.4	5.6	5.6	5.6	5.6	-	6.0	5.6	5.6	5.6	5.6
	S10	-	-	6.0	5.6	5.6	5.6	-	-	6.0	5.6	5.6	5.6	-	-	6.0	5.6	5.2	5.2
Inoculum Level		2 log cfu/ml						3 log cfu/ml						4 log cfu/ml					

This was attributed to the physiological heterogeneity of cells into a microbial population, as for their ability to survive in extreme conditions (Pascual et al., 2001) and to the fact that into a microbial population there is a distribution of injury over the individual cells (Pin and Baranyi, 2006). This distribution has as result that the larger the bacterial population is the more chances are that there will be a cell which will survive and will be able to grow and multiply (McKellar 1997, 2001; Baranyi, 1998; Robinson et al., 2001; Zhao et al., 2000; Metris et al., 2003).

The fact that some strains did not get affected at all comes in contrast with the findings of Koutsoumanis and Sofos (2005), who observed quite large differences between different inoculum sizes of *Listeria monocytogenes*. It is possible, however, that the difference between the two studies, is due to the use of different growth media and experimental conditions, while it may also be that at the above study, only one strain of the microorganism was tested.

In some publications, in order to choose the strain that will be used for the development of a "Growth/No Growth" model, takes place a screening of the strains (Vermeulen et al., 2007). However, our results indicate the occurrence of an intrastain growth variability, with different strains exhibiting the ability to grow in either low pH or water activity values or even a combination of those environmental factors. Therefore, distinguishing a certain strain as the most resistant is not possible, especially when taking in account that this variability is also affected by the experimental change of factors as temperature and initial inoculum level. Theoretically, the solution to this problem would be to develop a predictive growth model by using a mixed

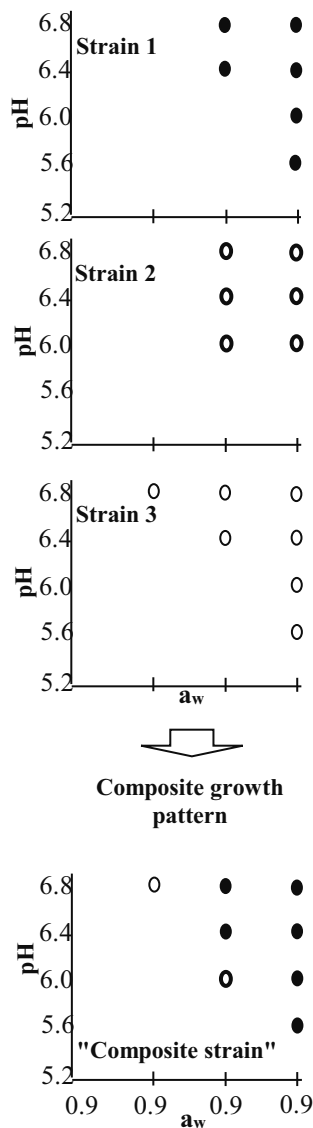
microbial culture, which would consist of the strains with the most extreme growth values. Vermeulen et al. (2007) however, observed that by using a mixed microbial culture, the growth boundary was the same, or sometimes even smaller, compared to the growth boundary which occurred by using an individual culture. This fact was attributed to the use of just the 1/5 of each individual culture, in order to create the mixed culture.

Development of the composite Growth/No Growth Model

Taking in account that during the screening procedure, no strain could be classified as the most resistant one, in either of the environmental factors examined, it was decided to develop a growth/no growth model using growth data of all the examined bacterial strains.

As shown in Figure 1, the growth profiles of the 10 strains were combined in a way that they get a unique "composite strain". This was done in order to avoid a possible failure of the model to predict growth in certain severe environmental conditions of different strains. For example, if there was growth observed in an extreme pH and a_w value for only one strain into one of its replications, then this would be one case over forty data sets (10 strains x 4 replications) providing a possibility of 2.5% to safely predict growth. Using a "composite" growth profile, this particular case would be one over four data sets (1 strain x 4 replications) providing a possibility of 25% to safely predict growth.

Figure 1: Conceptualization of the “composite” growth profile



The results of logistic regression and the estimated lower limits of pH and a_w that allow growth, as they were determined by these composite "Growth/No Growth" model, are shown in Tables 4 and 5 respectively. The following estimated values of pH and a_w are verified by both the observed experimental data and the literature.

The developed "Growth/No Growth" interface is shown in Figure 2. As it can be numerically approved by the values in Table 5 and visually observed in Figure 2, the developed model can successfully predict the growth of all tested strains of *Listeria monocytogenes*. Although the predicted values seem to be more conservative compared to the observed ones, this provides a safety margin so that none of the model's prediction fails. These predictions are called “fail safe” and have been described by numerous researchers (Vermeulen et al., 2010; Perez-Rodriguez and Valero, 2012; Polese et al., 2016; Khanipour et al., 2016).

Table 4: The estimated parameters and statistical indicators of the composite G/NG models. Where HL, the Hosmer-Lemeshow Test indicator

Composite models	Constant	pH	a_w	iL	pH x a_w	iL x pH	iL x a_w	HL (χ^2)
4°C	1324,63	-285,732	-1428,62	17,6622	304,596	1,22520	-24,6386	0,0101
	P	0,001	0,001	0,370	0,000	0,138	0,227	1,000
18°C	923,395	-297,060	-1262,12	151,064	366,596	-6,16116	-123,204	0,1570
	P	0,003	0,001	0,024	0,000	0,036	0,025	1,000

In order to better evaluate the potential of the composite model, we continued by developing individual predictive models for strains S5, S6 and S1, S7 for the temperature of 4°C and 18°C respectively (Model results not shown). For comparison purposes, these models were projected against the composite model as shown in Figure 3.

Figure 2: Growth/No Growth interface of *Listeria monocytogenes*, after incubation for 60 days at 4 and 18°C, as predicted by the composite models. With ○ are represented the points where no growth occurred and with ● the points where growth occurred for all of the ten strains used. Size of initial inoculum: (a, d) 2 log cfu/ml (b, e) 3 log cfu/ml (c, f) 4 log cfu/ml. Each kind of line represents a different growth probability, as shown in the legend.

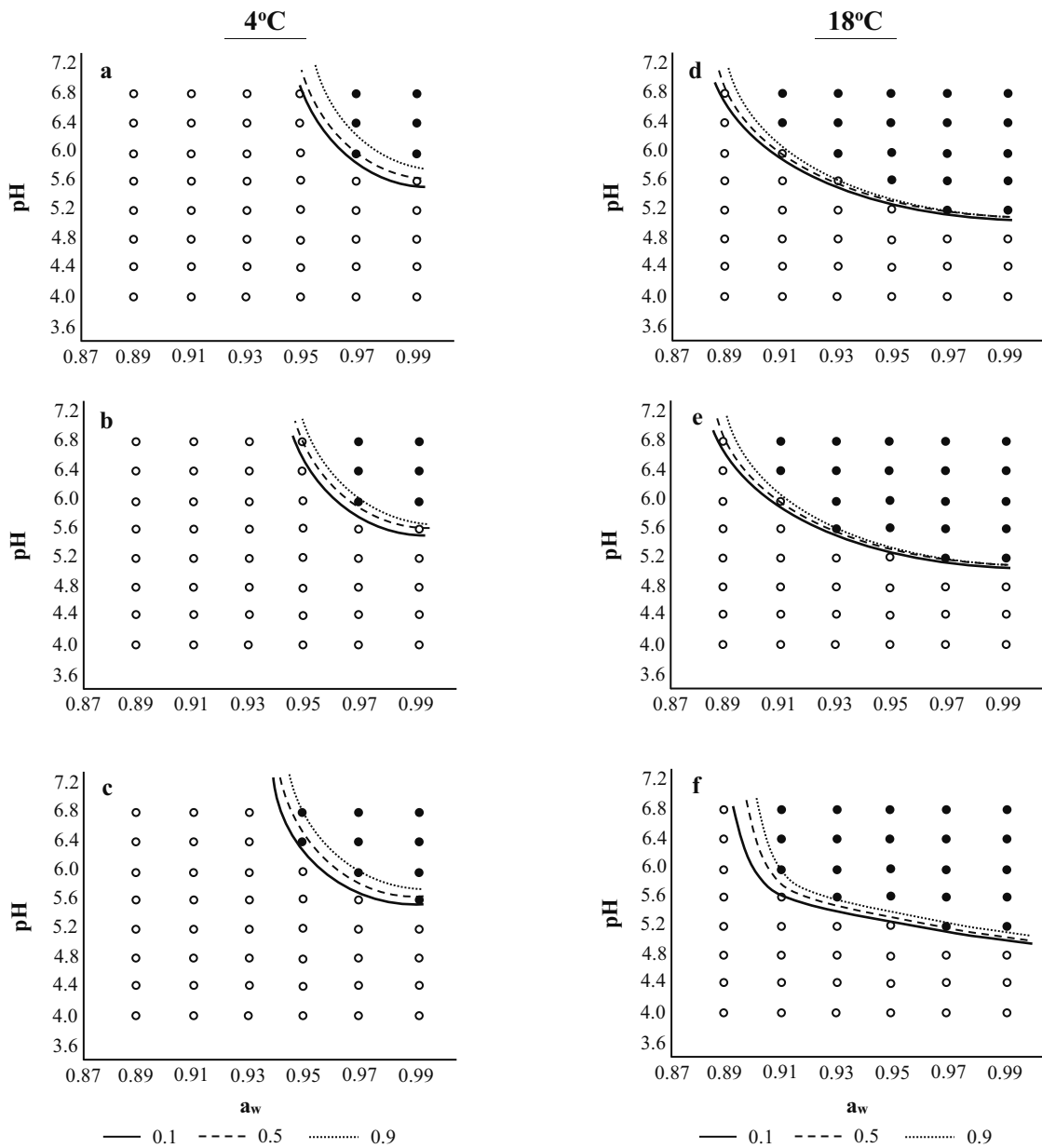
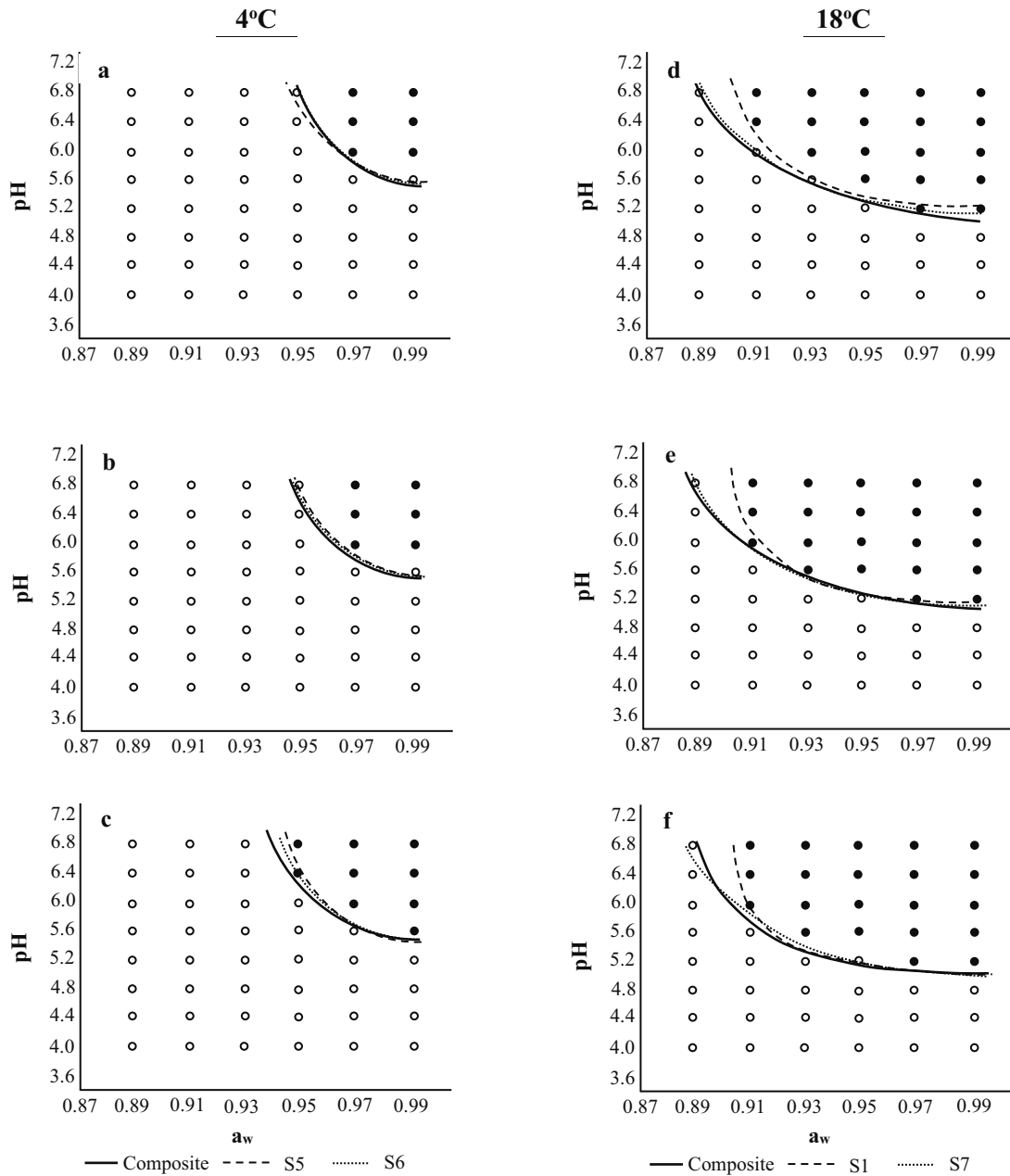


Table 5: The estimated lower limits that allow growth of *Listeria monocytogenes*, as they were determined by the composite G/NG models.

Composite Models	Predicted pH values			Predicted a_w values		
	2 log	3 log	4 log	2 log	3 log	4 log
4 °C	5,59	5,59	5,58	0,953	0,948	0,944
18 °C	4,99	5,02	5,06	0,891	0,892	0,893

Figure 3: Comparison of the composite model with the individual models of the most resistant strains (S) at each temperature. With ○ are represented the points where no growth occurred and with ● the points where growth occurred for all of the ten strains used. Size of initial inoculum: (a, d) 2 log cfu/ml (b, e) 3 log cfu/ml (c, f) 4 log cfu/ml. The probability value used was 0.1 (10%).



The composite model predicts (Figure 3) successfully the growth of *Listeria monocytogenes*, in factor combinations where the individual models fail to do so. For example, in Figure 3c, the individual model of strain S5 fails to predict growth at pH 6.4 and a_w 0.95, due to the fact that strain S5 did not grow in this specific environmental factor combination, even though that through the screening procedure this would be the strain that would be used to develop the predictive model. Additionally, even though the composite model keeps a safety prediction margin, the individual models tend to be even more conservative.

Conclusions

As the results indicate (Figure 3), the development of a "Growth/No Growth" model by using data of an individual

strain, would have resulted in a model failing to predict the full range of growth of *L. monocytogenes*. This was attributed to the fact that each strain adapts differently to changes of specific environmental factors as pH, water activity and temperature, while its adaptability is also affected by the initial inoculum level used. As shown in this experiment, the development of a predictive model using data of more than one strain can help surpass this strain variability and safely predict the growth of *L. monocytogenes*, while the fail-safe margin of the developed model provides us with the ability to further experiment with closer intervals regarding the environmental factors used.

REFERENCES

- Abdollahzadeh, E., Ojagh, S. M., Hosseini, H., Irajian, G., & Ghaemi, E. A. (2017). Predictive modeling of survival/death of *Listeria monocytogenes* in liquid media: Bacterial responses to cinnamon essential oil, ZnO nanoparticles, and strain. *Food Control*, 73, 954-965.
- Aryani, D. C., den Besten, H. M. W., Hazeleger, W. C., & Zwietering, M. H. (2015). Quantifying strain variability in modeling growth of *Listeria monocytogenes*. *International Journal of Food Microbiology*, 208, 19 – 29.
- Aryani, D.C., den Besten, H.M.W., Hazeleger, W.C., Zwietering, M.H., 2015. Quantifying variability on thermal resistance of *Listeria monocytogenes*. *International Journal of Food Microbiology*, 193, 130–138.
- Aryani, D.C., Den Besten, H.M.W., Hazeleger, W.C., Zwietering, M.H., (2015a). Quantifying strain variability in modelling growth of *Listeria monocytogenes*. *International Journal of Food Microbiology* 208, 19–29.
- Aryani, D.C., Den Besten, H.M.W., Hazeleger, W.C., Zwietering, M.H., (2015b). Quantifying variability and the effect of growth history on thermal resistance of *Listeria monocytogenes*. *International Journal of Food Microbiology* 193, 130–138.
- Augustin, J.-C., Bergis, H., Midelet-Bourdin, G., Cornu, M., Couvert, O., Denis, C., Huchet, V., Lemonnier, S., Pinon, A., Vialette, M., Zuliani, V., Stahl, V., (2011). Design of challenge testing experiments to assess the variability of *Listeria monocytogenes* growth in foods. *Food Microbiol.* 28, 746–754.
- Baranyi, J., (1998). Comparison of stochastic and deterministic concepts of bacterial lag. *Journal of Theoretical Biology*, 192, 403–408
- Bennion, J. R., Sorvillo, F., Wise, M. E., Krishna, S., & Mascola, L. (2008). Decreasing listeriosis mortality in the United States, 1990–2005. *Clinical infectious diseases*, 47(7), 867-874.
- Bover-Cid, S., N. Belletti, M. Garriga, T. Aymerich. (2011). Model for *Listeria monocytogenes* inactivation on dry-cured ham by high hydrostatic pressure processing. *Food Microbiology* 28, 804-809
- Boziaris, I.S. and Nychas, G.-J.E., (2006). Effect of nisin on growth boundaries of *Listeria monocytogenes* Scott A, at various temperatures, pH and water activities, *Food Microbiology* 23, 779–784
- Boziaris, I.S., Skandamis, P.N., Anastasiadi M. and Nychas, G.-J.E., (2006). Effect of NaCl and KCl on fate and growth/no growth interfaces of *Listeria monocytogenes* Scott A at different pH and nisin concentrations. *Journal of Applied Microbiology* 102, pp. 796–805.
- Buchanan, R.L., Golden, M.H., Whiting, R.C., (1993). Differentiation of the effects of pH and lactic or acetic acid concentration on the kinetics of *Listeria monocytogenes* inactivation. *Journal of Food Protection* 56, 474–478.
- Cole, M.B., Jones, M.V., and Holyoak, C., (1990). The effect of pH, salt concentration and temperature on the survival and growth of *Listeria monocytogenes*. *J. Appl. Bacteriol.*, 69: 63–72
- Den Besten, H. M., Aryani, D. C., Metselaar, K. I., & Zwietering, M. H. (2017). Microbial variability in growth and heat resistance of a pathogen and a spoiler: All variabilities are equal but some are more equal than others. *International journal of food microbiology*, 240, 24-31.
- Dinane, A., El Guendouzi, M., and Mounir, A., (2002). Hygrometric determination of water activities, osmotic and activity coefficients of (NaCl + KCl)(aq) at T = 298.15 K, *J. Chem. Thermodynamics*, 34, 423–441.
- Doyle, M.E., Mazzotta, A.S., Wang, T., Wiseman, D.W., Scott, V.N., 2001. Heat resistance of *Listeria monocytogenes*. *Journal of Food Protection*, 64, 410–429.
- Farber, J.M., Coates F., and Daley E., (1992). Minimum water activity requirements for the growth of *Listeria monocytogenes*. *Letters in Applied Microbiology* 15: 103-105.
- Farber, J.M., Coates F., and Daley E., (1992). Minimum water activity requirements for the growth of *Listeria monocytogenes*. *Letters in Applied Microbiology* 15: 103-105.
- Farber, J.M., Sanders, G.W., Dunfield, S. and Prescott, R., (1989). The effect of various acidulants on the growth of *Listeria monocytogenes*, *Letters in Applied Microbiology* 9, pp. 181–183
- Farber, J.M., Sanders, G.W., Dunfield, S. and Prescott, R., (1989). The effect of various acidulants on the growth of *Listeria monocytogenes*, *Letters in Applied Microbiology* 9, pp. 181–183
- George, S.M., Lund, B.M., and Brocklehurst, T.F. (1988). The effect of pH and temperature on initiation of growth of *Listeria monocytogenes*. *Letters in Applied Microbiology* 6: 153.
- George, S.M., Lund, B.M., and Brocklehurst, T.F. (1988). The effect of pH and temperature on initiation of growth of *Listeria monocytogenes*. *Letters in Applied Microbiology* 6: 153
- Gibson, A.M., Baranyi, J., Pitt, I., Eyles, M.J., Roberts, T.A., (1994). Predicting fungal growth: the effect of water activity in four species of *Aspergillus*. *International Journal of Food Microbiology* 23, 419–431.
- Greig, J. D., & Ravel, A. (2009). Analysis of foodborne outbreak data reported internationally for source attribution. *International journal of food microbiology*, 130(2), 77-87.
- Halkos, G., Kitsos, C.P., (2010). Exploring Greek Innovation activities: The adoption of Generalized Linear Models. MPRA Paper No 24392
- Hierro, E., Elvira Barroso, Lorenzo de la Hoz, Juan A. Ordonez, Susana Manzano, Manuela Fernandez (2011). Efficacy of pulsed light for shelf-life extension and inactivation of *Listeria monocytogenes* on ready-to-eat cooked meat products. *Innovative Food Science and Emerging Technologies* 12, 275–281
- Houhoula, D., Pirasmaki, D., Konteles, S., Kizis, D., Koussissis, S., Bratacos, M., Poggas, N., Charvalos, E., Tsakris, A., Papaparaskevas, J. (2012). High level of heterogeneity among *Listeria monocytogenes* isolates from clinical and food origin specimens in Greece, *Foodborne Pathogens and Disease*, 9(9), 848-851
- Khanipour, E., Flint, S. H., McCarthy, O. J., Palmer, J., Golding, M., Ratkowsky, D. A., Ross, T., Tamplin, M., (2016). Modelling the combined effect of salt, sorbic acid and nisin on the probability of growth of *Clostridium sporogenes* in high moisture processed cheese analogue. *International Dairy Journal* 57, 62 – 71.
- Koutsoumanis, K.P. and Sofos, J.N., (2005). Effect of inoculum size on the combined temperature, pH and aw limits for growth of *Listeria monocytogenes*. *International Journal of Food Microbiology* 104, 83–91.
- Koutsoumanis, K.P., Kendall, P.A., Sofos, J.N., (2004). A comparative study on growth limits of *Listeria monocytogenes* as affected by temperature, pH and aw when grown in suspension or on a solid surface. *Food Microbiol.* 21, 415–422.
- Koutsoumanis, K.P., Kendall, P.A., Sofos, J.N., (2004). A comparative study on growth limits of *Listeria monocytogenes* as affected by temperature, pH and aw when grown in suspension or on a solid surface. *Food Microbiol.* 21, 415–422.
- Le Marc, Y., Huchet, V., Bourgeois, C.M., Guyonnet, J.P., Mafart, P., and Thuault, D., (2002). Modelling the growth kinetics of *Listeria* as a function of temperature, pH and organic acid concentration. *International Journal of Food Microbiology*, 73: 219–237

- Lianou, A. and Koutsoumanis, K.P., (2011). A stochastic approach for integrating strain variability in modeling *Salmonella enterica* growth as a function of pH and water activity. *International Journal of Food Microbiology* 149, 254–261
- Lianou, A., Koutsoumanis, K.P., 2013. Strain variability of the behavior of foodborne bacterial pathogens: A review. *International Journal of Food Microbiology*, 167, 310 - 321.
- McClure, P.J., Roberts, T.A., Oguru, P.O., (1989). Comparison of the effects of sodium chloride, pH and temperature on the growth of *Listeria monocytogenes* on gradient plates and in liquid medium. *Lett. Appl. Microbiol.* 9, 95–99
- McKellar, R.C., (1997). A heterogeneous population model for the analysis of bacterial growth kinetics, *International Journal of Food Microbiology*, 36: 179
- McKellar, R.C., (2001). Development of a dynamic continuous–discrete–continuous model describing the lag phase of individual bacterial cells. *J. Appl. Microbiol.*, 90: 407.
- Metris, A., George, S.M., Peck, M.W., Baranyi, J., (2003). Distribution of turbidity detection times produced by single cell-generated bacterial population. *Journal of Microbiological Methods* 55, 821– 827.
- Nolan, D.A., Chamblin, D.C., Troller, J.A., (1992). Minimal water activity levels for growth and survival of *Listeria monocytogenes* and *Listeria innocua*. *International Journal of Food Microbiology* 16, 323–335.
- Parente, E., Giglio, M.A., Ricciardi, A., and Clementi, F., (1998). The combined effect of nisin, leucocin F10, pH, NaCl and EDTA on the survival of *Listeria monocytogenes* in broth. *International Journal of Food Microbiology*, 40: 65–74
- Pascual, C., Robinson, T.P., Ocio, M.J., Aboaba, O.O., Mackey, B.M., (2001). The effect of inoculum size and sublethal injury on the ability of *Listeria monocytogenes* to initiate growth under suboptimal conditions. *Letters in Applied Microbiology* 33, 357–361.
- Perez-Rodriguez, F., & Valero, A. (Eds.). (2012). *Predictive microbiology in foods*, New York. Heidelberg, Dordrecht, London: Springer Science & Business Media.
- Pin, C. and Baranyi, J., (2006). Kinetics of single cells: observation and modeling of a stochastic process. *Applied and Environmental Microbiology* 72, 2163–2169.
- Polese, P., Del Torre, M., Stecchini, M. L., (2016). Prediction of the impact of processing critical conditions for *Listeria monocytogenes* growth in artisanal dry-fermented sausages (salami) through a growth/no growth model applicable to time-dependent conditions. Article in Press, *Food Control* (2016), <http://dx.doi.org/10.1016/j.foodcont.2016.12.002>
- Robinson, T.P., Aboaba, O.O., Kaloti, A., Ocio, M.J., Baranyi, J., Mackey, B.M., (2001). The effect of inoculum size on the lag phase of *Listeria monocytogenes*. *International Journal of Food Microbiology* 70, 163–173.
- Ross, T., Dalgaard, P., (2004). Secondary models. In: McKellar, R.C., Lu, X. (Eds.), *Modelling Microbial Responses in Food*. CRC Press, Boca Raton, pp.63-150.
- Sant'Ana, A. S., Franco, B. D., & Schaffner, D. W. (2012). Modeling the growth rate and lag time of different strains of *Salmonella enterica* and *Listeria monocytogenes* in ready-to-eat lettuce. *Food microbiology*, 30(1), 267-273.
- Shakeri, G., Jamshidi, A., Khanzadi, S., & Azizzadeh, M. (2017). Modeling of *Salmonella typhimurium* growth under the effects of *Carum copticum* essential oil, temperature, pH and inoculum size. In *Veterinary Research Forum* (Vol. 8, No. 1, p. 59). Faculty of Veterinary Medicine, Urmia University, Urmia, Iran.
- Tienungoon, S., Ratkowsky, D.A., McMeekin, T.A., and Ross, T., (2000). Growth limits of *Listeria monocytogenes* as a function of temperature, pH, NaCl and lactic acid. *Applied and Environmental Microbiology* 66: 4979–4987
- Valero, A., Rodriguez, M., Carrasco, E., Perez-Rodriguez, F., Garcia-Gimeno, R.M. and Zurera, G., (2010). Studying the growth boundary and subsequent time to growth of pathogenic *Escherichia coli* serotypes by turbidity measurements. *Food Microbiology* 27, 819 – 828
- Vermeulen, A., Gysemans, K.P.M., Bernaerts, K., Geeraerd, A.H., Debevere, J., Devlieghere, F., Van Impe, J.F., (2009). Modelling the influence of the inoculation level on the growth/no growth interface of *Listeria monocytogenes* as a function of pH, aw and acetic acid. *International Journal of Food Microbiology*, 135, 83–89
- Vermeulen, A., Gysemans, K.P.M., Bernaerts, K., Geeraerd, A.H., Van Impe, J.F., Debevere, J., Devlieghere, F., (2007). Influence of pH, water activity and acetic acid concentration on *Listeria monocytogenes* at 7 °C: data collection for the development of a growth/no growth model. *International Journal of Food Microbiology* 114, 332–341
- Walker, S.J., Archer P., and Banks J.G., (1990). Growth of *Listeria monocytogenes* at refrigeration temperatures. *J. Appl. Bacteriol.* 68: 157–162.
- Whiting, R.C., Buchanan, R.L. (1993). A classification of models for predictive microbiology, *Food Microbiology*, Vol. 10 pp.175-7
- Zhao, L., Montville, T.J., and Schaffner, D.W., (2000). Inoculum size of *Clostridium botulinum* 56A spores influences time-to-detection and percent growth-positive samples, *Journal of Food Science*, 65, 1369
- Inglehart, D.L. and G.S. Shedler. (1983). "Simulation Output Analysis for Local Areas Computer Networks." Research Report RJ 4020 (45068), Research Division, IBM, San Jose, CA

Modeling and Simulation in Food Process Systems Engineering

PSE4GUT: INFLUENCE OF A LOW CALORIES DIET SHIFT ON GUT MICROBIOTA DYNAMICS - TOWARDS A PROCESS SYSTEMS ENGINEERING APPROACH

Theodora Akritidou, Cindy Smet, Philippe Nimmegeers, Simen Akkermans, Jan F.M. Van Impe*

BioTeC+ & OPTEC, Department of Chemical Engineering, KU Leuven
CPMF2, Flemish Cluster Predictive Microbiology in Foods
Gebroeders De Smetstraat 1, B-9000 Gent, Belgium

*E-mail: Jan.VanImpe@kuleuven.be

KEYWORDS

Intestinal microbiome, Model system, Human digestion

ABSTRACT

Sugars are more and more replaced with low- or non-calorie sweeteners. This change in diet does not only affect our own caloric intake but also the nutrients provided to our gut microbiota. The relationship between humans and their gut microbiota is mutualistic and the microbiota has an influence on the development of a wide variety of diseases such as obesity, type II diabetes and cancer. As such, diet changes affect our health in several ways through the effect on the gut microbiota. Consequently, an interesting approach would be to focus on characterizing and modeling the effect of a diet change, from high to low caloric content, on the behavior of a complex population of gut microbiota. On the other hand, realistic experiments (i.e., experiments that could also be performed *in vivo*) can be designed to estimate parameters which cannot be easily fixed upfront. In this article a review is presented on the current state of the art of model system development for microbial and physicochemical processes in the human small intestine. The emphasis is on how gut microbiota dynamics are influenced by a diet shift. The authors propose a novel process systems engineering approach for investigating the influence of a low calories diet change on gut microbiota dynamics.

INTRODUCTION

The World Health Organization (WHO) acknowledges the importance of reducing sugar consumption to tackle problems as obesity. Therefore, sugars are more and more replaced with low- or non-calorie sweeteners. This change in diet does not only affect our own caloric intake but also the nutrients provided to our gut microbiota. The relationship between humans and their gut microbiota is mutualistic and the microbiota has an influence on the development of a wide variety of diseases such as obesity, type II diabetes and cancer. Gut microbiota influence host health by modulating host immunity and by having an impact on the host metabolic health (Singh 2017). The human gut microbiota community consists of at least 10^{13} residents and it can be viewed as a metabolic 'organ' exquisitely tuned to human physiology, that performs functions that have not been evolved, so far (Bäckhed et al. 2004). For instance, some of the microorganisms residing in the gut encode proteins involved in functions important for the host's health, such as enzymes required

for the hydrolysis of otherwise indigestible dietary compounds, and the synthesis of vitamins (D'Argenio 2015). For instance, it has been revealed that members of the human intestinal *Bacteroides* genus harbor very broad saccharolytic potential, with some strains able to target dozens of different complex glycans, that are not degraded or absorbed as they pass through the stomach and small intestine, reaching the colon intact (Salyers et al. 1977). The close relationship between diet, gut microbiome and health suggests that a change in diet can have several unknown effects on our health. As such, changes from a normal to a low- or non-caloric diet are expected to have a variety of unexpected health effects.

Interesting results are found in literature indicating specific side effects of novel sweeteners through the gut microbiota. Several non- and low-caloric sweeteners are supplemented with dietary resistant maltodextrin (DRM) as a bulking agent. DRM is a novel water soluble, nonviscous and tasteless fiber, produced by the treatment of cornstarch with acid, enzymes, and heat (Fastinger et al. 2008). Baer et al. (2013) found that the consumption of DRM caused a significant increase of gut microbiota such as *Ruminococcus*, *Eubacterium*, *Lachnospiraceae*, *Bacteroides*, *Holdemania* and *Faecalibacterium*. This implicates that the DRM gives these microorganisms a competitive advantage for growth in the gut. Suez et al. (2014) tested the effect of non-caloric artificial sweeteners on the glucose resistance and gut microbiota of mice. When transferring the gut microbiota from saccharin consuming mice to germ free mice, they found impaired glucose intolerance compared to mice receiving control (glucose) microbiota. This demonstrates the effect of the non-caloric artificial sweeteners on glucose tolerance through their effect on the gut microbiota. Bertelsen et al. (2001) studied the fermentability of D-tagatose by 174 different species of human enteric bacteria and dairy lactic acid bacteria. The results demonstrated that D-tagatose is fermented by bacteria related to the genera *Enterococcus* and *Lactobacillus*.

This review examines the development of model systems that account for the microbial and physicochemical processes in the human small intestine, in order to investigate the effect of a diet shift on the gut microbiota dynamics. In the next section the most important parts and processes in the human digestive system are presented. Subsequently, a brief review is given on model systems for human digestion. The fourth section describes a novel process systems engineering approach for modeling and

studying the human microbial gut. The last section summarizes the conclusions of this review.

HUMAN DIGESTIVE SYSTEM

In order to unravel the impact of the gut microbiome on the human health, it is important to understand their role in the human digestive system. The human digestive system consists of the gastrointestinal tract and other organs facilitating digestion (Figure 1). The full process of digestion exists of many stages. In summary, after breakdown of the meal and its transformation into bolus by means of the saliva, the processed meal enters the stomach (Jalabert-Malbos et al. 2007). In the stomach, apart from a further mechanical breakdown, digestive enzymes and gastric juices facilitate the further chemical breakdown of macronutrients into its building blocks. Few (aerobic and facultative anaerobic) microbial species are present in the stomach due to its high acidity. Most of the digestion of the food takes place in the small intestine (duodenum, the jejunum and the ileum), with its main function to absorb the products of digestion into the bloodstream. The duodenum receives the chyme expelled from the stomach, which is a multiphase slurry that constitutes of a mixture of gases, liquid and solid particles (Lew et al. 1971), together with pancreatic juices and bile from the gall bladder, breaking down protein and emulsifying fats. Moreover, a mucus-rich alkaline secretion is produced, neutralizing the pH. In the jejunum, the midsection of the small intestine, products of the digestion (i.e., sugars, amino acids and fatty acids) are absorbed into the bloodstream. In the ileum, vitamin B12, bile acids and remaining nutrients are absorbed. The amount of gut microbiota increases in the small intestine (Drasar and Hill 1974).

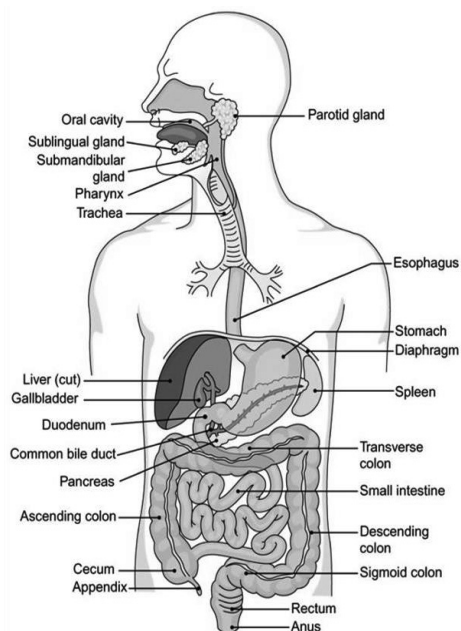


Figure 1. The human digestive system (Cohen and Wood 2000)

Finally, in the colon of the large intestine, water and some minerals are reabsorbed back into the blood. The waste products of digestion (feces) are defecated from the anus via the rectum. In the colon, the population of gut microbiota rapidly increases. The average cell counts in feces are around 10^{11} - 10^{12} CFU/g with an expected

number of species of more than 400, mainly anaerobic (O'Hara and Shanahan 2006).

MODEL SYSTEMS FOR HUMAN DIGESTION

Currently, changes in gut microbiota and/or diet are studied mainly in (bio)medical studies. Claessen et al. (2012) demonstrated that diet had an effect on gut microbiota composition. This was demonstrated by showing that elderly people in long-stay care had significantly less diverse gut microbiota than community dwellers. Bäckhed et al. (2004) found that transplanting gut microbiota from normal mice into germ-free mice increased their fat level (without an increase in food consumption). As such, research indicated that the composition of the gut microbiota may affect our caloric intake. Ley et al. (2006) found that a low caloric diet can alter the gut microbiome composition of obese people. A decrease in the amount of *Firmicutes* and an increase in the amount of *Bacteroidetes* was detected as the diet continued. These and several other studies demonstrate the links between diet, gut microbiota and health.

In addition, several (bio)medical studies are available discussing the effect of a diet on the human gut microbiota composition. The review of Graf et al. (2017) discussed the effects of (i) vegetarian diets, (ii) western diets, (iii) whole grain products, (iv) fruits and nuts, (v) vegetables and legumes, (vi) dietary fibers, (vii) fats, (viii) proteins and (ix) phytochemicals. The review of Scott et al. (2013) elaborated on the influence of (i) dietary carbohydrates, (ii) resistant starch and starch polysaccharides, (iii) prebiotics, (iv) proteins and (v) fats on the gut microbiota. However, the effects of, e.g., caloric intake or sugars were not discussed. As such, this very common and highly relevant diet change is generally overlooked in the currently available literature.

In addition, although (bio)medical studies generally allow the specific determination of the effect of diet changes on gut microbiota and health, they are limited with respect to the interpretation of the mechanisms behind these effects. This is a consequence of the fact that the studied system, i.e., the human gut system, is highly complex. Indeed, studying the multistage process of human digestion is a rather difficult procedure, costly and sometimes limited by ethical constraints. *In vivo* feeding methods, using animals or humans, usually provide the most accurate results, but they are time consuming and costly, which is why much effort has been devoted to the development of *in vitro* procedures (Boisen & Eggum 1991).

During the last decades, the development of model systems that describe and simulate the gastrointestinal tract has been an intriguing, yet challenging goal for several researchers. Some of their positive aspects are definitely their flexibility, their accuracy and their reproducibility (Guerra et al. 2012). In the human body, the largest microbial community is harbored in the gastrointestinal tract, where at least two orders of magnitude more genes than those found to our genome, derive from our gut microbiome (Egert et al. 2006; Qin et al. 2010). Models systems, such as the SHIME™ (Simulator of the Human Intestinal Microbial Ecosystem), originally developed at Ghent University (Molly et al. 1993) and brought on to the market by ProDigest (Gent, Belgium), the TIM Gastro-

Intestinal Model (Minekus et al. 1995) developed by TNO and the EnteroMix® colon simulator (Mäkivuokko et al. 2006) are among the most used *in vitro* methods that have been developed to investigate the effect of different products on the composition and activity of gut microbiota.

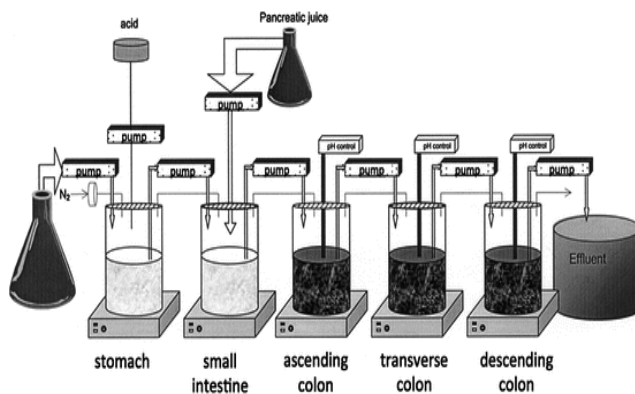


Figure 2. The SHIME™ model (Van de Wiele et al. 2015)

The SHIME™ is a multi-compartment dynamic simulator of the human gut that mimics the entire gastrointestinal tract by incorporating the stomach, the small intestine and the different colon regions (Figure 2). It consists of a succession of multi-compartment simulators or parts of the human gut, based on the awareness that fecal microbiota differ significantly from the *in vivo* colon microbiota in terms of community composition and metabolic activity (Van de Wiele et al. 2015). An improved version of the SHIME™ is the M-SHIME (mucosal-SHIME) (Van den Abbeele et al. 2011) which allows the study of the composition and functioning of the microbes that specifically reside on the mucosal surfaces of the gastrointestinal tract, by incorporating a mucosal environment containing mucin-covered microcosms. Furthermore, the presence and interaction with a mixed intestinal microbiota of the lumen is also allowed with the use of the M-SHIME (Van de Wiele et al. 2015).

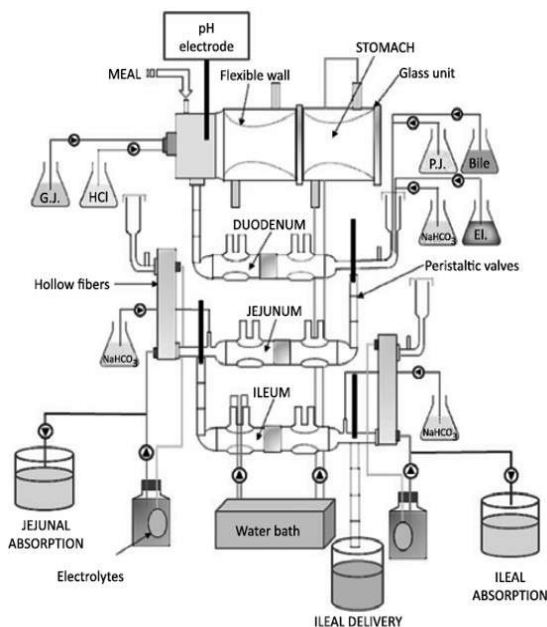


Figure 3. The TIM model (Guerra et al. 2012)

The TNO Gastro-Intestinal Model (TIM) is a multi-compartmental dynamic model designed to realistically simulate conditions in the lumen of the gastro-intestinal tract (Figure 3). It was developed in the early 1990s in response to industrial demand to study food products under more physiologically relevant conditions as compared to contemporary digestion models. The gastro-intestinal behavior of a wide variety of feed, food and pharmaceutical products is successfully studied with the use of TIM. Computer simulations of the conditions that take place *in vivo* during the transit and digestion of a meal in the lumen of the gut are the main tools on which the experiments in TIM are based on. These conditions include controlled parameters such as gastric and small intestinal transit, pH values, composition and flow rates of digestive fluids, and removal of water and metabolites. Specifically, TIM 1 mimics the upper digestive system by simulating the stomach and small intestine: duodenum, jejunum and ileum, while TIM 2 mimics the proximal colon of monogastric animals. Regarding TIM 1, fluid transportation from one vessel to another is executed by peristaltic valve pumps, while in a TIM 2 model system, a standardized microbial culture that derives from a fecal inoculum is initially inoculated to the model. The applications of the TIM 2 model correspond mostly to the investigation of the fermentation properties of dietary compounds such as fibers, pro- and prebiotics and antioxidants in the proximal part of the colon. During the past years, TIM has developed from an experimental lab setup, controlled by a PC of 8 MHz, into a platform of sequentially attached glass modules that are successfully used as model systems for an extensive range of studies, serving the feed, food and pharmaceutical industries. (Minekus 2015).

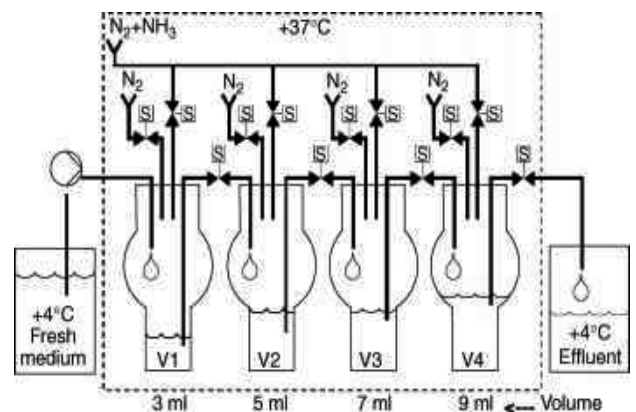


Figure 4. The EnteroMix® model (<https://www.guwsmedical.info>)

Finally, the EnteroMix® colon simulator is a semi-continuous device, with four parallel units, each comprised of four glass vessels connected consecutively and representing the ascending, transverse, descending and distal colon, respectively. An important advantage of this method is that it allows the implementation of four simultaneous simulations with the use of the same fecal inoculum, since the fluid consisting of media and the fecal slurry is mixed in the first vessel and 10 ml of the mixed culture is pumped into the next vessel in the chain. The vessels have small working volumes, enabling the

simulation of small concentrations of the tested substrate, and their pH levels are similar to the *in vivo* conditions. The EnteroMix® model has been used to study and evaluate the effects of fibers, probiotics and prebiotics and other bioactive compounds on immune health in the lower digestive tract (Mäkivuokko et al. 2005).

Despite the recent advances in the development of gastrointestinal model systems, there are still some limitations in modeling human gastrointestinal digestion, and some of the most significant ones are: (i) the absence of host response factors (Payne et al. 2012), (ii) the difficulty in modeling the complex mechanical forces and the complex gastric emptying pattern (Siegel et al. 1988; Kong and Singh 2008), (iii) the inadequacy in reproducing the conditions of healthy adults (Guerra et al. 2012), (iv) the weakness in simulating the overall digestive process (Anson et al. 2009; Fassler et al. 2006), and (v) the absence of microbial ecosystem (Booijink et al. 2012; Van den Bogert et al. 2011). The interest in assessing the interactions between the ingested compounds and the resident microbiota, though, is rapidly increasing and considering the great potential of the ‘-omics’ technologies, the need to include a gut microbiota model system in the gastrointestinal systems becomes a task of major importance (Guerra et al. 2012; Payne et al. 2012).

PROCESS SYSTEMS ENGINEERING APPROACH

“Process systems engineering (PSE) is concerned with the understanding and development of systematic procedures for the design and operation of chemical process systems, ranging from microsystems to industrial-scale continuous and batch processes” (Grossman and Westerberg 2000). Therefore, a novel approach would be to apply a PSE approach by simplifying the gut microbiota and their environment into a system that can be studied experimentally. The main advantages of such an approach are: (i) that this is a fully reproducible system, that it can minimize the variability of the system (ii) that it is not as expensive and time consuming as (bio)medical studies and (iii) that it does not raise ethical issues.

In this framework, a physicochemical model system can be developed, accounting for the physical transport processes and the chemical composition of a chyme that is representative for a ‘standard healthy meal’ that is being further digested in the small intestine. All the variables that characterize this model system, such as the pH, the temperature, the redox potential etc., can be controlled and kept constant. The term ‘standard healthy meal’ corresponds to a liquid mixture of the three basic nutrient compounds, i.e., carbohydrates, proteins and fats, in a ratio that is based on the nutritional guidelines for a healthy diet. Furthermore, a microbial system needs to be constructed, which will be representative for the gut microbiome present in the small intestine, by selecting key microbiota and by taking into account the diversity in the microbial community in the small intestine. The incorporation of the abovementioned model systems in a bioreactor setup will enable the investigation of the effect of a diet change to low caloric content on gut microbiota dynamics through a process systems engineering approach (Figure 5). According to previous studies, microbial communities present in the human gastrointestinal tract

have been analyzed and the results showed them to be extremely complex, with estimates of the number of different species present ranging from 500 to 1,000 (O’Hara and Shanahan 2006). Moreover, 16S rRNA gene-based analysis of the colonic microbiota has shown that as many as 80% of phylotypes defined by 16S rRNA gene sequences do not correspond to known cultured bacterial species, and more than half are entirely novel species (Wilson 2008). Consequently, the selection of the representative species for the development of the microbial model system can be a challenging task, since many parameters should be taken into account. The gut microbiota abundance, prevalence in the small intestinal segments and their role in human health and disease can constitute selection criteria for the representative microbial key groups. Nonetheless, the implementation of this simplified yet representative model system will enable mechanistic insight in the dynamics of gut microbiota and will allow the study of this system to an extent that has not been achieved up till now, since the development of a microbial model system that accounts for the small intestinal milieu is a completely novel aspect for the *in vitro* simulation of digestion.

Moreover, mathematical modeling techniques can be applied, leading to an improved understanding of the mechanisms behind the responses found in (bio)medical studies. As an initial modeling step, low complexity macroscopic models could be built to describe the growth and metabolism of the different gut microorganisms, covering only the main influencing substrates, biomass and metabolites mass balances.

The combination of experimental and modeling techniques can serve as a platform for reducing the number of *in vivo* and *in vitro* studies that is required to study related research questions.

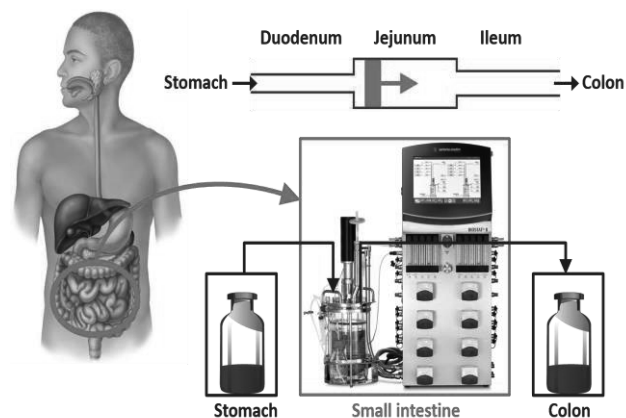


Figure 5. Schematic representation of the present approach

CONCLUSIONS

Nowadays, there is a tendency to a reduced sugar consumption by replacing sugars with low- or non-calorie sweeteners. As changes in diet also affect the nutrient intake of the human gut microbiota, the effect of a diet shift on human health and gut microbiome has gained interest. The current state-of-the-art in modeling the human digestive system lacks mechanistic knowledge on the gut microbiota, in order to achieve a good understanding and to describe/predict the effect of diet

shifts on the human gut microbiome. Moreover, a large number of test subjects are currently required to study the effects of a diet shift on gut microbiota. Such experiments are time consuming, expensive and also raise ethical questions. In this review the development of model systems accounting for the microbial and physicochemical processes in the human small intestine has been studied to overcome the current experimental limitations. Furthermore, a process systems engineering approach has been presented to investigate the effect of a diet shift on the human gut microbiota dynamics. With the presented approach, simplified, but still representative model systems are developed and studied to obtain mechanistic insight in the dynamics of gut microbiota. It is this simplification that allows the study of this system to extent that has not been achieved up till now. Furthermore, the development of predictive mathematical models will allow the description of the effect of a diet change on gut microbiota.

REFERENCES

- Anson, N.M. et al. 2009. Bioprocessing of wheat bran improves *in vitro* bioaccessibility and colonic metabolism of phenolic compounds. *Journal of Agricultural and Food Chemistry*, 57, 6148–6155.
- Bäckhed, F., Ding, H., Wang, T., Hooper, L.V., Koh, G.Y., Nagy, A., Semenkovich, C.F. and Gordon, J.I. 2004. The gut microbiota as an environmental factor that regulates fat storage. *PNAS*, 101 (44), 15718–15723.
- Baer, D.J., Stote, K.S., Henderson, T., Paul, D.R., Okuma, K., Tagami, H., Kanahori, S., Gordon, D.T., Rumpler, W.V., Ukhanova, M., Culpepper, T., Wang, X., and Mai, V. 2013. The Metabolizable Energy of Dietary Resistant Maltodextrin Is Variable and Alters Fecal Microbiota Composition in Adult Men. *The Journal of Nutrition*. 144(7), 1023-1029.
- Bertelsen, H., Andersen, H., Tvede, M. 2001. Fermentation of D-Tagatose by Human Intestinal Bacteria and Dairy Lactic Acid Bacteria. *Microbial Ecology in Health and Disease*, 13(2), 87-95.
- Boisen, S. and Eggum, B.O. (1991) Critical evaluation of *in vitro* methods for estimating digestibility in simple-stomach animals. *Nutrition Research Reviews*, 4, 141-162.
- Booijink, C.C. et al. 2010. High temporal and inter-individual variation detected in the human ileal microbiota. *Environmental Microbiology*, 12, 3213–3227.
- Claesson, M.J., Jeffery, I.B., Conde, S., Power, S.E., O'Connor, E.M., Cusack, S., Harris, H.M.B., Coakley, M., Lakshminarayanan, B., O'Sullivan, O., Fitzgerald, G.F., Deane, J., O'Connor, M., Harnedy, N., O'Connor, K., O'Mahony, D., Van Sinderen, D., Wallace, M., Brennan, L., Stanton, C., Marchesi, J.R., Fitzgerald, A.P., Shanahan, F., Hill, C., Ross, R.P., and O'Toole, P.W. 2012. *Nature*, 488, 178-185.
- Cohen, B. J. and Wood, D. L. 2000. Memmler's the human body in health and disease. 9th Edition. Philadelphia: Lippincot Williams and Wilkins.
- D'Argenio, V. and Salvatore, F. 2015. The role of the gut microbiome in the healthy adult status. *Clinica Chimica Acta* 451, 97–102.
- Drasar, B.S. and Hill, M.J. 1974. Human Intestinal Flora. Academic Press (London) Ltd
- Egert, M., De Graaf, A.A., Smidt, H., De Vos, W.M. and Venema, K. 2006. Beyond diversity: functional microbiomics of the human colon. *Trends in Microbiology* 14, 86–91.
- Fassler, C. et al. 2006. *In vitro* fermentability of differently digested resistant starch preparations. *Molecular Nutrition & Food Research*, 50, 1220–1228.
- Fastinger, N. D., Karr-Lilienthal, L.K., Spears, J.K., Swanson, K.S., Zinn, K.E., Nava, G.M., Ohkuma, K., Kanahori, S., Gordon, D.T., and Fahy, Jr, G.T. 2008. A novel resistant maltodextrin alters gastrointestinal tolerance factors, fecal characteristics, and fecal microbiota in healthy adult humans. *Journal of the American College of Nutrition*, 27(2), 356–366.
- Graf, D., Di Cagno, R., Fåk, F., Flint, H.J., Nyman, M., Saarela, M. and Watzl, B. 2015. Contribution of diet to the composition of the human gut microbiota. *Microbial Ecology in Health and Disease*. 26(1), 26164.
- Grossman, I.E. and Westerberg, A.W. 2000. Research Challenges in Process Systems Engineering. *AIChE Journal*, 46 (9), 1700-1703.
- Guerra, A., Etienne-Mesmin, L., Livrelli, V., Denis, S., Blanquet-Diot, S. and Alric, M. 2012. Relevance and challenges in modeling human gastric and small intestinal digestion. *Trends in Biotechnology*, 30 (11), 591-600.
- Jalabert-Malbosa, M.L., Mishellany-Dutoura, A., Wodaa, A., Peyron, M.A. 2007. Particle size distribution in the food bolus after mastication of natural foods. *Food Quality and Preference*.18 (5), 803-812.
- Kong, F. and Singh, R.P. 2008. Disintegration of solid foods in human stomach. *Journal of Food Science*, 73, 67–80.
- Lew, H.S, Fung, Y.C. and Lowenstein, C.B. 1971. Peristaltic carrying and mixing of chyme in the small intestine (an analysis of a mathematical model of peristalsis of the small intestine). *Journal of Biomechanics*,4, 297-315.
- Ley, R.E., Turnbaugh, P.J., Klein, S. and Gordon, G.J. 2006. Human gut microbes associated with obesity. *Nature*,444, 1022–1023.
- Mäkiyuokko, H.A., Saarinen, M.T., Ouwehand, A.C. and Rautonen, N.E. 2006. Effects of lactose on colon microbial community structure and function in a four-stage semi-continuous culture system. *Bioscience Biotechnology and Biochemistry*, 70, 2056–2063.
- Minekus M. (2015) The TNO Gastro-Intestinal Model (TIM). In: Verhoeckx K. et al. (eds) The Impact of Food Bioactives on Health. Springer, Cham
- Minekus, M., Marteau, P., Havenaar, R. and Huisintveld, J.H.J. 1995. A multicompartamental dynamic computer-controlled model simulating the stomach and small-intestine. *Atla- Alternatives to Laboratory Animals*, 23, 197–209.
- Molly, K., Woestyne, M.V. and Verstraete, W. 1993. Development of a 5-step multichamber reactor as a simulation of the human intestinal microbial ecosystem. *Applied Microbiology and Biotechnology*, 39, 254–258.
- O'Hara, A.M. and Shanahan, F. 2006. The gut flora as a forgotten organ. *Embo reports*, 7, 688-693.
- Payne, A.N. et al. 2012. Advances and perspectives in *in vitro* human gut fermentation modeling. *Trends in Biotechnology*, 30, 17–25.
- Qin, J.J., Li, R.Q., Raes, J., Arumugam, M., Burgdorf, K.S., Manichanh, C., et al. 2010. A human gut microbial gene catalogue established by metagenomic sequencing. *Nature*, 464, 59–65.
- Salyers, A.A., Vercellotti, J.R., West, S.E., and Wilkins, T.D. 1977. Fermentation of mucin and plant polysaccharides by strains of Bacteroides from the human colon. *Applied and Environmental Microbiology*, 33(2), 319-22.
- Siegel, J.A. et al. 1988. Biphasic nature of gastric emptying. *Gut*, 29,85–89.
- Singh, R.K., Chang, H.W., Yan, D., Lee, K.M., Ucmak, D., Wong, k., Abrouk, M., Farahnik, B., Nakamura, M., Zhu, T.H., Bhutani, T. and Liao, W. 2017 Influence of diet on the gut microbiome and implications for human health. *Journal of Translational Medicine*. 15 (73)
- Suez, J., Korem, T., Zeevi, D., Zilberman-Schapira, G., Thaiss, C.A., Maza, O., Israeli, D., Zmora, N., Gilad, S., Weinberger, A., Kuperman, Y., Harmelin, A., Kolodkin-Gal, I., Shapiro, H., Halpern, Z., Segal, E. and Elinav, E. 2014. Artificial sweeteners induce glucose intolerance by altering the gutmicrobiota. *Nature*, 514, 181-198
- Van de Wiele T., Van den Abbeele P., Ossieur W., Possemiers S., Marzorati M. 2015. The Simulator of the Human Intestinal Microbial Ecosystem (SHIME®). In: Verhoeckx K. et al. (eds) The Impact of Food Bioactives on Health. Springer, Cham
- Van den Abbeele, P., Grootaert, C., Marzorati, M., Possemiers, S., Verstraete, W., Gerard, P., et al. 2010. Microbial community development in a dynamic gut model is reproducible, colon region specific and selective for *Bacteroidetes* and *Clostridium* Cluster IX. *Applied and Environmental Microbiology*, 76, 5237–5246.
- Van den Bogert, B. et al. 2011. Microarray analysis and barcoded pyrosequencing provide consistent microbial profiles depending on the source of human intestinal samples. *Applied and Environmental Microbiology*, 77, 2071–2080.
- Wilson, M. 2008. *Bacteriology of Humans: an ecological perspective*. London, Blackwell Publishing Ltd. Chapter 9, 280.

WEB REFERENCES

<https://www.guwsmedical.info/intestinal-microbiota/info-nny.html>

SIMULTANEOUS DATA SCALING AND TRAINING OF DATA DRIVEN REGRESSION MODELS FOR QUALITY CONTROL OF BATCH PROCESSES

Carlos Andre Muñoz, Philippe Nimmegeers, Jan Van Impe
BioTeC+ & OPTEC, Department of Chemical Engineering, KU Leuven
CPMF2, Flemish Cluster Predictive Microbiology in Foods
Gebroeders De Smetstraat 1, B-9000 Gent, Belgium
email: jan.vanimpe@kuleuven.be

KEYWORDS

Simultaneous data scaling, soft sensors, quality prediction, partial least squares inversion

ABSTRACT

This contribution presents a novel approach for data scaling and training of Partial Least Squares (PLS) models, for use in applications of multivariate statistical process monitoring and control of batch processes. PLS models are intended for training soft sensors and for quality prediction. Additionally, aspects of model inversion are investigated to explore the use of the trained models for quality control. Batch processes are widely used in food industry as the preferred platform for the production of added value products due to the characteristics of the raw materials, i.e., natural elements with complex flow properties and compositions. This is also due to the nature of the most common transformations which involve bio-processes (e.g., fermentation) and the unit operations (e.g., drying) applied in the food industry. However, due to the complexity of their process' dynamics, quality control in the batch platform has traditionally been limited to the measurement of the end-product properties and the process control to the univariate monitoring in proven ranges. Data-driven models used in applications of fault identification, soft sensors, and quality prediction have been proven and exploited in the industry as they provide a solution for online monitoring and control. However, there are still many limitations on the existing data-driven methods that restrict their performance and application. In this contribution, it is demonstrated how the novel approach for simultaneous data scaling and model training results in significant improvements in the performance of the data-driven models. Advantages of the proposed algorithm regarding rank identification, the accuracy of the quality predictions and PLS model inversion are described.

INTRODUCTION

Latent variable methods, also known as (multi-)linear methods for decomposition and dimensionality reduc-

tion, are widely used to develop data-driven models in several fields (Fanaee-T and Gama 2016). In systems engineering, these models based on historical data have been used in applications of process monitoring, fault detection, and quality prediction. Moreover, data-driven approaches are an active research field in engineering in which developing methods that allow online data-driven process control is one of the current trends. Principal Component Analysis (PCA) and Partial Least Squares (PLS) are the most common latent variable methods exploited both in applications and research. PCA aims at projecting most of the variability present in a data set into a lower dimensionality space defined by the set of latent variables. This method is exploited in applications of process monitoring and fault detection. PLS is a regression modeling approach that allows to capture the maximum covariance between two data sets in the latent space, such that predictors for the output variables can be estimated (Luo et al. 2016). This approach is exploited to train soft sensors and for the prediction of end properties. One common limitation of these methods is that their performance depends on the scale of the data. As the data measured in production processes is obtained in different units and magnitudes (e.g., temperature, pressure) the variability present in the data is expressed in different scales. Thus, when applying latent variable methods the data scale operates as an inherent weighting factor that can result in models that preferentially capture the variability expressed at higher scales. Traditionally data pretreatment has been applied to normalize the scale along the batch data.

Autoscaling is the most widespread approach, it produces a data set that is mean centered and scaled to unit variance along all batches at each time point. However, it can be demonstrated how autoscaling reduces the results' accuracy and robustness. This because the original variance structure in the data is lost, noise is amplified under low signal-to-noise ratios and non-deterministic variability can be easily introduced due to a poor identification of the best rank approximation. Alternatives to this approach have been investigated, with variable scaling being one of these. This alternative maintains the physical interpretability of the trends and the original variance structure. However, this ap-

proach has failed to perform significantly better than autoscaling in applications of online monitoring (Westervhuis et al. 1999). In this regard, the present contribution develops a novel concept for data scaling that aims to solve the limitations mentioned before. A novel approach for simultaneous data scaling and model training is proposed. Through this approach, a more uniform distribution of error along the variables in the dataset is achieved. The main objective is to guarantee that the data-driven model is trained taking as much information as possible from the deterministic variability in each variable. Additionally, the novel approach results in a regularization of the rank approximation problem without diminishing the accuracy of the approximation as is the case when applying other regularization approaches.

In addition to studying the performance of the PLS models trained following the novel error scaling approach in direct applications (i.e., soft sensors and quality prediction), the problem of model inversion is investigated. This operation serves to estimate process conditions that lead to the desired output trend or quality condition, and it is relevant for process optimization and control applications. However, achieving this requires solving the challenges own of the model inversion, as being undermined for most of the cases (Ierapetritou et al. 2016). In this direction this contribution points out how the novel scaling approach helps on limiting the size of the null space, i.e., reducing significantly the number of possible solutions for a single problem and having more accurate solutions to the inversion problem. The first section of this contribution presents theoretical background on the traditional approach for constructing data-driven quality regression models based on PLS. The proposed novel simultaneous scaling and training approach is introduced in the second section. Then, an additional theoretical background is discussed regarding the model inversion problem. In the fourth section, the case study implemented to prove the concepts presented is described and the obtained results are discussed. Finally, the main conclusions of this work are presented and some comments on the direction for future work are presented.

TRAINING PLS MODELS

Traditionally, PLS models are applied to batch-wise unfolded data (Camacho et al. 2008). Following this approach the quality/output variables ($\mathbf{Y}_{[I \times L \times K]}$) are regressed to the process/input data ($\mathbf{X}_{[I \times J \times K]}$). This means that the tridimensional data (i.e., I batches \times J variables \times K time points) generated from historical measurements of multiple online sensors in batch processes are unfolded into matrices that kept the direction of the first dimension $Y_{(1),[I \times LK]}$ and $X_{(1),[I \times JK]}$ and decomposed into factor matrices that correlate them. For this, each matrix is expressed as the linear combi-

nation of two factor matrices. The loadings $P_{[JK \times R]}$ of the process data, and the loadings $Q_{[LK \times R]}$ of the quality variables, contain the R extracted features that define the directions of maximal variance between the two datasets. The scores $T_{[I \times R]}$ and $U_{[I \times R]}$ are matrices of R column vectors that represent the projection of the original data in the latent space (i.e., the latent variables or scores) for each batch. Therefore, this results in a regression model in which $X_{(1)}$ and its scores are good predictors of $Y_{(1)}$ (Wold et al. 2001). The transformation applied in PLS is depicted in equation (1). This equation shows the relation based on the weight matrix W that allows T to be a good predictor of the quality variables. The error matrices $E_{(1)}$, $F_{(1)}$, $H_{(1)}$ contain the residual variability that is not captured by the regression approximation.

$$\begin{aligned} X_{(1)} &= TP^T + E_{(1)} \\ Y_{(1)} &= UQ^T + H_{(1)} \\ Y_{(1)} &= TQ^T + F_{(1)} \\ T &= X_{(1)}W^* \\ W^* &= W(P^TW)^{-1} \end{aligned} \quad (1)$$

Data pretreatment is applied to the raw data, traditionally it consists of three operations, i.e., batch alignment, mean centering and scaling. In this contribution batch alignment is not investigated, and the indicator variable is considered the standard tool. The reader is referred to Wan et al. (2014) for details on this method and other alternatives. The main purpose of mean centering the data is to discard most of the non-linearities of the system which are common for all batches in the training dataset. Finally as mentioned before data rescaling is highly relevant due to the scale dependency in data-driven methods. Considering the general case as the one where the knowledge of the existing data correlations is limited, the standard idea for scaling is to try to make the variability present in each variable equal so that preferential learning is favored. For this purpose autoscaling has been widely applied. Scaling the data to unit variance, by dividing each time point for each variable by the standard deviation along all batches, transforms the data variability and gives it an equivalent magnitude at all points. However this method produces two unwanted results: firstly, the original trends of the variables and the original variance structure of the data are lost; and secondly, it can result in amplifying low amplitude variability, (generally being noise), while high amplitude variability, normally related with the systematic variability, is weakened. Alternatively, the variable scaling procedure aims to keep the original trends for each variable and therefore the original covariance. In this case, the scale given to each variable depends on the maximum and minimum values present in the data set for each variable.

Once the data has been pretreated it is used to train the PLS model that will be used for quality prediction

and/or the development of soft sensors. In this contribution, the PLS models were trained using the NIPALS method (Vandeginste et al. 1988) to determine iteratively the column vectors of the factor matrices. 'Leaving one out' cross validation is used to determine the approximation accuracy for the PLS models constructed. Wold's criterion (Gins et al. 2014) is used to establish the best rank approximation based on the mean square error (MSE) along with all variables and time points for the leave one out cross validation. In equation (2) the formulations for the MSE and Wold's criteria are presented for a PLS model using (R) latent variables for the rank approximation. Once the PLS model has been trained new process data is used as input to estimate either the end quality or the trend of the quality/output variables for which soft sensors have been trained. The Hotelling's T^2 statistics is used to define the region where the model is valid. T^2 is the distance to the center of the latent space of a new observation when it is projected to this reduced space. Equation (3) corresponds to the T^2 upper control limit. The upper control limit for T^2 follows the F -distribution with degrees of freedom equal to the number of validation batches (N_{val}) minus the rank of the approximation (R) (Gins et al. 2014). α and β in equations (2) and (3) determine the severity of the criteria.

$$MSE = F_1 F_1^T = (Y_1 - TQ^T)(Y_1 - TQ^T)^T$$

$$\frac{MSE(R+1)}{MSE(R)} > \alpha \quad (2)$$

$$T^2 = T \Sigma_T T^T$$

$$u_{T^2} = \frac{R(N_{val}^2 - 1)}{N_{val}(N_{val} - R)} F_{(R, N_{val} - R; \beta)} \quad (3)$$

SIMULTANEOUS DATA SCALING AND PLS MODEL TRAINING

The novel procedure proposed in this contribution for training PLS models consists of the simultaneous data scaling and training of the data-driven model resulting in a regularization approach. The aim is to overcome the limitations found when using a sequential approach based on autoscaling or variable scaling. Based on the concept of maximizing the availability of the information contained in the data and guaranteeing the best possible learning in all directions (i.e., from all variables of the system), an error based scaling is proposed. The principle of this approach is to find the appropriate scaling factors for each variable in the data set to guarantee that once the PLS model has been trained, the residual error has a unit variance distribution in the variables direction. An algorithmic procedure is proposed to achieve this objective. It is designed to iteratively converge to the appropriate scaling factors and model parameters simultaneously. At each iteration, the model is trained using data that has been scaled based on the error dis-

tribution of the previous iteration. The proposed algorithm is presented in Table 1. An initial model is trained starting from autoscaled data. In the next step the residual matrices for both the process data and quality variables are used to rescale the data. The variable-wise unfolded matrixes $X_{(2)}$ and $Y_{(2)}$ are scaled by the variance of each row in the residual tensors, unfolded in the same direction. A new model is trained with the scaled data and the loop is repeated until the system converges. The end point is achieved with the model that best approximates the scaled data and has a unit variance normal distributed residual for each variable in X and Y . Already at this point, the theoretical advantage of this approach with respect to the traditional scaling can be pointed out. Since the data is rescaled based on the variance of the residual for each variable, it is guaranteed that the data is rescaled to ensure that the model captures preferentially the deterministic variability present in each variable over taking stochastic behavior and therefore this improves choosing the right number of required latent variables to approximate the data.

Table 1: Algorithm simultaneous error scaling and PLS training.

1. Unfold \mathbf{X} and \mathbf{Y} into $X_{(1)}$ and $Y_{(1)}$
2. Mean center and normalize each column of both data sets
3. Compute the factor matrices W, T, P, Q for the PLS model of the autoscaled data. Equation (1)
4. While $\sigma_{E_{(2)}}^2 = \text{Variance}(E_{(2)}) \neq \vec{1}$ and $\sigma_{F_{(2)}}^2 = \text{Variance}(F_{(2)}) \neq \vec{1}$
 - 4.1 Establish new scaling parameters as $M = 1/\sigma_{E_{(2)}}^2$ and $N = 1/\sigma_{F_{(2)}}^2$
 - 4.2 Scale data via $X_{(2)}^T \odot M$ and $Y_{(2)}^T \odot N$
 - 4.3 Compute the factor matrices W, T, P, Q for the PLS model of the new scaled data.

End

PARTIAL LEAST SQUARES INVERSION

A PLS model, that has been trained based on historical data, can be used to estimate the required trajectories of the input variables to achieve certain desired conditions for the quality/output variables. To achieve this, the PLS model is inverted according to equation (4) where \mathbf{y}^{des} corresponds to the desired condition. The corresponding scores on the latent variable space \mathbf{t}^{des} are obtained inverting the model loadings for the output variables. The computed scores are then used to determine the input variables that would result on these projections (Bano et al. 2017). The major challenge of this approach lies in the correct interpretation and use of this solution as in most cases, especially in process monitoring and control, the obtained solution is not unique. In most of the cases the inversion of the PLS

model is an underdetermined problem due to the rank difference between the starting Y and resulting spaces X (Ierapetritou et al. 2016). The rank of the variability present in the output variables is in most of the cases lower than the rank of the input variability and therefore the estimated rank for the correlation between input and output variables is equal or higher than the rank of the input variables. Thus the solution obtained via direct inversion of the PLS model is only one of the possible infinite solutions contained in the *null space*. The *null space* of the problem corresponds to a sub space of the latent variable space along which the solution can move with no effect on the output variables (Ierapetritou et al. 2016).

$$\begin{aligned} \mathbf{t}^{des} &= (Q^T Q)^{-1} Q^T \mathbf{y}^{des} \\ \mathbf{x} &= \mathbf{t}^{des} P^T \end{aligned} \quad (4)$$

Therefore, the solution of the inversion problem requires a set of constraints that help to define a unique solution or at least limit the space where the possible solutions are located to a finite subspace in the null space. This implies formulating the inversion problem as an optimization problem. Ierapetritou et al. (2016) have presented a framework with 4 different scenarios to formulate the optimization problem and achieve the model inversion. In this contribution, an adapted formulation is used, considering the specific conditions of the case study and the aim of evaluating the performance of the two scaling approaches. This formulation is presented in equation (5) and considers that: (i) the desired output condition \mathbf{y}^{des} is completely defined, (ii) constraints are imposed over the model statistics to guarantee a solution located inside the region where the model is valid, and (iii) constraints are imposed on certain process variables ($\mathbf{x}_r(t)$) so a relevant unique solution is obtained. Bano et al. (2017) discussed how the constraints on the process conditions originate from process knowledge, physical feasibility or practical relevance. This optimization formulation is preferred in this contribution over others that use the process conditions directly as optimization variables. This implies a significant reduction in the number of decision variables for the optimization problem.

$$\begin{aligned} \min_{\mathbf{t}} \quad & \|\mathbf{y}^{des} - \mathbf{t}Q^T\|^2 \\ \text{subject to:} \quad & \\ & \mathbf{x} = \mathbf{t}P^T \\ & T^2 < u_{T^2}(\beta) \\ & \mathbf{x}_r(t) \leq \mathbf{c}_r \end{aligned} \quad (5)$$

RESULTS

Pensim case study

The Pensim model, from Birol et al. (2002) is used as a benchmark case study for the novel data-driven

monitoring framework. The Pensim model describes the fed-batch fermentation for the production of penicillin, which consists of a batch phase and a fed-batch phase which is started once the substrate concentration reaches a predefined lower bound. The 11 measured variables for process conditions X , i.e., during the reactor operation, are depicted in Table 2. The RAYMOND software package from Gins et al. (2014) is used for the implementation.

Two variables are considered as output/quality variables, i.e., the penicillin concentration and the biomass concentration. Soft sensors were trained for these variables considering that in normal operation they are not measured online and only the end condition is determined offline. A total of 50 batches were simulated for a period equivalent to 400 time points. 30 batches were used as training data set and 20 batches to test the trained PLS models using the classic approach and the novel simultaneous scaling/training approach. Three main aspects were evaluated: (i) the rank estimation and model training, (ii) offline quality prediction based on process parameters, and (iii) model inversion to estimate required process conditions to achieve a given desired output. Apart from the standard case (i.e. the benchmark conditions used in the Pensim reactor) two alternatives were evaluated. Firstly, a noise was introduced on one of the output variables (i.e., the biomass concentration), this to simulate lower accuracy for one of the quality measurements. Three values for signal to noise ratio were considered, 40dB, 20dB, and 10dB. Secondly, another data set was generated with extra variability. This was added to the feed rate by allowing variations on the set point during the fed-batch operation of the reactor. Normal distributed values between 0.05 and 0.07 L/h are given for the simulation of the 50 batches.

Table 2: Measured variables and initial conditions for Pensim case. study

Variable	Type of variable	Initial condition	Sensor noise (SN) / Disturbance (D)
Dissolved O_2 [mmol/L]	Dependent	1.16-1.18	$\sigma = 0.002$ (SN)
Volume [L]	Dependent	90-115	-
pH	Dependent	5	-
Temperature [K]	Dependent	298	-
Feed rate [L/h]	Independent	0 - 0.06	$\sigma = 0.005$ (D)
Aeration rate [L/h]	Independent	8	$\sigma = 0.3$ (D)
Agitation power [W]	Independent	30	$\sigma = 1$ (D)
Feed temp. [K]	Independent	296	$\sigma = 0.5$ (D)
Cooling water [L/h]	Dependent	-	-
Base flow [L/h]	Dependent	-	-
Acid flow [L/h]	Dependent	-	-

Rank estimation and training

The regression and dimensionality reduction via PLS requires estimating the rank to be used for the data decomposition. The selected rank is equivalent to the number of latent variables or in other words the dimensionality of the latent variable space. Traditionally, the relative increase of the prediction performance in terms of error reduction with each extra latent variable has been considered as a criterion. However, the challenge is to identify a well-defined limit for the rank where the approximation is good enough to reproduce the desired systematic variability while avoiding to capture non-systematic behavior that can lead to overfitting. Regularization techniques have been used to reduce the risk of overfitting. The extra regularization term is traditionally formulated to reduce the complexity of the model, e.g., by introducing non-structural sparsity to the factor matrices. In this way, an equilibrium between least squares minimum error of the approximation and the model complexity is obtained. As it was mentioned before the novel scaling approach can be seen as an alternative regularization method. Thus the first aspect investigated in the application of the Pensim case study is on the rank estimation. In Figs. 1 and 2 the training curves for PLS using standard autoscaled data (orange) and the proposed alternative using the simultaneous scaling-training approach (blue) are presented. In Fig. 1 the prediction error over the output variables is plotted together with the selected rank using Wold's criterion, marked with the dashed line. Figure 2 presents the MSE for the approximation of the process variables \mathbf{X} for each number of latent variables.

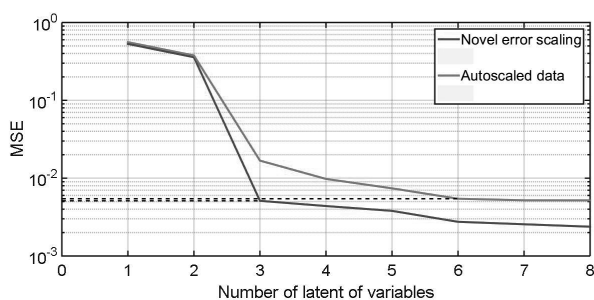


Figure 1: Training curves for PLS. Rank approximation vs. MSE on the output variables' prediction \mathbf{Y} .

As it can be seen in Fig. 1 the proposed novel approach produces a steeper reduction on the error at low ranks and reaches lower error at the point of no more significant improvement. Thus while for the autoscaled data Wold's criterion results in requiring 6 latent variables, the proposed scaling-training procedure only requires a rank 3 approximation. At the point of 3 latent variables, the error obtained via the proposed approach is almost one order of magnitude lower than that achieved with

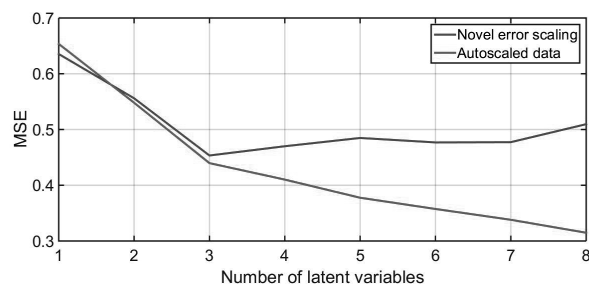


Figure 2: Training curves for PLS. Rank approximation vs. MSE on the process variables' approximation \mathbf{X} .

the same rank using the traditional approach. Finally it can be observed that both approaches offer similar performance for the first two latent variables. This means that those two latent variables capture the same variability independently of the method. In contrast the third latent variable is highly dependent on the scale of the data and in case of the novel scaling the model performance is significantly favored by the variability that is amplified in the data. Regarding the approximation of the process data it is observed that contrary to the results using autoscaled data, the training curve for the PLS model using the novel approach shows a change on the trend after 3 latent variables. This alerts on a possible overfitting if more latent variables are used. Fig. 3 shows the equivalent results when using the data set with extra variability on the feed rate. In this case it is not possible to determine the best rank approximation of the correlation using autoscaled data and up to 7 latent variables. In contrast for the model trained using the novel simultaneous scaling and training approach the identification is still as clear as it was for the standard case, only this time 4 latent variables are required. It is clear that the increase on the number of latent variables required, results from the extra deterministic variability introduced in the system. These results serve to validate the advantages of the proposed method on a dataset with different variability patterns. Moreover in this case the stronger presence of deterministic variability in the data makes clearer the advantages of the rank estimation via the novel scaling/training approach.

Quality prediction

The 20 batches simulated considering the same conditions used for the training data are used in this section to evaluate the performance of the trained PLS models. Quality prediction is performed using the direct form of the PLS model where the process data is fully defined and the model output are the conditions for the output/quality variables \mathbf{Y} . The PLS models trained in this contribution based on the in-silico Pensim case are intended to predict the complete trend of the output variables during the reactor operation, and in turn, the

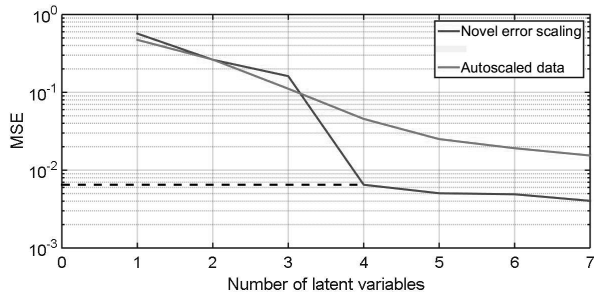


Figure 3: Training curves for PLS of the data with extra variability. Rank approximation vs. MSE on the prediction.

end quality is also obtained. Fig. 4 presents a fraction of the continuous trend predicted for the penicillin concentration and the approximate reactor volume during operation for a single batch. Fig. 5 presents the end point for the penicillin concentration, predicted for the 20 batches. These figures present the results for the standard Pensim case using two models trained with each scaling method. The numerical results obtained when implementing the models on the datasets with additional noise and extra variability of the feed rate are summarized in Table 3.

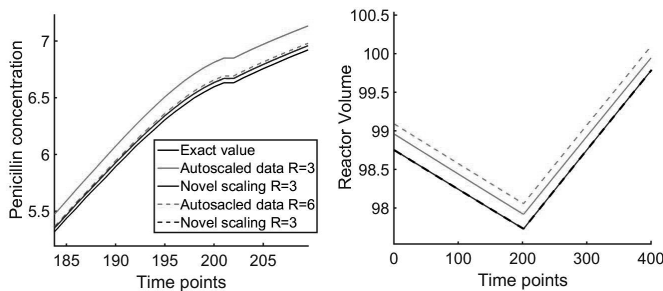


Figure 4: Prediction penicillin concentration and approximation reactor volume.

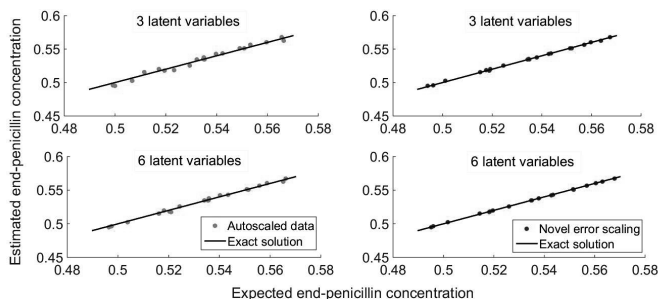


Figure 5: End point prediction penicillin concentration.

From these results, it is clear that a better prediction is obtained when using models trained with the proposed error based scaling. When looking at the single batch

Table 3: Prediction error for the two alternative scaling approaches on different data sets with R latent variables.

		a. Autoscaling, b. Novel error scaling		
		MSE Y	R^2 end point	MSE X
Stand. Pensim, R=3	a	0.53	0.978	8.73
	b	0.005	0.998	0.442
SNR 40, R=3	a	2.682	0.978	8.73
	b	0.114	0.998	0.442
SNR 20, R=3	a	10.407	0.979	8.73
	b	0.5149	0.998	0.442
SNR 10, R=3	a	11.632	0.981	8.73
	b	0.578	0.998	0.442
Extra variability	a	1.059	0.962	7.766
Feed rate, R=4	b	0.007	0.995	0.389

in Fig. 4, the worst prediction of the penicillin concentration is obtained when using the rank 3 PLS model of autoscaled data. Only with 6 latent variables, the traditional approach turns as accurate as the rank 3 approximation using the novel approach. Moreover, it is possible to obtain the exact solution only by a rank 6 model, based on the novel proposed scaling approach. In case of the approximated volume in the reactor, the rank 3 model is already sufficient to obtain the exact solution if the novel scaling approach is applied. Models based on autoscaled data present bias, it is even larger when the rank is increased. The numerical results confirm that these observations are applicable to the 20 batches. In general, the models based on the novel scaling approach perform more accurately in all cases. It is interesting to see that while the noise inclusion affects the performance of the two methods negatively, the addition of extra deterministic variability is accurately captured only by the model trained using the proposed scaling approach.

Regression process conditions

To compute the required process conditions that guarantee certain desired trend and/or the end point for the output variables, the PLS model has to be inverted. Therefore, in this case the known desired output becomes the input data and the required process conditions are the result obtained. As explained before the main limitation of using latent variable based models to compute regressors in many cases is the lack of uniqueness of the solution. Thus the first aspect evaluated in the present case study was the dimensionality of the null space for the different trained models. To do this the rank of the output data Y was estimated first. After applying singular value decomposition to the output data sets, it resulted that for all the cases, the standard Pensim, the case with added noise, and with added variability, the rank of the output variables equals 3. The same result was obtained for autoscaled data and data scaled using the novel approach. Therefore the dimen-

sionality of the null space corresponding to each case is the number of latent variables above 3 that each PLS model requires. Based on this, the features of different PLS models are presented in Table 4. Next, the direct inversion of the PLS models was applied to the given 20 batches that are not part of the training data but which are within NOC. The results obtained regarding the MSE of the estimated process condition (X) are as well depicted in Table 4.

Table 4: Regression error for the two alternative scaling approaches on different data sets a. Autoscaling, b.

Novel error scaling				
		Dimensions latent space	Dimensions null space	MSE X
Stand. Pensim	a	6	3	1.397
	b	3	-	0.443
SNR 40	a	6	3	0.446
	b	3	-	0.446
SNR 20	a	6	3	0.510
	b	3	-	0.455
SNR 10	a	6	3	0.531
	b	3	-	0.456
Extra variability	a	6	3	1.745
Feed rate	b	4	1	1.326

The direct inversion of the PLS models guarantees the minimum residual in the approximation of the desired output compare to the optimization approach, however the obtained solutions present limitations regarding other aspects. First, a relatively high error on the estimation of the required process conditions (MSE X), being lower for all cases where the novel scaling approach is applied. Secondly, for some batches, the direct inversion resulted in estimated scores that are located out of the validity region in the latent space. This problem was more frequently encountered in the case of the Pensim data with extra variability and when using the PLS model trained from autoscaled data. This can be related to the lower accuracy in the direct quality prediction obtained when using autoscaled data, and also due to the existence of a larger null space as result of the model inversion. To deal with this problem the inversion is tackled using the optimization form. First, the optimization problem with no constraints in X was applied. As it would be expected most of the solutions were the same obtained by the direct inversion, except for those that resulted in the violation of the validity region of the PLS model. Since the optimization formulation presented in equation (5) includes the constraint on the value T^2 , this method already overcomes that problem compared with the direct inversion.

The final volume in the reactor was chosen as the constraint to force the solution to comply with a unique solution within the null space. This approach allows to compare the trained models and see if the exact solution is feasible in the latent space, and if it implies accuracy

losses in the approximation of the other process conditions and/or the desired output conditions. To compare the solutions obtained following the three inversion approaches and evaluate the differences when using the novel scaling approach, the results for the Pensim case with extra variability in the feed rate are presented in Fig. 6 and Table 5. This figure shows the exact solution for the reactor volume and feed rate for one of the 20 batches evaluated in the inversion problem. In this figure, the solutions obtained through different approaches are as well depicted. In Table 5 the numerical results for the 20 batches are depicted, comparing the different approaches. The parameters evaluated are the accuracy of the solution evaluated as MSE of the trends of process conditions, and the MSE over the independent variables of the process (i.e. initial conditions and feed rate). Moreover, the number of violations of the validity region of the model in the latent space and the optimal value achieved for the loss function of the optimization problem are presented as well.

Table 5: Results model inversion for the estimation of required process conditions in the Pensim case with extra variability of the feed rate a. Autoscaling, b. Novel error scaling

		MSE X	MSE Ind. variables	Number of violations T^2	MSE Y
Direct inversion	a	1.744	0.696	10	0.0009
	b	1.323	0.810	5	0.0014
Unconstrained optimization	a	1.199	0.506	0	0.0015
	b	0.957	0.509	0	0.0017
constrained optimization	a	0.636	0.0018	0	0.0021
	b	0.388	0.0014	0	0.0073

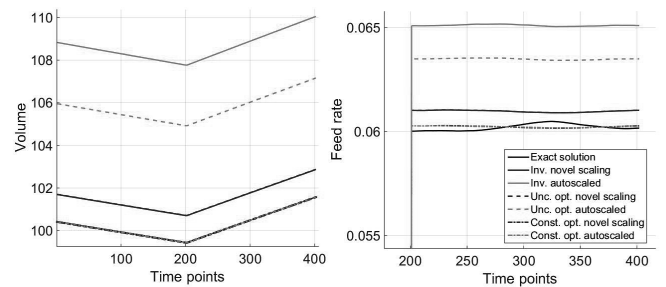


Figure 6: Estimation of the trend of the reactor volume and the step for the feed rate.

In Fig. 6 the solution obtained for the volume and the feed rate are presented. The results have shown how in every case the exact solution is feasible and is only obtained when the model inversion is applied through constrained optimization. In this case, both methods perform equally well. This proves that novel scaling approach does not affect the model inversion negatively and it offers results as good as those obtained with autoscaled data when an appropriate constraint is imposed

to obtain a unique solution. Different to this, when considering the direct model inversion or the unconstrained optimization problem, the solutions obtained through the novel approach seem to be more accurate than the others. These observations are supported by the results in Table 6. On the one hand, the MSE over process conditions X , was in all cases lower when using the novel scaling approach. On the other hand, the MSE over independent variables was the same in every case between the two approaches, except in the case of the direct model inversion. However, in that case, the inversion of the model based on autoscaled data resulted in a significantly larger amount of non-valid solutions due to the violation of the upper limit for T^2 .

CONCLUSIONS

A novel algorithm was presented to perform simultaneous data scaling and training of PLS regression models. The objective of this novel approach is to guarantee a better distribution of the approximation error along all variables present on the training data set, considering both process conditions and quality or output variables. Through the implementation of an industrially relevant case study and considering four different conditions, i.e. the standard case, 3 different noise levels and a case with extra variability, the proposed approach was validated and compared with the traditional approach using autoscaled data. It was demonstrated that due to the more appropriate scale given to the data when applying the proposed approach, the PLS models are trained taking the deterministic variability of the data preferentially. In turn, the best rank approximation for the correlation is identified clearer with significantly lower prediction errors during the cross validation procedure and resulting in less latent variables required for the model. The models trained using the novel error scaling approach perform more accurately for applications of quality prediction and soft sensors. In case of model inversion, it was discussed how the lower rank of the models results in the reduction of the dimensionality of the null space and therefore those models trained under this approach produce better estimations of the required process conditions when specific constraints for their trajectories cannot be imposed to guarantee a unique solution. In the other cases, these models performed equivalently to models trained based on autoscaled data. Future work in this direction will be on extending the proposed approach to online applications for quality prediction and process control of batch processes.

ACKNOWLEDGEMENTS

This work was supported by the Belgian Science Policy Office (DYSCO) [IAP VII/19] and KU Leuven PFV/10/002 Center-of-Excellence Optimization in Engineering (OPTEC). CAM holds a VLAIO-Baekeland

[HBC.2017.0239] grant.

REFERENCES

- Bano G.; Facco P.; Meneghetti N.; Bezzo F.; and Barolo M., 2017. *Uncertainty back-propagation in PLS model inversion for design space determination in pharmaceutical product development*. *Computers & Chemical Engineering*, 101, 110–124.
- Birol G.; Undey C.; and Cinar A., 2002. *A modular simulation package for fed-batch fermentation: penicillin production*. *Computers and Chemical Engineering*, 26, 1553–1565.
- Camacho J.; Pico J.; and Ferrer A., 2008. *Bilinear modelling of batch processes. Part II: A comparison of PLS soft-sensors*. *Journal of Chemometrics*, 22, no. 10, 533–547.
- Fanaee-T H. and Gama J., 2016. *Tensor-based anomaly detection: An interdisciplinary survey*. *Knowledge-Based Systems*, 98, 130–147.
- Gins G.; Vanlaer J.; Van den Kerkhof P.; and Van Impe J., 2014. *The RAYMOND simulation package Generating RAYpresentative MONitoring Data to design advanced process monitoring and control algorithms*. *Computers and chemical engineering*, 69, 108–118.
- Ierapetritou M.; Ramachandran R.; Sacher S.; and Kinnast J.G., 2016. *Process Simulation and Data Modeling in Solid Oral Drug Development and Manufacture*. Springer.
- Luo L.; Bao S.; Mao J.; and Tang D., 2016. *Quality prediction and quality-relevant monitoring with multilinear PLS for batch processes*. *Chemometrics and Intelligent Laboratory Systems*, 150, 9–22.
- Vandeginste B.G.M.; Sielhorst C.; and Gerritsen M., 1988. *NIPALS algorithm for the calculation of the principal components of a matrix*. *Trends in Analytical Chemistry*, 7, no. 8, 286–287.
- Wan J.; Marjanovic O.; and Lennox B., 2014. *Uneven batch data alignment with application to the control of batch end-product quality*. *ISA Transactions*, 53, no. 2, 584–590.
- Westerhuis J.; Kourti T.; and Macgregor J., 1999. *Comparing alternative approaches for multivariate statistical analysis of batch process data*. *Journal of Chemometrics*, 13, 397–413.
- Wold S.; Sjostrom M.; and Eriksson L., 2001. *PLS-regression: A basic tool of chemometrics*. *Chemometrics and Intelligent Laboratory Systems*, 58, no. 2, 109–130.

SMART SENSORS TO ASSESS AND TO ANTICIPATE FISH QUALITY EVOLUTION

Carlos Vilas, Míriam R. García, Eva Balsa-Canto, Antonio A. Alonso
Bioprocess Engineering Group. IIM-CSIC. c/ Eduardo Cabello,6. 36208 Vigo, Spain
email: antonio@iim.csic.es

KEYWORDS

Smart sensors, Quality assessment, Sensing technologies, Dynamic models, Physical/biochemical mechanisms, System's theory

ABSTRACT

Consumer's demands are currently the main drivers encouraging food industries to produce healthier food products that being at the highest possible quality standards, understood either as real or perceived, would not compromise safety standards. This necessarily leads to minimizing over-processing, as it might result into unacceptable quality losses, that in turn call for methods to ensure strict safety constraints satisfaction near its very low limits. Companies have oriented production strategies not only to meet the need for convenience but to offer fresher and healthier foods, compliant with consumer awareness of the links between nutrition and health. Food quality/safety assessment is central to this problematic.

In this note we will elaborate on current needs and trends in food sensing oriented to the on-line/in-line assessment of food quality and safety. We will identify the main obstacles and propose potential solutions which will happen to be found in the field of process system's theory.

INTRODUCTION

Nowadays, driven by consumers demands, food industries are encouraged to produce food products of the highest possible quality without compromising safety standars (Miri et al. 2008). In other words, consumers create incentives for companies to invest in means to preserve or to increase food quality. A quality label on a product increases its added-value what translates in larger sale turnovers and therefore benefits.

Real-time quality assessment and shelf-life forecast using non-invasive techniques is, therefore, an issue of paramount importance which can be approached from a system's theory perspective as illustrated in Figure 1. The main idea is to combine on-line measurements of relevant variables with dynamic models describing biological and biochemical mechanisms to derive shelf-life predictors capable of forecasting the evolution of

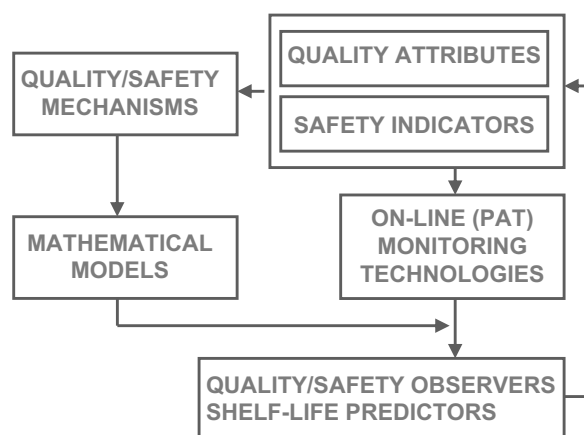


Figure 1: Block diagram illustrating the paradigm for real-time quality assessment

fish quality during processing, storage and distribution/transportation conditions.

A considerable research effort has been focused on both the identification of quality attributes and their correlation with available measurements (Harikedua et al. 2012). Quality is essentially a subjective concept which identifies the wishes and preferences of consumer's segments. However, typical quality attributes can be classified in nutritional (nutrient content) and organoleptic (flavor, color, odor, etc) attributes.

Any quality attribute is inferred by sets of measurements, which will be referred as *quality indicators*, directly or indirectly targeting particular factors. For example, color can be a quality indicator which, for a given food matrix, explains the result of a certain combination of pigments that have been produced under the action of some biochemical transformations.

Food quality attributes will be conditioned by the food matrix microstructure as well as by the magnitude of a number of stress variables that are influenced by transportation, storage or process conditions (Martins et al. 2008). For instance freshness deteriorates faster at higher temperatures due to the higher rates of degradation of nutrients, protein denaturalization or microbial enzymatic effects which also induce texture changes and may promote the appearance of odors and bad tastes.

Among the stress variables, of particular importance are temperature, water activity, pH, oxidant/antioxidant capacity ionic strength or light (frequency/intensity).

Quality attributes are employed to determine the shelf-life dating of a given food product, either to specify the last date when the product must be sold (“sell by date”); the “high-quality” period; or the date when the product must be removed from the store (Martins et al. 2008).

Mechanisms are the inter-relations between stress variables (temperature, pressure, water activity, pH, etc) and biological, chemical and bio-chemical factors related to quality and safety indicators. In the last instance mechanisms describe the underlying biochemistry and microbiology-physiology that determine the causal chains of implications.

In this context, models are quantitative descriptions of the mechanisms relating stress variables and quality factors. Such descriptions are expressed in terms of mathematical equations which can be derived from first principles when the knowledge of the system is good enough using correlation analysis when the mechanisms are not perfectly understood or a combination of both.

Sensing technologies consist of given instrumental/analytical devices to target quality indicators or stress variables related to such indicators plus correlations (chemometric models) to relate to quality attributes. In recent years a wide range of sensing technologies to assess the quality (meaning quality attributes), off-line and at real-time, have emerged (Mello and Kubota 2002, Su et al. 2011, Sliwinska et al. 2014, Oliveira and Pereira 2016).

From another point of view, models may also help manufacturers to design alternative formulations in food products in order to inhibit microbial growth, what surely will contribute not just to food safety but food quality as well. Safety and quality bounds may be used as state constraints in the formulation of optimal control or optimal design problems. Such formulation will provide the adequate systematic framework to achieve the goals of the process.

MECHANISMS AND MODELS

General aspects of what we refer to as mechanisms include the inter-relation between biological, chemical and bio-chemical factors (states) with the stress variables (inputs). Both define the input-state space. In the last instance mechanisms describe the underlying biochemistry and microbiology-physiology that determine causal set of implications. Parameters are present in the form of reaction constants, specific reaction rates or (mass and energy) transport coefficients.

Variability and uncertainty must be interpreted as the consequence of lack of knowledge on the food matrix, its variability (and complex structure), but also due to the multi-scale phenomena that takes place what demands to resort to mesoscopic or macroscopic descriptions.

Quantitative descriptions of the mechanisms are what we will refer to as *mathematical models* and will be critically reviewed here. Emphasis will be placed on the underlying multi-scale nature of (mass and energy) transport phenomena, chemical/biochemical kinetics, and microbial dynamics.

Formal description of quality and safety dynamics

Formally the system can be described by a set of differential operators describing the evolution of the states of the system (x):

$$\dot{x} = \mathcal{F}(x, u, \theta, \xi, t). \quad (1)$$

ξ and t represent the spatial coordinates and time, respectively. u stands for the stress variables whereas θ is the vector of parameters associated to the mathematical model which may include kinetic reaction constants, thermodynamic parameters, etc. A major challenge in food modeling is the estimation of parameters θ from available measurements. In this context, we have been working on a protocol for model calibration which includes identifiability analysis, parameter estimation and optimal experimental design (Vilas et al. 2017b).

Quality and safety are characterized by the values taken by the indicators (z) that are related to the system as:

$$z = \mathcal{Z}(x, u, \theta, \xi, t) \quad (2)$$

Finally the system is accessed via a set of measurements (y) also related to the states by functions of the form:

$$y = \mathcal{Y}(x, u, \theta, \xi, t) \quad (3)$$

Some measurements may coincide with quality/safety variables provided that a sensing technique (measurement device) is available to quantify such variable. However, in general, one would have only indirect access to the current quality/safety variable by means of measurements y which are employed to reconstruct the state x and from there the quality/safety indicators z . It is not always clear in many methods proposed in the literature how such reconstruction is performed or whether it is even possible to established such relation in a one-to-one (univocal) way. Such possibility is related to the concept of observability.

Evolution of physico-chemical variables

Concerning shelf-life assessment based on quality indicators for fish, some measurable physico-chemical properties such as total volatile basic-nitrogen (TVB-N), electrical conductivity (EC) or total aerobic count (TAC) can be employed as freshness indicators. For instance, EC values of intact muscles are very low, as the muscle tissues get decomposed, fluids flow out increasing the EC value (Yao et al. 2011).

Some adenosine triphosphate (ATP) degradation compounds enhance fish quality as they are related to the meaty and sweet flavor -for instance, inosine 5'-monophosphate (IMP)- whereas other such as hypoxanthine (Hx) are responsible for unpleasant bitterness (Surette et al. 1988, Li et al. 2015). In this regard, the K -value, related to the degree of degradation of ATP, became one of the most commonly employed indicators for fish freshness (Saito et al. 1959, Hong et al. 2017). The work by Lakshmanam and Gopakumar (1999) showed that the K -value correlates well with freshness in a large number of fish and shellfish species. Since the conversion of ATP to IMP is very fast, Karube et al. (1984) proposed another freshness indicator, the K_T -value, that only takes into account concentration of IMP, inosine and Hx. The work by Howgate (2005; 2006) investigated the degradation of IMP by assuming first order consecutive reactions. However, the degradation scheme may change from one species to another so the problem must be carefully addressed (Howgate 2006, Vilas et al. 2017a).

Traditionally, the assessment of physico-chemical properties of fish related to its quality during storage was based on statistical methods like the partial least-squares regression (PLS-R) -see (Harikedua et al. 2012)-. However during recent years, first principle based models for the description of the evolution of such physico-chemical properties have been proposed. First order models where the time constant is computed through a modified logistic Arrhenius equation are the most employed (Koutsoumanis and Nychas 2000, Tsironi et al. 2009, Yao et al. 2011). Such models can be used to describe the different indicators (K -value, EC, TVB, etc) by adjusting the parameters from experimental data.

Evolution of microbial populations

Microorganisms may be responsible for both quality and safety issues. Most of the models available to describe microorganism population growth are of deterministic nature and consider the temporal evolution of bacteria present in the foodstuff. Mechanistic models as the ones proposed by Baranyi and co-workers (Baranyi and Roberts 1994, Baranyi et al. 2009) over the last two decades are among the most popular to describe bacteria evolution at food storage conditions (low temperatures) as opposed to kinetic models used to describe thermal death during processing (in for example aseptic processing, pasteurization or sterilization). Based on these works García et al. (2015; 2017) predicted the evolution of quality for hake and cod, respectively. For a discussion on the effect of temperature see Halder et al. (2010). A critical analysis of the range of validity and their limits was discussed in McMeekin et al. (2006). The growth model suggested by Baranyi and Roberts (1994) uses a simple first order kinetic relation to describe the evolution of the cell population size (number

of cells or number of cells per volume). The growth rate in this work and others (Baranyi 1998, Kutalik et al. 2005, Baranyi et al. 2009) is multiplied by a logistic type function the authors refer to as the adjustment function. The role of such function is to describe the initial lag phase undergone by a homogeneous bacteria population inoculated into a growth-supporting environment. However lag parameters of bacterial population do not carry much information about the lag time of the individual cells what makes difficult to confront that hypothesis on practical experimental conditions.

Secondary growth models are usually complemented with a number of algebraic extra-relations (in many cases empirical correlations) to describe the effect of operation conditions, such as temperature, or the characteristics of the food matrix (chemical composition, water activity, pH, etc), on the growth (or death) rate constants.

A plethora of possible input-output type descriptions are available in the literature despite many criticisms, partly justified but partly not -see McMeekin et al. (2010)-. One such type of input-output description, widely employed to set up pasteurization or sterilization conditions on temperature ranges near 100 °C and even well above, is that relating temperature with inactivation rate constant through simple exponential (Arrhenius-type), decimal (TDT) relationships (Halder et al. 2010) or the Weibull model (Geeraerd et al. 2005). Of particular interest are the so-called growth/no growth models which relate environmental conditions (temperature, water activity, pH, etc) as inputs to a growth probability function as the output, indicating whether cells are likely to grow or not (Gysemans et al. 2007, Valero et al. 2007).

ON-LINE MONITORING TECHNOLOGIES

The aim of this section is to provide the reader with a general idea of the different types of sensors available for food quality assessment. Due to the huge amount of available technologies, performing an exhaustive review would require a complete paper so the reader is referred to the literature provided in this section and references therein for detailed descriptions.

On-line monitoring technologies can be roughly classified into (i) artificial senses; (ii) biosensors and chemical methods; (iii) physical methods.

Artificial senses are electronic devices that intend to mimic human senses (Sliwinska et al. 2014). They can be, in turn, classified into: (i) electronic noses; (ii) electronic tongues and (iii) computer vision devices. Electronic noses (Ghasemi-Varnamkhasti et al. 2009, Wilson 2013) and tongues (Escuder-Gilabert and Peris 2010) are basically a combination of a chemosensor, electronic devices and computer software. The sample is placed in a compartment, in which the amount of volatile compounds may increase using a thermostat, and an inert

gas is pumped into this compartment. The inert gas, together with the volatile compounds, are transported to the array of sensors changing their electric properties and generating a signal which is read using computer software. Electronic noses and tongues have been used for wide range of applications including, monitoring the fermentation in milk, wine or cheese; food freshness/quality assessment during storage or product authentication among other (Sliwinska et al. 2014). Systems of computer vision combine acquisition devices with processing and image analysis software (Timmermans 1998, Brosnan and Sun 2004). They are fast, non-invasive, may detect imperfections and can be used during food production, for instance for product discrimination or sorting.

Biosensor and chemosensor technologies (Mello and Kubota 2002, Su et al. 2011) integrate a recognition compound of biological nature with a transducer-receptor device. The interaction between the sample and the biological element changes its physico-chemical properties and such changes are detected by the transducer-receptor. They are sensitive, selective, do not require a sample pre-treatment and are relatively cheap and portable (Oliveira and Pereira 2016, Dragone et al. 2017). They offer the possibility of measuring microorganisms in real-time and they have also been used for chemical contaminants in food or the glucose concentration in the blood. The main advantages of chemosensors are their high sensitivity to specific chemical compounds, quick reactions, high reproducibility, robustness or easy calibration. Particular cases of chemosensors include Time-Temperature integrators (TTIs) able to recover the cumulative Time-Temperature history of a given process (Arias-Méndez et al. 2014).

A wide range of different technologies can be included in the physical methods. These range from texture analysis using acoustical devices (Chen and Opara 2013) to electrical techniques for detecting, for instance moisture or electrical conductivity, or optical techniques such as X-Ray or nuclear magnetic resonance (Xiaobo et al. 2016). Most of these methods are non-invasive and may detect food quality issues related to either external indicators, such as color or surface defects, or internal indicators such as firmness of internal defects (Chandrapala et al. 2012). An updated review of these methods, including future perspectives is provided in Xiaobo et al. (2016). As important as the sensors themselves are the techniques to analyze their signals. Data analysis demands multivariate pattern analysis with all the available statistical tools (PLS, ANOVA, MLR); Principal Component Analysis; Hierarchical Cluster Analysis; Support Vector Machines; Artificial Neural Networks, among others. The work by Sliwinska et al. (2014) provide us with a comprehensive review of the different methodologies used to analyze data from artificial senses devices although many of them are also used with another type of sensors.

ON-LINE ASSESSMENT AND PREDICTION OF FRESHNESS IN FISH

In this section we present two models used to forecast fish quality evolution. The first one, related to the K_I -value, is recommended for early storage whereas the second one should be used when bacteria spoilage is becoming to be noticed.

Freshness assessment at early storage stages

As mentioned above, K_I -value is a quality indicator that correlates well with freshness in a large number of fish species. The K_I -value is defined as:

$$K_I(\%) = \frac{[\text{Ino}] + [\text{Hx}]}{[\text{IMP}] + [\text{Ino}] + [\text{Hx}]} 100$$

Values below 20 % indicate fish of prime quality whereas values above 40 % mean that the fish is spoiled (Lakshmanam and Gopakumar 1999). In order to derive a model to forecast fish freshness at early storage stages, Vilas et al. (2017a) proposed a scheme, based on the work of Howgate (2005), describing the enzymatic degradation of IMP in sterile conditions. On the other hand, Vilas et al. (2018) studied the catalytic effect of bacteria on such degradation. The model, which considers first order reactions, is of the form:

$$\frac{d[\text{IMP}]}{dt} = -(r_1 + r_3 + r_4 + r_{1,bac}) - D[\text{IMP}] \quad (4)$$

$$\frac{d[\text{Ino}]}{dt} = r_1 + r_{1,bac} - (r_2 + r_{2,bac}) + D[\text{Ino}] \quad (5)$$

$$\frac{d[\text{Hx}]}{dt} = r_4 + r_2 + r_{2,bac} - D[\text{Hx}] \quad (6)$$

where $r_1 = k_1[\text{IMP}]$, $r_2 = k_2[\text{Ino}]$, $r_3 = k_3[\text{IMP}]$ and $r_4 = k_4[\text{IMP}]$. Coefficients k_1 , k_2 , k_3 and k_4 describe the effect of temperature using the Arrhenius equation:

$$k_i = A_i \exp\left(-\frac{E_{a,i}}{RT}\right); \quad \text{for } i = 1, 2, 3, 4 \quad (7)$$

Two types of bacteria were taken into account: *Pseudomonas spp* (Ps) and *Shewanella* (Sh). The effect of bacteria on the reaction rates is described using first order reactions of the form: $r_{1,bac} = k_{1,bac}(\text{Ps} + \text{Sh})[\text{IMP}]$ and $r_{2,bac} = k_{2,bac}(\text{Ps} + \text{Sh})[\text{Ino}]$. Bacterial growth is modeled using the standard logistic model where temperature dependence is described using the standard square-root model (see García et al. (2015) for details):

$$\frac{dx}{dt} = \log(10)\mu_x x \left(1 - \frac{x}{x^*}\right); \quad x = \{\text{Ps}, \text{Sh}\} \quad (8)$$

As shown in Figure 2 the model is able to predict the experimental evolution of the K_I -value.

Initial conditions for nucleotide and bacteria concentration are required to solve the model. Such conditions should be retrieved from experimental measurements. To that purpose sensors, as the ones mentioned in the previous section, are required.

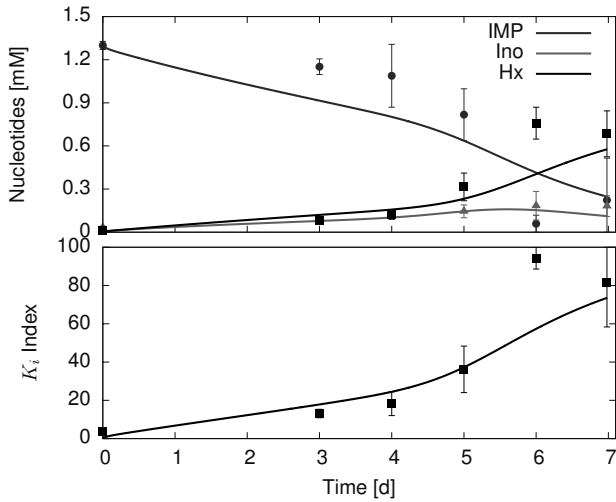


Figure 2: Top figure: evolution of nucleotides. Bottom figure: evolution of the K_i -value. Continuous lines represent model predictions whereas marks refer to experimental measurements.

Quality assessment during mid-term storage periods

Bacterial concentration is another index that correlates with fish quality. During the first days, at usual storage and transportation conditions, bacteria concentration is low. However, at mid-term storage stages bacteria is responsible for fish spoilage. The model described in García et al. (2015), see Eqn (8), was used for to model bacteria growth and its relation to fish quality. A validation experiment was used to evaluate the predictive capabilities of the model (see Figure 3). The blue bands in the figure represent model variability caused from measurement uncertainty. After optimal experimental design variability was reduced to admissible values.

Correlation between bacteria concentration and quality indicators such as the *Quality Sensory Method* (QSM) and the *Quality Index Method* (QIM) was explored (García et al. 2015). The relation between the QIM, ranging between 0-19 (Baixas-Nogueras et al. 2003), and bacterial concentration is given, for hake, by:

$$QIM = \text{nint}(10^{lQ}) - 1 \quad \text{where} \quad lQ = \alpha Ps + \beta Sh \quad (9)$$

where “nint” is the function that computes the nearest integer value. The QSM grades the quality of food (using different features of the skin, eyes, gills, peritoneum and flesh) in four categories: E (Extra-quality); A-quality; B-quality and NA (Not admitted). In García et al. (2015), the authors performed several experiments in which, a panel of experts evaluated the QIM and the QSM. From these data, the equivalences presented in Figure 4 were suggested. For example, as shown in the

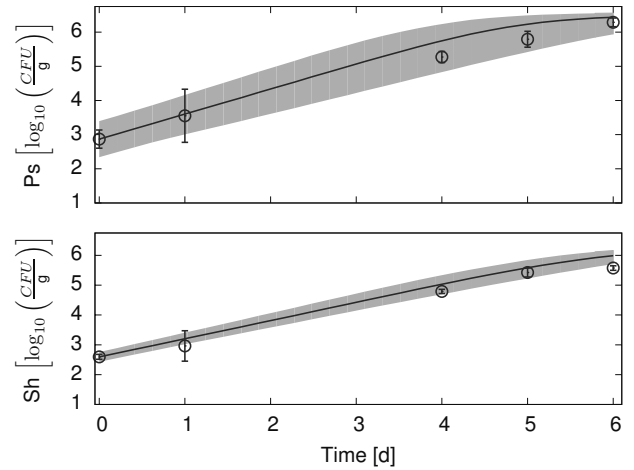


Figure 3: Comparison between model prediction for bacterial growth (continuous lines) and experimental data (marks) in a validation experiment. Blue regions represent model uncertainty.

figure, the E category corresponds to values of QIM between 0 and 3. Figure 4 also represents the QIM evolution predicted by the model. Model uncertainty in QIM forecast is computed from the uncertainty in Ps and Sh predictions (Figure 3).

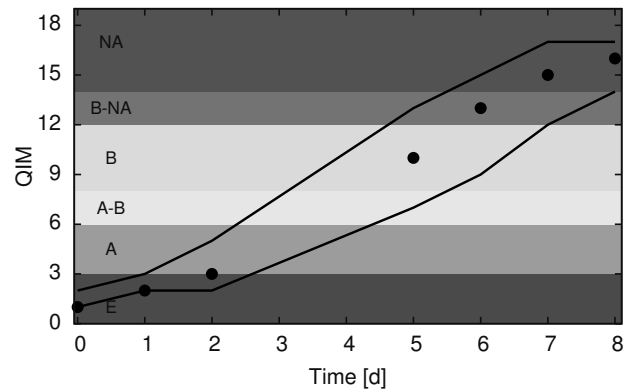


Figure 4: QIM evolution predicted by the model. Continuous lines represent the maximum and minimum QIM taking into account model uncertainty. Marks represent the most probable value. The background colors depict the QSM regions.

A panel of experts evaluated the QSM in a validation experiment. The model predictions coincided with the evaluation by experts (García et al. 2015). Shelf-life, understood as the time required to reach a not-admitted (NA) grade, can be obtained from the quality prediction model. Model uncertainty can be used to determine the moment when new measurements from the sensors are required to increase the confidence on model predictions.

This work was extended to develop a smart sensor with

capabilities of predicting all quality indexes standard in fish freshness (QIM, QSM and shelf-life) for cod (García et al. 2017). The smart sensor only requires measurements at the initial time of total volatile basic nitrogen (TVB-N) content and initial Psychrotrophic counts.

CONCLUSIONS AND FUTURE PERSPECTIVES

In this work we presented an approach to develop, from a system's theory perspective, a sensing technology for the assessment of food quality. By a sensing technology we mean a pack of reliable electronic devices together with a set of software components. Sensors, being the constituents of the hardware part, produce signals in response to the presence of some critical markers that suggest a given state of quality for the foodstuff. Software sensors, namely mathematical models describing mechanisms, are combined with the available measurements to infer or predict the evolution of other variables of interest. Inference implies the estimation of quality variables that cannot be directly accessed by the hardware sensors. Prediction of the temporal evolution of critical quality attributes over a future time horizon will determine features related to product shelf-life.

The state of the art of the different parts involved (sensors and mathematical models) has been summarized in the different sections of the manuscript. On the other hand, the reliability of mathematical models to forecast fish quality evolution was illustrated through two different examples: evolution of the K_I -value and relation between bacteria concentration and total volatile basic nitrogen content with quality indicators.

Research efforts are needed to integrate state-of-the-art sensors with mathematical and statistical models in order to extend the potentialities to do inference (software sensors) and dynamic predictions leading to the assessment of product shelf-life. In addition, the multiple sensor approach (that includes software sensors) will make it possible to develop further functionalities such as auto-checking, self-configuration, etc. In the last instance, this will lead to food sensing equipment requiring much less or none human intervention.

ACKNOWLEDGEMENTS

The authors acknowledge financial support from the Spanish Ministry of Science and Innovation (Projects ISFORQUALITY AGL2012-39951-C02-01 and RESISTANCE DPI2014-54085-JIN) as well as from EU Horizon 2020 research and innovation programme (COPRO project, grant agreement No 723575).

REFERENCES

Arias-Méndez A.; Vilas C.; Alonso A.A.; and Balsa-Canto E., 2014. *Time-Temperature integrators as*

predictive temperature sensors. Food Control, 44, 258–266.

Baixas-Nogueras S.; Bover-Cid S.; Veciana-Nogués T.; Nunes M.L.; and Vidal-Carou M.C., 2003.

Baranyi J., 1998. *Comparison of stochastic and deterministic concepts of bacterial lag. Journal of Theoretical Biology*, 192, 403–408.

Baranyi J.; George S.M.; and Kotalik Z., 2009. *Parameter estimation for the distribution of single cell lag times. Journal of Theoretical Biology*, 259, 24–30.

Baranyi J. and Roberts T.A., 1994. *A dynamic approach to predicting bacterial growth in food. International Journal of Food Microbiology*, 23, 277–294.

Brosnan T. and Sun D.W., 2004. *Improving quality inspection of food products by computer vision. Journal of Food Engineering*, 61, 3–16.

Chandrapala J.; Oliver C.; Kentish S.; and Ashokkumar M., 2012. *Ultrasonics in food processing food quality assurance and food safety. Trends in Food Science & Technology*, 26, no. 2, 88–98.

Chen L. and Opara U.L., 2013. *Texture measurement approaches in fresh and processed foods - A review. Food Research International*, 51, 823–835.

Dragone R.; Grasso G.; Muccini M.; and Torranin S., 2017. *Portable Bio/Chemosensoristic Devices: Innovative systems for Environmental Health and Food Safety Diagnosis. Frontiers in Public Health*, 5, 1–6.

Escuder-Gilabert L. and Peris M., 2010. *Review: highlights in recent applications of electronic tongues in food analysis. Anal Chim Acta*, 685, 15–25.

García M.R.; Cabo M.L.; Herrera J.R.; Ramilo-Fernandez G.; Alonso A.A.; and Balsa-Canto E., 2017. *Smart sensor to predict retail fresh fish quality under ice storage. Journal of Food Engineering*, 197, 87–97.

García M.R.; Vilas C.; Herrera J.R.; Bernárdez M.; Balsa-Canto E.; and Alonso A.A., 2015. *Quality and shelf-life prediction for retail fresh hake (Merluccius merluccius). International Journal of Food Microbiology*, 208, 65–74.

Geeraerd A.H.; Valdramidis V.P.; and Van Impe J.F., 2005. *GInaFit, a freeware tool to assess non-log-linear microbial survivor curves. International journal of food microbiology*, 102, no. 1, 95–105.

Ghasemi-Varnamkhasti M.; Mohtasebi S.S.; Siadat M.; and Balasubramanian S., 2009. *Meat quality assessment by electronic nose (machine olfaction technology). Sensors*, 9, no. 8, 6058–6083.

- Gysemans K.P.M.; Bernaerts K.; Vermeulen A.; Geeraerd A.H.; Debevere J.; Devlieghere F.; and Van Impe J.F., 2007. *Exploring the performance of logistic regression model types on growth/no growth data of Listeria monocytogenes*. *International Journal of Food Microbiology*, 114, 316–331.
- Halder A.; Black D.G.; Davidson P.M.; and Datta A., 2010. *Development of associations and kinetic models for microbiological data to be used in comprehensive food safety prediction software*. *Journal of Food Science*, 5, no. 75, 107–119.
- Harikedua S.D.; Wijaya C.H.; and Adawiyah D.R., 2012. *Relationship between sensory attributes of bakasang (a traditional Indonesian fermented fish product) and its physicochemical properties*. *Fish Science*, 78, 187–195.
- Hong H.; Regenstein J.M.; and Luo Y., 2017. *The Importance of ATP-related Compounds for the Freshness and Flavor of Post-mortem Fish and Shellfish Muscle: A Review*. *Critical Reviews in Food Science and Nutrition*, 59, no. 9, 1787–1798.
- Howgate P., 2005. *Kinetics of degradation of adenosine triphosphate in chill-storage rainbow trout (Oncorhynchus mykiss)*. *International Journal of Food Science and Technology*, 40, 579–588.
- Howgate P., 2006. *A review of the kinetics of degradation of inosine monophosphate in some species of fish during chilled storage*. *International Journal of Food Science and Technology*, 41, 341–353.
- Karube I.; Matsuoka H.; Suzuki S.; Watanabe E.; and Toyama K., 1984. *Determination of fish freshness with an enzyme sensor system*. *Journal of agricultural and food chemistry*, 32, no. 2, 314–319.
- Koutsoumanis K. and Nychas G.J.E., 2000. *Application of a systematic experimental procedure to develop a microbial model for rapid fish shelf life predictions*. *International Journal of Food Microbiology*, 60, 171–184.
- Kutalik Z.; Razaz M.; Elfwing A.; Ballagi A.; and Baranyi J., 2005. *Stochastic modelling of individual cell growth using flow chamber microscopy images*. *International Journal of Food Microbiology*, 105, 177–190.
- Lakshmanam P.T. and Gopakumar P., 1999. *K-value, an index for estimating fish freshness and quality*. *Current Science*, 76, no. 3, 400–404.
- Li K.F.; Luo Y.K.; and Shen H.X., 2015. *Postmortem Changes of Crucian Carp (Carassius auratus) During Storage in Ice*. *International Journal of Food Properties*, 18, no. 1, 205–212.
- Martins R.C.; Lopes V.V.; Vicente A.A.; and Teixeira J.A., 2008. *Computational shelf-life dating: complex systems approaches to food quality and safety*. *Food Bioprocess Technology*, 1, 207–222.
- McMeekin T.A.; Baranyi J.; Bowman J.; Dulgaard P.; Kirk M.; Ross T.; Schimid S.; and Zwietering M.H., 2006. *Information systems in food safety and management*. *International Journal of Food Microbiology*, 112, 181–194.
- McMeekin T.A.; Hill C.; Wagner C.; Dahl A.; and Ross T., 2010. *Ecophysiology of food-borne pathogens: essential knowledge to improve food safety*. *International Journal of Food Microbiology*, 139, S64–S78.
- Mello L.D. and Kubota L.T., 2002. *Review of the use of biosensors as analytical tools in the food and drink industries*. *Food Chemistry*, 77, 237–256.
- Miri T.; Tsoukala A.; Bakalis S.; Pistikopoulos E.N.; Rustem B.; and Fryer P.J., 2008. *Global optimization of process conditions in batch thermal sterilization of food*. *Journal of Food Engineering*, 87, 485–494.
- Oliveira A.E.F. and Pereira A.C., 2016. *Biosensor and Food Industry - Review*. *Rev Virtual Quim*, 8, no. 5, 1311–1333.
- Saito T.; Arai K.; and Matsuyoshi M., 1959. *A new method for estimating the freshness of fish*. *Bulletin of the Japanese Society of Scientific Fisheries*, 24, 749–750.
- Sliwinska M.; Wisniewska P.; Dymerski T.; Namiesnik J.; and Wardencki W., 2014. *Food Analysis Using Artificial Senses*. *Journal of Agricultural and Food Chemistry*, 62, no. 7, 1423–1448.
- Su L.; Jia W.; Hou C.; and Lei Y., 2011. *Microbial biosensors: A review*. *Biosensors and bioelectronics*, 26, 1788–1799.
- Surette M.E.; Gill T.A.; and LeBlanc P.J., 1988. *Biochemical basis of postmortem nucleotide catabolism in cod (Gadus morhua) and its relationship to spoilage*. *Journal of agricultural and food chemistry*, 36, no. 1, 19–22.
- Timmermans A.J.M., 1998. *Computer vision system for on-line sorting of pot plants based on learning techniques*. *Acta Horti*, 421, 91–98.
- Tsironi T.; Salapa I.; and P. T., 2009. *Shelf life modelling of osmotically treated chilled gilthead seabream fillets*. *Innovative Food Science and Emerging Technologies*, 10, 23–31.
- Valero A.; Hervás C.; García-Gimeno R.M.; and Zurera G., 2007. *Product unit neural networks models for predicting the growth limits of Listeria monocytogenes*. *Food Microbiology*, 24, 452–464.

- Vilas C.; Alonso A.A.; Herrera J.R.; Bernárdez M.; and García M.R., 2018. *A mathematical model to predict early quality attributes in hake during storage at low temperature. Journal of Food Engineering*, 222, 11–19.
- Vilas C.; Alonso A.A.; Herrera J.R.; García-Blanco A.; and García M.R., 2017a. *A model for the biochemical degradation of inosine monophosphate in hake (Merluccius merluccius). Journal of Food Engineering*, 200, 95–101.
- Vilas C.; Arias-Méndez A.; García M.R.; Alonso A.A.; and Balsa-Canto E., 2017b. *Towards predictive food process models: A protocol for parameter estimation. Critical Reviews in Food Science and Nutrition*, 58, no. 3, 436–449.
- Wilson A.D., 2013. *Diverse applications of electronic-nose technologies in agriculture and forestry. Sensors*, 13, 2295–2348.
- Xiaobo Z.; Xiaowei H.; and Povey M., 2016. *Non-invasive sensing for food reassurance. Analyst*, 141, 1587–1610.
- Yao L.; Luo Y.; Sun Y.; and Shen H., 2011. *Establishment of kinetic models based on electrical conductivity and freshness indicators for the forecasting of crucian carp (Carassius carassius) freshness. Journal of Food Engineering*, 107, 147–151.

INDUSTRIAL DESIGNS FOR MICROWAVE PASTEURIZATION OF LIQUID FOODS: A COMPUTATIONAL STUDY

Huseyin Topcam and Ferruh Erdogdu*

Department of Food Engineering, Ankara University, Ankara, Turkey

* Corresponding author

e-mail: ferruherdogdu@yahoo.com

KEYWORDS

Microwave heating, continuous microwave systems, rotational effects, design and optimization

ABSTRACT

In recent years, methods for processing liquid foods have changed from conventional to innovative techniques. In industry, convection heating of liquid foods with heat exchangers is still the most used method. However, demand for innovative methods is increasing constantly due to the possible advantages. Microwave processing provides volumetric heating, and it is regarded to be a green technology compared to conventional systems. Even if the microwave processing is considered to provide a volumetric heating, due to the non-uniform evolution of electromagnetic field, a certain non-uniformity in temperature distribution inside a product is still observed. In low viscosity products, this is not significant due to the buoyancy effect while, in high viscosity liquids, the non-uniformity might lead to over- or under-processing. Therefore, the objective of this study was to develop and experimentally validate a mathematical model for batch processing and use this model for further design of an industrial system design. For process designing, rotational effects (2.5 to 20 rpm) were also demonstrated. The increased rotation rate increased the temperature uniformity in high-viscous foods and used for alternative industrial process designing.

INTRODUCTION

Thermal processing of liquid foods generally depends on convection and conduction. Thus, non-uniform temperature distribution in product occurs and causes formation of over-processed and under-processed parts within the volume. Especially in viscous products, this temperature difference increases and might cause major problems in accordance to food safety and food quality. To overcome these problems, continuous-microwave systems are considered to be alternative to conventional systems especially due to their volumetric heating ability and reduced process times with energy savings and increased quality (Zhu et al. 2007; Wei et al., 2012; Yousefi et al., 2013). Continuous systems work under the fluid dynamic principles where the liquid product is

pumped through a microwave transparent tubing (e.g., Teflon) inside the microwave cavity, and the thermal processing is carried out. The objective is to get the thermally processed liquid food at the exit of the system. However, even in continuous microwave systems, non-uniform temperature distribution is observed due to cavity geometry, product location in cavity, temperature dependency of the dielectric properties, product viscosity and non-uniform electromagnetic field formation (Zhou et al., 1995, Basak and Meenakshi, 2006). Various studies were reported for low- and high-viscosity cases (Nikdel et al., 1993; Coronel et al., 2003; Kumar et al., 2008; Salvi et al., 2011; Tuta and Palazoglu, 2017). To overcome the temperature uniformity issue in high-viscosity liquids, rotational effects were hardly focused. Stratakos et al. (2016) used a continuous-flow microwave systems with a rotating tube to process tomato juice. The rotational effects are expected to increase the mixing in the liquid to enhance the temperature uniformity. Therefore, the objective of this study was first to develop and experimentally validate a mathematical model to determine the temperature change of a liquid during microwave heating with rotational effects and then to apply the developed model for designing industrial continuous systems. Since modelling of a natural convection phenomenon with the rotational effects is expected to be more complex compared to the case of forced convection under flow conditions, it was assumed that the experimental validation of the developed model might be further used to evaluate the process conditions of a continuous system.

MATERIAL & METHODS

Model development

The microwave heating model to determine the temperature distribution inside the liquid with rotational effects was developed using Comsol Multiphysics program (Comsol AB, V.5.2, Stockholm, Sweden). For this purpose, the microwave and fluid dynamic physics were used.

The governing equations solved were

- Maxwell equation (1) was used to evaluate electrical field changes at 915 (industrial system design) and 2450 (batch microwave system) MHz.

$$\nabla \times \left(\frac{1}{\mu} \nabla \times \vec{E} \right) - \frac{\omega^2}{c} (\epsilon' - i\epsilon'') \vec{E} = 0 \quad (1)$$

where \vec{E} is electric field intensity (V/m), ϵ' dielectric constant of a material, ϵ'' is relative dielectric loss of a material, ω is angular wave frequency ($2\pi f$, rad/s), μ is relative permeability of the material and c is speed of light in free space (3×10^8 m/s).

- To calculate temperature distribution within the product, energy equation (2) was solved:

$$\rho C_p \frac{\partial T}{\partial t} = \nabla(k \nabla T) + Q \quad (2)$$

where ρ is material density (kg/m³), c_p is specific heat (J/kg-K), k is thermal conductivity (W/m-K), T is temperature (K), and Q is the volumetric heat generation due to the incident microwave energy (W/m³).

- The absorption of electrical energy by product within the product was calculated by:

$$Q = \sigma |\vec{E}|^2 = \frac{1}{2} \omega \epsilon_0 \epsilon'' |\vec{E}|^2 \quad (3)$$

where σ is electrical conductivity of the material (S/m), ϵ_0 is free space permittivity (8.854×10^{-12} F/m).

- Velocity profiles in the heated liquid were obtained by solving the Navier–Stokes equation:

$$\frac{\partial \vec{v}}{\partial t} = -\nabla P + \mu \nabla^2 \vec{v} + \rho \vec{g} \quad (4)$$

where ∇P is the pressure force on element per unit volume (N/m²), \vec{g} is the acceleration due to gravity (m/s²), μ is viscosity (Pa.s) and \vec{v} is the velocity vector (m/s).

These equations were solved using the 'electromagnetic waves, frequency domain', 'laminar flow' and 'heat transfer in fluids' physics coupled in the Comsol Multiphysics program with $\approx 200,000$ elements used in the computational geometry.

Experimental studies

A modified domestic microwave oven was used for batch case modeling and experimental validation. Fig. 1 shows the modified domestic microwave oven and its computational geometry. The modification was carried out to place a PTFE cylinder within the system with enabled rotation.

The domestic microwave oven (with a system frequency of 2450 MHz) was 29.3×25.5×18 cm in size and it contains a cylindrical PTFE tube (17.5 cm in length and 2.5 cm in radius) to process liquids. The rotation mechanism of the oven enabled a 2.5 rpm rotation rate. The system works at the 2450 MHz frequency.

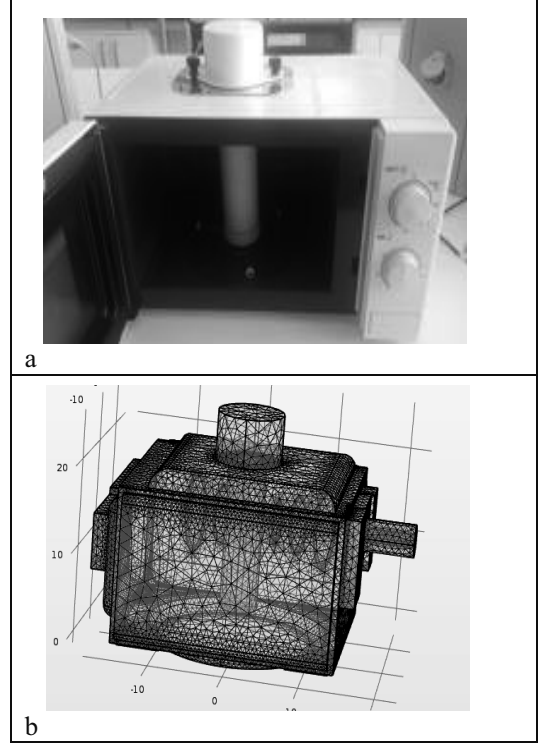


Figure 1: (a) Domestic Microwave Oven Modified for Experimental Studies; (b) Computational Geometry.

Pre-experiments with water load showed that the applied power was 375.19 W when 500 W setting was used. The microwave system worked with cycled heating, and cycles were recorded and applied in the developed model. For experimental validation studies, water and 0.5 % CMC (carboxymethyl cellulose) solution were used. Physical and thermal properties of the water were obtained from used Multiphysics program material library (Comsol AB, V.5.2, Stockholm, Sweden), and dielectric properties were experimentally measured at 2450 MHz frequency by using Network Analyzer (Agilent Technologies, ES061B ENA Series Network Analyzer, USA) with an open ended coaxial probe (Agilent Technologies, 85070E, USA) connection.

The required thermophysical and dielectric properties of 0.5% CMC solution were obtained from Tuta and Palazoglu (2017) and Coronel et al., (2003). Dielectric properties of water and 0.5% CMC as a function of temperature are shown in Table 1.

Table 1: Temperature dependent dielectric Constant (ϵ') and dielectric loss factor (ϵ'') values of 0.5% CMC solution at 2450 MHz.

T (°C)	Water		0.5% CMC	
	ϵ'	ϵ''	ϵ'	ϵ''
5	85.05	17.93	81.19	9.28
20	79.31	10.84	77.80	8.91
40	72.57	6.19	72.86	9.53
60	66.39	3.78	67.47	11.43
65	64.90	3.41	66.04	12.11

Temperature change of water and 0.5% CMC were obtained volumetrically at various intervals of the microwave working cycle, and results were compared with the model results. Temperature data were obtained using UMI-4 data acquisition system, FISO, Canada). As explained, the experimental studies were carried out in a 2450 MHz system while the industrial setting will be planned for 915 MHz.

These two frequencies are the generally applied settings of microwave systems domestic and industrial conditions. When moved from 2450 to 915 MHz, there are two significant changes. The first case is the reduction in the applied power (as also equation – 3 defines) and changes in the dielectric properties and possible increase in the penetration depth. These are expected to enable a better control of the process for the temperature increase and the temperature uniformity within the heated sample. Due to the higher temperature increases in the 2450 MHz application and the effect of natural convection, these systems are more difficult to mathematically evaluate, and the validated models might be easily applied to the continuous systems as explained above.

Industrial system design

For continuous flow industrial system (with a centralized pipe with 2.54 cm in radius and 40cm length), first a cylindrical cavity operating at 915 MHz at 4000 W power were simulated (Fig. 2). Processed liquid was assumed to be whole liquid egg (WLE). As explained in the experimental studies, the model validations were carried out at 2450 MHz using water and 0.5% CMC solution. These two liquids were specifically chosen to represent a two distinct viscosity range. With the easily formed natural convection effects in water, the mathematical evaluation was rather difficult compared to the viscous case. The experimental validation for these two conditions, on the other hand, was expected to suggest that the model might be used for any other liquid food. With the industrial significance of the liquid eff process, this sample was chosen to demonstrate in the industrial system conditions.

Thermophysical properties and dielectric properties were obtained from Coimbra et al. (2006) and Wang et al., (2009), respectively. Laminar flow rate was 0.05 m/s inlet velocity with an inlet temperature at 4°C. The walls were to have no slip condition and slip conditions with rotation rate up to 20 rpm. As explained in the previous section, the developed model was to be validated at 2.5 rpm rotation rate. Upon this validation, the model was to be used for higher rotation rates to demonstrate the effect of rotation.

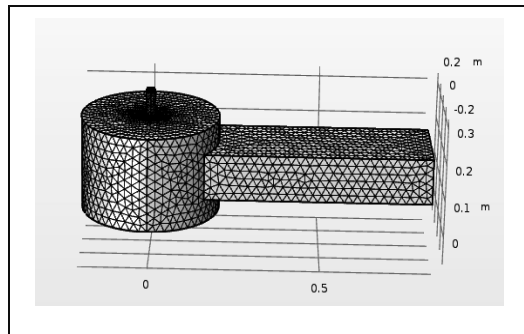


Figure 2: Computational Geometry of the Continuous Flow Industrial System.

RESULT & DISCUSSIONS

Experimental validation

As explained above, the mathematical model was developed using Comsol Multiphysics program. After preparing the computational geometry and solving the required governing equations with the given initial and boundary conditions, the volumetric temperature change of the liquid was compared with the model results. This comparison with the experimental data for water and 0.5% CMC can be observed in Figs. 3a-b, respectively. The experimental data, obtained at 2.5 rpm and 375.19 W power, were the average of three parallels with the standard deviation. The electromagnetic field distribution inside the system was shown in Fig. 4.

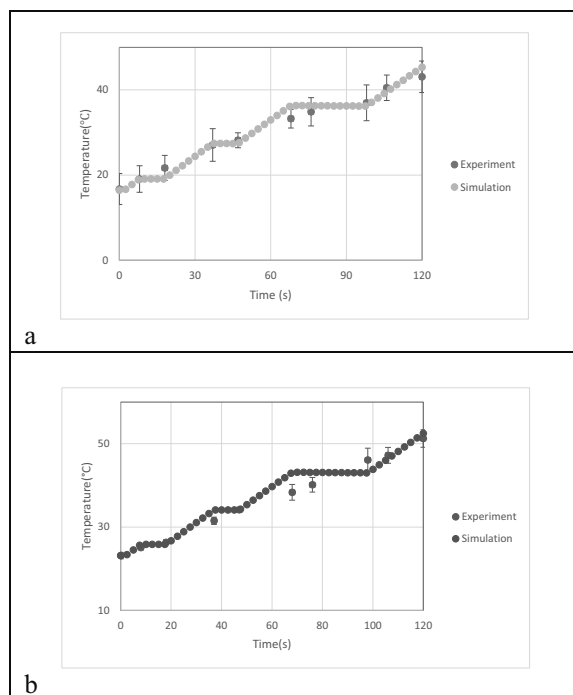


Figure 3. Comparison of Volume Averaged Experimental Temperature Data with Mathematical Model Results: (a) Water, (b) 0.5% CMC (°C).

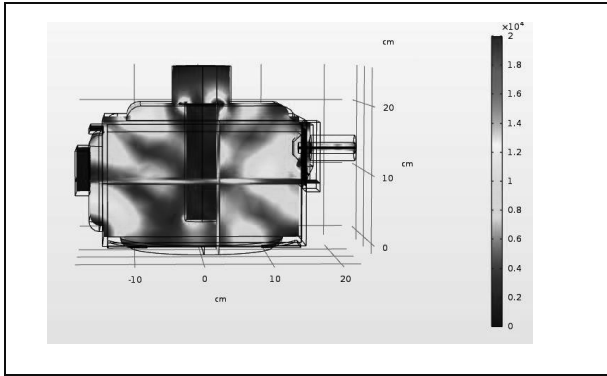


Figure 4: Electromagnetic Field Distribution inside the Domestic Microwave System (V/m).

Industrial system design

Continuous-flow case

The electromagnetic field configurations inside the industrial system and product were shown in Fig. 5. Surface average temperature at the theoretical exit of the system 0, 4, 8 and 20 rpm rotation were determined to be 61.21, 53.31, 53.47 and 53.68 °C, respectively. Temperature differences between maximum and minimum temperatures at the exit were reported in Table 2 to demonstrate the effect of rotation on enhancing temperature uniformity while temperature distribution velocity profile change at the exit were observed in Fig. 6.

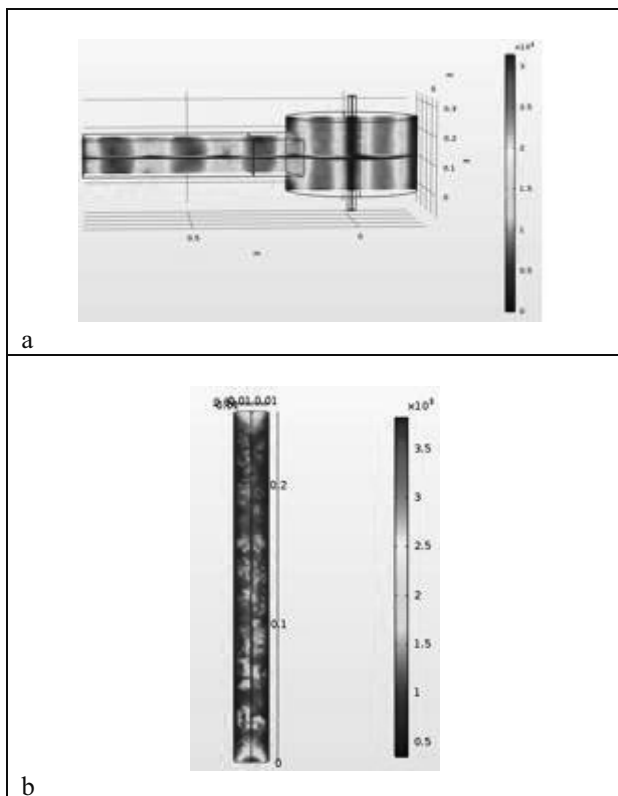


Figure 5: Electromagnetic Field Distribution in (a) The System Cavity (b) within the Liquid Product (V/m).

Table 2: Temperature Differences between Maximum and Minimum Outlet Temperatures at Different Rotation Rates.

Rotation rate (rpm)	Temperature Difference (°C)
0	5.6
4	3.1
8	1.4
20	0.2

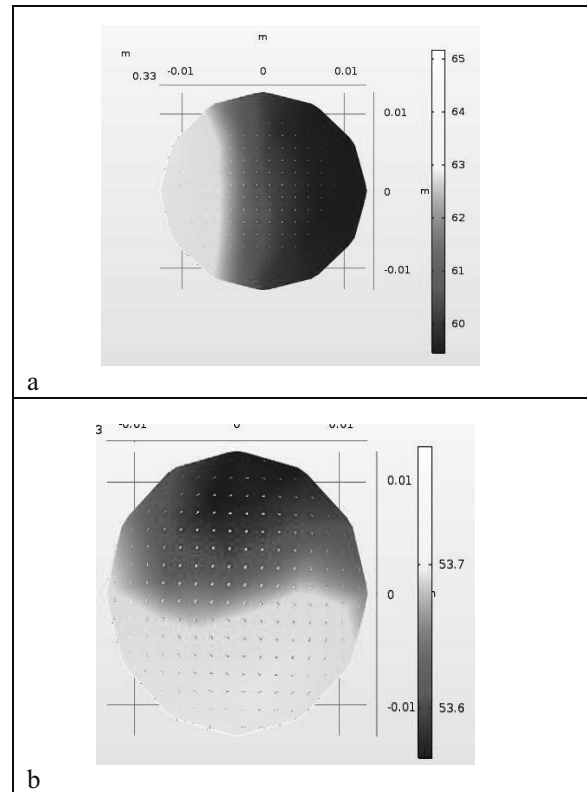


Figure 6: Velocity and Temperature Profiles of (a) 0 rpm and (b) 20 rpm Rotation Rate along the Theoretical Exit (°C).

Alternative designs for increased production volume

For an industrial system design to lead to increased production volume, multiple-pipe systems were considered, and effects of pipe quantity and location were evaluated. Two of the trials included 3- and 5- equally placed pipes located inside the cavity. While the latter case led to rather non-uniformity in temperature (Fig. 7a), rather uniform temperature change was obtained in the former case (Fig. 7b). In the 3-pipe design, center-focused electromagnetic field configuration is surrounded the pipes, and a uniform temperature among the pipes were obtained. The exit temperature was uniformly around to 35 °C. Therefore, it was concluded that either increased the system power or reduced inlet velocity should be used to achieve a required temperature of, for instance, 60 °C. The electromagnetic field

distributions for the 3-pipe configuration was shown in Fig. 8.

CONCLUSION

In this study, rotational effect on temperature distribution of liquids were determined using a mathematical model developed for a domestic microwave oven system and experimentally validated using water and 0.5% CMC. The model was then used for designing an industrial scale continuous microwave system using the demonstrated rotational effects. Besides, alternative continuous were demonstrated to achieve higher production capacity, and the pipe location and quantity effects on temperature increase were evaluated with an optimal processing condition.

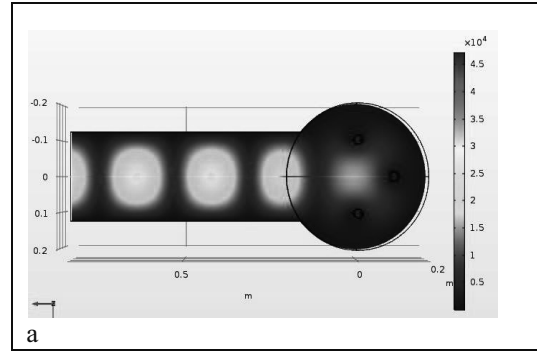


Figure 8: (a) Electromagnetic Field Distribution Obtained for the 3-Pipe Configuration (V/m).

ACKNOWLEDGEMENT

The authors gratefully acknowledge the Scientific Research Foundation, Ankara University, Turkey for supporting this project (Project No: 16H0443002).

REFERENCES

- Basak, T., & Meenakshi, A. 2006. A theoretical analysis on microwave heating of food slabs attached with ceramic plates: Role of distributed microwave incidence. *Food Research International*, 39(8), 932-944.
- Coimbra, J. S., Gabas, A. L., Minim, L. A., Rojas, E. E. G., Telis, V. R., & Telis-Romero, J. 2006. Density, heat capacity and thermal conductivity of liquid egg products. *Journal of Food Engineering*, 74(2), 186-190.
- Coronel, P., Simunovic, J., & Sandeep, K. P. 2003. Temperature Profiles Within Milk after Heating in a Continuous-flow Tubular Microwave System Operating at 915 MHz. *Journal of Food Science*, 68(6), 1976-1981.
- Kumar, P., Coronel, P., Truong, V. D., Simunovic, J., Swartzel, K. R., Sandeep, K. P., & Cartwright, G. 2008. Overcoming issues associated with the scale-up of a continuous flow microwave system for aseptic processing of vegetable purees. *Food Research International*, 41(5), 454-461.
- Nikdel, S., Chen, C. S., Parish, M. E., MacKellar, D. G., & Friedrich, L. M. 1993. Pasteurization of citrus juice with microwave energy in a continuous-flow unit. *Journal of Agricultural and Food Chemistry*, 41(11), 2116-2119.
- Salvi, D., Boldor, D., Aita, G. M., & Sabliov, C. M. 2011. COMSOL Multiphysics model for continuous flow microwave heating of liquids. *Journal of Food Engineering*, 104(3), 422-429.
- Stratakos, A. C., Delgado-Pando, G., Linton, M., Patterson, M. F., & Koidis, A. 2016. Industrial scale microwave processing of tomato juice using a novel continuous microwave system. *Food Chemistry*, 190, 622-628.

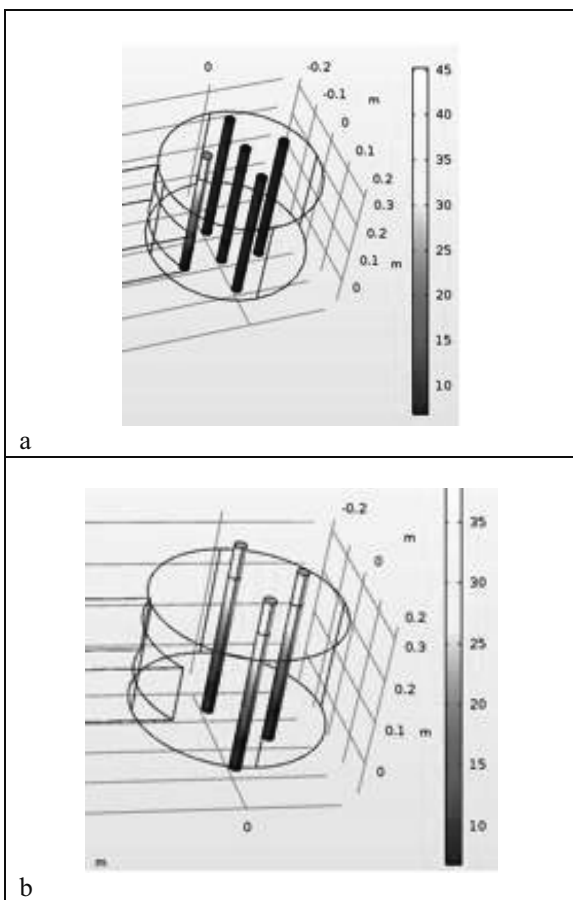


Figure 7: Temperature Profiles of (a) 5- Pipe and (b) 3- Pipe Configurations (°C).

- Tuta, S., & Palazoğlu, T. K. 2017. Finite element modeling of continuous-flow microwave heating of fluid foods and experimental validation. *Journal of Food Engineering*, 192, 79-92.
- Wang, J., Tang, J., Wang, Y., & Swanson, B. 2009. Dielectric properties of egg whites and whole eggs as influenced by thermal treatments. *LWT - Food Science and Technology*, 42(7), 1204-1212.
- Wei, W., Yin, H. M., & Tang, J. 2012. An optimal control problem for microwave heating. *Nonlinear Analysis: Theory, Methods & Applications*, 75(4), 2024-2036.
- Yousefi, T., Mousavi, S. A., Saghir, M. Z., & Farahbakhsh, B. 2013. An investigation on the microwave heating of flowing water: A numerical study. *International Journal of Thermal Sciences*, 71, 118-127.
- Zhou, L., Puri, V. M., Anantheswaran, R. C., & Yeh, G. 1995. Finite element modeling of heat and mass transfer in food materials during microwave heating—model development and validation. *Journal of Food Engineering*, 25(4), 509-529.
- Zhu, J., Kuznetsov, A. V., & Sandeep, K. P. 2007. Mathematical modeling of continuous flow microwave heating of liquids (effects of dielectric properties and design parameters). *International Journal of Thermal Sciences*, 46(4), 328-341.

A COUPLED CFD-HEAT TRANSFER MODEL FOR IN-PACKAGE SOLID FOOD PASTEURIZATION

Clarissa Detomi de Albuquerque
Sébastien Curet
Lionel Boillereaux
GEPEA ONIRIS (UMR CNRS 6144)
Site de la Géraudière CS 82225
44322 Nantes cedex 3, France
E-mail: clarissa.detomi@oniris-nantes.fr
E-mail: sebastien.curet@oniris-nantes.fr
E-mail: lionel.boillereaux@oniris-nantes.fr

KEYWORDS

modelling, pasteurization, heat transfer, CFD, microbial inactivation

ABSTRACT

This study deals with the modelling of thermal pasteurization of in-package solid food product immersed in hot water. The objective is to study the influence of dynamic heating temperatures on both thermal and inactivation kinetics. A severe dynamic heating rate (15 °C/min) is applied to a meat-based product relevant to thermal pasteurization without holding phase. For predicting thermal kinetics, the agreement between experimental and numerical temperatures of water and sample is noticeable. The thermal delay due to convection and conduction within water and solid food is discussed, justifying the interest of such an approach when heating rates are applied. This work demonstrates the necessity of predicting local thermal heterogeneities when modelling pasteurization within food products without holding phase at set point temperature. The model could be used for process optimization with the aim to ensure food safety by limiting as far as possible overtreatment.

INTRODUCTION

Modelling of thermal pasteurization of in-package solid food product presents several benefits to ensure optimal processing conditions for industry (Bottani et al. 2013; Hong et al. 2014). Indeed the challenge is to ensure food safety by limiting as far as possible quality loss due to overtreatment (Boillereaux et al. 2013).

Such an objective requires a multiphysics approach where CFD, heat transfer and microbial inactivation kinetics are coupled in a global model.

Traditional pasteurization processes combine successively heating, holding and cooling phases. In the literature, most microbial inactivation models are designed and validated during the holding phase at a reference temperature (Juneja et al. 1997; Valdramidis et al. 2005). In this work, attention is focused on the heating phase by considering a severe heating rate and its influence on inactivation kinetics.

MATERIAL AND METHODS

Samples of raw ground beef (3 g, 5% fat) inoculated with *E. Coli* K12 ($N_0 = 4.45 \cdot 10^6$ CFU/g) are packed in plastic

pouches immersed in a programmable Peltier-based effect water bath. (Hart Scientific AOIP, FC 9105, USA) and submitted to a 15 °C/min heating rate (initial temperature 7 °C) (Figure 1).



Figure 1. (a) experimental apparatus (b) heating vessel and in-package sample (c) sample packed in pouch.

A type-K thermocouple is introduced in the sample to control the treatment end temperature. Eight final temperatures were considered (50-52-54-56-58-60-62 and 64 °C). Temperatures are recorded by a data logger (AOIP datalog, 91133 RisOrangis, France) with output recordings every 1 second. Triplicates were carried out for each experiment.

Microbiology analysis are performed following the standard norm (ISO 16649-1:2001, 2001). The detection limit was fixed to 1 log CFU/g of the ground beef.

MODEL DESIGN

CFD and heat transfer model

A schematic description of the experimental apparatus is presented in Figure 2. To analyse the heat transport phenomena during pasteurization, the following assumptions were considered:

- *Assumption 1:* The product is homogeneous and isotropic with constant thermophysical properties.
- *Assumption 2:* The initial temperature of the food sample is homogeneous.

- *Assumption 3:* The mass transfer and shrinkage are negligible.
- *Assumption 4:* The geometry of the packaged sample is assimilated to an ellipsoid-cylinder, with axial symmetry.
- *Assumption 5:* The package thickness was sufficiently thin to neglect its impact on the heat transfer (low thermal resistance).

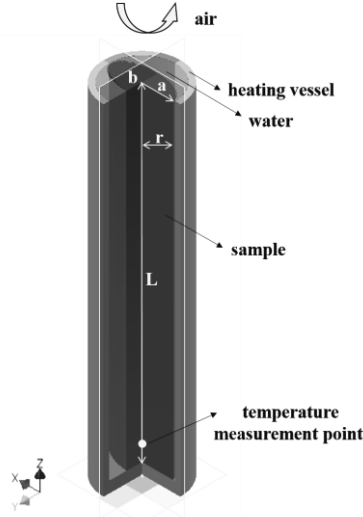


Figure 2. 3D view of heating vessel ($r=6$ mm; $L=60$ mm), ellipsoid-cylinder in-package food sample ($a=5.8$ mm; $b=2.8$ mm; $L=60$ mm) and probe location $(x, y, z)=(0, 0, 2.7)$ mm.

Heat transfer is based on the generalised heat equation which depends on thermophysical properties of the meat-based sample, as follows:

$$\rho_s C_p \frac{\partial T}{\partial t} = \text{div}(\lambda_s \nabla T) \quad (1)$$

For the heating fluid (water), natural convection is taken into account as follows:

$$\rho_w C_p \frac{\partial T}{\partial t} + \rho_w C_p \vec{u} \nabla T = \text{div}(\lambda_w \nabla T) \quad (2)$$

Navier-Stokes equations (Newtonian fluid and incompressible flow) enables to model the fluid mechanics within water:

$$\begin{cases} \frac{\partial u}{\partial x} + \frac{\partial v}{\partial y} + \frac{\partial w}{\partial z} = 0 \\ \rho_w \frac{d\vec{u}}{dt} = \rho_w \vec{g} - \nabla P + \mu_w \Delta \vec{u} \end{cases} \quad (3)$$

Where ρ is the density (kg/m^3), C_p the specific heat ($\text{kJ kg}^{-1} \text{K}^{-1}$), T the temperature ($^{\circ}\text{C}$), \vec{u} is the velocity field at any point of the 3D sample domain (u, v, w components), g is the gravitational constant (m/s^2), P the absolute pressure (Pa) and μ the dynamic viscosity (Pa.s). The subscripts s and w refers respectively to sample and water.

The CFD heat transfer model is solved with COMSOL®Multiphysics 5.3a and consists of two main

computational domains: *i*) liquid water filling the cylindrical vessel *ii*) ground beef sample located at the center of the vessel. The surfaces of the heating vessel are submitted to a temperature ramp at the wall (15°C/min). Natural convection at the surface of the food sample is considered from an empirical correlation dedicated to vertical cylinder (Churchill and Chu 1975).

Thermophysical properties of water are considered as temperature dependent (Green and Perry 2007). Thermophysical properties of ground beef are taken from literature (Pan and Singh 2001; Tsai et al. 1998): specific heat ($3.69 \text{ kJ kg}^{-1} \text{K}^{-1}$), thermal conductivity ($0.35 \text{ Wm}^{-1} \text{ }^{\circ}\text{C}^{-1}$) and density (1006 kg/m^3).

Initial and Boundary conditions

The initial and boundary conditions for the thermal and fluid mechanics model can be written as:

$$\begin{aligned} T &= T_0, \quad t = 0, \quad \forall (x, y, z), \quad T_0 = 7^{\circ}\text{C} \\ k \frac{\partial T}{\partial z} \Big|_{z=L} &= h_{air} (T - T_{\infty}), \quad \forall (x, y), \forall t > 0, \quad T_{\infty} = 20^{\circ}\text{C} \\ T_{wall} &= T_0 + \frac{dT}{dt} t, \quad \begin{cases} \text{for } x, y = R, \forall t > 0, \text{ for } z \in [0; L] \\ \text{for } z = 0, \forall t > 0, \forall x, y \end{cases} \\ u &= 0, P = P_{atm} + \rho_w g z \quad \text{at } t = 0, \forall x \forall y, \text{ for } z \in [0; L] \end{aligned}$$

Microbial inactivation model

Dynamic non log-linear model (Geeraerd et al 2000) was used to simulate microbial inactivation:

$$\frac{dN}{dt} = -k_{max} \left(\frac{1}{1 + C_c} \right) N \quad (4)$$

$$\frac{dC_c}{dt} = -k_{max} C_c \quad (5)$$

$$k_{max}(T) = \frac{\ln 10}{D_{ref}} \exp \left(\frac{\ln 10}{Z} (T - T_{ref}) \right) \quad (6)$$

The model parameters were taken from literature. So, physiological state of cells $C_c(0)$ is considered as 0.23 (Hamoud-Agha et al. 2013), decimal reduction time (D_{ref}) equal to 73 s, at reference temperature of 58°C and thermal resistance (Z) as 3.79°C , for ground beef 4.8% fat (Smith et al. 2001).

The microbial inactivation model is solved with MATLAB®7.10 from the 3D temperature-map predicted by COMSOL®Multiphysics 5.3a. This procedure enables to reduce considerably the computational time for predicting the microbial inactivation within the whole volume.

RESULTS

For model validation, experimental temperature of the ground beef sample is compared to the simulated one at the same location. Good agreement is found between experimental and predicted temperatures as can be observed on Figure 3. When ground beef is treated at a heating rate of 15°C/min , non-negligible thermal delays between water and

sample temperature (about 23 s) and setting temperature and sample (about 57 s) are remarked.

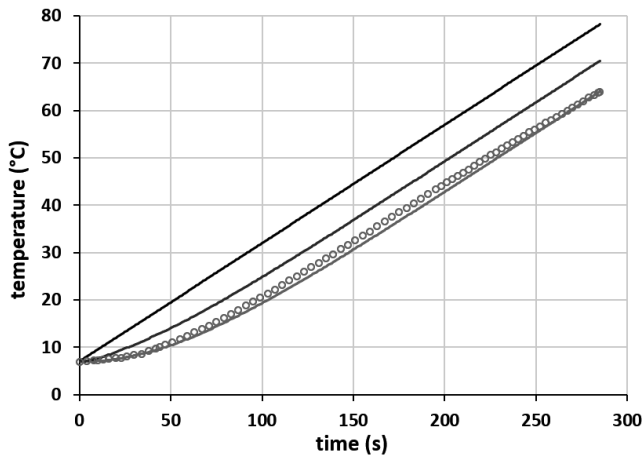


Figure 3. Thermal profiles: set temperature ramp of 15 °C/min (black line), sample experimental temperatures (red circle), sample (red line) and water (blue line) simulated temperatures.

The 3D modelling enables to compare the simulated temperatures following different cut lines located along the vertical axis (Figure 4) and at the end of the heating treatment

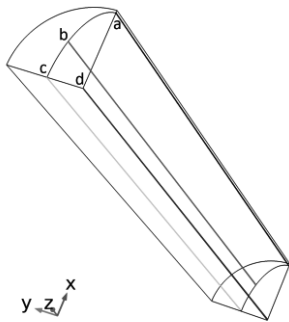


Figure 4. Cut lines in different positions on meat sample.

The Figure 5 depicts the evolution of predicted temperatures following the four different cut lines. It can be noticed that the temperature evolution is not homogeneous along the z -axis, justifying the necessity of 3D modelling for heat transfer with CFD.

The temperature gradients along the z -axis are less important when reaching the wall of the cylindrical vessel but remain the highest in terms of magnitude (black line in Figure 5).

A clear non homogeneous temperature distribution at the centre of the sample can be remarked (18.2 °C between the coldest and hottest points along the axis). The temperature profiles in the sample can be explained by the uneven distribution of the fluid flow and temperature around the sample.

More, the sample is cooled by external natural convection with ambient air close to the surface of the sample (z -axis = 60 mm).

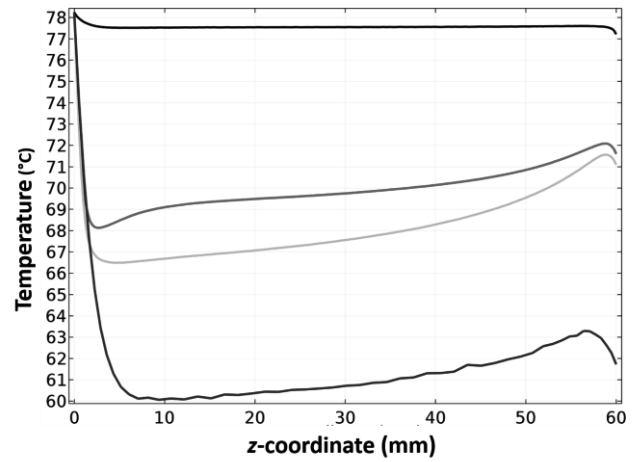


Figure 5. Temperature distribution along z -axis following different locations. As illustrated in Figure 4, position a (black line), b (red line), c (yellow line) and d (blue line).

The CFD modelling enables to predict the velocity fields due to natural convection around the sample. The Figure 6 depicts the norm of the velocity field following different processing times. Due to the temperature dependent thermophysical properties of water, fluid motion occurs, leading to natural convection phenomena around the sample. Recirculation of heating fluid (illustrated by black arrows in Figure 6) leads to more and more velocity field gradients appearing far from the wall of the cylindrical vessel.

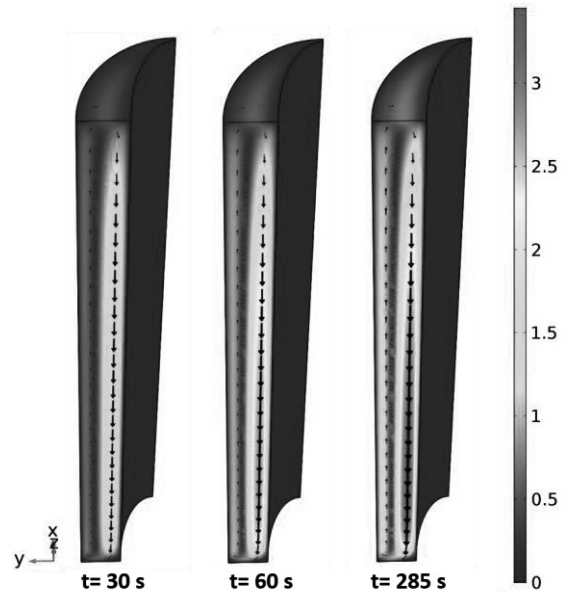


Figure 6. Velocity field of heating fluid (mm/s) following different simulation times.

The numerical simulation of CFD-heat transfer was used as a tool to complement the understanding of the results obtained experimentally and to illustrate 3D temperature distribution within both sample and heating fluid when a heating rate of the 15 °C/min is applied (Figure 7).

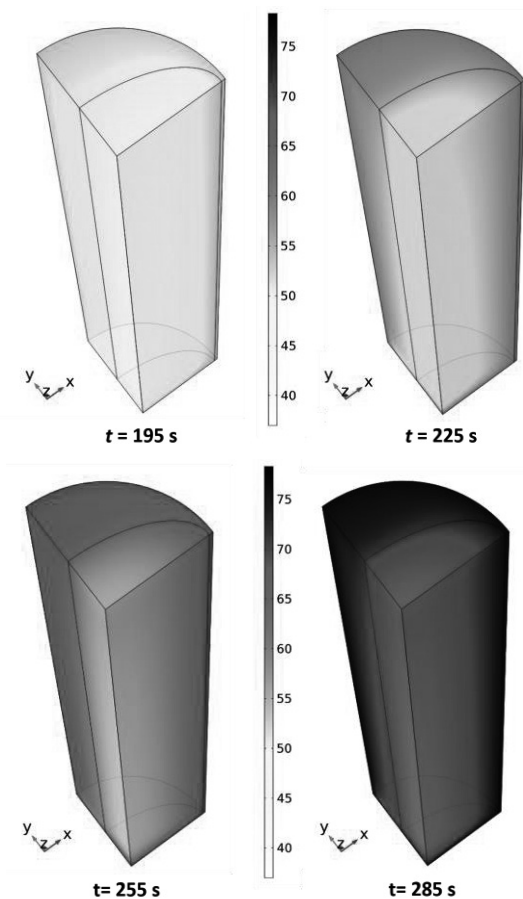


Figure 7. 3D distribution of temperatures (°C) at different simulated times for 15 °C/min.

The 3D distribution of temperatures indicate a thermal heterogeneity inducing different levels of local microbial inactivation within the processed sample. This observation cannot be experimentally validated in this study, because the microbiological analyses are performed on the total volume of the sample. As illustrated in Figure 8, only the volume average of the simulated inactivation data (black line) are compared with experiments data (red circle). However, the inactivation gradient were simulated and it is represented by the blue curve (minimal value) and by the red curve (maximal value).

Triplicated experiments display an acceptable repeatability of the microbiological analyses (Figure 8).

The (Geeraerd et al. 2000) inactivation model implemented with parameters issued from the literature (Smith et al. 2001) presents satisfying agreement with the experimental data.

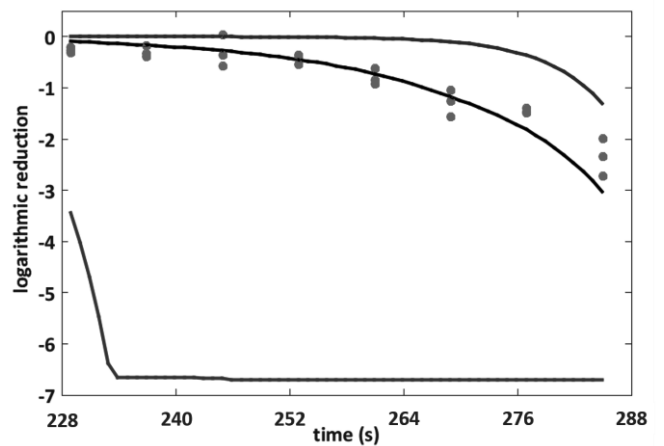


Figure 8. Triplicate experimental data (red circle), sample average volume (black line) and cold (blue line) and hot (red line) zone of the sample simulated logarithmic reduction of *E. coli*.

The simulated maximal and minimal inactivation results highlight a very important microbial inactivation heterogeneity in the volume. Indeed, even if an relevant inactivation ($-6.6 \log_{10}$) can be noticed after about 234 s, it is limited only to the peripheral area of the pouch (78 °C close to the vessel wall). In the remaining sample volume a partial inactivation of *E. coli* (less than $-2.5 \log_{10}$) was detected.

The heating rate of 15 °C/min induces a large thermal gradient occurring from the bottom to the top of the product is mainly responsible of this partial inactivation.

CONCLUSION

This contribution demonstrates that non-negligible microbial inactivation occurs during the heating phase when the lethal temperature is reached, underlining the importance of considering this stage in the modeling procedure. From a three-dimensional analysis of the problem, the large temperature gradients obtained at 15 °C/min without holding phase are able to explain the low level microbial inactivation.

The satisfying adequacy between model and experiments permits to foresee a model implementation in a process control procedure, allowing to supply the fair energy to reach the expected microbial inactivation while limiting heterogeneities. Such an objective could be reached for example by using combined energy sources (convection, microwaves, ohmic heating).

ACKNOWLEDGEMENTS

The authors are grateful to the National Council for Scientific and Technological Development (CNPq, Brazil) for Clarissa Detomi Albuquerque's PhD scholarship and financial support (process number 232767/2014-9).

REFERENCES

“ISO 16649-1:2001. Microbiology of Food and Animal Feeding Stuffs - Horizontal Method for the Enumeration of Beta-Glucuronidase-Positive Escherichia Coli - Part 1: Colony-Count Technique at 44 Degrees C Using Membranes and 5-

Bromo-4-Chloro-3-Indolyl.”

- Boillereaux, L., S. Curet, M. Hamoud-Agha, and H. Simonin. 2013. “Model-Based Settings of a Conveyorized Microwave Oven for Minced Beef Simultaneous Cooking and Pasteurization.” in *Computer Applications in Biotechnology (CAB 2013)*. Mumbai, India.
- Bottani, E., G. Ferretti, M. Manfredi, and G. Vignali. 2013. “Modeling and Thermo-Fluid Dynamic Simulation of a Fresh Pasta Pasteurization Process.” *International Journal of Food Engineering* 9(3):327–39.
- Churchill, S. W. and H. H. S. Chu. 1975. “Correlating Equations for Laminar and Turbulent Free Convection from a Vertical Plate.” *International Journal of Heat and Mass Transfer* 18(11):1323–29.
- Geeraerd, A. H., C. H. Herremans, and J. F. Van Impe. 2000. “Structural Model Requirements to Describe Microbial Inactivation during a Mild Heat Treatment.” *International Journal of Food Microbiology* 59(3):185–209.
- Green, D. W. and R. H. Perry. 2007. *Perry’s Chemical Engineering Handbook*. Eighth. The McGraw-Hill Companies, Inc.
- Hamoud-Agha, M. M., S. Curet, H. Simonin, and L. Boillereaux. 2013. “Microwave Inactivation of Escherichia Coli K12 CIP 54.117 in a Gel Medium: Experimental and Numerical Study.” *Journal of Food Engineering* 116(2):315–23.
- Hong, Y. K., J. T. Uhm, and W. B. Yoon. 2014. “Using Numerical Analysis to Develop and Evaluate the Method of High Temperature Sous-Vide to Soften Carrot Texture in Different-Sized Packages.” *Journal of Food Science* 79(4).
- Juneja, V. K., O. P. Snyder, and B. S. Manner. 1997. “Thermal Destruction of Escherichia Coli O157:H7 in Beef and Chicken: Determination of D- and Z-Values.” *International Journal of Food Microbiology* 35(3):231–37.
- Pan, Z. and R. Paul Singh. 2001. “Physical and Thermal Properties of Ground Beef during Cooking.” *LWT - Food Science and Technology* 34(7):437–44.
- Smith, S. E., J. L. Maurer, A. Orta-Ramirez, E. T. Ryser, and D. M. Smith. 2001. “Thermal Inactivation of *Salmonella* Spp., *Salmonella Typhimurium* DT104, and *Escherichia Coli* O157 : H7 in Ground Beef.” *Food Microbiology and Safety Thermal* 66(8):1164–68.
- Tsai, S. J., N. Unklesbay, K. Unklesbay, and A. Clarke. 1998. “Thermal Properties of Restructured Beef Products at Different Isothermal Temperatures.” *Journal of Food Science* 63(3):481–84.
- Valdramidis, V. P., K. Bernaerts, J. F. Van Impe, and A. H. Geeraerd. 2005. “An Alternative Approach to Non-Log-Linear Thermal Microbial Inactivation: Modelling the Number of Log Cycles Reduction with Respect to Temperature.” *Food Technology Biotechnology* 43(4):321–27.

BIOGRAPHIES

CLARISSA DETOMI DE ALBUQUERQUE was born in Belo Horizonte, Brazil and studied Food Engineering at the Federal University of Goiás, Brazil. In October 2015, she began a Ph.D in Food Process Engineering at ONIRIS, in GEPEA laboratory (Nantes, France). The thesis concerns the pasteurization of ground beef by the use of microwaves. The objective is to focus on the thermal and non-thermal effects during microwave processing and to propose an optimization of the process from both experimental and modelling approaches.

SÉBASTIEN CURET was born in Nantes, France. Graduated in 2005 as a process engineer (INSA Toulouse, France), he obtained his Ph.D in Food Process Engineering in 2008 (ENITIAA, Nantes, France). He has been an associate professor at ONIRIS (Nantes, France) since september 2008. His teaching activities are related to food process engineering (applied thermodynamic, unit operations and heat transfer). His research activities with the GEPEA laboratory are related to the optimization of microwave heating processes for the agri-food sector (modeling, numerical simulations and experimental investigations).

LIONEL BOILLEREAUX was born in Beaune, France. Graduated in Automatic in Grenoble (ENSIEG now ENSE) he obtained his Ph.D in 1996 at the National Polytechnic Institute (Grenoble, France). He has been working as a professor at ONIRIS with teaching activities related to process control and engineering. His research activities within the GEPEA laboratory are focused on the modeling, parameter estimation and process control strategies for thermal processes of the agri-food industry.

NUMERICAL MODELLING OF AIRFLOW AND HEAT TRANSFER IN A VENTED PALLET OF CHEESE

Anh Thu PHAM^(a,b,c), Jean MOUREH^(a), Denis FLICK^(a,b)

(a) IRSTEA, Génie des Procédés Frigorifiques (GPAN)

Antony, 92160, France, anh-thu.pham@irstea.fr

(b) AgroParisTech, Inra, Université Paris-Saclay, UMR Ingénierie, Procédés, Aliments (GENIAL)
Massy, 91300, France

(c) CNIEL, French Dairy Board – DirAST,
Paris, 75314, France

KEYWORDS

Heat transfer, temperature distribution, CFD, cheese, heat generating product.

ABSTRACT

During refrigerated transport and storage, cheese generates heat via respiration of the living microorganisms. Therefore, free/mixed convection phenomena are expected to occur within the pallet and to interact with forced convection around it. The resulting airflow should promote appropriate internal ventilation within the pallet to ensure the temperature homogeneity. This work aimed to study the influence of various parameters on the air flow and heat transfer within a pallet of cheese during forced air cooling. A 3-D computational fluid dynamics (CFD) model was developed to predict the temperature of the products in different configurations. Both forced and natural convection due to the heat generation of the produce were considered in the model. The numerical model can be potentially used as a design tool to improve the design of vented packages in order to reduce temperature differences of products within the pallet during the whole cold chain (cooling, transport, storage).

INTRODUCTION

The most important factor that affects the quality of the product during storage is the temperature (Defraeye et al. 2015, Ambaw et al. 2016). One of the reasons of heterogeneity is the over-ventilation in areas near the refrigerating unit with temperature close to the blowing temperature and the under-ventilation in the areas far from the refrigeration unit causing locally hot spots within the pallet (Moureh et al. 2009). Therefore, it is important to study the air pathways to better understand and to prevent the thermal heterogeneity. The experimental method is usually considered expensive, time-consuming and situation-specific (Zou et al. 2006). Moreover, when problem deals with biological materials, it is difficult to generalize the problem and control the experimental conditions (Delele et al. 2013). Numerical method is considered one of the most powerful alternative methods. Many authors chose CFD (Computational Fluid Dynamics) to study the airflow within a refrigerating enclosure: refrigerated truck (Moureh

et al. 2002), cold room (Hoang et al. 2015), refrigerated warehouse (Ho et al. 2010). In case of cheese product, the heat transfer becomes complex since it involves in aerodynamic and thermal interactions between the airflow around the pallet, and the natural convection inside the pallet generated by the internal production of heat by the microorganisms of the cheese.

The above state studies concerned forced convection cooling. To the best of author's knowledge, no numerical study has been carried out on a pallet of product generating heat. This study focused on studying the interaction between forced and free convection and their influence into the heat transfer within one layer of product by CFD method.

NUMERICAL MODELS

Computational domain

The modelling of the system was inspired by a standard industrial pallet of camembert (800mm x 1200mm x 1479mm) containing 54 cardboards evenly distributed into 9 layers, 6 cardboards per layer (figure 1.a). For each cardboard face, the total opening area (TOA) represents the ratio of the vented holes area to the considered face area. The TOA of both frontal face and side face (figure 1.b) are 5.1 %. There are 30 products per cardboard (3 layers of 10 products). Due to the complex geometry of the whole pallet, only one layer was modeled. The computational domain contained 1.15m x 1.75m x 2.14m air volume with one layer of products at the center. The detail dimensions were presented in figure 1. To simplify the problem and to reduce the number of mesh, several hypotheses were made:

- The system is symmetric so that only half of the layer was modelled
- There was no heat exchange between the different layers of the pallet in height direction
- There was no air gap between the cardboards
- In the real case, there are 3 layers of product per cardboards. In this model, these three layers was considered as a unique cylindrical bloc (110mm of diameter and 90mm of height)
- Three layers of product inside one cardboard is considered as one layer with the thickness equivalent of the thickness of three products

- The products distribute evenly in the cardboard
- The cardboard is considered adiabatic
- Cheese packaging was not considered in the model

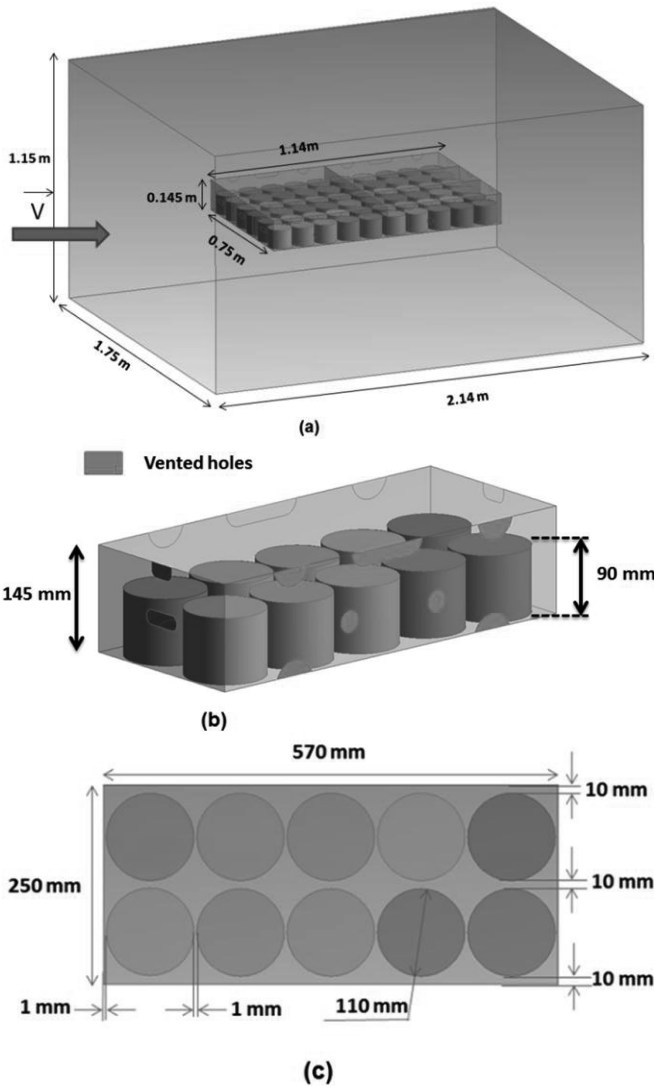


Figure 1 (a) computational domain, (b) geometry of one cardboard, (c) view from the top of cheeses in one cardboard

This layer of product is placed in a cold room where air is blown out from one lateral surface and evacuate by the opposite one. In the real warehouse, air is usually blown out by the evaporators so the blowing area is smaller than the warehouse walls. This modelling configuration corresponds with our test room in the laboratory.

Meshing

The difficulty related to our problem was that the space between two cheeses (1mm) was too small compared to the size of cheese (110mm of diameter). Therefore, the number of mesh becomes very large. In order to ensure the accuracy of the model, at least three meshes was modelled at the narrowest place (figure 2). A larger number of mesh is not possible due to the capacity of our computer. With this number of mesh, each simulation takes about two days in order to obtain the convergence.

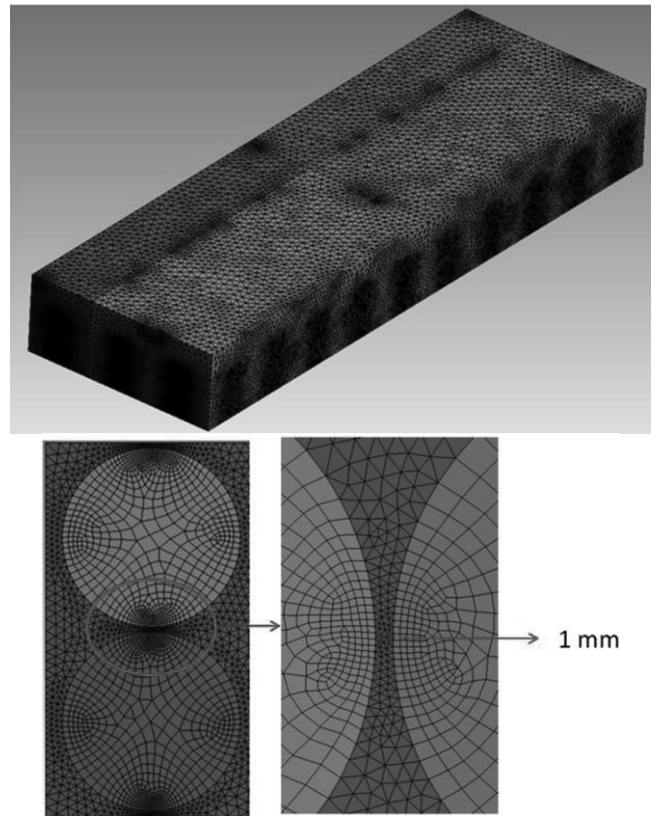


Figure 2: Mesh of half a layer of pallet

Due to the complexity of the geometry of the domain, unstructured meshes were used. The total number of mesh was 7.4 million meshes.

Boundary conditions

The heat flux generated by the product was fixed at 0.14W per cheese of 250g, the temperature of air ambient was 1°C. The air inflow velocity was 0.2m/s. Two models have been created: one that took account the free convection and the other without free convection. For this study, free convection was solved by using the Boussinesq approximation in which the variable density was allowed only in the buoyancy term. The top and the bottom of the studied layer were adiabatic. The simulations were performed with the CFD code ANSYS Fluent 17.0

RESULTS

The uniformity of the temperature was studied as well as the impact of the influence of natural convection to the heat exchange.

Mixed convection

The results presented in this part concerning the case where natural convection was included in the model, i.e. the air density varied in function of the temperature. The figure 3 represents the velocity vectors at the vented holes. The vectors were colored by the temperature scale. The blue color corresponded to the lowest temperature (1.0°C) and

the red one corresponded to the highest temperature (4.5°C).

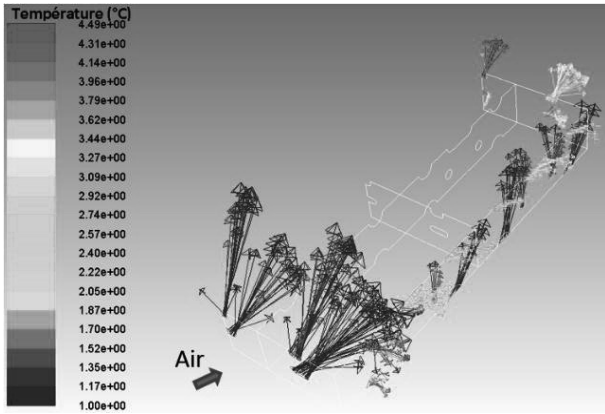


Figure 3 Velocity vectors at vented holes (with natural convection)

In the direction of inflow air, cold air entered the pallet by the vented holes of the first line of cardboard. Then air warmed up as it passed through the pallet. Hot air exited by the vented holes towards the end with smaller velocity. On the side faces, cold air entered through the bottom holes and mixed with hot air inside the pallet then hot air evacuated by the top holes. This air movement enhances heat exchange since heat can be evacuated not only by the main airflow direction but also by the side holes. It can be assumed that this air movement was driven by natural convection.

Figure 4 shows the temperature contour in the horizontal plane in the middle of the products. The temperature varied between 1.1°C (blue color) and 5.5°C (red color).

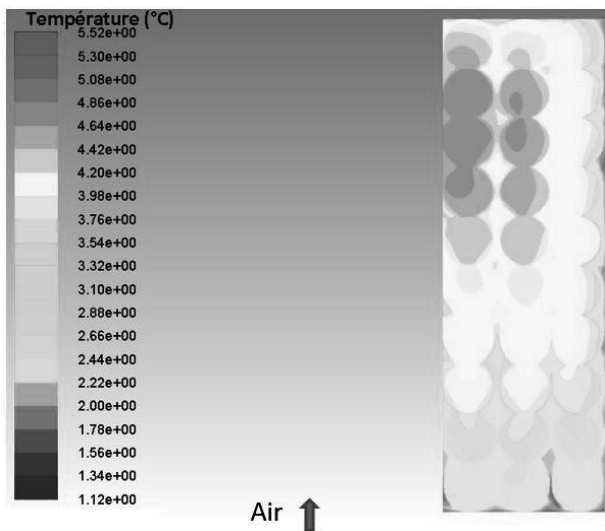


Figure 4: Product temperature contour (with natural convection)

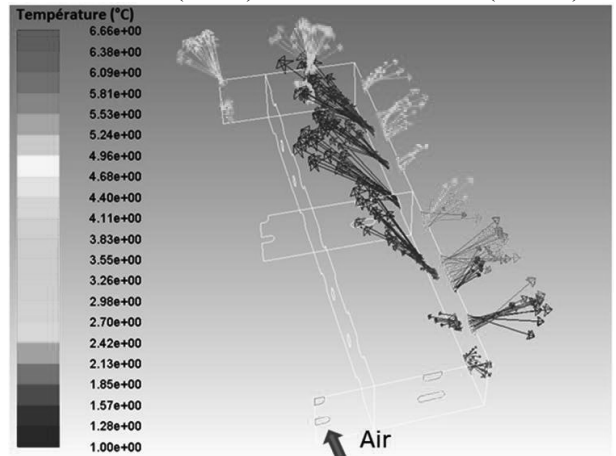
The general trend showed that the temperature rises along the main flow direction (from the ventilated face to the opposite one), hence blue and green colors for the first cheeses. However, the further the products are from the main entrance, the hotter they were, hence the presence of red color. In the first cardboard, the temperature rises

progressively. In the second cardboard, the maximal temperature is reached at the middle. After that the products temperature decreased. The reason of this decrease in temperature was that air accelerated towards outlet of the cardboard by passing vented holes which promoted the heat exchange. In the side direction, the further the products from the external wall of the pallet, the higher the product temperature is which is logical because heat exchange is due to the weak exchanges with the outside cold air.

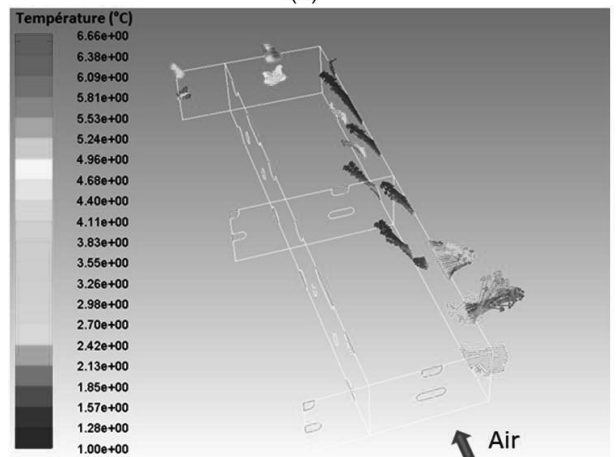
Forced convection (without free convection)

In order to study the influence of the natural convection on the heat exchange and airflow within the pallet, a study of an imaginary case has been carried out in which the density is constant, i.e. density does not depend on the temperature. Other boundary conditions were the same as in the previous case.

The figure 5 shows the velocity vectors at the side vented holes for both cases: with and without natural convection. The vectors are colored by the colors of the temperature: blue - the coldest (1.0°C) and red - the hottest (6.7 °C).



(a)



(b)

Figure 5 Velocity vectors at side vented holes (a) with natural convection (b) without natural convection

In the case without natural convection: air velocity was much lower compared to the case with natural convection. Air leaves the cardboard by the first two vented holes in blowing direction. From the third vented hole, cold air

entered by all the side holes with low velocity. Whereas in the case with natural convection, cold air entered only through the holes at the bottom and the hot air left through the holes at the top. This again confirmed that the upward and downward movements of the air were due to natural convection.

Figure 6 shows the contours of the temperature in the middle of the products in both cases: with and without natural convection. The temperature varies between 1.0°C (blue color) and 8.0°C (red color).

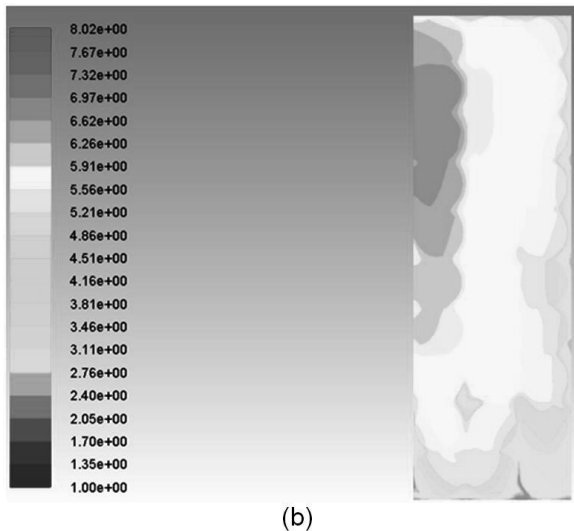


Figure 6: Product temperature contour: (a) with natural convection, (b) without natural convection

The product temperature is much more homogeneous in the case with the natural convection, which is due to a better circulation of the air: indeed, the maximum temperature is of 5.5 ° C (figure 4) whereas that of the case without convection natural is 8°C (figure 6). Moreover, considering the temperature evolution in the side direction in the case without natural convection, a clear difference can be observed between the first and the second cardboard. Products in the left side of the carton have higher temperature than those located at the same location in the case with natural convection. This is due to the fact that air velocity on the side direction is very low therefore heat exchange between two adjacent cardboard is very weak.

CONCLUSION

The airflow and heat transfer within one layer of products generating heat was studied numerically. The model took into account the natural convection due to the respiration activities of the products.

Two simulations were carried out: with and without natural convection. The results showed that the effect of natural convection was significant and cannot be neglected. Natural convection promotes the heat transfer by allowing cold air entering by bottom vented holes and hot air evacuating by top vented holes.

FUTURE WORK

For future work, a model of the whole pallet can be created based on this model. Instead of assuming that the upper and the lower part of the layer are adiabatic, there will be heat exchange between different layers. Due to the great number of mesh, it will not be possible to model the each product of the whole pallet. Therefore, milieu porous can be applied to the other layers. The model will also be validated by our experimental data.

REFERENCES

- Ambaw, A., Bessemans, N., Gruyters, W., Gwanpua, S. G., Schenk, A., De Roeck, A., Delele, M. A., Verboven, P. and Nicolai, B. M. (2016). "Analysis of the spatiotemporal temperature fluctuations inside an apple cool store in response to energy use concerns." *International Journal of Refrigeration* **66**: 156-168.
- Defraeye, T., Cronjé, P., Berry, T., Opara, U. L., East, A., Hertog, M., Verboven, P. and Nicolai, B. (2015). "Towards integrated performance evaluation of future packaging for fresh produce in the cold chain." *Trends in Food Science & Technology* **44**(2): 201-225.
- Delele, M. A., Ngcobo, M. E. K., Getahun, S. T., Chen, L., Mellmann, J. and Opara, U. L. (2013). "Studying airflow and heat transfer characteristics of a horticultural produce packaging system using a 3-D CFD model. Part I: Model development and validation." *Postharvest Biology and Technology* **86**: 536-545.
- Ho, S. H., Rosario, L. and Rahman, M. M. (2010). "Numerical simulation of temperature and velocity in a refrigerated warehouse." *International Journal of Refrigeration* **33**(5): 1015-1025.
- Hoang, H.-M., Duret, S., Flick, D. and Laguerre, O. (2015). "Preliminary study of airflow and heat transfer in a cold room filled with apple pallets: Comparison between two modelling approaches and experimental results." *Applied Thermal Engineering* **76**: 367-381.
- Moureh, J., Menia, N. and Flick, D. (2002). "Numerical and experimental study of airflow in a typical refrigerated truck configuration loaded with pallets." *Computers and Electronics in Agriculture* **34**(1-3): 25-42.
- Moureh, J., Tapsoba, M. and Flick, D. (2009). "Airflow in a slot-ventilated enclosure partially filled with porous boxes: Part II – Measurements and simulations within porous boxes." *Computers & Fluids* **38**(2): 206-220.
- Zou, Q., Opara, L. U. and McKibbin, R. (2006). "A CFD modeling system for airflow and heat transfer in ventilated packaging for fresh foods: I. Initial analysis and development of mathematical models." *Journal of Food Engineering* **77**(4): 1037-1047.

EDIBLE OIL HYDROGENATION: REVISITED VISCOSITY PREDICTION FOR ACCURATE PROCESS SIMULATION

Pierre Albrand, Anne-Marie Billet,
Carine Julcour and Vincent Gerbaud
Laboratoire de Génie Chimique
Université de Toulouse, CNRS
Toulouse, France
E-mail: pierre.albrand@ensiacet.fr

KEYWORDS

Edible oils, hydrogenation, viscosity, group contribution model

ABSTRACT

In food industry, the treatments applied to edible oils are of primarily importance, as the structure of fatty acid groups and their degree of saturation has a proved impact onto human health. Relevant models for the analysis and the optimization of native edible oil hydrogenation are needed, allowing the accurate account of the evolutive properties of oils during their processing.

A model based on group contribution is presented here to predict edible oil viscosity at given temperature and hydrogenated state. To use this model, the composition (in fatty acids) of the studied oil and its viscosity before hydrogenation have to be known at several temperatures.

INTRODUCTION

Hydrogenation consist of converting carbon-carbon double bounds (insaturations) into single bounds by addition of hydrogen in the presence of solid catalysts. This process is widely used in food industry to minimize edible oil rancidity, ease its packaging and improve the texture and consistency of processed foods. Traditional batch slurry reactors show selectivity issues, by producing high levels of fully saturated and trans fats which are harmful to human health. Thus current research on vegetable oil hydrogenation is focused on favoring partial conversion of the polyunsaturated fatty acids, while keeping *cis* configuration for the remaining double bonds. Innovative catalytic reactors, such as monolith reactor, might help tackle those goals by reducing mass transfer limitations and achieving controlled hydrodynamics (near plug flow behavior for the so-called "Taylor flow" regime). Computational fluid dynamic simulations have to be carried out in order to develop accurate enough sizing tools. These calculations are strongly linked to oil physical properties, especially to their viscosity, which strongly evolves during the reaction: a relevant model is needed to describe in detail its dependence on temperature and insaturation degree.

Various existing models and empirical equations describe temperature-dependence of fatty compound viscosity (Eiteman and Goodrum 1994); (Valeri and Meirelles, 1997); (Rabelo et al., 2000); (Fasina et al., 2006). Azian et al. (2001) predicted the viscosity of pure triacylglycerols constituted of three different fatty acids, based on that of single fatty acid triacylglycerols.

Ceriani et al. (2007) made use of a large database (763 experimental values) to optimize a group contribution model

able to predict temperature-dependent viscosity of triacylglycerols (TAG), which are the major components (>95%) of edible oils. While this model indeed gave satisfying results for pure triacylglycerols with less than 5% of average deviation, its extension to edible oils (of known composition) was much more uncertain with average deviation ranging from 2.8% for corn oil to 28.6% for grapeseed oil. This double observation raises the need of a new model for edible oil undergoing hydrogenation. In this work, we develop a model which uses the same decomposition groups and related parameters of the triacylglycerol molecule as used by the model derived by Ceriani et al. (2007), but refers to known viscosity values of the native (unhydrogenated) oil over a given temperature range.

MATHEMATICAL NOTATIONS AND EQUATIONS

Triacylglycerols (TAG) are esters based on glycerol and fatty acid molecules. Figure 1 shows their general chemical formula.

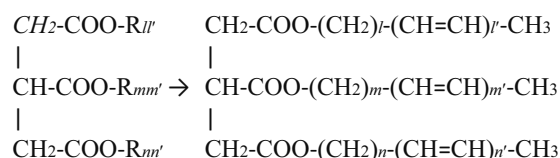


Figure 1: Triacylglycerol Chemical Formula (Ceriani et al. 2007)

Table 1 shows the group decomposition of a TAG molecule as described by Ceriani et al. (2007).

Table 1: Group Decomposition of General TAG Molecule according to Ceriani et al. (2007)

Group	Number
-CH ₂ -CH-CH ₂ -	1
-COO-	3
-CH ₂ -	$l + m + n$
-CH=	$l' + m' + n'$
-CH ₃	3

Therefore, only -CH₂- and -CH= groups vary from one TAG to another depending on the three fatty acids composing them. Knowing the fatty acid composition of a given vegetable oil, an equivalent fatty acid, corresponding to the average numbers of -CH₂- groups (p) and insaturations (p' equal to half the number of -CH= groups), can be deduced, and thus an equivalent TAG composed of three equivalent fatty acids. The equivalent TAG decomposition is displayed in Table 2.

Table 2: Group Decomposition of an Equivalent TAG Molecule according to Ceriani et al. (2007)

Group	Number
-CH ₂ -CH-CH ₂ -	1
-COO-	3
-CH ₂ -	3 <i>p</i>
-CH=	6 <i>p</i> '
-CH ₃	3

Equation (1) gives the temperature-dependent viscosity model proposed by Ceriani et al. (2007).

$$\ln \mu = \sum_k N_k (A_{1k} + \frac{B_{1k}}{T} - C_{1k} \ln T - D_{1k} T) + M [\sum_k N_k (A_{2k} + \frac{B_{2k}}{T} - C_{2k} \ln T - D_{2k} T)] + Q \quad (1)$$

where N_k is the number of k groups and A_{1k} to D_{2k} correspond to optimized coefficients. M is the molecular weight of the considered molecule and Q a corrective term which depends on temperature and varies with the molecule. During hydrogenation, p' groups convert into p groups while carbon number in TAG ($N_{C,TAG}$) remains constant (see Equation (2)).

$$N_{C,TAG} = 9 + 3p + 6p' \quad (2)$$

Knowing the composition of the studied oil before reaction, and therefore $N_{C,TAG}$, Equation (1) is only function of p' and T . By introducing the hydrogenation degree X as defined in Equation (3) where p_0' is the value of p' for the unhydrogenated oil, Equation (1) is now function of X and T (see Equation (4)).

$$X = \frac{p'_0 - p'}{p'_0} \quad (3)$$

$$\ln \mu = K_0 + K_1 X + K_2 X^2 \quad (4)$$

where

$$K_i = A_i + \frac{B_i}{T} - C_i \ln T - D_i T, i = \{0; 1; 2\} \quad (5)$$

In the present work, A_0 to D_0 parameters are identified from the known viscosity values of various raw (unhydrogenated) edible oils, taken at different temperatures, using Matlab R2016b. A_1 to D_1 and A_2 to D_2 are obtained from Equation (1) as a function of Ceriani et al.'s parameters and $N_{C,TAG}$. In other words, the model being specifically calibrated with the oil of interest prior to hydrogenation so as to account for the effect of complex TAG mixture and impurities (up to 4%), it then should give a reliable estimate of viscosity evolution during the reaction through TAG optimized parameters.

VISCOSITY PREDICTION OF HYDROGENATED SUNFLOWER OIL

The model presented above is applied to a refined sunflower oil whose fatty acid composition is given in Table 3. This leads to values for p and p_0' of 12.95 and 1.477, respectively; hence $N_{C,TAG}$ is equal to 56.72.

Table 3: Fatty Acid Composition of Unhydrogenated Sunflower Oil measured at Institut des Corps Gras, Pessac, France in 2017

Fatty Acid	Weight percentage (%)
14:0	0.08
16:0	6.59
16:1	0.14
18:0	3.24
18:1	29.74
18:2	58.75
18:3	0.06
20:0	0.24
20:1	0.16
22:0	0.70
24:0	0.26

Table 4 indicates the viscosity of this sunflower oil measured over the 20°C-80°C range by capillary viscometer.

Table 4: Dynamic Viscosity of Unhydrogenated Sunflower Oil measured at LFCR, Pau, France in 2017

T (°C)	μ (mPa.s)
20	64.00±0.08
40	29.38±0.03
60	16.06±0.02
80	9.95±0.01

Table 5 then gives the calculated parameters for K_0 expression.

Table 5: Parameters of K_0 Expression (Temperature-Dependence of Viscosity for Unhydrogenated Oil)

A_0	-548.78
B_0	20,824
C_0	-90.555
D_0	0.11091

Figures 2 and 3 show the results of Ceriani et al.'s model and of the present model, respectively, for different hydrogenation yields and temperatures. Note that highly hydrogenated sunflower oil might be solid at low temperature. Therefore model prediction in those conditions is not plotted on the figures.

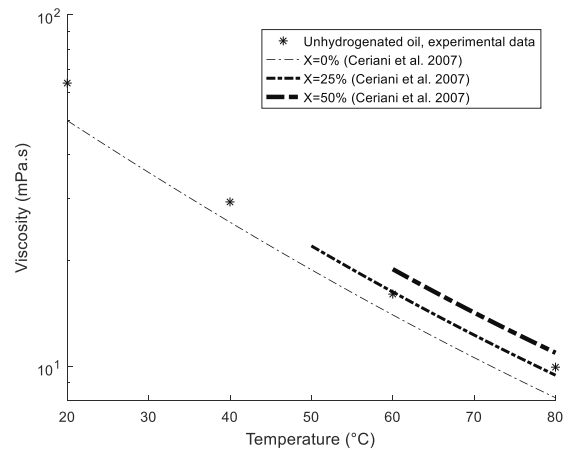


Figure 2: Viscosity Predictions for Partially Hydrogenated Oil according to Ceriani et al. (2007).

The model of Ceriani et al. (2007) underestimates measured raw oil viscosities by 22% at 20°C and by 18% at 80°C.

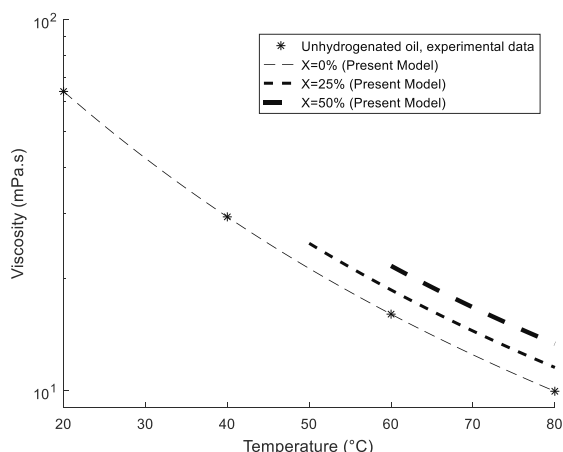


Figure 3: Viscosity Predictions for Partially Hydrogenated Oil for the Present Model.

As it was set on measured viscosities for unhydrogenated oil, the present model corrects this gap. The increase with hydrogenation degree is then similar for both models as expected. For instance, viscosity at 80°C is found to increase by 34% (3,4 cP) at 50% conversion (as compared to raw oil) according to our model. In the range where hydrogenated oil remains liquid, temperature effect is only moderately amplified. To assess model accuracy, partial hydrogenation of refined sunflower oil was carried out in a batch stirred reactor using commercial Pd/Al₂O₃ beads (Alfa Aesar) as a catalyst. Hydrogenation degree was determined from gas chromatography analysis of the processed oil. Its viscosity is available in Table 6. Experimental data for raw and hydrogenated oils are also displayed in Figure 4 along with the predictions of the two models. The average relative deviation for the hydrogenated oil is reduced from 20% to 3.7% with the proposed correction.

Table 6: Dynamic Viscosity of Partially Hydrogenated Sunflower Oil measured at IMFT, Toulouse, France in 2017

T (°C)	μ (mPa.s)
60	19.3
40	15.4
60	12.1
80	9.9

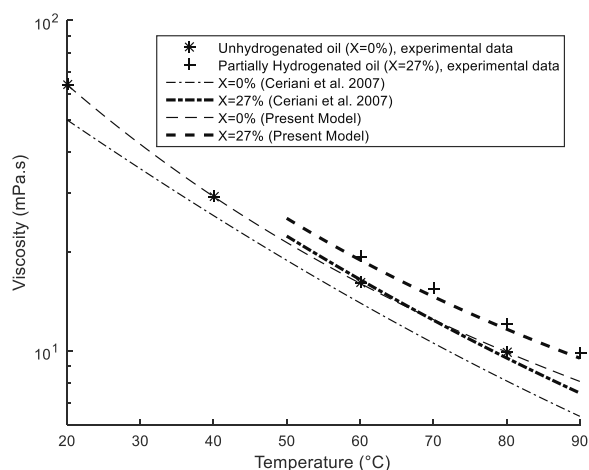


Figure 4: Comparison of the Models - (Ceriani et al., 2007) and present one - with respect to Experimental Data for Raw and Partially Hydrogenated Oils.

CONCLUSION

This revisited model gives satisfying results for sunflower oil and will be further evaluated by the authors for different types of edible oils after partial hydrogenation. Similar approach will be also applied for the prediction of surface tension, based for instance on the work of Diaz-Tovar et al. (2011). These models will be then implemented into a CFD code for the simulation of gas-liquid flows in hydrogenation reactors.

REFERENCES

- Azian, M. N.; Mustafa Kamal, A. A.; Panau, F. & Ten, W. K. "Viscosity estimation of triacylglycerols and of some vegetable oils, based on their triacylglycerol composition" *Journal of the American Oil Chemists' Society*, 2001, 78, 1001-1005
- Ceriani, R.; Gonçalves, C. B.; Rabelo, J.; Caruso, M.; Cunha, A. C. C.; Cavaleri, F. W.; Batista, E. A. C. & Meirelles, A. J. A. "Group Contribution Model for Predicting Viscosity of Fatty Compounds" *Journal of Chemical & Engineering Data*, 2007, 52, 965-972
- Díaz-Tovar, C.-A.; Gani, R. & Sarup, B. "Lipid technology: Property prediction and process design/analysis in the edible oil and biodiesel industries" *Fluid Phase Equilibria*, 2011, 302, 284 - 293
- Eiteman, M. A. & Goodrum, J. W. "Density and viscosity of low-molecular weight triglycerides and their mixtures" *Journal of the American Oil Chemists' Society*, 1994, 71, 1261
- Fasina, O. O.; Hallman, H.; Craig-Schmidt, M. & Clements, C. "Predicting temperature-dependence viscosity of vegetable oils from fatty acid composition" *Journal of the American Oil Chemists' Society*, 2006, 83, 899
- Rabelo, J.; Batista, E.; Cavaleri, F. v. W. & Meirelles, A. J. A. "Viscosity prediction for fatty systems" *Journal of the American Oil Chemists' Society*, 2000, 77, 1255-1262
- Valeri, D. & Meirelles, A. J. A. "Viscosities of fatty acids, triglycerides, and their binary mixtures" *Journal of the American Oil Chemists' Society*, 1997, 74, 1221-1226

Optimal control of fructo-oligosaccharide production

J. Schorsch¹, M. Kinnaert¹, R. Fekih-Salem², L. Dewasme³, C. C. Castro⁴, A. Vande Wouwer³

¹ Department of Control Engineering and System Analysis, Université libre de Bruxelles (Belgium)

² LAMSIN, University of Tunis El Manar (Tunisia)

³ Automatic Control Laboratory, University of Mons (Belgium)

⁴ Applied Chemistry and Biochemistry Department, University of Mons (Belgium)

email: laurent.dewasme@umons.ac.be

KEYWORDS

Pontryagin maximum principle, bang bang control, biotechnology

Abstract

The objective of this study is to determine an optimal substrate feed rate for optimizing the fructo-oligosaccharide production by *Aureobasidium pullulans* in a fed batch reactor. The feed profile is characterized by the feed start time, rate and end time. The optimization is carried out based on a simple dynamic model of the process and using Pontryagin maximum principle in the framework of singular control problems. The resulting control law is of the bang-bang type. The bioreactor is first filled-up at maximum feed rate, followed by a batch phase.

Introduction

Fructo-oligosaccharides (FOS) are dietary carbohydrates, which can be used as an alternative to sugar, offering 30% relative sweetness, and a selective increase of the probiotic bacteria development, with a preventive effect on gastrointestinal diseases, colorectal cancer and diabetes (Tomomatsu 1994). Naturally, FOS can, for instance, be harvested in significant quantities in honey, bananas and rye. However, their industrial production is delicate since several processes are required to reach acceptable degrees of purity (Nobre et al. 2015; 2016).

A convenient way to produce FOS in bioreactors arises from transfructosylation of sucrose (GF), composed of the monosaccharides glucose (G) and fructose (F), through microbial enzymes (fructosyltransferase and β -fructofuranosidase) present in microorganisms such as *Aureobasidium pullulans* (Dominguez et al. 2012) or *Aspergillus* sp. (Rocha et al. 2009). These enzymatic activities produce complex sugars, namely 1-Kestose (GF₂), Nystose (GF₃) and 1-Fructofuranosyl Nystose (GF₄) which constitute the FOS family.

Based on a simple dynamic model of the FOS production in a fed-batch reactor, the objective of this study is to maximize the FOS concentration by manipulating the substrate feed rate. The approach is based on Pontryagin maximum principle, a method that has received considerable attention in the context of bioprocess optimization and control (see e.g.

Van Impe and Bastin (1995), Smets et al. (2004)).

This paper is organized as follows. In Section 2, the dynamic model of fed-batch FOS production is presented. Section 3 deals with the optimal control problem, conclusions are drawn in Section 4.

Modeling FOS production

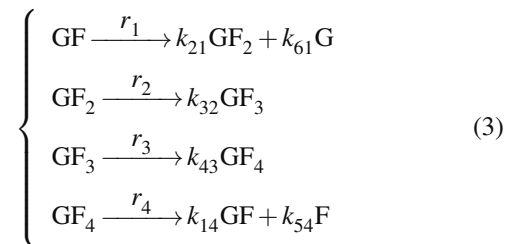
Based on a set of experimental data collected in batch and fed batch experiments, it is possible to derive the minimum number of reactions explaining the data using maximum likelihood principal component analysis (Mailier et al. 2013). A step by step parameter identification procedure can then be followed to estimate the reaction stoichiometry and kinetics. More precisely, the final model involves 8 kinetic parameters and 6 pseudo-stoichiometric coefficients and the mass balance differential equation system is as follows:

$$\begin{cases} [\dot{\text{GF}}] &= -r_1 + k_{14}r_4 + \frac{1}{V}(\text{GF}_{in} - [\text{GF}])Q \\ [\dot{\text{GF}}_2] &= -r_2 + k_{21}r_1 - \frac{[\text{GF}_2]}{V}Q \\ [\dot{\text{GF}}_3] &= -r_3 + k_{32}r_2 - \frac{[\text{GF}_3]}{V}Q \\ [\dot{\text{GF}}_4] &= -r_4 + k_{43}r_3 - \frac{[\text{GF}_4]}{V}Q \\ [\dot{\text{F}}] &= k_{54}r_4 - \frac{[\text{F}]}{V}Q \\ [\dot{\text{G}}] &= k_{61}r_1 - \frac{[\text{G}]}{V}Q \\ \dot{V} &= Q \end{cases} \quad (1)$$

where $[\alpha]$ denotes the concentration (in g.L^{-1}) of the component α . Q represents the substrate feed rate (in L.h^{-1}), which is the manipulated variable. GF_{in} is the substrate concentration (in g.L^{-1}) and V the broth volume (in L). The reaction rates (in $\text{g.L}^{-1}.\text{h}^{-1}$) are defined by Monod laws:

$$r_i = \mu_i^{\max} \frac{[\text{GF}_i]}{K_{m_i} + [\text{GF}_i]}, \text{ with } i = 1, 2, 3, 4, \quad (2)$$

where μ_i^{\max} denotes the maximum rate (in $\text{g.L}^{-1}.\text{h}^{-1}$) of the reaction i . K_{m_i} (in g.L^{-1}) represents the half-saturation constant associated to component i . The corresponding reaction scheme is given by:



Optimization of FOS production

The dynamic model is affine in the input Q and can be cast in the general nonlinear form

$$\frac{dX}{dt} = f(X) + g(X)Q \text{ with } t_0 \leq t \leq t_f \quad (4)$$

with the state vector $X = [GF, GF_2, GF_3, GF_4, F, G, V]$. Function f represents the reaction kinetics while g characterizes the hydrodynamics. At $t = t_0$, the process is initiated with initial concentrations and volume $X(t_0) = X_0$. The final condition is related to the maximum volume V_{\max} (in L) which should be reached at final time:

$$\Omega = V(t_f) - V_{\max} = 0. \quad (5)$$

The performance index J represents the FOS amount at final time:

$$J(t_f) = [GF_2](t_f) + [GF_3](t_f) + [GF_4](t_f) \equiv h(X), \quad (6)$$

The substrate feed rate Q is limited by the feed pump capacity. Let Q_{\max} and Q_{\min} be the upper and lower bounds respectively:

$$Q_{\min} \leq Q \leq Q_{\max}. \quad (7)$$

The objective is to find an admissible control function, $Q(t)$, which yields a system (4) trajectory satisfying (5) and (7) while maximizing the performance index J . Pontryagin maximum principle states that this problem is equivalent to the maximization of the Hamiltonian H (Bryson and Ho 1969):

$$H = \phi + \psi Q \quad (8)$$

where functions $\phi = \lambda^\top f(X)$ and $\psi = \lambda^\top g(X)$.

The costate vector λ is given by:

$$\frac{d\lambda^\top}{dt} = -\frac{\partial H}{\partial X} = -\lambda^\top \frac{\partial f}{\partial X} - \lambda^\top \frac{\partial g}{\partial X} Q. \quad (9)$$

with transversality conditions:

$$\lambda(t_f) = \frac{\partial h(X)}{\partial X} + \nu \frac{\partial \Omega(X)}{\partial X} \quad (10)$$

providing $\lambda_{GF,G,F}(t_f) = 0$, $\lambda_{GF_2,GF_3,GF_4}(t_f) = 1$ and $\lambda_\nu(t_f) = \nu$ with $\nu \in \mathbb{R}$ where λ_α is the costate associated to the state α .

The Hamiltonian (8) is affine in the control input, which is subject to the linear inequality constraints 7, and a "bang-bang" solution exists, consisting in a control sequence made of minimum and maximum input levels and singular arcs. Based on the sign of the Hamiltonian partial derivative with respect to the input Q , i.e. the value of ψ , the "bang-bang" control results from:

$$\begin{cases} \text{if } \psi < 0, \text{ then } Q = Q_{\min}, \\ \text{if } \psi = 0, \text{ then } Q = Q_s, \\ \text{if } \psi > 0, \text{ then } Q = Q_{\max}. \end{cases} \quad (11)$$

The singular control law Q_s is obtained by taking the second time derivative of ψ (see e.g. Bryson and Ho (1969)):

$$Q_s = -\frac{\lambda^\top \left(\frac{\partial q}{\partial X} f - \frac{\partial f}{\partial X} q \right)}{\lambda^\top \left(\frac{\partial q}{\partial X} g - \frac{\partial g}{\partial X} q \right)} \quad (12)$$

Table 1: Optimal control: hardware constraints and initial conditions.

Hardware constraints		Initial conditions	
GF_{in}	280 g.L ⁻¹	$[GF](t_0)$	200 g.L ⁻¹
V_{\max}	3 L	$V(t_0)$	1 L
Q_{\max}	0.5 L.h ⁻¹	$[G](t_0)$ and $[F](t_0)$	0 g.L ⁻¹
Q_{\min}	0 L.h ⁻¹	$[GF_{2,3,4}](t_0)$	0 g.L ⁻¹

under the condition that $\lambda^\top \left(\frac{\partial q}{\partial X} g - \frac{\partial g}{\partial X} q \right) \neq 0$, where q is

$$q = \frac{\partial g}{\partial X} f - \frac{\partial f}{\partial X} g. \quad (13)$$

This criteria is based on the necessary optimality conditions including

$$\frac{\partial H}{\partial Q} = \lambda^\top g = 0. \quad (14)$$

Based on this development, the following 5-step algorithm is proposed:

1. Guess t_f , ν and a substrate feed rate Q respecting the final condition (5), and integrate forward the model defined in (4).
2. Determine λ by integrating backward Equation (9).
3. Integrate forward the model defined in (4) using singular control (11).
4. Repeat Steps 2 and 3, considering $\nu = \nu + \delta\nu$, with $\delta\nu$ as small as required, until $\Omega = 0$.
5. Repeat Steps 2 to 3 with a new guess of t_f in order to maximize the performance index J (6) and nullify Hamiltonian (8).

Numerical results

The dynamic model (1), as well as another candidate model proposed in (Jung et al. 1989) and identified so as to match the available experimental data, are used in the optimization procedure. Initial conditions and constraints are listed in Table 1.

The two optimization problems (based on the two candidate models) lead to similar input trajectories (i.e., the feed rate represented in subplot A of Fig. 1): a fed-batch phase of approximately 4 hours at maximum flow rate $Q_{\max} = 0.5 \text{ L.h}^{-1}$ until the bioreactor is completely filled, followed by a batch phase ($Q_{\min} = 0 \text{ L.h}^{-1}$). This profile maximizes the productivity of GF_2 , direct by-product of the inlet substrate GF.

Model (1) suggests a reaction rate r_1 which always remains below the maximum value μ_1^{\max} , and a global reaction rate, defined by $f_{GF_2} + f_{GF_3} + f_{GF_4}$, increasing even after the fed-batch phase and reaching a maximum within 10 hours (see subplot C in Fig. 1). The model of (Jung et al. 1989) behaves slightly differently with r_1 first at its maximum, thus implying a maximal global reaction rate (subplot C in Fig. 1) during the fed-batch phase followed by a decrease when the bioreactor is no longer fed. Consequently, the predicted productivity and yield (given by Equations (15)) are 2.75

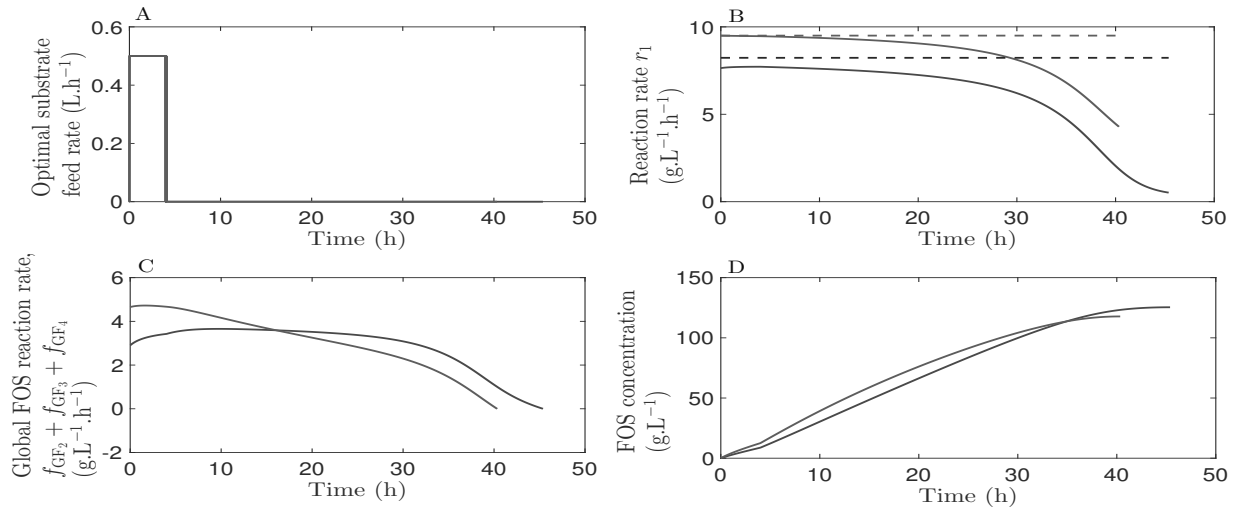


Figure 1: Subplot A shows the optimal substrate feed rate. Subplot B shows the reaction rates (continuous lines) and the associated maximum rates (dotted line). The global FOS production rate is displayed in subplot C. Subplot D shows the evolution of the FOS concentrations. The blue and red colors correspond respectively to model (1) and the model from (Jung et al. 1989).

$\text{g.L}^{-1}.\text{h}^{-1}$ and 49.3% with model (1). These numbers have to be compared to the prediction based on the model of (Jung et al. 1989), which is a slightly higher productivity of $2.92 \text{ g.L}^{-1}.\text{h}^{-1}$ and lower yield of 46.5%. Indeed, in the first case, 125 g.L^{-1} of FOS are obtained after 45.4 hours while in the second case, 118 g.L^{-1} are obtained after 40.3 hours.

$$\begin{cases} \mathcal{P}(t_f) = \frac{[\text{GF}_2](t_f) + [\text{GF}_3](t_f) + [\text{GF}_4](t_f)}{V(t_f)}, \\ \mathcal{Y}(t_f) = V_{\max} \frac{[\text{GF}_2](t_f) + [\text{GF}_3](t_f) + [\text{GF}_4](t_f)}{[\text{GF}](t_0)V(t_0) + \text{GF}_{\text{in}}(V_{\max} - V(t_0))}. \end{cases} \quad (15)$$

Conclusion

A bang-bang control strategy is proposed for the optimization of the FOS production, which consists in a fed-batch phase at maximum flow rate followed by a batch phase.

Acknowledgements

The authors gratefully acknowledge the financial support from the F.R.S.-FNRS, the Belgium National Fund for the Scientific Research, (PDR: T.0196.13).

References

Bryson A.E. and Ho Y.C., 1969. *Applied optimal control*. Ginn and Co, Waltham, Mass.

Dominguez A.; Nobre C.; Rodrigues L.R.; Peres A.M.; Rocha I.; Lima N.; and Teixeira J.A., 2012. *New improved method for fructooligosaccharides production by Aureobasidium pullulans*. *Carbohydrate Polymers*, 89, no. 4, 1174–1179.

Jung K.; Run J.W.; Kang K.R.; Lim J.Y.; and Lee J.H., 1989. *Mathematical model for enzymatic production of fructo-*

oligosaccharides from sucrose. *Enzyme Microb Technol*, 11, 491–494.

Mailier J.; Remy M.; and Vande Wouwer A., 2013. *Stoichiometric identification with maximum likelihood principal component analysis*. *J Math Biol*, 67, 739–765.

Nobre C.; Castro C.; Hantson A.L.; Teixeira J.; De Weireld G.; and Rodrigues L., 2016. *Strategies for the production of high-content fructo-oligosaccharides through the removal of small saccharides by co-culture or successive fermentation with yeast*. *Carbohydrate polymers*, 136, 274–281.

Nobre C.; Teixeira J.A.; and Rodrigues L.R., 2015. *New trends and technological challenges in the industrial production and purification of fructo-oligosaccharides*. *Critical Reviews in Food Science and Nutrition*, 55, 1444–1455.

Rocha O.; Nobre C.; Dominguez A.; Torres D.; Faria N.; Rodrigues L.; Teixeira J.A.; Ferreira E.C.; and Rocha I., 2009. *A dynamical model for the fermentative production of fructooligosaccharides*. *Computer Aided Chemical Engineering*, 27, 1827–1832.

Smets I.Y.; Claes J.E.; November E.J.; Bastin G.P.; and Van Impe J.F., 2004. *Optimal adaptive control of (bio)chemical reactors: past, present and future*. *Journal of Process Control*, 14, 795–805.

Tomomatsu H., 1994. *Health effects of oligosaccharides*. *Food Technol*, 48, 61–65.

Van Impe J.F. and Bastin G., 1995. *Optimal adaptive control of fed-batch fermentation processes*. *Control Eng Practice*, 3, no. 7, 939–954.

Modeling and Simulation in Innovative Food Production and Processing Technologies

MODELLING AND VALIDATION OF TIME-TEMPERATURE HISTORY AND ENZYME INACTIVATION IN THE CONTINUOUS FLOW MICROWAVE-ASSISTED PASTEURIZATION OF APPLE JUICE

Érica S. Siguemoto, Carmen C. Tadini and Jorge. A. W. Gut
Dept. Chemical Engineering, Escola Politécnica
FoRC – Food Research Center / University of São Paulo
05508-010, São Paulo,
Brazil
E-mail: jorgewgut@usp.br

KEYWORDS

Chemical engineering, Differential equations, Model evaluation, Validation.

ABSTRACT

Modelling the time-temperature history of a continuous flow thermal process is useful to evaluate temperature induced changes such as inactivation of microorganisms/enzymes or degradation of quality/sensory attributes. In this work the microwave assisted pasteurization of a low viscosity liquid food is modelled considering tubular heat exchangers, single mode microwave applicator and holding tube. Temperature distribution was determined based on overall heat transfer coefficients and mean residence times. Model validation was carried on for the processing of cloudy apple juice at three temperatures (70 °C, 80 °C and 90 °C), two flow rate levels and two heating modes (conventional and microwave) using a pilot scale unit. Polyphenol oxidase (PPO) inactivation was determined using kinetic parameters. Measured temperatures after heating, holding and cooling steps agreed with model predictions, as well as the residual PPO activity after processing. Focused microwave heating provided high heating rates, providing enzymatic inactivation similar to that from an ideal process with no over-processing.

INTRODUCTION

Continuous flow focused microwave heating is an emerging technology in food processing and an attractive alternative to heat exchangers in food pasteurization due to fast volumetric heating and lower tube surface temperature (Zhu et al., 2007). Consequently, microwave-assisted pasteurization has a potential to reduce nutritional and sensorial losses that occurs in conventional thermal processing (Tang, 2015).

Proper design of a pasteurization process requires the selection of optimal conditions to achieve the safety requirements and to minimize food quality degradation (Ling et al., 2015). Kinetic models help to understand the mechanisms of change during food processing and allow optimizing and predicting the final product characteristics. These mathematical models describe the inactivation of biochemical parameters, such as microorganisms, enzymes and chemical compounds, or physical changes (van Boekel, 2008). The biochemical parameters most used to assess the

quality of pasteurized apple juice are enzymes (Siguemoto et al., 2018a) and microorganisms (Tajchakavit et al., 1998; Cañumir et al., 2002; Gentry and Roberts, 2005).

The polyphenoloxidase (PPO) activity in fruit juice is associated with the decrease of consumer acceptance due to changes of nutritional (oxidation of phenolic compounds, carotenoids and ascorbic acid) and organoleptic (oxidation of sugars and enzymatic browning) properties (Aka et al., 2013). Apple enzymes showed to be more thermal resistant than microorganisms, then PPO activity was used as an indicator for pasteurization of apple juice (Siguemoto et al., 2018a).

Continuous flow thermal processing of liquid foods has three steps: heating, holding and cooling. For food safety purposes, the target microorganism inactivation is evaluated only in the holding tube at maximum velocity (tube centre) and lower temperature (tube outlet). However, the residence time in the heating step and compensation for temperature drop at holding tube also contribute with thermally induced changes (Aguilar and Gut, 2014).

In order to properly evaluate the changes in thermal processing, the whole time-temperature history of the product must be known, as well as the kinetics equations and parameters. The objectives of this work were to: 1) model the time-temperature history and quality change of a low viscosity liquid food processed in a microwave-assisted pasteurizer; 2) validate the modelling for apple juice processing using polyphenol oxidase (PPO) as a time-temperature integrator (Tucker, 1999); 3) compare results from conventional and microwave heating modes.

MODELLING OF TIME-TEMPERATURE HISTORY

Figure 1 presents a diagram of the microwave assisted pasteurization process, which is based on the pilot-scale unit Lab25-UHT/HTST EHVH (MicroThermics, Raleigh, USA). Processed product was cloudy apple juice (*Malus domestica* Borkh, cv Fuji Suprema). Heater 1 and Cooler are counter-current coil heat exchangers linked to an 18 kW hot water and a 3.5 kW cold water circuits, respectively. Heater 2 is a microwave heater with a single mode cavity connected to a 6 kW magnetron (2450 MHz). With tuning, microwaves were focused on a central ceramic tube with minimal reflected power (< 20 W). The holding section was a thermally insulated holding tube with the residence time of

18 s (bulk velocity) at nominal flow rate of 0.5 L/min. There were nine temperature transmitters (TT in Fig. 1) and data were recorded every 10 s. Temperature at TT3 was automatically controlled by manipulating the power level of the hot water circuit whereas temperature TT4 was controlled by the manipulation of the magnetron power level.

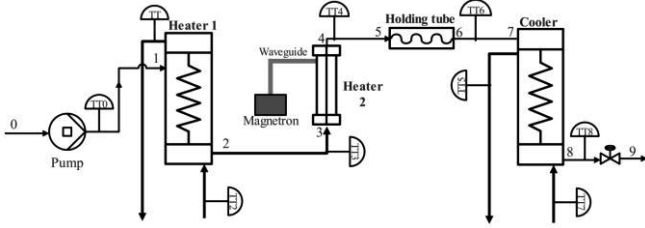


Figure 1: Diagram of pilot-scale microwave pasteurizer

The time-temperature history was determined based on the average velocity of the product along its path. Based on the internal volumes, the average residence times from points 1 to 8 in Fig. 1 were determined from the ratio between volume and volumetric flow rate (Siguemoto et al., 2018b).

For the prediction of the average temperature profile, steps 1-2, 2-3, 3-4, 4-5 and 6-7 were assumed isothermal because of their short length or low heat loss. For the heat exchangers (steps 1-2 and 7-8), the overall heat transfer coefficient was defined in order to determine the internal temperature profile. Correlations adjusted by Siguemoto et al. (2018b) for water were used:

$$q = U \cdot A_e \cdot \Delta T_{lm} \quad (1a)$$

$$\frac{1}{U \cdot A_e} = a + \frac{b}{Re^c} \quad (1b)$$

where q is the heat load, U the overall heat transfer coefficient, $A_e = \pi \cdot d_o \cdot L$ the reference heat transfer area, d_o the external diameter, L the tube length, ΔT_{lm} the logarithmic mean temperature difference, $Re = d_i \cdot v \cdot \rho / \mu$ the Reynolds number, d_i the internal diameter, $v = 4 \cdot Q / \pi \cdot d_i^2$ the average velocity, Q the volumetric flow rate, ρ the density and μ the viscosity. Parameters determined for Heater 1 were $a = 1.65 \cdot 10^{-3}$ K/W, $b = 1.02$ K/W and $c = 0.866$ ($4.2 \cdot 10^3 \leq Re \leq 8.1 \cdot 10^3$), while parameters for Cooler were $a = 3.53 \cdot 10^{-3}$ K/W, $b = 1.05$ K/W and $c = 0.706$ ($3.5 \cdot 10^3 \leq Re \leq 8.4 \cdot 10^3$). Thermo-physical properties of apple juice were calculated for the average temperature using correlations from Constenla et al. (1989) and Gentry and Robert (2005).

A linear temperature change was assumed in Heater 2, from point 3 to the TT4 set-point, because of the short residence time in the applicator (2 s at 0.5 L/min). In the holding tube, heat loss with $U = 8$ W/K.m² (Siguemoto et al, 2018b) was considered, independent of the flow rate since forced internal convection is not the limiting thermal resistance.

Temperature profiles of the hot and cold fluids in Heater 1 and Cooler were determined from Eqs.(2a) and (2b):

$$\frac{dT_{cold}(x)}{dx} = \frac{U \cdot \pi \cdot d_o}{\dot{m}_{cold} \cdot C_{p,cold}} \cdot (T_{hot} - T_{cold}) \quad (2a)$$

$$\frac{dT_{hot}(x)}{dx} = \frac{U \cdot \pi \cdot d_o}{\dot{m}_{hot} \cdot C_{p,hot}} \cdot (T_{hot} - T_{cold}) \quad (2b)$$

where $\dot{m} = \rho \cdot Q$ is the mass flow rate and x the axial coordinate. Properties of water were evaluated at average temperature using correlations compiled by Gut and Pinto (2003). By discretizing the tube length in 100 slices with thickness $\Delta x = L/100$, temperature profile was estimated using a finite difference method (Beers, 2006):

$$T_{cold}(x + \Delta x) \cong T_{cold}(x) + \frac{dT_{cold}}{dx} \cdot \Delta x \quad (3a)$$

$$T_{hot}(x + \Delta x) \cong T_{hot}(x) + \frac{dT_{hot}}{dx} \cdot \Delta x \quad (3b)$$

Similarly, temperature profile in the holding tube was obtained from Eqs. (2a) and (3a) considering the surrounding air as the cold fluid.

To numerically solve these equations, boundary conditions were needed. At Heater 1, inlets were specified based on average measurements of TT0 and TT2 (Fig. 1). For the holding tube, the inlet T_5 was the TT4 set-point. At Cooler, inlets came from calculated T_6 and measurements of TT7. Since flow is counter-current in the exchangers, the outlets of the utility fluids were adjusted at $x = 0$ using Excel 2016 Solver (Microsoft, Redmond, USA) to result in the desired inlet at $x = L$.

MODELING OF ENZYMATIC INACTIVATION

Siguemoto et al. (2018a) studied the thermal inactivation of polyphenol oxidase (PPO) in cloudy apple juice and adjusted a first order kinetic model with two isoenzymes (thermolabile and thermostable). This model has five parameters: $D_{l,ref}$ and $D_{s,ref}$ are the reference D-values of the thermolabile and thermostable isoenzymes; z_l and z_s are the z-values of the thermolabile and thermostable isoenzymes; and α is the initial activity fraction due to the thermolabile isoenzyme (Liing and Lund, 1978). For an isothermal process at temperature T for time t , Eqs.(4), (5a) and (5b) provide the residual enzymatic activity:

$$\frac{A}{A_0} = \alpha \log\left(\frac{-t}{D_l}\right) + (1 - \alpha) \log\left(\frac{-t}{D_s}\right) \quad (4)$$

$$D_l = D_{l,ref} \log\left(\frac{T_{ref} - T}{z_l}\right) \quad (5a)$$

$$D_s = D_{s,ref} \log\left(\frac{T_{ref} - T}{z_s}\right) \quad (5b)$$

where A is the enzymatic activity in the time t , A_0 the initial activity and $\log()$ the antilogarithm function.

The reported kinetic parameters of PPO inactivation at $T_{ref} = 80$ °C by conventional heating were $\alpha = 0.148$, $D_{l,ref} = 27.7$ s, $D_{s,ref} = 42.3$ s, $z_l = 3.52$ °C and $z_s = 50.7$ °C, while for PPO inactivation by microwave heating $\alpha = 0.147$, $D_{l,ref} = 48.9$ s, $D_{s,ref} = 57.8$ s, $z_l = 7.42$ °C and $z_s = 94.6$ °C (Siguemoto et al., 2018a).

For a non-isothermal process with a time-temperature history $T(t)$, the equivalent processing time at the reference temperature or integrated lethality (F_{ref}) can be calculated from Eqs.(6a) and (6b) for each isoenzyme. Therefore, the predicted residual activity for a non-isothermal treatment can be determined from Eq. (7).

$$F_{l,ref} = \int_0^t \text{alog} \left(\frac{T(t) - T_{ref}}{z_l} \right) dt \quad (6a)$$

$$F_{s,ref} = \int_0^t \text{alog} \left(\frac{T(t) - T_{ref}}{z_s} \right) dt \quad (6b)$$

$$\frac{A}{A_0} = \alpha \text{alog} \left[\frac{\int_0^t \text{alog} \left(\frac{T(t) - T_{ref}}{z_l} \right) dt}{D_{l,ref}} \right] + (1 - \alpha) \text{alog} \left[\frac{\int_0^t \text{alog} \left(\frac{T(t) - T_{ref}}{z_s} \right) dt}{D_{s,ref}} \right] \quad (7)$$

The time-temperature history obtained from the model described in the previous section was included in Eq.(7) and the integrals were numerically solved by the trapezium method.

MODEL SIMULATION AND EXPERIMENTAL VALIDATION

Twelve experiments of cloudy apple juice pasteurization were conducted: three processing temperatures (70 °C, 80 °C and 90 °C), two flow rates and two heating modes (conventional – C and microwave – M). These processing conditions were based on commercial pasteurization of apple juice (Tajchakavit et al., 1998; Sinha, 2012) and heat resistance of apple juice enzymes (Siguemoto et al., 2018a). Table 1 presents the conditions with corresponding flow rates and set-points for TT3 and TT4. These temperature set-points were chosen so that the desired processing temperature could be obtained at TT6, compensating heat losses along the product path.

Table 1: Flow Rate and Temperature Set-Points for Cloudy Apple Juice Pasteurization by Conventional (C) and Microwave (M) Heating

Id.	Flow rate (L/min)	Temperature (°C)	Set-point TT3 (°C)	Set-point TT4 (°C)
C1	0.5	70	73.5	–
C2	0.9	70	72.3	–
C3	0.5	80	84.3	–
C4	0.9	80	82.6	–
C5	0.5	90	94.8	–
C6	0.9	90	93.0	–
M1	0.4	70	30.0	71.5

M2	0.8	70	30.0	71.2
M3	0.4	80	30.0	82.4
M4	0.8	80	30.0	81.5
M5	0.4	90	30.0	92.6
M6	0.8	90	30.0	91.6

For the microwave assisted pasteurization runs, Heater 1 was used as a pre-heater to obtain a temperature of 30 °C at the inlet of Heater 2. Tested flow rates were 0.4 and 0.8 L/min. For the conventional heating runs, the microwave heater was off. Since the internal volume of Heater 2 contributes with holding, the flow rate in conventional runs was increased by 12% (0.45 L/min had to be rounded up to 0.5 L/min because 0.1 L/min was the allowable flow rate step-change).

Equipment start-up was made with water and the juice was introduced after steady-state. Only after the maximum residence time of the process at the given flow rate (Siguemoto et al., 2018b) was exceeded, 500 mL samples of processed juice were collected at the outlet. Treated apple juices were immediately stored in a plasma freezer 349FV (Fanem, São Paulo, Brazil) at - 30 °C, and later thawed for PPO activity assay.

Polyphenol oxidase (PPO) activity was assessed spectrophotometrically in quadruplicates as described by Siguemoto and Gut (2017), measuring the absorbance at 420 nm during the reaction of the juice sample with pyrocatechin (Sigma Aldrich, St Louis, USA).

The simulation of the model provided values for product temperatures from points 1 to 8 in Fig. 1, which were combined with the mean residence times of each step to generate the time-temperature history of the product. The relative absolute error between model prediction and measurements for T_3 , T_6 and T_8 were calculated for each experimental run for comparison and validation. The measured residual activity at the end of the process was compared with the model prediction based on the time-temperature history and kinetics.

RESULTS AND DISCUSSION

Figure 2 shows, as example, the measured temperatures along the product path and the predicted temperature profiles from the model simulation for pasteurized apple juice by conventional and microwave heating at processing conditions of C3 and M3, respectively. It can be seen that the processing temperature is achieved half-way through the heat exchanger in C3; consequently, the product is exposed to high temperature more than necessary. This happened because this heat exchanger was designed to reach higher temperatures (excess area). On the other hand, a fast increase in product temperature was observed in microwave pasteurization (M3) (52 °C raise in 2.4 s).

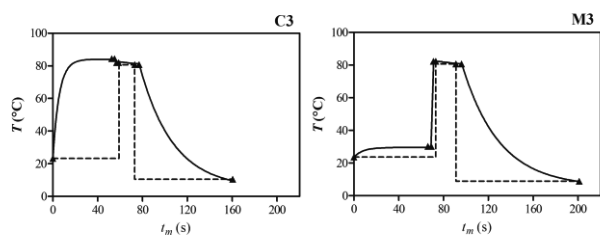


Figure 2: Temperature Profiles of Pasteurized Apple Juice at Experiments C3 and M3, Showing Measured Temperatures (▲), Model Prediction (—) and Ideal Case (---).

Figure 2 also includes dashed lines showing a hypothetical ideal process with instantaneous heating and cooling steps and isothermal holding. In this unit the heating step is close to ideal when using Heater 2. This could reduce the over-processing associated with long come-up times and increase product quality (Tang, 2015). The prediction of temperature profile at other processing conditions were similar to that presented in Fig. 2.

For both heating modes, predicted temperatures at the outlet of Heater 1 (T_3), Holding tube (T_6) and Cooler (T_8) are in good agreement with the experimental data. The average relative error on the pasteurization temperature prediction (T_6) was only 0.2%, while the largest average relative error (19.0%) was on the prediction of the exit temperature (T_8). The modelling slightly underestimated the exit temperature; however, the lethality contribution from the end of the cooling section is negligible, thus not compromising the evaluation of enzymatic inactivation.

The experimental residual activities of PPO were measured at the end of the process (step 9 in Fig. 1) and compared to residual activities predicted by the model. Table 2 presents the results for each processing condition. Results of residual activity were lower than ideal due to over-processing (non-isothermal tube and contribution from heating and cooling steps).

Table 2: Experimental and Model Predicted Residual PPO Activity after Processing and Ideal Values

Id.	Experimental	Model	Ideal
C1	0.22 ± 0.01	0.18	0.66
C2	0.40 ± 0.01	0.30	0.79
C3	0.09 ± 0.01	0.01	0.40
C4	0.00 ± 0.01	0.06	0.61
C5	0.00 ± 0.01	0.00	0.24
C6	0.00 ± 0.01	0.02	0.42
M1	0.13 ± 0.01	0.18	0.63
M2	0.24 ± 0.01	0.33	0.79
M3	0.12 ± 0.01	0.05	0.47
M4	0.00 ± 0.01	0.20	0.69
M5	0.00 ± 0.01	0.02	0.34
M6	0.00 ± 0.01	0.12	0.54

Figure 3 shows the parity charts of predicted versus experimental values of A/A_0 . The calculated residual activities of PPO were close to the predictions obtained from

model simulation for both conventional and microwave heating.

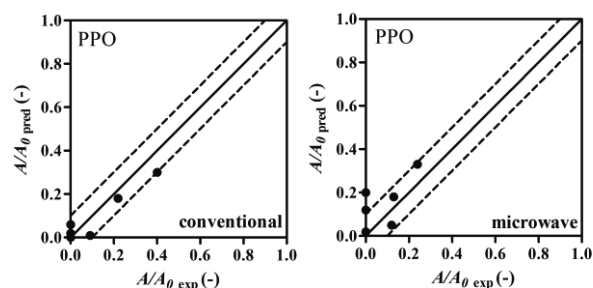


Figure 3: Parity Charts for PPO Residual Activities under Conventional and Microwave Processing. Dashed Lines Indicate ± 10%

CONCLUSIONS

The proposed model provided the time-temperature history for the cloudy apple juice pasteurization and predicted residual activity of PPO at the outlet. Twelve conditions were experimentally tested and temperature and activity predictions are close to experimental values. Since microwave heating was faster, over-processing was smaller than when using the heat exchanger. Evaluation of nutritional or quality parameters, as bioactive compounds, vitamins, colour and volatile compounds, are needed to assess improvements from microwave-assisted processing.

REFERENCES

- Aguilar, H.F. and Gut, J.A.W. 2014. "Continuous HTST pasteurization of liquid foods with plate heat exchangers: Mathematical modeling and experimental validation using a time-temperature integrator". *Journal of Food Engineering*, 123, 78-86.
- Aka, J.P.; Courtois, F.; Louarme, L.; Nicolas, J.; and Billaud, C. 2013 "Modelling the interactions between free phenols, L-ascorbic acid, apple polyphenoloxidase and oxygen during a thermal treatment". *Food Chemistry*, 138, 1289-1297.
- Beers, K.J. 2006. *Numerical Methods for Chemical Engineering*. Cambridge University Press, Cambridge.
- Cañumir, J.A.; Celis, J.E.; de Bruijn, J.; and Vidal, L.V. 2002. "Pasteurisation of apple juice by using microwaves". *LWT - Food Science Technology*, 35(5), 389-392.
- Constenla, D.T.; Lozano, J.E.; and Crapiste, G.H. 1989. "Thermophysical properties of clarified apple juice as a function of concentration and temperature". *Journal of Food Science*, 54 (3), 663-668.
- Gentry, T.S. and Roberts, J.S. 2005. "Design and evaluation of a continuous flow microwave pasteurization system for apple cider". *LWT - Food Science Technology*, 38(3), 227-238.
- Gut, J.A. and Pinto, J.M. 2003. "Modeling of plate heat exchangers with generalized configurations". *International Journal of Heat and Mass Transfer*, 46(14), 2571-2585.
- Liing, A.C. and Lund, D.B. 1978. "Determining kinetic parameters for thermal inactivation of heat-resistant and heat-labile isoenzymes from thermal destruction curves". *Journal of Food Science*, 43 (4), 1307-1310.
- Ling, B.; Tang, J.; Kong, F.; Mitcham, E.J.; and Wang, S. 2015. "Kinetics of food quality changes during thermal processing: a review". *Food and Bioprocess Technology*, 8(2), 343-358.

- Siguemoto, É.S. and Gut, J.A.W. 2017. "Validation of spectrophotometric microplate methods for polyphenol oxidase and peroxidase activities analysis in fruits and vegetables". *Food Science and Technology (Campinas)*, 37, 148-153.
- Siguemoto, É.S.; Pereira, L.J.; and Gut, J.A.W. 2018a. "Inactivation kinetics of pectin methylesterase, polyphenol oxidase and peroxidase in cloudy apple juice under microwave and conventional heating to evaluate non-thermal microwave effects". *Food Bioprocess and Technology*, under review.
- Siguemoto, É.S.; Pires, M.N.; Funcia, E.S.; and Gut, J.A.W., 2018b. "Evaluation of a continuous flow microwave pasteurization unit for liquid foods: residence time distribution, heat transfer and integrated lethality". *Journal of Food Engineering*, under review.
- Sinha, N.K. 2012. "Apples". In: *Handbook of fruits and fruit processing*, N. K. Sinha; J. S. Sidhu; J. Barta, J. S. B. Wu; and M. Pilar Cano (Eds.), John Willey & Sons, New York, 265-278.
- Tajchakavit, S.; Ramaswamy, H.S.; and Fustier, P. 1998. "Enhanced destruction of spoilage microorganisms in apple juice during continuous flow microwave heating". *Food Research International*, 31(10), 713-722.
- Tang, J. 2015. "Unlocking potentials of microwaves for food safety and quality". *Journal of Food Science*, 80(8).
- Tucker, G. 1999. "A novel validation method: Application of time-temperature integrators to food pasteurization treatments". *Food and Bioprocess Processing*, 77(3), 223-231.
- Van Boekel, M.A., 2008. *Kinetic modeling of reactions in foods*. CRC press, Boca Raton.
- Zhu, J.; Kuznetsov, A.V.; and Sandeep, K.P. 2007. "Mathematical modeling of continuous flow microwave heating of liquids (effects of dielectric properties and design parameters)". *International Journal of Thermal Sciences*, 46(4), 328-341.

ACKNOWLEDGEMENT

The authors acknowledge the financial support from the São Paulo Research Foundation – FAPESP (grants numbers 2013/07914-8 and 2014/06026-4).

AUTHOR BIOGRAPHIES

ÉRICA S. SIGUEMOTO is a food engineer and obtained her master degree in public health nutrition at the University of São Paulo (2013). Now she is a Ph.D. student at the Department of Chemical Engineering, University of São Paulo, under the supervision of Professor Jorge A. W. Gut. Her Ph.D. research focuses on the microwave-assisted pasteurization of fruit juices. E-mail: erica.siguemoto@usp.br, ORCID: 000-0003-3868-5984

CARMEN C. TADINI is a food engineer and obtained her Ph.D. at University of São Paulo (1994). Currently is full professor at the Chemical Engineering Department of USP and is vice-coordinator of the Food Research Center (FoRC) since 2013. Field of study is novel food processing technologies and innovation. E-mail: catadini@usp.br, ORCID: 0000-0002-0811-5430

JORGE A. W. GUT is a chemical engineer and obtained his Ph.D. at University of Sao Paulo (2003). Currently is associate professor at the Chemical Engineering Department of USP and studies continuous processing of liquid foods. Email: jorgewgut@usp.br, ORCID: 0000-0001-6447-8490

A Long-Short-Term Memory Network Model for Biscuit Baking

Alberto Tonda, Nathalie Perrot
UMR 782 GMPA, Team MALICES, INRA
1 av. Lucien Brétignières, 78850, Thiverval-Grignon, France
email: {alberto.tonda,nathalie.perrot}@inra.fr

KEYWORDS

Food process modelling, Neural networks, LSTM, Biscuit baking

ABSTRACT

Long-Short-Term Memory (LSTM) networks are a relatively recent addition to the field of Artificial Neural Networks (ANNs). LSTM networks are specifically tailored for machine learning of time series, where the outputs of a system are not just a function of their inputs, but also of an internal state. The state itself can be seen as dependent on the historical series of all inputs seen by the system up to that point in time. In this paper, we present an application of LSTM networks to the modeling of biscuit baking. Starting from 16 real-world time series of biscuit baking, gathered by the United Biscuits company under different conditions, we show how the proposed LSTM network can correctly predict unseen values. Remarkably, the network is also able to reproduce a dynamic behavior up to variations that might be overlooked as noise.

INTRODUCTION

The process of baking biscuits in industrial ovens involves several biochemical and physical phenomena, including gelatinization of starch, denaturation of proteins, and Maillard reactions. Given this complexity, creating a physically accurate mathematical model of the biscuit baking process seems a daunting task. A possible alternative is to use a data-driven approach, for example a machine learning technique, to derive a black-box model of the whole process from experimental data, to then test its prediction capabilities on unseen data. Such an approach would also ease the difficulty in modeling outputs such as biscuit color, that are traditionally hard to describe mathematically. While most machine learning approaches are unable to deal with time-dependent systems, a specific class of Artificial Neural Networks (ANNs), called Long-Short-Term memory (LSTM) networks, currently represent the state of the art for several applications related to time series.

This paper presents a LSTM-based approach to machine learning the biscuit baking process. Starting from a training dataset of real-world time series of biscuit

baking, collected by the company United Biscuits, the proposed approach learns the dynamics of two output variables of interest, color and weight loss, and it is then tested on an unseen test dataset.

BACKGROUND

In this section, minimal information about biscuit baking and LSTM Networks are given, in order to introduce the scope of the present work.

Biscuit baking

Industrial biscuit baking aims to transform raw biological materials into a final product which satisfies multiple criteria. For example, thickness and weight of the biscuits can create issues for packaging, if they are not constrained between specific thresholds; on the other hand, the color of the product must be pleasant to the eye of the customer. The transformation process from dough to biscuit is performed in tunnel ovens, and it is the result of complex coupled biochemical and physical phenomena still not completely understood and controlled (Savoye et al. (1992)).

The principal biochemical reactions in the process are gelatinization of starch, denaturation of proteins, and Maillard reactions, that give browned food its distinctive flavor; all these phenomena are linked to temperature, humidity, and water activity inside the biscuit (Wade (1988)). Moreover, conduction, radiation and convection contribute to different degrees to baking, depending on the design of the industrial baking oven. A precise mathematical description of such heat-mass transfers is far from trivial, as the properties of the product change constantly during the process, and little information about the thermal properties of commercial doughs is available. Finally, it would be extremely useful to include the evolution of sensory characteristics of biscuits, such as loss of moisture, formation of color, and change in mass, in the mathematical description of the process; but describing a relationship between such characteristics and the control variables is not straightforward.

Given this complexity, it is not surprising that several approaches have been proposed to model and control the industrial baking process, ranging from fuzzy logic (Per-

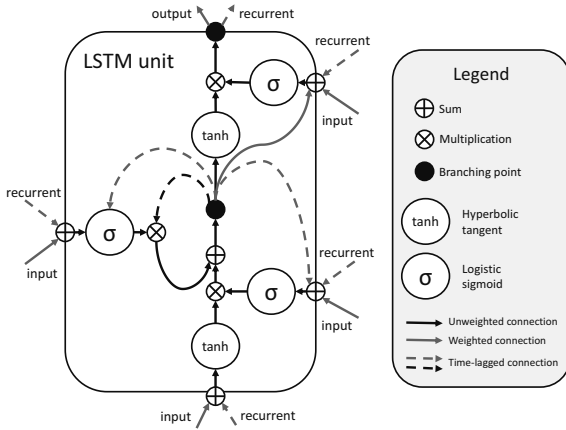


Figure 1: Basic unit of a LSTM network.

rot et al. (2000), Perrot et al. (2006)), to heat-transport models (Sablani et al. (1998), Trystram et al. (1993)), to models tackling air properties in tunnel ovens (Mirade et al. (2004)).

LSTM networks

LSTM networks (Hochreiter and Schmidhuber (1997), Gers et al. (1999)) are a category of ANNs, more specifically belonging to the class of Recurrent Neural Networks (RNNs). Classical ANNs (Rosenblatt (1958)) are machine learning approaches loosely inspired by neural networks in the brain, that can work as general function approximators. ANNs are composed by a series of units called *artificial neurons* connected to each other, able to receive and send signals. Usually, the signal at a connection between artificial neurons is a real number, and the output of each artificial neuron is calculated by a non-linear function of the weighted sum of its inputs. Like other machine-learning approaches, ANNs can *learn* to approximate an unknown function by tuning the weights in the artificial neurons from a dataset featuring several combinations of inputs and outputs for a target phenomenon, termed *training set*. ANNs are then usually tested on a dataset of unseen values, called *test set*, to verify whether they were able to learn a configuration of weights that generalizes well.

While ANNs are an effective approach, routinely used in applications ranging from games (Silver et al. (2016)) to image classification (Sermanet et al. (2013)), they can only model processes for which the outputs depend exclusively on the current inputs. In several real-world process, however, the outputs are also a function of an internal state, that is itself dependent on the history of inputs until that point. RNNs (Hopfield (1987)) try to address this issue, by adding connections between units to form directed cycles. Thanks to this feedback mechanisms, RNNs can exhibit dynamic temporal behavior, and are used in issues where the sequence of inputs is

relevant for the outputs, such as speech recognition or natural language analysis. Among the different types of RNNs, LSTM networks are one of the most recent proposed paradigms. In a LSTM network, each unit is considerably more complex than a simple artificial neuron in an ANN (see Figure 1). A common LSTM unit is composed of a cell, an input gate, an output gate and a forget gate. The cell is responsible for storing values over an arbitrary time interval, while each gate regulates the flow of values that goes through the connections of the LSTM: the input gate controls the extent to which a new value flows into the cell, the forget gate controls the extent to which a value remains in the cell and the output gate controls the extent to which the value in the cell is used to compute the output activation of the LSTM unit. Thanks to the ability of storing information over variable intervals of time, LSTM currently represent the state of the art in several domains, such as speech recognition (Xiong et al. (2017)).

DATASET

Sixteen time series of biscuit cooking under different conditions have been gathered by United Biscuits, Inc.¹, in the scope of the DREAM FP7 European Project Axellos (2009-2013). The oven used during the experiments features four different zones, with different temperatures. During the cooking process, biscuits are slowly moved from one zone to the next on metal trays, while the heat flux in the oven is manually regulated by an employee. The considered input variables are: tf (heat flux measured in the top part of the oven, W/m^2), bf (heat flux measured in the bottom part of the oven, W/m^2), z_c (nominal heat flux in the current zone of the oven, W/m^2), and $z_{p1} \dots z_{p4}$ (nominal heat flux in the previous zones of the oven that the biscuit tray has already passed, W/m^2). The considered output variables are: c (color of the biscuits, based on the reflected light measured in lm), and wl (weight loss of the biscuits, measured in g). Each variable is measured every 5 s, with each baking process lasting 350 s, giving a total of 70 points per time series. Color is always measured on the same individual reference biscuit during the whole time series, weight loss is taken as an average on the same 3 reference biscuits during the experiment. Additionally, the initial conditions of variables c , and wl are used as inputs during the experiments.

Out of the 16 time series, several are repetitions of an experiment under the same conditions (in groups of 3, 3, 2, 3, 2, 3 time series, respectively). Table 1 summarizes the features of the dataset. Figure 2 shows an example of time series, highlighting the non-negligible differences even between repetitions under the same conditions. Another notable feature is that output variable wl presents a behavior that, at a first glance, seems ex-

¹United Biscuits, <http://www.unitedbiscuits.com/>

Table 1: Summary of the 16 time series on biscuit cooking gathered by United Biscuits. During the experiments, the temperature in different zones of the oven is changed, in order to explore several possible behaviors.

ID	Training?	Heat flux (W/m^2)				
		z1	z2	z3	z4	z5
std-1	yes	2500	3500	4000	4000	2000
std-2	yes	2500	3500	4000	4000	2000
stdval	no	2500	3500	4000	4000	2000
T1-1	yes	4000	3500	4000	4000	2000
T1-2	yes	4000	3500	4000	4000	2000
T1val	no	4000	3500	4000	4000	2000
T2-1	yes	2500	3500	4000	4000	3000
T2-2	yes	2500	3500	4000	4000	3000

ID	Training?	Heat flux (W/m^2)				
		z1	z2	z3	z4	z5
T3-1	yes	2500	3500	6000	4000	2000
T3-2	yes	2500	3500	6000	4000	2000
T3val	no	2500	3500	6000	4000	2000
T4-1	yes	2500	3500	4000	6000	2000
T4-2	yes	2500	3500	4000	6000	2000
T5-1	yes	2500	5000	1000	5000	2000
T5-2	yes	2500	5000	1000	5000	2000
T5val	no	2500	5000	1000	5000	2000

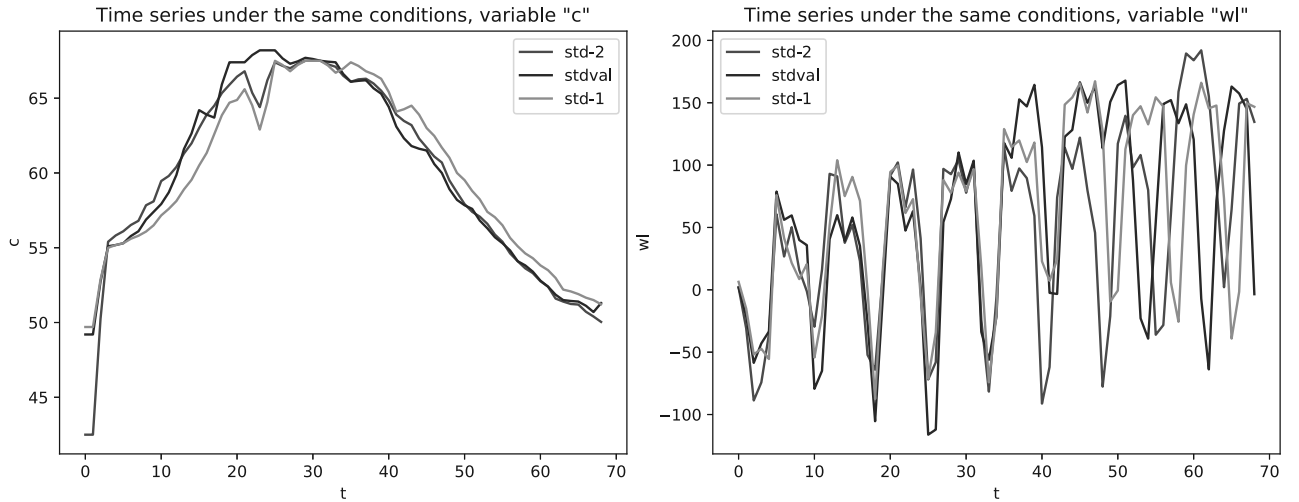


Figure 2: Comparison of three time series run under the same conditions (labeled **std-1**, **std-2**, **stdval**). It is immediately noticeable how the series differ from each other. Interestingly, the behavior of output variable wl seems to indicate the presence of a considerable amount of noise.

tremely noisy.

EXPERIMENTAL RESULTS

The 16 time series are split into a training set (12 time series) and a test set (4 time series), that will be unseen by the LSTM network during the training phase. The test set has been selected among the repetitions of experiments in conditions already present in the training set. All variables have been normalized by subtracting the mean and scaling to unit variance, on the basis of the values contained in the training set. After a few tentative runs, the parameters of the network are configured as follows: 8 inputs (all previously described input variables plus the initial conditions for the 2 output variables), 50 units in a single hidden layer, 2 outputs (all output variables); `tanh` activation function, 3000 training epochs, RMSprop gradient descent optimizer (Hinton et al. (2014)). All the code of the machine learning algorithm is implemented in the Keras (Chol-

let et al. (2015)) and `scikit-learn` (Pedregosa et al. (2011)) Python libraries.

The final model has excellent fitting on the test set, with mean squared error $MSE = 0.015$ and $R^2 = 0.9863$. An interesting result is that, visually, the model is able to reproduce trends in unseen data that at a first glance might be mistaken for noise: for example, in Figure 3, the model is able to closely predict the behavior of wl , showing that the signal-to-noise ratio is better than what a human expert could have considered from a superficial analysis of the data.

CONCLUSIONS

In this paper, a new data-driven approach to modeling biscuit cooking is presented. Exploiting a class of artificial neural networks known as long-short-term memory networks, the approach is tested on a real-world dataset collected by the company United Biscuits. The proposed methodology is proved capable of accurately pre-

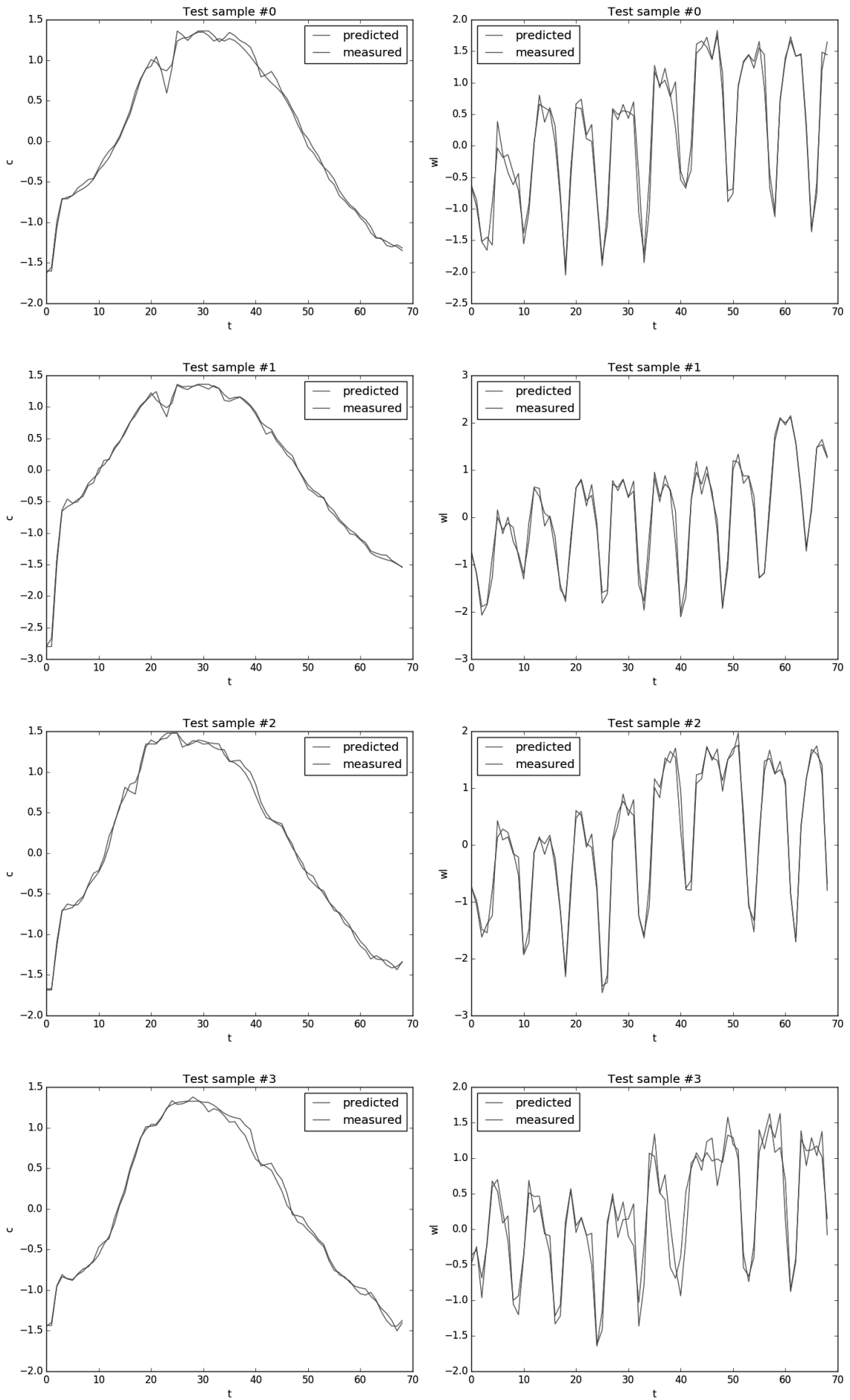


Figure 3: Predictions of the trained model on the unseen test data of the time series labeled **stdval**. The scale is different from the previous plots, as all variables have been normalized.

dicting the dynamics of biscuit cooking, even for features that are classically hard to predict, such as the color of the biscuits. Future works will focus on testing the approach under different conditions, focusing first on the variation of humidity.

REFERENCES

- Axellos M., 2009-2013. *DREAM - Design and development of REAListic food Models with well-characterised micro- and macro-structure and composition*.
- Chollet F. et al., 2015. *Keras*. <https://github.com/fchollet/keras>.
- Gers F.A.; Schmidhuber J.; and Cummins F., 1999. *Learning to forget: Continual prediction with LSTM*.
- Hinton G. et al., 2014. *Neural Networks for Machine Learning*. http://www.cs.toronto.edu/~tijmen/csc321/slides/lecture_slides_lec6.pdf.
- Hochreiter S. and Schmidhuber J., 1997. *Long short-term memory*. *Neural computation*, 9, no. 8, 1735–1780.
- Hopfield J.J., 1987. *Neural networks and physical systems with emergent collective computational abilities*. In *Spin Glass Theory and Beyond: An Introduction to the Replica Method and Its Applications*, World Scientific. 411–415.
- Mirade P.; Daudin J.; Ducept F.; Trystram G.; and Clement J., 2004. *Characterization and CFD modelling of air temperature and velocity profiles in an industrial biscuit baking tunnel oven*. *Food research international*, 37, no. 10, 1031–1039.
- Pedregosa F.; Varoquaux G.; Gramfort A.; Michel V.; Thirion B.; Grisel O.; Blondel M.; Prettenhofer P.; Weiss R.; Dubourg V.; Vanderplas J.; Passos A.; Cournapeau D.; Brucher M.; Perrot M.; and Duchesnay E., 2011. *Scikit-learn: Machine Learning in Python*. *Journal of Machine Learning Research*, 12, 2825–2830.
- Perrot N.; Ioannou I.; Allais I.; Curt C.; Hossenlopp J.; and Trystram G., 2006. *Fuzzy concepts applied to food product quality control: A review*. *Fuzzy sets and systems*, 157, no. 9, 1145–1154.
- Perrot N.; Trystram G.; Guely F.; Chevré F.; Schoeseters N.; and Dugre E., 2000. *Feed-back Quality Control in the Baking Industry Using Fuzzy Sets*. *Journal of food process engineering*, 23, no. 4, 249–279.
- Rosenblatt F., 1958. *The perceptron: A probabilistic model for information storage and organization in the brain*. *Psychological review*, 65, no. 6, 386.
- Sablani S.; Marcotte M.; Baik O.; and Castaigne F., 1998. *Modeling of simultaneous heat and water transport in the baking process*. *LWT-Food Science and Technology*, 31, no. 3, 201–209.
- Savoie I.; Trystram G.; Duquenoy A.; Brunet P.; and Marchin F., 1992. *Heat and mass transfer dynamic modelling of an indirect biscuit baking tunnel-oven. Part I: Modelling principles*. *Journal of food engineering*, 16, no. 3, 173–196.
- Sermanet P.; Eigen D.; Zhang X.; Mathieu M.; Fergus R.; and LeCun Y., 2013. *Overfeat: Integrated recognition, localization and detection using convolutional networks*. *arXiv preprint arXiv:13126229*.
- Silver D.; Huang A.; Maddison C.J.; Guez A.; Sifre L.; Van Den Driessche G.; Schrittwieser J.; Antonoglou I.; Panneershelvam V.; Lanctot M.; et al., 2016. *Mastering the game of Go with deep neural networks and tree search*. *nature*, 529, no. 7587, 484–489.
- Trystram G.; Fahloul D.; Duquenoy A.; and Al-lache M., 1993. *Dynamic modelling and simulation of the biscuit baking oven process*. *Computers & Chemical Engineering*, 17, S203–S208. doi: 10.1016/0098-1354(93)80230-k. URL [https://doi.org/10.1016/0098-1354\(93\)80230-k](https://doi.org/10.1016/0098-1354(93)80230-k).
- Wade P., 1988. *Biscuit, cookies and crackers: The principles of the craft. Vol. I*.
- Xiong W.; Wu L.; Alleva F.; Droppo J.; Huang X.; and Stolcke A., 2017. *The Microsoft 2017 Conversational Speech Recognition System*. Tech. rep.

On the quantification of the impact of natural antimicrobials on the growth kinetics of *Listeria* in complex food models

**Katherine Costello
Madeleine Bussemaker
Eirini Velliou***

Bioprocess and Biochemical
Engineering group (BioProChem),

Department of Chemical and
Process Engineering,
University of Surrey,
Guildford GU2 7XH, UK

Jorge Gutierrez-Merino

Department of Nutritional
Sciences,

University of Surrey,
Guildford GU2 7XH, UK

**Maria Baka
Jan Van Impe**

Chemical and Biochemical
Process Control Laboratory
(BioTeC⁺), KU Leuven,
Sustainable Chemical Process
Technology,
Campuses Ghent & Aalst,
Gebroeders de Smetstraat 1,
9000 Ghent, Belgium

* Corresponding author: Dr ir Eirini Velliou, e.veliou@surrey.ac.uk, Fax: 0044-(0)-1483683010

KEYWORDS

Antimicrobial resistance, predictive modelling, *Listeria*, food microstructure, Xanthan gum, nisin.

ABSTRACT

Recent studies report an increase in antimicrobial resistance (AMR) in *Listeria* species. Most available studies on the AMR of *Listeria* are conducted in liquid systems, however *Listeria* can be present in solid or structured food products, e.g. soft cheeses, salmon or meat products. Food structure can affect the bacterial dynamics and/or antimicrobial resistance. In this work, we systematically study the growth kinetics of *Listeria*, as influenced by the natural antimicrobial nisin on complex food models. *L. innocua* was grown in colonies on solid matrices comprising Tryptic Soy Broth with Xanthan gum, Whey protein isolate, or both (biphasic system), in the presence or absence of nisin at 10°C, 30°C and 37°C. The growth kinetics of *Listeria* were affected by the structure of the matrices, and by the presence of nisin. The action of nisin on *Listeria* was different depending on the system composition and the temperature. Our findings give an insight into the growth of *Listeria* in the presence of nisin in model systems of varied structural complexity, and highlight the importance of accounting for stress adaptation in solid/structured systems when designing decontamination processes with natural antimicrobials.

INTRODUCTION

There is an increasing demand for foods that are minimally processed in order to retain their natural colouring, nutritional content, taste and texture (Ale et al., 2015; Valdramidis and Koutsoumanis, 2016). To achieve this, there is great interest in minimal food processing, such as the treatment of food products with natural antimicrobial compounds (Troy et al., 2016). Minimal processing is less harsh when compared to classical sterilisation, pasteurisation or antibiotics, and so there is the potential for such processing conditions to present a mild, sublethal stress,

inducing an adaptive response in bacteria consequently allowing post-treatment survival (EFSA, 2015). Antimicrobial resistance in food-borne pathogenic bacteria is an emerging threat to public health worldwide, with an increase in resistant bacterial strains – particularly *Listeria monocytogenes* – reported in recent years (Escolar et al., 2017). This is of concern as the effective treatment of listeriosis infections in humans may become compromised resulting in higher mortality rates (EFSA, 2015). Thus, it is important to understand how AMR is developed in bacteria in response to such treatments for the effective use of natural antimicrobials in food processing.

Most studies on the AMR of *Listeria* are conducted in liquid systems, with the effect of the (food) system structure on the development of AMR in microorganisms still poorly understood. In real food products, *Listeria* can be found in solid or solid(like)/structured food systems, e.g., soft cheeses, ice cream, fish and meat products. Cells grown in a solid system grow in colonies and experience a completely different environment to planktonic growth in liquid systems. Cells grown as colonies experience diffusional limitations of oxygen and nutrients and accumulation of (acidic) metabolic products around the colony, causing a self-induced (acid) stress that may affect the microbial kinetics and the microbial environmental response (Wilson et al., 2002; Velliou et al., 2013, Skandamis & Jeanson, 2015). Furthermore, microorganisms could display a different level of AMR development. Bacteria found in foods are also likely to grow in co-culture which can result in stress due to competition and/or extracellular metabolic products. For example, lactic acid bacteria (LAB) are natural producers of nisin, an antimicrobial, and LAB are found in similar foods to *Listeria*. Therefore, in order to achieve a fundamental understanding of the AMR development of *Listeria* in food systems in response to nisin it is important to conduct kinetic experiments in model systems that mimic as accurately as possible the microstructure of solid or solid(like) food systems.

The present work is a systematic comparative study of the microbial dynamics of *Listeria*, as influenced by the presence of nisin, i.e. a natural antimicrobial produced by

lactic acid bacteria on solid(like)/structured systems of various structural complexities at a range of growth temperatures.

MATERIALS AND METHODS

Inoculum preparation

L. innocua ATCC 33090 stock cultures were provided by the University of Surrey, and stored at -20°C in liquid medium containing Tryptic Soy Broth (TSB), supplemented with glycerol. Frozen cultures were thawed and a loopful was precultured in 15 ml of TSB (Oxoid Ltd., Basingstoke, UK) supplemented with 0.6% w/v yeast extract (Oxoid Ltd., Basingstoke, UK) (TSBYE) for 9.5 hours at 37°C. 20 µL was transferred to a fresh 15 ml of TSBYE and cultured for 15 hours at 37°C until early stationary phase (10⁹ CFU/ml).

Preparation of structured food models

Monophasic solid food model systems were prepared using Xanthan gum as per the method of Ale et al. (2015). For the conduction of microbial growth experiments the solid medium was removed from the falcon tube to a sterile petri plate, and cut into discs approximately 5 mm thickness.

For biphasic food model systems, Whey protein isolate (WPI) (Prolacta® 95 Instant Native Whey Protein Isolate, Bacarel, UK) was added to TSBYE at a concentration of 10% w/v and stirred for 1 hour until dissolved using a magnetic stirrer plate (HB502, Bibby Sterilin Ltd, UK). 5% w/v Xanthan gum in TSBYE was added in a 1:1 ratio, and the mixture mechanically stirred for 6 min, then prepared as for the monophasic gel systems.

For experiments *in the presence of nisin*, a sublethal level of nisin (140 IU/ml) was added to the monophasic Xanthan gum systems to represent an additional (mild) stress. Nisin was added after autoclaving as its' stability is jeopardized at high temperatures. Experiments with nisin took place for 3% and 5% Xanthan gum but not for 7% Xanthan gum nor for the biphasic system, as a homogeneous distribution of nisin in those two later systems was not possible due to their structural complexity.

Confocal Microscopy

For Xanthan gum gels, 300 µL of the appropriate viscoelastic gel was transferred into a well chamber, inoculated with 10³ CFU/ml cells and incubated at the appropriate temperature until early stationary phase. Surface colonies were visualised using DAPI (Sigma Aldrich, Germany): 20 µL of a 1 µg/ml solution was added to each well chamber for 20 min, before rinsing with phosphate buffered saline (PBS, Oxoid Ltd., UK). Samples were imaged using a commercial laser scanning confocal microscope (CLSM) (Ti-Eclipse Inverted Microscope System, Nikon Instruments Europe, 60x magnification, oil immersion).

For the Xanthan gum/Whey protein system, phase separation was visualised by adding 20 µL of a 0.01% w/v Rhodamine B solution (Sigma Aldrich, Germany) to 40 ml of biphasic mixture during gel preparation before the autoclaving step. Rhodamine B binds to the protein phase only, allowing for definition between the two phases (Boons et al., 2013a,

2014; Tromp et al., 2001). Samples were prepared and surface colonies were visualised in the same way as for monophasic systems. The colony size/distribution followed a similar pattern for all temperatures under study, therefore images are shown in this paper only for 37°C.

Growth experiments

Growth curves at 10°C, 30°C and 37°C were obtained for the growth of *L. innocua* on 3%, 5%, and 7% Xanthan gum (XG) gelified systems, and also on the 5% Xanthan gum / 10% Whey protein (XG/WPI) mixture. The initial cell density was adjusted to 10³ CFU in 50 µL of inoculum. 50 µL of inoculum was dropped and distributed onto the surface of a disc. A sample was processed every hour (30°C, 37°C), or twice a day (10°C) by transferring the sample to a stomacher bag (BA6040, Seward, UK) and adding a suitable volume of PBS for an initial dilution of 1/10. The contents were stomached for 1 min (Colworth Stomacher 80, Seward, UK), and 100 µL taken from the bag using pipettes for viscous media (MICROMAN® E, Gilson Ltd, USA). Decimal dilutions were prepared in TSBYE (900 µL), and surface plated on TSAYE agar (Oxoid Ltd., UK) for enumeration of *L. innocua*. Plates were incubated for 24 hours at 37°C before enumeration.

Estimation of growth parameters and statistical analysis

Growth data were natural log-transformed and plotted as a function of time. The Baranyi and Roberts growth model was fitted to the data:

$$\frac{dN(t)}{dt} = \frac{Q(t)}{1 + Q(t)} \cdot \mu_{max} \cdot \left[1 - \left(\frac{N(t)}{N_{max}} \right)^m \right] \cdot N(t)$$
$$\frac{dQ}{dt} = \mu_{max} \cdot Q \quad (1)$$

With N(t) (CFU/ml) the cell density at time t; N_{max} (CFU/ml) the maximum value for N(t) when the model is fitted independently to each species in co-culture; Q(t) the physiological state of the cells; μ_{max} (1/h) the maximum specific growth rate (Baranyi & Roberts, 1994). Matlab version R2017a (The Mathworks Inc., Natick, USA) was used for these plots and for data analysis. Optimisation of the model fit was achieved by using the function lsqnonlin. The variance-covariance matrix was used to obtain standard deviations of the parameter estimates.

RESULTS & DISCUSSION

Microbial spatial organisation

The distribution and size of stationary phase *L. innocua* colonies at 37°C on 3%, 5% and 7% monophasic XG systems as well as on the 5%XG/10%WPI biphasic system was investigated using CLSM. The most representative images are displayed in Figure 1.

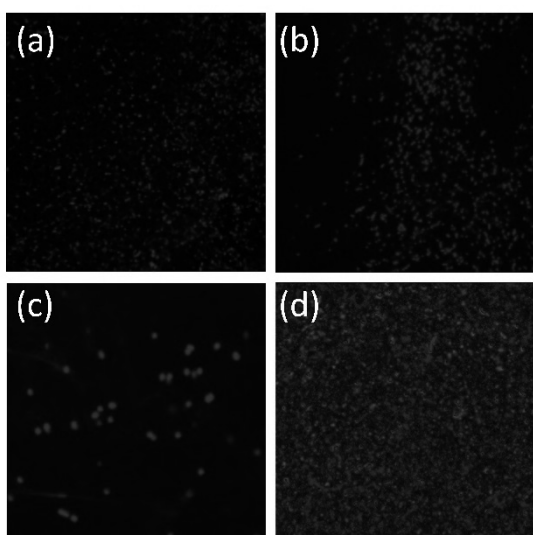


Figure 1: CLSM images showing surface growth of *L. innocua* at 37°C for (a) 3%XG, (b) 5%XG, (c) 7%XG monophasic systems, and (d) 5%XG/10%WPI biphasic system. Colonies are dyed with DAPI (blue), the WPI phase with Rhodamine B (red), while XG is not dyed (black).

For the **biphasic 5%XG/10%WPI system** *L. innocua* is observed to grow only on the protein phase (WPI) (Figure 1d). More specifically, bacterial localisation on the protein phase is confirmed as it is clear that DAPI positive areas (blue), i.e., colonies, are always located only on the top of the Rhodamine-positive area (red) which surrounds them (Figure 1d).

This finding, to the best of our knowledge, is the first observation of the selectivity of Listeria towards the protein phase on a biphasic XG/WPI system, and the first study for microbial surface growth on such a system. There are only two studies previously investigating microbial growth in biphasic protein/polysaccharide systems, but not for surface growth nor for *Listeria*. Boons et al. (2013a, 2014) investigated the immersed growth of *E. coli* at 23.5°C in a dextran/gelatin phase-separated system of varying composition, and observed selective growth in the dextran phase, reversely to our observations. Léonard et al. (2013) observe preferential immersed growth of *L. lactis* in the protein phase of a complex liquid caseinate/alginate biphasic system. There are several potential explanations for our observation of the preferential localisation of *L. innocua* on the WPI phase (Figure 1d). The adhesion of bacterial cells to surfaces is known to be related to surface properties such as hydrophobicity and electrostatic interactions (Léonard et al., 2013). More specifically, when whey proteins are heated at temperatures higher than 70°C, the structure unfolds resulting in the surfacing of hydrophobic protein groups and the development of a generally hydrophobic molecule following gelation (Liu et al., 2005). Xanthan gum is known to be a hydrophilic polymer (Kar et al., 2010), and *Listeria* species are known to be hydrophobic (Takahashi et al., 2010). Thus, hydrophobic/hydrophilic interactions make it more preferable for *Listeria* to attach to the hydrophobic protein phase of the current system (as observed on Figure 1d). It is noted that all phases in the current study have a negative electrostatic charge (Briandet et al., 1999; Zhang et al., 2014), thus hydrophobicity is the more important

interaction (rather than electrostatic interactions between the media and the cells).

For microbial growth at 37°C on the **XG monophasic systems**, colony size is observed to increase as the Xanthan gum concentration increases (Figure 1a, 1b, 1c), suggesting that viscosity affects the colony size on the system. The increase in concentration of XG is linked to surface tension, changes of which could directly cause an increase in colony size. More specifically, it has been shown that the surface tension of a XG system decreases as the XG concentration increases (Muthamizhi et al., 2014). As the concentration of XG increases, the contact angle of the colony to the XG surface reduces, which could facilitate the outward growth of a bacterial colony to a larger diameter than the one that would be reached at a lower concentration/higher contact angle, as observed in the present study. Our findings are in agreement with Be'er et al. (2009) who showed that *P. dendritiformis* colonies on agar are larger on systems containing a higher concentration of surfactant, i.e. lower surface tension. Similarly, Rook and Bruckman (1953) showed that *E. coli* colonies growing on gelatin become larger as various surfactants, which act to decrease surface tension, are added.

Microbial dynamics in the food models

The growth kinetics of *L. innocua* were obtained for growth on the monophasic 3%, 5%, and 7% XG systems and on the biphasic 5%XG/10%WPI system at 10°C, 30°C, and 37°C. Figure 2 shows the fits of the Baranyi and Roberts microbial growth model on the mean experimental data.

The influence of temperature on the growth parameters is evident for all systems in this study; generally, as expected, it is observed that *L. innocua* grows faster at higher temperatures (Figure 2).

No significant differences are observed for any of the growth parameters in the various XG gel systems for a specific temperature (Figure 2a, 2b, 2c) thus indicating that the system viscosity had little or no effect on the surface growth kinetics. The lack of differences on the microbial dynamics could be attributed to (i) the gelling agents used or (ii) the high concentration of XG used in these systems in comparison to other studies. More specifically, very few food models study the microbial growth kinetics using XG as a gelling agent (Ale et al., 2015; Boons et al., 2013b). Instead most studies use gelatin at a concentration range of 1-35% w/v (for example, Aspridou et al., 2014; Boons et al., 2013b; Brocklehurst et al., 1997; Smet et al., 2015) or agar at a concentration range of 1-10% w/v (for example, Flourey et al., 2013; Robinson et al., 1991; Skandamis et al., 2007; Stecchini et al., 2001). Xanthan gum, gelatin and agar have significantly different rheological properties which could affect the microbial growth dynamics. In the present study high concentrations of XG were used (3-7% w/v) in comparison to previous studies using the same gelling agent where a maximum of 2.5% w/v XG was used (Ale et al., 2015; Boons et al., 2013b). This indicates that it is likely there is a “threshold” below which variations in the concentration of Xanthan gum affect the growth kinetics of *L. innocua*, and above which no differences are observed.

Microbial dynamics in the food models in the presence of nisin

As previously mentioned, a sublethal level of nisin was added to the monophasic 3% and 5% XG systems to represent an additional (mild) stress. The microbial growth kinetics were monitored at all three temperatures under study. The Baranyi & Roberts model fits on the mean experimental data are shown in Figure 2.

For all conditions under study, as previously noted for nisin-free systems, the maximum growth rate μ_{max} decreases as the temperature decreases, with no significant differences observed for μ_{max} with varied XG concentration at a specific temperature (as with nisin-free systems), as can be seen in Figures 2b and 2c. A more significant inhibitory effect of nisin on growth is observed at 10°C (Figure 2a), where a significant disturbance in growth is observed as the concentration of XG is increased, with effectively no growth occurring on the 5% XG nisin-rich system (Figure 2a). Additionally, while growth is observed for the 3% XG nisin-rich system, it is greatly affected by the presence of nisin, with a significant reduction in N_{max} of approximately 4 ln CFU/ml in comparison to the nisin-free system (Figure 2a). This observation suggests a significant influence of system structure/stiffness in combination with nisin at suboptimal temperatures. As discussed previously (microscopy section), larger surface colonies are observed as the concentration of XG increases, related to a reduction in surface tension which facilitates the outward growth of colonies to a larger diameter (Figure 1a, 1b, 1c). This suggests that, as the colony becomes larger at higher concentrations of XG (Figure 1c), more cells are in contact with the 5% XG surface containing nisin thus there is more interaction between the colony and nisin. This greater exposure level of cells to nisin at higher concentrations of XG is reflected in the kinetics (Figure 2a). It is therefore suggested that *a synergistic effect exists between the viscoelastic surface, the presence of nisin, and suboptimal temperatures, thus negatively impacting surface growth, i.e. acting as a hurdle.* More specifically, as also reported in literature for other stresses, when stress factors are combined (i.e. low temperatures, nisin, and a viscoelastic environment) a synergistic combined effect is observed with growth being more inhibited than if each stress factor was applied individually (see as examples Baka et al., 2015; Leistner, 2000; Smet et al., 2015).

CONCLUSIONS

Here, we present for the first time that *Listeria* surface growth is selective on the protein phase of a biphasic 5% Xanthan gum/10% Whey protein system. Furthermore, significant differences are observed in the colony size and distribution in the monophasic Xanthan gum-based systems depending on the gelling agent concentration. Generally, while only a few differences in the growth kinetics of *Listeria* were observed in all model systems under study, significant differences were observed regarding colony spatial organization and size, suggesting an effect of structural composition and complexity on a microscopic scale.

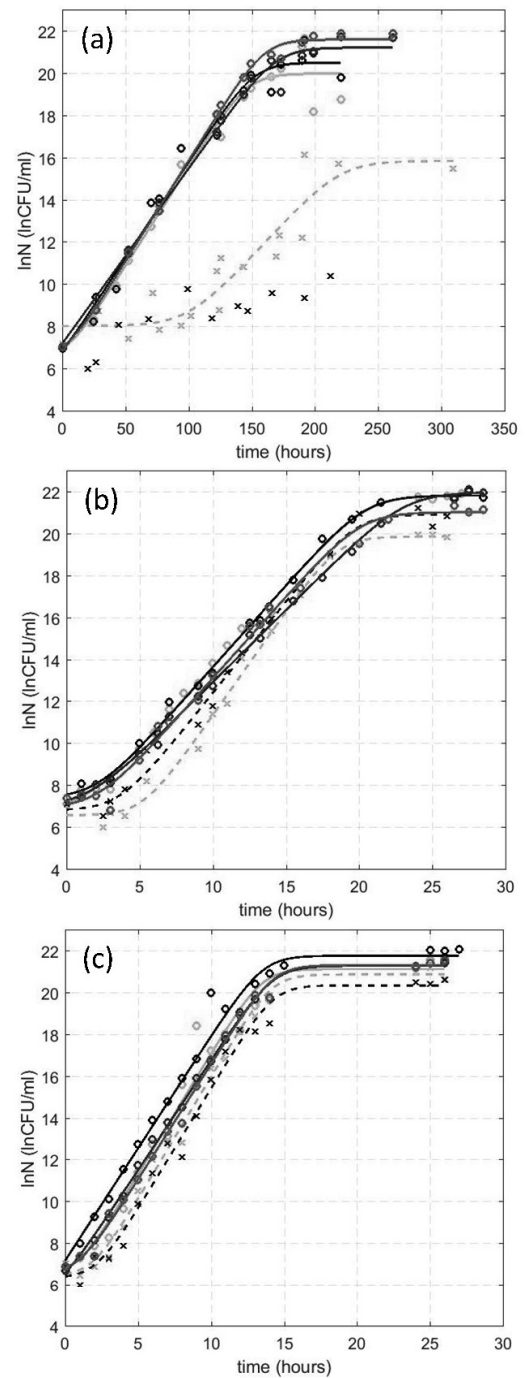


Figure 2: Fits of the Baranyi and Roberts growth model on the experimental data obtained for *L. innocua* surface growth at (a) 10°C, (b) 30°C, (c) 37°C for monophasic 3%XG (o,-), nisin-rich 3%XG (o,-), 5%XG (o,-), nisin-rich 5%XG (o,-), 7%XG (o,-) and biphasic 5%XG/10%WPI (o,-) systems.

Furthermore, our findings show that the system viscosity in monophasic XG based systems had an inhibitory effect for surface growth at 10°C. Overall, our findings are of importance, especially when investigating the efficacy of novel treatment approaches, as the environmental stress within a colony is directly affected by the colony size and location which could result in different levels of cross-protection in systems of varying structural complexity, leading to different survival rates of *Listeria* in these systems.

FUTURE WORK

Future investigations using appropriate molecular stress biomarkers will allow a topological mapping of the stress response of *Listeria* to nisin at colony level, allowing a fundamental understanding of the interconnections between structure and single cell microbial stress response. Furthermore co-culture experiments with Lactic acid bacteria (which produce nisin) will allow a better understanding of cross-talk phenomena between pathogens and food microflora.

ACKNOWLEDGEMENTS

This work was supported by the Department of Chemical and Process Engineering of the University of Surrey as well as an Impact Acceleration Grant (IAA-KN9149C) of the University of Surrey, an IAA-EPSRC Grant (RN0281J), and the Royal Society.

REFERENCES

- Ale, P., Paul, S., Gutierrez, J., Velliou, E.G., 2015. On the quantification of the impact of natural antimicrobials on the growth kinetics of *Listeria*: a comparison between liquid and gelified systems, 29th EFFoST International Conference Proceedings.
- Aspidou, Z., Moschakis, T., Biliaderis, C.G., Koutsoumanis, K.P., 2014. Effect of the substrate's microstructure on the growth of *Listeria monocytogenes*. *Food Res. Int.* 64, 683–691.
- Baka, M., Noriega, E., Tsakali, E., Van Impe, J.F.M., 2015. Influence of composition and processing of Frankfurter sausages on the growth dynamics of *Listeria monocytogenes* under vacuum. *Food Res. Int.* 70, 94–100.
- Baranyi, J., Roberts, T.A., 1994. A dynamic approach to predicting bacterial growth in food. *Int. J. Food Microbiol.* 23, 277–294.
- Be'er, A., Smith, R.S., Zhang, H.P., Florin, E.-L., Payne, S.M., Swinney, H.L., 2009. *Paenibacillus dendritiformis* Bacterial Colony Growth Depends on Surfactant but Not on Bacterial Motion. *J. Bacteriol.* 191, 5758–5764.
- Boons, K., Mertens, L., Van Derlinden, E., David, C.C., Hofkens, J., Van Impe, J.F., 2013a. Behavior of *Escherichia coli* in a heterogeneous gelatin-dextran mixture. *Appl. Environ. Microbiol.* 79, 3126–3128.
- Boons, K., Van Derlinden, E., Mertens, L., Peeters, V., Van Impe, J.F., 2013b. Effect of Immobilization and Salt Concentration on the Growth Dynamics of *Escherichia coli* K12 and *Salmonella* Typhimurium. *J. Food Sci.* 78, 567–574.
- Boons, K., Noriega, E., Van den Broeck, R., David, C.C., Hofkens, J., Van Impe, J.F., 2014. Effect of Microstructure on Population Growth Parameters of *Escherichia coli* in Gelatin-Dextran Systems. *Appl. Environ. Microbiol.* 80, 5330–5339.
- Briandet, R., Meylheuc, T., Maher, C., Bellon-Fontaine, M.N., 1999. *Listeria monocytogenes* Scott A: cell surface charge, hydrophobicity, and electron donor and acceptor characteristics under different environmental growth conditions. *Appl. Environ. Microbiol.* 65, 5328–5333.
- Brocklehurst, T.F., Mitchell, G.A., Smith, A.C., 1997. A model experimental gel-surface for the growth of bacteria on foods. *Food Microbiol.* 14, 303–311.
- EFSA, 2015. The European Union summary report on trends and sources of zoonoses, zoonotic agents and food-borne outbreaks in 2014. *EFSA.* 13, 1–190.
- Escolar, C., Gómez, D., del Carmen Rota García, M., Conchello, P., Herrera, A., 2017. Antimicrobial Resistance Profiles of *Listeria monocytogenes* and *Listeria innocua* Isolated from Ready-to-Eat Products of Animal Origin in Spain. *Foodborne Pathog. Dis.* 14, 357–363.
- Floury, J., Jeanson, S., Madec, M.-N., Lortal, S., 2013. Porosity of *Lactococcus lactis* subsp. *lactis* LD61 colonies immobilised in model cheese. *Int. J. Food Microbiol.* 163, 64–70.
- Kar, R., Mohapatra, S., Bhanja, S., Das, D., Barik, B., 2010. Formulation and In Vitro Characterization of Xanthan Gum-Based Sustained Release Matrix Tablets of Isosorbide-5-Mononitrate. *Iran. J. Pharm. Res.* 9, 13–19.
- Leistner, L., 2000. Basic aspects of food preservation by hurdle technology. *Int. J. Food Microbiol.* 55, 181–186.
- Léonard, L., Gharsallaoui, A., Ouaali, F., Degraeve, P., Waché, Y., Saurel, R., Oulahal, N., 2013. Preferential localization of *Lactococcus lactis* cells entrapped in a caseinate/alginate phase separated system. *Colloids Surf B Biointerfaces* 109, 266–272.
- Liu, X., Powers, J.R., Swanson, B.G., Hill, H.H., Clark, S., 2005. Modification of whey protein concentrate hydrophobicity by high hydrostatic pressure. *Innov. Food Sci. Emerg. Technol.* 6, 310–317.
- Muthamizhi, K., Kalaichelvi, P., Tukaram Powar, S., Jaishree, R., 2014. Investigation and modelling of surface tension of power-law fluids. *RSC Adv.* 4, 9771–9776.
- Robinson, T.P., Wimpenny, J.W.T., Earnshaw, R.G., 1991. pH gradients through colonies of *Bacillus cereus* and the surrounding agar. *J. Gen. Microbiol.* 137, 2885–2889.
- Rook, J.J., Bruckman, H.W.L., 1953. On the suitability of gelatin for plate cultures. II. *Antonie Van Leeuwenhoek* 19, 394–362.
- Skandamis, P.N., Brocklehurst, T.F., Panagou, E.Z., Nychas, G.-J.E., 2007. Image analysis as a means to model growth of *E. coli* O157:H7 in gel cassettes. *J. Appl. Microbiol.* 103, 937–947.
- Skandamis, P.N., Jeanson, S., 2015. Colonial vs. planktonic type of growth: Mathematical modeling of microbial dynamics on surfaces and in liquid, semi-liquid and solid foods. *Front. Microbiol.* 6, 1–9.
- Smet, C., Noriega, E., Van Mierlo, J., Valdramidis, V.P., Van Impe, J.F., 2015. Influence of the growth morphology on the behavior of *Salmonella* Typhimurium and *Listeria monocytogenes* under osmotic stress. *Food Res. Int.* 77, 515–526.
- Stecchini, M.L., Del Torre, M., Donda, S., Maltini, E., Pacor, S., 2001. Influence of agar content on the growth parameters of *Bacillus cereus*. *Int. J. Food Microbiol.* 64, 81–88.
- Takahashi, H., Suda, T., Tanaka, Y., Kimura, B., 2010. Cellular hydrophobicity of *Listeria monocytogenes* involves initial attachment and biofilm formation on the surface of polyvinyl chloride. *Lett. Appl. Microbiol.* 50, 618–625.
- Tromp, R.H., Van de Velde, F., Van Riel, J., Paques, M., 2001. Confocal scanning light microscopy (CSLM) on mixtures of gelatine and polysaccharides. *Food Res. Int.* 34, 931–938.
- Troy, D.J., Shikha, K., Kerry, J.P., Tiwari, B.K., 2016. Sustainable and consumer-friendly emerging technologies for application within the meat industry: An overview. *MESC* 120, 2–9.
- Valdramidis, V.P., Koutsoumanis, K.P., 2016. Challenges and perspectives of advanced technologies in processing, distribution and storage for improving food safety. *Curr. Opin. Food Sci.* 12, 63–69.
- Velliou, E.G., Noriega, E., Van Derlinden, E., Mertens, L., Boons, K., Geeraerd, A.H., Devlieghere, F., Van Impe, J.F., 2013. The effect of colony formation on the heat inactivation dynamics of *Escherichia coli* K12 and *Salmonella* Typhimurium. *Food Res. Int.* 54, 1746–1752.
- Wilson, P.D.G., Brocklehurst, T.F., Arino, S., Thuault, D., Jakobsen, M., Lange, M., Farkas, J., Wimpenny, J.W.T., Van Impe, J.F., 2002. Modelling microbial growth in structured foods: Towards a unified approach. *Int. J. Food Microbiol.* 73, 275–289.
- Zhang, S., Zhang, Z., Vardhanabhuti, B., 2014. Effect of charge density of polysaccharides on self-assembled intragastric gelation of whey protein/polysaccharide under simulated gastric conditions. *Food Funct.* 5, 1829–1838.

EFFECT OF XANTHAN GUM ON PHYSICOCHEMICAL AND TEXTURAL PROPERTIES OF GLUTEN-FREE BATTER AND BREAD

Christian R. Encina-Zelada
José A. Teixeira

Centre of Biological Engineering
School of Engineering
University of Minho
Portugal

Fernando Monteiro

Department of Electrical Engineering, School of
Technology and Management
INESC-TEC Institute for Systems and Computer
Engineering, Technology and Science, Porto
Portugal

Ursula Gonzales-Barron
Vasco Cadavez

CIMO Mountain Research Centre, School of Agriculture
Polytechnic Institute of Bragança
Portugal

E-mail: ubarron@ipb.pt

KEYWORDS

Quinoa flour, Rheology, Texture profile analysis, Crumb image analysis

ABSTRACT

The objective of this study was to evaluate the effect of xanthan gum (XG) on physicochemical, rheological and textural properties of gluten-free batter and bread. Batches of gluten-free bread used a base formulation of rice, corn and quinoa flour, and different levels of XG (1.5, 2.5 and 3.5%) and water content (WC; 90, 100 and 110%) in a full factorial design. Although in interaction with water, higher XG doses tended to produce batters of lower stickiness, work of adhesion, strength-cohesiveness; which, when baked, produced loaves of lower specific volume and baking loss; and bread crumb of lower Aw, pH, hardness, springiness, firmness, mean cell area, void fraction, mean cell aspect ratio, and higher firmness, consistency, cohesiveness, adhesiveness, chewiness, resilience, cell density, cell size uniformity and mean cell compactness ($p < .001$). Gluten-free loaves of good appearance in terms of high specific volume, low crumb hardness, high crumb springiness, and open grain visual texture were obtained in formulations with 110% WC and XG doses between 1.5-2.5%.

INTRODUCTION

To target the 0.5–1.0% of the world's population estimated to be affected by coeliac auto-immune disease (Gujral et al., 2012), a number of food products that avoid the use of wheat (gliadin), rye (secalins), barley (hordein) and oats (avidins) have been lately developed. There has been particularly an upsurge in the development of gluten-free bread.

Xanthan gum (XG), a high molecular weight polysaccharide produced by the bacterium *Xanthomonas*

campestris, is largely used in gluten-free breadmaking, because it can hydrate in cold water and produce a viscous solution with strong shear thinning flow behaviour. The xanthan molecule has a cellulosic backbone with side chains that wraps around the backbone and make it rigid, enabling its emulsifying and foaming properties (Naji and Razavi, 2014). In low amounts, XG has been found to increase loaf volume, and improve bread rheological and sensory properties (Hager and Arendt, 2013). Optimising textural and sensory attributes, researchers have recommended doses of XG in gluten-free bread, that, in general, range between 0.5% up to 7.0% (flour weight), yet this is strongly linked to bread formulation and water content. The objectives of this study were: (i) to assess the effect of both xanthan and water on the rheological properties of batter, and the physicochemical and textural properties of bread formulated with a mixture of rice, corn and quinoa flours; and (ii) to get an insight into the relationships among all the quality attributes measured.

MATERIALS AND METHODS

Bread elaboration

The effects of GG (three doses tested) and water content (WC; three levels tested) were evaluated using a full factorial design. Thus, nine batches of gluten-free bread, with two replicates, were produced using a base formulation of rice flour (50%), corn flour (50%) and quinoa flour (20%), sunflower oil (6% flour weight), white sugar (3% flour weight), refined salt (1.5% flour weight), instant yeast (3% flour weight), GG (1.5, 2.5 or 3.5% flour weight) and water (90, 100 or 110% flour weight). To make the batters, XG was purchased from TecPan (Portugal), while the other ingredients were purchased from a local supermarket. Demineralised water (pH=6.8) kept at 5°C overnight was used. All ingredients were mixed for 6 min in a professional food processor (SilverCrest SKMP-1200, Germany) equipped with a batter blade. Two hundred and eighty grams were then poured into in oiled and floured square

tins, and allowed to proof at 30°C and 85% of relative humidity for 60 min in a climatic chamber (Climacell 222, Germany). Afterwards, all moulds from the same batch were placed in a pre-heated convection oven (Princess, 2000 W, The Netherlands) for 60 min at 190°C. Bread loaves were un-moulded when reaching ambient temperature, and all analyses were performed after 24 h. The rheology of batter and bread were characterised using a texture analyser TA-XT plus (Stable Micro Systems, UK) fitted with specific fixtures, namely, the SMS/Chen-Hoseney stickiness rig for dough stickiness analysis; the 35 mm-diameter perspex flat rig, and a standard size back extrusion cylindrical container (50 mm diameter, capacity of 115 g approx.) for the back-extrusion analysis; and a 36 mm-diameter aluminium probe (model P/36R) for the texture profile analysis.

Batter rheology

Several batter rheological properties were studied, including: 1) stickiness analysis (Agrahar-Murugkar et al., 2015), which produced measurements of: stickiness (STIba, g), work of adhesion (ADHba, g.s), and strength-cohesiveness (SCOba, mm); and 2) back extrusion analysis (Juszczak et al., 2012), which rendered measurements of: firmness (FIRba, g), consistency (CONba, g.s), cohesiveness (COHba, g) and viscosity index (VISba, g.s).

Bread crumb quality properties

The bread loaf specific volume (SVObr, ml/g) was calculated as loaf volume divided by loaf weight 24 h after baking, while the baking loss (BLObr, %) was computed as [initial loaf weight before baking - the loaf weight after 24 h baking x 100] / initial loaf weight before baking. Such physical properties were measured in triplicate. Water activity (Aw) and pH of bread crumb were quantified in quintuplicate as in Machado-Alencar et al. (2015) and Hashemi et al. (2016), respectively. Texture profile analysis (TPA) (Martínez and Gomez, 2017) was employed to obtain the bread crumb rheological properties of hardness (HARbr, g), adhesiveness (ADHbr, g.s), springiness (SPRbr, mm), cohesiveness (COHbr, g), chewiness (CHEbr, g.mm), resilience (RESbr, dimensionless) and firmness (FIRbr, g).

Bread crumb image analysis

Slices of bread were scanned (Canon Pixma MG-2550, Vietnam) with -10% brightness and +15% contrast with a resolution of 350 dpi, and a 4.0 cm x 4.0 cm field-of-view from the centre of the image was cropped and saved in png format for posterior analysis. Several grain crumb features were computed using the automated thresholding technique proposed in Gonzales-Barron and Butler (2006) and Gonzales-Barron and Butler (2008), coded in Matlab software (ver. R2015a, The Mathworks, USA). These were: mean cell area (MCA, mm²); cell density (CD, number of cells/mm²); uniformity (UNI, dimensionless), calculated as the rate between the number of cells ≤ 5 mm² and number of cells > 5 mm²; void fraction (VFR, dimensionless), calculated as the proportion of the space occupied by the pores/cells; mean cell compactness (COM, dimensionless), with compactness defined as the ratio of the area of the cell to the area of a circle having the same perimeter; and mean

cell aspect ratio (ARA, dimensionless), with aspect ratio defined as the ratio of the major axis to the minor axis of a cell.

Statistical analysis

Data were analysed using the R software version 3.3.1 (R Core Team, 2017). Analyses of variance were applied to assess the effect of XG and WC on the response variables: pH, Aw, BLObr, batter stickiness and batter extrusion. On the other hand, for the response variables: specific volume, TPA, firmness and features of bread crumb acquired by image analysis, a linear mixed model was used assuming that the measurements taken from the same loaf were clustered. Statistical analyses were conducted using the packages “plyr”, “ggplot2”, “lme4” and “lmerTest” for the linear models; and the packages: “rmisc”, “rcmdmisc”, “plyr”, “ggplot2”, “car”, “multcompView” and “lsmeans” for the linear mixed models.

RESULTS AND DISCUSSION

Batter properties

Both XG and WC affected the rheology of gluten-free batter, as per the results of the batter stickiness analysis (Figure 1) and the back-extrusion analysis (Figure 2). The batter stickiness properties of STIba, ADHba and SCOba, ranged from 28.81 to 55.90 g, from 3.19 to 4.57 g.s and from 2.42 to 3.67 mm, respectively. At a constant XG level, higher WC consistently ($p < .001$) increased the STIba, ADHba and SCOba measures, while at a constant WC level, higher XG contents consistently ($p < .001$) decreased those stickiness measures (Figure 1). This occurs because xanthan gum has the capacity to bind large amounts of water into the dough matrix.

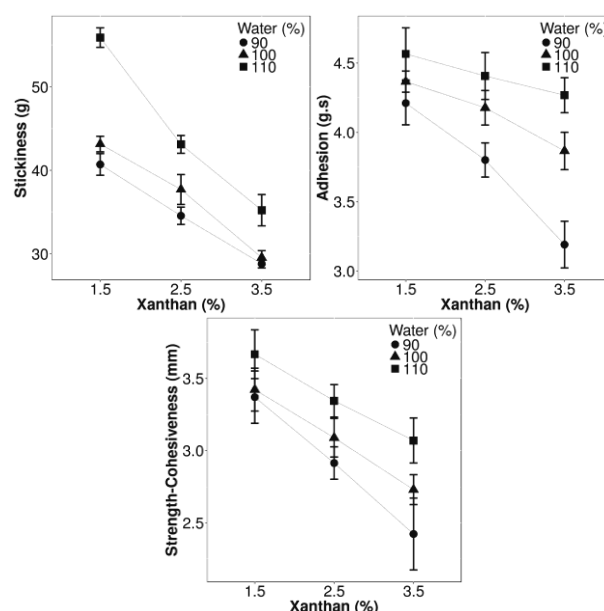


Figure 1: Effect of Xanthan Gum and Water Content on the Gluten-Free Batter Stickiness Properties of STIba (top left), ADHba (top right) and SCOba (bottom)

The back extrusion analysis values ranged for FIRba from 359.08 to 1990.04 g, for CONba from 3494.17 to 17363.37

g□s, for COHba from -260.59 to -1098.89 g and for VISba from -1249.64 to -4691.52 g□s. Higher XG contents increased ($p<.001$) FIRba and CONba, and decreased ($p<.001$) COHba and VISba while higher WC levels had an opposite effect, reducing ($p<.001$) FIRba and CONba, and increasing ($p<.001$) COHba and VISba (Figure 2). Using the same level of water (110%), Sciarini et al. (2010) obtained lower batter firmness values, from 50.8 to 1252 g, for a mixture of corn/soy (90:10) and rice/soy (80:20), respectively. They concluded that rice/soy mixtures required higher force to extrude, because soy proteins have the ability to absorb cold water, resulting in a decrease of free water in the batter mixture. In our case, quinoa proteins may have lent a greater cold water absorption capability, hence producing batters of higher firmness than those with soy proteins.

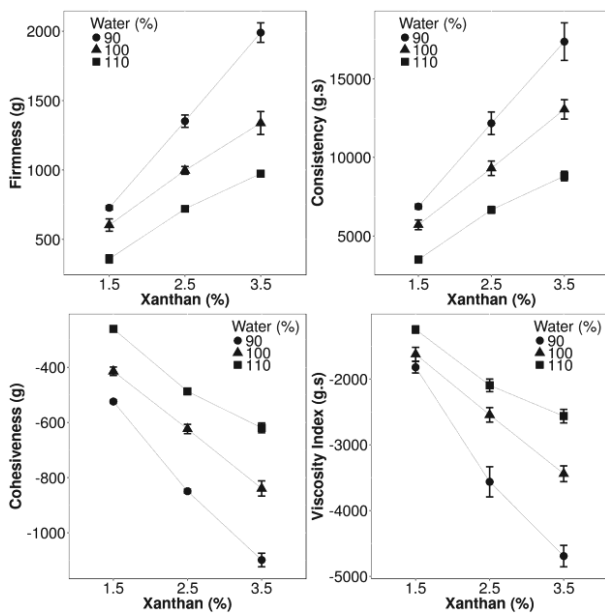


Figure 2: Effect of Xanthan Gum and Water Content on the Gluten-Free Batter Back-Extrusion Properties of FIRba (top left), CONba (top right), COHba (bottom left) and VISba (bottom right)

Compared between 1.5 and 2.5% of xanthan in a GF fresh filled pasta batter, Sanguinetti et al. (2015) observed that a higher dose of XG resulted in a more cohesive, less adhesive and more elastic batter. Sabanis and Tzia (2010) and Turkut et al. (2016) reported that higher consistency values and viscosity index in their GB batters led to lower specific volume. This finding was corroborated in the present study, where 3.5% XG doses produced loaves of lower specific volume (1.69 ml/g) compared to those obtained from treatments with 1.5% xanthan (1.78 ml/g) (Figure 3).

Bread crumb physicochemical properties

Moisture loss during baking ranged from 11.9 to 14.5%, increasing ($p<.001$) with higher WC, and decreasing ($p<.001$) with higher XG content (Figure 4). However, although higher XG amounts reduce baking loss, it can negatively affect the volume of loaves (Figure 4). The specific volume of bread ranged from 1.58 to 1.91%, and

decreased ($p<.001$) with higher XG content, and increased ($p<.001$) with higher WC.

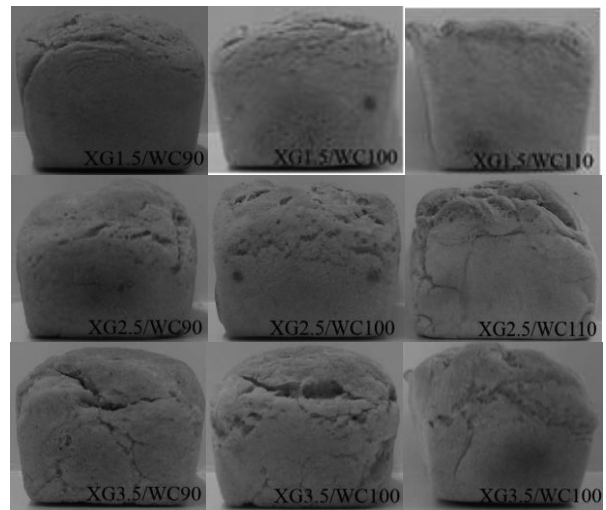


Figure 3: Photographs of Gluten-Free Bread Loaves Produced with Varying Xanthan Gum (XG) and Water Content (WC) Showing Height and Crust Appearance

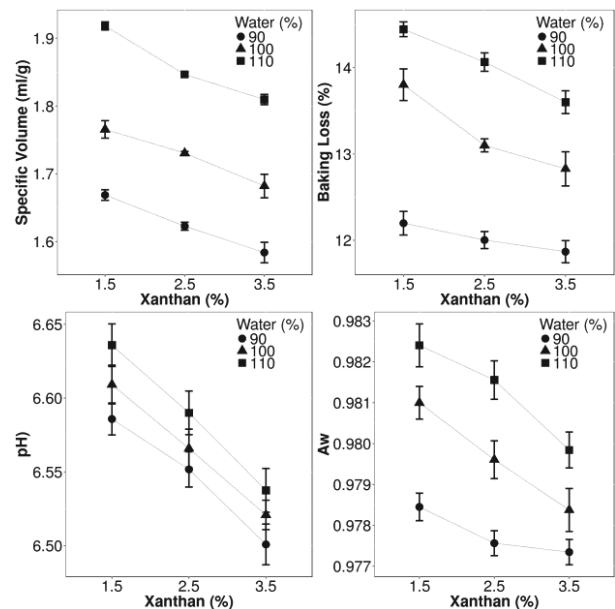


Figure 4: Effect of Xanthan Gum and Water Content on the Gluten-Free Bread Physicochemical Properties of SVObr (top left), BLObr (top right), pH (bottom left) and Aw (bottom right)

The positive impact of high WC was readily evident in the specific volume of breads, as explained by de la Hera et al. (2014), due to the plasticizer effect of the water which contributes to the extensional properties of the batter during mixing allowing the hydration of the particles. Nonetheless, Han et al. (2012) reported that excessive water can cause overexpansion during baking resulting in large volume breads or collapsed loaves. Onyango et al. (2011) explained that, as gas leaks out of the bubbles, it forces its way through the weakly connected particles and channels formed by gas pressing the particles apart. Since, in our experiments, small-sized bread loaves were mostly associated to lower baking losses; we can conclude that,

regardless of the XG dose, batters with low WC tended to proof insufficiently, resulting in bread loaves of lower volume. In relation to the other physicochemical properties, bread acidity was also influenced by the addition of XG ($p < .001$) and WC ($p < .001$), with more acidic crumbs produced by higher doses of XG. As expected, the amount of free water in the crumb decreased with the addition of higher concentrations of XG ($p < .001$) and lower WC amounts ($p < .001$).

Bread crumb textural properties

Having produced firmer and less viscous batters, lower WC levels consequently yielded tougher breads (Figure 5). According to the TPA, loaves with the lowest WC content (90%) were significantly harder (5130 g), less cohesive (0.477) and less springy (0.833) than the treatments with 100 and 110% WC. The addition of higher amounts of water can improve crumb texture, since the 110% WC treatments produced softer breads, with lower values of HARbr (1995 g) and CHEbr (911 g·mm), ADHbr (-12.80 g·s – in absolute value), and higher values of SPRbr (0.884 mm), COHbr (0.517) and RESbr (0.217), compared to those obtained from the lower WC treatments of 90 and 100%. Although, to a lower extent than WC, XG also had an impact on bread crumb texture.

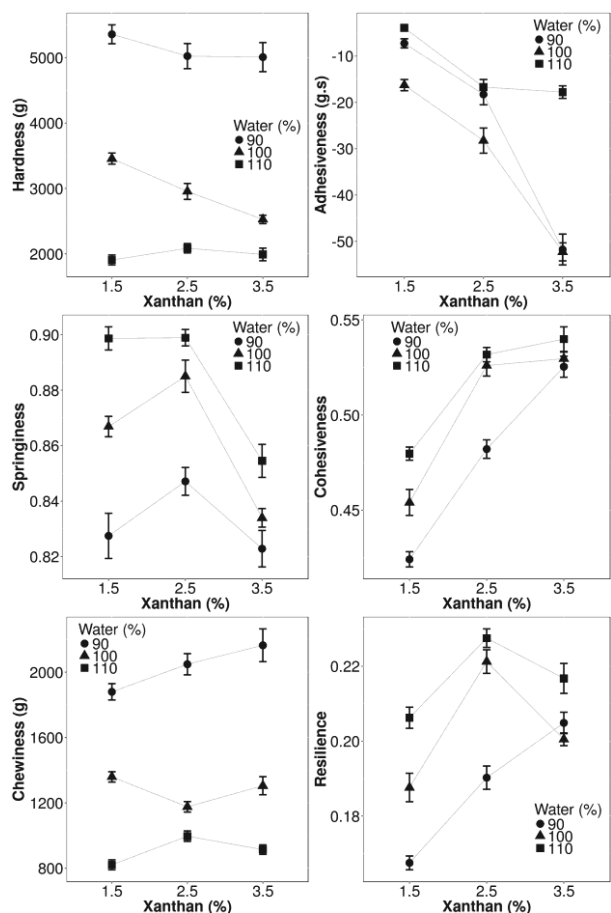


Figure 5: Effect of Xanthan Gum and Water Content on the Gluten-Free Bread Instrumental Textural Properties of HARbr (top left), ADHbr (top right), SPRbr (middle left), COHbr (middle right), CHEbr (bottom left) and RESbr (bottom right)

Loaves formulated with the lowest XG dose (1.5%) produced crumb with higher values of HARbr (3574 g) and SPRbr (0.864 mm), and lower values of ADHbr (-9.14 g·s – in absolute value), COHbr (0.453), CHEbr (1353 g·mm) and RESbr (i.e., 0.187), compared to those obtained from 2.5 and 3.5% XG. Apart from hardness, resilience and springiness are important quality properties as they characterise crumb elasticity or the ability of the material to return to its shape after stress (Onyango et al., 2011), which is a desired attribute empirically assessed by the consumer. In our results, RESbr and SPRbr were found to be linked, having both a quadratic trend with XG dose, and optimum (higher) values were around 2.5% XG. In addition, bread of these desired properties were obtained at the highest WC of 110%. Apart from the separate effects of XG and WC, statistical analysis evidenced interactions ($p < .001$) between XG and WC on all of TPA measurements, being the strongest for resilience.

Image analysis features of crumb grain

Digital images (Figure 6) of gluten-free bread crumb grains, showed visual differences among the nine formulations. While higher WC formulations produced more open grain textures, lower WC formulations produced the opposite, closer crumbs of smaller pores. Such differences were statistically corroborated in all of the image grain features analysed. Values were in the range of 0.73 – 1.89 mm² for MCA; 0.200 – 0.319 cells/mm² for CDE; 10.54 – 63.09 for UNI; 0.217 – 0.339 for VF; 0.755 – 0.776 for COM; and 1.666 – 1.770 for ARA.

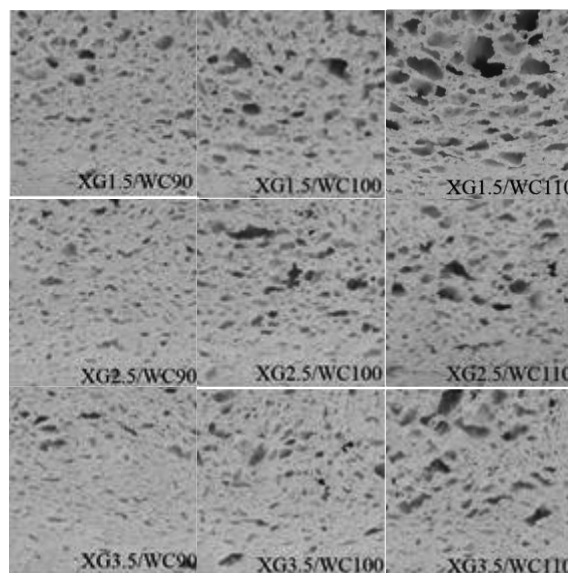


Figure 6: Crumb Grain of Gluten-Free Bread Produced by Varying Xanthan Gum (XG) and Water Content (WC)

According to Figure 7, when XG increased, MCA, VF and AR values decreased ($p < .001$) while CDE, UNI and COM increased ($p < .001$). This means that at a constant level of water in the formulation, increasing XG doses only produces smaller bread loaves. These smaller loaves tend to have a compact visual texture, formed of a greater number of cells, but of smaller size. Because of this, the cell size uniformity is greater but the void fraction is lower. Smaller

loaves of denser or more compact texture also have the characteristic of having more rounded cells (i.e., higher cell compactness) and less elongated cells (i.e., lower aspect ratio). Loaves of lower XG contents (1.5%) presented crumbs with larger pores, with higher values of MCA (1.35 mm²), VF (0.29) and AR (1.75), and lower values of CD (0.25 cells/mm²), UNI (20.5) and COM (0.76) compared to those obtained with higher XG levels of 2.5 and 3.5%.

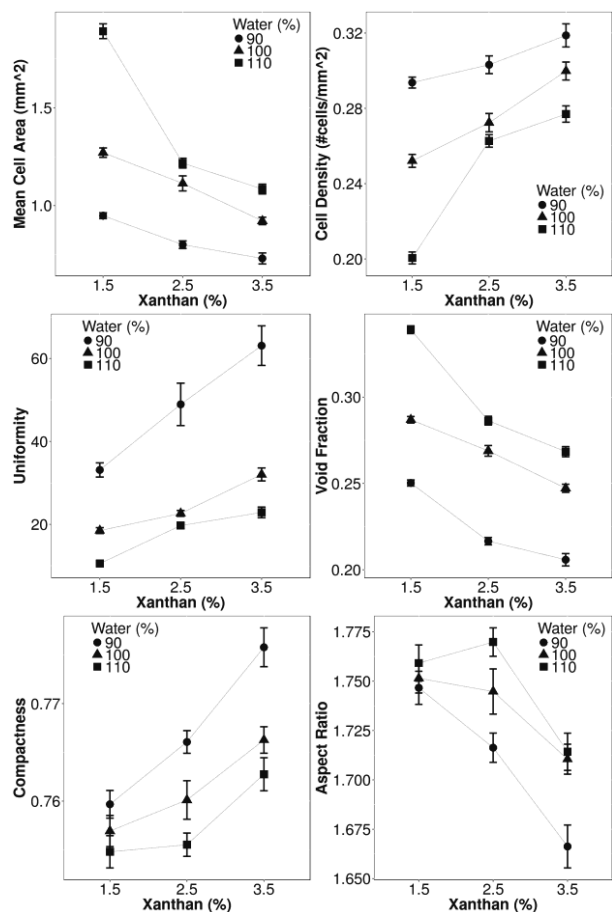


Figure 7: Effect of Xanthan Gum and Water Content on the Gluten-Free Bread Crumb Grain Features of MCA (top left), CD (top right), UNI (middle left), VFR (middle right), COM (bottom left) and ARA (bottom right)

On the other hand, when higher proportions of WC were added, the opposite was observed; this is, values of CD (0.25 cells/mm²), UNI (17.5) and COM (0.758) were lower ($p < .001$), while values of MCA (1.38 mm²), VF (0.30) and AR (1.75) were higher when breads were formulated with 110% WC, in comparison with those obtained with the lower WC treatments of 90 and 100%. This signifies that, when loaves undergo a better proofing, expanding more during fermentation and baking, facilitated by the greater amount of water, the final visual texture of the bread crumb has altogether a different crumb grain. As breads were formulated with a constant XG dose and increasing WC levels, crumb grains appeared more open; in other words, crumb made of cells of greater size and less compact and more elongated shape. This in turn leads to a less uniform grain (since the number of large cells is greater) and a higher void fraction.

A denser bread crumb grain can also be effectively evaluated by the measurements of cell size uniformity and mean cell compactness or aspect ratio. Notice that higher values of UNI and COM were obtained with higher amounts of XG (3.5%) and lower values of WC (90%), corresponding in both cases to a denser structure (Figure 7). Thus, when during proofing and baking, batter expands more and steadily, a greater number of large cells is produced, therefore bringing down the ratio small-to-large cells (UNI), while due to coalescence, the large cells tend to be more elongated and less compact, thereby bringing down the values of COM.

From the nine formulations, the more open crumb grain was attained by the formulation with 1.5% XG and 110% WC (2.25 mm²; Figure 7), whereas the formulation with 3.5% XG and 90% WC produced the smallest mean cell size (0.56 mm²), characterising the denser structure obtained, which was also reflected by the lowest specific volume of this formulation (1.59 ml/g; Figure 3). For de la Hera et al. (2014), if gluten-free breads are elaborated with excessive water, large holes can appear in the crumb, as was also attested in our experiments for the formulation XG1.5/WC110 (Figure 6). In this study, using XG as the only batter thickener, it was possible to obtain crumbs with open grain structures at a high level of water (110%) and a low level of XG (1.5%). The presence of larger cells can also be linked to a spongier crumb structure, which is a desirable quality property yet not typically found in gluten-free breads. Similar to our findings were those reported by Schober et al. (2005) who encountered that sorghum bread with a fine crumb structure was tougher than bread with a coarse and open crumb structure.

4. CONCLUSION

Higher amounts of xanthan gum, in gluten-free bread formulated with a mixture of rice, maize and quinoa flours, have in principle the capacity to retain more water; however, at a constant water level, higher doses of xanthan gum produce less viscous and sticky batters but of increased firmness, that translates into baked loaves of smaller volume with a more cohesive and less springy crumb texture. The highest water content of 110% and XG between 1.5 and 2.5% produced loaves of good quality in terms of high specific volume, low hardness, high springiness, low cell density, low cell size uniformity, high void fraction and high mean cell area.

REFERENCES

Agrahar-Murugkar, D.; Gulati, P.; Kotwaliwale, N.; and Gupta, C. 2015. "Evaluation of nutritional, textural and particle size characteristics of dough and biscuits made from composite flours containing sprouted and malted ingredients". *Journal of Food Science and Technology*, 52(8), 5129–5137.

de la Hera, E.; Rosell, C.M.; and Gomez, M. 2014. "Effect of water content and flour particle size on GF bread quality and digestibility". *Food Chemistry* 151, 526–531.

- Gujral, N.; Freeman, H.J.; and Thomson, A.B.R. 2012. Celiac disease: prevalence, diagnosis, pathogenesis and treatment. *World Journal of Gastroenterology*, 18 (42), 6036–6059.
- Hager, A.S.; and Arendt, E.K. 2013. “Influence of hydroxypropylmethylcellulose (HPMC), xanthan gum and their combination on loaf specific volume, crumb hardness and crumb grain characteristics of gluten-free breads based on rice, maize, teff and buckwheat”. *Food Hydrocolloids*, 32, 195–203.
- Han, H.M.; Cho, J.H.; Kang, H.W.; and Koh, B.K. 2012. “Rice varieties in relation to rice bread quality”. *Journal of the Science of Food and Agriculture*. 92, 1462–1467.
- Hashemi, M.; Afshari, A.; Aminzare, M.; Raeisi, M.; and Sahranavard, T. 2016. “Evaluation of pH and common salt content in bread samples produced in mashhad, Iran”. *Journal of Food Quality and Hazards Control* 3, 73–75.
- Juszczak, L.; Witzcak, T.; Ziobro, R.; Korus, J.; Cieslik, E.; and Witzcak, M. (2012). “Effect of inulin on rheological and thermal properties of gluten-free dough”. *Carbohydrate Polymers* 90, 353–360.
- Machado-Alencar, N.M.; Steel, C.J.; Alvim, I.D.; Carvalho de Morais, E.; and Andre-Bolini, H.M. (2015). “Addition of quinoa and amaranth flour in gluten-free breads: Temporal profile and instrumental analysis. *LWT - Food Science and Technology* 62, 1011–1018.
- Martínez, M.M.; and Gómez, M. 2017. “Rheological and microstructural evolution of the most common gluten-free flours and starches during bread fermentation and baking”. *Journal of Food Engineering* 197, 78–86.
- MATLAB. 2015. “Version 8.5.0.197613 (R2015a)”. Natick, Massachusetts, The MathWorks Inc., USA.
- Naji, S.; and Razavi, S.M.A. 2014. “Functional and textural characteristics of cress seed (*Lepidium sativum*) gum and xanthan gum: Effect of refrigeration condition”. *Food Bioscience* 5, 1–8.
- Onyango, C.; Mutungi, C.; Unbehend, G.; and Lindhauer, M.G. 2011. “Modification of gluten-free sorghum batter and bread using maize, potato, cassava or rice starch”. *LWT - Food Science and Technology*, 44(3), 681–686.
- R Core Team. 2017. “R: A Language and Environment for Statistical Computing”. R Foundation for Statistical Computing, Vienna, Austria. URL <http://www.R-project.org>.
- Sanguinetti, A.M.; Secchi, N.; Del Caro, A.; Fadda, C.; Fenu, P.A.M.; Catzeddu, P.; and Piga, A. 2015. “Gluten-free fresh filled pasta: The effects of xanthan and guar gum on changes in quality parameters after pasteurisation and during storage”. *LWT - Food Science and Technology* 64, 678–684.
- Schober, T.J.; Messerschmidt, M.; Bean, S.R.; Park, S.H.; and Arendt, E.K. 2005. “Gluten-free bread from sorghum: quality differences among hybrids”. *Cereal Chemistry*, 82, 394–404.
- Sciarini, L.S., Ribotta, P.D., Leon, A.E., and Perez, G.T. 2010. “Influence of gluten-free flours and their mixtures on batter properties and bread quality”. *Food Bioprocess Technology* (3), 577–585.

BIOGRAPHIES

CHRISTIAN R. ENCINA-ZELADA, a Peruvian national, attended the National Agricultural University of La Molina (UNALM, Lima, Peru), where he obtained his Bachelor degree (2003) and Food Industries Engineering title (2005). Before obtaining his Master degree in Food Technology (2006), he started lecturing at the UNALM Food Technology Department in 2004. He is currently pursuing PhD studies at the University of Minho, Portugal, and conducting experimental work at the CIMO Mountain Research Centre, IPB, Portugal. He is a fluent science communicator in English and Spanish.

URSULA GONZALES-BARRON, a Peruvian-Irish national, graduated with first-class honours in the Faculty of Food Industries at the National Agricultural University La Molina, Peru (1999), and later on, she obtained her doctoral degree at the Biosystems Engineering Department of University College Dublin, Ireland (2006). She is currently an Investigator Fellow at CIMO Mountain Research Centre, IPB, Portugal. Her expertise resides in diverse areas of food quality and safety, including mathematical modelling, predictive microbiology, food safety meta-analysis, risk assessment of pathogens, shelf-life determination and sensory analysis. Dr. Gonzales-Barron has published > 60 peer-reviewed articles, and >100 proceedings communications; with an H-index of 17. She serves as Editor in the *LWT – Food Science and Technology Journal*, and is a fluent science communicator in English, Portuguese and Spanish.

VASCO CADAVEZ, a Portuguese national, obtained his first degree in Animal Science in 1993 at the Portuguese University of Trás-os-Montes e Alto Douro. After a novel research on carcass composition and quality using ultrasound, he obtained his PhD degree in 2004. He is currently a Professor at the Animal Science Department of the Polytechnic Institute of Braganza (IPB), Portugal, and an active researcher at the CIMO Mountain Research Centre, IPB. Dr. Cadavez is very knowledgeable in a wide range of mathematical and statistical modelling techniques applied to agriculture, animal science, and food quality and safety. He is a fluent science communicator in English and Portuguese.

CREATING, REFINING AND VALIDATING A MODEL DESCRIBING SPATIOTEMPORAL DYNAMICS IN CHEESE DURING RIPENING

Thorsten Stefan

Institute of Applied Mathematics and Statistics,
University of Hohenheim, Schloss Hohenheim, Westhof-Süd, 70599 Stuttgart

E-mail: Thorsten.Stefan@uni-hohenheim.de

KEYWORDS

Spatiotemporal Predictive Modelling in Food, Reaction-Diffusion Equations, Model Validation, Optimisation.

ABSTRACT

In a project aimed at demonstrating the feasibility of a novel method of cheese production, we created a spatiotemporal model that tracks changes in concentrations of microorganisms and their metabolites during cheese ripening. The model was built using a Multiphysics software that includes an interfaces for handling CFD (computational fluid dynamics) in porous media. The method used creating this model could be readily applied to other food products that are solid or heterogeneous, overcoming the restricted use of traditional, well-mixed approaches in predictive microbiology. We further demonstrate how experimental results can be obtained to refine and validate this model, and how the model can be used to optimise the injection strategy of a bacterial suspension.

INTRODUCTION

Recent decades have seen a substantial growth in the use of mathematical models in the food industry, as advances in processing power of modern computers have made previously infeasible calculations quick and inexpensive. This is in particular true for computational fluid dynamics (CFD), a numerical method that is increasingly used in food process simulation (Norton and Sun, 2006), in particular when modelling thermal processes (Bouvier et al., 2014; Norton et al., 2013; Plana-Fattori et al., 2016).

Despite gaining prominence in the food industry in general, models involving CFD are still uncommon in food microbiology, with the exception of bacterial inactivation (Denys et al., 2005; Norton et al., 2013). Most of the models designed to predict bacterial growth, however, have been validated in homogeneous broth medium, even though the importance of spatially explicit models has been acknowledged (Dens and Van Impe, 2000, 2001). This limits predictions of bacterial growth to homogeneous environments, like broths and fluid foods. Predictions for solid foods or heterogeneous food products can therefore in most cases only be made experimentally, which might be both time-consuming (Skinner et al., 1994) and expensive, and prevents an understanding of the underlying processes regarding bacterial growth, metabolism and spatial colony dynamics (Bernaerts et al., 2004).

In the context of a project involving a novel technology platform for cheese production, we demonstrate how a

complex model of spatial and temporal changes in a solid cheese matrix during the ripening period can be created, and how it can be refined and validated with experimental data. As the novel technology platform requires the inoculation of a solid, extruded cheese with a starter culture of lactic acid bacteria in a number of different positions at the start of the ripening period, a number of centres of bacterial activity exist, making a spatially explicit model indispensable.

Most of the parameters the model requires were initially taken from the literature; these parameters were updated with experimental values as soon as the latter became available, thus refining the predictive quality of the model. Finally, we show an approach to validate the model by comparing the spatial pattern of the pH at the end of the ripening period to the pH-distribution predicted by the model. Our final aim is to use the refined and validated model to identify the optimal injection strategy, which depends on the injection positions and the method of inoculation, as well as the amount and concentration of the bacterial suspension injected.

METHODS

Governing Equations

The model was created with COMSOL Multiphysics®, a commercial Multiphysics software that includes physics interfaces for CFD (computational fluid dynamics) and diffusion processes in porous media. Regarding cheese as a porous medium (Keব্য and Morris, 1990), we used the software to explicitly model the temporal and spatial dynamics of the substrate (lactose) and the main fermentation products lactic acid and lactate, as well as the local pH. Furthermore, the local concentrations of salt (NaCl) and of the components of a hypothetical acid/salt buffer that emulates the buffer systems present in milk were included in the model. The final component of the model was the concentration of the starter culture, which also depended both on the spatial location and time. We assumed a stable cheese structure and thus constant effective diffusion coefficients and cheese porosity.

Bacterial growth, dispersal and spatiotemporal changes in the chemical species were modelled by a system of nonlinear PDEs of reaction-diffusion type. The spatiotemporal concentration changes for each species X (e.g. lactate) are governed by equation (1):

$$\frac{\partial[X](x, t)}{\partial t} = D_x \nabla^2[X](x, t) + r_x(x, t) \quad (1)$$

The species-specific reaction terms $r_X(x, t)$ characterise the biochemical reactions, such as the production of lactic acid from lactose by lactic acid bacteria or the dissociation of lactic acid into lactate and H^+ . In case of the lactic acid bacteria, the reaction terms specify local bacterial growth according to equation (2):

$$r_B(x, t) = \mu_{max} \cdot \frac{Q(t)}{1 + Q(t)} \cdot [B](x, t) \cdot [S](x, t) \quad (2)$$

$$\cdot f_{pH}([H](x, t)) \cdot f_{aw}([NaCl](x, t))$$

Here, μ_{max} is the maximum bacterial growth rate, $Q(t)$ is the physiological state of the lactic acid bacteria (Baranyi and Roberts, 1994), $[B](x, t)$ and $[S](x, t)$ denote concentrations of bacteria and substrate (lactose), and $f_{pH}([H](x, t)) \in [0, 1]$ as well as $f_{aw}([NaCl](x, t)) \in [0, 1]$ are functions that specify the inhibiting effect of a low pH and low values of water activity (aw) on bacterial growth, respectively. The reaction term $r_B(x, t)$ is inspired by a general class of substrate- and product-limited microbial growth models (Van Impe et al., 2005; Poschet et al., 2005), as it explicitly takes nutrient exhaustion and metabolic waste product effects into account.

Initial Conditions and Boundary Conditions

At the start of the ripening period, a solid, extruded cheese matrix is inoculated with a starter culture of lactic acid bacteria in a number of different positions. Two different sets of initial conditions were examined. The first set assumed that the injection of the bacterial suspension resulted in a spherical distribution of the injected solution in the pores of the cheese, centred on the tip of the injection needle (figure 1, left). This was modelled as a decrease in all spatial directions according to a trivariate normal distribution, as the suspension would reach more distant pores less likely than pores close to the injection centre. The second set of initial conditions assumed that the bacterial suspension filled the canal of the injection needle quickly, and thus resulted in a cylindrical distribution of the injected solution from the tip of the injection needle along the entire injection canal. This, in turn, was modelled as a decrease in all directions orthogonal to the injection canal, and a half-spherical distribution below it (figure 1, right). The model further assumes a boundary condition of no flux on all boundaries of the cheese matrix.

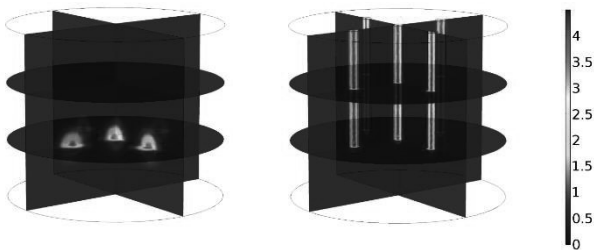


Figure 1: The initial concentrations of lactic acid bacteria (shades of red, yellow and light blue) in a cylindrical cheese matrix. The spherical distribution of the starter cultures (left) and the cylindrical distribution (right) were the two borderline cases investigated.

For the model refinement and validation, we performed experiments that inoculated a cylindrical cheese shape with a suspension of lactic acid bacteria (~170M cfu/mL) in five

different locations, arranged like the five dots on one side of a dice (figure 1, top view). The injection needle penetrated two thirds of the cheese matrix, which was acidulated with lactic acid to a pH of 5.7 before the ripening period.

We examined the spatial distribution of the pH within the cheese matrix at the end of the ripening period as a representative of the achieved homogeneity, and thus the quality of the cheese.

Experimental Determination of Effective Diffusion Coefficients and the Spatial pH-Distribution

The effective diffusion coefficients of lactose, lactic acid and NaCl were determined using the touching semi-infinite cylinder method (Wilde et al., 2001). A two-chamber diffusion tube is stored in an incubation box for several days at 10°C; at the end of the incubation period, the samples are cut into 2 mm thick slices, which are subsequently analysed. The resulting concentration profile allows for the calculation of the effective diffusion coefficients. This procedure was validated by determining D_{eff} of NaCl in cheese, where precise literature estimates exist.

The spatial pH-distribution at the end of the ripening period of 56 days was obtained by slicing the cylindrical cheese matrix horizontally into three slices of equal size, which were further sliced into 9 pieces each (see figure 3, top). Each of the 27 pieces was pureed, and its pH measured with a pH-electrode, yielding the average pH for each piece.

RESULTS AND DISCUSSION

Fine-tuning the Model Parameters using Experimental Results

Initially, all parameters used in the model were taken from the literature, as experimental measurements were not yet available. This applied in particular to the effective diffusion coefficients, which strongly influenced the spatiotemporal distribution of substrate, metabolites, pH and NaCl, and thus the quality of the ripened cheese. The literature estimates for lactose and lactic acid / lactate were $D_{eff}(\text{lactose}) = 1.3 \cdot 10^{-10}$ and $D_{eff}(\text{lactic acid, lactate}) = 2.4 \cdot 10^{-10}$ (Floury et al., 2010; Silva et al., 2013).

Measurements of the effective diffusion coefficients of lactose and lactic acid were conducted as outlined above, which resulted in the improved values of $D_{eff}(\text{lactose}) = 1.65 \cdot 10^{-9}$ and $D_{eff}(\text{lactic acid, lactate}) = 3 \cdot 10^{-11}$. Using these values in an updated model resulted in a markedly different prediction of the spatial distribution of the main fermentation product, lactic acid / lactate, at the end of the ripening period (figure 2).

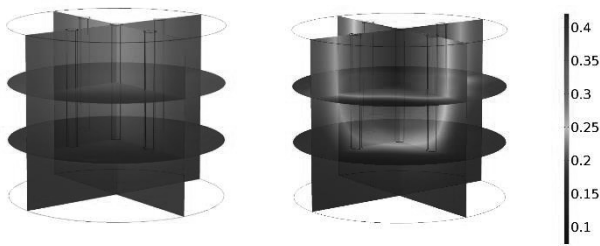


Figure 2: Spatial distribution of the sum of the concentrations of lactic acid and lactate at the end of the ripening period, in mol/L. The literature estimates for the effective diffusion coefficients of lactose and lactic acid / lactate would lead to a more even distribution of the main fermentation product (lactic acid and lactate; left) after ripening, while the final spatial product distribution using the experimentally determined diffusion coefficients was more uneven (right).

The experimental determination of the effective diffusion coefficients of lactose and lactic acid / lactate was performed to improve the estimates of D_{eff} of the most important chemical species used in the model. This was necessary as no precise estimates of diffusivity of these species in cheese were available. The literature estimates originated from a linear regression of D_{eff} on the molecular weight, based on previous experimental work (Floury et al., 2010; Silva et al., 2013), and assuming that a linear dependency exists.

The uneven distribution of the fermentation products in figure 2 (right) compared to the much more even distribution in figure 2 (left) mainly originated from the reduced diffusivity of lactic acid / lactate (the experimentally determined value of D_{eff} was nearly an order of magnitude smaller than the estimation based on the molecular weight, see above). This more than compensated for the increased diffusivity of lactose, which was more than an order of magnitude higher than its literature-based estimate. The latter, however, resulted in an increased conversion of lactose (and thus in a higher yield of lactic acid / lactate), as lactose diffused much quicker to the centres of metabolic activity.

Validation of the Model

The first step to validate the model was the measurement of the average pH at the end of the ripening period (56 days) for 27 pieces of the cheese matrix (figure 3). One of the important findings of this validation was the substantial influence of the initial spatial distribution of the lactic acid bacteria. The pH-distribution at the end of the ripening period appears to be consistent with an injection assumption roughly intermediate between the two borderline cases shown in figure 1, but somewhat closer to the cylindrical injection assumption (figure 3, bottom right) than to the spherical (figure 3, bottom left). Direct spatial measurements of the concentration of the injected bacteria were impractical, as the concentration decreased quickly from the injection point.

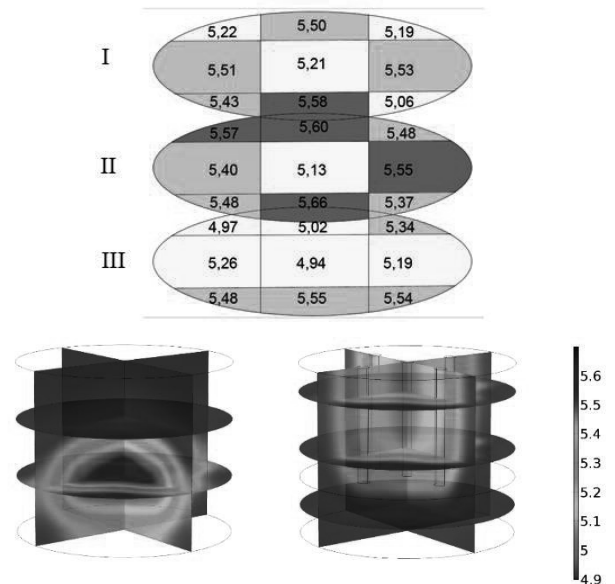


Figure 3: Measured (top) and modelled (bottom) pH-values in the cheese matrix after 56 days of ripening. The top figure shows three different layers (top, central, bottom) of the cheese matrix, each of which is further cut into 9 pieces, whose experimentally determined average pH is shown. The bottom left figure shows the assumption of a spherical initial injection of the bacterial suspension, while the bottom right figure shows the assumption of a cylindrical initial injection.

While the experiment shows some deviations from the expected symmetry, the model predictions nevertheless are not contradicted by the experimentally determined spatial pH-distribution.

Optimisation of the Injection Pattern

A preferably uniform distribution of fermentation products in the cheese matrix at the end of the ripening period is an important indicator of cheese quality. As long as the distribution of fermentation products of a cheese is not even enough, the injection strategy has to be adapted. This can be achieved by varying the number of injections (which is generally chosen to be as low as possible), the injection pattern (i.e. the injection positions), or the bacterial suspension injected in terms of its volume or concentration. Choosing these factors carefully is therefore crucial, and grows in importance with increasing complexity of the cheese geometry.

The necessity to perform a potentially large number of experiments to achieve a “good” injection pattern practically precludes a purely experimental approach. However, as the number of model runs necessary for this inverse optimisation problem might be large as well, an efficient model with manageable run-time is required.

CONCLUSIONS AND FUTURE WORK

Three-dimensional, spatially explicit models that take the dynamic changes in the concentrations of microorganisms and substrates, metabolites and other chemical species in time and space into account are to date rarely used in predictive microbiological models. This is regrettable, as the results obtained so far show that employing models based on CFD

can make a valuable contribution to predictive microbiology in many practical applications.

The new technology platform for cheese production allowed for an investigation into the effects of localised centres of bacterial activity on the overall fermentation rate, as well as the spatial distribution of fermentation products over time. In the current context of the project, this is important in order to obtain a sufficient cheese quality, which requires either an optimisation of the injection strategy, or a good estimate for the required ripening period for a given injection pattern. In addition, new cheese shapes can be modelled based on the parameters obtained from a previously analysed cheese shape, thus shortening development time, which could enable even small enterprises with limited financial resources to create competitive niche products.

However, applications are not limited to the new method for cheese production proposed. Whenever spatial locations of microorganisms are important, these models can considerably improve predictions made by traditional microbiological models. Applications might include ripening of cheese using traditional production methods if the spatial distribution and size of colonies is known (Jeanson et al., 2011) or uneven (Reinbold et al., 1958), and meat curing. As soon as well-adjusted models exist, they can substantially save time compared to an experimental approach, in particular if, as was the case here, lengthy fermentation processes are modelled.

The next step in this project will be the spatial measurements of the pH, substrate, fermentation products and bacterial concentrations at *different* points in time during the ripening period, analogous to figure 3 (top). This will allow for a better fine-tuned, more realistic spatiotemporal model of cheese ripening for the investigated new cheese-production method. As soon as the model is sufficiently close to the experimental results, optimisation of the injection strategy for arbitrary cheese shapes will be the final modelling exercise.

REFERENCES

- Baranyi, J., and Roberts, T.A. (1994). A dynamic approach to predicting bacterial growth in food. *Int. J. Food Microbiol.* 23, 277–294.
- Bernaerts, K., Dens, E., Vereecken, K., Geeraerd, A.H., Standaert, A.R., Devlieghere, F., Debevere, J., and Van Impe, J.F. (2004). Concepts and tools for predictive modeling of microbial dynamics. *J. Food Prot.* 67, 2041–2052.
- Bouvier, L., Moreau, A., Ronse, G., Six, T., Petit, J., and Delaplace, G. (2014). A CFD model as a tool to simulate β -lactoglobulin heat-induced denaturation and aggregation in a plate heat exchanger. *J. Food Eng.* 136, 56–63.
- Dens, E.J., and Van Impe, J.F. (2000). On the importance of taking space into account when modeling microbial competition in structured food products. *Math. Comput. Simul.* 53, 443–448.
- Dens, E.J., and Van Impe, J.F. (2001). On the need for another type of predictive model in structured foods. *Int. J. Food Microbiol.* 64, 247–260.
- Denys, S., Pieters, J.G., and Dewettinck, K. (2005). Computational fluid dynamics analysis for process impact assessment during thermal pasteurization of intact eggs. *J. Food Prot.* 68, 366–374.
- Floury, J., Jeanson, S., Aly, S., and Lortal, S. (2010). Determination of the diffusion coefficients of small solutes in cheese: A review. *Dairy Sci. Technol.* 90, 477–508.

- Van Impe, J.F., Poschet, F., Geeraerd, A.H., and Vereecken, K.M. (2005). Towards a novel class of predictive microbial growth models. *Int. J. Food Microbiol.* 100, 97–105.
- Jeanson, S., Chadoeuf, J., Madec, M.N., Aly, S., Floury, J., Brocklehurst, T.F., and Lortal, S. (2011). Spatial distribution of bacterial colonies in a model cheese. *Appl. Environ. Microbiol.* 77, 1493–1500.
- Kebary, K.M.K., and Morris, H.A. (1990). Porosity, Specific Gravity and Air Content in Blue Cheeses. *Food Struct.* 9, 57–60.
- Norton, T., and Sun, D.-W. (2006). Computational fluid dynamics (CFD) – an effective and efficient design and analysis tool for the food industry: A review. *Trends Food Sci. Technol.* 17, 600–620.
- Norton, T., Tiwari, B., and Sun, D.W. (2013). Computational Fluid Dynamics in the Design and Analysis of Thermal Processes: A Review of Recent Advances. *Crit. Rev. Food Sci. Nutr.* 53, 251–275.
- Plana-Fattori, A., Flick, D., Ducept, F., Doursat, C., Michon, C., and Mezdoor, S. (2016). A deterministic approach for predicting the transformation of starch suspensions in tubular heat exchangers. *J. Food Eng.* 171, 28–36.
- Poschet, F., Vereecken, K.M., Geeraerd, A.H., Nicolai, B.M., and Van Impe, J.F. (2005). Analysis of a novel class of predictive microbial growth models and application to coculture growth. *Int. J. Food Microbiol.* 100, 107–124.
- Reinbold, G.W., Hussong, R. V., and Stine, J.B. (1958). Distribution of Propionibacteria in Swiss Cheese. *J. Dairy Sci.* 41, 606–610.
- Silva, J.V.C., Peixoto, P.D.S., Lortal, S., and Floury, J. (2013). Transport phenomena in a model cheese: the influence of the charge and shape of solutes on diffusion. *J. Dairy Sci.* 96, 6186–6198.
- Skinner, G.E., Larkin, J.W., and Rhodehamel, E.J. (1994). Mathematical Modeling of Microbial Growth: a Review. *J. Food Saf.* 14, 175–217.
- Wilde, J., Baumgartner, C., Fertsch, B., and Hinrichs, J. (2001). Matrix effects on the kinetics of lactose hydrolysis in fermented and acidified milk products. *Chem. Biochem. Eng. Q.* 15, 143–147.

BIOGRAPHY

THORSTEN STEFAN was born in Graz, Austria. He studied Mathematics and Chemistry at the University of Graz (Austria) and Mathematical Biology at the University of York (UK). He obtained his PhD at the University of Glasgow (UK) in 2016 with a thesis that investigated reasons for the diversity of the MHC, which is a highly polymorphic genetic region in the vertebrate genome. While in Glasgow, he mostly worked at the interface of mathematical modelling, population genetics and immunology. In January 2015, he moved to the University of Hohenheim, Stuttgart (Germany), where he started doing research in the area of predictive modelling in foods in addition to tackling research questions from a theoretical point of view in the wider biological subject area.

INFLUENCE OF COLD ATMOSPHERIC PLASMA ON THE MICROBIAL DYNAMICS OF SALMONELLA TYPHIMURIUM DURING STORAGE AT DIFFERENT TEMPERATURES

Cindy Smet¹, Maria Baka¹, James Walsh², Vasilis Valdramidis³ and Jan F.M. Van Impe^{1,*}

¹ BioTeC+ & OPTEC, Department of Chemical Engineering, KU Leuven, Gent, Belgium

¹ CPMF2, Flemish Cluster Predictive Microbiology in Foods

² Department of Electrical Engineering and Electronics, University of Liverpool, Liverpool, UK

³ Department of Food Studies and Environmental Health, University of Malta, Msida, Malta

* E-mail: Jan.VanImpe@kuleuven.be

KEYWORDS

Cold atmospheric plasma, storage temperature, osmotic stress, suboptimal pH.

ABSTRACT

Microbial decontamination by means of cold atmospheric plasma (CAP) offers great potential for treatment of heat-sensitive food products, extending their storage life. CAP is created by applying a high voltage to a gas stream, resulting in microbial inactivation according to different mechanisms. This paper assesses the influence of CAP on the storage life of food model systems inoculated with *Salmonella* Typhimurium. (Food) model systems, with varying intrinsic factors (pH, salt concentration, (micro)structure), are treated for 5 minutes using a dielectric barrier discharge reactor generating a helium-oxygen plasma. Following treatment, the impact of extrinsic factors is evaluated by storage at 8°C or 20°C. During storage, cell densities are determined. Data are fitted with predictive (growth or inactivation) models. CAP treatment can result in microbial reductions and prolongs storage, however its rate of success is dependent on both extrinsic and intrinsic factors. An important factor is the storage temperature, as recovery of CAP treated cells proves more difficult when stored at 8°C. At 20°C, cell growth is merely slowed down. Additionally, at pH 5.5, 6% (w/v) NaCl, osmotic stress is induced on the microorganisms, which results in low cell recovery or further inactivation. However, the food (micro)structure has a limited impact during storage.

INTRODUCTION

The use of CAP represents a novel technology with high potential for decontamination of heat sensitive foods products, like fruits and vegetables. Nowadays, the microbiological safety of these products is often ensured by the use of a washing treatment in combination with chemical biocides (Aharoni et al. 1997; Goodburn and Wallace 2013). The high water consumption together with the possible formation of carcinogenic halogenated by-products, constitute a major disadvantage regarding the use of this technique. Therefore, the innovative CAP technology could result as effective alternative, due to its short treatment at room temperature (Korachi et al. 2010; Moisan et al. 2001).

CAP is produced by the excitation of a gas stream with a high voltage, at room temperature and under atmospheric

pressure. This excitation results in a mixture of electrons, ions, atomic species, free radicals, and UV photons (Deng et al. 2006; Perni et al. 2007). Reactive species and charged particles accumulate at the surface of the cell membrane and bombard it, inducing lesions. The (toxic) reactive species diffuse through cell membranes, or penetrate through lesions, and interact with macromolecules, causing local damage. In addition, UV photons modify the DNA of the microorganisms by inducing the formation of thymine dimers (Fernandez and Thompson 2012; Gallagher et al. 2007; Moisan et al. 2002).

The CAP efficacy, together with its impact on the storage life, depends on several parameters. Next to the CAP set-up, plasma characteristics or operating parameters (like power, frequency, voltage, gas flow or composition) are of major importance (Ehlbeck et al., 2011; Deng et al., 2006; Han et al., 2014; Fernandez and Thompson, 2012). Additionally, the target microorganism, the microbial load and growth phase have an effect on the CAP treatment (Afshari and Hosseini, 2012; Fernandez et al., 2012). Finally, it was recently proved that also the (food) sample properties determine the success of the treatment. Firstly, the topography of the sample influences CAP treatment (Fernandez et al., 2013). Secondly, factors intrinsic to the sample (e.g., food microstructure, saline concentration, pH) can exert stresses on the microorganisms and impact the efficacy of CAP treatment (Kayes et al., 2007; Rowan et al., 2007; Smet et al., 2016, 2017a).

For microorganisms, stress includes all conditions deviating from their optimal growth conditions, and can lead to damaging the cell or even cell death. Stress resistance is related to the possibility of cells to handle these stress factors after exposure. Additionally, cross protection can arise, as cells exposed to a certain type of stress can gain resistance towards subsequent stresses (Archer, 1996). Microorganisms can suffer from stress during different stages in the food production chain: (i) when they survive in an environment where a limited number of nutrients are present, before they contaminate the food product (e.g., survival in water or in equipment), (ii) when surviving on a food product with intrinsic factors far from the optimal for growth (e.g., suboptimal pH, low aw), (iii) during treatment of the product (e.g. pasteurization, HHP, CAP), and (iv) during storage (e.g., low storage temperatures).

The objective of this work is to assess the influence of CAP on the storage life of a (food) model system with varying intrinsic properties, based on the microbial behavior of *S. Typhimurium* at different storage temperatures. Survival or growth of this important foodborne pathogen during the storage is characterized and compared with microbial dynamics of untreated cells. The impact of osmotic stress and suboptimal pH (pH 7.4, 0% (w/v) NaCl or pH 5.5, 6% (w/v) NaCl), and food (micro)structure (liquid or solid(like) system) are incorporated in the experimental plan.

MATERIALS AND METHODS

Salmonella enterica serovar Typhimurium SL1344 was kindly provided by the Institute of Food Research (IFR, Norwich, UK). The culture was stored at -80°C in Tryptone Soya Broth (TSB (Oxoid LTd., Basingstoke, UK)) supplemented with 25% (v/v) glycerol (Acros Organics, NJ, USA). For every experiment, a fresh purity plate was prepared from the frozen stock culture by spreading a loopful onto a Tryptone Soya Agar plate (TSA (Oxoid Ltd., Basingstoke, UK)) incubated at 37°C for 24 h. One colony from this plate was transferred into 20 mL TSB and incubated under static conditions at 37°C for 8 h (Binder KB series incubator; Binder Inc., NY, USA). Next, 200 µL from this stationary phase culture was added to 20 mL of fresh TSB and incubated under the same conditions for 16 h. Following this protocol, cell cultivation yielded early-stationary phase populations ($9 \log_{10}(\text{CFU/mL})$), which were used for further inoculation.

In a following step, *S. Typhimurium* was grown under different experimental conditions (see Introduction). In summary, cells were grown at 20°C in petri dishes under static conditions, planktonically in a liquid system (Tryptic Soya Broth (TSB)), or as surface colonies (TSB, supplemented with 5% (w/v) gelatin). All systems had a specific salt concentration and the pH was adapted. Once the cells reached the stationary growth phase, samples were diluted and re-inoculated before inactivation, in either the liquid model system ($5.5 \log(\text{CFU/mL})$) or on the solid(like) model system ($5.5 \log(\text{CFU/cm}^2)$) and were CAP treated.

A Dielectric Barrier Discharge (DBD) reactor (Figure 1) was used to study microbial inactivation, similar as described in Smet et al. (2016). In summary, an enclosure (22.5 cm x 13.5 cm x 10 cm) around the electrode increased the residence time of the plasma species around the sample and provided a more controlled environment. The residence time in the enclosure, not airtight, was approximately 45 s. The plasma was generated in a gas mixture of helium (purity 99.996%, at a flow rate of 4 L/min) and oxygen (purity $\geq 99.995\%$, at a flow rate of 40 mL/min). Thus, the total flow rate of this 99% helium, 1% oxygen gas mixture is 4.04 L/min. Samples were placed between the 0.8 cm gap of the DBD electrodes, and after flushing the reactor with the helium-oxygen gas mixture for 4 min, the plasma was generated. Samples were treated for 5 minutes at a peak-to-peak voltage around 7 kV, frequency of 15 kHz and dissipated plasma power of 7.45 W. The temperature increase of the sample, measured directly after treatment using a thermometer, was about 2°C.

After treatment, petri dishes were immediately sealed with parafilm, and stored in a temperature controlled incubator at either 8 or 20°C. In some cases, the liquid carrier significantly evaporated due to the CAP generated, thus (for all samples of this type) 100 µL of dilution medium at the same experimental conditions was added prior to storage. Control tests, executed without current, confirmed that this evaporation was because of the CAP generation and not due to the gas flow itself (Smet et al., 2017b). During the storage period (10 days if stored at 20°C, 30 days if stored at 8°C) sampling took place at regular time intervals (ranging from every couple of hours to a few samples a week, depending on the storage temperature). The cell density during storage was determined via viable plate counting on Tryptic Soy Agar plates, using the drop plating technique (Miles et al. 1938). For cells inactivated in a liquid carrier, 900 µL of saline solution (0.85% (w/v) NaCl) was added to the sample. Afterwards, the diluted sample (1 mL) was collected from the petri dish and transferred to a sterile Eppendorf tube, in order to prepare serial decimal dilutions. For cells inactivated on the solid(like) surface, the content of the petri dish was transferred to a stomacher bag, liquefied in a thermostatic water bath at 37°C and homogenized in the stomacher for 30 seconds. 1 mL was taken from this bag, and serial decimal dilutions were prepared with saline solution. For each sample, 3-6 dilutions were plated in duplicate onto TSA plates, which placed at 37°C for 24 h before counting.

The microbial dynamics observed during storage were fitted with the model of Baranyi et al. (1994) or Geeraerd et al. (2000). If growth was observed, experimental data were fitted with the primary growth model of Baranyi and Roberts (1994):

$$\begin{aligned} \frac{dN(t)}{dt} &= \frac{Q(t)}{1+Q(t)} \cdot \mu_{max} \cdot \left(1 - \frac{N(t)}{N_{max}}\right) \cdot N(t) \\ \frac{dQ(t)}{dt} &= \mu_{max} \cdot Q(t) \end{aligned} \quad (1)$$

where $N(t)$ [CFU/mL] is the cell density at time t [h], N_{max} [CFU/mL] is the maximum cell density at the stationary phase, μ_{max} [h⁻¹] is the maximum growth rate and $Q(t)$ [-] is a measure of the physiological state of the cells.

The model of Geeraerd et al. (2000), was used to fit experimental data in case inactivation was observed. This model describes a microbial inactivation curve consisting of a shoulder, a loglinear inactivation phase and a tail:

$$\begin{aligned} \frac{dN(t)}{dt} &= -\frac{1}{1+C_c(t)} \cdot k_{max} \cdot \left(1 - \frac{N_{res}}{N(t)}\right) \cdot N(t) \\ \frac{dC_c(t)}{dt} &= -k_{max} \cdot C_c(t) \end{aligned} \quad (2)$$

where $N(t)$ [CFU/mL] is the cell density at time t [h], N_{res} [CFU/mL] is the residual cell density at the tailing phase, k_{max} [h⁻¹] is the maximum inactivation rate and $C_c(t)$ [-] is a measure of the physiological state of the cells.

Parameters of both models were estimated via the minimization of the sum of square errors (SSE), using the *lsqnonlin* routine of the Optimization Toolbox of Matlab version R2009b (The Mathworks Inc.). Simultaneous with parameter estimation, the parameter estimation errors were determined based on the Jacobian matrix. The Root Mean

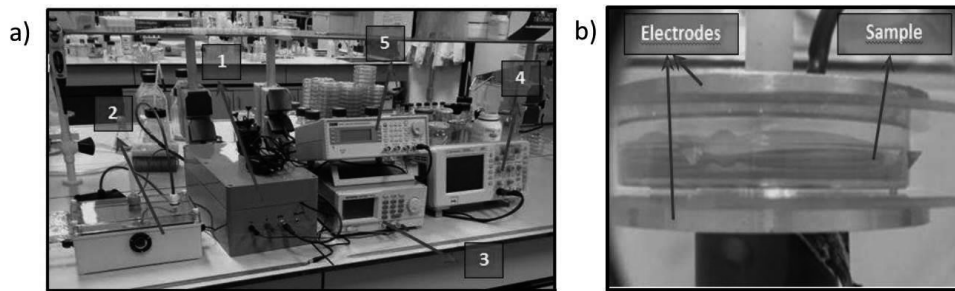


Figure 1: a) the CAP set up: (1) plasma power source, (2) Dielectric Barrier Discharge reactor, (3) DC power supply, (4) oscilloscope and (5) function generator. b) DBD electrode inside reactor.

Squared Error (RMSE) was added as an absolute measure of the goodness of the model fit to the actual observed data.

RESULTS AND DISCUSSION

The growth and inactivation curves in Figure 2 illustrate the influence of CAP treatment (\diamond) as compared to untreated controls (x), for both liquid and solid(like) model systems, under different experimental (pH 7.4, 0% (w/v) NaCl (pink), pH 5.5, 6% (w/v) NaCl (blue)) and storage conditions (8 and 20°C). The experimental data were fitted with either the Baranyi and Roberts (1994) (growth) or the Geeraerd et al. (2000) model (inactivation). The growth (N_0 , lag (length of lag time), μ_{max} , N_{max}) or inactivation parameters (N_0 , t_l (length of shoulder), k_{max} , N_{max}), are represented in Table 1.

Figure 3 provides a visual interpretation of the different tendencies.

Regardless of the experimental growth or storage conditions, CAP treatment extends the storage life of the treated (model) systems, indicating the CAP treatment itself does not induce cell resistance. In most cases, this extension is realized by slowing down microbial growth, as it is the case for all experiments at 20°C and for pH 7.4, 0% (w/v) NaCl at 8°C. In the other cases, the cell densities are even further reduced (8°C, pH 5.5, 6% (w/v) NaCl). Noteworthy, for pH 5.5, 6% (w/v) NaCl at 8°C (severe stress), also untreated control samples display an inactivation of the cell level.

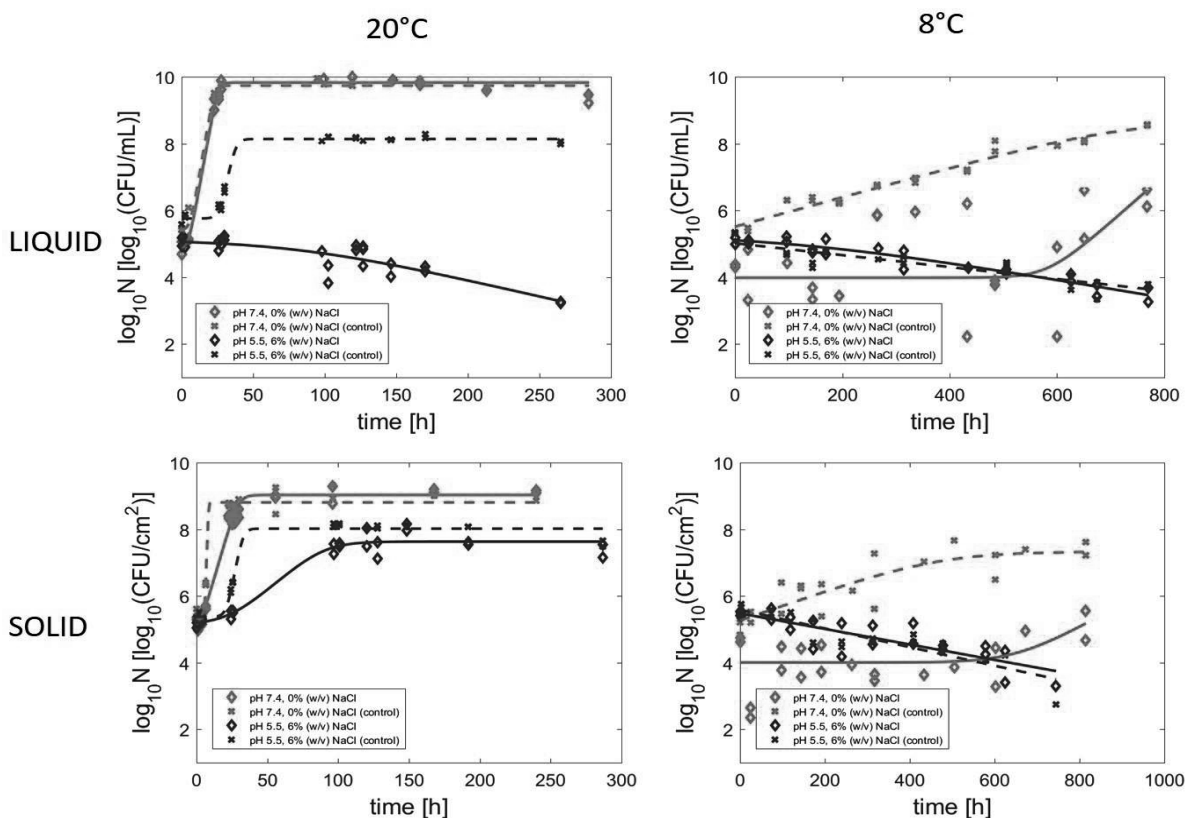


Figure 2: Growth/ inactivation curves of *S. Typhimurium*, both for CAP treated samples and untreated controls, stored for 10 d at 20 °C (left) or for 30 d at 8 °C (right). Cells were inactivated in a liquid (top) or on a solid(like) (bottom) model system. Prior to CAP treatment, cells were grown at pH 7.4, 0% (w/v) NaCl or pH 5.5, 6% (w/v) NaCl. Experimental data (symbols) and global fit of the Baranyi and Roberts model (growth), or the Geeraerd et al. model (inactivation): CAP treated samples (\diamond , solid line) and controls (x, dashed line).

Table 1: Growth ($\log_{10}N_0$ (\log_{10} (CFU/mL or \log_{10} (CFU/cm²), lag (h), μ_{max} (1/h), $\log_{10}N_{res}$ (\log_{10} (CFU/mL or \log_{10} (CFU/cm²)) and inactivation ($\log_{10}N_0$ (\log_{10} (CFU/mL or \log_{10} (CFU/cm²), t_l (h), k_{max} (1/h), $\log_{10}N_{res}$ (\log_{10} (CFU/mL or \log_{10} (CFU/cm²)) parameters for *S. Typhimurium* stored at 20°C and 8°C. Cells were grown, inactivated and stored in a liquid carrier or on a solid(like) surface. Cells were grown at pH 5.5, 6% (w/v) NaCl or at pH 7.4, 0% (w/v) NaCl. Both CAP treated samples and untreated controls were stored.

Temperature	Experimental condition	(Micro)structure	Treatment	Inactivation parameters				RMSE	
				$\log_{10}N_0$	t_l	k_{max}	$\log_{10}N_{res}$		
20°C	pH 5.5, 6% (w/v) NaCl	LIQUID	CAP treated	5.1 ± 0.1	85.6 ± 27.2	0.029 ± 0.004	-	0.287	
			Control	Growth parameters				RMSE	
		SOLID	CAP treated	5.2 ± 0.1	24.4 ± 9.8	0.087 ± 0.019	7.6 ± 0.1		0.2482
			Control	5.4 ± 0.1	21.2 ± 2.6	0.522 ± 0.346	8.0 ± 0.0	0.1704	
	pH 7.4, 0% (w/v) NaCl	LIQUID	CAP treated	4.9 ± 0.2	4.7 ± 2.1	0.545 ± 0.053	9.8 ± 0.1	0.2495	
			Control	5.4 ± 0.2	5.9 ± 2.7	0.582 ± 0.087	9.7 ± 0.1	0.2287	
		SOLID	CAP treated	5.1 ± 0.1	3.0 ± 2.1	0.338 ± 0.026	9.0 ± 0.1	0.2244	
			Control	5.3 ± 0.1	5.8 ± 27.0	3.335 ± 129.141	8.8 ± 0.1	0.2522	
	8°C	pH 5.5, 6% (w/v) NaCl	LIQUID	CAP treated	5.1 ± 0.1	169.1 ± 95.7	0.006 ± 0.001	-	0.1887
				Control	5.0 ± 0.1	-	0.004 ± 0.000	-	0.2389
SOLID			CAP treated	5.5 ± 0.1	-	0.005 ± 0.002	-	0.3738	
			Control	5.6 ± 0.1	-	0.007 ± 0.001	-	0.3123	
pH 7.4, 0% (w/v) NaCl					Growth parameters				RMSE
					$\log_{10}N_0$	lag	μ_{max}	$\log_{10}N_{max}$	
		LIQUID	CAP treated	4.0 ± 0.3	582.7 ± 92.9	0.033 ± 0.022	-	1.3576	
			Control	5.5 ± 0.1	0.0 ± 63.6	0.010 ± 0.001	8.7 ± 0.3	0.2216	
		SOLID	CAP treated	4.0 ± 0.2	654.3 ± 148.2	0.017 ± 0.016	-	0.7153	
			Control	5.3 ± 0.3	0.0 ± 204.2	0.010 ± 0.006	7.3 ± 0.3	0.5073	

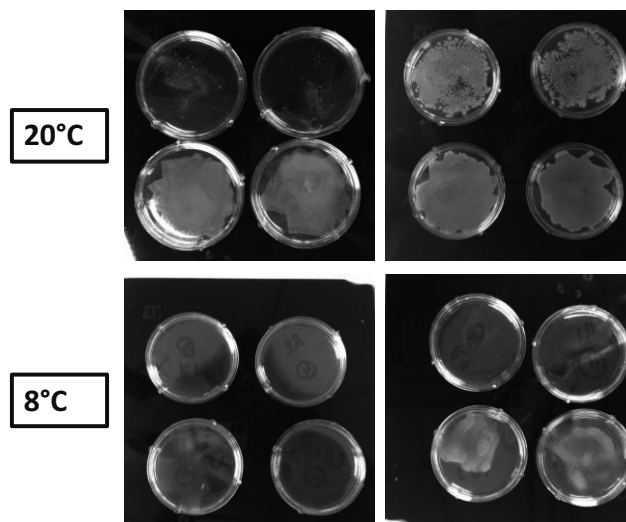


Figure 3: CAP treated samples (top, duplicates) and controls (bottom, duplicates) for *S. Typhimurium* cells inactivated on a solid(like) surface: 20°C) Cells grown at pH 7.4, 0% (w/v) NaCl, stored at 20°C for 10 days (images after 1 day (left) and 10 days (right) of storage). 8°C) Planktonic cells grown at pH 7.4, 0% (w/v) NaCl, stored at 8°C for 30 days (images after 8 (left) and 30 days (right) of storage).

When assessing storage parameters (Table 1) for experimental cases where growth was observed, large differences in lag phase duration were only observed at 8°C, where CAP treated samples have longer lag phases as compared to the controls. Differences in maximum specific growth rates between CAP treated samples and the untreated controls depend on the experimental condition. For the most optimal growth condition, pH 7.4, 0% (w/v) NaCl at 20°C, growth patterns for CAP treated samples and controls are much alike, therefore μ_{max} values are not significantly different. μ_{max} values are alike for this optimal experimental condition at 8°C, as the difference in growth behavior is mainly caused by the extension of the lag phase. If growth during storage resulted in a stationary phase, N_{max} values are either similar for both CAP treated samples and controls, or lower for treated samples. When inactivation is observed during storage, a shoulder phase is rarely present (or short). Again, differences in inactivation rates (k_{max}) depend on the experimental condition. At 20°C and for cells grown at pH 5.5, 6% (w/v) NaCl (inactivation in a liquid carrier) only CAP treated cells resume to inactivate during storage. For all experiments at pH 5.5, 6% (w/v) NaCl and 8°C, both CAP treated samples and controls (further) inactivate during storage. However, differences in k_{max} are limited. For pH 5.5, 6% (w/v) NaCl at 8°C, the residual cell densities in the tail are the lowest for CAP treated samples.

The positive influence of CAP treatment on food (model) storage has also been reported in literature. Surowsky et al. (2014) illustrated that additional storage of CAP (plasma jet, Ar/O₂ mixture) treated apple juice (2 mL samples) inoculated with *Citrobacter freundii* further reduces the microbial counts. Lacombe et al. (2015) studied the influence of CAP treated blueberries on native microbiota, after storage up to 7 days at 4°C, using a jet system operating with ambient air. Cell reduction persists throughout the complete storage period. Similar results are reported by Klockow and Keener (2009), for storage of spinach leaves at 5°C for 24 hours, using a DBD set-up working with air and oxygen. This further decrease in cell level during storage is comparable to findings reported for experiments at pH 5.5, 6% (w/v) NaCl stored at 8°C (or in some cases even when stored at 20°C). Tappi et al. (2016) studied the effect of CAP (DBD, working with air) on storage of melons (at 10°C during 4 days) and observe a delayed growth of spoilage mesophilic and psychrotropic microflora if CAP treated. In this study, a delayed cell growth was observed for the optimal growth condition (pH 7.4, 0% (w/v) NaCl) if stored at 8°C, and for most experimental conditions stored at 20°C.

The beneficial effect of CAP treatment on the elongation of the storage period is very distinct, and proved by both literature and the presented results. However, the results in Figure 2 also indicate that the impact of CAP on the microbial kinetics during storage is highly affected by the storage temperatures. Additionally, intrinsic factors of the food (model) system prove to have an effect. The impact of all of these factors on (food) preservation by CAP treatment are discussed in more detail in the following sections.

Influence of Storage Temperature

Temperature is an important extrinsic factor influencing microbial dynamics. During storage at 20°C, *S. Typhimurium* cells are almost always able to grow, CAP treated or not. At 8°C, the low temperature affects the cells ability to recover and grow, possibly even resulting in further inactivation (pH 5.5, 6% (w/v) NaCl).

For experimental conditions where growth is observed for both storage temperatures, the impact of the temperature on the parameters is evident (Table 1). At 8°C (suboptimal temperatures), microbial growth is slowed down as compared to the results at 20°C, resulting in a reduction of growth rates and maximum cell densities together with an elongation of the lag phase. This is due to a decrease of enzymatic reactions within the microbial cell, in combination with changes in its membrane structure (Adams and Moss, 2006; Swinnen et al., 2004). When for both temperatures the cell level further reduces during storage (pH 5.5, 6% (w/v) NaCl for samples treated on a liquid carrier), the impact of the temperature on the parameters is not significant.

When assessing the relation between CAP treated samples and controls at both temperatures, it can be concluded that storage at a lower temperature prolongs the positive effect of CAP treatment on the microbial kinetics. This effect is illustrated at pH 7.4, 0% (w/v) NaCl. After storage of 30 days following CAP treatment, cells at 8°C are not able to reach a stationary phase, while control samples do. At 20°C, the stationary phase is reached within 48 hours, for both CAP treated samples and controls. The additional effect of temperature on the microbial behavior after CAP treatment is as well notable at pH 5.5, 6% (w/v) NaCl for cells inactivated on a solid(like) surface. At 20°C, CAP treatment reduces growth as compared to the controls, while at 8°C both CAP treated samples and controls are no longer able to survive. Regardless of the experimental conditions, the relation in microbial growth behavior between CAP treated samples and untreated controls completely adapts according to the temperature, indicating the additional benefit of a low storage temperature after CAP treatment.

Similar findings regarding the effect of the storage temperature after CAP treatment, in comparison to the controls, have previously been reported by Song et al. (2015). In that study, using N₂ as a working gas, 10 days of storage of CAP treated lettuce results in a further reduction of the *E. coli* cell level when stored at 4°C, while growth is observed when stored at 10°C. Inactivation on lettuce (pH 6.0-6.5, a_w up to 1.0) can be best compared to our system of surface colonies grown at pH 7.4, 0% (w/v) NaCl, for cells inactivated on a solid(like) surface. In this case, regardless of the storage at 8 or 20°C, a (reduced) growth is always observed (as both temperatures selected are not as severe as 4°C). Furthermore, in Song et al. (2015) the controls follow the same trend as the treated samples at both temperatures tested. This is in contrast with results reported at 20°C for pH 5.5, 6% (w/v) NaCl (inactivation for CAP treated samples, growth for controls). Differences with findings from literature already indicate the additional influence of other (intrinsic) factors on the storage behavior after CAP treatment.

Influence of Intrinsic Factors

Next to the storage temperature, also the intrinsic factors (e.g., pH and salt level) of the food product or model system influence microbial dynamics during storage. Whereas for the optimal experimental condition (pH 7.4, 0% (w/v) NaCl) (slow) growth is always observed for CAP treated samples and untreated controls, increasing the acidic and osmotic stress level (pH 5.5, 6% (w/v) NaCl) slows down growth and can even result in a shift towards microbial inactivation.

As at 8°C, both growth (pH 7.4, 0% (w/v) NaCl) and inactivation (pH 5.5, 6% (w/v) NaCl) occur, the effect of a stressing experimental condition becomes abundantly clear. Similar findings were reported at 20°C, when inactivated in a liquid carrier. For the conditions at 20°C expressing growth, the optimal condition introduces shorter lag phases, higher μ_{max} values and higher maximum cell densities during the storage period as compared to the condition at pH 5.5 and 6% (w/v) NaCl.

Similar results were reported for both planktonic cells and surface colonies in Boons et al. (2013) and Smet et al. (2015), where the influence of osmotic and acidic stress on the growth morphology of *S. Typhimurium* cells is studied. The addition of the salt in the medium reduces the water activity, exerting severe stresses on the microorganisms and possibly resulting in cell death (O'Byrne and Booth, 2002). As in Smet et al. (2015), the suboptimal pH values selected in this study are mild and far from growth limits, as *S. Typhimurium* has a pH_{min} of 3.8 and pH_{max} of 9.5 (ICMSF, 1996). Therefore, the pH influence on the storage behavior is likely to be lower as compared to the impact due to osmotic stress. In summary, as for temperature, also (stressing) media conditions influence the microbial dynamics and are able to amplify the effect of CAP, further extending the storage period.

A final intrinsic factor potentially affecting storage is the influence of the food (micro)structure (liquid model system vs. solid(like) model system). The influence of the (micro)structure is mainly important during treatment, as it affects the cells growth morphology and influences the delivery mode of CAP active species to the microbial contamination (Smet et al. 2017b). The results indicate only a small influence of the food (micro)structure during the subsequent storage after CAP treatment. However, the results in Figure 2 and Table 1 indicate that in rare cases the (micro)structure can also influence the microbial kinetics during subsequent storage, as recovery proved more difficult for the liquid samples (pH 5.5, 6% (w/v) NaCl), stored at 20°C. This can be explained by the fact that more long lived reactive species (e.g., H₂O₂) are produced in this liquid model system. In addition, low pH values are known to enhance the antimicrobial effect of H₂O₂, explaining why the phenomenon was not observed at pH 7.4, 0% (w/v) NaCl (Raffellini et al. 2007). However, the two support systems are not directly comparable, as the liquid carrier exists of only 100 μ L of media. Together with the difference in volume, the nutrient level available in the liquid carrier is different to the solid(like) surface, and might not be sufficient for microbial recovery and growth of CAP treated cells under certain experimental stressing conditions (pH 5.5, 6% (w/v) NaCl). This fact could contribute to differences

observed between the different support systems at 20°C and pH 5.5, 6% (w/v) NaCl.

CONCLUSIONS

CAP treatment prolongs the storage life of the model systems treated. Intrinsic factors have been previously reported to influence the CAP inactivation efficacy, as stressing intrinsic factors can create cells resistant to CAP. However, the stressing CAP treatment itself does not induce cells resistant to stressing storage conditions, as the beneficial effect of CAP during the storage life is obvious for all experimental conditions. Moreover, the results indicate that the microbial storage behavior is influenced by both intrinsic and extrinsic factors. As expected, a low storage temperature prolongs the positive effect of CAP treatment on the microbial kinetics, as cell recovery proves to be more difficult at low storage temperatures as compared to storage at room temperatures. Next to the storage conditions, the intrinsic factors of the sample itself again play an important role. Stressing media conditions, e.g., osmotic stress or a suboptimal pH value, can also amplify the positive CAP effect further extending the storage life. Finally, the food model system (micro)structure's impact on the storage life is minimal.

Even though the model systems do not fully mimic real food products (e.g., with respect to composition, volume, roughness, contamination level), and validation studies for real food products are required, this study already indicates that the novel CAP technology could also extend the storage life of food products. Furthermore, although the results obtained are valid for the specific DBD set-up used, this study can be regarded indicative for other systems (e.g., gliding arcs or corona discharges, other gas mixtures, or DBD systems with different electrode gaps). This research indicates CAP treatment is able to extend the storage time of a food product, depending on the storage conditions and intrinsic parameters of the product. Next to the ability of CAP to obtain high microbial reductions, the additional prolonged food storage enhances the suitability of CAP to be applied in the food industry.

ACKNOWLEDGEMENTS

This work was supported by project PFV/10/002 (Center of Excellence OPTEC-Optimization in Engineering) and by Post-Doctoral Mandate PDM/16/125 (Maria Baka) of the KU Leuven Research Council. It was also partly supported by a Marie Curie FP7-Reintegration-Grant within the 7th European Community Framework Programme under the project Development of novel Disinfection Technologies for Fresh Produce (DiTec) (303939), the COST ACTION TD1208, the COST ACTION FA1202 BacFoodNet (1202), and The Engineering & Physical Sciences Research Council (EPSRC), UK, grant EP/J005894/1 and EP/N021347/1.

REFERENCES

- Adams, M.R.; and M.O. Moss. 2006. "Food Microbiology. (2nd ed.)." Cambridge, UK: The Royal Society of Chemistry.
- Afshari, R.; and H. Hosseini. 2012 "2012 Atmospheric Pressure Plasma Technology: A New Tool for Food Preservation."

- International Conference on Environment, Energy and Biotechnology*, 33, 275-278
- Archer, D.L. 1996. "Preservation microbiology and safety: Evidence that stress enhances virulence and triggers adaptive mutations." *Trends in Food Science and Technology*, 7, 91-95.
- Aharoni, Y.; E. Fallik; A. Copel; M. Gil; S. Grinberg; and J.D. Klein. 1997. "Sodium bicarbonate reduces postharvest decay development on melons." *Postharvest Biology and Technology*, 10, 201-206.
- Baranyi, J.; T.A. Roberts. 1994. "A dynamic approach to predicting bacterial growth in food." *International Journal of Food Microbiology*, 23, 277-294.
- Boons, K.; E. Van Derlinden; L. Mertens; V. Peeters; and J.F. Van Impe. 2013. "Effect of Immobilization and Salt Concentration on the Growth Dynamics of *Escherichia coli* K12 and *Salmonella* Typhimurium." *Journal of Food Science*, 78, M567-M574.
- Deng, X.; J.J. Shi; and M.G. Kong. 2006. "Physical mechanisms of inactivation of *Bacillus subtilis* spores using cold atmospheric plasmas." *IEEE Transactions on Plasma Science*, 34, 1310-1316.
- Ehlbeck, J.; U. Schnabel; M. Polak; J. Winter; Th. von Woedtke; R. Brandenburg; T. von dem Hagen; and K-D. Weltmann. 2011. "Low temperature atmospheric pressure plasma sources for microbial decontamination." *Journal of Physics D: Applied Physics*, 44, 013002.
- Fernandez, A.; and A. Thompson. 2012. "The inactivation of *Salmonella* by cold atmospheric plasma treatment." *Food Research International*, 45, 678-684.
- Fernandez, A.; N. Shearer; D.R. Wilson; and A. Thompson. 2012. "Effect of microbial loading on the efficiency of cold atmospheric gas plasma inactivation of *Salmonella enterica* serovar Typhimurium." *International Journal of Food Microbiology*, 152, 175-180.
- Fernandez, A.; E. Noriega; and A. Thompson. 2013. "Inactivation of *Salmonella enterica* serovar Typhimurium on fresh produce by cold atmospheric gas plasma technology." *Food Microbiology*, 33, 24-29.
- Gallagher, M.K.; N. Vaze; S. Gangoli; V.N. Vasilets; A.F. Gutsol; T.N. Milovanova; S. Anandan; D.M. Murasko; and A.A. Fridman. 2007. "Rapid inactivation of airborne bacteria using atmospheric pressure dielectric barrier grating discharge." *IEEE Transactions on Plasma Science*, 35(5), 1501-1510.
- Geeraerd, A.; C. Herremans; and J.F. Van Impe. 2000. "Structural model requirements to describe microbial inactivation during a mild heat treatment." *International Journal of Food Microbiology*, 59, 185-209.
- Goodburn, C. and C. Wallace. 2003. "The microbiological efficacy of decontamination methodologies for fresh produce: A review." *Food Control*, 32, 418-427.
- Han, L.; S. Patil; K.M. Keener; P. Cullen; and P. Bourke. 2014. "Bacterial Inactivation by High Voltage Atmospheric Cold Plasma: Influence of Process Parameters and Effects on Cell Leakage and DNA." *Journal of Applied Microbiology*, 116, 784-794.
- ICMSF. 1996. "Micro-organisms in foods 5. In: Characteristics of microbial pathogens." London, UK: Blackie Academic & Professional.
- Kayes, M.M.; F.J. Critzer; K. Kelly-Wintenberg; J.R. Roth; T.C. Montie; and D.A. Golden. 2007. "Inactivation of Foodborne Pathogens Using a One Atmosphere Uniform Glow Discharge Plasma." *Foodborne pathogens and disease*, 4, 50-59.
- Klockow, P.A.; K.M. Keener. 2009. "Safety and quality assessment of packaged spinach treated with a novel ozone-generation system." *LWT - Food Science and Technology*, 42, 1047-1053
- Korachi, M.; C. Gurol; and N. Aslan. 2010. "Atmospheric plasma discharge sterilization effects on whole cell fatty acid profiles of *Escherichia coli* and *Staphylococcus aureus*." *Journal of Electrostatics*, 68, 508-512.
- Lacombe, A.; B.A. Niemira; J.B. Gurtler; X. Fan; J. Sites; G. Boyd; and H. Chen. 2015. "Atmospheric cold plasma inactivation of aerobic microorganisms on blueberries and effects on quality attributes." *Food Microbiology*, 46, 479-484.
- Miles, A.A.; S.S. Misra; and J.O. Irwin. 1938. "The estimation of the bactericidal power of the blood." *The Journal of Hygiene*, 38(6), 732-749.
- Moisan, M.; J. Barbeau; S. Moreau; J. Pelletier; M. Tabrizian; and L. Yahia. 2001. "Low-temperature sterilization using gas plasmas: a review of the experiments and an analysis of the inactivation mechanisms." *International Journal of Pharmaceutics*, 226, 1-21.
- Moisan, M.; J. Barbeau; M.-C. Crevier; J. Pelletier; N. Philip; and B. Saoudi. 2002. *Plasma sterilization. Methods and mechanisms*. Pure Applied Chemistry, 74, 349-358.
- O'Byrne, C.P.; and I.R. Booth. 2002. "Osmoregulation and its importance to foodborne microorganisms." *International Journal of Food Microbiology*, 74, 203-216.
- Perni, S.; G. Shama; J.L. Hobman; P.A. Lund; C.J. Kershaw; G.A. Hidalgo-Arroyo; C.W. Penn; X.T. Deng; J.L. Walsh; and M.G. Kong. 2007. "Probing bactericidal mechanisms induced by cold atmospheric plasmas with *Escherichia coli* mutants." *Applied Physics Letters*, 90, 073902.
- Raffellini, S.; S. Guerrero; and S.M. Alzamora. 2007. "Effect of hydrogen peroxide concentration and pH on inactivation kinetics of *Escherichia coli*." *Journal of Food Safety*, 28, 514-533.
- Rowan, N. J.; S. Espie; J. Harrower; J.G. Anderson; L. Marsili; and S.J. MacGregor. 2007. "Pulsed-Plasma Gas-Discharge Inactivation of Microbial Pathogens in Chilled Poultry Wash Water." *Journal of Food Protection*, 70, 2805-2810.
- Smet, C.; E. Noriega; J. Van Mierlo; V.P. Valdramidis; and J.F. Van Impe. 2015. "Influence of the growth morphology on the behavior of *Salmonella* Typhimurium and *Listeria monocytogenes* under osmotic stress." *Food Research International*, 77, 515-526.
- Smet, C.; E. Noriega; F. Rosier; J.L. Walsh; V.P. Valdramidis; and J.F. Van Impe. 2016. "Influence of food intrinsic factors on the inactivation efficacy of cold atmospheric plasma: impact of osmotic stress, suboptimal pH and food structure." *Innovative Food Science and Emerging Technologies*, 38(B), 393-406.
- Smet, C.; M. Baka; A. Dickenson; J. Walsh; V. Valdramidis; and J. Van Impe. 2017a. "Antimicrobial efficacy of cold atmospheric plasma for different intrinsic and extrinsic parameters." *Plasma Processes and Polymers*, art.nr. e1700048.
- Smet, C.; E. Noriega; F. Rosier; J.L. Walsh; V.P. Valdramidis; and J.F. Van Impe. 2017b. "Impact of food model (micro)structure on the microbial inactivation efficacy of cold atmospheric plasma." *International Journal of Food Microbiology*, 240, 47-56.
- Song, A.Y.; Y.J. Oh; J.E. Kim; K.B. Song; D.H. Oh; and S.C. Min. 2015. "Cold Plasma Treatment for Microbial Safety and Preservation of Fresh Lettuce." *Food Science and Biotechnology*, 24(5), 1717-1724.
- Surowsky, B.; A. Fröhling; N. Gottschalk; O. Schlüter; and D. Knorr. 2014. "Impact of cold plasma on *Citrobacter freundii* in apple juice: Inactivation kinetics and mechanisms." *International Journal of Food Microbiology*, 174, 63-71.
- Swinnen, I.A.M.; K. Bernaerts; E.J.J. Dens; A.H. Geeraerd; and J.F. Van Impe. 2004. "Predictive modelling of the microbial lag phase: a review." *International Journal of Food Microbiology*, 94, 137-159.
- Tappi, S.; G. Gozzi; L. Vannini; A. Berardinelli; S. Romani; L. Ragni; and P. Rocculi. 2016. "Cold plasma treatment for fresh-cut melon stabilization." *Innovative Food Science and Emerging Technologies*, 33, 225-233.

INFLUENCE OF PLASMA CHARACTERISTICS ON THE EFFICACY OF COLD ATMOSPHERIC PLASMA (CAP) FOR INACTIVATION OF BIOFILMS DEVELOPED BY *LISTERIA MONOCYTOGENES* AND *SALMONELLA* TYPHIMURIUM

M. Govaert, C. Smet, M. Baka and J.F.M. Van Impe *

BioTeC+ & OPTEC, Department of Chemical Engineering, KU Leuven
CPMF2, Flemish Cluster Predictive Microbiology in Foods
Gebroeders De Smetstraat 1, B-9000 Gent, Belgium
* E-mail address: Jan.VanImpe@kuleuven.be

KEYWORDS

Cold Atmospheric Plasma, inactivation, biofilms, *Listeria monocytogenes*, *Salmonella* Typhimurium, sub-lethal injury

ABSTRACT

The biofilm mode of growth of pathogenic bacteria such as *Listeria monocytogenes* and *Salmonella* Typhimurium protects them from currently applied disinfection methods for food contact surfaces. As a result, viable cells remain on the surface and become a contamination source. To avoid contamination of food products, new inactivation methods such as Cold Atmospheric Plasma (CAP) can be used. However, knowledge concerning the influence of different plasma characteristics, such as those investigated in this study, i.e., the applied plasma electrode and the oxygen level of the gas flow, on the efficacy of CAP for biofilm inactivation is still required. In this research, two electrodes (Surface Barrier Discharge (SBD) and Dielectric Barrier Discharge (DBD) electrode) and three oxygen levels (He + 0.0/0.5/1.0 (v/v) % O₂) were tested. Based on the obtained results, the DBD electrode has the highest biofilm inactivation efficacy and the oxygen level of 0.0 (v/v) % results in the highest log-reductions. At these specific conditions, approximately 3.5-log reductions have been obtained (on general medium), which is promising for the application of CAP for biofilm inactivation.

INTRODUCTION

During the last decades, food safety became a major concern for producers, consumers, and government. Food products are considered safe if they do not contain any chemical, physical, and microbiological contaminants. With respect to microbiological safety, the occurrence of foodborne pathogens (including bacteria, viruses, molds, yeasts, prions, and protozoa) can be a real threat for human health (Martinović 2016). Within the European Union (EU), bacterial species account for the highest number of foodborne illnesses/zoonoses. According to the foodborne illnesses reported in 2015 within the EU, salmonellosis (caused by *S.* (Typhimurium)) has a high notification rate (21.2/100,000 capita) and a relatively high fatality rate (0.24 %). On the contrary, listeriosis (caused by *L. monocytogenes*) has a relatively low notification rate

(0.46/100,000 capita), but a very high fatality rate (17.7 %) (EFSA and ECDC 2017). Consequently, it is important to avoid and/or control contamination of food products with these pathogenic microorganisms.

In the food processing plant, food contact surfaces are a primary area of concern as contamination source (Marriott and Gravani 2006). This is mainly because (pathogenic) bacteria, such as *Listeria monocytogenes*, *Salmonella enterica* and *Escherichia coli*, grow predominantly as biofilms on surfaces, rather than as planktonic cells or colonies (Giaouris et al. 2014). Biofilms are functional consortiums of microorganisms attached to a surface and the biofilm-associated cells are embedded in a matrix of self-produced extracellular polymeric substances (EPS) (Kumar and Anand 1998). The matrix has several functions, i.e., (i) it can retain water and nutrients, which prevents cells from dehydration and starvation, (ii) it keeps the cells attached to the surface, i.e., they can withstand shear forces, and (iii) it protects the cells from antimicrobial agents due to a limited diffusion of these components into the 3-dimensional biofilm structure (Conserton et al. 1987; Kumar and Anand 1998). Biofilm-associated cells can also undergo physiological changes, i.e., they become metabolically dormant cells with a reduced growth rate and a decreased consumption of nutrients and oxygen. Since antimicrobial agents (and antibiotics) are far more effective towards actively growing cells (such as planktonic cells), these dormant cells cannot get (completely) inactivated using antimicrobial agents (e.g., chlorine or hydrogen peroxide) (Kumar and Anand 1998; Gómez-López 2012). As a result, currently applied decontamination methods are not efficient enough for inactivation of biofilms and new methods should be considered.

CAP is one of the promising (non-thermal) technologies (Giaouris et al. 2014). In general, plasma is often referred to as an ionized gas, consisting of ions, photons, free electrons, and activated neutral species (excited and radical) (Banu et al. 2012; Fernández and Thompson 2012). Plasma can be generated in different ways, e.g., using an electric discharge in a gas at room temperature and at atmospheric pressure. This plasma type (i.e., CAP) has some important advantages, e.g., (i) it is fast, (ii) it can be created at a low

temperature, (iii) plasma components fade out immediately after treatment, and (iv) cells can be inactivated in multiple ways (Misra et al. 2011; Banu et al. 2012; Fernández and Thompson 2012). However, further research is required to fully assess the efficacy of this technology when applied for biofilm inactivation. In addition, the possible induction of sub-lethally injured cells following CAP treatment should be investigated as well since sub-lethal injury of bacterial cells has been reported already following treatment with currently applied (thermal) technologies. Under optimal conditions, these cells can recover and may cause public health concerns (Noriega et al. 2013).

In literature, different plasma characteristics have been reported to have an influence on the inactivation efficacy of CAP, e.g., the set-up (electrode), the gas flow, the gas composition, and the plasma intensity (Lerouge et al. 2001; Deng et al. 2007; Ehlbeck et al. 2011; Fernández and Thompson 2012; Han et al. 2014; Smet et al. 2017). More knowledge concerning the (combined) influence of these parameters on the CAP inactivation efficacy will aid to improve the inactivation of bacterial species which have developed the ability to grow as biofilms.

Therefore, the goal of this research was to obtain knowledge regarding the influence of (i) the applied electrode and (ii) the oxygen level of the gas flow on the efficacy of CAP for inactivation of model biofilms developed by *L. monocytogenes* and *S. Typhimurium*. The influence of these characteristics has been determined as function of time, i.e., for each combination of variables, different treatment times (0-30 min) were applied. Additionally, sub-lethal injury has been assessed for all experimental conditions and predictive models were implemented to analyse the data.

MATERIALS AND METHODS

Experimental Design

For both pathogenic bacteria, i.e., *L. monocytogenes* and *S. Typhimurium*, strongly adherent and mature model biofilms were developed. Subsequently, biofilms were treated with CAP while altering the applied electrode and the oxygen level of the gas flow. Two different types of electrodes were tested, i.e., the Surface Barrier Discharge (SBD) and the Dielectric Barrier Discharge (DBD) electrode. For each of the experiments, a gas mixture consisting of Helium and Oxygen ($\text{He} + \text{O}_2$) was used. However, three different oxygen levels were examined, i.e., 0.0, 0.5 and 1.0 (v/v) %. For each combination of plasma characteristics, the influence on the inactivation efficacy was determined as function of time, i.e., model biofilms were treated for different treatment times (0, 1, 2, 5, 7.5, 10, 15, 20, 25, and 30 min). Following CAP treatment, cell densities were determined via plate counts on both general and selective medium.

Microorganism, Pre-culture Conditions, and Model Biofilm Development

In this research, *L. monocytogenes* LMG 23775 and *S. Typhimurium* LMG 14933, both acquired from the

BCCM/LMG bacteria collection of Ghent University in Belgium, were used. Stock-cultures were stored at -80°C (U101 Innova, New Brunswick Scientific Co., USA) in Tryptic Soy Broth (TSB, Becton Dickson, US) supplemented with 20% (v/v) glycerol (VWR International, Belgium).

For every experiment, a purity plate was prepared by spreading a loopful of stock-culture onto an agar plate (Lennox Luria Bertani Agar (Becton Dickson, USA) supplemented with 5 g/l NaCl (Sigma-Aldrich, US)). Agar plates were incubated (Binder BD115, VWR International, Belgium) for 24 h at 30°C (*L. monocytogenes*) or 37°C (*S. Typhimurium*), which are the optimal growth temperatures for these microorganisms (BCCM 2017).

Pre-cultures were prepared by transferring one colony from the incubated purity plate into an Erlenmeyer containing 20 mL of fresh growth medium (Lennox Luria Bertani broth (Becton Dickson, US) supplemented with 5 g/l NaCl). Pre-cultures were again incubated for 24 h at 30°C (*L. monocytogenes*) or 37°C (*S. Typhimurium*). After incubation, stationary phase cultures were obtained with a cell density of approximately 10^9 CFU/mL.

These pre-cultures were 100-fold diluted in fresh growth medium to obtain an inoculum with a cell density of approximately 10^7 CFU/mL. Brain Heart Infusion (BHI, VWR chemicals, Belgium) and 20-fold diluted TSB were used as dilution medium for *L. monocytogenes* and *S. Typhimurium*, respectively. These media were selected based on a preliminary optimization procedure. Small polystyrene Petri dishes (50 mm diameter, 9 mm height, Simport, Canada) were inoculated with 1.2 mL of inoculum, after which they were closed and gently shaken to make sure the inoculum covered the entire surface. Finally, Petri dishes were incubated for 24 h at 30°C (*L. monocytogenes*) or 25°C (*S. Typhimurium*). As for the dilution media, incubation temperatures were selected based on preliminary tests.

CAP Equipment and Inactivation Procedure

A schematic overview of the two applied electrodes can be observed in Figure 1 (DBD and SBD electrode in Figure 1A and 1B, respectively).

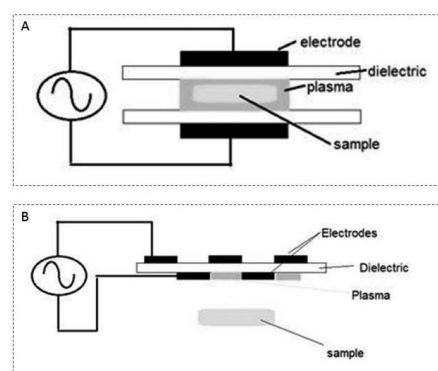


Figure 1 Schematic representation of Dielectric Barrier Discharge (DBD, A) and Surface Barrier Discharge (SBD, B) electrode

For both electrodes, the discharge is generated between two electrodes (DBD electrode diameter = 5.5 cm; SBD electrode diameter = 5.0 cm), covered by a dielectric layer (diameter 7.5 cm). Around both electrodes, an enclosure has been provided to increase the residence time of the plasma species and to obtain a more controlled environment. Both enclosures (22.5 cm x 13.5 cm x 10 cm and 10 cm x 10 cm x 4 cm for the DBD and SBD electrode, respectively) were not airtight, which could result in the presence of traces of oxygen and nitrogen from the environment. In case of the DBD, the electrode gap was set at 0.8 cm and the sample was placed between the electrodes prior to treatment. In case of the SBD, there is no electrode gap, i.e., both electrodes are located on the top of the enclosure. Here, the sample was placed below the two electrodes while ensuring a similar distance between the sample and the electrodes as was the case for the DBD.

For all experiments, the plasma was generated in a gas mixture of helium (purity 99.996%, at a flow rate of 4 L/min) and oxygen (purity $\geq 99.995\%$). Three different oxygen levels were tested, i.e., 0.0, 0.5 and 1.0 (v/v) %, resulting in oxygen flow rates of 0, 20, and 40 mL/min, respectively. The helium and oxygen flow rates were mixed before entering the plasma enclosures. The plasma power supply transforms a low voltage DC input (0-60 V) into a high voltage AC signal (0-20 kV), at a frequency up to 30 kHz. In this research, the input voltage and the frequency were set at 21.88 V and 15 kHz, respectively. The input voltage was selected based on preliminary tests since this input voltage resulted in the creation of a stable and reactive plasma.

After placing the sample between or below the electrodes, the reactor chamber was flushed (4 and 2 min for DBD and SBD, respectively) to ensure a homogeneous gas composition in the enclosures. Finally, the high-voltage power source was energized, and the plasma was generated. Samples, which were rinsed 3 times with sterile Phosphate Buffered Saline (PBS) solution (to remove the remaining planktonic cells) and which were allowed to dry for 15 min prior to treatment, were treated up to 30 min.

Microbiological Analysis

Following CAP treatment of the model biofilms, the cell scraping method was used to remove the remaining biofilm-associated cells from the surface. Therefore, 2 mL of sterile PBS solution was added to the treated Petri dishes and a cell scraper (blade width 20 mm, Carl Roth GmbH+Co, Germany) was used to remove the biofilm. After this, serial decimal dilutions (in 0.85 (m/v) % NaCl solution) of the obtained cell suspensions were prepared and plated on agar plates. BHI Agar (BHIA, BHI supplemented with 14 g/l biological agar, VWR Chemicals, Belgium) and PALCAM agar (VWR Chemicals, Belgium) were used for *L. monocytogenes*, while Tryptic Soy Agar (TSA, TSB supplemented with 14 g/l biological agar) and Xylose Lysine Deoxycholate Agar (XLDA, Merck & Co, USA) were used for *S. Typhimurium*. Three drops (20 μ L/drop) of each serial dilution were plated on both media for each microorganism (Miles et al. 1938). Before counting the colonies, BHI and PALCAM agar plates were

incubated for (at least) 24 h at 30°C and TSA and XLD agar plates were incubated for 24 h at 37°C.

Modelling, Parameter Estimation and Estimation of Sub-lethal Injury

The model of Geeraerd et al. (2000) was used to fit the experimental data. This model describes a microbial inactivation curve consisting of a log-linear inactivation phase and a tail (Equation 1).

$$N(t) = (N_0 - N_{res}) \cdot e^{-k_{max} \cdot t} + N_{res} \quad (1)$$

Where $N(t)$ [CFU/cm²] is the cell density at time t [min], N_0 [CFU/cm²] the initial cell density, N_{res} [CFU/cm²] is a more resistant subpopulation and k_{max} [1/min] the maximum specific inactivation rate. Based on the difference between $\log_{10} N_0$ and $\log_{10} N_{res}$, the final log-reduction has been calculated for each combination of plasma characteristics.

The parameters of the Geeraerd et al. (2000) model were estimated via the minimization of the sum of squared errors (SSE), using the lsqnonlin routine of the Optimization Toolbox of Matlab version R2015b (The Mathworks, Inc.). At the same time, the parameter estimations were determined based on the Jacobian matrix. The Root Mean Squared Error (RMSE) served as an absolute measure of the goodness of the model to fit the actual obtained data.

Finally, to calculate the percentage of sub-lethal injury (% SI), theoretical concentrations obtained from the model of Geeraerd et al. (2000) were used for both the general and selective counts. The equation of Busch and Donnelly (1992) (Equation 2) was used to determine the percentage of injured cells at each treatment time. As a result, the percentage of sub-lethal injury has been plotted as function of the treatment time.

$$\%SI = \frac{CFU \text{ general medium} - CFU \text{ selective medium}}{CFU \text{ general medium}} \cdot 100 \quad (2)$$

Statistical Analysis

Analysis of variance (ANOVA) test was performed to determine whether there are any significant differences amongst means of the estimated model parameters, at a 95.0% confidence level ($\alpha = 0.05$). Fisher's Least Significant Difference (LSD) test was used to distinguish which means were significantly different from others. The analyses were performed using the anova1 routine of the Statistical Toolbox of Matlab version R2015b (The Mathworks, Inc.). For each parameter of the Geeraerd et al. (2000) model, different ANOVA tests (for each microorganism separately) were performed. Initially, a comparison has been made between all values obtained for a certain parameter (i.e., 12 values in total). For this test, significant differences have been indicated with small letters (e.g., a). For the influence of the electrode, a separate test has been performed for each oxygen concentration and each medium. In this case, significant differences have been indicated with a capital letter (e.g., A). For the influence of the oxygen level, a separate test has been performed for each electrode and each medium. Here, significant differences have been indicated with a number (e.g., 1).

RESULTS AND DISCUSSION

In Figure 2A (*L. monocytogenes*) and 2B (*S. Typhimurium*), the biofilm cell density on general and selective medium is expressed as function of the treatment time when applying the DBD and SBD electrode at different oxygen concentrations, i.e., 0.0, 0.5, and 1.0 (v/v) %. In Figure 3A (*L. monocytogenes*) and 3B (*S. Typhimurium*), the percentage of sub-lethally injured cells is expressed as function of the treatment time when applying both electrodes at the same oxygen concentrations. In Table 1, all estimated parameters of the Geeraerd et al. (2000) model are represented for both electrodes and both species.

In general, several observations can be made independently from the applied electrode and the examined oxygen level.

First of all, it can be observed that the shape of the inactivation curves (Figure 2) is similar for both microorganisms, i.e., the curves contain a log-linear inactivation phase followed by a tail. Therefore, the same model can be used to fit the data. Secondly, the initial cell density ($\log_{10} N_0$) is different for both microbial species, i.e., a higher cell density (on both general and selective media) can be observed for the *L. monocytogenes* biofilm compared to the *S. Typhimurium* biofilm (Table 1). This can be explained due to a different stationary cell density of the mature biofilm for both bacterial species and should be considered when assessing (possible) differences between the CAP efficacy for inactivation of these microbial species.

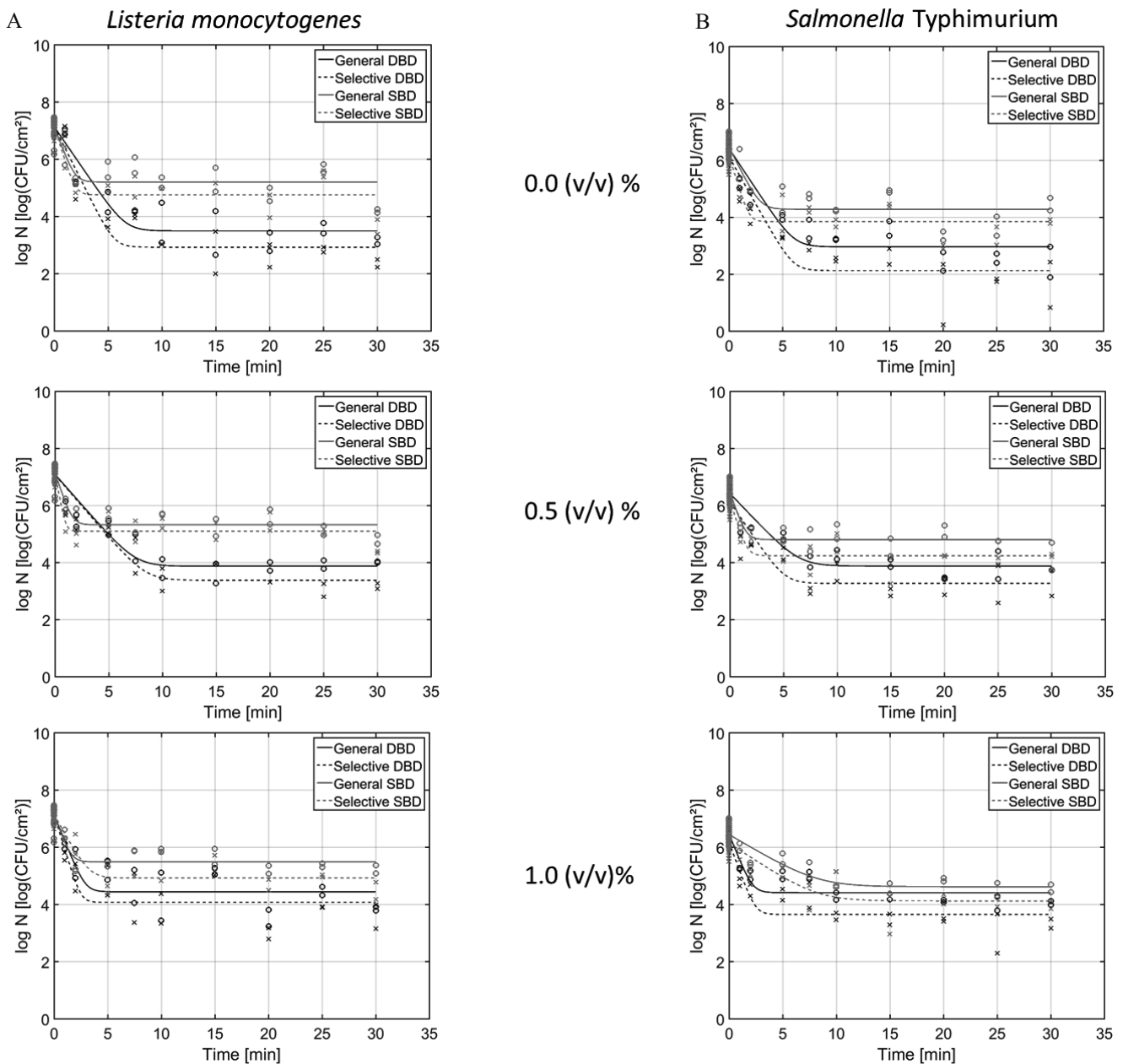


Figure 2 Cell density ($\log(\text{CFU}/\text{cm}^2)$) as function of the treatment time when applying two different electrodes (DBD/SBD) and three different oxygen levels (0.0/0.5/1.0 (v/v) %). Experimental data (symbols) and global fit (line) of the Geeraerd et al. (2000) model: total viable population on general medium (o, solid line) and uninjured viable population on selective medium (x, dashed line). A: results *L. monocytogenes* biofilms and B: results *S. Typhimurium* biofilms.

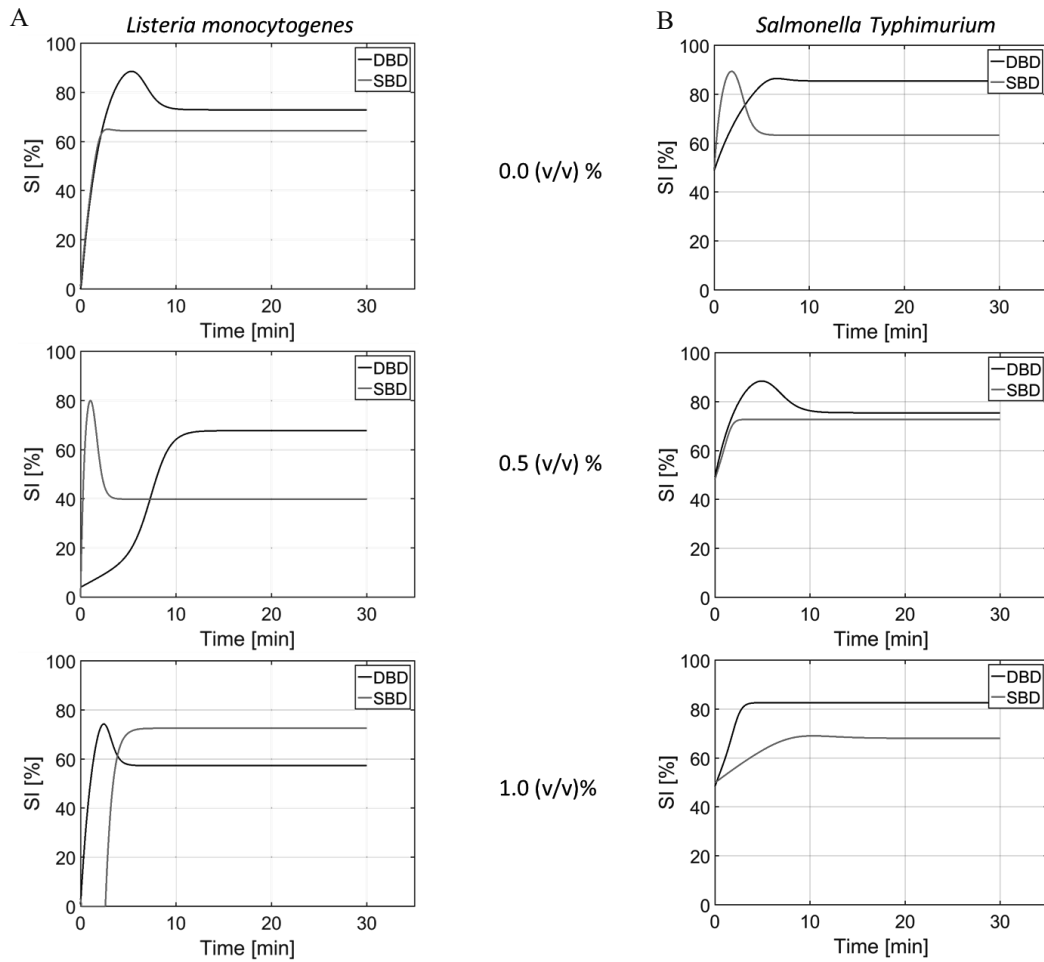


Figure 3 Percentage (%) of sub-lethally injured cells as function of the treatment time for both investigated electrodes (DBD/SBD) and all three examined oxygen concentrations (0.0/0.5/1.0 (v/v) %). A: results *L. monocytogenes* biofilms and B: results *S. Typhimurium* biofilms.

Table 1 Estimated model parameters Geeraerd et al. (2000) model for all examined combinations of plasma characteristics (electrodes/oxygen levels) and both microorganisms (*L. monocytogenes* and *S. Typhimurium*).

	<i>L. monocytogenes</i>					
	DBD 0.0 (v/v) % oxygen	SBD 0.0 (v/v) % oxygen	DBD 0.5 (v/v) % oxygen	SBD 0.5 (v/v) % oxygen	DBD 1.0 (v/v) % oxygen	SBD 1.0 (v/v) % oxygen
${}^1_2 \text{Log}_{10} N_0$ general medium ³ (log(CFU/cm ²))	A ₁ 7.1±0.1 ^a	A ₁ 7.2±0.1 ^a	A ₁ 7.1±0.1 ^a	A ₁ 7.2±0.1 ^a	A ₁ 7.2±0.1 ^a	A ₁ 7.2±0.1 ^a
${}^1_2 \text{Log}_{10} N_0$ selective medium ³ (log(CFU/cm ²))	A ₁ 7.2±0.1 ^a	A ₁ 7.2±0.1 ^a	A ₁ 7.1±0.1 ^a	A ₁ 7.2±0.1 ^a	A ₁ 7.2±0.1 ^a	A ₁ 7.2±0.1 ^a
${}^1_2 k_{max}$ general medium ³ (1/min)	A ₁ 1.265±0.142 ^a	B ₁ 2.343±0.577 ^{b,c,d}	A ₁ 0.985±0.106 ^a	B ₁ 2.606±0.596 ^d	A ₂ 2.141±0.403 ^{b,c,d}	A ₁ 2.440±0.588 ^{c,d}
${}^1_2 k_{max}$ selective medium ³ (1/min)	A ₂ 1.735±0.172 ^{a,b,c}	B ₁ 2.771±0.491 ^d	A ₁ 1.007±0.090 ^a	B ₂ 4.754±1.097 ^e	B ₃ 2.809±0.434 ^d	A ₁ 1.549±0.272 ^{a,b}
${}^1_2 \text{Log}_{10} N_{res}$ general medium ³ (log(CFU/cm ²))	A ₁ 3.5±0.1 ^b	B ₁ 5.2±0.1 ^{h,i}	A ₂ 3.9±0.1 ^c	B _{1,2} 5.3±0.1 ^{h,i}	A ₃ 4.4±0.1 ^e	B ₂ 5.5±0.1 ^j
${}^1_2 \text{Log}_{10} N_{res}$ selective medium ³ (log(CFU/cm ²))	A ₁ 2.9±0.1 ^a	B ₁ 4.8±0.1 ^f	A ₂ 3.4±0.1 ^b	B ₂ 5.1±0.1 ^{g,h}	A ₃ 4.1±0.1 ^d	B _{1,2} 4.9±0.1 ^{f,g}
${}^1_2 \text{Log-reduction}$ general medium ³ (log(CFU/cm ²))	B ₃ 3.6±0.2 ^e	A ₂ 2.0±0.1 ^b	B ₂ 3.2±0.1 ^f	A _{1,2} 1.8±0.1 ^{a,b}	B ₁ 2.7±0.2 ^e	A ₁ 1.7±0.1 ^a
${}^1_2 \text{Log-reduction}$ selective medium ³ (log(CFU/cm ²))	B ₃ 4.2±0.1 ^h	A ₂ 2.4±0.1 ^d	B ₂ 3.7±0.1 ^g	A ₁ 2.0±0.1 ^{b,c}	B ₁ 3.1±0.2 ^f	A _{1,2} 2.2±0.1 ^{c,d}
RMSE general medium (l)	0.4354	0.4322	0.3899	0.3471	0.4770	0.3314
RMSE selective medium (l)	0.4329	0.3942	0.3989	0.3213	0.4855	0.3255
	<i>S. Typhimurium</i>					
	DBD 0.0 (v/v) % oxygen	SBD 0.0 (v/v) % oxygen	DBD 0.5 (v/v) % oxygen	SBD 0.5 (v/v) % oxygen	DBD 1.0 (v/v) % oxygen	SBD 1.0 (v/v) % oxygen
${}^1_2 \text{Log}_{10} N_0$ general medium ³ (log(CFU/cm ²))	A ₁ 6.4±0.1 ^b	A ₁ 6.5±0.1 ^b	A ₁ 6.4±0.1 ^b	A ₁ 6.5±0.1 ^b	A ₁ 6.5±0.1 ^b	A ₁ 6.4±0.1 ^b
${}^1_2 \text{Log}_{10} N_0$ selective medium ³ (log(CFU/cm ²))	A ₁ 6.1±0.1 ^a	A ₁ 6.2±0.1 ^a	A ₁ 6.1±0.1 ^a	A ₁ 6.2±0.1 ^a	A ₁ 6.2±0.1 ^a	A ₁ 6.2±0.1 ^a
${}^1_2 k_{max}$ general medium ³ (1/min)	A ₁ 1.308±0.154 ^{a,c}	A ₂ 1.747±0.351 ^{b,c,d,e}	A ₁ 0.912±0.122 ^{a,b}	B ₂ 2.553±0.619 ^{d,e,f}	B ₂ 2.178±0.369 ^{c,d,e,f}	A ₁ 0.516±0.075 ^a
${}^1_2 k_{max}$ selective medium ³ (1/min)	A ₁ 1.534±0.198 ^{a,d}	B ₂ 2.876±0.584 ^f	A ₁ 1.284±0.227 ^{a,c}	B ₂ 2.768±0.661 ^{e,f}	B ₂ 2.370±0.416 ^{c,d,e,f}	A ₁ 0.573±0.110 ^a
${}^1_2 \text{Log}_{10} N_{res}$ general medium ³ (log(CFU/cm ²))	A ₁ 3.0±0.1 ^b	B ₁ 4.3±0.1 ^{f,g}	A ₂ 3.9±0.1 ^e	B ₂ 4.8±0.1 ^h	A ₃ 4.4±0.9 ^g	A ₂ 4.6±0.1 ^h
${}^1_2 \text{Log}_{10} N_{res}$ selective medium ³ (log(CFU/cm ²))	A ₁ 2.1±0.2 ^a	B ₁ 3.8±0.1 ^e	A ₂ 3.3±0.1 ^c	B ₂ 4.2±0.1 ^{f,g}	A ₃ 3.6±0.1 ^d	B _{1,2} 4.1±0.1 ^f
${}^1_2 \text{Log-reduction}$ general medium ³ (log(CFU/cm ²))	B ₃ 3.4±0.1 ^h	A ₂ 2.2±0.1 ^{d,e}	B ₂ 2.5±0.1 ^f	A ₁ 1.7±0.1 ^a	A ₁ 2.0±0.1 ^{c,d}	A ₁ 1.8±0.1 ^{a,b}
${}^1_2 \text{Log-reduction}$ selective medium ³ (log(CFU/cm ²))	B ₂ 4.0±0.2 ⁱ	A ₂ 2.3±0.1 ^{e,f}	B ₂ 2.9±0.2 ^g	A ₁ 1.9±0.1 ^{b,c}	B ₁ 2.5±0.1 ^f	A _{1,2} 2.0±0.2 ^{b,c,d}
RMSE general medium (l)	0.4198	0.3961	0.4614	0.3256	0.4374	0.2900
RMSE selective medium (l)	0.5468	0.4249	0.3464	0.3852	0.3279	0.4306

¹ Influence electrode: for each microorganism, oxygen concentration and growth medium, model parameters bearing different superscripts (no uppercase capital letters in common) are significantly different ($P \leq 0.05$)

² Influence oxygen concentration: for each microorganism, electrode and growth medium, model parameters bearing different superscripts (no lowercase numbers in common) are significantly different ($P \leq 0.05$)

³ Combined effect electrode and oxygen concentration: for each microorganism, model parameters bearing different superscripts (no uppercase small letters in common) are significantly different ($P \leq 0.05$)

When comparing the obtained log-reductions for both species, it could be concluded that almost no differences can be observed, except for the DBD at 0.5 and 1.0 (v/v) %. In this case, higher log-reductions have been observed for *L. monocytogenes* compared to *S. Typhimurium* (Table 1). This could be related to the higher initial cell density of the *L. monocytogenes* biofilm and/or due to the different composition of their cell wall (PennState 2018). Finally, when comparing the initial cell densities on general and selective medium, it can be observed that the initial cell density for *L. monocytogenes* using general medium is the same as using selective medium (Table 1). Consequently, (almost) no sub-lethal injury should be observed for these biofilm-associated cells prior to treatment, which is indeed the case (Figure 3A). In contrary, significantly higher initial cell densities for *S. Typhimurium* are obtained on general medium compared to the selective medium, which should result in a significant amount of sub-lethally injured cells prior to treatment. This can be observed in Figure 3B, since approximately 50% of the biofilm-associated cells are sub-lethally injured following 0 min of CAP treatment.

The difference in sub-lethal injury prior to treatment between both bacterial species could possibly be the result of the microenvironment present in the biofilm. Since *L. monocytogenes* is in general a more resistant microorganism (Marriott and Gravani 2006; Food and Drug Administration 2012), local changes in the pH of the biofilm could for example result in sub-lethal injury of the *S. Typhimurium* biofilm-associated cells, but not for those present in *L. monocytogenes* biofilms. Another possible explanation could be that the provided, and required, growth medium for *S. Typhimurium* results already in an induction of sub-lethally injured cells.

Influence of the Electrode

For both microorganisms, the electrode has an influence on the k_{max} value, the residual population, and the obtained log-reductions following treatment (Table 1 and Figure 2).

The initial inactivation rates (k_{max}) are (significantly) higher when applying the SBD electrode for both media, except for the highest oxygen concentration of 1.0 (v/v) %. In this case, there are no significant differences (general medium *L. monocytogenes*) or the k_{max} value is higher while applying the DBD electrode (selective medium *L. monocytogenes*; general and selective medium *S. Typhimurium*). Consequently, the inactivation of biofilm-associated cells is initially faster, at almost all conditions, when applying the SBD electrode. Nevertheless, this log-linear inactivation phase has only a short duration period (Figure 2), i.e., following less than 5 min (except for *S. Typhimurium* at 1.0 (v/v) % oxygen), a residual constant population can be observed while applying the SBD electrode. Considering this short duration and the relatively high standard deviation of the k_{max} values obtained while applying the SBD electrode, significant differences between the k_{max} values obtained with both electrodes could be related to the model fit (and the low number of data points within this short log-linear inactivation phase).

Significant differences can also be observed concerning the obtained log-reductions (and residual cell densities)

following CAP treatment with the two examined electrodes (Table 1). Independently from the oxygen level and the treated microorganism, (significantly) higher log-reductions are obtained while applying the DBD electrode (Table 1 and Figure 2). For *L. monocytogenes*, log-reductions between 2.7 and 4.2 log(CFU/cm²) are obtained with the DBD electrode, while log-reductions between 1.7 and 2.4 log(CFU/cm²) are obtained with the SBD electrode. For *S. Typhimurium*, the obtained log-reductions range between 2.0 and 4.0 log(CFU/cm²) and 1.66 and 2.34 log(CFU/cm²) for the DBD and SBD electrode, respectively. As a result, it could be concluded that the DBD electrode is more effective for inactivation of biofilms.

However, the obtained log-reductions are in all cases higher when using selective medium compared to general medium. As a result, a residual percentage of sub-lethally injured cells can be observed following CAP treatment with both electrodes (Figure 3). In almost all cases, except for *L. monocytogenes* biofilms at 1.0 (v/v) % oxygen, using the DBD electrode results in a higher percentage of sub-lethally injured cells (up to 80%). This should be considered since this could result in an overestimation of inactivated cells when only selective medium is used. Nevertheless, the highest completely kill efficacy is still obtained using the DBD electrode, and this for all oxygen concentrations and both microorganisms, since the highest log-reductions on general medium (indicating both injured and un-injured viable cells) have been obtained with this electrode.

Based on the higher log-reductions obtained with the DBD electrode, it can be concluded that this electrode is more effective for inactivation of biofilms. The lower efficacy applying the SBD electrode can be explained based on the research of Olszewski et al. (2014). In this research, it was mentioned that one of the drawbacks of the SBD configuration is the inefficient transport of reactive species towards the sample. Since applying the SBD electrode results in an indirect CAP treatment, the most reactive species, which have the shortest lifetime, recombine before they reach the sample. With the DBD electrode, a direct treatment is conducted, resulting in more reactive species reaching the sample and a higher inactivation efficacy (Olszewski et al. 2014). However, depending on the targeted application, it could still be advised to use the SBD electrode since its more practical scale-up aspect for industrial applications (Olszewski et al. 2014). Nevertheless, a compromise should be considered between applicability and efficacy.

Influence of the Oxygen Concentration

As for the influence of the applied electrode, significant differences are observed regarding the k_{max} values, the residual populations, and the obtained log-reductions following CAP treatment at different oxygen concentrations (Table 1).

For the DBD electrode, the highest k_{max} values are obtained at an oxygen level of 1.0 (v/v) % oxygen, and this is observed for both microorganisms and both media. For the SBD electrode, the influence of the oxygen concentration is depending on the microorganism and the medium. For

L. monocytogenes, the lowest k_{max} value is obtained at 1.0 (v/v) %, and this for both media. For *S. Typhimurium*, the oxygen level has no influence on the k_{max} value (general medium) or is the highest at 0.5 (v/v) % (selective medium). However, as for the influence of the electrode, the short duration period of the log-linear inactivation phase should be considered. Due to a low number of data points within this short period, significant differences could be the result of the model fit.

For both microorganisms and for both electrodes, (significantly) higher log-reductions are obtained at 0.0 (v/v) % of oxygen, and this for both media. This is in contradiction with previous research reported in literature. According to Laroussi (2005) and Fernández and Thompson (2012), the presence of oxygen enhances the killing efficacy of CAP. Oxygen-based reactive species have been reported to have a strong oxidative effect on the outer surfaces of the cells, i.e., unsaturated fatty acids present in the membrane of the cells can react with oxygen-based reactive species such as hydroxyl radicals (OH \cdot), resulting in a compromised function of the membrane lipids. Atomic oxygen on the other hand, can oxidize proteins, resulting in structural changes and malfunctioning of proteins/enzymes (Laroussi 2005). Nevertheless, previously mentioned studies were not performed using bacterial cells growing as biofilms. Consequently, investigating the biofilm inactivation mechanism of CAP could possibly improve understanding the influence of the oxygen concentration on the CAP inactivation efficacy for biofilms in particular.

Finally, when comparing the percentage of sub-lethally injured cells obtained for all three oxygen levels (Figure 3), differences can be observed between the two electrodes and between both microorganisms. For the DBD, the lowest amount of sub-lethal injury is observed at 1.0 and 0.5 (v/v) % for *L. monocytogenes* and *S. Typhimurium*, respectively. For the SBD electrode, using 0.5 and 0.0 (v/v) % of oxygen results in the lowest amounts of sub-lethal injury for *L. monocytogenes* and *S. Typhimurium*, respectively. Nevertheless, for both microorganisms and both electrodes, the highest completely kill efficacy is still obtained while using the lowest oxygen concentration of 0.0 (v/v) %.

Most Efficient Combination of Plasma Characteristics

When the model parameters of all possible combinations of plasma characteristics are compared, it can be concluded that for both microorganisms, the highest log-reductions are obtained following treatment with the DBD electrode at 0.0 (v/v) % of oxygen. In this case, the log-reductions on general medium are 3.6 and 3.4 log(CFU/cm 2) for *L. monocytogenes* and *S. Typhimurium*, respectively.

CONCLUSIONS

The goal of this study was to investigate the influence of the applied electrode (DBD/SBD) and the oxygen level of the gas flow (He + 0.0 - 1.0 (v/v) % O $_2$) on the CAP inactivation efficacy for biofilms. It could be concluded that the highest log-reductions have been obtained while using the DBD electrode. For the oxygen level, the highest

efficacy has been obtained at an oxygen concentration of 0.0 (v/v) %. The obtained log-reductions (approximately 3.5 log(CFU/cm 2)) at these conditions, i.e., DBD at 0.0 (v/v) % oxygen, where promising with respect to CAP application for disinfection of abiotic surfaces.

FUTURE RESEARCH

In future research, the effect of another plasma characteristic will be investigated, i.e., the plasma intensity, since this has been reported in literature to have a significant influence on the inactivation efficacy of CAP (Deng et al. 2007; Han et al. 2014), which has been confirmed by preliminary tests.

ACKNOWLEDGEMENTS

This work was supported by project PFV/10/002 (Center of Excellence OPTEC-Optimization in Engineering) and by Post-Doctoral Mandate PDM/16/125 (Maria Baka) of the KU Leuven research council.

REFERENCES

- Banu, M. S., Sasikala, P., Dhanapal, A., Kavitha, V., Yazhini, G. and Rajamani, L. (2012). Cold plams as a novel food processing technology. *International Journal of Emerging trends in Engineering and Development Issue 2, Vol. 4*, 803-818.
- BCCM, Belgian Co-ordinated Collections of Micro-organisms (2017). Bacterial cultures.
- Busch, S.V. and Donnelly, C.W. (1992) Development of a repair-enrichment broth for resuscitation of heat-injured *Listeria monocytogenes* and *Listeria innocua*. *Applied Environmental Microbiology* 58, 14-20.
- Conserton, J., Cheng, K., Geesey, G., Ladd, T. I., Curtis Nickel, J., Dasgupta, M. and Marrie, T. J. (1987). Bacterial biofilms in nature and disease. *Annual Review of Microbiology* 41, 435-464.
- Deng, S., Ruan, R., Mok, C. K., Huang, G., Lin, X. and Chen, P. (2007). Inactivation of *Escherichia coli* on Almonds Using Nonthermal Plasma. *Journal of Food Science* Vol. 72, Nr. 2, 62-66.
- EFSA and ECDC (2017). The European Union summary report on trends and sources of zoonoses, zoonotic agents and food-borne outbreaks in 2015. *EFSA Journal* 2016; 14(12):4634, 231pp.
- Ehlbeck, J., Schnabel, U., Polak, M., Winter, J., von Woedtk, Th., Brandenburg, R., von dem Hagen, T. and Weltmann, K.-D. (2010). Low temperature atmospheric pressure plasma sources for microbial decontamination. *Journal of Physics D: Applied Physics* 44, 1-18.
- Fernández, A. and Thompson, A. (2001). The inactivation of *Salmonella* by cold atmospheric plasma treatment. *Food Research International* 45, 678-684.
- Food and Drug Administration. (2012). Bad BugBook, Foodborne Pathogenic Microorganisms and Natural Toxins. Second Edition.
- Geeraerd, A. H., Herremans, C. H. and Van Impe, J. F. (2000). Structural model requirements to describe microbial inactivation during a mild heat treatment. *International Journal of Food Microbiology* 59, 185-209.
- Giaouris, E., Heir, E., Hébraud, M., Chorianopoulos, N., Langsrud, S., Mørseth, T., Habimana, O., Desvaux, M., Renier, S.

and Nychas, G.-J. (2014). Attachment and biofilm formation by foodborne bacteria in meat processing environments: Causes, implications, role of bacterial interactions and control by alternative novel methods. *Meat Science* 97, 298-309.

Gómez-López, V. M. (2012). *Decontamination of Fresh and Minimally Processed Produce*. John Wiley & Sons, Inc.

Han, L., Patil, S., Keener, K. M., Cullen, P. and Bourke, P. (2014). Bacterial Inactivation by High Voltage Atmospheric Cold Plasma: Influence of Process Parameters and Effects on Cell Leakage and DNA. *School of Food Science and Environmental Health*, 1-30.

Kumar, G. C. and Anand, S. K. (1998). Significance of microbial biofilms in food industry: a review. *International Journal of Food Microbiology* 42, 9-27.

Laroussi, M. (2005). Low Temperature Plasma-Based Sterilization: Overview and State-of-the-Art. *Plasma Processes and Polymers* (2), 391-400.

Lerouge, S., Wertheimer, M. R. and Yagia, L. (2001). Plasma Sterilization: A Review of Parameters, Mechanisms, and Limitations. *Plasmas and Polymer* 6 (3), 175-188.

Marriott, N. G. and Gravani, R. B. (2006). *Principles of food sanitation - Fifth edition*. Springer.

Martinović, T., Andjelković, U., Šrajer Gajdošik, M., Rešetar, D. and Josić, D. (2016). Foodborne pathogens and their toxins. *Journal of Proteomics*, 226-235.

Miles, A. A., Misra, S. S. and Irwin, J. O. (1938). The estimation of bactericidal power of the blood. *Epidemiology & Infection* 38, 732-749.

Misra, N. N., Tiwari, B. K., Raghav Rao, S. M. and Cullen, P. J. (2011). Nonthermal Plasma Inactivation of Food-Borne Pathogens. *Food Eng Rev* 3, 159-170.

Noriega, E., Velliou, E., Van Derlinden, E., Mertens, L. and Van Impe, J. F. (2013). Effect of cell immobilization on heat-induced sublethal injury of *Escherichia coli*, *Salmonella* Typhimurium and *Listeria innocua*. *Food Microbiology* 36, 355-364.

Olszewski, P., Li, J. F., Liu, D. X. and Walsh, J. L. (2014). Optimizing the electrical excitation of an atmospheric pressure plasma advanced oxidation process. *Journal of Hazardous Materials* 279, 60-66.

PennState (2018). Elementary Microbiology - Gram stain.

Smet C., Baka M., Dickenson A., Walsh J., Valdramidis V. and Van Impe J. (2017). Antimicrobial efficacy of cold atmospheric plasma for different intrinsic and extrinsic parameters. *Plasma Processes and Polymer*, art.nr. e1700048.

MODELLING MICROBIOLOGICAL AND QUALITY MARKER RESPONSES TO ENHANCE COLD PLASMA CEREAL GRAIN PROCESSING

Dana Ziuzina¹, Agata Los¹, Simen Akkermans², Daniela Boehm¹,
Patrick J. Cullen¹, Jan F.M. Van Impe², Paula Bourke¹

¹ Plasma Research Group

School of Food Science and Environmental Health
Dublin Institute of Technology, Ireland

² BioTeC+ - Chemical & Biochemical Process Technology & Control
Department of Chemical Engineering
KU Leuven, Gent, Belgium

KEYWORDS

Plasma, response surface modelling, polynomial, wheat, barley, germination, bacteria, fungi, spores.

ABSTRACT

This study employed response surface modelling to establish key process parameters for high voltage dielectric barrier discharge (HVDBD) atmospheric cold plasma (ACP) decontamination of cereal grains that were in alignment with maintenance of product critical quality parameters. Response surface modelling of experimental data probed the key factors in relation to microbial control and seed germination promotion. Depending on treatment parameters and target intrinsic characteristics, significant reduction of microbial contamination on wheat and barley grains was achieved. The efficacy of the plasma treatment (20 min) against microorganisms decreased in the following order: *E. coli* > *P. verrucosum* (spores) > *B. atrophaeus* (vegetative cells) > *B. atrophaeus* (endospores). Germination percentage of samples treated for up to 5 min was not affected, but it was decreased after 20 min of treatment. Overall, ACP was effective for cereal grain decontamination, however the diverse native micro-flora may pose greater resistance to the closed surface decontamination approach than the individual fungal or bacterial challenges.

INTRODUCTION

Contamination of cereal grains with insects or microorganisms is a persistent concern for the grain industry due to irreversible damage to quality and safety characteristics and economic losses. Conventional techniques for controlling spoilage of cereal grains include thermal and chemical sterilization methods, however, these methods can negatively affect the quality and functional properties of cereals and cereal products; moreover, complete elimination of mycotoxins from food product by processing can rarely be achieved

(Karlovsky et al., 2016; Oghbaei, Prakash, & Yildiz, 2016). ACP presents an alternative to conventional grain decontamination methods owing to the high antimicrobial potential generated during the treatment with chemical and bioactive radicals, e.g. reactive oxygen species (ROS) and reactive nitrogen species (RNS), which cause damage to proteins and nucleic acids, as well as lesions in cellular membranes (Laroussi and Leipold 2004). The plasma treatment efficacy for microbial inactivation is under investigation in a number of food systems. As a non-thermal process, ACP causes minimal or no thermal damage to the food product treated (Niemira 2012).

The aim of this work was to apply polynomial response surface models to cereal grains' microbiological and quality criteria in response to HVDBD ACP contained treatment to improve safety whilst maintaining grain quality. For this, antimicrobial efficacy of ACP against background microflora of barley and against challenge pathogens, such as *E. coli*, *B. atrophaeus* (vegetative cells and endospores) and *P. verrucosum* (spores) inoculated on barley was investigated. To study the mechanisms responsible for the potential enhancement of early wheat growth, response surface models were applied to examine the influence of ACP treatment on wheat quality parameters, such as germination rate and mean germination time.

METHODOLOGY

Cereal Grains

Organic wheat and barley grains were purchased from a local retailer. Barley grains were sterilized by autoclaving at 121°C for 15 min and used to study the effect of ACP on inactivation of challenge pathogens. In order to assess ACP treatment efficacy for the reduction of background microbiota, unsterilized barley grains were used. Germination studies were performed using unsterilized wheat grains.

Microbiological Criteria

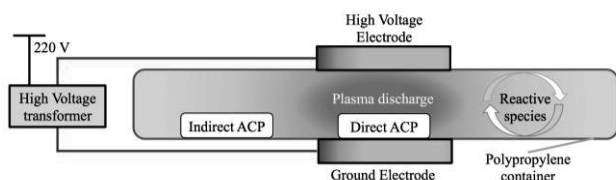
E. coli NCTC 12900, *B. atrophaeus* var. *niger* ATCC 9372 and *P. verrucosum* DSM 12639 were used in this work. Sterilized barley grains (10 g) were sprayed with a suspension of selected microorganism (0.5 ml) and air-dried for 1 h. To evaluate the effect of ACP treatment on grain background microbiota, unsterilized and un-inoculated wheat and barley grains were used.

Quality Parameters

To investigate the impact of ACP on physiological properties of wheat grains germination percentage (G%) and mean germination time (MGT) were calculated: $G\% = (n \times 100\%) / N_t$, and mean germination time: $MGT = \sum (n \times d) / N$, where n is number of grains germinated on each day, N_t – total number of grains, N is total number of grains germinated at the termination of the experiment and d is the number of days from the beginning of the test. All germination experiments were performed at least three times.

Experimental Design

The HVDBD ACP system (Fig. 1) used in this study was previously described by Ziuzina et al. (2015). Wheat or barley grains (2 g) were treated inside the sealed container, which was used to provide a contained environment during and post treatment. The samples were subjected to either direct or indirect ACP treatment for 5–20 min at 80 kV under atmospheric pressure and air and analysed for microbiological (plate count) and functional characteristics (G% and MGT) immediately or after storage for 0, 2 or 24 h post treatment to monitor effects of retention time on ACP treatment efficacy. All experiments were performed in duplicate and replicated at least



three times.

Fig. 1. Schematic of the experimental set-up for DBD plasma system

Statistical Analysis

Statistical analysis was performed using IBM SPSS statistics 21 Software (SPSS Inc., Chicago, USA). All data was subjected to analysis of variance (ANOVA). Means of ACP treated and untreated controls were compared according to the method of Fisher's Least Significant Difference-LSD at the 0.05 level.

Response Surface Modelling

The datasets of the microbial inactivation and germination studies were modelled using polynomial response surface models. These mathematical models were fitted to the datasets using the *lsqnonlin* routine of the Optimization Toolbox of Matlab version 7.14 (The Mathworks Inc.). The mathematical model for the effect of treatment time (tt) and retention time (rt) on the inactivation of microorganisms on barley and wheat was formulized as: $\delta(tt, rt) = a_1 \cdot tt + a_2 \cdot rt + a_3 \cdot tt \cdot rt$, where δ is the decimal reduction of the microbial population as calculated by comparing the microbial quantities with the average of the controls. The parameters a_1 to a_3 are regression coefficients. The response surface model for the effect of treatment time, retention time and incubation time (it) on the germination rate γ was described as: $\gamma(tt, rt, it) = a_1 + a_2 \cdot tt + a_3 \cdot rt + a_4 \cdot it + a_5 \cdot tt \cdot rt + a_6 \cdot tt \cdot it + a_7 \cdot rt \cdot it$. The 95% confidence bounds on the model parameter estimates were determined using the *nlparci* Matlab function. A more detailed description of the calculation of confidence bounds on the parameter estimates is available in Walter & Pronzato (1997).

RESULTS

Inactivation of Barley Background Microflora

Significant reductions in barley background microflora were only achieved after longer treatment for 20 min in combination with 2 h retention time or after either 5 or 20 min of treatment in combination with an extended retention time of 24 h ($p < 0.05$), with no statistical difference between surviving populations of the treated groups recorded. In terms of the effects of mode of plasma exposure, direct treatment always resulted in

slightly higher reductions of both mesophilic bacteria and fungi on grains (Fig. 2).

Inactivation of Challenge Microorganisms

The reduction of microorganisms inoculated on barley grains is presented in Fig. 3. ACP treatment efficacy was strongly affected by the type of microorganism studied. The efficacy of the plasma treatment of barley grains inoculated with microorganisms decreased in the following order: *E. coli* > *P. verrucosum* (spores) > *B. atrophaeus* (vegetative cells) > *B. atrophaeus* (endospores).

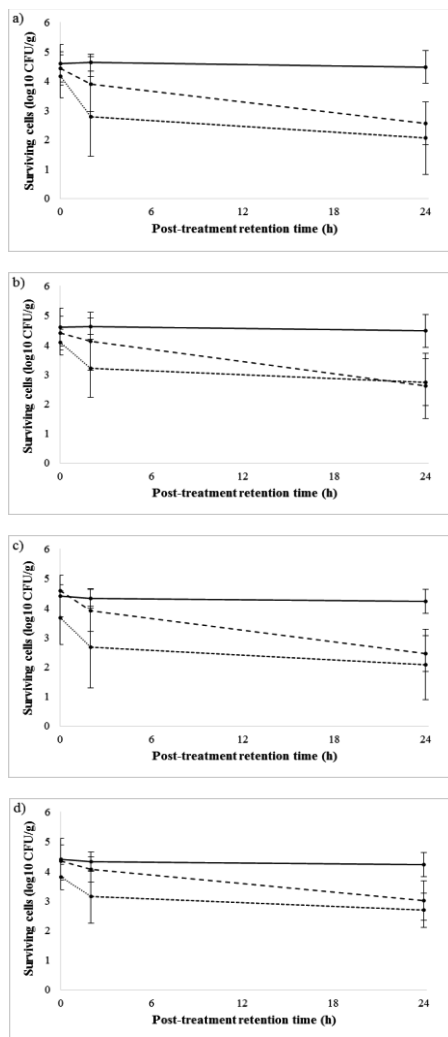


Fig. 2. Surviving barley microflora: mesophilic bacteria – direct (a) and indirect (b) treatment, yeasts and moulds – direct (c) and indirect (d) treatment; —●— - control, - -●- - 5 min treatment, ···· - 20 min treatment.

The highest resistance was observed for *B. atrophaeus* endospores. For other microorganisms tested, 20 min of treatment

with 24 h retention time was the most efficient combination.

Modelling Analysis

The modelling results with respect to the inactivation of naturally present fungi and mesophilic bacteria in barley are presented in Table 1, where the magnitude of each coefficient indicates the influence of the related term on the decimal reduction.

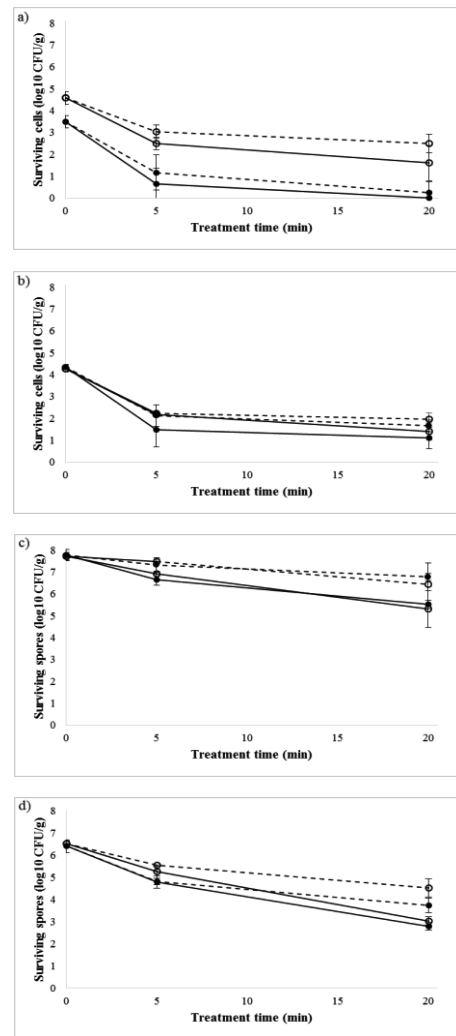


Fig. 3. (a) *E. coli*, (b) *B. atrophaeus* vegetative cells, (c) *B. atrophaeus* spores and (d) *P. verrucosum* spores; post-treatment retention time: 2 h - ○ - direct treatment and - -○- - indirect treatment, 24 h - ● - direct treatment and - -●- - indirect treatment. Vertical bars represent standard deviation.

The 95% confidence bounds on the parameter estimates were omitted as all parameters had a high accuracy. The relatively low values of all coefficients confirm that naturally present

microorganisms have a high resistance against the applied ACP treatment.

The modelling analysis confirm that the endospores of *B. atrophaeus* were considerably more resistant against ACP treatment than the vegetative cells. These results also demonstrate that the effect of treatment time itself is comparable between *E. coli* and *P. verrucosum* spores. The modelling analysis also indicates that the challenge microorganisms used were much more susceptible to the ACP treatments than the background microbiota. Even though the effect of treatment time itself was always lower for the indirect treatment, the combined effect of treatment time and retention time can still be similar, however, this was not the case for *B. atrophaeus* spores.

Table 1. Response surface model coefficients

Grain type	Microorganism	Mode of plasma exposure					
		Direct			Indirect		
		tt	rt	tt-rt	tt	rt	tt-rt
Barley	<i>B. atrophaeus</i> spores	0.077	-0.004	1.39E-03	0.019	0.001	7.56E-04
	<i>B. atrophaeus</i> cells	0.181	0.044	-1.29E-03	0.154	0.109	-5.44E-03
	<i>E. coli</i>	0.176	0.083	-4.31E-04	0.124	0.145	-2.86E-03
	<i>P. verrucosum</i>	0.193	0.023	-6.56E-04	0.114	0.070	-1.94E-03
	Fungi	0.056	0.018	2.05E-03	0.043	0.081	-2.18E-03
	Mesophilic bacteria	0.039	0.020	3.30E-03	0.045	0.085	-2.16E-03
	Fungi	0.114	0.031	3.82E-04	0.094	0.069	-2.90E-03
Wheat	Mesophilic bacteria	0.088	0.032	-8.97E-04	0.007	0.056	-4.67E-04

Wheat Grain Germination

In general, 5 min of treatment had minimal effect on the grain germination rate, regardless of mode of exposure or retention time used, whereas 20 min of direct treatment significantly decreased germination for most samples ($p < 0.05$) (Fig. 4). By Day 7, no significant differences were observed between the samples subjected to 5 min of plasma treatment, with either 2 or 24 h retention time, and the control samples ($p < 0.05$). The parameter estimates and 95% confidence bounds of the response surface model for the effect of treatment, retention and incubation time on the germination rate is presented in Table 2. The Root Mean Squared Error (RMSE) of each model is also presented. This error is an estimate of the standard deviation of the error between the model and the measurements.

Response surface models were compared with average measured germination rates. The effect of the treatment time itself is much

higher with the direct treatment than with the indirect treatment (more than a factor of 2 higher).

Also the retention time has a larger effect on the germination rate for the direct treatment. In case of the indirect treatment, it is mostly the interaction between the treatment time and retention time that impacts the germination rate. The standard deviation of the difference between the response surface model and the measurements, as approximated by the RMSE, is relatively high for both models. In this case, the high RMSE points to high variability of the germination rate, given the same experimental conditions.

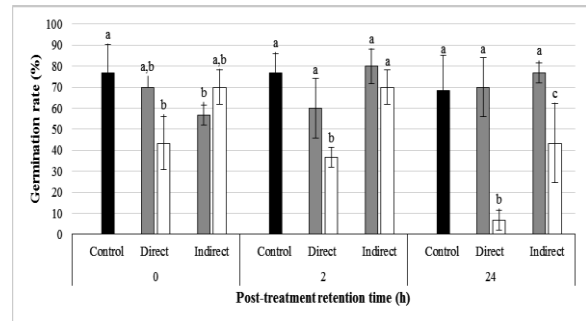


Fig. 4. G% measured on day 7: ■ - untreated control, after ■ - 5 and □ - 20 min of treatment.

Table 2. Response surface model parameter

Model term	Direct	Indirect
Constant	39.851 ± 41.716	47.864 ± 44.076
tt	-2.304 ± 0.309	-0.808 ± 0.326
rt	0.302 ± 0.174	-0.158 ± 0.183
it	5.651 ± 1.945	3.837 ± 2.055
tt-rt	-0.030 ± 0.001	-0.075 ± 0.001
tt-it	0.032 ± 0.013	0.116 ± 0.014
rt-it	-0.089 ± 0.007	0.034 ± 0.008
RMSE	14.94	15.35

DISCUSSION

The polynomial response surface models were used to study the effect of HVDBD ACP critical control parameters on microbiological safety and quality attributes of grains. The modelling demonstrated that contained HVDBD ACP treatment combined with 24 h of retention time significantly reduced the number of microbial counts on grains. A closed process combined with post treatment retention allowed the extended interaction of the plasma generated reactive species with the sample. This facilitated antimicrobial action of long lived reactive species and it explains why

in our study extending post-treatment retention time was generally more efficient for microbial inactivation, which is important for translation to process design. However, ACP microbial inactivation efficacy depended on many different factors, such as plasma mode, process parameters, type of microorganism and its physiological state. By modelling microbial response, this work demonstrated that background microflora of grains and *B. atrophaeus* endospores exhibited higher resistance to plasma than other challenge microorganisms tested. The complex spore coat structure of *B. atrophaeus* has been identified as a resistance mechanism against various chemicals, particularly oxidizing agents (Sella et al. 2014). In this study, fungal spores were more resistant to treatment than Gram-negative *E. coli* and less resistant than both vegetative cells and spores of Gram-positive *B. atrophaeus*. Similarly, Eissa et al. (2014) demonstrated higher resistance of bacterial spores to peroxyacetic acid and hydrogen peroxide as compared to *B. subtilis* spores.

When comparing the effect of the mode of treatment on the microbial inactivation, the observed differences were limited. In case of applying the indirect treatment, all treatments that resulted in a significant reduction of the microbial load also showed antagonistic interactions between the effects of treatment and retention time. As such, combining both a long treatment time and retention time may not be efficient. Thus, it is advised to combine shorter treatment times with longer retention times to achieve the required inactivation efficacy. This work also demonstrated that the mode of exposure can be exploited to modulate the impact of reactive species on the functional properties of grains and seeds, with the potential to modulate quality while enhancing or maintaining microbiological safety.

CONCLUSION

This work established that response surface modelling of microbiological challenge data and quality indicators can be employed for optimisation of cold plasma based interventions applied to cereal grains. The efficacy of ACP treatment was dependent on processing parameters and the type and physiological state of microorganisms.

Through modelling, it has been demonstrated that combining shorter treatment times and longer retention times, sufficient microbial inactivation can be achieved, with minimal negative impacts on germination parameters of grains. The highest resistance to plasma was observed for native microflora present on grains followed by *B. atrophaeus* endospores, which could be further employed as biomarkers to address microbiological parameters for process understanding and control. Therefore, contained HVDBD ACP technology in conjunction with modelling can be a promising tool for effective cereal grain decontamination and modulation of functional properties.

FUTURE RESEARCH

Mathematical modelling of the biological and physicochemical responses to cold plasma application may be used as a process control mechanism.

ACKNOWLEDGEMENTS

Science Foundation Ireland (SFI) Grant Number 14/IA/2626 and the project PFV/10/002 of the KU Leuven Research Council.

REFERENCES

- Laroussi, M. and Leipold, F. 2004. Evaluation of the roles of reactive species, heat, and UV radiation in the inactivation of bacterial cells by air plasmas at atmospheric pressure. *International Journal of Mass Spectrometry*, 233(1-3), 81–86.
- Eissa, M.E.; Abd El Naby, M.; and Beshir, M.M. 2014. Bacterial vs. fungal spore resistance to peroxygen biocide on inanimate surfaces. *Bulletin of Faculty of Pharmacy, Cairo University*, 52(2), 219–224.
- Karlovsky, P.; Suman, M.; Berthiller, F.; De Meester, J.; Eisenbrand, G.; Perrin, I. and Dussort, P. 2016. Impact of food processing and detoxification treatments on mycotoxin contamination. *Mycotoxin Research*, 32(4), 179–205.
- Niemira, B.A. 2012. Cold Plasma Decontamination of Foods *. *Food Science Technology*, 3, 125–142.
- Oghbaei, M.; Prakash, J. and Yildiz, F. 2016. Effect of primary processing of cereals and legumes on its nutritional quality: A comprehensive review. *Cogent Food & Agriculture*, 2(1), 1–14.

Sella, S.R.; Vandenberghe, L.P.S.; and Soccol, C.R. 2014. Life cycle and spore resistance of spore-forming *Bacillus atrophaeus*. *Microbiological Research*, 169(12), 931–939.

Ziuzina, D.; Han, L.; Cullen, P.J.; and Bourke, P. 2015. Cold plasma inactivation of internalised bacteria and biofilms for *Salmonella enterica*

serovar typhimurium, *Listeria monocytogenes* and *Escherichia coli*. *International Journal of Food Microbiology*, 210, 53–61.

Walter, E.; and Pronzato, L. 1997. Identification of parametric models from experimental data. Springer, Paris

CHARACTERIZATION OF FISH BASED MODEL FOOD SYSTEMS FOR MICROWAVE HEATING MODELING

Ferruh Erdogdu^{1*}, Huseyin Topcam¹, Ozan Altin¹, Davy Verheyen², Jan F. Van Impe², Ti Kian Seow²,
Dagbjørn Skipnes³ and Torstein Skåra³

¹Department of Food Engineering,
Ankara University

Golbasi Kampusu, Golbasi-Ankara, 06830 Turkey

* e-mail address: ferruherdogdu@yahoo.com

²KU Leuven, Department of Chemical Engineering,
BioTeC+ & OPTEC & CPMF²

Gebroeders de Smetstraat 1, B-9000 Ghent, Belgium

e-mail address: Jan.VanImpe@kuleuven.be

³Nofima, P.O. Box 8034,
4068 Stavanger, Norway
e-mail address: Torstein.Skara@nofima.no

KEYWORDS

Microwave heating, modelling, dielectric properties, fish based model food systems

ABSTRACT

Food products can be classified into six categories of food architectures: liquids, aqueous gels, oil-in-water emulsions, water-in-oil emulsions, gelled emulsions, and surfaces. For studies of microwave (MW) heating, model foods with consistent and predictable dielectric properties (e.g. tylose) are frequently used. In this study, the dielectric properties of five fish based model food systems were characterised, and one of these, a liquid with added xanthan, was used for modelling of MW heating, and compared to tylose. The preliminary results indicate a more homogeneous heating for tylose, than for the Xanthan. Besides, as such, the fish based model systems may show a closer resemblance to real food.

INTRODUCTION

Microwave heating has been a promising technology for food industry due to its plethora of possible food processing applications, e.g., thawing of frozen meats, pre-cooking for fast food chains, and pasteurization of pre-packaged foods (Decareau, 1985). All these processes started taking off with microwave heating recent decades. When a food product is subjected to microwave heating, electromagnetic energy penetrates into the product and is converted to heat by interactions with charged particles and polar molecules (Buffler, 1992). The penetration depth is strongly influenced by applied frequency (915 or 2450 MHz in most food processing cases) and dielectric properties, which are also function of frequency and temperature. Compared to conventional thermal treatments used in food industry, microwave heating leads to significantly shorter processing times due to the direct interaction between food materials and electromagnetic waves, resulting in less damage to the physico-chemical and nutritional properties of thermally processed foods (Datta and Hu, 1992; Soto-Reyes et al., 2015). However, temperature uniformity still continues to be a concern, and forced rotation of the product within the cavity is one of the common ways to increase the temperature uniformity (Li and Sun, 2002).

Heat transfer and resulting temperature distribution of foods is influenced by different factors related to the product, package, process and used equipment, e.g., shape, size, composition, multiple components, physical state,

and dielectric properties (Datia and Davidson, 2000; Salazar-González et al., 2012; Vadivambal and Jayas, 2010). Among these factors, the dielectric properties of a food product (i.e., the dielectric constant ϵ' , expressing the ability of a material to store electric energy, and the dielectric loss factor ϵ'' , expressing the conversion of microwave energy into thermal energy) are of major importance in relation to microwave heating (Tang, 2015). As stated, they both are functions of applied frequency and evolved temperature.

In addition, dielectric properties of foods are affected by food composition (e.g., moisture content, salt, fat content). Hence, dielectric properties must be determined for each specific food product or food product group as a function of temperature and frequency (Guan et al., 2004; Tang, 2015). Due to the limitations related to the use of real food products (e.g., each batch of food can only be used once, difficult to use for periodical tests), model foods with consistent and predictable dielectric properties are used frequently in microwave studies (Llave et al. 2015, 2016). Materials used for the creation of model foods in previous studies include bentonite water pastes (Luan et al., 2015), agar gel (Sakai et al., 2005), tylose (Llave et al. 2015, 2016), and whey protein gel (Wang et al., 2009). However, similarities between these model systems and real foods are rather limited, often requiring validation in the target food product (Llave et al., 2016).

In this study, microwave heating was modelled in fish based model food systems (Verheyen et al., 2017), i.e., more complex model food systems than used in previous studies. Due to their high heat sensitivity and resulting quality loss induced by traditional thermal inactivation techniques (Rosnes et al., 2011), fish products are of significant interest for microwave studies. Considering the increased use of MW heating for pasteurization and sterilization purposes, the use of fish based models is expected to give an idea on the use of microwave systems for innovative processing purposes. To develop the mathematical model, the model systems were characterized for their dielectric and thermal properties, and resulting temperature difference was compared with a conventional model system of tylose gel (77% moisture content – wet basis).

MATERIALS AND METHODS

Model systems

The fish-based model systems were prepared as described by Verheyen et al. (2017). These were two liquid systems (with and without xanthan gum), an emulsion (with 1%

fat), an aqueous gel and a gelled emulsion. They were compositionally designed in such a way that the micro-structural effect could be isolated, and all model systems were suitable for common growth and mild thermal inactivation experiments.

Density

Density of the samples was measured at room temperature recording the mass of a 100 mL volume.

Specific heat capacity

The specific heat capacity was determined by Differential scanning Calorimetry (DSC), using the sapphire method (Anon., 1981, 2010). Since this parameter is expected to be temperature dependent (Darros-Barbosa et al., 2003), measurements were recorded in the range between 0-10 °C and 60-70 °C, and four measurements, between 3-7 °C and 63-67 °C, respectively, were used to determine the c_p value at 5 and 65 °C.

Thermal conductivity

Thermal conductivity of the samples was measured by a line heating source probe and instrument KD2 (Decagon devices inc, Pullman, WA, USA) at 4, 60 and 70 °C.

Dielectric properties

The dielectric properties were measured by using a network analyzer (Agilent Technologies ES061B ENA Series Network Analyzer, ABD) in the frequency range of 915 to 2450 MHz. The network analyzer used an open ended coaxial-line probe (Agilent Technologies, 85070E, ABD), and dielectric constant (ϵ') and loss factor (ϵ'') were measured within a temperature range of 2 to 80 °C. Temperatures of the solutions were adjusted in a water bath (Mettler, Germany). All measurements were carried out in triplicate, and the open ended coaxial-line probe was calibrated by measuring the properties of air, the short-circuit block (metallic short block) and distilled water at corresponding measurement temperatures.

Modelling

The modelling study was carried out using the properties of xanthan and tylose (as a common example used in various model validation studies). Dielectric and thermal properties of tylose gel were obtained from Llave et al. (2015, 2016). The mathematical model to determine the electromagnetic field distribution within a microwave cavity and temperature distribution within the sample was developed using Comsol Multiphysics program (V.5.1 - Comsol AB, Stockholm, Sweden). Figure 1 illustrates the computational geometry of the microwave cavity. The cylindrical sample (tylose and xanthan) dimensions placed in the cavity were 6.6 cm; in diameter and 3.8 cm in height.

For model development, microwave heating physics (electromagnetic waves and heat transfer in solids) was used with following governing equations for electromagnetic and temperature distributions with the applied boundary conditions.

Electromagnetic Waves:

$$\nabla \times \left(\frac{1}{\mu} \nabla \times \vec{E} \right) - \frac{\omega^2}{c} (\epsilon' - i\epsilon'') \vec{E} = 0$$

Boundary conditions:

- Perfect Electromagnetic Conductor for cavity and waveguide walls,
- 2450 MHz frequency and variable power due to the on-off cycles of the microwave system (Figure 2 shows the on-off cycles within the given process time) with TE₁₀ mode rectangular type port, and
- Dielectric properties of the samples were function of temperature through the frequency-transient solver.

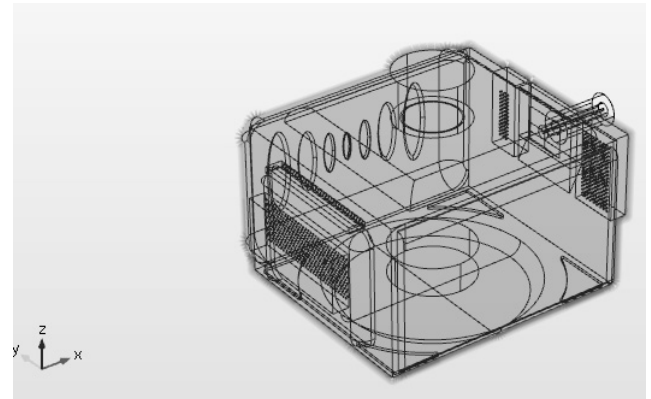


Figure 1. The computational geometry of the microwave cavity in the applied modeling study.

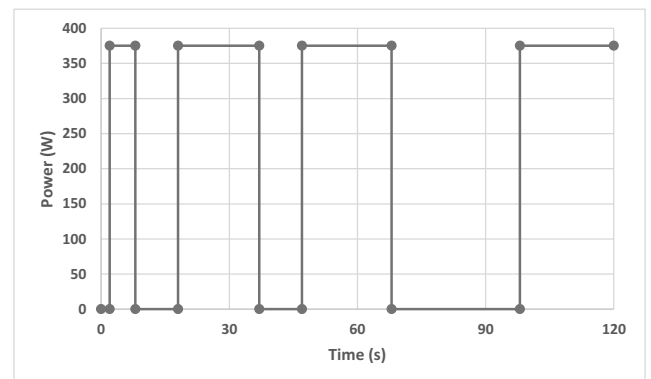


Figure 2. The on – off cycle of the microwave system used in the modeling study.

Heat Transfer in Solid;

$$\rho C_p \frac{\partial T}{\partial t} = \nabla(k\nabla T) + Q$$

Where absorbed power, Q was:

$$Q = \sigma |\vec{E}|^2 = \frac{1}{2} \omega \epsilon_0 \epsilon'' |\vec{E}|^2$$

Boundary conditions:

- Fixed and uniform initial temperature distribution,
- Convective heat transfer for surface of sample with a heat transfer coefficient of $h = 25 \frac{W}{m^2K}$.

RESULTS AND DISCUSSION

Thermophysical properties

Density and thermal conductivity values are reported in Tables 1 and 2, respectively. Density values ranged from

800 to 920 kg/m³ for different fish based model systems at 20 °C while the emulsion and the xanthan had the lowest density and highest density, respectively. Specific capacity values at 5 °C ranged from 0.51 to 3.30 J/g-K, at 5 °C, and

from 2.30 to 3.44 J/g-K at 65 °C. The liquid system showed the highest specific heat capacity at both temperatures.

Table 1: Density and specific heat capacity of the model systems.

Sample\Temperature [°C]	Density [kg/m ³]		Specific Heat Capacity, c _p [J/g*K]			
	20	5	5	65	65	65
Xanthan	920	1.90 ± 0.02	2.30	±	0.01	
Liquid	910	3.30 ± 0.00	3.44	±	0.05	
Aqueous gel	850	2.90 ± 0.00	3.17	±	0.01	
Emulsion	800	2.38 ± 0.01	2.95	±	0.01	
Gelled emulsion	880	0.51 ± 0.00	2.69	±	0.09	

Table 2: Thermal conductivity of the model systems.

Sample\Temperature [°C]	Thermal conductivity [W/m*K]					
	4	60	70	70	70	70
Xanthan	0.19 ± 0.01	0.60 ± 0.00	0.67 ± 0.03			
Liquid	0.34 ± 0.00	0.46 ± 0.03	0.73 ± 0.02			
Aqueous gel	0.13 ± 0.00	0.45 ± 0.03	0.55 ± 0.01			
Emulsion	0.06 ± 0.00	0.45 ± 0.02	0.60 ± 0.02			
Gelled emulsion	0.33 ± 0.00	0.53 ± 0.01	0.56 ± 0.02			

Table 3: Dielectric constant and dielectric loss factor of the model systems at 2450 MHz

Temperature [°C]	2	25	42	61	81
	Dielectric constant				
Xanthan	81.5 ± 0.09	71.6 ± 0.39	67.1 ± 4.11	66.7 ± 0.61	50.4 ± 5.05
Liquid	75.8 ± 0.15	83.2 ± 0.81	65.1 ± 4.07	67.0 ± 1.46	59.7 ± 1.44
Aqueous gel	83.6 ± 0.55	71.7 ± 0.12	76.4 ± 1.96	61.7 ± 0.91	60.5 ± 7.00
Emulsion (1%fat)	76.4 ± 4.09	57.3 ± 0.17	59.6 ± 6.40	64.7 ± 0.22	57.5 ± 5.10
Gelled emulsion	79.3 ± 0.37	72.5 ± 11.54	64.1 ± 1.16	69.9 ± 0.02	60.3 ± 3.04
	Dielectric loss factor				
Xanthan	35.4 ± 0.05	31.6 ± 0.05	34.5 ± 4.30	43.5 ± 1.44	41.3 ± 4.01
Liquid	31.5 ± 2.78	34.5 ± 0.86	30.0 ± 3.39	41.4 ± 2.76	52.6 ± 1.06
Aqueous gel	30.9 ± 0.07	41.3 ± 0.02	40.5 ± 0.91	34.7 ± 1.22	43.0 ± 0.35
Emulsion (1%fat)	30.8 ± 1.78	27.4 ± 0.20	31.0 ± 1.45	40.1 ± 0.54	49.4 ± 2.79
Gelled emulsion	34.4 ± 0.03	31.1 ± 5.87	27.5 ± 0.66	43.2 ± 0.01	42.0 ± 3.12

Dielectric properties

The dielectric properties as a function of temperature at 2450 MHz frequency are shown in Table 3.

Modelling of microwave heating

The tylose and xanthan samples were assumed to be located in a microwave cavity (Fig. 1) and the results were compared under the same conditions. Figures 3 and 4 show the surface temperature distribution of the samples after MW heating for 90 s for tylose and 20 s for xanthan. The local surface temperature increase for the xanthan samples was rather high with the localized hot spots compared to the tylose sample even at the earlier stage of heating. After 20 s of heating, xanthan surface temperature increased over 100 C, and it was required to include the latent heat of vaporization to have a reasonable data. Since the objective of the study was to demonstrate the effect of dielectric properties and penetration depth on the temperature increase, the temperature distributions at the given times were compared. The surface temperature

distribution (T_{surface}) and volume average temperature (T_{avg}) changes of the samples are shown in Figures 5 and 6, respectively.

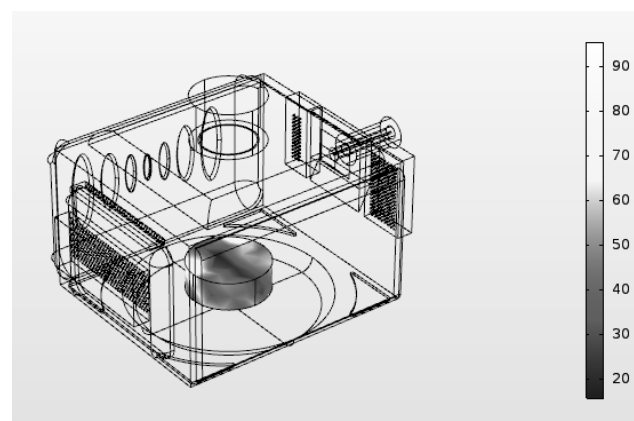


Figure 3. Surface temperature distribution of the tylose sample after 90 s of the microwave heating (temperature scale is in °C).

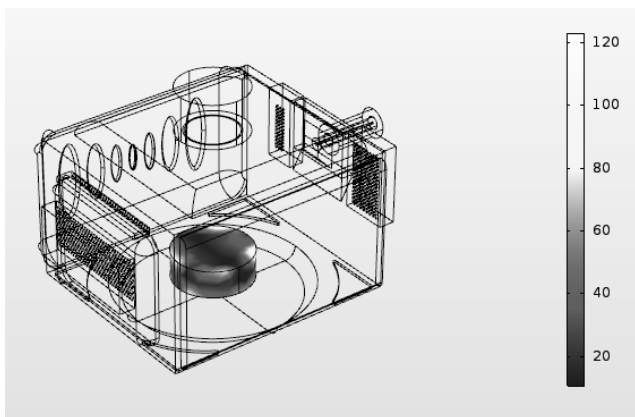


Figure 4. Surface temperature distribution of the Xanthan sample after 20 s of the microwave heating (temperature scale is in °C).

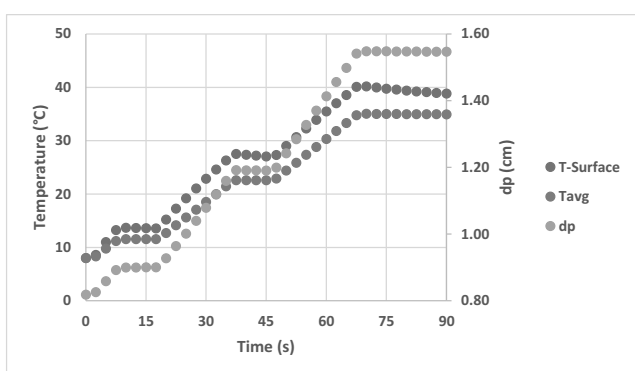


Figure 5. Surface (T_{surface}) and volume average temperature (T_{avg}) changes of tylose sample with its penetration depth (secondary y-axis) during 90 s of heating.

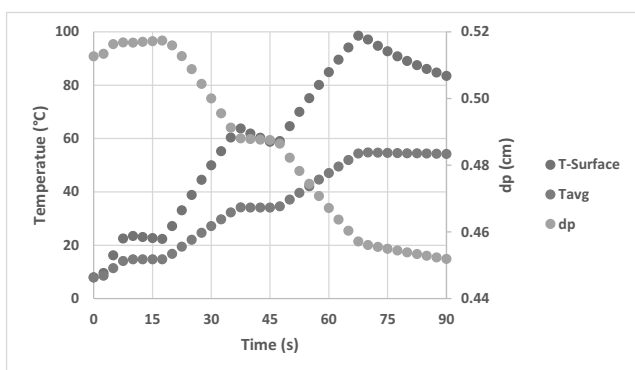


Figure 6. Surface (T_{surface}) and volume average temperature (T_{avg}) changes of xanthan sample with its penetration depth (secondary y-axis) during 90 s of heating.

As observed in these figures, for the tylose sample, the difference between surface and volume average temperature was rather small (Figure 5) compared to the xanthan, where rather significant differences were observed (Figure 6). This was due to local (over) heating of the surface. As explained below, penetration depth is strongly influenced by applied frequency and dielectric properties. Hence, in the same figures, change of penetration depth (dp) is also demonstrated:

$$d_p = \frac{c}{2\pi f \sqrt{2\epsilon'} \sqrt{1 + \left(\frac{\epsilon''}{\epsilon'}\right)^2 - 1}}$$

The penetration depth is defined as the depth at which the intensity of the electromagnetic effect is reduced to its 1/e (37%). It increased up to 1.6 cm for the case of tylose while it decreased from 0.52 to 0.45 cm for Xanthan sample, indicating a shorter penetration depth. Since the electromagnetic effect was limited to demonstrate a volumetric heating for the case of Xanthan, local surface heating with hot spots was more common with the limited volume average temperature increase compared to the case of tylose. Figures 7 and 8 show the effect of penetration at 20 s of the process for the samples in the xz plane.

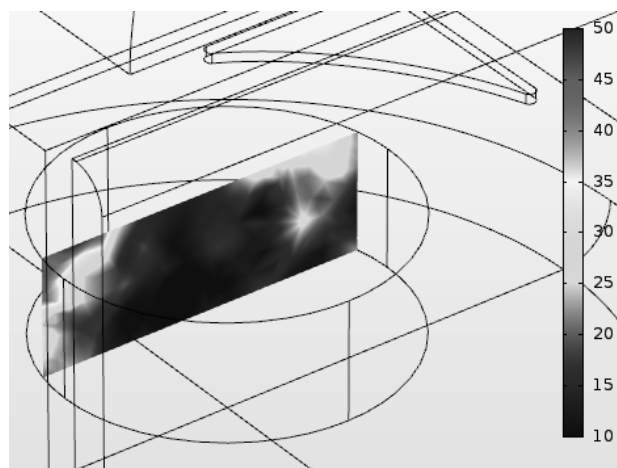


Figure 7. Effect of penetration depth at 20 s of the process for tylose sample in the xz plane (temperature scale is in °C).

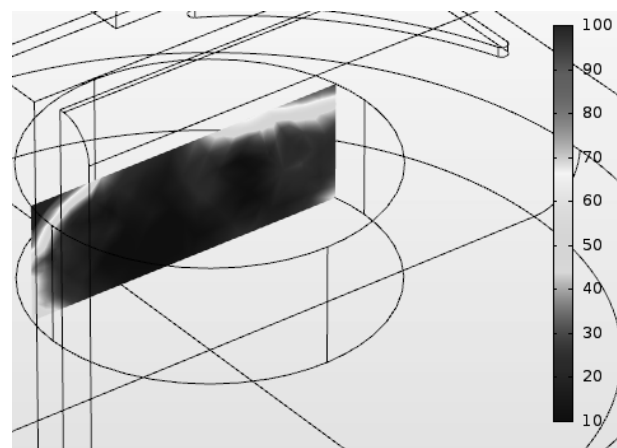


Figure 8. Effect of penetration depth at 20 s of the process for xanthan sample in the xz plane (temperature scale is in °C).

As observed, the tylose samples demonstrate a better uniformity while a certain surface heating starts for the xanthan sample at a rather early stage of the process. In addition to the effect of dielectric properties and penetration depth on heating rate, specific heat value was another factor. Specific heat values of xanthan changed from 1.90 to 2.30 J/g-K from 5 to 65 °C while it was 3.65 J/g-K for tylose. This shows that xanthan sample requires less heat energy to increase in its temperature. This also

demonstrates the significant effect of specific heat capacity during microwave heating.

CONCLUSIONS AND FUTURE RESEARCH

In this study, the dielectric properties of five fish based model food systems were characterised, and one of these, a liquid with added xanthan, was used for modelling of MW heating, and compared to tylose. The preliminary results indicate a more homogeneous heating for tylose, than for the Xanthan. But as such, the fish based model systems may show a closer resemblance to real food. In addition, the model systems open for modifications and adjustments, both to study effects on the microwave heating, and also on the inactivation of microorganisms

REFERENCES

- Anon. 1981. Specific Heat Capacity Measurements Using DSC I. Application Brief.
- Anon. 2010. Measuring specific heat capacity. Thermal Analysis UserCom.
- Buffler, C.R. 1992. Microwave cooking and processing: engineering fundamentals for the food scientist. Van Nostrand Reinhold, New York, USA.
- Darros-Barbosa, R., Balaban, M.A. and Teixeira, A.A. (2003). Temperature and concentration dependence of heat capacity of model aqueous solutions. *Int J Food Prop.* 6(2): 239-258.
- Datia, K.D. and P.M. Davidson. 2000. Microwave and radio frequency processing. *J. Food Sci.* 65(s8): 32-41.
- Datta, A.K. and W. Hu. 1992. Optimization of quality in microwave heating. *Food Technol.* 46(12): 53-56.
- Guan, D., M. Cheng, Y. Wang and J. Tang. 2004. Dielectric properties of mashed potatoes relevant to microwave and radio-frequency pasteurization and sterilization processes. *J. Food Sci.* 69: 30-37.
- Li, B. and D.W. Sun. 2002. Novel methods for rapid freezing and thawing of foods – A review. *J. Food Eng.* 54: 397-405.
- Liu, S., X. Yu, M. Fukuoka and N. Sakai. 2014. Modeling of fish boiling under microwave irradiation. *J. Food Eng.* 140: 9-18.
- Llave, Y.; Liu, S.; Fukuoka, M. and Sakai, N. 2015. Computer simulation of radiofrequency defrosting of frozen foods. *Journal of Food Engineering*, 152, 32-42.
- Llave, Y., M. Katsuya, D. Kambayashi, M. Fukuoka, and N. Sakai. 2016. Dielectric properties and model food application of tylose water pastes during microwave thawing and heating. *Journal of Food Engineering* 178:20-30.
- Luan, D., J. Tang, F. Liu, Z. Tang, F. Li, H. Lin and B. Stewart. 2015. Dielectric properties of bentonite water pastes used for stable loads in microwave thermal processing systems. *J. Food Eng.* 161: 40-47.
- Rosnes, J. T., T. Skåra, and D. Skipnes. 2011. Recent advances in minimal heat processing of fish: Effects on microbiological activity and safety. *Food Bioprocess. Technol.* 4: 833-848.
- Sakai, N., W. Mao, Y. Koshima and M. Watanabe. 2005. A method for developing model food system in microwave heating studies. *J. Food Eng.* 66: 525-531.
- Salazar-González, C., M.F. San Martín-González, A. López-Malo, M.E. Sosa-Morales. 2012. Recent studies related to microwave processing of fluid food. *Food Bioprocess. Technol.* 5(1): 31-46.
- Soto-Reyes, N., A.L. Temis-Pérez, A. López-Malo, R. Rojas-Laguna and M.E Sosa-Morales. 2015. Effects of shape and size of agar gels on heating uniformity during pulsed microwave treatment. *J. Food Sci.* 80(5): E1021-E1025.
- Tang, J. 2015. Unlocking potentials of microwaves for food safety and quality. *J. Food Sci.* 80(8): E1776-E1793
- Vadivambal, R. and D.S. Jayas. 2010. Non-uniform temperature distribution during microwave heating of food materials – a review. *Food Bioprocess. Technol.* 3: 161-171.
- Verheyen, D., M. Baka, S. Glorieux, B. Duquenne, I. Fraeye, T. Skåra, and J. F. Van Impe. 2018. Development of fish-based model systems with various microstructures. *Food Res Int*:In press.
- Wang, Y., J. Tang, B. Rasco, S. Wang, A.A. Alshami and F. Kong. 2009. Using whey protein gel as a model food to study dielectric heating properties of salmon (*Oncorhynchus gorbuscha*) filets. *Food Sci. Technol.* 42: 1174-1178.

Multi-Scale Modeling Methods

A SEMI-AUTOMATIC MODELLING APPROACH FOR THE PRODUCTION AND FREEZE-DRYING OF LACTIC ACID BACTERIA

Thomas Chabin, Marc Barnabé, Alberto Tonda, Nadia Boukhelifa, Fernanda Fonseca
Eric Dugat-Bony, H el ene Velly, Evelyne Lutton, Nathalie M ejean Perrot
UMR 782 GMPA, INRA
1 av. Lucien Br etign eres, 78850, Thiverval-Grignon, France
email: {firstname.lastname}@inra.fr

KEYWORDS

Complex Systems, Multiscale Modelling, Interactive Modelling, Optimisation, Expert Knowledge, Visualisation, Freeze-Drying of Lactic Acid Bacteria.

ABSTRACT

The production system of freeze-dried lactic acid bacteria involves several processes, but its impact on bacteria resistance is still not well understood. This system can be defined as a complex one since it depends on multiple scales: the Genomic, the Cellular and the Population scale. The scarcity of data available for building models leads us to propose an approach that makes use of expert knowledge. In this paper we present a semi-automatic modelling tool, LIDEOGRAM and discuss how it contributes to insight formulation and rapid hypothesis testing. New results show that LIDEOGRAM is able to produce more robust modelling hypotheses when experts can interact and revisit the genomic data preprocessing.

INTRODUCTION

Complex systems are found in many features of nature and science, ranging from the economic and social structure of a city to the global climate, or from the behaviour of a single cell to the behaviour of the intricate interactions of the human brain. Complex systems involve numerous components linked by non-trivial relationships, and are challenging to study. Modelling such complex systems, by summarising available knowledge into a mathematical or computational representation, is not a trivial task.

Concentrates of Lactic Acid Bacteria (LAB) are widely used in the food industry for manufacturing products such as yoghurt, cheese, fermented meat, vegetables and fruit beverages. The production of freeze-dried LAB is a complex food system due to its multi-scale and multi-step properties. One of the main challenges that need to be tackled ahead is to understand the origin of the LABs resistance and/or their sensitivity to the whole production system. Models describing parts of the system for a specific strain of bacteria are found in the

literature (Passot et al. (2011)). However, to the best of our knowledge, no models have been proposed to represent the whole process.

Automatic modelling approaches have already been proposed for complex systems such as metabolic networks (Schmidt et al. (2011)), or for various multi-scale processes (Hasenauer et al. (2015)). These approaches often require a significant amount of data, however, gathering data on the freeze-drying process of LAB is expensive and time-consuming. Little amount of data is thus generally available, and this is a major issue for automatic modelling. To compensate for the lack of data, expert knowledge on the process can be exploited. We show in this paper how such knowledge can be integrated within a modelling process, based on a semi-automatic scheme. The paper is organised as follows: First we present some background on complex systems, on semi-automatic modelling and on expert knowledge integration. The target system and the dataset are then described. Next we detail our semi-automatic modelling software and show some experimental results. Finally, results are discussed and conclusions are drawn.

BACKGROUND

Complex Systems in Biology and Food Systems: Expert Knowledge Integration Methods

A complex system is defined as a system made of multiple processes, entities, and nested subsystems. Global properties emerge through a series of phenomena occurring at different scales (Ladyman et al. (2013)). Appropriate descriptions with high expressiveness and little uncertainty of the underlying mechanisms is needed to elucidate such systems. Building models of complex systems is crucial, but highly difficult. It usually requires a robust framework, with strong iterative interaction combining computational intensive methods, formal reasoning and experts from different fields. In such context, optimisation plays an important role (Lutton et al. (2016)). Properties of food systems (such as uncertainty and variability, heterogeneity of data, coexistence of qualitative and quantitative information, conjunction of different perspectives) raise the focus on another es-

sential issue, that can be called the *human factor*. In order to gain a better understanding of food systems, human expertise and decision making are of major importance, and should thus be integrated into automatic modelling approaches (Lutton and Perrot (2015)). Numerous papers propose to take advantage of a structured prior knowledge of a system to improve machine learning methods. Among those, prior knowledge was used to improve the predictions of neural networks model of chemical systems (Thompson and Kramer (1994)), or to build a genetic network using Bayesian methods (Le et al. (2004)). Expert knowledge was also used by Baudrit et al. (2010) to improve the quality of a cheese ripening process model using Bayesian networks. In other studies, structured knowledge about the topic of interest is not well defined and exist more in the form of insights. In such cases, approaches relying on visual exploration of the data, and interactions through software have been proposed (Turkay et al. (2017), Cancino et al. (2012) and Krause et al. (2014)). In this way, it is possible to confirm and elucidate new hypotheses.

In this context, this work aims at presenting in the following sections a new approach for modelling multi-scale systems, interactively and iteratively, through visual exploration, machine learning and knowledge integration.

PRODUCTION AND FREEZE-DRYING OF LACTIC ACID BACTERIA

Concentrates of LAB, also called starters, are food ingredients widely used for producing fermented meat, vegetables, fruit and dairy products. The commercialisation of these starters requires the application of successive operations: fermentation, concentration and preservation by freezing or freeze-drying (or lyophilisation). The viability and acidification activity of the cells are the two main quality attributes of the starters. They depend on many control parameters of the multi-steps process: Fermentation, Concentration, Formulation, Freeze-Drying and Storage, See Carvalho et al. (2004) for a detailed description.

The bacteria's levels of resistance to the processes is also dependent on the biochemical and biophysical properties and organisation of their membrane, which in turn is determined by the expression of the bacterial genome. This case study is based on the work of Velly et al. (2015) about the resistance of *Lactococcus lactis* subsp. *lactis* *TOMSC161* to freeze-drying. This strain, very sensitive to freeze-drying, is used for the manufacture of *Tomme de Savoie*, a French cheese, for its texturing and acidification characteristics. Several bacterial properties were measured for two fermentation temperatures (22 C and 30 C), and two cell growth phases (at the beginning of the stationary growth phase and 6 hours later). The dataset features 12 data points, corresponding to previous detailed four fermentation conditions and three biological repetitions of each experimental condition. Dif-

ferent scales were considered:

- Genomic: Transcriptomic data obtained on 2744 genes by RNA-seq,
- Cellular: Relative composition of main fatty acids present in the bacterial membrane determined by Gas Chromatography-Mass Spectrometry after extraction and the Anisotropy of the membrane (rigidity) assessed by flow cytometry,
- Population: Viability by numbering on agar plates and acidification activity in milk quantified using the CINAC system at the end of the following steps: Concentration, Freezing, Drying, and three months of Storage.

LIDEOGRAM

Experts of the domain seek answers about how a given bacterial strain becomes resistant to the process. Mathematical tools, including mathematical formulas are generally used to help them address these questions. But finding reliable formulas linking the different variables of such a system is indeed challenging. In biological data, repetitions of a given experimental condition are often highly variable. Moreover, experiments are usually time-consuming and expensive, resulting in few data being obtained, which makes the task of characterising the existing variability difficult.

LIDEOGRAM (*Life-based Interactive DEvelopment Of GRAphical Models*) tries to address these challenges with an original approach based on semi-automatic modelling (See Chabin et al. (2017a;b) for details). The goal of LIDEOGRAM is to provide experts with a design tool for modelling their complex process. Each non-input variable is modelled by a mathematical formula involving other variables of the system. It is then possible to create a multi-scale model where each scale of the process is defined with variables of a lower scale and with experimental conditions. A global model is therefore a concatenation of mathematical equations that figure relationships between different variables at different scales. This is similar to other successful multi-scale modelling approaches such as for grape berries ripening by Dai et al. (2007) or for cow's milk production by Cros et al. (2003): the global model is made of stacked sub-models.

However, it is difficult to find the "right" equation in a context of high variability in the dataset. It is for instance frequent to come up with over-fitted equations that perfectly represent a dataset including its noise. In order to rule out over-fitted equations, our strategy is to involve experts in the course of the modelling process rather than splitting the (small) available dataset into training and test subsets. The expectation is that experts are able, thanks to their knowledge of the pro-

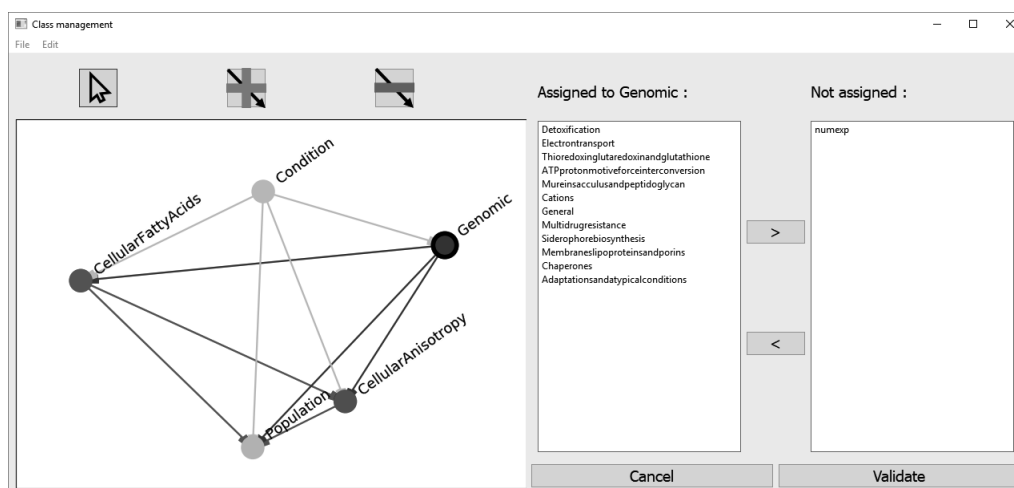


Figure 1: Screenshot of the interface where users choose the authorised links between the defined classes. A link between two classes means that all variables associated to the parent class can be involved in the equations for all variables of the child class. The displayed graph represents the selected constraints chosen for this experiment. The selected class here is the Genomic class (circled in black). The variables assigned to this class can be seen on the right side.

cess, to identify over-fitted, under-fitted or inappropriate equations.

Therefore, as a first optimisation step, LIDEOGRAM runs Orthogonal Matching Pursuit (OMP) on each variable. This technique introduced by Pati et al. (1993) is a linear regression that makes it possible to choose the number of predictive variables used in an equation. Using this approach, a set of candidate equations with different levels of complexity and fitting error is associated to each variable. Constraints can be defined beforehand by the user, using the interface presented in Figure 1. It makes it possible to attribute each variable to a given class of variables, and to authorise or forbid links between them, in the sense that only the variables from a parent class can be used for calculating the variables of the child class.

A qualitative view of the proposed equations is then presented to the user as a graphical network (See Figure 2). The purpose of this view is to help the user identify the critical variables, where expert feedback is most needed. Nodes of the graph represent variables. Colours of nodes correspond to their attributed class. A link between two variables means that the parent node is used at least once in the set of equations of the child node. Colours of links correspond to a numerical value computed using all mathematical equations featuring the parent node in the child node. A green link corresponds to a good mean fitting of the data for the corresponding equations. Conversely, a red link represents a poor fitting. The network may be difficult to read, since the displayed graphical network can have a considerable amount of links. A slider filters the links based on a level of importance. This level of importance is defined for a link by the number of equations in the child node that use the parent

node, divided by the total number of equations of the child node.

When a node is selected, the equations found by OMP are displayed on the top-right side (See Figure 2). Similarly, a click on an equation triggers the corresponding plot of experimental versus predicted data. The user can then interact with the system by deleting an equation, deleting a link between a parent node and a child node (i.e. all equations using the parent node in the child node are deleted), or deleting a variable (in this case all equations using the deleted variable are deleted). After this, few or no equations may remain for some nodes, the user can choose to restart the OMP on any node, with new constraints. After this, an evolutionary optimisation builds a global model by selecting one equation for each variable, thus taking into account the coherence between the scales.

USING EXPERT KNOWLEDGE VIA A SEMI-AUTOMATIC MODELLING SCHEME

The first step when starting LIDEOGRAM is to organise the set of variables into classes and to define the possible links between classes. Five classes of variables, linked to the different scales of the process, were designed: Condition, Genomic, CellularFattyAcids, CellularAnisotropy and Population. The authorised links between the classes are presented in Figure 1.

A preprocessing of the variables at the Genomic scale was needed before running LIDEOGRAM on them. With 2744 genes measured by transcriptomics and with a high variance in the measurements, it is hard to explore and make sense of the function of each individual gene in a model. For this purpose, two solutions

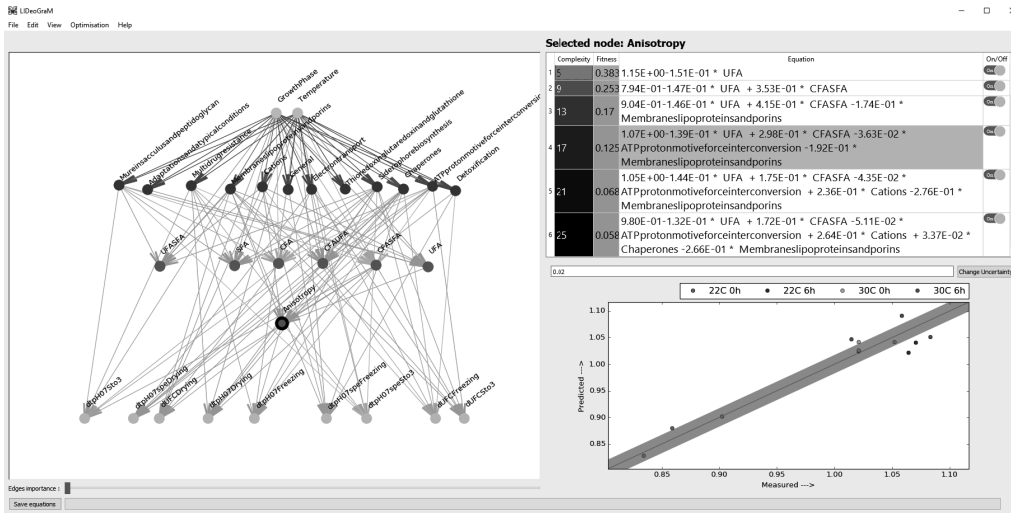


Figure 2: Screenshot of LIDEOGRAM. Left: graphical model representing the mean fitness for all local models. Top-right: list of equations proposed for the selected node (Anisotropy); Bottom-right: plot of the measured versus predicted data corresponding to the selected equation.

were explored using human expertise. The first pre-processing (PP1) is a classification proposed by Bolotin et al. (2001). The 82 functional classes of genes were reviewed by the experts in order to keep the most relevant ones. Twelve functional classes were selected at the genomic level. For each functional class, the sum of the genes expressions corresponding to this functional class is computed. Following experts advices, a second pre-processing (PP2) was performed to select only the genes showing a strong differential expression with respect to the conditions of fermentation. The selection criterion, computed for each gene, is the variance calculated on the mean expression for each condition, divided by the maximum of the variances calculated for each fermentation condition. Only the genes with a criterion larger than 2 were kept, which yielded 26 genes. LIDEOGRAM was used to rapidly access the best way to pre-process the genomic data for the modelling step. Results are reported in Table 1, where 0 represents the best possible prediction and 1 the worst one.

Table 1: Experimental results on the local and global models using PP1 and PP2.

	PP1	PP2
Mean of the Local models at the Genomic Scale	All variables > 0.7	All variables < 0.5
Global Fitness on 10 runs	0.702 var. 1.4×10^{-4}	0.283 var. 5.0×10^{-5}

From these results, it seems that the variance criterion approach (PP2) for the Genomic scale performs better, both in terms of local and global model. These

two hypotheses were explored in less than an hour, giving users a convenient and versatile way to test various modelling hypotheses. The equations proposed for the Anisotropy were also explored, using PP1 (shown in top-right side of Figure 2). Each equation was evaluated by the experts, who stated that the first three equations were compatible with their knowledge. Indeed, it was shown by Velly et al. (2015) that the anisotropy associated to membrane rigidity is anti-correlated with the Unsaturated Fatty Acids (UFA), but correlated to the ratio between Cyclic Fatty Acids and Saturated Fatty Acids (CFASFA). In the third equation, it is proposed that the anisotropy is also anti-correlated with the expression of genes that are associated to the membrane's lipoproteins and porins. According to our experts, this could be explained by the localisation of such proteins anchored (lipoproteins) to the membrane and crossing it (porins), respectively. One can thus hypothesise that their interactions with membrane components such as fatty acids could possibly modify membrane physical properties with a lowering effect on anisotropy (rigidity). Finally, some of the proposed equations were hard to validate. Our hypothesis is that these are over-fitted equations which may not represent the underlying reality. Such equations can then be discarded by the expert.

DISCUSSION AND CONCLUSION

We have presented above a semi-automatic approach for multi-scale modelling, that relies on both expert knowledge and automatic optimisation. LIDEOGRAM lets domain experts easily test various modelling hypotheses for multi-scale systems. Tests have been made on a production system for freeze-dried Lactic Acid Bacteria. LIDEOGRAM is also used for other applications, for ex-

ample, for modelling a cheese ripening ecosystem, and for modelling a grape berry maturity prediction system. Future improvements will be focused on the graphical interface and the various views: new interaction techniques will be proposed for analysing and modifying the proposed models. Indeed, it has been suggested that providing a variety of views and interactions (including change of focus of interest) is an excellent manner to engage users, reduce their fatigue and boost their creativity (Lutton et al. (2003), Boukhelifa et al. (2016)). Non-linear local models will be implemented in a future version of the software. We actually expect a better accuracy with the proposed models. Previous attempts using non-linear models provided promising results, however technical difficulties make the full use of a non-linear modelling approach more complex. Pareto front exploration of the local models is another important issue that will be developed in a further work.

REFERENCES

- Baudrit C.; Sicard M.; Willemin P.H.; and Perrot N., 2010. *Towards a global modelling of the Camembert-type cheese ripening process by coupling heterogeneous knowledge with dynamic Bayesian networks*. *Journal of Food Engineering*, 98, no. 3, 283–293.
- Bolotin A.; Wincker P.; Mauger S.; Jaillon O.; Malmare K.; Weissenbach J.; Ehrlich S.D.; and Sorokin A., 2001. *The complete genome sequence of the lactic acid bacterium *Lactococcus lactis* ssp. *lactis* IL1403*. *Genome research*, 11, no. 5, 731–753.
- Boukhelifa N.; Bezerianos A.; Tonda A.; and Lutton E., 2016. *Research prospects in the design and evaluation of interactive evolutionary systems for art and science*. In *CHI workshop on Human Centred Machine Learning*. np.
- Cancino W.; Boukhelifa N.; and Lutton E., 2012. *Evo-graphdice: Interactive evolution for visual analytics*. In *Evolutionary Computation (CEC), 2012 IEEE Congress on. IEEE*, 1–8.
- Carvalho A.S.; Silva J.; Ho P.; Teixeira P.; Malcata F.X.; and Gibbs P., 2004. *Relevant factors for the preparation of freeze-dried lactic acid bacteria*. *International Dairy Journal*, 14, no. 10, 835–847.
- Chabin T.; Barnabe M.; Boukhelifa N.; Fonseca F.; Tonda A.; Velly H.; Lemaitre B.; Perrot N.; and Lutton E., 2017a. *LIDeOGraM: an interactive evolutionary modelling tool*. In *Biennial International Conference on Artificial Evolution (EA-2017)*. np.
- Chabin T.; Barnabe M.; Boukhelifa N.; Fonseca F.; Tonda A.; Velly H.; Perrot N.; and Lutton E., 2017b. *Interactive evolutionary modelling of living complex food systems: freeze-drying of lactic acid bacteria*. In *Proceedings of the Genetic and Evolutionary Computation Conference Companion*. ACM, 267–268.
- Cros M.J.; Duru M.; Garcia F.; and Martin-Clouaire R., 2003. *A biophysical dairy farm model to evaluate rotational grazing management strategies*. *Agronomie*, 23, no. 2, 105–122.
- Dai Z.W.; Vivin P.; and Génard M., 2007. *Modelling the effects of leaf-to-fruit ratio on dry and fresh mass accumulation in ripening grape berries*. In *VIII International Symposium on Modelling in Fruit Research and Orchard Management 803*. 283–292.
- Hasenauer J.; Jagiella N.; Hross S.; and Theis F.J., 2015. *Data-driven modelling of biological multi-scale processes*. *Journal of Coupled Systems and Multiscale Dynamics*, 3, no. 2, 101–121.
- Krause J.; Perer A.; and Bertini E., 2014. *INFUSE: interactive feature selection for predictive modeling of high dimensional data*. *IEEE transactions on visualization and computer graphics*, 20, no. 12, 1614–1623.
- Ladyman J.; Lambert J.; and Wiesner K., 2013. *What is a complex system?* *European Journal for Philosophy of Science*, 3, no. 1, 33–67.
- Le P.P.; Bahl A.; and Ungar L.H., 2004. *Using prior knowledge to improve genetic network reconstruction from microarray data*. In *in silico biology*, 4, no. 3, 335–353.
- Lutton E.; Cayla E.; and Chapuis J., 2003. *ArtiE-fract: The artists viewpoint*. In *Workshops on Applications of Evolutionary Computation*. Springer, 510–521.
- Lutton E. and Perrot N., 2015. *Complex systems in food science: Human factor issues*. *6th International Symposium on Delivery of Functionality in Complex Food Systems Physically-Inspired Approaches from the Nanoscale to the Microscale*.
- Lutton E.; Perrot N.; and Tonda A., 2016. *Evolutionary Algorithms for Food Science and Technology*. John Wiley & Sons.
- Passot S.; Fonseca F.; Cenard S.; Douania I.; and Trelea I.C., 2011. *Quality degradation of lactic acid bacteria during the freeze drying process: Experimental study and mathematical modelling*.
- Pati Y.C.; Rezaifar R.; and Krishnaprasad P.S., 1993. *Orthogonal matching pursuit: Recursive function approximation with applications to wavelet decomposition*. In *Signals, Systems and Computers, 1993. 1993 Conference Record of The Twenty-Seventh Asilomar Conference on. IEEE*, 40–44.
- Schmidt M.D.; Vallabhajosyula R.R.; Jenkins J.W.; Hood J.E.; Soni A.S.; Wikswo J.P.; and Lipson H., 2011. *Automated refinement and inference of analytical models for metabolic networks*. *Physical biology*, 8, no. 5, 055011.
- Thompson M.L. and Kramer M.A., 1994. *Modeling chemical processes using prior knowledge and neural networks*. *AIChE Journal*, 40, no. 8, 1328–1340.
- Turkay C.; Slingsby A.; Lahtinen K.; Butt S.; and Dykes J., 2017. *Supporting theoretically-grounded model building in the social sciences through interactive visualisation*. *Neurocomputing*.
- Velly H.; Bouix M.; Passot S.; Penicaud C.; Beinsteiner H.; Ghorbal S.; Lieben P.; and Fonseca F., 2015. *Cyclopropanation of unsaturated fatty acids and membrane rigidification improve the freeze-drying resistance of *Lactococcus lactis* subsp. *lactis* TOMSC161*. *Applied microbiology and biotechnology*, 99, no. 2, 907–918.

A generalized NURBS based dynamic metabolic flux analysis framework: deciphering intracellular pathway activation from extracellular measurements

Philippe Nimmegeers, Simen Akkermans, Wouter Gijsen, Dries Telen, Jan Van Impe
 BioTeC+ & OPTEC, Department of Chemical Engineering, KU Leuven
 CPMF2, Flemish Cluster Predictive Microbiology in Foods
 Gebroeders de Smetstraat 1, B-9000 Gent, Belgium
 E-mail address: Jan.VanImpe@kuleuven.be

KEYWORDS

Dynamic metabolic flux analysis, Metabolic networks, Parameter estimation, Splines

ABSTRACT

Current macroscopic population balance models are not sufficient to obtain a profound understanding in the complex behaviour of microbial responses in food. Including metabolic network information in mathematical models leads to an improved mechanistic insight in microbial processes. The main difficulty in including such information is the high number of fluxes and metabolites and the number of ordinary differential equations that has to be added to the model equations. To reduce the number of mass balance differential equations, pseudo steady state is assumed and the intracellular mass balances are replaced by an underdetermined system of algebraic equations. Dynamic metabolic flux analysis estimates intracellular time-dependent flux distributions from available measurements, by parameterizing the fluxes as a function of time. In this article, a novel DMFA technique based on a non-uniform rational B-splines (NURBS) parameterization of the free fluxes (NDMFA) is presented. This NDMFA technique can be seen as a generalization of previously introduced state of the art DMFA techniques.

INTRODUCTION

A metabolic network is an elegant representation of the interactions occurring between the different components within a cell. Such a network consists of m nodes, corresponding with the m intra- and extracellular metabolites (i.e., the chemical compounds consumed/produced by a cell) and n edges denoting the n fluxes, which can be biochemical reactions between the metabolites, exchange fluxes or reactions between cell and environment or transport throughout the cell. The stoichiometric matrix $\mathbf{S} \in \mathbb{R}^{(m+1) \times n}$ comprises the information of these interactions by stacking the stoichiometric coefficient of a metabolite i in reaction j in the element S_{ij} (i.e., on the i -th row and j -th column of the stoichiometric matrix). In Figure 1 a toy example is presented to show

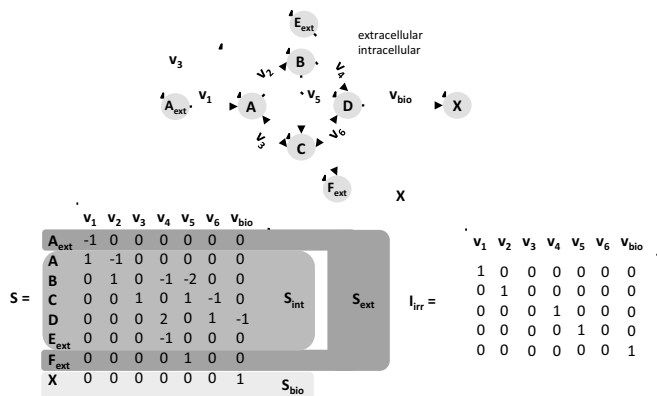


Figure 1: Example of a metabolic network and matrices characterizing such a network.

the different components of a metabolic network and matrices used to describe such networks.

Dynamic metabolic flux analysis (DMFA) can be seen as an example of a multi-scale model structure exploiting information at the macroscopic (extracellular) level and microscopic (intracellular) level by means of metabolic networks. This model structure allows (under certain assumptions) to estimate time-dependent fluxes in metabolic networks, based on available measurements (e.g., exchange fluxes between cells and their environment, metabolite concentrations, etc.). Different techniques for dynamic metabolic flux analysis have been developed throughout the last decades and a thorough review on metabolic flux analysis techniques has been presented by Antoniewicz (2015). Dai and Locasale (2016), presented an overview of the different software tools that exist for metabolic flux analysis, together with a methodology to resolve metabolic fluxes from stable isotope labeling.

The current state of the art in dynamic metabolic flux analysis is to parameterize the dynamic fluxes mathematically as a function of time. The first *generic* dynamic metabolic flux analysis methodology has been proposed by Leighty and Antoniewicz (2011), describing the dynamic fluxes are described by a piecewise linear parameterization. A fully nonlinear dynamic parameter

estimation approach has been presented by Vercammen et al. (2014), in which the dynamic fluxes are parameterized by B-splines and a direct simultaneous discretization approach based on orthogonal collocation has been followed to construct a NLP. This algorithm has also been applied to a temperature induced lag phase of an *E. coli* strain Vercammen et al. (2017). A generalization of the DMFA technique of Leighty and Antoniewicz (2011) to B-splines, together with a new heuristic algorithm for knot insertion has been presented by Martínez et al. (2015). Fernandes de Sousa et al. (2016) applied convex analysis (positive algebra) together with cubic flux smoothing to determine bounded intervals for each dynamic intracellular flux (without introducing additional constraints or objective function). The remainder of this work is structured as follows. The next section covers the formulation of DMFA as an optimization problem. Subsequently, the generalized NURBS based DMFA framework is introduced, clearly indicating that current state of the art parameterizations are a subset of this framework. In the *Results and discussion* section the NURBS based DMFA framework is implemented for a benchmark DMFA case study from Vercammen et al. (2014). Finally, the *Conclusions* section summarizes the main contributions and results of this work, together with perspectives for future research.

DMFA PROBLEM FORMULATION

Before introducing the DMFA optimization problem, the following two assumptions need to be made. Firstly, all cells are considered to be equal to one average cell. This implies that all cells express the same flux pattern $\mathbf{v}(t)$. Secondly, the medium is considered to be liquid and perfectly mixed. This assumption results in equal biomass and extracellular metabolite concentrations for each cell.

The following model structure comprises the macroscopic extracellular, biomass and microscopic intracellular mass balances while assuming batch conditions (i.e., no liquid inflow or outflow). Note that these balances are coupled via the flux vector \mathbf{v} :

$$\frac{d\mathbf{c}_{\text{ext}}}{dt} = \mathbf{S}_{\text{ext}}\mathbf{v}c_{\text{bio}} \quad (1)$$

$$\frac{dc_{\text{bio}}}{dt} = \mathbf{S}_{\text{bio}}\mathbf{v}c_{\text{bio}} \quad (2)$$

$$\frac{d\mathbf{c}_{\text{int}}}{dt} = \mathbf{S}_{\text{int}}\mathbf{v} - \mu\mathbf{c}_{\text{int}} \quad (3)$$

with $\mathbf{c}_{\text{ext}} \in \mathbb{R}^{m_{\text{ext}}}$ (expressed in [mmol/L]) and $\mathbf{c}_{\text{int}} \in \mathbb{R}^{m_{\text{int}}}$ (expressed in [mmol/gDW]) the extracellular and intracellular metabolite concentration vector, c_{bio} (in [gDW/L]) the biomass concentration, $\mathbf{S}_{\text{ext}} \in \mathbb{R}^{m_{\text{ext}} \times n}$, $\mathbf{S}_{\text{bio}} \in \mathbb{R}^{1 \times n}$ and $\mathbf{S}_{\text{int}} \in \mathbb{R}^{m_{\text{int}} \times n}$ the extracellular, biomass and intracellular partitions of the stoichiometric matrix $\mathbf{S} \in \mathbb{R}^{m \times n}$, $\mathbf{v} \in \mathbb{R}^n$ the flux vector (expressed as specific fluxes in [mmol/gDW/h]) and μ ([1/h]) the

scalar specific growth rate of the microorganism or also called the *pseudo-reaction rate to biomass*.

In DMFA, dynamic (i.e., time dependent) flux profiles are estimated without the need for kinetic functions. Two simplifications are made regarding the mass balance in Equation (3): (i) the second term in Equation 3, a dilution term caused by cell growth, is discarded as it is typically smaller than the reaction term and (ii) intracellular pseudo-steady state is assumed as it has been empirically motivated in Stephanopoulos et al. (1998) that intracellular dynamics are much faster than extracellular dynamics. These two assumptions simplify the intracellular mass balance to the following linear system in the fluxes:

$$\mathbf{S}_{\text{int}}\mathbf{v} = \mathbf{0} \quad (4)$$

with the null vector $\mathbf{0} \in \mathbb{R}^{m_{\text{int}}}$. The system in Equation (4) is underdetermined, such that the rank (\mathbf{S}_{int}) is not full, since the number of intracellular metabolites is for the majority of metabolic networks smaller than the number of fluxes (i.e., $m_{\text{int}} < n$). From basic linear algebra, the fluxes in the flux vector \mathbf{v} can be written as a linear combination of $d = n - \text{rank}(\mathbf{S}_{\text{int}})$ linearly independent degrees of freedom, called *free fluxes* and comprised in the *free flux vector* $\mathbf{u} \in \mathbb{R}^d$. By neglecting the dilution term related to cellular growth and following the *pseudo steady state assumption*, the following generic model structure is derived:

$$\frac{d\mathbf{c}_{\text{ext}}}{dt} = \mathbf{S}_{\text{ext}}\mathbf{v}c_{\text{bio}} \quad (5)$$

$$\frac{dc_{\text{bio}}}{dt} = \mathbf{S}_{\text{bio}}\mathbf{v}c_{\text{bio}} \quad (6)$$

$$\mathbf{S}_{\text{int}}\mathbf{v} = \mathbf{0} \quad (7)$$

Consider $\mathbf{K} \in \mathbb{R}^{n \times d}$ a basis for the null space of the intracellular stoichiometric matrix \mathbf{S}_{int} (i.e., $\mathbf{K} = \text{null}(\mathbf{S}_{\text{int}})$), then the fluxes \mathbf{v} can be formulated as a function of the free fluxes \mathbf{u} :

$$\mathbf{v} = \mathbf{K}\mathbf{u} \quad (8)$$

In case that the network can be made fully determined by available measurements, the system can be simulated by dynamic metabolic flux analysis, i.e., estimating the free flux parameters and initial extracellular concentrations from these measurement data \mathbf{y}_m .

Consider the state vector $\mathbf{x} = [\mathbf{c}_{\text{ext}} \quad c_{\text{bio}}]^\top$, the augmented extracellular stoichiometric matrix $\mathbf{S}_{\text{aug,ext}} = [\mathbf{S}_{\text{ext}} \quad \mathbf{S}_{\text{bio}}]^\top$ and the measurable output $\mathbf{y} \in \mathbb{R}^{n_y}$ which is described as a function of the states, free fluxes, optimization parameters and time by $\mathbf{h}(\mathbf{x}, \mathbf{u}, \mathbf{p}, t)$, then the DMFA optimization problem is formulated over the time interval $t \in [0, t_f]$ as follows:

$$\min_{\mathbf{P}, \mathbf{c}_0} \sum_{j=1}^{n_{tm}} \left(\sum_{i=1}^{n_{m,c}} \left(\frac{c_{i,j} - c_{i,j,m}}{\sigma_{i,j,m}} \right)^2 + \sum_{i=1}^{n_{m,r}} \left(\frac{r_{i,j} - r_{i,j,m}}{\sigma_{i,j,m}} \right)^2 \right)$$

$$\text{s.t.} \begin{cases} \frac{dx}{dt} = \mathbf{S}_{\text{aug,ext}} \mathbf{K} \mathbf{u}(\mathbf{p}) c_{\text{bio}} \\ x_i(0) = x_{i,0} \\ \mathbf{I}_{\text{irr}} \mathbf{v} \geq \mathbf{0} \quad \text{with } \mathbf{I}_{\text{irr}} \in \mathbb{R}^{n_{\text{irr}} \times n_v} \\ \mathbf{v} = \mathbf{K} \mathbf{u}(\mathbf{p}) \\ c_i = c_{0,i} + \mathbf{S}_{\text{ext},i} \cdot \mathbf{K} \cdot \mathbf{u}(t, \mathbf{p}) \\ r_i = \mathbf{S}_{\text{aug,ext},i} \cdot \mathbf{K} \cdot \mathbf{u}(t, \mathbf{p}) \end{cases} \quad (9)$$

with the DMFA objective function being a weighted sum of squared errors (with the inverse of the measurement variances as weights), $t_{m,i}$ the i -th measurement time point, n_{tm} the number of measurement time points and n_{irr} the number of irreversible fluxes and $\mathbf{I}_{\text{irr}} \in \mathbb{R}^{n_{\text{irr}} \times d}$ the irreversibility matrix which selects the irreversible fluxes from the flux vector \mathbf{v} . Note that other constraints can be added on the fluxes and concentrations as stated in e.g., Llaneras and Picó (2008).

A NURBS BASED DMFA FRAMEWORK

Non-uniform rational B-splines (NURBS)

Splines are smooth, piecewise polynomial functions of the following form:

$$\Gamma(t) = \sum_{i=0}^{n_{\Gamma}} \phi_i(t) \mathbf{P}_i \quad (10)$$

with n_{Γ} the number of basis functions, $\phi_i(t)$ the basis functions and \mathbf{P}_i the control points.

B-splines are smooth, piecewise polynomial functions which are constructed using the B-splines basis functions, $N_{i,q}(t)$. The B-spline basis functions of q -th degree, i.e., $(q+1)$ -th order, are defined by the Cox-de Boor recursive relation given in Equations (11) and (12) (de Boor (2001)).

$$N_{i,0}(t) = \begin{cases} 1 & \text{if } t_{k,i+1} \leq t \leq t_{k,i} \\ 0 & \text{otherwise} \end{cases} \quad (11)$$

$$N_{i,q}(t) = \frac{t - t_{k,i}}{t_{k,i+q} - t_{k,i}} N_{i,q-1}(t) + \frac{t_{k,i+q+1} - t}{t_{k,i+q+1} - t_{k,i+1}} N_{i+1,q-1}(t) \quad (12)$$

with $t_{k,i}$ the knot locations. Non-uniform rational B-splines (NURBS) are a generalization of B-splines and are very popular in computer aided design and manufacturing applications (CAD/CAM). NURBS are constructed by using rational basis functions, $R_{i,q}$. These rational basis functions are formulated using the B-spline basis functions and a weight vector (Equation (13)).

$$R_{i,q}(t) = \frac{N_{i,q}(t) \cdot w_i}{\sum_{j=0}^{n_{\Gamma}} N_{j,q}(t) \cdot w_j} \quad (13)$$

The NURBS curve is constructed as a sum of these different rational basis functions. The NURBS curves are thus defined by \mathbf{P}_i , $t_{k,i}$ and the additional w_i .

NURBS based DMFA problem formulation

Currently, two state-of-the-art parameterization techniques exist for dynamic metabolic flux analysis: linear dynamic metabolic flux analysis (Leighty and Antoniewicz (2011)) and B-spline dynamic metabolic flux analysis (Martínez et al. (2015)). A more general parameterization would be with NURBS as these are mathematically more complex than B-splines and enable even more complex shapes. As B-splines are a special case of NURBS and piecewise linear functions (as used in linear dynamic metabolic flux analysis) are a special case of B-splines, it is clear that a NURBS based dynamic metabolic flux analysis framework generalizes these two methods. More specifically, NURBS are reduced to B-splines if the weight vector is completely equal to 1 (BDMFA). If the order q is set to 1, then the method reduces further to LDMFA. .

In the NURBS based DMFA framework (NDMFA), the free fluxes $u_i(t)$ are described as:

$$u_i(t) = \sum_{i=0}^{n_{\Gamma}} \mathbf{P}_i \cdot R_{i,q}(t) \quad (14)$$

Using the new definition for the free fluxes, the concentrations can be expressed explicitly as follows:

$$c_i = c_{i,0} + \mathbf{S}_{\text{ext},i} \cdot \mathbf{K} \cdot \mathbf{P} \cdot \mathbf{IR}(t_{\mathbf{k}}, t) \quad (15)$$

with $t_{\mathbf{k}}$ the knot vector and

$$\mathbf{P} = [\mathbf{P}_0 \quad \cdots \quad \mathbf{P}_{n_{\text{tk}}-q-2}] \quad (16)$$

$$\mathbf{R}(t) = \begin{bmatrix} R_{0,q+1}(t) \\ \cdots \\ R_{n_{\text{tk}}-q-2,q+1}(t) \end{bmatrix} \quad (17)$$

$$\int \mathbf{R}(t) dt = \mathbf{IR}(t) \quad (18)$$

Unlike in BDMFA it is not possible to obtain an analytical expression for the time integral for $\mathbf{R}(t)$, therefore the integral is called \mathbf{IR} and calculated numerically. \mathbf{S} and \mathbf{K} are the same as for BDMFA. The optimization parameters of this problem are the initial concentrations, \mathbf{c}_0 ; the control points of each metabolite for each basis function; \mathbf{P} , the knot locations, $t_{\mathbf{k}}$; and the weight vector, \mathbf{w} . Therefore the optimization problem is non-linear with respect to the optimization parameters. If the knots and the weights are fixed and known the problem is linear with respect to the optimization parameters and the problem can be solved analytically in one step.

Algorithm for solving the NDMFA problem

A way to solve this optimization problem is to use a method where the Matlab function $Fmincon$ is used to solve the non-linear problem for each number of knots. To reduce the calculation time of $Fmincon$, gradients of the constraints and the objective function need to be added. The gradients of $\mathbf{R}(t)$ can be found analytically but the gradients of $\mathbf{IR}(t)$ have to be calculated numerically. Combined with the large number of parameters, this means that the calculation time is very large.

Another way to solve this optimization problem is to use the same heuristic approach as in BDMFA (Martínez et al. (2015)). An additional heuristic aspect has to be treated as there is also a trial-and-error search for the weights. The algorithm is then completely the same as for BDMFA except that for a fixed set of knots the optimal solution is found via a heuristic algorithm that finds the optimal weight set. For a fixed knot set and a fixed weight set the Matlab function $Lsqlin$ is used to find the optimal solution. The effect of the weights is the highest around 1. There is less distinction between the NURBS-curves if the weights become very small or very large. Therefore a relative search based on the weight values is proposed, i.e. the weights are varied with a fraction a , around the current weight value. In this article the a -value is set to 10%.

Algorithm 1 Heuristic algorithm for NURBS weight allocation

Input: Specify a .

Output: Optimal weight vector w_i^* .

Step 1: Set all weights equal to 1: $w_i = 1, \forall i$.

Step 2: Solve the NDMFA problem with this weight set, resulting in x^* and SSE^* , set $i = 1$.

Step 3: while $i < n_w$ (with n_w the number of weights) do:

$$w_{Li} = (1 - a)w_i \rightarrow x_L, SSE_L$$

$$w_{Ui} = (1 + a)w_i \rightarrow x_U, SSE_U$$

if $\min(SSE_L, SSE^*, SSE_U) == SSE_L$ do:

$$SSE^* = SSE_L, w_i^* = w_{Li}$$

else if $\min(SSE_L, SSE^*, SSE_U) == SSE_U$ do:

$$SSE^* = SSE_U, w_i^* = w_{Ui}$$

while $w_i^* == w_{Li}$ or $w_i^* == w_{Ui}$

and $tol_l \leq w_i^* \leq tol_u$ do:

if w_i^* has been updated do:

recalculate weights of k control points back:

$$i = \max(1, i - k),$$

if $i == 1$, do:

$$i = i + 1 \text{ and go to Step 3 for } w_i.$$

else:

$$i = i + 1$$

RESULTS AND DISCUSSION

The NURBS based DMFA framework is applied to the benchmark small scale DMFA problem from Vercammen et al. (2014). The biological network consists of three extracellular metabolites, A_{ext} , E_{ext} and F_{ext} , the biomass, X , and four intracellular metabolites, A , B , C and D . These metabolites are linked by seven fluxes. The seven fluxes described in this problem are specific to the amount of biomass. This network is the same as depicted in Figure 1.

The concentration measurements for the extracellular metabolites and the biomass are simulated per time steps of 1 hour during a period of 20 hours by solving the mass balance differential equations. The reference fluxes used in this simulation are v_1 , v_4 and v_5 and are formulated as in Equations (19), (20) and (21). Noise is added to these concentrations at each time point to obtain a realistic setting.

$$v_{1,\text{ref}} = \frac{c_{A_{\text{ext}}}}{1.5 + c_{A_{\text{ext}}}} \quad (19)$$

$$v_{4,\text{ref}} = 0.2 \cdot \frac{c_{E_{\text{ext}}}}{3 + c_{E_{\text{ext}}}} \quad (20)$$

$$v_{5,\text{ref}} = \frac{1}{1 + c_{F_{\text{ext}}}} \quad (21)$$

NDMFA is applied to the benchmark DMFA case study and simulated data sets have been used to which noise has been added as described in Vercammen et al. (2014). The 95% confidence intervals for the concentration profiles and the flux profiles are depicted in Figure 2 and 3 respectively.

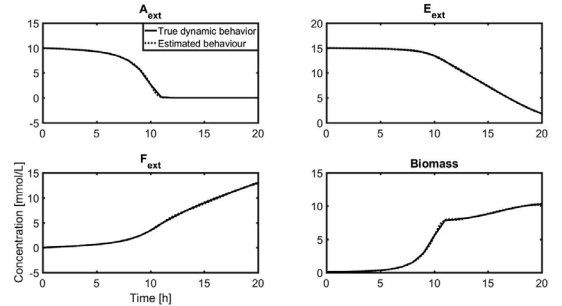


Figure 2: 95% confidence intervals of the fitted concentration profiles using NDMFA on the medium-scale case study.

These Figures indicate that the concentration measurements are accurately and precisely fitted. The constraints on the concentrations and the irreversible fluxes are also satisfied. Due to the high number of degrees of freedom NURBS have, smooth flux profiles can be reconstructed. However, the cost for such flux estimates is very high. A comparison has been made with a linear and B-spline free flux parameterization, using the

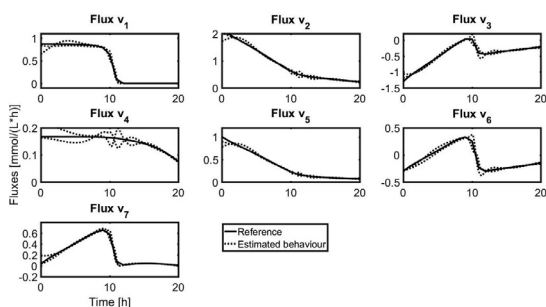


Figure 3: 95% confidence intervals of the fitted flux profiles using NDMFA on the medium-scale case study.

same framework in which constraints are imposed on the concentrations and fluxes. The mean value and the standard deviation for the SSE, calculation time and the number of parameters (n_p) for the solutions for the simulated data sets are shown in Table 1. From Table 1, it is clear that for this case study a linear or B-spline flux parameterization are sufficient and requires less computation time. Note that a lower number of optimization variables is needed in the NURBS based algorithm but that the heuristic weight determination algorithm significantly increases the computation time.

Table 1: SSE, number of optimization variables and CPU time for different flux parameterizations.

	Linear	B-spline	NURBS
SSE	24.65	56.08	70.52
n_p	69	37	34
CPU time (s)	31.66	25.03	75682

CONCLUSIONS AND FUTURE WORK

Estimating dynamic fluxes in metabolic networks is useful for obtaining a better process understanding and enables an improved process control. The goal of this article was to introduce a generalized NURBS based framework in which the current state-of-the-art methods can be formulated and extended with improvements regarding the implementation of constraints on fluxes and concentrations. The presented NURBS based DMFA framework enables the estimation of physically possible time dependent metabolic fluxes by imposing constraints, which the current state of the art techniques do not guarantee.

Currently, a user-friendly tool for dynamic flux estimations in metabolic networks is not available. NDMFA can serve as a generalized framework for DMFA, with high flexibility regarding the shape of dynamic flux profiles. In addition, an algorithm that recognizes the required complexity for describing a studied system would be a useful feature. Such algorithm could be used to

make the heuristic weight determination algorithm obsolete or to automatically choose the required spline order.

ACKNOWLEDGEMENTS

This work was supported by KU Leuven [PFV/10/002] Center-of-Excellence Optimization in Engineering (OPTEC) and the Belgian Science Policy Office (DYSCO) [IAP VII/19].

REFERENCES

- Antoniewicz M.R., 2015. *Methods and advances in metabolic flux analysis: A mini-review*. *J Ind Microbiol Biotechnol*, 42, 317–325.
- Dai Z. and Locasale J.W., 2016. *Understanding metabolism with flux analysis: From theory to application*. *Metabolic Engineering*.
- de Boor C., 2001. *A Practical Guide to Splines*. Springer-Verlag, New York, USA.
- Fernandes de Sousa S.; Bastin G.; Jolicoeur M.; and Vande Wouwer A., 2016. *Dynamic metabolic flux analysis using a convex analysis approach: Application to hybridoma cell cultures in perfusion*. *Biotechnology and Bioengineering*, 113, 1102–1112.
- Leighty R.W. and Antoniewicz M.R., 2011. *Dynamic metabolic flux analysis (DMFA): A framework for determining fluxes at metabolic non-steady state*. *Metabolic Engineering*, 13, no. 6.
- Llaneras F. and Picó J., 2008. *Stoichiometric modelling of cell metabolism*. *Journal of Bioscience and Bioengineering*, 105, no. 1.
- Martínez V.S.; M B.; Gray P.; Nielsen L.K.; and Quek L.E., 2015. *Dynamic metabolic flux analysis using B-splines to study the effects of temperature shift on CHO cell metabolism*. *Metabolic Engineering Communications*, 2, 46–57.
- Piegl L. and Tiller W., 1996. *The NURBS Book*. Monographs in Visual Communication. Springer Berlin Heidelberg.
- Vercammen D.; Logist F.; and Van Impe J., 2014. *Dynamic estimation of specific fluxes in metabolic networks using non-linear dynamic optimization*. *BMC Systems Biology*, 8, no. 132.
- Vercammen D.; Telen D.; Nimmegeers P.; Janssens A.; Akkermans S.; Noriega Fernandez E.; Logist F.; and Van Impe J., 2017. *Application of a dynamic metabolic flux algorithm during a temperature-induced lag phase*. *Food and Bioprocess Processing*, 102, no. 1-19.

Ghost Competition: On the Reliability of Quorum Sensing as an Information Source for Bacterial Species

Ihab Hashem, Philippe Nimmegeers, Satyajeeet Bhonsale, Carlos André Muñoz López, Jan Van Impe
BioTeC+ & OPTEC, Department of Chemical Engineering, KU Leuven
CPMF2, Flemish Cluster Predictive Microbiology in Foods
Gebroeders de Smetstraat 1, B-9000 Gent, Belgium
*E-mail address: Jan.VanImpe@kuleuven.be

KEYWORDS

Quorum sensing, Game theory, Signaling theory, Gene regulation

ABSTRACT

Given the immense evolutionary pressure in bacterial communities, microbial species have developed simple, yet efficient, information gathering systems to coordinate the regulation of their genes. By producing small diffusible chemical molecules, known as quorum signals, a microbial species could assess the density of its population in order to timely express its costly traits. However, this poses the question of whether such information processing systems could be vulnerable to manipulation by competing strains such that the quorum-regulated species can not infer the true state of their environment. This "ghost competition" could eventually lead to wasteful production of costly compounds as targeted bacteria can no longer tune their gene regulation to best suit their own interests. Using an ecological competition model between a toxin producer and toxin sensitive strain, we find that bacteria could indeed gain from producing quorum signals to disrupt the gene regulation systems of their ecological competitors. It has been also found that there will be an optimal cost for signal production that offers a balance between a minimal impact on growth and maximal protection against false signaling.

INTRODUCTION

Quorum sensing is the simplest biological communication system on earth, yet it gives rise to probably some of its most complex phenomena. To assess their population density, bacteria produce chemical compounds to accumulate in their environment. Eventually, when the signals' concentration reaches a certain threshold, *quorum*, bacterial cells respond by altering the regulation of their genes, usually to express a costly trait which is only beneficial at high densities. Quorum sensing has been found to increase the evolutionary stability of cooperative microbial phenotypes by controlling the production of extracellular enzymes (Schluter et al. (2016)). It is

also instrumental for pathogenic bacteria as they need to coordinate the expression of virulence factors to inflict maximum damage on other cells or their host (Bucci et al. (2011)). Given such importance, a considerable attention has been given to investigate the properties of quorum sensing systems, including the metabolic cost of the molecules and the influence of targeting those systems on the biomass growth (Diggle et al. (2007), Janssens et al. (2007)). Signaling molecules are known to be metabolically cheap molecules compared to other toxins and enzymes (Harrington and Sanchez (2014)). However, some recent experimental evidence indicates that a significant metabolic cost could be involved in synthesizing such molecules (Ruparell et al. (2016)).

The decisive role played by quorum sensing in the competition between microbes poses a natural question: could this information source be manipulated to reduce the fitness of quorum-regulated species? This could happen via a competing strain which produces the same type of signals as the quorum regulated one, in order to deteriorate the reliability of their major information gathering mechanism, as in Figure 1. We define such situations in which a focal species can not reliably infer the state of its environment due to interference from a competing species as *ghost competition*.

In this paper, we aim to explore using a simple population model the potential and the extent of occurrence of such tactics in the microbial world.

MODEL

We extend the model from Bucci et al. (2011) in which a toxin producing strain is competing with a sensitive, non-producer, strain in a simple batch culture. Here, the producer strain also uses quorum signaling to regulate the bacteriocin production. Delaying their attack could give the producer cells a competitive edge over their rivals as the toxin becomes most effective at high cell densities. However, this communication mechanism could be prone to exploitation from the sensitive strain if it produces the same type of quorum signals. The model dynamics can be described by the following set of equations (Bucci et al. (2011), Cornforth and Foster (2013)):

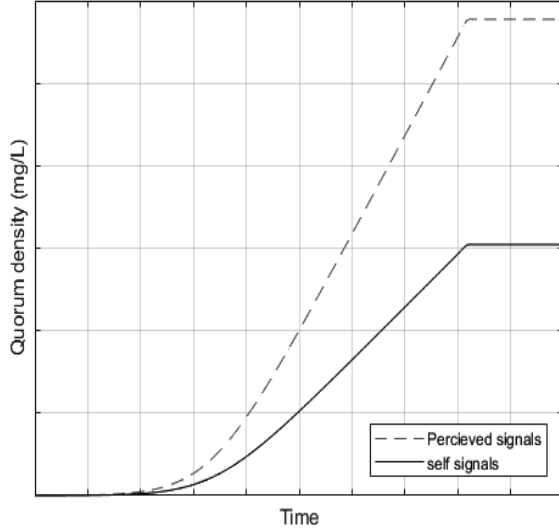


Figure 1: Radio jamming in bacteria: the self-density perceived by a quorum-regulated species could be higher than reality due to dishonest signals by competing species

$$\frac{dP}{dt} = (1 - fH(Q - Q_{th}))(\mu - q_p C)H(\mu - q_p C)P \quad (1)$$

$$\frac{dS}{dt} = ((\mu - q_s C)H(\mu - q_s C) - K_T T)S \quad (2)$$

$$\frac{dT}{dt} = H(Q - Q_{th})\alpha f(\mu - q_p C)H(\mu - q_p C)P - \beta_T T \quad (3)$$

$$\frac{dN}{dt} = \frac{-1}{Y}\mu(P + S) \quad (4)$$

$$\frac{dQ}{dt} = q_p P H(\mu - q_p C) + q_s S H(\mu - q_s C) \quad (5)$$

$$\mu = \mu_{max} \frac{N}{N + K_N} \quad (6)$$

With P the concentration of the toxin producer strain, S the concentration of the sensitive strain, T , N and Q are the concentrations of the toxin, nutrient and quorum signals respectively. μ is the growth rate of bacteria in absence of toxin or quorum production, with μ_{max} as the maximum specific growth rate and K_N the half saturation constant. f is the relative metabolic investment in toxin production by the producer strain, Q_{th} is the quorum threshold concentration, above which toxin production is activated. C is the cost of production of quorum signals. q_p and q_s are the stoichiometric coefficients of the production of quorum molecules for the producer and sensitive strains respectively. K_T is the killing rate of the toxin, while β_T is the rate of toxin decay in the environment. α is the stoichiometric coefficient for the toxin production and Y is the biomass yield.

In this model, the toxin production is regulated using a heaviside step function H , equal to 1 when its argument is positive and zero otherwise, such that the release of bacteriocin starts only after the concentration of quorum signals in the system reaches a certain threshold. Both the producer and the sensitive strain have the potential to produce quorum signals. However, while the producer strain actually uses the quorum mechanism to regulate its gene expression, the sensitive strain produces quorum signals only to disrupt the decision making machinery of its counterpart. Production of quorum signals inflicts a fixed cost on the growth of the bacterial species and it stops when the growth rate is very low. In all simulations, the batch culture is inoculated by 1 mg/l of each strain. The initial nutrient concentration is 2000 mg/l and the model is run for 500 hours. The values of the rest of the parameters can be found in Table 1 (Bucci et al. (2011), Cornforth and Foster (2013)).

Table 1: Parameters used

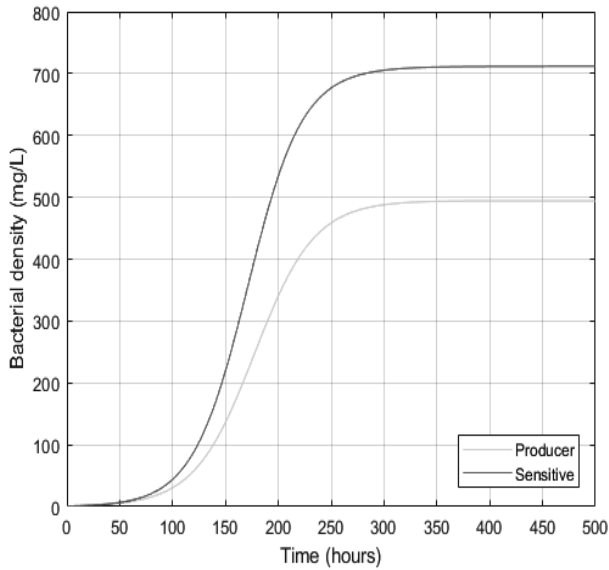
Parameter	Value
f	0.1
K_N	$5 * 10^{-4}$ (mg/l)
K_T	$1.5 * 10^{-4}$ (1/mg toxin/hr)
β_T	10^{-1} (/hr)
μ_{max}	1 (/hr)
Y	0.7 (mg bacteria/ mg nutrients)
α	4 (mg bacteria/ mg nutrients)

RESULTS AND DISCUSSION

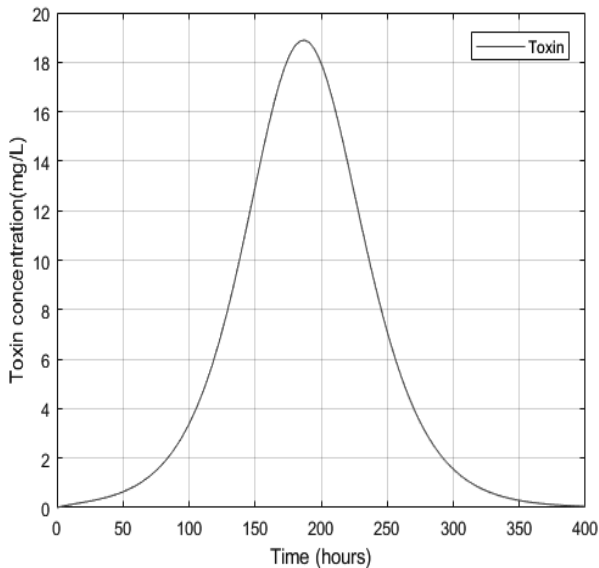
To illustrate why bacteria have evolved quorum sensing as a means to regulate their behavior, we first show the case when a constitutive toxin producer grows against a sensitive strain, thus, no quorum production takes place and both q_s and q_p are equal to zero. Figure 2 shows how the sensitive strain outgrows its competitor in this case as the producer strain invests its resources in toxin production too early, while the concentration of bacteria is too low. In a sparse system, the toxin can not be effective. Hence, the strain that does not produce toxin has the chance to increase its biomass, consume more nutrients and dominate the batch culture by the end.

The dynamics of the system change drastically when the toxin producer uses quorum sensing to regulate its activity as in Figure 3. Here, the stoichiometric coefficient for quorum signals released by the toxin producer $q_p = 1 * 10^{-3}$ mg quorum/mg bacteria/hr, with cost $C = 0.01$ mg growth/mg quorum. The quorum threshold Q_{th} is set to 5 mg quorum/l and no interference from the sensitive strain is involved. Toxin production hereby starts as a sharp signal once the quorum threshold is reached in the system. This assures high toxin lethality and the producer strain gains advantage from investing in toxin production, outgrowing its rival.

We highlight how the tuning of the quorum system affects the fitness of the toxin producer strain in Figure



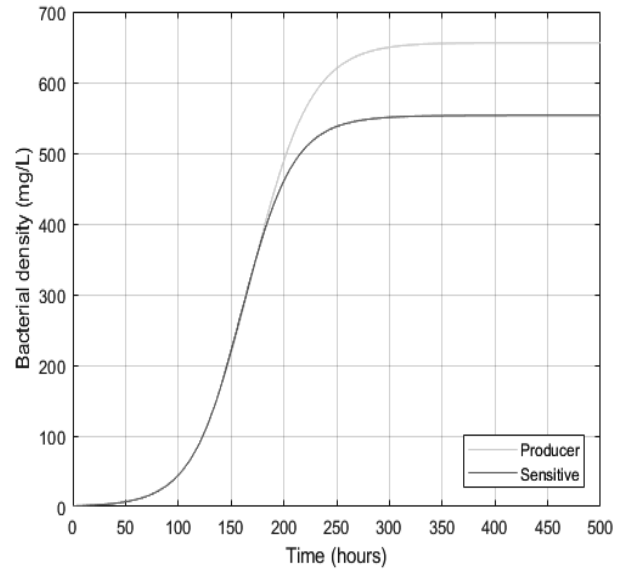
(a) Bacterial concentrations



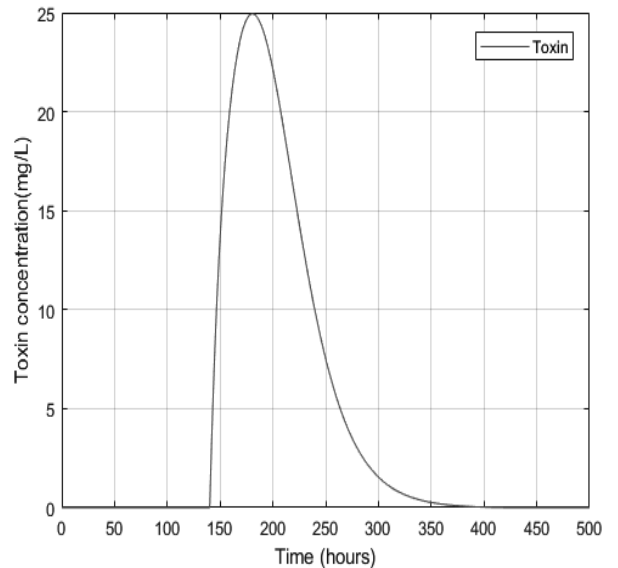
(b) Toxin concentration

Figure 2: Competition between constitutive toxin producer and a sensitive strain

4. A very low rate of production of quorum signals could render toxin obsolete as its activation would happen at very low growth rates, as nutrients become scarce, rendering insignificant amounts of toxin to be produced. On the other hand, reaching the quorum threshold too early would result in investing in toxin while bacterial densities are too low in the system. The toxin decays and the competition balance is tipped in favor of non producers. Therefore, for a quorum-regulated bacteria to be successful, it has to produce quorum signals in a close to optimal rate to maximize



(a) Bacterial concentrations



(b) Toxin concentration

Figure 3: Competition between quorum-regulated toxin producer and a sensitive strain

the gain from investing in costly traits. This kind of dynamics, along with the crucial benefits of quorum regulation, suggests that a cunning tactic that could be used in the "microbe-kill-microbe" world is clouding the information received by the quorum-regulated species through the production of false signals, which only aim to hasten the activation of costly traits, rendering the quorum sensing concept useless. In the next simulation, we investigate an example of ghost competition.

In Figure 5, the sensitive strain is as well producing

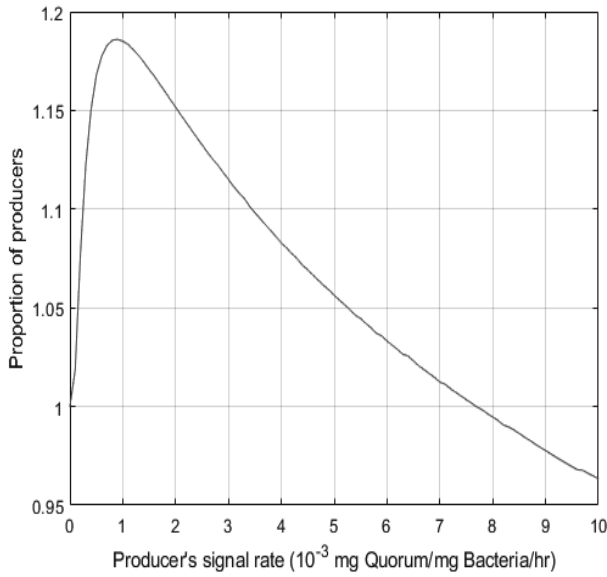
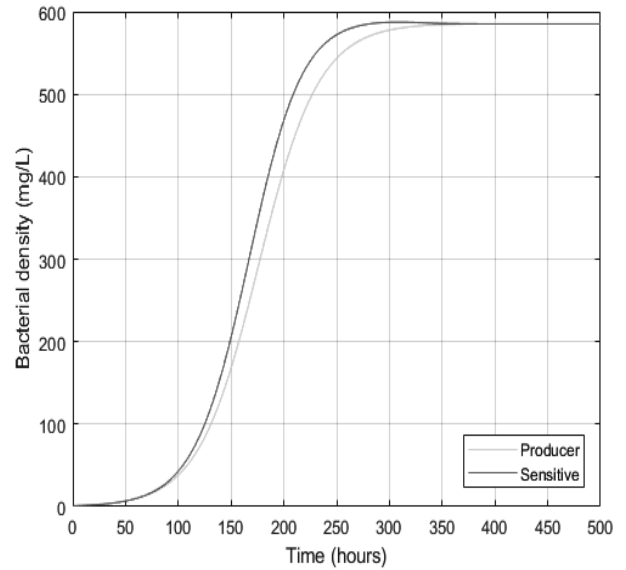


Figure 4: Relationship between the signal rate of a quorum-regulated toxin producer and its success in competition with a sensitive strain

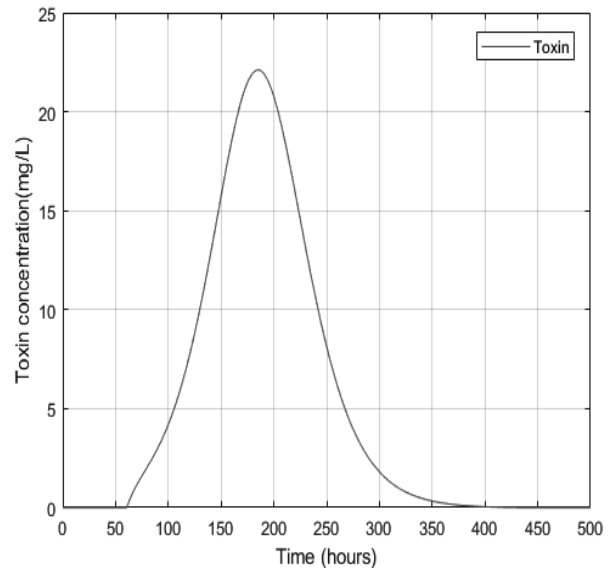
quorum signals, with $q_s = 20 * 10^{-3}$ mg quorum/mg bacteria/hr. The sole fitness advantage that it gains from such trait is to interfere with gene regulation of potential ecological competitors using the same signal. The result is an early expression of the bacteriocin release genes of the producer strain, and the strain that does not produce costly toxin and instead produces the relatively cheaper chemical signals can again achieve a fitness improvement in the system.

Next, we investigate the influence of varying the cost of the production of the quorum signals on the potential for production of false signals. Signaling theory predicts that the more costly the signal, the less it is vulnerable to exploitation. In Figure 6, it is found that indeed when increasing the quorum signals' cost, C , the ghosting gain, improvement in the final proportion of sensitive strain relative to the case with no false signals, decreases as false signals production increases. This means that the sensitive strain loses in fitness if it evolved/activated a quorum signal production system, as the cost of signals required to effectively toggle the gene regulation of the producer strain is too high that it outweighs the benefits of such strategy.

However, one must be careful before concluding that bacteria should evolve costly signals to ensure a reliable information gathering system. Metabolically expensive quorum signals would indeed protect the producer strain from exploitation, yet this will hamper its growth rate. Figure 7 shows that in case of costly signals, the producer strain loses in fitness compared to a sensitive strain in case of low false signals production rates by the sensitive, dishonest, strain. Therefore, sig-



(a) Bacterial concentrations



(b) Toxin concentration

Figure 5: Competition between quorum-regulated toxin producer and a sensitive strain that produces quorum signals only to "confuse" its competitors

nals that are most immune to ghost competition will make their producers lose the simple competition.

It is observed that an intermediate value of C would give the best balance between protection from false signals and competitive growth rate, occurs here at $C = 0.05$. In this value, false signaling could still exist as the sensitive strain gains from producing quorum signals in an average rate. However, the quorum regulation system becomes resilient against further exploitation. It is still to be investigated if this behavior would be maintained in different parametric regions.

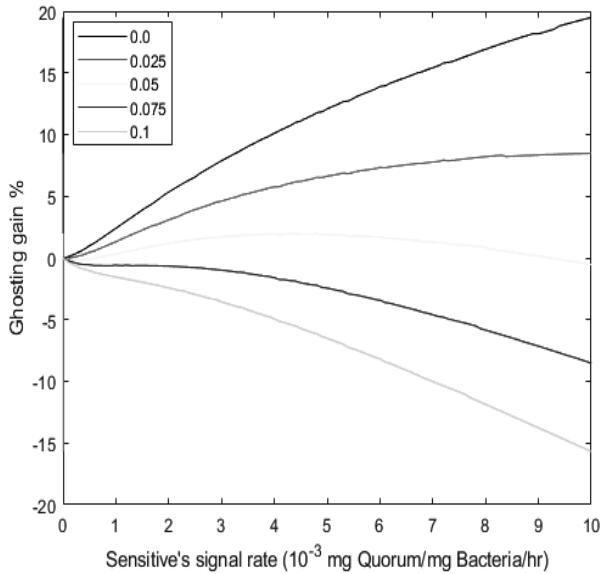


Figure 6: Relationship between the rate of dishonest signals produced by the sensitive strain and its gain in competition for different values of the signal's cost C

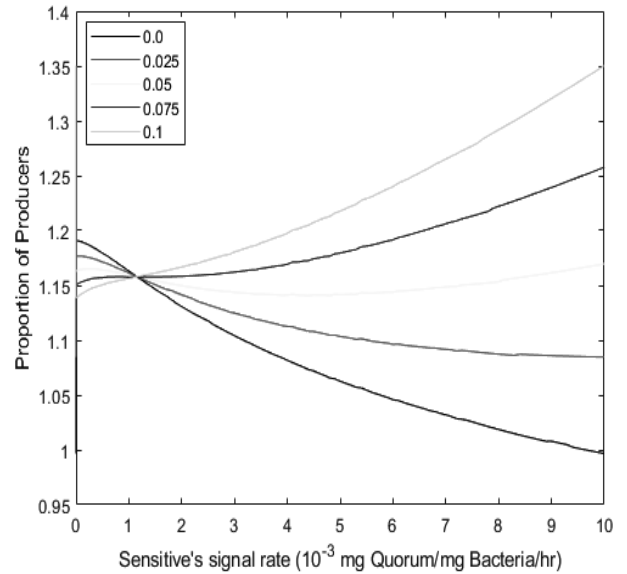


Figure 7: Relationship between the rate of dishonest signals produced by the sensitive strain and the final proportion of producers for different values of the signal's cost C

CONCLUSION

In this paper, we investigated the potential of deploying dishonest signaling in microbial communities. Bacteria use quorum signaling to regulate a wide range of activities which are vital to their survival, from sharing growth enzymes among population of the same genotype till the coordination of bacteriocin production against other species. This immense impact of such information gathering system on the growth dynamics in microbial communities suggests that there is a strong evolutionary interest for microbes to develop quorum production systems, not for their self-signaling, but to interfere with signaling systems for other species. Here, we opted to investigate possibly the simplest system under which ghost competition could occur: two strain system in a batch culture, with one strain using quorum signals to regulate its toxin production.

It has been found that producing false signals could indeed be beneficial for the sensitive strain by reducing the impact of toxin produced due to in-timely regulation. Switching to the production of more costly signals will protect the information system from exploitation, however, it reduces the fitness of the quorum producer. Many questions are still to be investigated in further research. It is expected that the cost of signals would probably correlate with the growth advantage given by the regulated behavior. More potent toxins or more beneficial growth enzymes should be regulated using more expensive, less potential to be exploited, signals.

The initial nutrient concentration as well as the quorum threshold are expected to influence the results. Moreover, the effects of the spatial distribution of species have the potential to drastically change the results. In future work, we aim to investigate ghost competition in the context of multi-species biofilm growth. Being one of the most diverse ecological system on earth, bacteria in biofilms are known to use quorum sensing to navigate their ultra-competitive environment. Clustering and diffusion constraints usually play a part in the evolution of cooperative and competitive strategies in biofilms. Due to the complexity of these biological systems, we will use an Individual based Modeling approach to investigate how the results from our simple model here could be altered in a spatially structured community.

We would expect that some of the key conclusions of this paper to be generalizable. Given the importance of quorum sensing, we predict that some strains will evolve the capacity to produce quorum signals, not to respond to them, but in an effort to reduce the efficiency of the regulation systems of their opponents. A significant metabolic cost should be invested in signals which regulate key population activities of a microbial strain. And finally, a quorum-regulated strain will always use the metabolically cheapest signals possible in order to remain competitive despite ghost competition, but not any cheaper.

ACKNOWLEDGEMENTS

IH is supported by FWO-SB grant 1S54217N. This work was supported by KU Leuven [PFV/10/002] Center-of-Excellence Optimization in Engineering (OPTEC) and the Belgian Science Policy Office (DYSCO) [IAP VII/19].

REFERENCES

- Bucci V.; Nadell C.D.; and Xavier J.B., 2011. *The evolution of bacteriocin production in bacterial biofilms. The American Naturalist*, 178, no. 6, E162–E173.
- Cornforth D.M. and Foster K.R., 2013. *Competition sensing: the social side of bacterial stress responses. Nature Reviews Microbiology*, 11, no. 4, 285.
- Diggle S.P.; Gardner A.; West S.A.; and Griffin A.S., 2007. *Evolutionary theory of bacterial quorum sensing: when is a signal not a signal? Philosophical Transactions of the Royal Society B: Biological Sciences*, 362, no. 1483, 1241–1249.
- Harrington K.I. and Sanchez A., 2014. *Eco-evolutionary dynamics of complex social strategies in microbial communities. Communicative & integrative biology*, 7, no. 1, e28230.
- Janssens J.; Steenackers H.; Metzger K.; Daniels R.; Ptacek D.; Verhoeven T.; Hermans K.; Vanderleyden J.; De Vos D.; and De Keersmaecker S., 2007. *Interference with the quorum sensing systems of Salmonella enterica serovar typhimurium: possibilities and implications. Communications in agricultural and applied biological sciences*, 72, no. 1, 35–39.
- Ruparell A.; Dubern J.F.; Ortori C.A.; Harrison F.; Halliday N.M.; Emtage A.; Ashawesh M.; Laughton C.A.; Diggle S.P.; Williams P.; et al., 2016. *The fitness burden imposed by synthesising quorum sensing signals. Scientific reports*, 6, 33101.
- Schluter J.; Schoech A.P.; Foster K.R.; and Mitri S., 2016. *The evolution of quorum sensing as a mechanism to infer kinship. PLoS computational biology*, 12, no. 4, e1004848.

Multi-scale Modeling to explain Wine Fermentation

D. Henriques^{1,†}, R. Minebois^{2,†}, R. Pérez-Torrado², E. Balsa-Canto^{1,*} and A. Querol^{2,*}

¹(Bio)process engineering group, IIM-CSIC, Vigo, Spain

²Grupo de Biología de Sistemas en Levaduras de Interés Biotecnológico, IATA-CSIC, Valencia, Spain

[†] Equal contributors

*email: ebalsa@iim.csic.es; aquerol@iata.csic.es

KEYWORDS

Wine fermentation, yeast, kinetic models, genome-scale models, flux-balance analysis

ABSTRACT

This work addresses the multi-scale modelling of wine fermentation driven by a particular wining yeast, *S. cerevisiae* T73. Basically, we define an extracellular kinetic model which describes the dynamics of relevant metabolites and use the model to constrain a genome-scale metabolic model. The model is solved using dynamic flux balance analysis approach. The flux distribution is computed at each instant by solving a linear programming problem which considers the extracellular model as constraints and biomass maximization as the cellular objective.

The model successfully explains growth and cell death measured in terms of OD600, biomass dry-weight and number of colony forming units as well as the relevant extracellular metabolites, measured by high-performance liquid chromatography. Also, the model provides the metabolic flux dynamics compatible with experimental data.

INTRODUCTION

The winemaking industry is facing various challenges due to new trends in consumer preferences, increased concerns on the effects of alcohol consumption on health and road safety and the impact of global climate change on grape ripening and wine composition.

Yeasts have an essential role in reducing wine alcohol levels and/or astringency and improving the aroma profile. In this context, the modern wine industry uses specific yeasts to inoculate grape must. This approach allows not only controlling the fermentation but reducing the risk of contamination and increasing the reproducibility of particular characteristics.

Typically, industrial fermentations are performed as batch or fed-batch processes. In such fermentations, a dynamic interaction occurs between yeasts metabolism and the environment. As the processes evolve com-

plex combinations of stresses affect the dynamics of the biomass itself as well as the yields of the different products (ethanol, glycerol, acetate, aromas, etc.).

The modeling of wine fermentation has received substantial attention. Cramer et al. (2002), Malherbe et al. (2004) or Coleman et al. (2007) adopted a macroscopic scale modeling approach to address the role of assimilable nitrogen in ethanol and CO₂ production. More recently Henriques et al. (2018) proposed an essentially macroscopic model to predict the performance of cold fermentations.

A multi-scale mathematical modeling of the process brings the possibility of understanding the evolution of yeast metabolism in a time-varying environment, comparing the fermentation performance of several species under different environmental conditions (must composition, temperature) and, eventually, designing optimal processes.

Sainz et al. (2003) proposed the idea of combining kinetic models with stoichiometric modeling to explain wine fermentation by *Saccharomyces cerevisiae* under nitrogen starvation. The model, which included around 40 reactions, was able to describe fermentation profiles qualitatively. To improve the quality of predictions, Vargas et al. (2011) expanded the metabolic model to genome-scale, in what the authors called the idFV715 model, which includes 1181 metabolic reactions comprising 590 components.

In this work, we propose using a similar approach to describe wine fermentation by a commercial yeast wine strain. We combine a kinetic model with a genome-scale metabolic model embedded into a dynamic flux balance analysis approach (Sánchez et al. 2014, Hjersted et al. 2007). In addition, since we have counts for colony forming units (CFUs) and biomass measurements we are able to distinguish between viable cells which can ferment and those which can reproduce and this distinction is explicitly incorporated in the model.

EXPERIMENTAL METHODS

Yeast and medium selection

We selected a commercial strain, T73 (Lalvin T73 from Lallemand Montreal, Canada), as our wine *S. cerevisiae* representative. All fermentations were performed in 3x replicates in 250 mL flasks that contained 200 mL of grape must.

High Performance Liquid Chromatography

Residual sugars (glucose and fructose) and relevant products were determined by HPLC (Thermo Fisher Scientific, Waltham, MA. USA) using a refraction index detector and a HyperREZTM XP Carbohydrate H+ 8 μ m column (Thermo Fisher Scientific) equipped with a HyperREZTM XP Carbohydrate Guard (Thermo Fisher Scientific). Samples were diluted to maintain our target compounds within the allowed range of detection, filtered through a 0.22 μ m nylon filter (Symta, Madrid, Spain) and injected in duplicate. The analysis conditions were: eluent, 1.5 μ M of H₂SO₄; 0.6 mL/min flux and a 50°C oven temperature.

Biomass measurements

A volume of sample in a pre-weighted 2 ml Eppendorf tube was centrifuged at maximum speed (13.200 rpm) in a MiniSpin centrifuge (Eppendorf, Spain) for 10 minutes. The supernatant was carefully removed, the pellet washed twice with Milli-Q water and centrifuged in the same conditions. After washing, the aqueous supernatant was removed carefully and the tube placed in a 65°C oven for 72h. Finally, the DW was obtained by measuring mass weight difference of tubes with a Sartorius BP121S analytical balance.

OD600 measurement at each sampling point was carried out using a diluted volume of sample and an Eppendorf Biophotometer spectrophotometer (Eppendorf, Germany).

200 μ L of a diluted volume of the samples were plated in triplicates in YPD solid medium (2% glucose, 2% Agar, 0.5% peptone, 0.5% yeast extract) and incubated two days at 25°C. After what, the resulting colonies were counted with a Comecta S.A Colony Counter. Only plates with CFUs between 30 and 300 were used to calculate the CFUs of the original sample.

THEORETICAL METHODS: THE MODELING PIPELINE

Dynamic flux balance analysis

Flux balance analysis (FBA) Varma and Palsson (1994), Orth et al. (2010) is a modelling framework based on knowledge of reaction stoichiometry and mass balances.

The framework is based on the so-called pseudo steady-state assumption, i.e. there is no metabolite accumulation. This is captured by the well known expression:

$$\mathbf{S} \cdot \mathbf{v} = \mathbf{0} \quad (1)$$

where \mathbf{S} is stoichiometric matrix of (n metabolites by m reactions) and \mathbf{v} is a vector of metabolic fluxes. The number of unknown fluxes is higher than the number of equations and thus the system is undetermined. Still it is possible to find a unique solution under the assumption that cells metabolism evolves to pursue a predetermined goal such as biomass formation, i.e., to maximize growth rate:

$$\max \mu \quad (2)$$

$$s.t. : \quad (3)$$

$$\mathbf{S} \cdot \mathbf{v} = \mathbf{0} \quad (4)$$

$$\mathbf{LB} < \mathbf{v} < \mathbf{UB} \quad (5)$$

In its dynamic version, the FBA approach is solved iteratively through time and constraints are updated to take into account the dynamics of the cellular environment, for example, extracellular metabolites consumption or formation rates (Mahadevan and Doyle III 2002).

Several yeast genome-scale metabolic models (GEMs) have been published and are currently used for metabolic engineering and elucidating biological interactions (Sanchez and Nielsen 2015). Here we use the YEAST 5 GEM first refined version of YEAST 4 (the first consensus GEM) which includes improved sphingolipid metabolism. YEAST 5 accounts for more than 1500 metabolites and more than 2000 reactions (Heavner et al. 2012). The corresponding FBA problem is solved using the COBRA toolbox for MATLAB Heirendt et al. (2017).

Parameter estimation

Parameters for the kinetic model describing external metabolites are estimated by solving a nonlinear optimization problem. The aim is to find the unknown kinetic parameter values that minimize the least squares function - which accounts for the distance between model predictions and experimental data- subject to the system dynamics - the model- and parameter bounds (Vilas et al. 2018).

To automatize the modeling pipeline we used the AMIGO2 toolbox (Balsa-Canto et al. 2016).

RESULTS

Modeling hexoses transport

We modeled the transport of hexoses using a Michaelis-Menten (MM) type kinetics with competitive ethanol inhibition as follows (Hjersted et al. 2007):

$$v_{tr,H} = -X_f \cdot k_H \cdot H \cdot \frac{1}{1 + E/K_{Ei}} \quad (6)$$

where k_H regards the Michaelis constant, H refers to the relevant hexoses (glucose and fructose), X_f is the number of cells with fermentation capacity. K_{Ei} defines the strength of the ethanol inhibitory effect and E is the ethanol concentration.

Modeling production of extracellular metabolites

The production of extracellular metabolites is assumed to be proportional to the amount of transported hexoses (Sánchez et al. 2014):

$$v_{Ex} = -X_f \cdot k_{Ex} \cdot (v_G + v_F) \cdot \frac{MW_H}{MW_{Ex}} \quad (7)$$

where Ex refers to the extracellular metabolite, k_{Ex} controls the magnitude of metabolite production and MW_H

MW_{Ex} is the ratio of hexoses and extracellular metabolite molecular weights.

Ordinary differential equations

The dynamic model distinguishes viable non-fermenting from fermenting cells. We assume that a viable cell can ferment even if it not able to divide. The experimental data show a large difference in the dynamics of the number of colonies forming units and the other biomass measurements, dry weight and OD600 (see Figure 1). We, therefore, represent cell viability decay due to ethanol accumulation with a Hill-type kinetics:

$$\dot{X}_v = \mu \cdot X_v - X_v \cdot k_{Edeth} \cdot \frac{E^n}{E^n + k^n} \quad (8)$$

where X_v represents the number of viable cells, μ is the specific growth rate obtained with the constraint based model and k_{Edeth} , n and k are the parameters controlling susceptibility to ethanol. On the other hand the decay of cells with fermentative capacity is affected by a linear expression and is not dependent on ethanol:

$$\dot{X}_f = \mu \cdot X_v - X_f \cdot k_{death}; \quad (9)$$

where X_f represents the number fermenting cells and k_{death} is the parameter controlling the decay in fermenting cells.

Finally, the dynamics of hexoses ($\dot{H} = v_{tr,H}$) and other extracellular metabolites ($\dot{E}x$) are represented by the fluxes $v_{tr,H}$ and v_{Ex} .

Dynamic constraints

Constraints in form of fluxes were added to the genome-scale model. The fluxes (given in $\text{mmol} \cdot \text{gDW}^{-1} \cdot \text{h}^{-1}$) are computed as for hexoses transport:

$$v_{tr,H^*} = \frac{v_{tr,H}}{MW_H \cdot X_f \cdot DW_{perCell}} \quad (10)$$

where MW_H is the hexose molecular weight and $DW_{perCell}$ is estimated dry weight per cell. Similarly, constraints for extracellular metabolites were added

$$v_{Ex^*} = \frac{v_{Ex}}{MW_{Ex} X_f \cdot DW_{perCell}} \quad (11)$$

where MW_{Ex} is the molecular weight of the corresponding extracellular metabolite.

Colony forming units, OD600 and dry weight

To reconcile the different biomass measurements with the model, we have estimated the dry-weight per fermenting cell (*gramsPerCell*) and the number of fermenting cells per OD unit (*cellsPerOD*). The biomass and OD600 are assumed to be proportional to these parameters. The number of viable cells was considered to be the same as the number of CFUs.

Best model trajectories

Figure 1 presents model predictions of extracellular metabolites. The model can satisfactorily explain biomass trajectories biomass in terms of dry weight, number and OD600 as well as the relevant external metabolites.

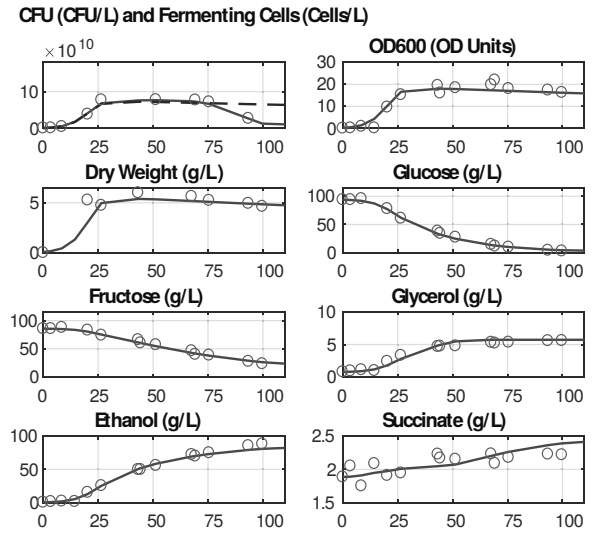


Figure 1: Model predictions and experimental data corresponding to external metabolites. The dashed line in the top-left subplot represents the estimated number of cells with fermentative capacity.

Figure 2 shows the dynamics of the 20 fluxes with highest mean value.

48.8991021	47.33207079	42.05873803	31.02330011	20.65459903	13.76005631	6.153742393	5.898287385	4.556276245	1010_ethanol transport
48.8991021	47.33207079	42.05873803	31.02330011	20.65459903	13.76005631	6.153742393	5.898287385	4.556276245	1009_ethanol exchange
47.39855465	45.87966851	40.76850942	30.07258183	20.07285721	13.34042033	5.967968616	5.720353215	4.419474059	148_phosphoglycerate kinase
44.16868243	42.7534199	37.99100006	28.02475886	18.66068834	12.43417518	5.564574546	5.333832636	4.121544205	214_pyruvate decarboxylase
37.10836644	35.91904384	31.91691882	23.54171504	15.67259009	10.45983111	4.676240076	4.482012649	3.461699436	149_phosphoglycerate mutase
39.27328792	38.01470451	33.77951491	24.9165879	16.58914273	11.0519098	4.943001142	4.73783282	3.455123044	217_pyruvate kinase
10.21960863	9.892306989	8.790924283	6.868088699	4.320335893	2.880589225	1.29172854	1.238340565	0.957774624	920_carbon dioxide exchange
10.21960863	9.892306989	8.790924283	6.868088699	4.320335893	2.880589225	1.29172854	1.238340565	0.957774624	173_phosphoserine phosphatase (L-serine)
10.21960863	9.892306989	8.790924283	6.868088699	4.320335893	2.880589225	1.29172854	1.238340565	0.957774624	147_phosphoglycerate dehydrogenase
9.798212949	9.484228558	8.427657175	6.216584936	4.139104044	2.757709441	1.233675788	1.182488815	0.913571868	174_phosphoserine transaminase
9.798212949	9.484228558	8.427657175	6.216584936	4.139104044	2.757709441	1.233675788	1.182488815	0.913571868	245_sedoheptulose 1,7-bisphosphate D-glyceraldehyde-3-phosphate-lyase
10.79122948	10.4437498	9.281558773	6.846053464	4.357692687	3.036073493	1.357396042	1.301021329	1.004872432	143_phosphofructokinase (7p)
10.76459768	10.42633324	9.288123737	6.906665701	4.670034009	3.183182794	1.534585701	1.4748365178	1.179926746	916_bicarbonate formation
8.669280263	8.391543316	7.456948877	5.801134721	3.663501272	2.441594073	1.093429161	1.048140019	0.810175497	911_bicarbonate exchange
7.30774579	7.266798245	6.45995551	4.759215441	3.164902509	2.104764473	0.935603449	0.896381329	0.694489226	388_D-fructose transport
15.10797486	14.61709046	12.96517681	9.507789804	6.258325268	4.09727028	1.721362656	1.642481798	1.230801426	1079_H+ exchange
13.45041346	13.01945427	11.56925809	8.534456823	5.683024501	3.787004005	1.695131606	1.62486526	1.255684812	145_phosphoglucuronate dehydrogenase
21.69109754	20.99606872	18.65726657	13.7628922	9.164241316	6.106430171	2.732793933	2.619482699	2.024130844	420_glucose transport
									142_phosphofructokinase
									309_triose-phosphate isomerase

Figure 2: Dynamic flux profile for selected reactions: top 20 average flux. As time progresses (from sampling time 1 to 9), the estimated intracellular fluxes tend to decrease as so does the rate of hexoses transport.

CONCLUSIONS

This work presents the combination of a kinetic model and the YEAST 5 genome-scale metabolic model within a parameter identification and a dynamic flux balance

analysis framework to explain wine fermentation by *S. cerevisiae* T73 wine yeast.

The proposed model effectively describes yeast population growth and decay and a number of extracellular metabolites, such as glucose, fructose, ethanol, glycerol, succinate, lactate and acetate at 25 °C.

The combination of micro-vinification experiments with high-performance liquid chromatography and multi-scale modelling has the potential to serve as a powerful tool in understanding the metabolic idiosyncrasies of particular wine strains and species currently used in the wine industry. We aim to apply this strategy to other non-conventional yeast species to explore their metabolic differences in wine fermentation.

ACKNOWLEDGEMENTS

This project has received funding from the Spanish government (MINECO) and the European Regional Development Fund (ERDF) through the projects IMPROWINE (grant numbers AGL2015-67504-C3-1-R; AGL2015-67504-C3-2-R) to AQ and EBC. RM was supported by a FPI grant from the Ministerio de Economía y Competitividad, Spain (grant number AGL2015-67504-C3-1-R).

REFERENCES

- Balsa-Canto E.; Henriques D.; Gabor A.; and Banga J., 2016. *AMIGO2, a toolbox for dynamic modeling, optimization and control in systems biology. Bioinformatics*, 32(21), 3357–3359.
- Coleman M.; Fish R.; and Block D., 2007. *Temperature-Dependent Kinetic Model for Nitrogen-Limited Wine Fermentation. Appl Environ Microbiol*, 73, no. 18, 5875–5884.
- Cramer A.; Vlassides S.; and Block D.E., 2002. *Kinetic model for nitrogen-limited wine fermentations. Biotechnol Bioeng*, 77, no. 1, 49–60.
- Heavner B.; Smallbone K.; Barker B.; Mendes P.; and Walker L.P., 2012. *Yeast 5 – an expanded reconstruction of the *Saccharomyces cerevisiae* metabolic network. BMC Syst Biol*, 6(1), 55.
- Heirendt L.; Arreckx S.; Pfau T.; Mendoza S.N.; Richelle A.; Heinken A.; Haraldsdottir H.S.; Keating S.M.; Vlasov V.; Wachowiak J.; et al., 2017. *Creation and analysis of biochemical constraint-based models: the COBRA Toolbox v3.0. arXiv preprint arXiv:171004038*.
- Henriques D.; Alonso-del Real J.; Querol A.; and Balsa-Canto E., 2018. **Saccharomyces cerevisiae* and *S. kudriavzevii* Synthetic Wine Fermentation Performance Dissected by Predictive Modeling. Front Microbiol*, 9, 88.

- Hjersted J.; Henson M.; and Mahadevan R., 2007. *Genome-scale analysis of Saccharomyces cerevisiae metabolism and ethanol production in fed-batch culture. Biotechnol & Bioeng*, 97, no. 5, 1190–1204.
- Mahadevan R. and Edwards J.S. and Doyle III F., 2002. *Dynamic flux balance analysis of diauxic growth in Escherichia coli. Biophys J*, 83, no. 3, 1331–1340.
- Malherbe S.; Fromion V.; Hilgert N.; and Sablayrolles J.M., 2004. *Modeling the effects of assimilable nitrogen and temperature on fermentation kinetics in enological conditions. Biotechnol Bioeng*, 86(3), 261–272.
- Orth J.; Thiele I.; and Palsson B., 2010. *What is flux balance analysis? Nat Biotechnol*, 28, no. 3, 245.
- Sainz J.; Pizarro F.; Prez-Correa J.R.; and Agosin E., 2003. *Modeling of yeast metabolism and process dynamics in batch fermentation. Biotechnol & Bioeng*, 81, no. 7.
- Sanchez B. and Nielsen J., 2015. *Genome scale models of yeast: towards standardized evaluation and consistent omic integration. Integr Biol*, 7, 846–858.
- Sánchez B.J.; Pérez-Correa J.R.; and Agosin E., 2014. *Construction of robust dynamic genome-scale metabolic model structures of Saccharomyces cerevisiae through iterative re-parameterization. Metabol Eng*, 25, 159–173.
- Vargas F.A.; Pizarro F.; Pérez-Correa J.R.; and Agosin E., 2011. *Expanding a dynamic flux balance model of yeast fermentation to genome-scale. BMC Syst Biol*, 5, no. 1, 75.
- Varma A. and Palsson B., 1994. *Stoichiometric flux balance models quantitatively predict growth and metabolic by-product secretion in wild-type Escherichia coli W3110. App Environ Microbiol*, 60, no. 10, 3724–3731.
- Vilas C.; Arias-Mndez A.; Garcia M.; Alonso A.; and Balsa-Canto E., 2018. *Towards predictive food process models: A protocol for parameter estimation. Crit Rev Food Sci & Nut*, , no. 58(3), 436–449.

TWO-EQUATION OXYGEN DIFFUSIVITY OF APPLE CORTEX TISSUE FOR MULTISCALE MODELING OF GAS EXCHANGE

Siem Janssen
 Pieter Verboven
 Bart Nicolai
 Department of Biosystems, KU Leuven
 Willem de Croylaan 42
 B 3000, Leuven, Belgium
 E-mail: siem.janssen@kuleuven.be

Susana Zorrilla
 Instituto de Desarrollo Tecnológico para
 la Industria Química, CONICET
 Universidad Nacional del Litoral
 Güemes 3450
 3000, Santa Fe, Argentina

KEYWORDS

Finite volume method, microscale model, effective diffusivity, porous media

ABSTRACT

A two-equation multiscale model was developed for diffusive oxygen transport in apple cortex tissue. Effective diffusivity of oxygen in both the pore and the cell phase was computed for the 3D microstructure of Jonagold cortex. Microstructure images were obtained with high resolution X-ray CT, and used in microscale simulations of gas diffusion with a voxel based finite volume method. The effective diffusivity of the liquid phase was as expected normally distributed, while the effective diffusivity of the gas phase showed a bimodal distribution. This was caused by the low pore connectivity of some of the 3D microstructures as 10 out of the 16 used samples did not show any open porosity. The 3D microstructure of the apple tissue imposed a significant reduction in the gaseous diffusivity. A comparison was made with the effective tissue diffusivity of a one-equation model for oxygen diffusion, assuming phase equilibrium. Good correspondence was found between the two models for the microscale properties of the tissues used. The large variation in the equilibrium effective tissue diffusivity that was obtained earlier could thus be explained by the variability in open porosity of apple cortex tissue.

INTRODUCTION

Gas exchange between a fruit and its environment is of crucial importance for metabolic processes such as respiration. During respiration, sugars and other reducing metabolites are oxidized by molecular oxygen to water and carbon dioxide. Apple fruit may deteriorate quickly after harvest due to respiration-driven ripening and senescence. To prolong storage life, respiration is minimized by low temperature, decreased oxygen partial pressure and slightly increased carbon dioxide partial pressure in so called controlled atmosphere (CA) storage. Conservation under CA conditions intends to avoid severe quality losses such as reduction of firmness and loss of green color, flavor and aroma. Moreover, it also reduces the risk of storage disorders such as superficial scald. As a result, a year round supply of high quality fruit is possible (Kays 1991; Lurie and Watkins 2012). However, caution is advised as suboptimal storage conditions can lead to physiological disorders such as internal browning in the fruit (Franck et al. 2007; Herremans et al. 2014; Ho et al. 2014).

Due to the consumption of oxygen and the production of carbon dioxide during respiration, concentration gradients develop in bulky organs such as apples, in which diffusion is limited (Cameron and Yang 1982). Gas diffusion is related to the porosity and the microstructure of the fruit tissue, and more specifically to the network of intercellular pores and cells (Ho et al. 2011; Verboven et al. 2008). A restricted oxygen supply through the skin and hypanthium in combination with low external oxygen conditions during CA storage can lead to local hypoxic (very low oxygen) and even anoxic (no oxygen) conditions inside the fruit (Ho et al. 2011). These conditions may eventually result in development of off-flavors and storage defects as a consequence of a dominating fermentative metabolism (Franck et al. 2007).

As experimental analysis of internal gas profiles in fruit is tedious, a multiscale gas transport model of fruit has been suggested. With this approach, the fruit is regarded as a continuum (macroscale model) in which the gas transport is described by effective (or apparent) gas transport parameters of the tissues. These parameters are calculated from simulations on the microscale, modeling gas transport through pores and cells of tissue samples. Ho et al. (2011) proposed a one-equation macroscale model for the description of gas transport in fruit, written here for diffusion and reaction:

$$\alpha_i \frac{\partial c_{i,g}}{\partial t} = \nabla D_{i,tissue}^{eff} \nabla c_{i,g} + R_i \quad (1)$$

with

$$\alpha_i = \varepsilon_t + (1 - \varepsilon_t) RTH_i \quad (2)$$

α_i is the tissue gas capacity for the respiratory gas i , ε_t the total porosity of the tissue, R_i ($\text{mol m}^{-3} \text{s}^{-1}$) the tissue respiration rate, $c_{i,g}$ (mol m^{-3}) the gas concentration expressed in gas partial pressures, R ($\text{Pa m}^3 \text{mol}^{-1} \text{K}^{-1}$) the universal gas constant, T (K) the temperature, H_i ($\text{mol m}^{-3} \text{Pa}^{-1}$) Henry's constant for the gas and $D_{i,tissue}^{eff}$ ($\text{m}^2 \text{s}^{-1}$) the effective tissue diffusivity. The latter is an effective lumped diffusivity of the apple tissue, encompassing the effect of porosity and tortuosity, and was estimated with a finite volume microscale model solved on 3D X-ray images of the porous microstructures.

In apple tissue, two large-scale phases can be identified: the pore phase and the cell phase. Both phases have a significantly

different capacity in transporting oxygen, as the pore phase is filled with air and the cell phase can be considered as water. This is expressed in the diffusivity values of oxygen in both phases (Table 1). This might imply a significant difference in concentration between the two phases, called a large-scale mass non-equilibrium, for which Cherblanc et al. (2007) suggested a two-equation model to be more appropriate. This model simulates gas transport separately for each phase, coupled by an interphase mass transfer coefficient. Moreover, when the less diffusive phase (i.e. the cell phase) is considered as stagnant, a mobile-immobile two-equation model is recommended (Cherblanc et al. 2003; Orgogozo et al. 2010). The mass transfer between the two phases is controlled by a diffusive process and is often macroscopically described by a first-order kinetics (Orgogozo et al. 2010).

In this paper a two-equation multiscale model is developed for describing diffusive oxygen transport in apple tissue. The effective diffusion parameters of this model are estimated and evaluated in comparison to the one-equation diffusivity.

MATERIAL AND METHODS

Macroscale Non-Equilibrium Model

In apple, oxygen may diffuse through pores and cells, both phases provide tortuous pathways for gas diffusion. Interphase transfer occurs through the cell wall and cell membranes. A two-equation macroscale model for oxygen exchange in apple is proposed for the pore and cell phase, respectively:

$$\varepsilon_t \frac{\partial c_{O_2,g}}{\partial t} = \nabla \cdot (\varepsilon_t D_{O_2,g}^{eff} \nabla c_{O_2,g}) - W \quad (3)$$

$$(1 - \varepsilon_t) \frac{\partial c_{O_2,l}}{\partial t} = \nabla \cdot ((1 - \varepsilon_t) D_{O_2,l}^{eff} \nabla c_{O_2,l}) + R_{O_2} + W \quad (4)$$

Parameters $D_{O_2,g}^{eff}$ and $D_{O_2,l}^{eff}$ ($m^2 s^{-1}$) are the effective diffusivities of oxygen in the gas and liquid phase respectively, $C_{O_2,l}$ ($mol m^{-3}$) is the oxygen concentration in the liquid phase, R_{O_2} ($mol m^{-3} s^{-1}$) the tissue respiration rate of oxygen and W ($mol m^{-3} s^{-1}$) the macroscale mass transfer coefficient between the two large-scale phases.

Equation (5) gives a proposed flux formulation for W , incorporating cell wall and cell membrane permeability (Davit et al. 2012; Chastanet and Wood 2008) into the overall resistance of the interphase. The mass transfer was assumed driven by a diffusive process and is described by a first-order kinetics.

$$W = \frac{a_v}{\left(\frac{L_w}{D_{O_2,w}} + \frac{L_{mem}}{D_{O_2,mem}} \right)} (RTH_{O_2} c_{O_2,g} - c_{O_2,l}) \quad (5)$$

Parameter a_v (m^{-1}) is the specific interfacial area of pore and cell phase (per unit of volume), L_w and L_{mem} (m) represent

the thickness of cell wall and membrane, respectively, and $D_{O_2,w}$ and $D_{O_2,mem}$ ($m^2 s^{-1}$) the liquid based diffusivity of those structures. Table 1 gives the values of the known parameters of the proposed two-equation macroscale model. The following unknowns were determined from a microscale analysis:

- the microstructural parameters a_v and ε_t , and
- the effective diffusivity of the gas phase $D_{O_2,g}^{eff}$ and of the cell phase $D_{O_2,l}^{eff}$.

Table 1: Physical Properties of the Two-Equation Model (at 293 K)

Model constants	
L_w (m)	$1,67 \times 10^{-5}$ (*)
L_{mem} (m)	$8,00 \times 10^{-8}$ (*)
$D_{O_2,w}$ ($m^2 s^{-1}$)	$2,01 \times 10^{-9}$ (*)
$D_{O_2,mem}$ ($m^2 s^{-1}$)	$2,91 \times 10^{-10}$ (*)
R ($Pa m^3 mol^{-1} K^{-1}$)	8,3144
H_{O_2} ($mol m^{-3} Pa^{-1}$)	$1,37 \times 10^{-5}$
$D_{O_2,air}$ ($m^2 s^{-1}$)	$1,60 \times 10^{-5}$
$D_{O_2,water}$ ($m^2 s^{-1}$)	$2,01 \times 10^{-9}$

(*) From Ho et al. (2014)

Microscale Model

The effective diffusivities of the tissue $D_{O_2,g}^{eff}$ and $D_{O_2,l}^{eff}$ were estimated by solving Fick's law of diffusion in both phases over voxelized 3D microstructure geometries of pores and cells of tissue samples obtained from X-ray micro-CT, which is described in Ho et al. (2011) and further detailed below. The model assumed steady state conditions and ignored respiration. Fickian diffusion of oxygen in pore (air) and cell (water) phase was then separately solved by Equation (6) and (7), respectively.

$$0 = \nabla D_{O_2,air} \nabla c_{O_2,g} \quad (6)$$

$$0 = \nabla D_{O_2,water} \nabla c_{O_2,l} \quad (7)$$

$D_{O_2,air}$ and $D_{O_2,water}$ ($m^2 s^{-1}$) are the diffusivity of oxygen in air and water, respectively (Table 1).

Equations (6) and (7) were discretized based on the voxel volumes (voxel based finite volume method) resulting in a linear set of equations on the unknown oxygen concentration at the voxels (Ho et al. 2011). A concentration gradient of 30% to 5% oxygen partial pressure was applied in the z-direction of the 3D microstructures. The set of equations was solved for $C_{O_2,g}$ and $C_{O_2,l}$ using the generalized minimum residual method available in Matlab (The Mathworks, Natick, MA, USA).

Given the distribution of oxygen throughout the samples, the mass flow of oxygen in both phases was calculated in the direction of the applied concentration gradient. The effective diffusivity of the pore and cell phase was determined by

Fick's law of diffusion in the z-direction of the 3D microstructures (Equation (8) and (9)).

$$D_{O_2,g}^{eff} = -\frac{n_{O_2,g}\Delta z}{\varepsilon_t A \Delta C_{O_2,g}} \quad (8)$$

$$D_{O_2,l}^{eff} = -\frac{n_{O_2,l}\Delta z}{(1-\varepsilon_t) A \Delta C_{O_2,l}} \quad (9)$$

where $\Delta C_{O_2,g}$ and $\Delta C_{O_2,l}$ (mol m⁻³) were the applied equilibrium concentration gradients in the z-direction, Δz (m) the thickness of the tissue sample in that direction, A (m²) the area of the samples perpendicular to Δz and $n_{O_2,g}$ and $n_{O_2,l}$ (mol s⁻¹) the mass flow rates of oxygen in the z-direction in the gas and liquid phase, respectively.

3D Microstructure Of Apple Cortex Tissue

3D microstructures of 16 Jonagold (*Malus x domestica* 'Jonagold') apple cortex samples were used for microscale model simulations to determine the parameters of the two-equation model. These samples were taken from previous research concerning the one-equation model and were obtained with high resolution X-ray CT (Ho et al. 2011). The 3D sample dimensions are (1.28 mm)³ with a voxel size of (5 μm)³. Structural parameters a_v and ε_t were calculated with the image analysis software Avizo (Thermo Fisher Scientific, Bordeaux, France). Additionally, the open porosity (ε_o) is calculated as well i.e. the pores that connect both sides of the 3D samples where the concentration gradient is applied. It is calculated with a dedicated program written in Matlab.

RESULTS AND DISCUSSION

Microstructure Properties

The left image of Figure 1 shows a slice of one of the Jonagold scans where the black spots identify pores while the greyish area identifies the cell tissue. With image editing software, a 3D representation of the microstructures was obtained which was used in the microscale model (Figure 1, right).

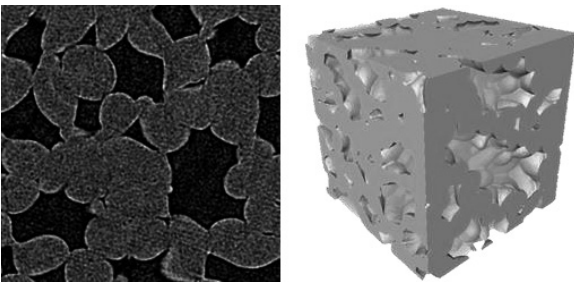


Figure 1: Slice of a Jonagold Scan (left) and a 3D Representation of one of the Samples (right)

Based on these images, the microstructural properties ε_t , ε_o and a_v were calculated (Table 2). The total porosity was calculated as the ratio of the pore volume to the total volume of the sample. The specific interfacial area was calculated as the ratio of contact surface between the two phases over the total sample volume. Both ε_t and a_v were relatively large

which indicated that the porosity in the sample is well distributed, resulting in a large contact area with the cell volume. The open porosity was only calculated in the direction of the applied oxygen gradient over the Jonagold cortex samples. It should be noted that 10 out of the 16 samples did not have any open porosity ($\varepsilon_o=0$).

Comparing the porosity of the 6 samples that showed an open porosity, the total porosity was still 10 times the open porosity. For all samples the difference was 20-fold. Therefore, it can be concluded that overall, the 3D pore microstructures have a very low pore connectivity. This may raise questions whether the used sample size is representative for the tissues. Connectivity may be enhanced over larger samples, be it across more tortuous paths. To explore such features, micro-CT of the large samples will be required and representative elementary volume analysis revisited.

Microscale Simulations

A concentration gradient was applied on the Jonagold samples and the distribution of oxygen was calculated in both phases. Figure 2 shows the results for the porous oxygen concentration in a sample without (top) and with (bottom) an open porosity in the direction of the applied gradient. The latter shows a distinct porous channel in which oxygen is easily transported. An effective oxygen diffusivity of $1,42 \times 10^{-6}$ m² s⁻¹ was estimated for this sample, while this was only $8,96 \times 10^{-10}$ m² s⁻¹ for the former sample due to lack of pore connectivity.

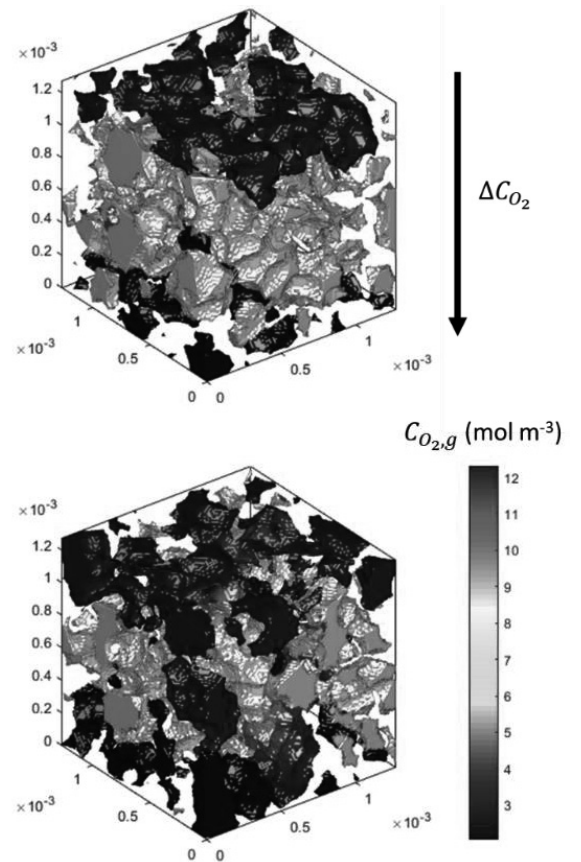


Figure 2: Oxygen Distribution in the Pore Space of a Sample without (top) and with (bottom) an Open Porosity in the Direction of the Applied Oxygen Gradient

Effective Diffusivity

Table 2 shows the estimated parameters for the two-equation model. $D_{O_2,g}^{eff}$ was estimated two orders of magnitude lower than $D_{O_2,air}$, meaning that, compared to oxygen diffusion in open air, the tissue microstructure imposed a significant reduction in the ease of gaseous oxygen diffusion. An opposite trend was found for $D_{O_2,l}^{eff}$, which was estimated slightly higher than $D_{O_2,water}$. This trend implied that the tissue microstructure facilitated liquid oxygen diffusion. In the microscale model, oxygen transfer between the two phases was possible. Therefore, dissolved oxygen was able to be partly transported through the pores of the samples, bypassing the liquid phase where the diffusion is slower. This phenomenon resulted in an overall higher diffusivity in the liquid phase compared to oxygen diffusion in pure water.

Distributions of the common logarithms of $D_{O_2,g}^{eff}$ and $D_{O_2,l}^{eff}$ are shown in Figure 3. While a relatively narrow and normal distribution was found for $\log_{10}(D_{O_2,l}^{eff})$, this was not the case for $\log_{10}(D_{O_2,g}^{eff})$, which was characterized by a bimodal distribution over a large range of values. This bimodality resulted from the effect of open porosity of the samples on the estimation of $D_{O_2,g}^{eff}$. An open porosity equal to zero, i.e. no direct porous path between the two ends of the sample, resulted in very low values of $D_{O_2,g}^{eff}$, more or less 2 orders of magnitude lower compared to the samples with open porosity.

Table 2: Estimated Parameters for the One- and Two-Equation Model

Parameter	Mean \pm St.dev
ε_t (%)	$26,58 \pm 1,83$
ε_0 (%)	$1,22 \pm 2,09$
a_v (m ⁻¹)	$(921 \pm 30) \times 10^1$
$D_{O_2,g}^{eff}$ (m ² s ⁻¹)	$(1,70 \pm 3,48) \times 10^{-7}$
$D_{O_2,l}^{eff}$ (m ² s ⁻¹)	$(2,70 \pm 0,06) \times 10^{-9}$
$D_{O_2,tissue}^{eff}$ (m ² s ⁻¹)	$(4,60 \pm 10,02) \times 10^{-8}$ (*)

(*) Estimated by Ho et al. (2011)

Comparison Of The One- And Two-Equation Model Parameters

$D_{O_2,tissue}^{eff}$ of the one-equation model is given in Table 2 (Ho et al. 2011). The value was obtained from a direct simulation of the two-phase transport in the microscale geometry, including the interphase transport. The one-equation model diffusivity also has a large variation, indicating the effect of non-connectivity of the pore network in some of the samples. The sum of Equations (3) and (4) will lead to Equation (1) if we assume gas-liquid equilibrium and

$$\varepsilon_t D_{O_2,g}^{eff} + (1 - \varepsilon_t) RTH_{O_2} D_{O_2,l}^{eff} = D_{O_2,tissue}^{eff} \quad (10)$$

Using the average values in Table 2, the term on the left hand side will equal to 4.53×10^{-8} m² s⁻¹. This value corresponds closely to the effective tissue diffusivity value given in Table

2. A one-on-one comparison of the left and right hand term of Equation (10) is given for the whole dataset (Figure 4). The axes are expressed in the common logarithm and the red line represents identical values. There was a good correspondence between the two terms. This implied that the equilibrium condition appeared valid and that the large variations seen in $D_{O_2,g}^{eff}$ and $D_{O_2,tissue}^{eff}$ originated from the same source, namely the differences in pore connectivity of the Jonagold microstructures.

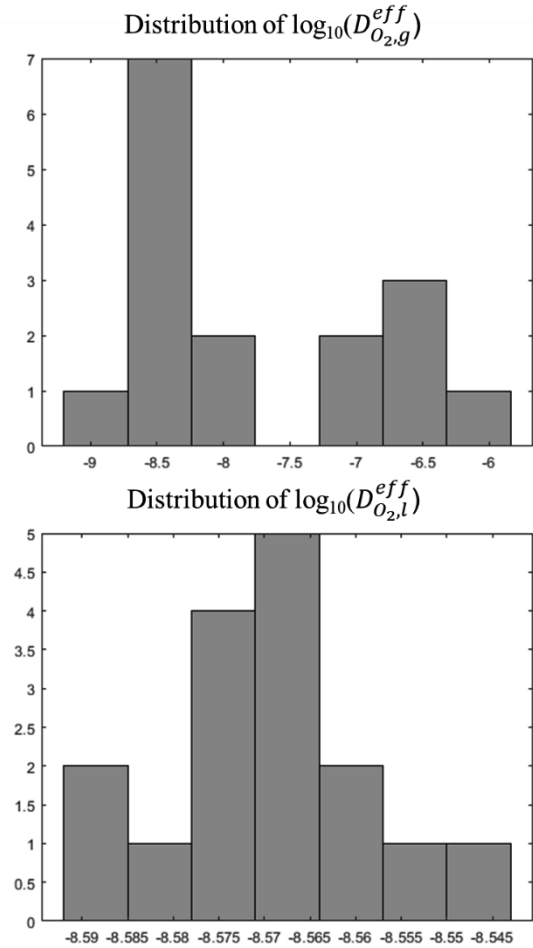


Figure 3: Distribution of the Common Logarithms of $D_{O_2,g}^{eff}$ (top) and $D_{O_2,l}^{eff}$ (bottom)

CONCLUSION

This research showed that the pore connectivity in the Jonagold samples had an enormous influence on the estimation of the effective diffusivity of oxygen in the pore space. The presence of an open porosity divided the samples in two groups, resulting in a bimodal distribution for the diffusivity in the gas phase. The microstructure of the apple cortex was found to significantly limit the diffusivity in the gas phase, while slightly enhancing the diffusivity in the liquid phase. The latter effect was explained by oxygen dissolved in the liquid phase taking a shortcut through the pores of the sample, where transport is faster.

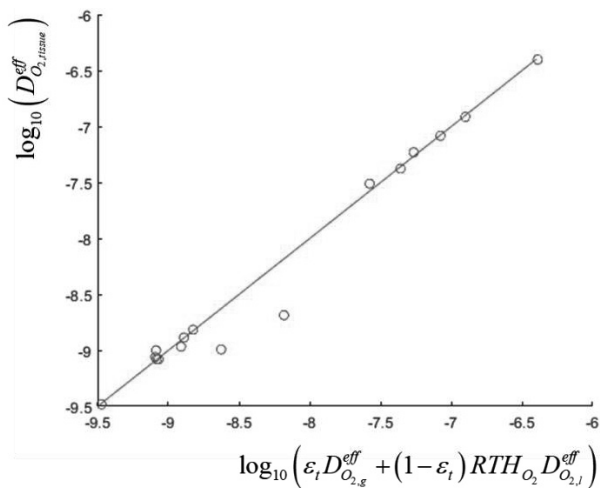


Figure 4: One-on-One Comparison of the Left and Right Hand Term of Equation (10) for all the Jonagold Samples (Axes are expressed in the Common Logarithm and the Red Line represents Identical Values)

FUTURE RESEARCH

Studying the microstructural parameters of the apple samples, and their effect on the estimated parameters of the two-equation model, brought to light that the used sample size might not be representative for the apple tissue. A sensitivity analysis is in order to determine how sample size will influence the pore connectivity, which is found a determining parameter in the estimation of effective diffusivities.

The two-equation model will next be used in multiscale simulations predicting oxygen concentrations in entire fruits. Here, respiration is taken into account as seen in equations (3) and (4). Further steps include the modeling of carbon dioxide diffusion and the addition of permeation effects on gas transport inside the fruit. The two-equation multiscale model will be compared to the one-equation model (Ho et al. 2011). Stochastic simulations of the spatial variability of diffusivity and transient simulations will be targeted.

ACKNOWLEDGEMENTS

A great thanks goes out to professor Susana Zorrilla from the 'Universidad Nacional del Litoral', Argentina, who initiated this research topic when she visited our research facility (MeBioS) in Leuven. In addition, her further guidance and supervision regarding this research remains extremely insightful to this day. Acknowledgement also goes out to the KU Leuven for supplying the funding to pursue this interesting topic (project C16/16/002).

REFERENCES

Cameron, A C, and S F Yang. 1982. "A Simple Method for the Determination of Resistance to Gas Diffusion in Plant Organs." *Plant Physiology* 70: 21–23.

Chastanet, J., and Brian D. Wood. 2008. "Mass Transfer

Process in a Two-Region Medium." *Water Resources Research* 44: 1–16.

Cherblanc, F., A. Ahmadi, and M. Quintard. 2003. "Two-Medium Description of Dispersion in Heterogeneous Porous Media: Calculation of Macroscopic Properties." *Water Resources Research* 39 (6): 1–20.

Cherblanc, F., A. Ahmadi, and M. Quintard. 2007. "Two-Domain Description of Solute Transport in Heterogeneous Porous Media: Comparison between Theoretical Predictions and Numerical Experiments." *Advances in Water Resources* 30: 1127–43.

Davit, Y., B. D. Wood, G. Debenest, and M. Quintard. 2012. "Correspondence Between One- and Two-Equation Models for Solute Transport in Two-Region Heterogeneous Porous Media." *Transport in Porous Media* 95: 213–38.

Franck, Christine, Jeroen Lammertyn, Quang Tri Ho, Pieter Verboven, Bert Verlinden, and Bart M. Nicolaï. 2007. "Browning Disorders in Pear Fruit." *Postharvest Biology and Technology* 43 (1): 1–13.

Herremans, Els, Pieter Verboven, Thijs Defraeye, Seppe Rogge, Quang Tri Ho, Maarten L A T M Hertog, Bert E. Verlinden, Evi Bongaers, Martine Wevers, and Bart M. Nicolai. 2014. "X-Ray CT for Quantitative Food Microstructure Engineering: The Apple Case." *Nuclear Instruments and Methods in Physics Research, Section B: Beam Interactions with Materials and Atoms* 324. Elsevier B.V.: 88–94.

Ho, Quang Tri, Pieter Verboven, Solomon W. Fanta, Metadel K. Abera, Moges A. Retta, Els Herremans, Thijs Defraeye, and Bart M. Nicolaï. 2014. "A Multiphase Pore Scale Network Model of Gas Exchange in Apple Fruit." *Food and Bioprocess Technology* 7: 482–95.

Ho, Quang Tri, Pieter Verboven, Bert E Verlinden, Els Herremans, Martine Wevers, Jan Carmeliet, and Bart M Nicolaï. 2011. "A Three-Dimensional Multiscale Model for Gas Exchange in Fruit." *Plant Physiology* 155 (3): 1158–68.

Kays, Stanley J. 1991. *Postharvest Physiology of Perishable Plant Products*. New York, US: London Van Nostrand Reinhold.

Lurie, Susan, and Christopher B. Watkins. 2012. "Superficial Scald, Its Etiology and Control." *Postharvest Biology and Technology* 65. Elsevier B.V.: 44–60.

Orgogozo, Laurent, Fabrice Golfier, Michel Buès, and Michel Quintard. 2010. "Upscaling of Transport Processes in Porous Media with Biofilms in Non-Equilibrium Conditions." *Advances in Water Resources* 33: 585–600.

Verboven, Pieter, Greet Kerckhofs, Hibru Kelemu Mebatsion, Quang Tri Ho, Kristiaan Temst, Martine Wevers, Peter Cloetens, and Bart M Nicolaï. 2008. "Three-Dimensional Gas Exchange Pathways in Pome Fruit Characterized by Synchrotron X-Ray Computed Tomography." *Plant Physiology* 147 (2): 518–27.

ESTIMATION OF INTRINSIC VISCOSITY OF APPLE CELLS BY NUMERICAL SIMULATION

Artemio Plana-Fattori (*), Christophe Doursat, Giana Almeida,
Gabrielle Moulin, Cassandre Leverrier, Even Ou, and Denis Flick

UMR Ingénierie Procédés Aliments,
AgroParisTech, INRA, Université Paris-Saclay, 91300 Massy, France

(*) author corresponding address: AgroParisTech, Dept. MMIP, 16 rue Claude Bernard, 75231 Paris
E-mail: artemio.planafattori@agroparistech.fr

KEYWORDS

relative viscosity, intrinsic viscosity, apple cells,
extensional flow, Einstein equation, COMSOL Multiphysics

ABSTRACT

A numerical simulation approach was proposed to estimate the intrinsic viscosity of particles with complex geometry. The approach is based upon the solution of the mass and the momentum conservation equations for an incompressible Newtonian fluid under steady-state creeping flow around the particle. The reliability of the approach is demonstrated after solving the problem for fluid flow around a small sphere, whose effect is known after theoretical work. The approach is then applied in solving the same problem for different apple cells. The intrinsic viscosity varies with the particle shape and its orientation, between 2.6 and 4.6.

INTRODUCTION

Understanding the rheology of food materials is essential for the standardized characterization of raw materials and innovative products, as well as for optimized industrial processing (Fischer and Windhab 2011). In the case of apple purees, bulk measurements have allowed to evaluate the influence of particles size and insoluble solids content on the suspension rheological properties (Espinosa-Muñoz et al. 2013); further, direct observation has demonstrated the ability of apple cells to compress and decrease their volume when the concentration of the suspension increases (Leverrier et al. 2017). As a complement to experimental work, numerical simulation can provide useful information linking these two scales (bulk and cell). Indeed, the rheology of particle-fluid suspensions through numerical simulation has been studied since the 1990's, for instance by solving the dynamics of the solid particles combined with a Lattice Boltzmann approach for the fluid phase in the case of spheres, cylinders, or disks (Ladd and Verberg 2001).

It is clear that many of the complex phenomena associated with a flowing suspension cannot be explained by using a classical Newtonian description of a fluid with an ef-

fective viscosity. The volume fraction of the particles in a suspension (volume occupied by particles per unit volume of suspension) has often been assumed to be the only variable that influences the observed rheological properties of the suspension. Experimental evidence has shown that this is incorrect and that other factors, such as the shape and size distribution of the particles, the presence of electrical charges, and the type of flow being experienced must be considered (Jeffrey and Acrivos 1976). The study of the hydro-dynamical contributions of non-Brownian particles to the rheology of suspensions usually starts with diluted systems, i.e., those in which there are so few particles that occasional collisions between particles can be ignored. In such case everything one needs to know can be obtained from studying the flow around a single particle (Mewis and Wagner 2012, p.41).

Einstein (1906) has shown that the viscosity η of a diluted suspension of rigid spheres, treated as an incompressible homogeneous liquid, divided by the viscosity η_ℓ of the pure liquid, can be expressed as a linear function of the volume fraction of particles, ϕ :

$$\eta / \eta_\ell = 1 + \alpha \phi . \quad (1)$$

The parameter α is called intrinsic viscosity, being equal to 2.5 for very diluted spherical particles. Since then, much work has been devoted in describing the relative viscosity of disperse systems as a function of the concentration of the dispersed phase: equations have been developed on a theoretical foundation; theoretical equations have been adapted to empirical results; and empirical expressions have been reformulated in such a way that the Einstein equation (1) is obtained at very low concentration. Fifty years ago, dozens of formulas were already available (Rutgers 1962).

Theoretical computation of the relative viscosity due to very diluted ellipsoidal particles has demonstrated that the parameter α in the Einstein equation (1) can assume values from 2 up to 10 depending on the particle shape and orientation (Jeffery 1922). These findings have provided a physical, micro-structural explanation of observations, including changes of rheological regime as the volume fraction increases (Mueller et al. 2010).

Looking for a method to investigate the role played by the particle shape on the intrinsic viscosity, we propose a numerical simulation approach for studying the effect on the flow of a liquid around a particle suspended in it. In this contribution two kinds of particles are considered: spheres, as a way to assess the reliability of the approach; and some apple cells, in order to explore the potential of our approach in the case of irregularly-shaped particles.

METHODS

Particles in the liquid constitute obstacles to fluid flow; hence their presence distorts the flow field. Further, there is friction at the surface of particles. Both effects are expected to increase the energy dissipation during flow, and hence the apparent viscosity, above that of the pure suspending medium (Mewis and Wagner 2012, p.46).

Our rationale is based on the thought experiment of Einstein (1906) in his theoretical analysis dealing with the viscosity of diluted suspensions. In a first step, we solve an extensional stationary fluid flow problem associated with the presence of a very small particle placed in the center of a volume of incompressible Newtonian liquid. The viscous dissipation W is calculated by integrating $\eta_\ell(\dot{\gamma})^2$ over the liquid volume under consideration, where η_ℓ is the viscosity of the liquid phase, and $\dot{\gamma}$ is the shear rate field. The second step involves the solution of the problem but without the particle in the liquid volume. This second problem is associated with a smaller viscous dissipation W_ℓ , due to a shear rate field $\dot{\gamma}_\ell$ which does not exhibit the features characterizing the flow disturbances occurring in the first problem. The relative viscosity η/η_ℓ due to the presence of the particle in the liquid volume is finally obtained by computing the ratio W/W_ℓ .

The mass and momentum conservation equations for an incompressible Newtonian fluid under stationary conditions can be written as:

$$\nabla \cdot \mathbf{u} = 0 \quad (2)$$

$$\rho(\mathbf{u} \cdot \nabla) \mathbf{u} = \nabla \cdot (-p\mathbf{I} + \eta_\ell(\nabla \mathbf{u} + (\nabla \mathbf{u})^T)), \quad (3)$$

where \mathbf{u} is the velocity (magnitude in $\text{m}\cdot\text{s}^{-1}$) and p the pressure (Pa); ρ is the liquid density ($\text{kg}\cdot\text{m}^{-3}$) and η_ℓ its viscosity (Pa.s).

Following Einstein, here we consider extensional flow around the particle. The computational domain is a cube; two opposite faces are associated with outflow, while the four remaining ones correspond to inflow. At the particle surface, the velocity field is assumed to vanish. At the two outlet boundaries, the pressure p is assumed to vanish under no viscous stress. At the four inlet boundaries, the velocity components u , v , w are prescribed as:

$$u = A(x - x_0), \quad v = B(y - y_0), \quad w = C(z - z_0), \quad (4)$$

where the coordinates (x_0, y_0, z_0) indicates the barycenter of the particle. On account of the incompressibility of the liq-

uid, the constants A , B , and C must fulfill the condition $A + B + C = 0$. Three scenarios are here considered:

- $A = 1, B = C = -1/2$; outflow through the cube faces which are parallel to the plane YZ;
- $B = 1, A = C = -1/2$; outflow through the cube faces which are parallel to the plane XZ; and
- $C = 1, A = B = -1/2$; outflow through the cube faces which are parallel to the plane XY.

Only one scenario is required in assessing the relative viscosity due to spheres. In the case of apple cells, the application of these scenarios is equivalent to consider three arbitrary orientations for the particle in respect to the fluid flow. The liquid is characterized by the density $\rho = 1000 \text{ kg}\cdot\text{m}^{-3}$ and the dynamic viscosity $\eta_\ell = 0.001 \text{ Pa}\cdot\text{s}$ (similar to pure water at 20°C). This problem is solved under creeping regime: Reynolds number is smaller than 1.5 for all the cases.

Equations (2) and (3) need to be solved firstly with the particle at the center of the computational domain, and later in its absence. These equations are solved through the finite-element method as implemented in the simulation package COMSOL Multiphysics software (version 5.2.0.220; COMSOL, Inc., Burlington, Massachusetts) (Zimmerman 2006). Three-dimensional domains are commonly approximated by a mesh of polyhedrons in the process of setting up the equations for finite-element analysis. In this study the domains are subdivided into large numbers of small, non-overlapping tetrahedrons, which allow suitable geometrical approximations of virtually any three-dimensional shape. Discretization of equations (2) and (3) considers first-order Lagrange finite elements for the velocity components and the pressure. The solution of the linear system obtained after discretization of governing equations is reached through the direct solver PARDISO (Schenk and Gartner 2004). Satisfactory convergence of the numerical model is reached in looking for a relative tolerance smaller than 10^{-6} .

SPHERES

Figure 1A illustrates the computational domain, built around a sphere corresponding to the volume fraction of 0.4%. Figure 1B displays model predictions of the velocity field, after solving the fluid flow problem in the presence of that sphere. Velocities vanish in the vicinity of the sphere, as a consequence of friction (no slip condition at the particle surface). This leads to distortion of the flow field, which is put in evidence in Figures 1C and 1D.

Model predictions of the relative viscosity were obtained at different mesh resolutions. Solving the problem with the coarser mesh required less than 2 Gb-RAM and few seconds; the application of the finer mesh required above 190 Gb-RAM, and results were available after some days of work on a Windows-7 64-bit SP1, Intel Xeon CPU ES-2630 v3 @ 2.40 GHz, 192 Gb-RAM computer.

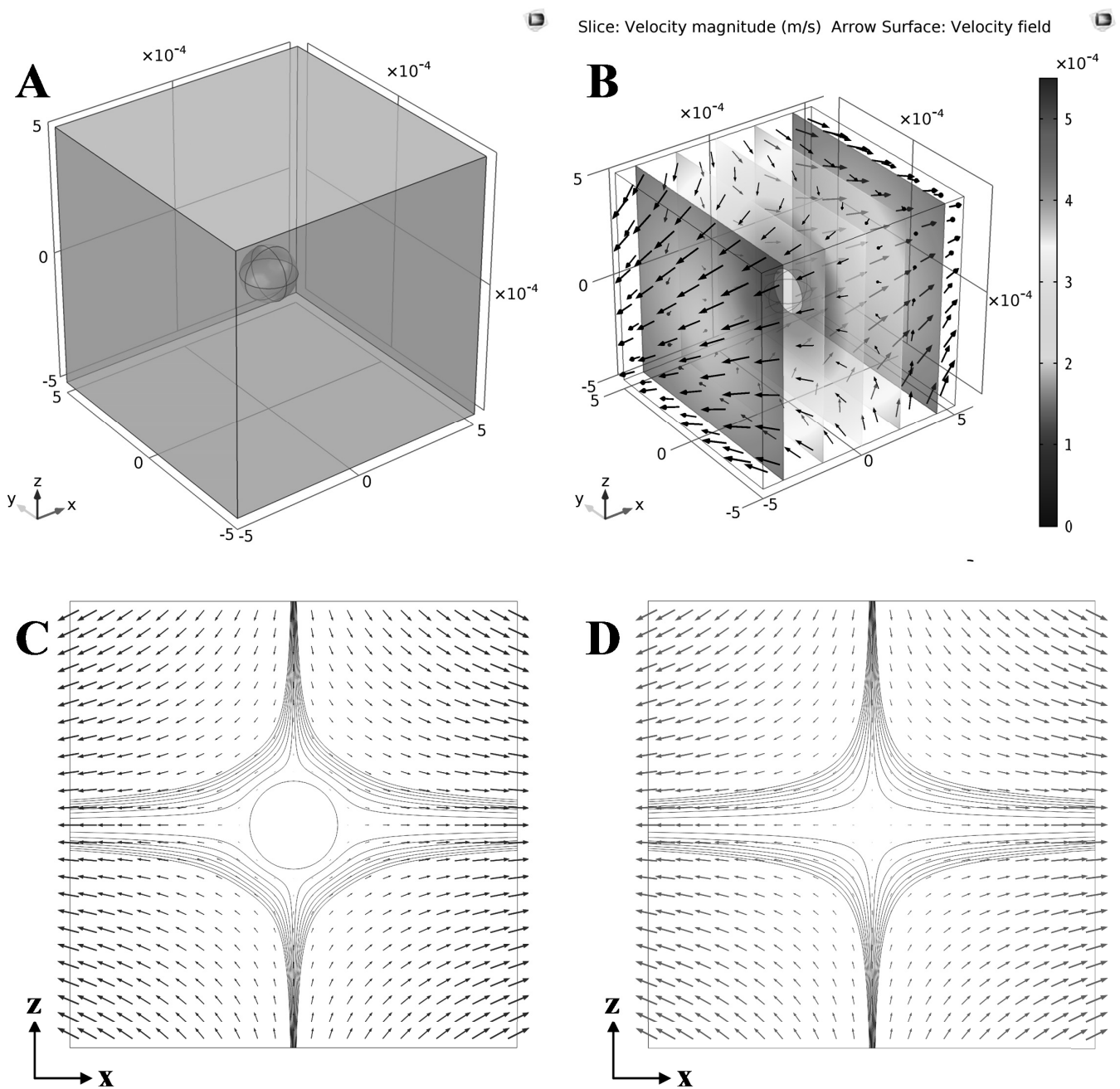


Figure 1: Display **A** shows the computational domain for a sphere corresponding to the volume fraction of 0.4 %, where the blue faces indicate domain outlets when outflow boundary conditions correspond to $A = 1$. Display **B** presents model predictions of the velocity field around such a sphere, in 3D representation; the same model predictions are presented in display **C** with the help of streamlines and velocity vectors in the plane $Y = 0$. Display **D** presents model predictions of the velocity field in the absence of the sphere. Dimensions are expressed in meters.

Figure 2 summarizes results obtained for spheres corresponding to the volume fractions of 0.1 % and 0.4 %. Model results converged with the mesh resolution, and the values predicted for the relative viscosity due to such spheres became quite stable above 5×10^5 mesh elements. Even applying the highest mesh resolution, there is a difference between values predicted for the relative viscosity from the model and those from the Einstein equation (1); further, such a difference increases with the volume fraction. In fact, the intrinsic viscosity is defined for infinitely small volume fraction as $\alpha = \lim_{\phi \rightarrow 0} (\eta - \eta_\ell) / (\eta_\ell \phi)$. Assuming a volume fraction of 0.4 % in numerical simulation leads to slightly overestimate the intrinsic viscosity, $\alpha_{0.4\%} \sim 2.54$, whereas using 0.1 % gives $\alpha_{0.1\%} \sim 2.50$.

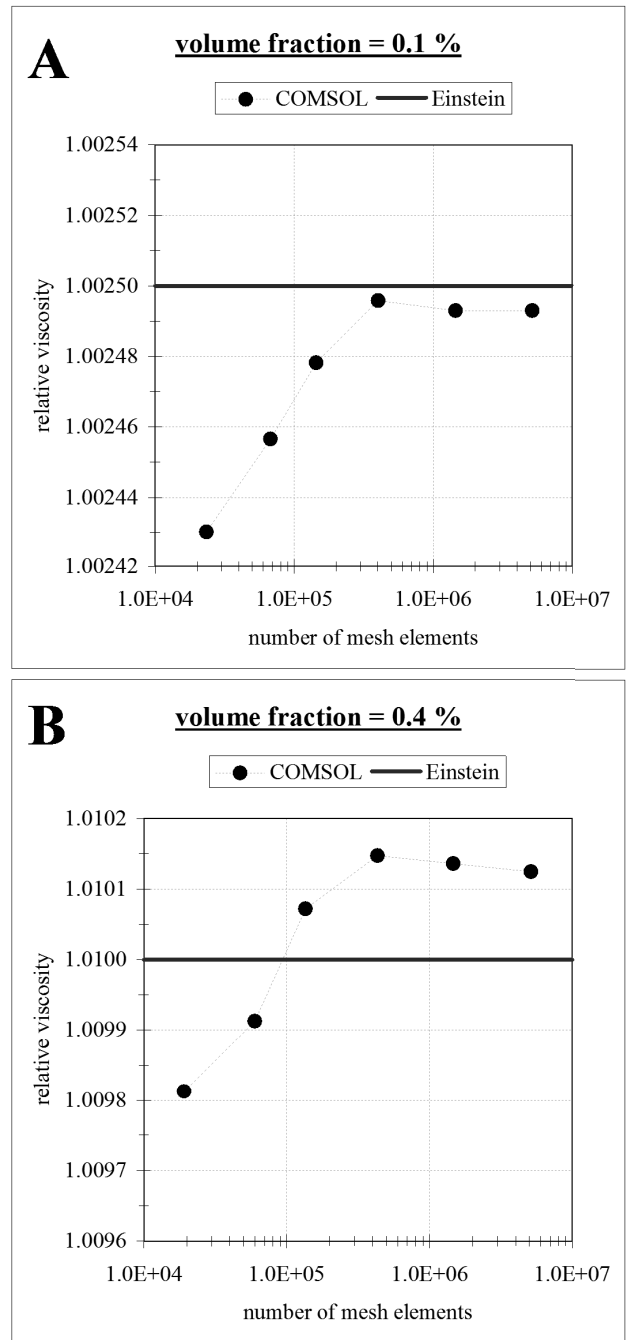


Figure 2: Model predictions of the relative viscosity due to spheres, after assuming a volume fraction of 0.1 % (A) and 0.4 % (B), as function of the number of mesh elements. Blue lines indicate the value as estimated from the Einstein equation (1) for $\alpha = 2.5$.

APPLE CELLS

The application of numerical modeling to problems involving real food particles constitutes a challenging task. On one hand, the irregularly-shaped particles that we found in real-world problems can exhibit very complex geometrical features. Under such conditions, the construction of the computational domain needs to include a realistic representation of the particles of interest as provided by image acquisition and post-processing. On the other hand, meshing algorithms can forbid the construction of relatively coarse meshes for detailed geometries. As noted above, higher is the resolution in meshing the computational domain, larger is the computer memory required and longer is the simulation time needed for reaching a satisfactory solution.

Our numerical modeling approach was applied to three apple cells (Leverrier et al., 2017). The volume occupied by each apple cell was about 1.36, 3.40 and $1.27 \times 10^6 \mu\text{m}^3$, respectively; the geometry of each cell was obtained using confocal microscopy and three-dimensional reconstruction. These apple cells were sampled from a moderately diluted apple puree (0.47 g of insoluble solids per 100 ml of suspension; volume fraction of 0.43); the cells are expected do not change their shape under fluid flow.

Three steps were conducted in order to consider those apple cells in our numerical approach.

- Firstly, the volume associated with each cell was subdivided into a large number of tetrahedrons. This was performed through the Simpleware software environment and its +FE Mesh Generation Module (version 2016.09-SP1; Synopsis, Inc., Mountain View, California). Looking for a detailed representation of the cells, a relatively high meshing resolution was considered; the resulting volume meshes are constituted by about 1.8 , 3.7 , and 2.3×10^6 tetrahedrons.
- Secondly, the file containing the volume mesh generated by Simpleware was imported into the COMSOL environment, in which we created a 3D representation of the apple cell considered. The results obtained can be appreciated in Figure 3.
- Lastly, a cubic computational domain was built, whose center coincides with the cell barycenter. The volume fraction corresponding to the cell is assigned, hence the cube volume becomes a multiple value of the cell volume (say, 250 times higher for a volume fraction of 0.4 %).

The standard options of the COMSOL Multiphysics mesh generator gave origin to great heterogeneity in the size of elements. Hence, the subdivision of the computational domain was customized in order to generate a large number of tetrahedrons with similar size. The shortest edge of mesh elements was set to be a sub-multiple of the side L of the liquid

cube representing the computational domain; and the ratio of their longest edge to the shortest edge was set to be 4.

Figure 4 shows results reached for the apple cells after assuming the volume fraction $\phi = 0.1 \%$ and 0.4% , taking into account the three sets of flow boundary conditions. Sensitivity tests were performed on the mesh resolution in solving the flow problem for the three apple cells in the case of boundary conditions associated with $A = 1$. Quite stable results were obtained above 10^6 mesh elements; hereafter only the results obtained with the finest mesh are discussed.

Table 1 translates model predictions of relative viscosity into estimates of intrinsic viscosity. All the values are higher than 2.5, associated with the Einstein equation (1). This was expected as a consequence of the irregular, non-spherical shape of particles under consideration. Essentially the same estimates of intrinsic viscosity are obtained from model simulations performed for $\phi = 0.1 \%$ and 0.4% . Table 1 indicates that, for a given particle, the intrinsic viscosity depends on the particle orientation with respect to the flow boundary conditions. The relative standard deviation (or coefficient of variation) of α is smaller for one cell (#1) than for the other two, without any apparent reason from the visual inspection of their 3D appearance. As shown in Figure 3, each apple cell exhibits a variety of geometrical features, including convex and concave regions, as well as rugged and smooth areas. It seems difficult to anticipate the influence of the geometrical features exhibited by an apple cell on its intrinsic viscosity.

SUMMARY AND FUTURE WORK

- Results obtained for spheres demonstrated the reliability of our approach for volume fractions below 0.4%. Differences between model results and estimates from the Einstein equation (1) remained below 2 % of the intrinsic viscosity value (2.54 instead 2.5 for $\phi = 0.4\%$).
- Model predictions of the intrinsic viscosity due to an isolated apple cell are higher than for a sphere. Such an increase depends on the cell shape as well as on its orientation with respect to the extensional flow.

Results presented above were obtained after placing the cube center at the particle barycenter. In fact, we should consider the position at which the forces exerted by the fluid on the particle exhibit null resultant. Such a steady-state position of the particle could differ slightly from its barycenter. Further, only three different orientations were considered in obtaining the results shown above. Two conditions deserve attention regarding the estimation of the intrinsic viscosity. At low shear (Peclet number < 1), thermal agitation dominates, and the particle orientation is random. Therefore the intrinsic viscosity at low shear should be based on the averaged value obtained from numerous orientations. Inversely, at high shear (Peclet number > 100), thermal agitation becomes negligible; the particle orientation is expected to be in

the direction corresponding to the lowest viscous dissipation, say to the lowest intrinsic viscosity. The latter could also be obtained by turning the particle until the torque vanishes. Finally, a larger set of apple cells should be considered in order to obtain statistically significant values.

The determination of the intrinsic viscosity of apple cells can be useful to estimate the volume fraction which is occupied by solid particles in apple juices or apple purees. Indeed, one could progressively dilute the apple-based food product, searching conditions where the suspension viscosity becomes a linear function of the concentration; then, knowing the viscosity of the continuous phase (e.g. the supernatant after centrifugation), the volume fraction could be estimated from the measurement of the suspension viscosity.

ACKNOWLEDGEMENTS

Authors kindly acknowledge Prof. Gérard Couvelier for his inspiring comments about our work.

REFERENCES

- Einstein, A. 1906. "Eine neue bestimmung der molekül-dimensionen". *Annalen der Physik* 19, 289-306. [Corrections are provided in Einstein (1911); the content in English of both articles is provided in Einstein (1956); the reader can be also interested on the Remarks section in Farris (1968) as well as on the section #12 in Jeffrey and Acrivos (1976)]
- Einstein, A. 1911. "Berichtigung zu meiner arbeit: Eine neue bestimmung der moleküldimensionen". *Annalen der Physik* 34, 591-592.
- Einstein, A. 1956. *Investigation on the Theory of the Brownian Movement*. Unabridged and unaltered republication of the 1st English edition (1926). Dover, New York.
- Espinosa-Muñoz, L., C. M. G. C. Renard, R. Symoneaux, N. Biau, and G. Couvelier. 2013. "Structural parameters that determine the rheological properties of apple puree". *Journal of Food Engineering* 119, 619-626.
- Farris, R. J. 1968. "Prediction of the viscosity of multimodal suspensions from unimodal viscosity data". *Transactions of the Society of Rheology* 12, 281-301.
- Fischer, P. and E. J. Windhab. 2011. "Rheology of food materials". *Current Opinion in Colloid and Interface Science* 16, 36-40.
- Jeffery, G. B. 1922. "The motion of ellipsoidal particles immersed in a viscous fluid". *Proceedings of the Royal Society, series A (Mathematical, Physical and Engineering Sciences)* 102, 161-179.
- Jeffrey, D. J. and A. Acrivos. 1976. "The rheological properties of suspensions of rigid particles". *American Institute of Chemical Engineers Journal* 22, 417-432.
- Ladd, A. J. C. and R. Verberg. 2001. "Lattice-Boltzmann simulations of particle-fluid suspensions". *Journal of Statistical Physics* 104, 1191-1251.
- Leverrier, C., G. Moulin, G. Couvelier, and G. Almeida. 2017. "Assessment of deformability of soft plant cells by 3D imaging". *Food Structure* 14, 95-100.
- Mewis, J. and N. J. Wagner. 2012. *Colloidal Suspension Rheology*. Cambridge University Press, New York.
- Mueller, S., E. W. Llewellyn, and H. M. Mader. 2010. "The rheology of suspensions of solid particles". *Proceedings of the Royal Society of London A: Mathematical, Physical and Engineering Sciences* 466, 1201-1228.
- Rutgers, R. 1962. "Relative viscosity and concentration". *Rheologica Acta* 2, 305-348.
- Schenk, O. and K. Gartner. 2004. "Solving unsymmetric sparse systems of linear equations with PARDISO". *Future Generation Computer Systems* 20, 475-487.
- Zimmerman, W. B. J. 2006. *Multiphysics Modelling with Finite Element Methods*. World Scientific, Singapore.

AUTHOR BIOGRAPHIES

ARTEMIO PLANA-FATTORI studied Atmospheric Sciences in the Universidade de Sao Paulo and later in the Université de Lille. After 20 years teaching and conducting research in Brazil, he joined AgroParisTech in 2010, where he has working with numerical modeling applied to food engineering.

DENIS FLICK is Full Professor at AgroParisTech. He conducts research in modeling and numerical simulation of coupled phenomena in food processes (heat and mass transfer, fluid flow and product deformation, product transformation), with applications in food cold chain equipment, heat exchangers, cooking and baking, dairy products, bread, and ice cream. His teaching area includes transport phenomena, thermodynamics, and numerical modeling.

CHRISTOPHE DOURSAT and GIANA ALMEIDA are Professors, CASSANDRE LEVERRIER is Assistant Professor, and GABRIELLE MOULIN is Assistant Engineer, all at AgroParisTech.

EVEN OU contributed to this study in the scope of his research internship at AgroParisTech.

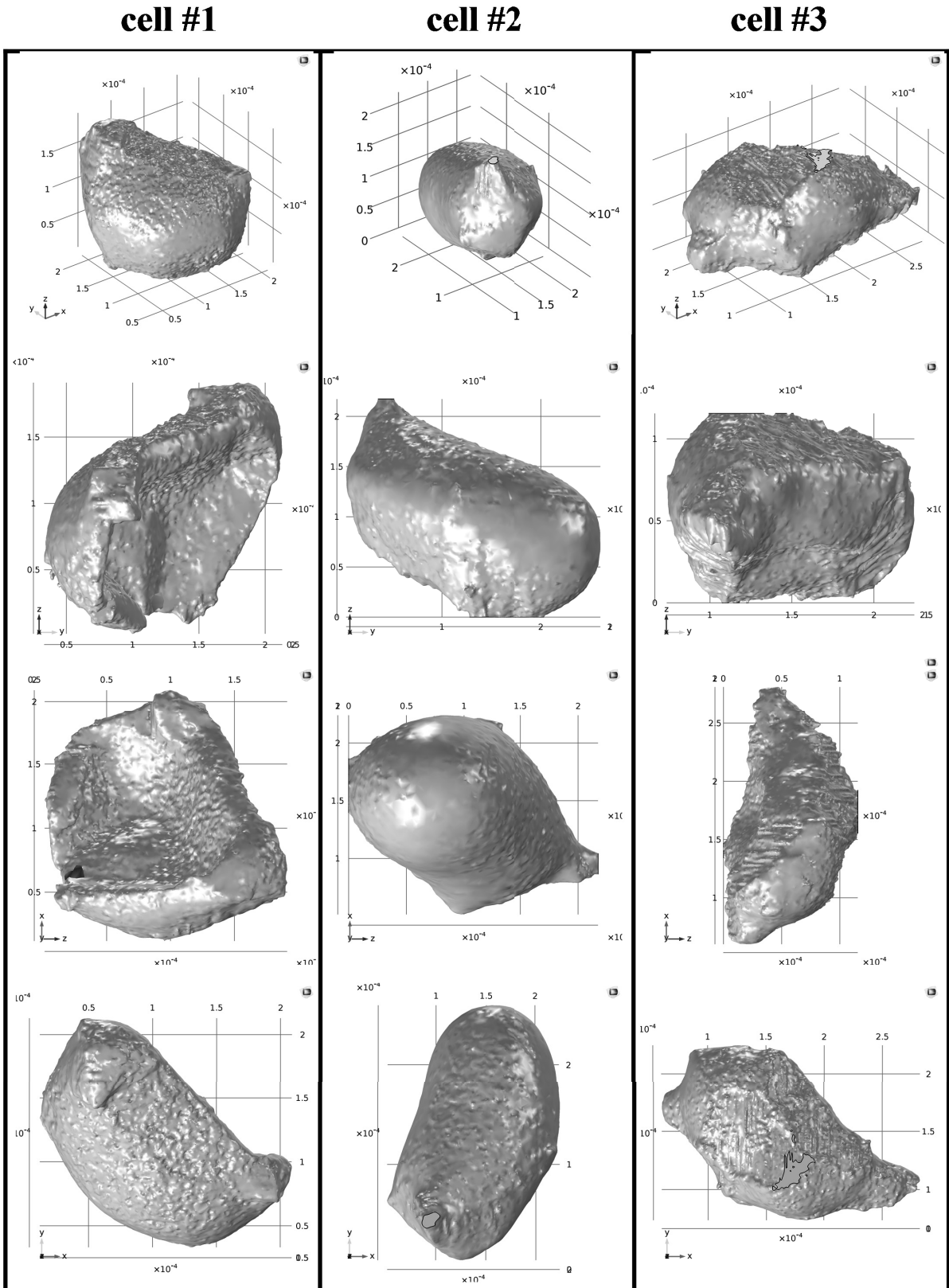


Figure 3: The apple cells here considered, after 3D reconstruction by the COMSOL Multiphysics geometry builder. The second, third, and fourth rows from the top exhibit the apple cells facing one of the cube outlets, when applying the flow boundary conditions associated with $A = 1$, $B = 1$, and $C = 1$, respectively (see METHODS). Dimensions are expressed in meters.

$\phi = 0.1 \%$					
cell	$A = 1$	$B = 1$	$C = 1$	average	RSD
#1	4.47	4.25	4.53	4.42	0.03
#2	2.67	3.42	2.92	3.00	0.13
#3	3.75	3.24	2.92	3.31	0.13

$\phi = 0.4 \%$					
cell	$A = 1$	$B = 1$	$C = 1$	average	RSD
#1	4.55	4.33	4.62	4.50	0.03
#2	2.70	3.46	2.95	3.04	0.13
#3	3.81	3.30	2.97	3.36	0.13

Table 1: Estimates of the intrinsic viscosity α , from the results displayed in Figure 4. RSD stands for relative standard deviation (i.e. coefficient of variation).

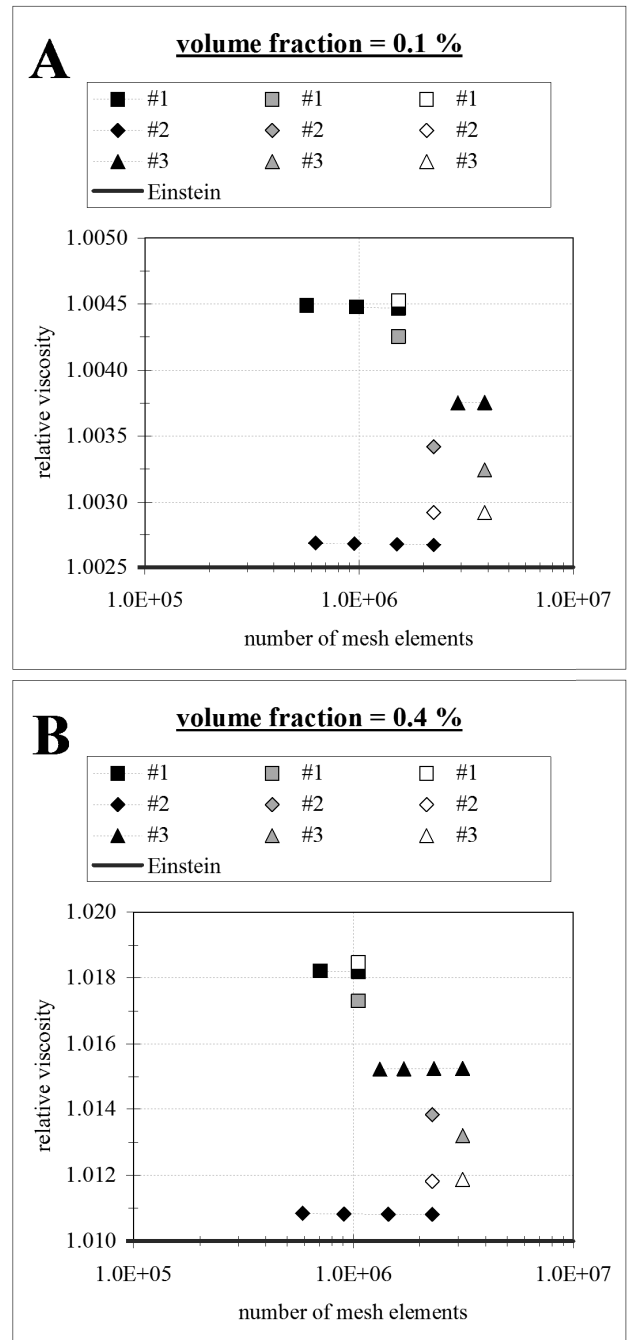


Figure 4: Model predictions of the relative viscosity due to the three apple cells as a function of the number of mesh elements, by assuming a volume fraction of 0.1 % (A) and 0.4 % (B). Blue lines indicate values associated with the Einstein equation (1) for $\alpha = 2.5$. Black, gray, and open symbols indicate results obtained after assuming the flow boundary conditions associated with $A = 1$, $B = 1$, and $C = 1$, respectively.

MODELING OF MICROWAVE HEATING IN A CYLINDRICAL CAVITY SYSTEM: EFFECT OF ROTATION AND SAMPLE LOCATION ON TEMPERATURE UNIFORMITY

Ozan Altin¹, Ferruh Erdogdu^{1*}, Dagbjørn Skipnes² and Torstein Skåra²

¹Department of Food Engineering,
Ankara University
Golbasi-Ankara, 06830 Turkey

* Corresponding author
e-mail: ferruherdogdu@yahoo.com

²Nofima, P.O. Box 8034
4068 Stavanger, Norway

KEYWORDS

Microwave heating, rotational effects, cavity geometry, temperature uniformity

ABSTRACT

In conventional thermal processing, heat transfer is generally carried out by conduction and convection, and significant temperature non-uniformity within the sample is observed. Longer processing times are also required with extensive use of energy. Microwave (MW) heating is an innovative thermal process and accepted to provide volumetric heating compared to the conventional processes by reducing the required process time and energy. However, non-uniform electromagnetic field within the MW cavity leads to a non-uniform temperature distribution within the product. In this study, sample temperature distribution during MW heating was examined as a function of sample location within the MW cavity and rotation rates applied to the sample during the process. In addition, compared to the generally approaches in the literature, a cylindrical cavity was considered. The developed mathematical model was experimentally validated with a comparatively uniform electric field distribution within the cylindrical microwave cavity, and experimental results demonstrated that the location of the sample and the rotational effects significantly influenced the sample temperature distribution. The results of this study is expected to be further used for industrial system design and optimization purposes.

INTRODUCTION

In conventional thermal processing, heat transfer is generally carried out by conduction and convection, and a significant temperature non-uniformity within the sample is observed. Microwave (MW) heating is an innovative thermal process to apply in various food processes from thawing to heating, from pasteurization to sterilization. Microwave frequency range within the electromagnetic spectrum is from 300 MHz to 300 GHz. Federal Communication Commission (FCC) allows 915

MHz (with a wavelength $\lambda=32.79$ cm) and 2450 ($\lambda=12.24$ cm) MHz frequencies for industrial and domestic microwave systems, respectively.

Heating in a microwave cavity occurs when electromagnetic field penetrates the sample. This process is highly affected by dielectric properties of the sample: the dielectric constant (ϵ') representing absorbed electromagnetic energy by the sample and the loss factor (ϵ'') representing the converted electromagnetic energy into heat. Temperature increase, due to the absorption of electromagnetic energy, occurs volumetrically with dipolar rotation and ionic conduction.

MW heating is accepted to provide a volumetric heating compared to the conventional processes and reduce process time. However, non-uniform electromagnetic field in a MW cavity leads to a non-uniform temperature distribution within the product.

In the literature (Zhang and Datta 2005; Raj et al. 2011; Chen et al. 2016), effects of some parameters like applied cyclic or invert power, sample geometry and rotation in a cavity have been focused to determine optimum conditions to obtain a uniform temperature distribution within the sample. In various studies, MW cavity was generally considered to have a rectangular shape with the wave guide opens into the cavity through the sides. Some exceptions for the side – located wave guides were about the use of flatbed microwave systems (Liu et al., 2014). While effects of these parameters on temperature distribution of the samples were generally determined experimentally, interest in mathematical modelling has increased in recent decades to better understand the electromagnetic distribution in the cavity and its interaction with the sample for power absorption and heat generation with the evolved temperature increase. The rotation effect was one parameter often focused in the literature to increase the temperature uniformity of the sample. A number of studies are available that determine the rotational effects on temperature distribution during MW heating (Geedipalli et al., 2007; Raj et al. 2011; Liu et al. 2013; Chen et al. 2016). The rotation in these mathematical models has not been solved continuously, and it was generally assumed to make several angular

movement rather than including a continuous rotation coupled with the electromagnetic and heat transfer physics.

Developing an experimentally validated mathematical model is assumed to be an appropriate approach for process design and optimization purposes (Knoerzer et al. 2008; Erdoğan et al. 2017), and a fully coupled model with rotation might be useful to better determine the effects of sample location within the cavity interacted with the electromagnetic field distribution. Besides the effect of rotation within the cavity, nearly all MW systems consist of a rectangular cavity. Since the electromagnetic field distribution is formed by reflection of electromagnetic waves from the walls of the cavity, the cavity shape might also be considered to have a certain effect.

Therefore, in this study, different sample position (center and off-center) in a cylindrical MW cavity (with a circular cross-section) and continuous rotational effects during process are focused to develop a mathematical model and validate with experimental data within a cylindrical microwave cavity.

MATERIAL AND METHOD

The MW system used in the experiments was built by Gigatherm (Flawil, Switzerland) at 2450 MHz and 1 kW power with an inverter magnetron. Figure 1 shows this system with its computational geometry. Tylose gel (77% moisture content - wb), located in a cylindrical baker (diameter =6.6 cm; height =3.8 cm), was the experimental sample used in the heating experiments. Tylose is widely used in MW and RF experiments as experimental material. Tylose can easily be shape to container shape, also it has dielectric properties similar to meat (Llave et al., 2016).

A mathematical model to determine the electromagnetic field distribution within the system and temperature distribution within the sample was developed using Comsol Multiphysics program (V.5.1 - Comsol AB, Stockholm, Sweden). Dielectric and thermal properties of tylose gel were obtained from Llave et al. (2015, 2016). Sample top surface temperature distribution was obtained using a MobIR® M8 Thermal Camera (Wuhan Guide Infrared Co., Ltd., China) and local temperature measurements were obtained using fiber optic probes in a OPTOCOM AG Fiber Optic Temperature Sensor TS3 (Dresden, Germany) data acquisition system. For model development, microwave heating physics (electromagnetic waves and heat transfer in solids) were coupled with the moving mesh physics. The governing equations solved are listed below with the applied boundary conditions.

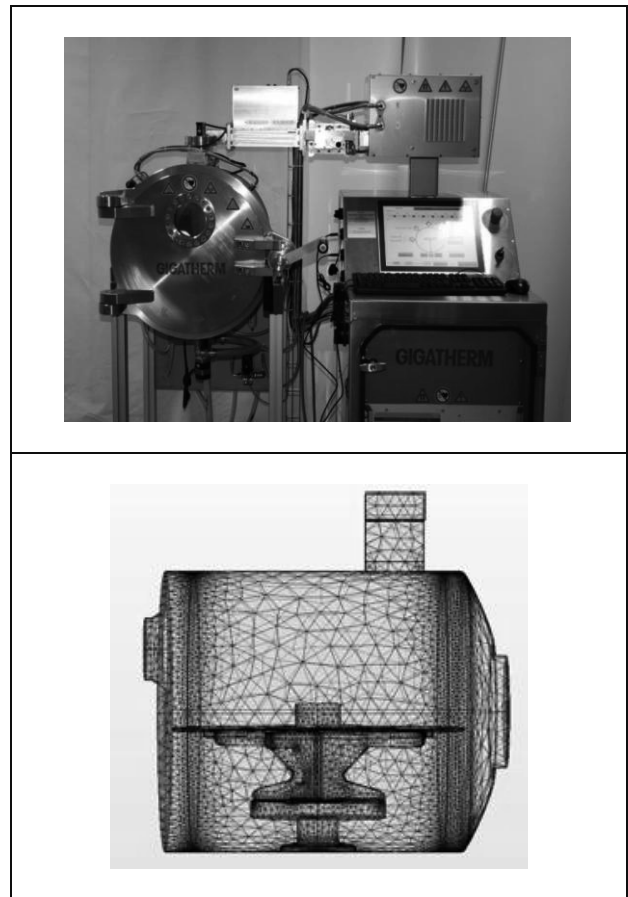


Figure 1. Computational geometry of the microwave system used in the experiments.

Electromagnetic Waves:

- Maxwell equation (1) was used to evaluate electric field distribution in MW cavity:

$$\nabla \times \left(\frac{1}{\mu} \nabla \times \vec{E} \right) - \frac{\omega^2}{c^2} (\epsilon' - i\epsilon'') \vec{E} = 0 \quad (1)$$

where \vec{E} is electric field intensity (V/m), ϵ' dielectric constant of a material, ϵ'' is relative dielectric loss of a material, ω is angular wave frequency ($2\pi f$, rad/s), μ is relative permeability of the material and c is speed of light in free space (3×10^8 m/s).

Boundary conditions:

- Perfect Electromagnetic Conductor for cavity and waveguide walls,
- 2450 MHz frequency, 1 kW power, TE₁₀ mode, rectangular type port,
- Scattering boundary condition for turntable (Teflon material), and
- Dielectric properties of the sample were a function of temperature through the frequency-transient solver.

Heat Transfer in Solid;

- To calculate temperature distribution within product, heat transfer energy equation (2) was solved:

$$\rho c_p \frac{\partial T}{\partial t} = \nabla(k \nabla T) + Q \quad (2)$$

Where absorbed power (3), Q was:

$$Q = \sigma |\vec{E}|^2 = \frac{1}{2} \omega \epsilon_0 \epsilon'' |\vec{E}|^2 \quad (3)$$

and ρ was material density (kg/m³), c_p was specific heat (J/kg-K), k was thermal conductivity (W/m-K), T was temperature (K), and Q was the volumetric heat generation due to the incident microwave energy (W/m³). Equation (3); σ was electrical conductivity of the material (S/m), ϵ_0 was free space permittivity (8.854*10⁻¹² F/m).

Boundary conditions:

- Fixed and uniform initial temperature distribution, and
- Convective heat transfer for surface of sample with a heat transfer coefficient of $h = 25 \frac{W}{m^2K}$.

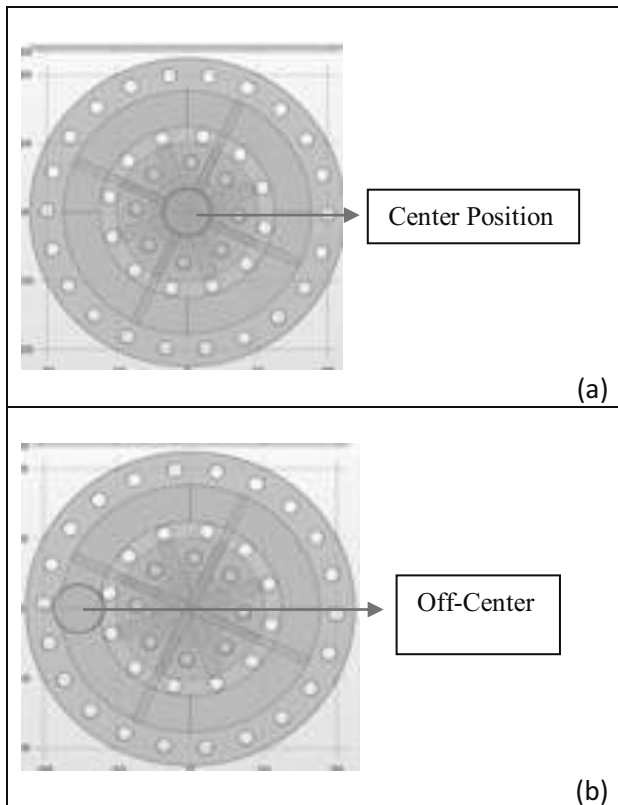


Figure 2. Tylose sample position in the cavity located on the turn-table (a) on-center, (b) off-center.

Moving Mesh;

- Cylindrical coordinate system was used to carry out the continuous rotation process
- The rotation rate was $2 * \pi * rpm * sys2.r$ (where rpm=3.67 rpm (revolutions per minute), measured experimentally and sys2.r was the rotation radius)
- The rotation within the system does not continue in the same direction during the whole process. The rotation movement is performed at clockwise direction for 330°, and then the sample returns to its starting position at a given rotation rate.

The computational geometry (Figure 1) was prepared applying Nyquist criteria (4):

$$S_{max} < \frac{\lambda}{2} = \frac{c}{2f\sqrt{\epsilon'\mu'}} \quad (4)$$

where λ is wavelength (m), f is frequency (Hz), μ' is relative permeability.

This study consisted of 2 steps: for the effect of sample position on the turn-table (on- and off-center; Figure 2) and rotation rate.

RESULTS AND DISCUSSION

Model validation results are shown in Figures 3 to 5. In the first part of the validation experiments, time-temperature data obtained at local measurements were compared with the model results (Figure 3) while, in the second part, thermal camera images of the surface temperature of the sample were compared for on-center with no-rotation (Figure 4) and off-center with rotation (Figure 5).

As can be observed in these figures, the model data correlated well with the experimental results. A better correlation was obtained based on the local temperature measurements while reasonable results were obtained based on the thermal camera measurements. The observed hot spots on top surface of the sample corresponded with the electromagnetic field formed within the cavity (Figure 6). Due to limitations in available computational power, the electromagnetic field was assumed to be in steady state. With the applied moving mesh physics, only the sample within the cavity was forced to rotate at the pre-determined rotation rate. In addition, metal sheets placed on turntable affecting the electromagnetic field distribution was not fully included in the rotating model. Therefore, certain deviance might be observed with the model data and thermal images. For the off-center with rotation, tylose sample faced to a more variable electromagnetic field compared to the center – no-rotation case. Therefore, a more homogeneous temperature distribution was obtained

(Figure 5 vs 4). A continuous rotation was carried out in this study. Chen et al. (2016) used the Matlab program for rotating mash potato, and rotation was carried out step by step rather than as a continuous process.

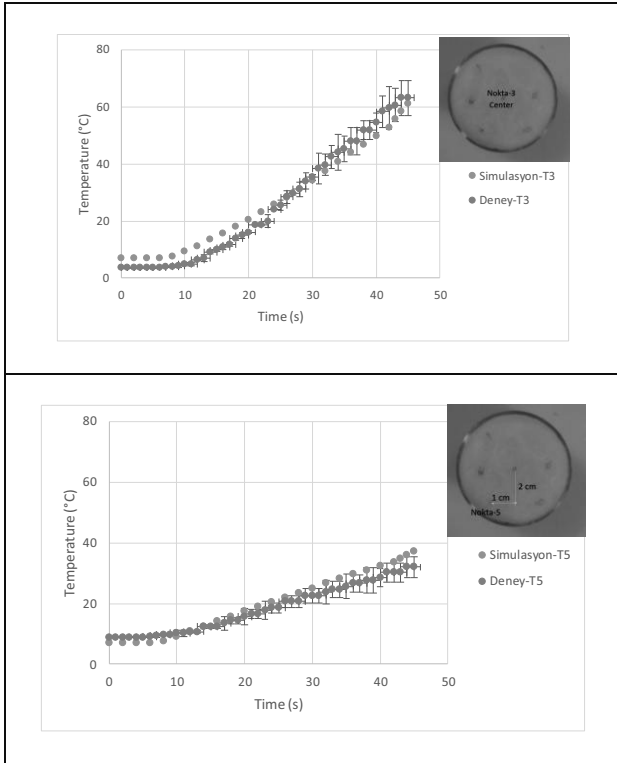


Figure 3. Local comparison of experimentally obtained time temperature data with the model results.

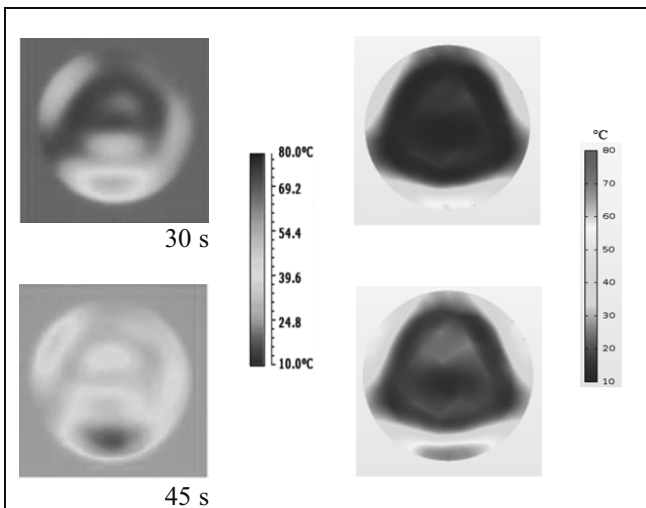


Figure 4. Comparison of surface temperature thermal camera images (left) with model results (right) for on-center with no-rotation at 30 and 45 s of heating.

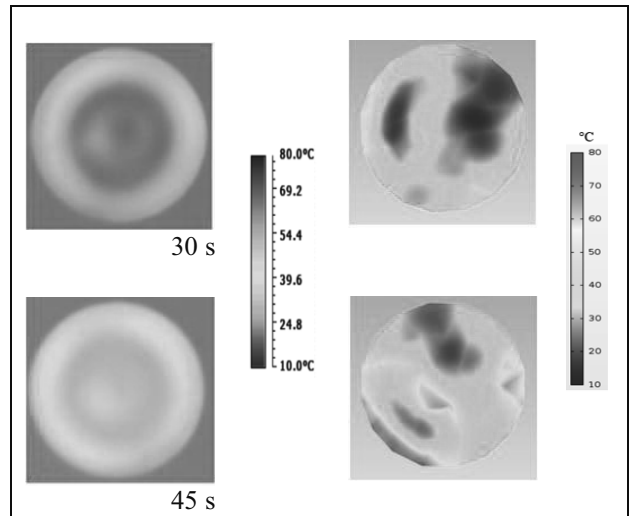


Figure 5. Comparison of surface temperature thermal camera images (left) with model results (right) for off-center with rotation at 30 and 45 s of heating.

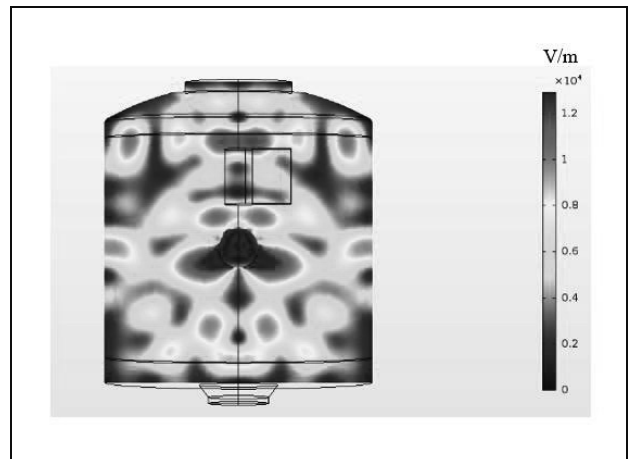


Figure 6. Electromagnetic field formed within the microwave system cavity (xz-view).

The absorbed power by mash potato was reported to oscillate due to rotation, and a similar effect was observed in the current study. Figure 7 shows absorbed power during the process for center no-rotation and off-center with rotation cases. As observed, after the initial heating period, the center sample's power absorption with no-rotation was rather stable while certain oscillations were observed due to the effect of rotation and sample's facing with the variable electromagnetic field distribution during the continuous rotation.

Comparisons for center and off-center cases for rotation and no-rotation processes were also done with respect to center-rotation process (as a more chosen case). Figure 8 shows this comparison. A higher temperature distribution

was obtained for center no-rotation case due to the limited facing of the electromagnetic field compared to the both rotation cases.

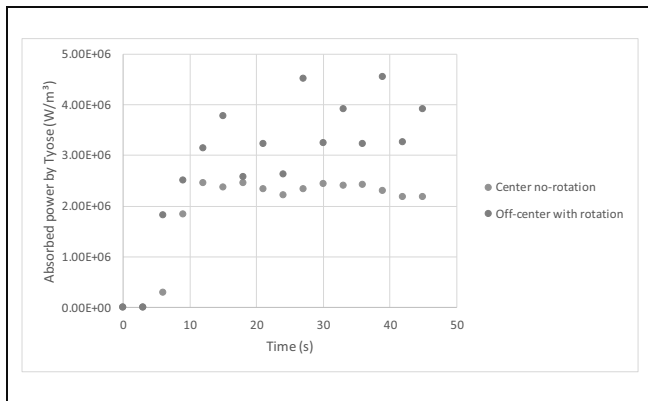


Figure 7. Absorbed power during the process for center no-rotation and off-center with rotation cases.

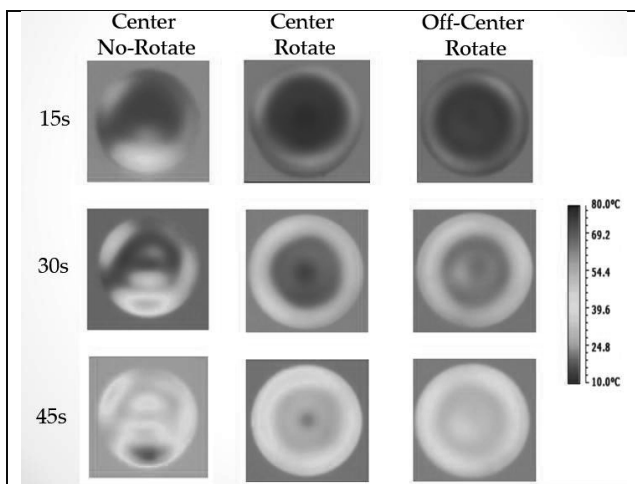


Figure 8. Comparisons for center and off-center cases for rotation and no-rotation processes were also done with respect to center-rotation process

CONCLUSIONS

A mathematical model was developed for MW heating process in a specially designed microwave system. The model was validated with experimental data, and effects of rotation and sample location within the cavity were investigated using the experimental data and validated model results.

Based on these:

- Sample position in the cavity combined with rotation affected the temperature distribution significantly.

- The rotation process enabled a longer facing with the variable electromagnetic field leading to a more uniform temperature distribution over the sample surface. Non-homogenous electric field in the cavity led to hot and cold spots within the sample and especially of the sample surface.
- Due to the facing with the variable field, energy absorbed by the surface of sample oscillated during the process compared to the no-rotation case.

The developed and experimentally validated mathematical model is planned to be used for industrial scale system design and process optimization purposes.

ACKNOWLEDGEMENT

The authors gratefully acknowledge the Erasmus+ Program of the Ankara University through the Ankara Consortium for New Work Experiences (YITAK) for the long-term scholarship to complete this study in Nofima Research Center, Stavanger, Norway. The Norconsery foundation is also kindly acknowledged for funding the project.

REFERENCES

- Chen, F., Warning, A. D., Datta, A. K. and Chen, X. 2016. Thawing in a microwave cavity: Comprehensive understanding of inverter and cycled heating. *Journal of Food Engineering*, 180, 87-100.
- Erdogdu, F.; Altin, O.; Marra, F. and Bedane, T. F. 2017. A computational study to design process conditions in industrial radio-frequency tempering/thawing process. *Journal of Food Engineering*, 213, 99-112.
- Geedipalli, S.S.R.; Rakesh, V. and Datta, A. K. 2007. Modeling the heating uniformity contributed by a rotating turntable in microwave ovens. *Journal of Food Engineering*, 8, 359-368.
- Knoerzer, K.; Regier, M. and Schubert, H. 2008. A computational model for calculating temperature distributions in microwave food applications. *Innovative Food Science & Emerging Technologies*, 9, 374-384.
- Liu, S.; Fukuoka, M. and Sakai, N. 2013. A finite element model for simulating temperature distributions in rotating food during microwave heating. *Journal of Food Engineering*, 115, 49-62.
- Liu, S. Ogiwara, Y., Fukuoka, M. and Sakai, N. 2014. Investigation and modeling of temperature changes in food heated in a flatbed microwave oven. *Journal of Food Engineering*, 131, 142-153.
- Llave, Y.; Liu, S.; Fukuoka, M. and Sakai, N. 2015. Computer simulation of radiofrequency defrosting of frozen foods. *Journal of Food Engineering*, 152, 32-42.

- Llave, Y.; Mori, K.; Kambayashi, D.; Fukuoka, M. and Sakai, N. 2016. Dielectric properties and model food application of tylose water pastes during microwave thawing and heating. *Journal of Food Engineering*, 178, 20-30.
- Raj, J. D.; Birla, S.; Pitchai, K.; Subbiah, J. and Jones, D. 2011. Modeling of Microwave Heating of a Rotating Object in Domestic Oven. *In Excerpt from the Proceedings of the 2011 Comsol Conference*, Boston, MA, USA.
- Zhang, H. and Datta, A. K. 2005. Heating concentrations of microwaves in spherical and cylindrical foods: Part Two: In a cavity. *Food and Bioprocess Processing*, 83(1), 14-24.

Modeling and Simulation in Food Business and Economics

AN EVALUATION OF THE EFFECT OF DIFFERENT TEMPERING CONDITIONS ON DARK CHOCOLATE COMPOSITIONS

Jewel Ann Joseph¹, Jan F.M. Van Impe^{1,*}, Monika Polanska¹
BioTeC+ & OPTEC & BiFTec, Department of Chemical Engineering, KU Leuven
CPMF2, Flemish Cluster Predictive Microbiology in Foods
Gebroeders De Smetstraat 1, B-9000 Gent, Belgium
* E-mail: Jan.VanImpe@kuleuven.be

KEYWORDS

Chocolate tempering, cocoa butter crystallization, temper index

ABSTRACT

The optimal tempering condition to obtain a superior quality chocolate with good contraction, gloss and texture without forming any fat bloom during storage can vary for each product depending on its composition. For a standard chocolate having an average fat dosage, the temper index (TI) for a well-tempered condition is between 4 and 6. This may differ for more extreme recipes such as a high-fat and low-fat chocolate. In such a case, the lesser undercooling required for a high-fat chocolate may become an advantage for minimizing energy consumption within the production line. This study evaluates the effect of tempering conditions on chocolates with different fat compositions by using a standard cocoa butter seed addition (CBSA) technique used by Cargill® and conventional tempering by Aasted temper unit. The results indicated that the high-fat chocolate tempered to TI 2.0 showed an equivalent quality to TI 5.0 in terms of hardness and fat bloom stability whereas, a TI of 7.0 was necessary for the low-fat chocolate to attain a better bloom stability than TI 5.0. Therefore, this study demonstrates that the faster crystallization power of high-fat chocolates and the slower crystallization power of low-fat chocolates necessitates the adaptation of the temper indexes.

INTRODUCTION

Chocolate is produced from *Theobroma cacao* beans and often the manufacturing is considered as a complex process. Chocolate is a complex matrix consisting of fine solids such as sugar and cocoa particles which are dispersed in a fat based continuous medium (Afoakwa, Paterson, Fowler, & Vieira, 2008a) with additional ingredients such as emulsifiers and flavourings. This continuous fat based medium is mostly cocoa butter and its functionality is responsible for the overall quality of a chocolate. High quality chocolates are in extensive demand within the consumers and are marked by properties such as hardness, glossiness and snap. Cocoa butter has at least six crystalline polymorphs (I-VI) characterised by its structure and melting point. Tempering chocolate is required to obtain only form V, the most desirable in terms of it exhibiting the best appearance and taste. This form has a shiny appearance, produces an audible snap when broken, melts in the mouth, and has a smooth texture. Unfortunately, it is not

the most stable of the six morphs and requires tempering in order to maintain the required structure. The sensorial property of this complex product is dependent on the polymorphic behaviour of the fat present within it and $\beta(V)$ is proven to be the right crystal form to provide the best product characteristics (Ollivon, 2004; Timms, 2002). The formation of the various crystalline structures is based on the different triglycerides present within the fat. Cocoa butter, which is a mixture of different triglycerides has the ability to solidify at temperatures below 25°C but can melt easily at body temperature (Whitefield, 2005; Beckett, 2008). The crystallization behaviour of chocolate is greatly influenced by the minor changes in the Triacylglycerol (TAG) profile and the solid fat content within the product. Most of the TAG's are mono-unsaturated which is responsible for the polymorphic behaviour along with small amounts of di-unsaturated, tri-saturated and tri-unsaturated TAG's (Foubert, 2003). A cocoa butter containing more saturated fats solidifies faster (Lechter, 2009). Therefore, the compositional differences within the chocolate are expected to have a severe impact on its structure and bloom stability. This can be the baseline in determining optimal tempering conditions for different chocolate compositions, especially regarding their fat content. Such a plausible condition which is repeatable in the production line may help in reducing the consumption of energy and time

The fat percentage of chocolates generally constitutes between 25% and 35%, and a chocolate having a fat content below 23% is considered as a paste (Beckett, 2000). The recipe of a chocolate has a major influence on the rate of crystal formation during the tempering process (Beckett, 2017; Brown, 2015) and the amount of fat present in the chocolate during manufacture influences the degree of crystallinity and the crystal size distribution (CSD) (Afoakwa, 2010). These crystals can be generated within the chocolate by using a conventional tempering unit and crystal seed addition method. The transition of the crystal forms occurs irreversibly from the least stable α to the most stable triclinic parallel packed $\beta(VI)$ form with density differences and increasing melt temperatures (Martini, Awad, & Marangoni 2006). In a conventional tempering process, ample quantities of chocolate are pumped through a tempering unit which consist of different zones. The temperatures in these zones are controlled for cooling to induce nucleation and crystal growth followed by reheating to eliminate the less stable crystals. The seed tempering process is equipped with a simpler heat exchanger compared to the conventional method. In this method, a precise amount of pre-made

crystal seeds are added into the chocolate maintained below 34°C to ensure $\beta(V)$ crystals. The seed tempering technique is expected to generate a well-tempered chocolate by the addition of 0.2-1% of crystal seeds. Kinta and Hartel (2009) studied the influence of the quantity of seeds added on the tempering quality. The study showed that the higher the amount of crystals added into the chocolate, faster is the crystallization. Such a condition resulted in a faster formation of smaller β crystals. The addition of pre-made seeds in the molten chocolate provides multiple nucleation sites (Svanberg, Ahrné, Lorén, and Windhab, 2011). The bloom formation seen on the under tempered chocolates having fewer amount of seeds are caused by the phase separation of both particles and fat occurring during the crystal growth.

A substantial amount of research is carried out in the field of chocolate tempering and the crystallization in chocolates. However, there is limited study performed on the utilization of a multi-stage tempering unit for attaining good tempering conditions for varied dark chocolate compositions and its impact on the physical properties. This may be because a tempering unit principally functions as a heat exchanger to build crystals within a product and the processing conditions required for each machine can be unique. It will depend on various process parameters for which no standard condition is used hitherto.

MODELLING OF CRYSTALLIZATION KINETICS OF FATS

The crystallization kinetics of fats (particularly the rate of crystallization and the rate of change from one polymorph to another) are as important as the equilibrium behaviour of fats and their mixtures since they are relevant to real systems of chocolate production. While the fundamentals of nucleation, fat crystallization and polymorphism are widely covered in the literature, modelling of the crystallization kinetics of fats could be more emphasized and explored. A number of different models exist to describe the kinetics however, they allow only to certain extent for controlled operations concerning crystallization of fat components under certain conditions. These equations find their basis in thermodynamics and because thermodynamic properties are not often known, they are thereby not always easy to use in practice. Several models have been proposed by different authors over the years: the Avrami model and to a lesser extent the Gompertz model, are most popular however, neither of the models are being perfect. The Avrami model (Kawamura, 1979, Dibildox-Alvarado & Toro-Vazquez, 1997, Kerti, 1998, Metin & Hartel, 1998, Toro-Vazquez et al., 2000) was the first one to be used on isothermal cocoa butter crystallization by Ziegleder (1990). However, this model is limited to a single component system. The right type, size and the amount of crystals determine the correct solidification and melting properties of a chocolate. The Avrami model (and its modifications) is the most widely used approach for the description of isothermal phase transition kinetics and provides a theoretical basis with underlying assumptions, which are not often met in the

case of fat crystallization. Therefore, it is important to understand the influence of the various ingredients and processes on the physical and sensorial properties of the chocolate to ensure superior quality. Some authors use a modified Avrami equation, also called the Avrami-Erofeev equation (Herrera et al., 1999a, Herrera et al., 1999b, Ng & Oh., 1994 and Toro-Vazquez & Dibildox-Alvarado, 1997). On the other hand, the Gompertz model provides a better fit by a straightforward physical interpretation of the parameters, however has a weak theoretical basis. Kloek et al. (2000) and Vanhoutte (2002) used a reparameterized Gompertz equation to describe their crystallization curves. Berg and Brimberg (1983) proved that empirical equations used for aggregation and flocculation can also be used to describe fat crystallization. There is certainly a need to develop a new model to describe the crystallization kinetics of fats. Foubert et al. (2002) described a new model in the form of differential equation allowing use under dynamic temperature variations. It describes the crystallization process as if it is a reversible reaction with a first order forward reaction and a reverse reaction of order n . The model provides an analytical solution under isothermal conditions that simplifies parameter estimation. Following this an extension of the Foubert model has been developed to facilitate the description of two-step processes (Foubert et al., 2006). The model is built based on the assumptions of the presence of an isosbestic point indicating that the first step involves crystallization of part of the melt in the α polymorph and the second step involves a polymorphic transformation from α to β' with no β' crystals formed directly from the melt. Performed simulation experiments demonstrated the role of different model parameters and proved that parameter estimation on the different data sets resulted in a good fit.

AIM

This study describes the pre- and post-crystallization of dark chocolates with high and low-fat compositions and its influence on the final product quality. Modelling is proposed as a future perspective requiring further studies and research.

MATERIALS AND METHODS

All the chocolate samples used in this study were manufactured by Cargill cocoa and chocolate, Moeskroen, Belgium. This study focused on dark chocolates containing high and low fat to determine the influence of the amount of fat content on tempering conditions and the product quality. Standard chunks of dark chocolate were kept in an oven overnight at 45-50°C to ensure the complete melting of crystals present in the chocolate, which could otherwise influence the tempering process.

The study involved two different tempering methods: (i) CBSA (Cargill protocol) and (ii) Conventional tempering (AMC50-CTS, DK-3520, Aasted-Mikroverk ApS, Farum, Denmark). Both the methods were applied on each chocolate recipe to attain a TI of 2.0 and 5.0 for high-fat, and a TI of 5.0 and 7.0 for a low-fat sample. The temper

quality was determined by using a temper meter (MultiTherm TC, Buhler, Switzerland). The quality of the final product was confirmed by conducting a texture analysis (TA-XT plus Stable Micro Systems, Surrey, England) and fat bloom evaluation both visually and using a scanning electron microscope (Hitachi Tabletop Microscope TM-1000, Tokyo, Japan). The solidification kinetics of the chocolate was measured using MCR 302 (Anton Paar GmbH, Ostfildern, Germany). The trend for demouldability observed in the rheological method was compared with a lab-scale cooling process utilizing pre-conditioned polycarbonate moulds of dimension 100×50×5 mm (type CW 2017, Chocolate World, Antwerp, Belgium) in a climate chamber (CTS GmbH, Hechingen, Germany).

RESULTS AND DISCUSSION

Tempering by CBSA Method

The standard method currently used by Cargill involves the addition of approximately 1% of crystal seeds. However, during the study it was noticed that a TI of 5.0 was obtained for the high-fat chocolate with 0.75% crystal seeds while compared to a low-fat chocolate which required 1%.

Tempering by Aasted Temper Unit

The Aasted temper unit consists of three zones with heat exchange plates which are equipped with scrapers to ensure a controlled heat exchange within the chocolate. A TI of 5.0 ± 0.1 was achieved for the high-fat chocolate by adjusting the zone 1, 2 and 3 temperatures to 33.5°C, 23.8°C and 29.5°C respectively with a scraper speed of 100%. To attain a TI of 2.0 ± 0.1 , the zone 2 and 3 temperatures were increased. Similarly, for a low-fat chocolate a TI of 5.0 ± 0.4 and 7.0 ± 0.3 was achieved by adjusting the zone 2 and 3 temperatures.

Evaluation of Solidification Kinetics Using Rheometer

A rheological analysis was performed for high-fat and low-fat chocolates to analyse the solidification kinetics and the demouldability of tempered chocolate. The crystallization speed attained from the rheological study showed that the onset of contraction and the total time for demouldability changes within the same recipe when subjected to different temper indexes. The total time for solidification and demoulding is longer for the chocolate with TI 2.0. In the case of the low-fat chocolates, the TI 7.0 shows faster induction than TI 5.0. Therefore, a faster solidification and demoulding is noticed for the chocolate with TI 7.0.

Cooling and Demouldability of Tempered Chocolates

The tempered chocolates from CBSA method and Aasted were cooled under two different temperatures and relative humidity (RH) to determine the demouldability time. These included cooling at $10 \pm 1^\circ\text{C}/55\%$ and $20 \pm 1^\circ\text{C}/35\%$ in climate chambers. The aim of this method was to select the best parameter attained from the detachment of chocolate during realistic cooling that can be correlated to the results attained from the rheological method. The two parameters determined during the realistic cooling were

the onset time of detachment and the time for complete detachment of chocolate from the mould. The high-fat dark chocolates tempered to TI 2.0 and 5.0 by CBSA were cooled at 20°C and 10°C. It was seen from the results that the chocolate tempered to TI 2.0 exhibited a slower onset of detachment compared to TI 5.0 when cooled at 20°C. A similar trend was noticed for the onset and the complete detachment of the chocolates at TI 2.0 when cooled at 10°C as shown in Figure 1.

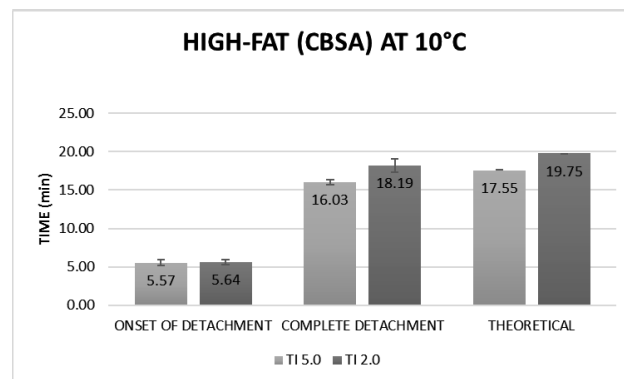


Figure 1: Onset of detachment, complete detachment and theoretical point of demouldability for high-fat chocolates tempered to TI 5.0 and TI 2.0 by CBSA method and cooled at 10°C

The low-fat dark chocolate when tempered to TI 5.0 and 7.0 were cooled at 20°C and 10°C. The chocolate with TI 7.0 when cooled at 20°C exhibited a slower onset of detachment than the TI 5.0. However, as seen in Figure 2, the TI 7.0 showed a faster onset and complete detachment from the mould than TI 5.0 when the chocolate was cooled at 10°C. Hence, the best parameters that can be correlated well with the theoretical point of demouldability attained from the rheometer measurements are the onset time of detachment and time for complete detachment from realistic cooling as shown in Figures 1 and 2.

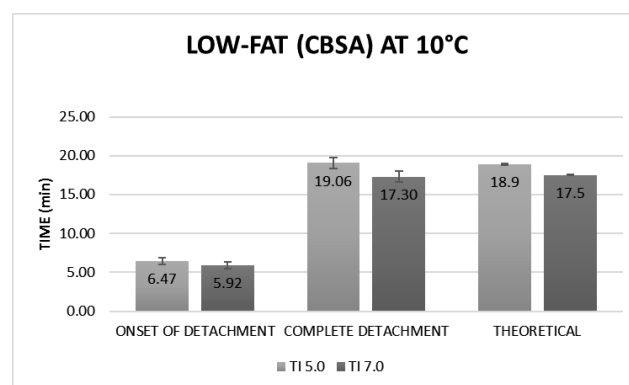


Figure 2: Onset of detachment, complete detachment and theoretical point of demouldability for TI 5.0 and TI 7.0 of low-fat chocolates tempered by CBSA and cooled at 10°C

Hardness of Chocolate

The hardness of the high-fat (TI 2.0 and TI 5.0) and low-fat (TI 5.0 and TI 7.0) chocolates tempered by CBSA and Aasted method were determined by conducting a texture analysis. A notable difference was not observed in terms of hardness within similar recipes having different temper indexes using both methods as indicated in the Figures 3 and 4.

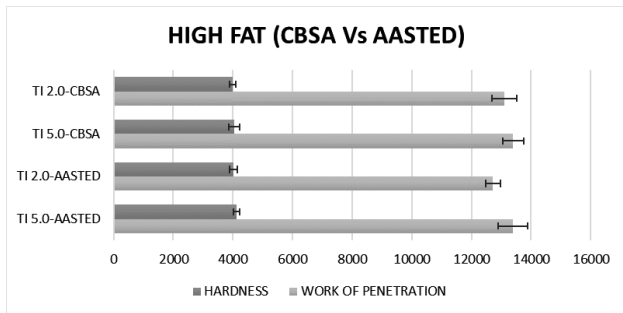


Figure 3: Comparison of hardness measurements of CBSA and Aasted tempered samples of high-fat chocolate using texture analyser

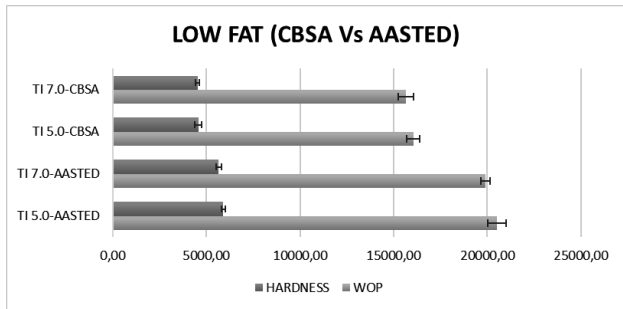


Figure 4: Comparison of hardness measurement of CBSA and Aasted tempered samples of low-fat chocolate using texture analyser

Fat Bloom Analysis

Two sets of samples were prepared for each chocolate type by the CBSA and Aasted method which were cooled in a climate chamber at $20^{\circ}\text{C}\pm 1^{\circ}\text{C}$ with 35% RH. The tempered high-fat (TI 2.0 and 5.0) and low-fat (TI 5.0 and TI 7.0) dark chocolates showed good gloss and demouldability directly after cooling. A chocolate bar from each set was stored in climate chambers controlled at $25^{\circ}\text{C}/40\%$ and $20^{\circ}\text{C}/35\%$ (the reference) respectively after demoulding. The samples stored at 25°C were compared with the samples at 20°C from day 1 up to 3 months to record the changes in their appearance. A scale from 0 to 4 was used for the visual evaluation of fat bloom in the tempered dark chocolates which is in accordance with a protocol followed by Cargill. The bloomed samples were evaluated using the electron scanning microscope to compare with the standard. The consolidated results from the visual evaluation of high-fat and low-fat samples as shown in Table 1 indicated similar blooming stability for high-fat chocolate tempered to TI 2.0 and TI 5.0. However, it was noticed that the low-fat chocolate with TI 7.0 exhibited a better bloom stability in comparison with TI 5.0.

Table 1: Consolidated results from the visual evaluation of CBSA and Aasted tempered samples cooled at 20°C

SAMPLE	TI	STABILITY
HIGH-FAT	2.0	Similar
	5.0	Similar
LOW-FAT	5.0	Low
	7.0	High

The SEM analysis showcased similar results as the visual evaluation. It was seen from the SEM images as shown in

Figures 5 and 6 that the bloom formation in high-fat chocolate with TI 2.0 and 5.0 were similar whereas, in the case of low-fat chocolate a TI of 7.0 showed less bloom compared to TI 5.0.

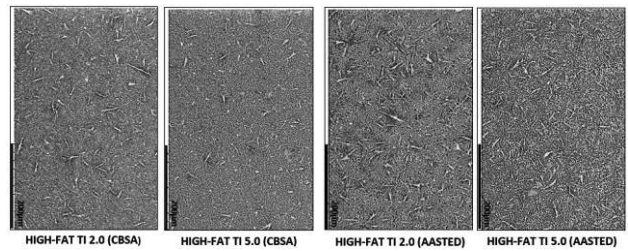


Figure 5: SEM images of CBSA and Aasted tempered samples of high-fat chocolate cooled at 20°C

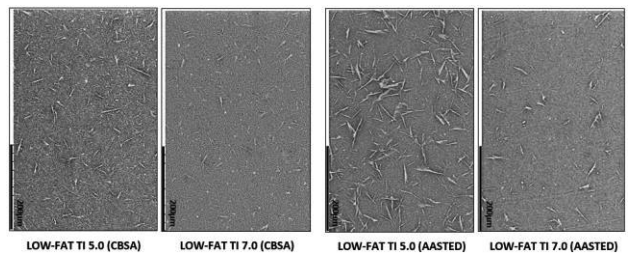


Figure 6: SEM images of CBSA and Aasted tempered samples of low-fat chocolate cooled at 20°C

CONCLUSION AND FUTURE PERSPECTIVES

Several discrepancies were noticed for the Aasted tempered high and low-fat chocolates. However, a more homogeneous tempering achieved by the seed addition method showed almost equivalent characteristics for both chocolates when tempered to varied temper indexes. The onset time of detachment and time for complete detachment was determined during cooling and was chosen as the best parameters which can be compared to the theoretical point of demouldability attained from the rheometer analysis. The high-fat chocolate tempered to TI 2.0 by CBSA exhibited an equivalent bloom stability compared to TI 5.0. However, a variation was observed for these chocolates when tempered using the Aasted machine followed by a slow cooling. It was noticed that TI 2.0 bloomed faster than TI 5.0 in this case. It may imply that the chocolate was tempered too low within the Aasted and a higher TI of 3.0 might be required to produce a well-tempered chocolate. But, considering a homogeneous tempering such as the CBSA method, the results confirm that the high-fat chocolate when tempered to TI 2.0 can exhibit the properties of a well-tempered chocolate such that a TI of 5.0 is not required. In the case of the low-fat chocolate the results indicated that a TI of 7.0 requires a lower induction time compared to TI 5.0. The fat bloom study which is an appropriate method to analyse the quality of a tempered chocolate clearly reveals that the low-fat chocolate tempered to TI 7.0 exhibit a higher stability than TI 5.0. The optimization of cooling at 10°C by the installation of a camera inside the climate chamber favoured a controlled cooling of the chocolate without the need for opening the door of the cooling unit. However, various parameters mainly, the cooling rate influences the time required for the chocolate to detach

from the mould and this may differ in an industrial cooling tunnel. Therefore, it would be ideal to perform an industrial cooling study to achieve a corroboration for the lab-scale findings.

In conclusion, the present study showed that a lower TI of 2.0 for the high-fat and a higher TI of 7.0 for the low-fat chocolates, still delivered a good temper quality similar to a well-tempered standard recipe with TI 5.0. Therefore, by knowing the differences in crystallization power of a chocolate recipe, the temper index needs to be adjusted to achieve an optimally tempered chocolate. It was possible to elucidate in this study that a high-fat chocolate with higher crystallization power can be tempered to a TI of 2.0 instead of TI 5.0 and a low-fat chocolate with a lower crystallization power is required to be tempered to a TI 7.0 instead of TI 5.0 to achieve a well-tempered chocolate.

Modelling approach of crystallization kinetics of fats should further be studied to improve and modify the existing models. While the fundamentals of nucleation, fat crystallization and polymorphism are widely covered in the literature, modelling of the crystallization kinetics of fats could be more emphasized and explored. The existing models and their modifications allow to certain extent for controlled operations concerning crystallization of fat components under certain conditions, neither of the models is however being perfect.

ACKNOWLEDGEMENTS

This work was funded by Cargill R&D Centre, Brussels under the European Master of Science in Food Science, Technology and Business (BiFTec) co-funded by the Erasmus+ Programme of the European Union. We are grateful to Jeroen De Paepe (Cargill) and Ellen Huizenga (Godiva Chocolatier) for their support in the successful completion of this project.

REFERENCES

Afoakwa, EO., Alistair P., and Mark F., and Joselio V. 2008a. "Particle size distribution and compositional effects on textural properties and appearance of dark chocolates", *Journal of Food Engineering*, 87(2), 181-190.

Afoakwa, EO. 2010. *Chocolate Science and Technology*, 1st edition, Chichester, U.K, John Wiley & sons Ltd.

Beckett, ST. 2008. *The Science of Chocolate*, 1st edition, Cambridge, U.K., The Royal Society of Chemistry Publishing.

Beckett, ST., Fowler, MS., and Ziegler, GR. 2017. *Beckett's Industrial Chocolate Manufacture and Use*, 5th edition, Oxford, U.K., Wiley-Blackwell publishing.

Beckett, ST. 2000. *The Science of Chocolate*, Vol. 22, London U.K., The Royal Society of Chemistry Publishing.

Berg, TGO., and Brimberg, UI. (1983). "Über die Kinetik der Fettkristallisation", *Fat Science Technology*, 85, 142-149.

Brown, A. 2015. *Understanding food: principles and preparation*, Stamford, CT: Cengage Learning.

Dibildox-Alvarado, E., and Toro-Vazquez, JF. 1997. "Isothermal crystallization of tripalmitin in sesame oil", *Journal of the American Oil Chemists' Society*, 74, 69-76.

Foubert, I., Vanrolleghem, P., Vanhoutte, B., and Dewettinck, K. 2002. "Dynamic mathematical model of the crystallization kinetics of fats", *Food Research International*, 35, 945-956.

Foubert, I. 2003. "Modelling isothermal cocoa butter crystallization: influence of temperature and chemical composition" Gent, Universiteit Gent.

Foubert, I., Dewettinck, K., Janssen, G., Vanrolleghem, PA. 2006. "Modelling two-step isothermal fat crystallization", *Journal of Food Engineering*, 75, 551-559

Herrera, ML., De Leon Gatti, M., and Hartel, RW. 1999a. "A kinetic analysis of crystallization of a milk fat model system", *Food Research International*, 32, 289-298.

Herrera, ML., Falabella, C., Melgarejo, M., and Anon, MC. 1999b. "Isothermal crystallization of hydrogenated sunflower oil: II. Growth and solid fat content", *Journal of the American Oil Chemists' Society*, 76, 1-6.

Kawamura, K. 1979. "The DSC thermal analysis of crystallization behavior in palm oil", *Journal of the American Oil Chemists' Society*, 56, 753-758.

Kerti, K. 1998. "Thermal analysis of cocoa butter and cocoa butter alternatives. Crystallisation using DSC Method", 2nd International workshop on control applications in postharvest and processing technology, Budapest, Hungary, June 3-5, 1998, p.173-176.

Kinta, Y., and Hartel, RW. 2010. "Bloom Formation on Poorly-Tempered Chocolate and Effects of Seed Addition", *Journal of the American Oil Chemists' Society*, 87(1), 19-27.

Kloek, W., Walstra, P., and Van Vliet, T. 2000. "Crystallization kinetics of fully hydrogenated palm oil in sunflower oil mixtures", *Journal of the American Oil Chemists' Society*, 77, 389-398.

Lechter, A. 2009. "Tempering chocolate - a review", *The manufacturing confectioner*, 53-58. <http://www.gomc.com/firstpage/200901053.pdf>

Martini, S., Awad, T., and Marangoni, AG. 2006. "Chapter 8: Structure and properties of fat crystal networks". In *Modifying Lipids for Use in Food*, 1st edition, 142-69.

Metin, S., and Hartel, RW. 1998. "Thermal analysis of isothermal crystallization kinetics in blends of cocoa butter with milk fat or milk fat fractions", *Journal of the American Oil Chemists' Society*, 75, 1617-1624.

Ng, WL., and Oh, CH. 1994. "A kinetic study on isothermal crystallization of palm oil by solid fat content measurements", *Journal of the American Oil Chemists' Society*, 71, 1135-1139.

Ollivon, M. 2004. "Chocolate, a mysteriously appealing food", *European Journal of Lipid Science and Technology*, 106(4), 205-06.

Svanberg, L., Ahrné, L., Lorén, N. and Windhab, E. 2011. "Effect of sugar, cocoa particles and lecithin on cocoa butter crystallisation in seeded and non-seeded chocolate model systems", *Journal of Food Engineering*, 104(1), 70-80.

Timms, RE. 2002. "Oil and fat interactions Theory, problems and solutions", *The Manufacturing Confectioner*, 82(6), 50-64.

Toro-Vazquez, JF., and Dibildox-Alvarado, E. 1997. "Parameters that determine tripalmitin crystallization in sesame oil", *Journal of Food Lipids*, 4, 269-282.

Toro-Vazquez, JF., Briceno-Montelongo, M., Dibildox-Alvarado, E., Charo-Alonso, M., and Reyes-Hernandez, J. 2000. "Crystallization kinetics of palm stearin in blends with sesame seed oil", *Journal of the American Oil Chemists' Society*, 77, 297-310.

Vanhoutte, B. 2002. "Milk fat crystallisation: fractionation and texturisation", PhD thesis, Gent, Belgium, Ghent University, 365p.

Whitefield, R. 2005. *Making chocolates in the factory*, 1st edition, London, UK Kennedy's Publications Ltd.

Ziegler, G. 1990. "DSC-Thermal analysis and kinetics of cocoa butter crystallization", *Fett Wissenschaft Technologie - Fat Science Technology*, 92(12):481-485

TECHNO-ECONOMIC EVALUATION OF β -CYCLODEXTRIN PRODUCTION FROM CASSAVA TUBERS

Nikolaos Vacharakis, Anastasia Louizaki, Chrysi Charalambous, Stylianos Raphaelides and Alexandros Koulouris*

Department of Food Technology
Alexander Technological Education Institute
P.O. Box 141, 57400 Thessaloniki
Greece

*E-mail: akoul@food.teithe.gr

KEYWORDS

Cassava, Cyclodextrins, Techno-Economic Analysis, Process Simulation.

ABSTRACT

Cassava is one of the most important food crops in wet tropical places containing one of the most pure forms of starch (called tapioca). Cyclodextrins are products resulting from a simple enzymatic conversion of starch (a renewable natural material) and used in a variety of applications in the food and pharmaceutical industry. The objective of this paper is to present a techno-economic feasibility study for the production of β -cyclodextrin from tapioca starch obtained from cassava tubers. The proposed process with a capacity of 20 metric tons/h of cassava was modeled in SuperPro Designer v10 (a process design software tool). The results obtained by solving the mass and energy balance equations (to calculate the material and energy requirements and estimate the process yield) and performing economic calculations are presented and discussed. The analysis indicates that the proposed plant requiring capital investment of approximately 65 million € presents an economically viable process with revenues around 113 million €/yr and operating expenses around 75 million €/yr.

INTRODUCTION

Cassava (*Manihot esculenta*), also called manioc or yuca, is one of the most important food crops in wet tropical places, particularly suited to low availability of nutrients in the soil and able to survive drought. It is one of the oldest crops of products from South America, but nowadays it spreads to all the tropical and subtropical regions of the planet. Although the leaves of the cassava are sometimes consumed, the main edible part is the tuber, which is essentially the root of the plant (Tonukari, 2004). A significant limitation of cassava production is the rapid alteration of the tuber after harvesting which limits tuber storage only to a few days (Tonukari, 2004).

Although cassava is an important food, it contains toxic and antiseptic substances that interfere with the digestion and intake of nutrients. Cyanogens are found in 3 forms in the cassava, in cyanogenic glycoside (95% linamarin and 5% in lotaustratin), cyanohydrins and free cyanide (Montagnac et al., 2009).

Over two-thirds of total cassava production is used as food for humans, while the rest is used for industrial purposes (Tonukari, 2004). Cassava is also used for the production of a starch called tapioca which is a basic food in many parts of the world. The starch content of a new cassava root ranges from 25-30%. Tapioca is one of the most pure forms of starch and production varies from region to region. Commercially, starch is converted into various forms: hot soluble powder, pre-cooked thin or thick flakes, rectangular sticks and spherical "pearls" (Gustafson, 2015). Tapioca starch can be converted to maltotriose, maltose and glucose as well as other modified sugars and organic acids. It can be used to prepare fructose syrups and to form gelatin capsules. The use of tapioca as a raw material for the production of ethanol for fuel is already being investigated and is very promising (Gustafson, 2015).

Cyclodextrins are a group of cyclic oligosaccharides. The most well-known natural cyclodextrins are α -, β - and γ -cyclodextrins: α -cyclodextrin consists of 6 molecules of glucopyranose, β -cyclodextrin of 7 and γ -cyclodextrin of 8. They are produced from starch (a renewable natural material) through a multi-step enzymatic process involving different enzymes with cyclodextrin glycosyltransferase (CGTase) produced by microorganisms such as *Bacillus macerans* and *Bacillus circulans* being the most commonly used enzyme. Today, with the help of genetic engineering, a series of enzymes specialized for the industrial production of cyclodextrins have been developed.

The food and drug industries are the main users of cyclodextrins because of their favorable properties which include: stability at high processing temperatures, resistance to oxidation and thermal denaturation, color stability and ease of handling. The food industry in particular consumes 80-90% of world production of cyclodextrins in foods for a variety of purposes: (i) to protect lipophilic food ingredients that are sensitive to oxygen and light and heat; (ii) to stabilize fragrances, flavors, vitamins and essential oils from degradation, (iii) to suppress unpleasant flavors and odors; (iv) to convert the liquid food ingredient into a solid powder; (v) to dissolve vitamins and food color; (vi) to control the release of certain food ingredients and remove contaminants (vii) to preserve the quality of the food during storage with improved packaging technology. There are several regulatory principles that control the use of various cyclodextrins regarding safety (GRAS, Generally Recognized as Safe), addition limit, acceptable daily intake, etc. The molecular

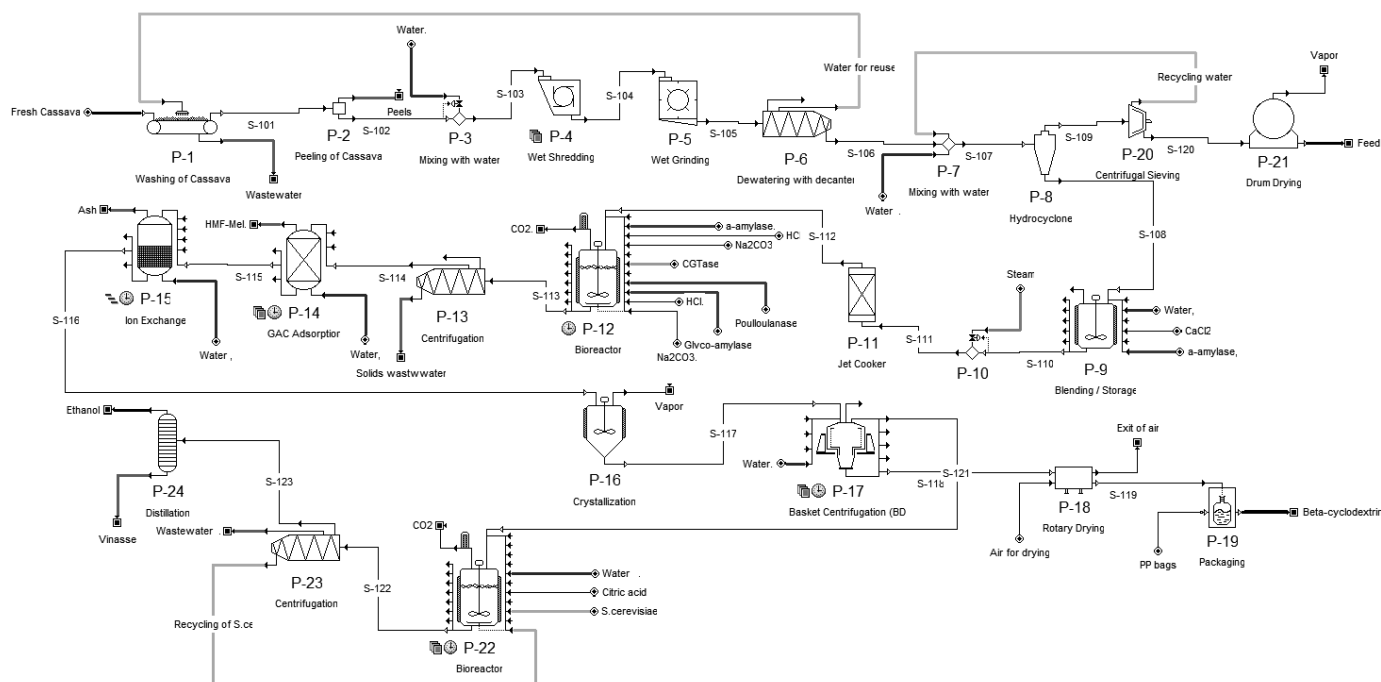


Figure 1. Process Flowsheet for a Plant Producing β -Cyclodextrin from Cassava Tubers

encapsulation of flavor components in the cyclodextrin cavity has proven to be the most effective method of stabilizing the taste in food and thus providing protection from heat and evaporation (Li et al., 2014; Das, 2013; Saenger, 1980).

Cyclodextrins are not metabolised as fast as starch. This is because they break down more slowly into linear C-1,4 glucanohydrate dextrans and are not hydrolyzed by enzymes that affect the end groups. All toxicity tests have shown that the oral consumption of α - and γ -cyclodextrin is harmless. According to the FAO reports, enzymatically modified starch derived from cyclodextrins is also toxicologically harmless. (<http://www.fao.org>)

Council Regulation (EU) 231/2012 states that β -cyclodextrin (E 459) is produced by the action of CGTase obtained from *B. circulans*, *P. macerans* or the *B. licheniformis* SJ1608 recombinant strain for partially hydrolyzed starch. Only the bacterial species listed in Regulation (EU) No 231/2012 can be used.

Beta-cyclodextrin (E 459) is a food additive approved in accordance with Annex II and Annex III to Regulation (EC) No 1333/2008. Council Regulation (EC) (EC) No 1333/2008 and the specific purity criteria are laid down in Commission Regulation (EU) 231/2012. In 1996, the Scientific Committee on Food (SCF) evaluated the safety of β -cyclodextrin as a carrier and stabilizer, produced by the activity of glucose-transferase (CGTase) obtained from *Bacillus circulans* in partially hydrolysed starch. The recommended maximum level of β -cyclodextrin intake from food is 5 mg per kg of body weight per day. For α - and γ -cyclodextrins no acceptable daily intake (ADI) was reported due to their non-toxicological profiles (www.efsa.europa.eu).

For the industrial production of cyclodextrins, starches with high amylopectin content are preferred. Corn and wheat starches contain higher percentage of amylose and impurities and are therefore not suitable. Tapioca starch and waxy corn starch consist of almost 80% amylopectin and would be ideal substrates.

Two different types of cyclodextrin production processes can be identified: solvent and non-solvent processes. In solvent processes, an organic complexing agent precipitates selectively one type of cyclodextrin and drives the enzymatic reaction to produce mainly this type of cyclodextrin. In non-solvent processes, no complexing agent is added and, therefore, a mixture of different cyclodextrins is produced with their relative ratio being dependent on the CGTase used and on the reaction conditions. Because of the lower enzymatic reaction yield and the production of a mixture of cyclodextrins, non-solvent processes compared with solvent processes require a more complex downstream purification process (including a crystallization step), have higher energy demands and produce a large number of by-products. However, non-solvent processes avoid all the drawbacks resulting from the use of a potentially flammable, toxic or expensive solvent whose presence in the final product may limit its usability in food applications. In addition, the cost of cyclodextrin production is high if the solvent isn't nearly completely recovered and reused making solvent processes quite expensive especially if solvents with high boiling point are used (Biewer et al., 2002).

The objective of this paper is to present a complete techno-economic feasibility study for the production of β -cyclodextrin from tapioca starch obtained from cassava tubers and evaluate its potential for commercial production. The proposed technology is a non-solvent process which yields a product free of toxic solvent residues while

exploiting most by-products in an attempt to annihilate the economic drawbacks of non-solvent processes.

The proposed process flow sheet was developed and solved on SuperPro Designer v10, a commercial process simulation software tool by Intelligen, Inc. (www.intelligen.com). The use of SuperPro Designer as a simulation tool for designing pharmaceutical, biotech, food and other types of processes has been reported in numerous publications in the scientific and technical literature. However, there exist only few reported SuperPro Designer models using cassava as raw material (Knight, 2011; Quintero et al., 2015) and, to the best of our knowledge, none for the production of cyclodextrins.

A thorough description of the proposed process is presented next followed by an analysis of the results obtained by solving the mass and energy balances and performing economic analysis.

PROCESS DESCRIPTION

Figure 1 presents a complete flow diagram of a continuous process for the production of β -cyclodextrin from cassava. Cassava tubers are fed through an inclined conveyor belt to a three-stage blade washing machine (P-1). The blade washing mechanism adopts the principle of sweep cleaning. The heavier sand and dirt sink to the bottom of the basin, as opposed to the lower density tubers that float and move to the next stage of mechanical peeling (P-2). A Brush Roller Cassava Peeler (www.dornow.de) is used to remove the brown peel of the tuber by scraping. Then the peeled tubers are washed (P-3) and inserted into a cassava root chopping machine (P-4) where they are chopped to ensure efficient wet milling (P-5). This is the first step of extracting the starch where the goal is to open all the tuber cells so that all the starch granules are released. In this process, treatment water has to be added to dilute the slurry and extract the cyanogen glucosides by releasing them into the water. This whole process is carried out on a Rasper machine. In the next step, a two-phase Decanter type separation (P-6) is carried out, where the aqueous phase containing the cyanogenic glucosides is separated at the outlet of the liquid, and the starch paste which contains proteins and fibers is removed from the solids outlet. The slurry is then mixed with excess water in a blender (P-7) at a concentration of about 20% w/w.

It is believed that the amount of fibers remaining in the slurry is negligible (less than 2%) so the slurry is directly passed to the hydrocyclone purification step (P-8). At this stage the slurry is fed to an array of ten hydrocyclones arranged in series. This centrifugal separation leads to the separation of the heavier starch removed from the bottom outlet and the hydrated (by about eight times) proteins are removed from the upper outlet. At the end of this process a dense slurry of starch (40% w/w moisture) is received. The mixture of proteins is fed into a centrifugal screening device (P-20) where the total solids are separated from the water. The solids are fed to an atmospheric drum dryer (P-21) where they are dehydrated while the water resulting from the centrifugal separation is recycled back. The resulting

dehydrated solids can be used either for cattle feed or for biotechnological antibiotic production processes.

After the tapioca starch purification step, the suspension produced is introduced into a stirred tank (P-9) where the starch concentration is standardized by adding water so that after the jet cooking stage the final suspension concentration is 30% w/w. CaCl_2 (to a final concentration of 30 ppm) and the *B. licheniformis* α -amylase enzyme (1.8 kg of enzyme solution -1,4- α -D-Glucan- glucanohydrolase Termamyl® 300L- per 1000 kg of starch) are also added. While stirred, the tank contents are also pre-heated to 70°C (Slominska et al., 2013). Live steam is then injected into the starch suspension (P-10) and the heated mixture is fed into a jet cooker (P-11). Steam injection is carried out by means of a pneumatic system which allows precise measurement and addition of the required quantity of steam to achieve the desired temperature of 105 °C. The residence time of the suspension in the jet cooker is 5 minutes. The addition of α -amylase prior to the gelatinization and liquefaction step aims at the faster reduction of the viscosity of the suspension during the starch hydrolysis step (P-12) at 95°C. At the end of hydrolysis, the starch has been converted into low molecular weight dextrins with dextrose equivalent (DE) of about 20. Subsequently, the α -amylase enzyme is inactivated by adjusting the pH to 3 (by adding an HCl solution) for 3 minutes. The pH adjustment in the hydrolysed product is carried out by cooling to 50°C and neutralization by addition of sodium carbonate with a final pH of 5. This inactivation leads to the denaturation of the α -amylase enzymes and the formation of the precipitate in the hydrolysis product (www.biokemi.org).

Enzyme CGTase-glucosyltransferase from *B. Thermoanaerobacter* sp. (TORUZYME®) is then added to the bioreactor at a ratio of 50mg /100kg of starch. This is a solvent-free method of cyclization avoiding the problems of toxicity or specificity to other forms of cyclodextrin that some solvents (such as toluene or ethanol) exhibit (Biwer et al., 2002). The CGTase enzyme cyclizes however only 30% of the starch in α -, β -, and γ -cyclodextrins in a ratio of 3: 5: 2 at 90°C, pH 5 and for 4 h (Norman and Jorgensen, 1992; Biwer et al., 2002). Glucoamylase and poulloulanase enzymes are then added to hydrolyze remaining dextrins to glucose at 60°C for 1 h (Hii et al., 2012). Glucoamylase cleaves dextrins into glucose to facilitate subsequent purification of β -cyclodextrin. All enzymes are then inactivated by adding HCl to pH 3 and by heating to 80°C for 3 minutes. The pH adjustment in the product produced is carried out by cooling to 50°C and neutralization by adding calcium carbonate with a final pH of 7. This inactivation leads to the formation of a sediment composed of altered enzymes. Removal of the precipitate is accomplished by decanter-type centrifugation (P-13) (Norman and Jorgensen, 1992).

The next step is to treat the mixture by filtration on activated charcoal filters (P-14). This filtration is intended to discolour the mixture and remove the caramelization products generated at the high dextrinization and fermentation temperatures of cyclodextrins (Biwer et al., 2002). An ion

exchange step (P-15) follows for the removal of ions which were added into the bioreactor. The purified solution containing the cyclodextrins and sugars is then led to a continuous crystallizer (P-16) where solids are first concentrated to 60% and then cooled to 25°C to crystallize β -cyclodextrin (Biwer et al., 2002). Separation of the crystals from the mother liquor is then carried out by centrifugal Basket type filtration (P-17). Separated crystals are washed in the cake to remove all impurities. The mother liquor is then led to a stirred batch fermentor (P-22) where water (to a final concentration of 17.5% in sugars), citric acid (to a final pH of 4.5), and yeast of *S. cerevisiae* in the form of a dry baker's yeast (at a concentration of 2% w/v) are added. Fermentation is carried for 32 h at 30°C to produce ethanol. The fermented broth is sent to a three-phase decanter centrifuge (P-23) where an ethanol-rich solution is taken from the light phase outlet while a large fraction of yeast is separated from the solids phase and recycled back to the fermentor (Lima et al., 1998; Mojovic et al., 2005). The light phase is led to a fractional distillation column (P-24) where a commercial product containing 96% v/v ethanol is obtained as distillate. Bioethanol can be sold as a fuel or as an additive for the preparation of alcoholic beverages and perfumes.

The produced vinacas containing both α - and γ -cyclodextrins are led from the column bottom to the waste treatment plant. Isolation of α - and γ -cyclodextrins from the waste stream could be achieved only via a complex and expensive chromatographic step with low yields and a range of by-products (Biwer et al., 2002) so it was deemed uneconomical and was not pursued.

The high-purity crystals of β -cyclodextrin obtained from the basket centrifuge are fed into a rotary dryer (P-18) suitable for drying of crystalline products. Drying is carried out using hot air at 120°C. The moisture content of the final product should be less than 14% (wet basis). The dried powdered crystals are then packaged in polypropylene bags of a net weight of 20 kg in a vertical packaging machine (P-19).

TECHNO-ECONOMIC ANALYSIS

Table 1 shows the material requirements for a plant processing 20 metric tons of cassava per hour. The plant produces 600kg/h of high-purity β -cyclodextrin packaged in 20-kg polypropylene bags. The plant is assumed to operate 330 days per year.

Table 1: Material Requirements Per 20kg Product Bag

Material	kg
alpha-amylase	0.56
CaCl ₂	0.01
Cassava	687.27
Citric acid	0.31
Glyco-amylase	1.30
Na ₂ CO ₃	0.03
Poulloulanase	0.07
Saccharomyces s	0.55
HCl 20%	0.10
Water	1,128.96

Table 2: Utility Requirements Per 20kg Product Bag

Utility	kg
Steam	1030
Chilled Water	98940

The annual product throughput is around 230,500 bags of β -cyclodextrin per year. In addition, the plant produces around 15,000,000 L(STP) of bio-ethanol and 5,000,000 kg of animal feed (the protein/fiber-rich stream separated from cassava) per year.

The process has significant cooling and heating utility requirements as shown in Table 2.

With respect to economics, the total equipment cost for a plant of the above capacity is estimated to be around 7.7 million €, with the bioreactors being the most expensive equipment. The total plant cost is around 22 million € with a physical cost breakdown shown in Figure 2. The total capital investment (including direct and indirect costs, working capital etc.) is estimated to be around 65 million €.

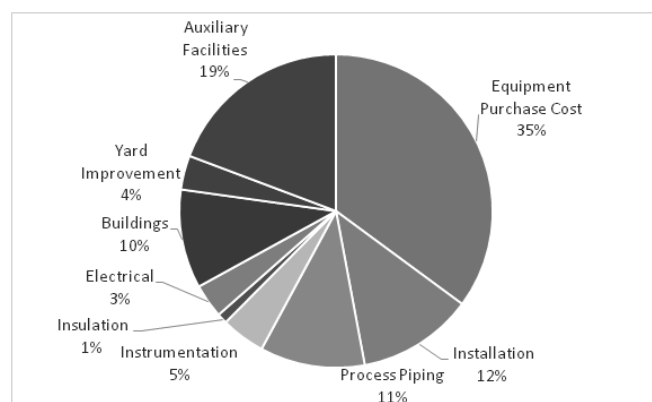


Figure 2. Direct (Physical) Cost Breakdown.

The operating cost is around 75 million €/yr (including depreciation) with the material cost being its most significant component (about 50% of the total cost) as shown in the pie-chart cost breakdown in Figure 3. The purchasing price at the time of analysis (end of 2017) for cassava was 0.22€/kg.

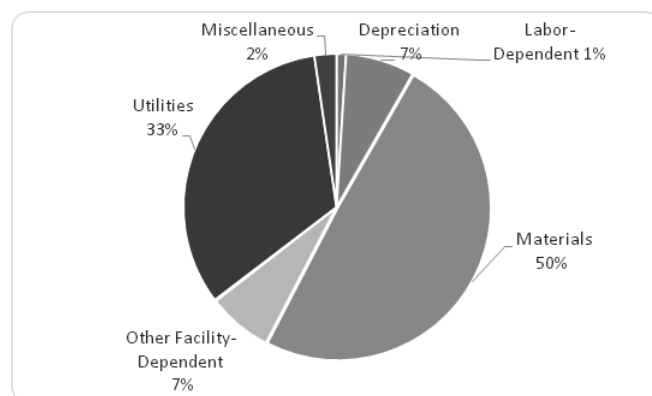


Figure 3. Annual Operating Cost Breakdown.

Table 3: Selling prices of main product and by-products

Product	€
β-cyclodextrin	22.25 /kg
Bioethanol	0.7 /L(STP)
Animal Feed	0.076 /kg

Table 3 shows the assumed selling prices of all products. These values were obtained through a web-search at the time of the analysis on products of similar composition. Expected revenues from β-cyclodextrin are in the order of 102.5 million €/yr assuming a selling price of 22.25€/kg. Additional revenues of 10.8 million €/yr can result from selling the process by-products (bioethanol and animal feed). The resulting gross profit margin is 34%.

Based on all above economic results, the process seems to be economically viable with a Return on Investment (ROI) index at 44.2%, payback time of 2.26 years and Net Present Value of 201 Million € at 7% interest rate.

CONCLUSIONS

A commercial feasibility study was conducted using SuperPro Designer on a plant that uses casava tubers to produce β-cyclodextrin. The proposed technology is a non-solvent process; it yields a product free of toxic solvent residues and, at the same time, it exploits most by-products in order to take advantage of the full economic potential of the process. The model mass and energy balance equations were solved to calculate the material and energy requirements and a detailed economic analysis on the process was performed. Results from this preliminary techno-economic analysis indicate that the process is technically feasible and economically viable.

REFERENCES

- Biwer A.; G. Antranikian; and E. Heinzle. 2002. "Enzymatic production of cyclodextrins." *Appl Microbiol Biotechnol*, 59(6), 609–617.
- Das S.K.; R. Rajabalaya, S. David; N. Gani; J. Khanam; and A. Nanda. 2013. "Cyclodextrins-The Molecular Container." *Research Journal of Pharmaceutical, Biological and Chemical Sciences*, 4(2), 1694-1720.
- Gustafson A.Y. 2015. "Wastewater to renewable energy at a tapioca factory in Vietnam." MSc Thesis. Department of Chemical Engineering, Lund University, Sweden.
- Hii S.L; J.S. Tan; T.C. Ling; and A.B. Ariff. 2012. "Pullulanase: Role in Starch Hydrolysis and Potential Industrial Applications." *Enzyme Research*, Vol. 2012, 1-14.
- Knight, J. 2011. "Commercialization of a method for the preparation of glucose syrup from whole cassava for use as a fixed carbon source for the fermentative production of algal oil." MSc Thesis. Department of Chemistry, Case Western Reserve University, USA.
- Li Z.; S. Chen; Z. Gu; J. Chen; and J. Wu. 2014. "Alpha-cyclodextrin: Enzymatic Production and Food Applications." *Trends in Food Science & Technology*, 35, 151-160.
- Lima H.O.; F. Moraes; and G. Zanin. 1998. "Beta-Cyclodextrin Production by Simultaneous Fermentation and Cyclization." *Appl Biochem Biotechnol*, 70-72, 789-804.

- Mojovic L.; S. Nikolic; M. Rakin; and M. Vukasinovic. 2006. "Production of Bioethanol from Corn Meal Hydrolyzates." *Fuel*, 85, 1750-1755.
- Montagnac J.A.; C.R. Davis; and S.A. Tanumihardjo. 2009. "Processing Techniques to Reduce Toxicity and Antinutrients of Cassava for Use as a Staple Food." *Comprehensive Reviews In Food Science And Food Safety*, 8(1), 17-27.
- Norman B.E and S. Jorgensen. 1992. "Thermoanaerobacter sp CGTase: its Properties and Application." *Denpun Kagaku*, 39(2), 101-108.
- Quintero J.A; Cardona C.A; Felix E.; Moncada J.; and Higuera J.C. 2015. "Techno-economic analysis of fuel ethanol production from cassava in Africa: The case of Tanzania." *African Journal of Biotechnology*, 14 (45), 3082-3092.
- Saenger W. 1980. "Cyclodextrin Inclusion Compounds in Research and Industry." *Angew. Chem. Int.*, 19, 344-362.
- Slominska L.; D. Wisniewska; and A. Grzeskowiak A. 2013. "Liquefaction of Starch by Thermostable Alpha-Amylase." *Technologia Alimentaria*, 2(2), 17-26.
- Tonukari N. J. 2004. "Cassava and the Future of Starch." *Electronic Journal of Biotechnology*, 7 (1) 1-4.

WEB REFERENCES

- www.biokemi.org
- www.efsa.europa.eu
- www.fao.org
- www.dornow.de
- www.intelligen.com

MODELING A BREWERY: CAPACITY AND COST ANALYSIS

Alexandros Koulouris*,
Department of Food Technology
Alexander Technological Education Institute
P.O. Box 141, 57400 Thessaloniki
Greece

Albert Roussos and Demetri Petrides
Intelligen, Inc.
2326 Morse Avenue
Scotch Plains, NJ 07076
USA

*E-mail: akoul@food.teithe.gr

KEYWORDS

Beer Production, Simulation, Techno-Economic Analysis.

ABSTRACT

A brewery simulation model is presented in this paper for an industrial-scale beer production and filling facility. The model was developed on SuperPro Designer, a process design software tool, and used for capacity estimation, process scheduling and economic analysis. The fermentation process was identified as the plant bottleneck; with the introduction of extra equipment units, the process cycle time was improved and the throughput increased. As demonstrated by the economic analysis, the improved plant capacity yields an economically viable process.

INTRODUCTION

Computer-aided process design (CAPD) and simulation tools could have a tremendous impact in process development for batch food industries, as they have had since the early sixties in the bulk chemicals and oil sectors. Their most important advantage is that they allow fast, inexpensive and easily documentable experimentation with numerous alternative scenarios that would be impossible to evaluate by hand calculations or experimentally (Koulouris and Petrides, 2002). Computer-generated models can be used to calculate material and energy requirements and the expected process yield, estimate plant capacity, cycle times and production cost, pinpoint the economic "hot-spots", i.e. the steps of high capital and operating cost or low yield throughput, or to identify the environmental hot-spots such as materials that are costly to dispose. The findings from such analyses can be used in process design, process and product development, technology transfer and process fitting, production scheduling and resource utilization and, in general, streamlining of manufacturing operations. At the end, all these can have a profound impact on the business bottom-line.

This paper presents a simulation model of an industrial-scale beer production and filling facility. The model was developed on SuperPro Designer v10, a commercial process design software tool by Intelligen, Inc. (www.intelligen.com). The objective of the model is to optimize the plant's throughput and perform a thorough economic analysis. For the development of the model, process data for the brewing process were taken from Bamforth (2003) and Goldammer (2008).

PROCESS DESCRIPTION

The brewery process is separated into three sections, namely: brewhouse, fermentation/aging, and filling/packaging. Figure 1 shows the flowsheet of the entire process excluding the filling/packaging section. For the selected beer recipe, two different carbohydrate sources are employed, specifically malted barley and corn grits. In the model, they are represented as mixtures whose assumed composition (Goode and Arendt, 2006) is shown in Table 1.

Table 1: Feed Composition

Component	Barley Malt (%w/w)	Corn Grits (%w/w)
Starch	70	73
Proteins	11	8
Fibers	8	10
Fat	2	3
Minerals	1	1
Water	8	5

The processing capacity of the modeled process is 12 metric tons (MT) of malted barley and 6 MT of corn grits per batch. Using the procedure/equipment names shown in Figure 1, the process is as follows. Malted barley is grinded in Mill-1 and collected in the SB-101 solids bin. Likewise, corn grits are grinded in Mill-1 and collected in solids bin SB-102. The next step is the mashing stage. Mashing is the process of mixing the milled barley malt and cereal adjuncts (corn grits) with hot water and letting the mixture stand at an appropriate temperature, while the enzymes degrade the proteins and starch to yield the malt extract (i.e., the wort) that is used as the substrate for fermentation. The corn grits are mashed-in first because of the higher temperature that is required for the gelatinization of corn starch. The contents of SB-102 are transferred into the mash vessel (MK-1) where they are mixed with hot water. A small quantity of barley malt (around 20% by weight of corn grits) is also added at this stage. After the completion of the adjunct mashing stage, sparge water of ambient temperature is added to the vessel to cool down the contents. The malted barley is then transferred into the mashing vessel and is mashed according to the following schedule:

- Heat to 45°C and hold for 15 min. This stage represents the proteolysis reaction where the protein content is extracted from the malt and transferred into the wort.
- Heat to 65°C and hold for 180 min. This stage represents the saccharification reaction where the starch is broken down to sugars which are dissolved

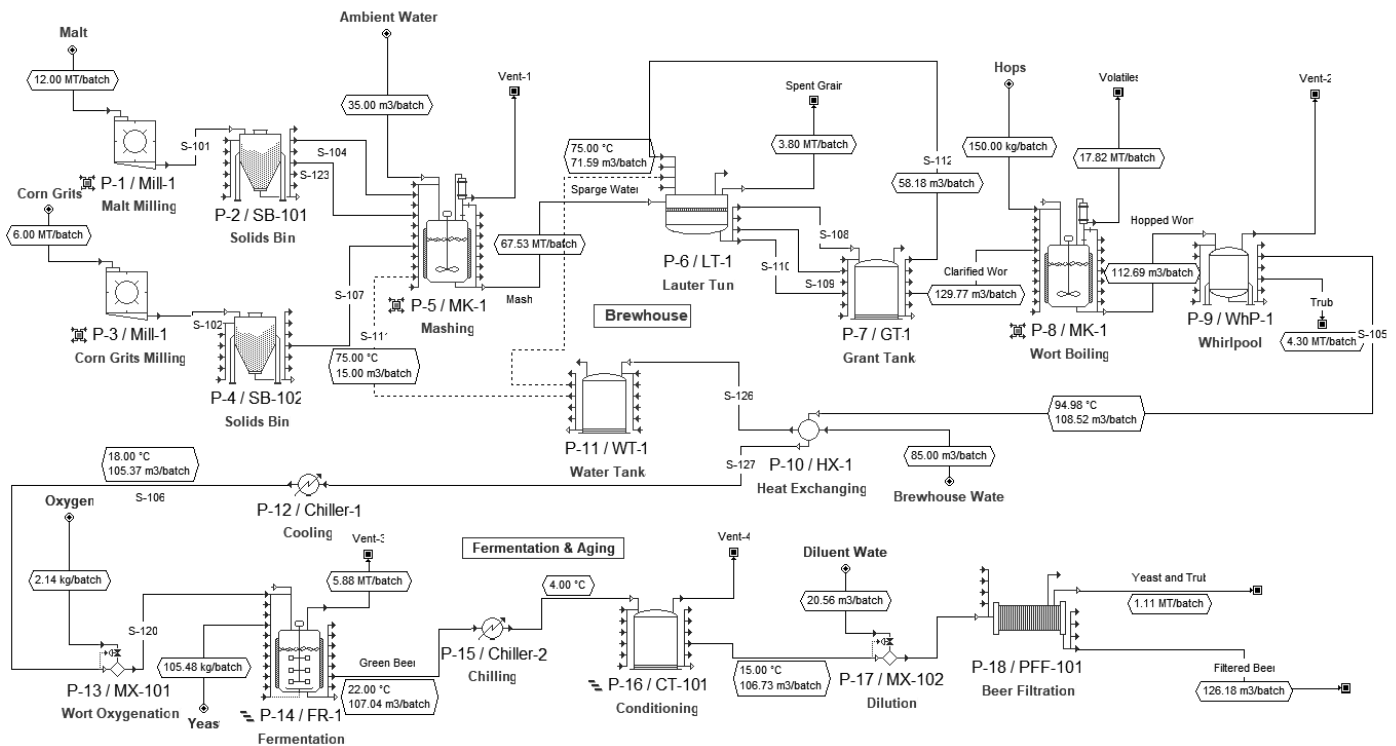


Figure 1. The Process Flowsheet of the Brewery Model.

in the wort. The conversion of starch into sugars is represented by the following mass stoichiometry:



The component Glucose in the reaction products represents a variety of fermentable and non fermentable sugars that are extracted from the malt into the wort (e.g., maltose, dextrins, maltotriose, glucose, fructose and sucrose). The extent of the reaction is set to 90% with respect to starch to indicate that, on average, 90% of the starch contained in the barley malt and corn grits is extractable.

- Heat to 75°C and hold for 10 min in order to terminate enzyme activity, reduce the viscosity and promote the coagulation of particles, thereby improving the fluidity of the mash.

Next, the mash is transferred to the lauter tun (LT-1) where the separation of the wort from the solids is performed. The solid-liquid separation is represented by a filtration operation accompanied by a recycling of the wort until a desired clarity is achieved. In the end, the solids bed that remains in the lauter tun is washed with sparge water in order to increase the yield of the process.

The clarified wort is then transferred back to the mash vessel (MK-1) where hops are added and the resulting mixture is boiled. The boiling of the wort serves a number of purposes including sterilization, extraction of the bittering and aromatic compounds (iso- α -acids) from the hops, as well as coagulation of excess proteins and other undesirable flavoring substances. The Mashing (P-5) and Wort Boiling (P-8) procedures utilize the same vessel (MK-1). Before the

fermentation stage, the hops and hot trub that are formed during wort boiling are removed by sedimentation in a Whirlpool (WhP-1).

The clarified wort from the whirlpool is cooled down by heating the water utilized in the brewhouse section (P-10 / HX-1). Heat integration improves the economics of the process and its environmental foot print. The cooling of the wort is completed using Chiller-1 where it is cooled down to 18°C in and then oxygenated in MX-101 to a dissolved oxygen concentration of 0.02 g/L. The oxygenated wort is transferred to a fermentor (FR-101) where brewing yeast is pitched to a concentration of 1 g/L (corresponding to approximately 6×10^9 cells/L). The fermentation of sugars to ethanol is represented by the following mass stoichiometry (Bamforth, 2003):



The extent of the fermentation reaction is set to 88% to indicate that only a portion of the sugars contained in the wort are actually fermentable. Fermentation lasts for 5 days and the temperature is maintained at 22°C by flowing chilled water in the jacket of the fermentor. After the completion of fermentation, the immature (green) beer is cooled to 4°C in Chiller-2 during its transfer to the conditioning tank CT-101. The fermentor is cleaned using both caustic (NaOH) and acid (H₃PO₄) solutions. The conditioning and aging of the beer in CT-101 takes about a week. Next, the beer is diluted in mixer MX-102 with water to 5% alcohol by volume (4% w/w) prior to filtration in PFF-101. The plate and frame filter (PFF-101) removes all suspended solids.

It is assumed that 20% of the produced beer is packaged in 50L kegs while the remaining 80% is bottled in 0.5L glass

bottles. The beer of the keg-line is pasteurized in bulk form while the pasteurization of the bottled beer is performed inside the bottles. The filled and pasteurized bottles are labeled and then packed in dozen-bottle cartons.

THROUGHPUT ANALYSIS

The modeled process as described above produces approximately 126,000 L of beer per batch. The process cycle time (i.e. the time lag between the start of two consecutive batches) is 8.57 days, which allows for a maximum of 37 batches per year (assuming a 330-day annual operation) and an annual throughput of 4,670,000 L of filtered beer. From a simple comparison of the process times of all equipment, it can be easily verified that the fermentation step is the process bottleneck while the brewhouse equipment and the filling lines are underutilized. It is possible to reduce the cycle time of the process and increase its throughput by installing additional fermentors and conditioning tanks operating in staggered mode (out of phase). Figure 2 shows the equipment occupancy Gantt chart of the main equipment for 16 consecutive batches for a plant with 6 fermentors (FR-1 to FR-6), 10 conditioning tanks (CT-101 to CT-110) and 2 filtered beer tanks (FBT-1 and FBT-2) operating in stagger mode. In this case, the minimum cycle time of the process has been reduced to 20.93 hours. Rounding the cycle time to 24 h (i.e. start a new batch every day), results in 315 batches per year and an annual throughput of 39,758,000 L of filtered beer. This represents a throughput increase of 750% compared to the base case.

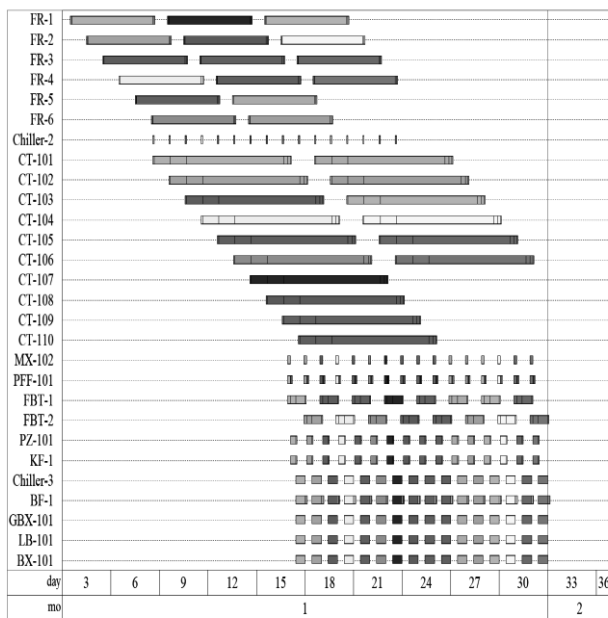


Figure 2. The Equipment Occupancy Gantt Chart.

COST ANALYSIS

Table 2 displays the material requirements in kg/batch. Based on the material demands per batch and the number of batches that can be executed per year, the annual material cost can be estimated to be around \$5 million. The assumed purchasing price for barley malt was 0.2\$/kg, for corn grits 0.15\$/kg and for hops 1.5\$/kg.

Table 2: Material Requirements Per Batch

Material	kg/batch
Water	211,828
Barley Malt	12,000
Hops	150
Corn Grits	6000
Brewing Yeast	106
NaOH (2.5% w/w)	20,084
H3PO4 (0.2M)	19,971

The estimated annual operating cost (including materials, utilities, labor and facility-dependent costs such as depreciation and maintenance), is \$24.2 million, which translates to a unit cost of \$0.61 per kg of filtered beer. With an assumed selling price of \$6 per twelve half-liter-beer-bottle cartons and of \$20 per 50 L beer kegs, the total annual revenues are estimated to be around \$34.8 million resulting in a gross margin of 30.8%.

Using vendor quotations and empirical cost models, the total equipment cost for a plant of this capacity (39,758,000 L of filtered beer per year) was estimated at around \$8.8 million resulting in a total capital investment of around \$60.9 million.

Based on all above economic results, the process seems to be economically viable with a Return on Investment (ROI) index at 20%, payback time of 5 years and Net Present Value of \$21.9 million at 7% interest rate.

CONCLUSIONS

A process model of an industrial-scale batch brewery process was presented. The model mass and energy balances were solved to calculate the material and energy requirements, the cycle time was estimated and improved to increase process throughput and an economic analysis on the process was performed. The improved process is economically viable. Such a model can be used for further process and product development at the design phase or streamline manufacturing operations on an existing brewery facility.

REFERENCES

Bamforth C. 2003. *BEER – Tap Into the Art and Science of Brewing*. Oxford University Press.
 Goldammer, T. 2008. *The Brewer’s Handbook – The complete Book to Brewing Beer*. Apex Publishers.
 Goode D. L. and E.K. Arendt. 2006. “Developments in the Supply of Adjunct Materials for Brewing”. In *Brewing: NewTechnologies*, C. Bamforth (Ed.). Woodhead Publishing, Cambridge, 30-67.
 Koulouris, A.; and D.P. Petrides. 2002. “See the Optimum- Batch Process Optimization via CAPD and Simulation,” *Process Worldwide*, 2, 38-40.

WEB REFERENCES

www.intelligen.com

Short Paper

Design and CFD Simulation of a Parabolic Solar Fruit Dryer

Joshua Wanyama¹, Cyrus Galyaki¹, John Muyonga², Nicholas Kiggundu¹ and Noble Banadda^{1,3*}

¹Department of Agricultural and Bio-Systems Engineering, Makerere University, P.O. 7062, Kampala, Uganda

²Department of Food Science and Technology, Makerere University, P.O. 7062, Kampala, Uganda

³Department of Agricultural and Biosystems Engineering, Iowa State University, 1340 Elings Hall, Ames, Iowa 50011-3270, USA

*Email: banadda@caes.mak.ac.ug

KEYWORDS

CFD Simulation, Solar dryer, fruit drying, fruits, food quality

ABSTRACT

Several solar drying technologies exist in Uganda, but marred with multiple challenges such as inefficient conversion of trapped solar radiations into thermal energy, low throughput, poor quality construction materials, poor heat and mass transfer, air flow, heat penetration and heat distribution, prolonged drying times to mention but a few. In this study, a state of the art solar dryer that overcomes such difficulties and can be constructed from materials that are locally available was designed. The dryer consists of a concrete base of 7m × 5m × 10cm, with a parabolic frame made of painted mild steel and covered with a 198 μm transparent UV-stabilized visqueen. Simulations built on Computational Fluid Dynamics (CFD) were made to predict air flow and temperature distribution inside the drying chamber using ANSYS FLUENT V14.0. Simulation results were validated by experimental investigation of temperature and air flow distribution inside the dryer, followed by statistical comparison of simulation and the observed results. Further the dryer was tested with three full batches (120±7 kg) of fresh pineapple slices of 2-3 mm thickness and diameter 10±1.5 cm for the sunshine period of 8:00 am to 6:00 pm, continued to the following day until the desired moisture content of 15% wb was reached. CFD simulations predicted air flow and temperature to be 0.68±0.07 ms⁻¹ and 51±3°C, respectively. These results were validated experimentally and were found to be 0.47±0.02 ms⁻¹ and 57.8±10°C for inside air flow and temperature, respectively.

INTRODUCTION

Fruit drying is further faced with increasing necessity to meet; stricter quality specifications, higher production rates, and stern environmental regulations. To resolve the challenges faced in fruit drying, it is important to consider the fundamentals of heat, mass and momentum transfer coupled with knowledge of fruit drying properties when designing a dryer or drying systems. Studies such as Misha *et al.*, 2013) show that use of Computational Fluid Dynamics (CFD) analysis techniques can replace costly and time consuming experiments to; optimize, retrofit, improve equipment and processing approaches. CFD techniques precisely predict air flow distribution, temperature profiles, and momentum flow in the design of dryers and/ or drying systems. CFD thus provides means for creative innovation and ingenuity in the food drying industry. The main objective of this study was to design and simulate heat and mass transfer profiles in solar fruit dryer with aid of CFD software.

MATERIALS AND METHODS

Building a CFD based prototype

Building a CFD based prototype followed four steps: a) Selection of dryer type; b) Sizing of the dryer; Generation of 3D model using Computer Aided Design (CAD) software; and Analysis of 3D model for air flow fields and temperature distribution. A greenhouse type of dryer with a parabolic shape was selected (Figure 1). The model was selected

because it can easily be constructed out of locally available materials and scaled up to accommodate big drying loads. Further, the parabolic shape was chosen to adapt the dryer to strong wind loads, increase area for light transmission and to enhance the esthetics of the design. The wet produce is placed under the transparent enclosure where solar radiations are entrapped. The solar radiation is directly absorbed by the drying produce and some is absorbed and irradiated by a black painted concrete floor. Heat gradually gained by drying produce affects moisture removal to the surfaces. The stream of air from the inlet vents carries the vapor away through the outlet vents to the surrounding environment.

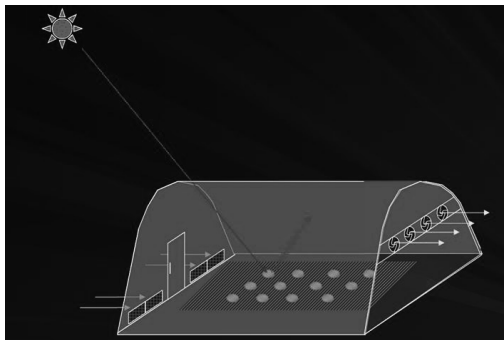


Figure 1: A greenhouse type solar dryer model

Sizing of the dryer

The drying area is determined considering energy required to dry anticipated mass of wet produce and estimating the solar radiation collection area that meets the energy requirement. This is because the collector absorbs the solar radiation and converts them into hotter long wave radiations by principle of black body radiation, to provide the enthalpy requirement for drying the food produce.

Experimental procedure

The dryer was tested using fresh pineapple slices of 2-3 mm thickness and diameter 10 ± 1.5 cm. Three full batches of 120 ± 7 kg of fresh sliced pineapple pulp were dried. For each batch, drying was started at 8:00

am and continued to 6:00 pm. Drying was continued to the following day until the desired moisture content of 15% wb was reached. At the end of every batch, the dry sold weight of samples was determined by oven method at 103°C for 24 h. Temperature and relative humidity were measured using a Hygrothermograph, HTC-1 (accuracy $\pm 1^\circ\text{C}$ and $\pm 5\%$ for temperature and relative humidity respectively). The air velocity was measured using an air flow meter (Air flow, model 323, accuracy $\pm (3\% + 3 \text{ ms}^{-1})$). Product mass loss was monitored using an analytical balance (Rawang, AS60/220.R2, accuracy $\pm 0.1\text{g}$).

RESULTS AND DISCUSSIONS

The CFD model output results

A summary of the CFD simulations results is shown in Figure 2. Temperature is uniform inside the dryer. The collector concrete heated to a maximum of 327K, while the entrapped air in the drying chamber reached an average of 324K compared to the 315K obtained by Adeniyi et al. (2012) in a simple passive indirect solar dryer. These results closely agree with the 318 K obtained by Yunus and Al-Kayiem (2013) as mean temperature of the air inside the drying chamber.

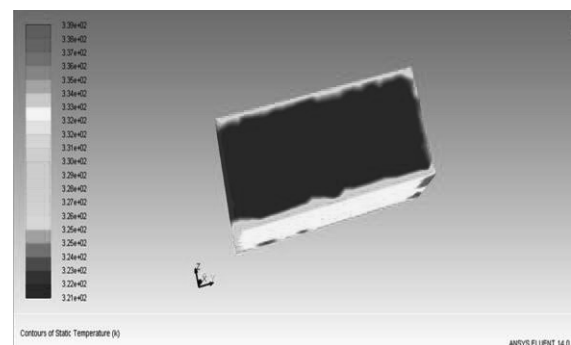


Figure 2: Contours of static temperature (K)

Velocity magnitude contours show uniform distribution air flow (Figure 3), although regions of higher velocity

streams exist at the entry point and exit point of the drying chamber. It can also be noticed that the velocity is homogeneous in a vertical plane in the solar collector and drying chamber. Air in the drying chamber has an average velocity of 0.68 ms⁻¹ compared to 2.00 ms⁻¹ of inlet air and the 13.6 ms⁻¹ as it enters the discharge pipe. This behavior of temperature and velocity is necessary for drying purposes, since it ensures a high-quality and homogeneous drying process.

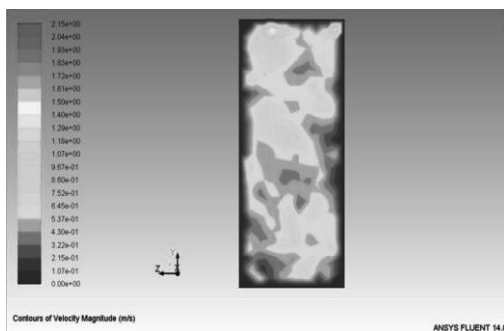


Figure 3: Contours of Velocity magnitude (ms⁻¹).

Results from testing of the dryer

The drying rate of the pineapple samples were initially high because the moisture content was high, but decreased rapidly to almost the same rate in the course of drying (Figure 2). This was due to the free moisture near the surface of the slices and subsequently slows down because the evaporating surface will have moved to below the slice surface and due to increase in internal forces.

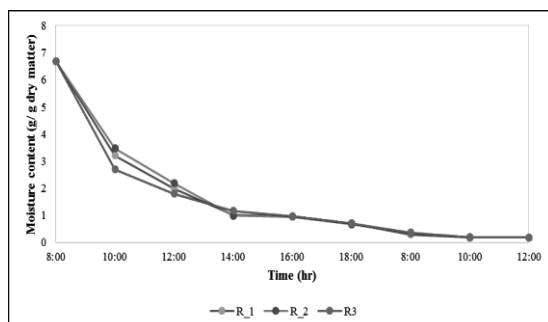


Figure 4: The drying curve for pineapple slices

CONCLUSIONS

Based on field finding a more appropriate solar dryer model was designed, built and tested. A CFD based model of the new design was developed and validated by comparing no load results with CFD output results. The model results closely agreed ($R^2=0.9995$) with the experimental testing results for inside temperature and from the prototype tested, results were indicative of uniform air flow and temperature distribution which are vital for uniform product drying.

REFERENCES

1. Adeniyi, A. A., Mohammed, A., and K. Aladeniyi. 2012. Analysis of a solar dryer box with ray tracing CFD technique. *International Journal of Scientific & Engineering Research*, 3(10), 1–5.
2. Amanlou, Y. and Zomorodian, A. 2010. “Applying CFD for designing a new fruit cabinet Dryer.” *Journal of food engineering*, 101(1), 8-15.
3. Yunus, Y. M. and H.H. Al-Kayiem. 2013. Simulation of Hybrid Solar Dryer. In *IOP Conference Series: Earth and Environmental Science* (Vol. 16, No. 1, p. 012143). IOP Publishing.

Author Listing

AUTHOR LISTING

Akkermans S.....	95/125/145/229	Evans J.....	60
.....	248	Fekih-Salem R.....	184
Akritidou T.....	145	Fenton O.....	77
Albrand P.....	181	Flick D.....	177/269
Almeida G.....	269	Fonseca F.....	243
Alonso A.A.....	130/158	Foster A.....	60
Altin O.....	235/277		
Alvarez G.....	60	Galyaki C.....	301
Angarano V.....	125	García M.R.....	130/158
		Gatt R.....	113
Baka M.....	117/125/199/	Gerbaud V.....	181
.....	214/221	Gijsen W.....	248
Bakalis S.....	52	Gonzales-Barron U.....	204
Balcázar J.L.....	71	Gortzi O.....	104
Balsa-Canto E.....	158/259	Govaert M.....	221
Banadda N.....	301	Gut J.A.W.....	189
Barnabé M.....	11/243	Gutierrez-Merino J.....	199
Bhonsale S.....	25/29/253		
Billet A.-M.....	181	Hashem I.....	25/253
Boehm D.....	229	Healy M.G.....	77
Boillereaux L.....	172	Henriques D.....	259
Borrego C.M.....	71	Houhoula D.....	81/135
Boskou G.....	104		
Boukhelifa N.....	11/243	Janssen S.....	264
Bourke P.....	41/229	Joseph J.A.....	285
Bruggeman F.....	5	Julcour C.....	181
Bussemaker M.....	199		
		Kiggundu N.....	301
Cadavez V.....	204	Kinnaert M.....	184
Castro C.C.....	184	Kojić P.....	57
Chabin T.....	11/243	Konteles S.....	135
Charalambous C.....	290	Koulouris A.....	290/295
Chieffi A.....	125		
Clarke R.....	77	Leducq D.....	60
Coldrey P.....	60	Leverrier C.....	269
Costello K.....	199	Los A.....	229
Cullen P.J.....	229	Louizaki A.....	290
Cummins E.....	41/71/74/77	Lutton E.....	11/243
Curet S.....	172		
		Mac Kernan D.....	33
Damas A.....	60	Méjean Perrot N.....	11/243
Detomi de Albuquerque C.....	172	Merai M.....	108
.....		Mexi A.....	81
Dewasme L.....	184	Minebois R.....	259
Djekić I.....	19	Molenaar D.....	5
Doursat C.....	269	Monteiro F.....	204
Dugat-Bony E.....	243	Moulin G.....	269
		Moureh J.....	60/177
Encina-Zelada C.R.....	204	Muñoz López C.A.....	25/150/253
Erdogdu F.....	166/235/277	Muyonga J.....	301

AUTHOR LISTING

Nefel Simou V.	81	Tonda A.	11/194/243
Nicolaï B.	264	Topcam H.	166/235
Nimmegeers P.	25/29/95/145/	Tsakali E.	104/135
.....	150/248/253	Tsaknis J.	104
O´ Flaherty E.	71	Tsironi T.	81
Ou E.	269	Vacharakis N.	290
Pant A.F.	89	Valdramidis V.P.	41/113/214
Pérez-Torrado R.	259	Van Impe J.F.M.	19/25/41/29/95/
Perrot N.	194	117/125/135/
Petrides D.	295	145/150/199/
Pham A.T.	177	214/221/229/
Plana-Fattori A.	269	235/248/253/
Planqué B.	5	285
Pojić M.	57	Vande Wouwer A.	184
Polańska M.	41/285	Velliou E.	199
Querol A.	259	Velly H.	243
Raphaelides S.	290	Verboven P.	264
Reinelt M.	89	Verheyen D.	117/235
Režek Jambrak A.	19	Vilas C.	158
Roche A.	11	Vladimirov L.	81
Roussos A.	295	Walsh J.	214
Salliou N.	46	Wanyama J.	301
Sardella D.	113	Youbi-Idrissi M.	60
Schnäckel W.	41	Ziuzina D.	229
Schorsch J.	184	Zorrilla S.	264
Seow T.K.	235		
Shevlin D.	74		
Siguemoto É. S.	189		
Skåra T.	117/235/277		
Skipnes D.	235/277		
Smet C.	125/145/214		
.....	221		
Souliotis A.	104		
Stamatis K.	81		
Stathopoulos P.	135		
Stefan T.	210		
Swennen D.	11		
Tadini C.C.	189		
Teixeira J.A.	204		
Telen D.	29/248		
Teusink B.	5		
Thomas-Danguin T.	11		
Thomopoulos R.	46/52		
Timpis D.	104/135		